DETECTING AND MONITORING LAND DEGRADATION FEATURES AND [illegible] IN THE [illegible]BA VALLEYS, [illegible]

[illegible]

ITC
Publication
Number 36

Graciela Isabel Metternicht

DETECTING AND MONITORING LAND DEGRADATION FEATURES AND PROCESSES IN THE COCHABAMBA VALLEYS, BOLIVIA A SYNERGISTIC APPROACH

GRACIELA ISABEL METTERNICHT

Publication
Number 36

International Institute for Aerospace Survey and Earth Science (ITC)
PO Box 6, 7500 AA Enschede, The Netherlands
ISBN 90 6164 118 7

PREFACE

This publication is the PhD thesis of Mrs. Graciela Metternicht, successfully defended on 14 May 1996, at the University of Ghent, Belgium.

The thesis deals with the identification and characterization of indicators suitable to describe, map and monitor land degradation processes in the semiarid environment of the Cochabamba Valleys, in the eastern Andean cordillera of Bolivia. Salinization-alkalinization and gully formation are among the main land degradation phenomena in the above valleys.

The susceptibility of land to degradation is strongly controlled by the origin and nature of the landscape. This is why the thesis of Mrs. Metternicht properly starts reconstituting the differential tectonic and depositional evolution of the Cochabamba Valleys during the Quaternary. This evolution led to geopedologic conditions which promote salinization-alkalinization in the Punata-Cliza valley, while they favor accelerated water erosion in the Sacaba valley.

Because of the scarce vegetation cover and the bright soil reflectance dominating in the area, remotely-sensed data provide an efficient way to identify, delineate and monitor surface features caused by salinization-alkalinization and by accelerated water erosion. However, detailed field and laboratory data are needed to accurately map salt-affected topsoils, explain the formation of rills and gullies, and identify the areas potentially exposed to land degradation. The thesis meets this need of integrating data from various sources and levels of resolution. The author goes one step further by attempting to
quantitatively assess the efficiency and cost-effectiveness of different modes of data synergy.

Soil salinization-alkalinization and accelerated soil erosion are often affected by large spatial variations at short distance, generating diffuse limits between cartographic units. The thesis solves this problem through data modelling using fuzzy sets and expert rules for monitoring salinization-alkalinization and predicting soil erosion hazard.

By combining a landscape-based approach, different modes of data synergy and fuzzy modelling, the thesis of Mrs. Metternicht represents an original and rich contribution to the study of land degradation in general. Due to the unusual width and depth devoted to the treatment of the subject, guiding this thesis was a particularly stimulating venture for the promotors.

Prof. Dr. M. De Dapper
Prof. Dr. J.A. Zinck

ABSTRACT

In the Cochabamba valleys, central Bolivia, factors such as the introduction of large-scale irrigation, deforestation, population growth, drought periods and highly erosive precipitations led, over the past decades, to land degradation through salinization and alkalinization, accelerated soil erosion, flooding and torrential burying of agricultural lands. From the above degradation processes, land salinization and alkalinization and accelerated soil erosion were selected for analysis.

The study area comprises the Central, Sacaba and Punata-Cliza basins, with a total extension of 96,500 ha. Land degradation phenomena such as salinization, alkalinization, soil erosion and flash-floods affect 23% of the total area. The valleys are located at altitudes between 2500 and 3600 masl, belong to the mesothermic interandean valleys. They originated from tectonic depressions filled in by Quaternary lacustrine, glacio-lacustrine and alluvio-lacustrine sediments.

The core objective of this study is to identify and characterize indicators suitable to describe, map and monitor land degradation processes in the semiarid environment of the valleys. For this purpose, a synergistic approach combining data extracted from various types of remote sensing documents (aerial photographs, Landsat TM and JERS-1 SAR) and field observations, at multi-scale level, was used. To achieve the main goal, research focused on the following specific objectives:

1. Land degradation indicators: detection and description of land degradation features; analysis and evaluation of the spectral discrimination of soil properties and surface degradation features; identification of land degradation indicators, and investigation of the relationships between land degradation features, indicators, mechanisms and processes in selected landscape components.
2. Land degradation processes: delimitation and monitoring of the salinization-alkalinization process; assessment of soil susceptibility to erosion.
3. Mapping land degradation processes and evaluating the research approach: estimating the intensity, rate and spatial distribution of the land degradation processes; and testing the relevance of the synergistic approach for mapping and monitoring land degradation processes.

ACKNOWLEDGMENTS

This dissertation could not have been completed without the cooperation and assistance of many persons and institutions. First of all, I am very grateful to both promotors, Prof. Dr. J.Alfred Zinck and Prof. Dr. Morgan De Dapper, for their contributions at all stages of the research. I received stimulating guidance from Prof. Zinck, who demonstrated a belief in interdisciplinary work. He supported and encouraged my decision to go through the 'soils' world after my specialization in geoinformatics. I learned much about using the right words to express my ideas. I hope I have done it in the proper way!. I thank Prof. De Dapper for his willingness to act as promotor. He fulfilled this task with dedication and always followed the progress of the work with interest .

The Netherlands Fellowship Program (NFP) financially supported this three-year research project. I am indebted to the Universidad Nacional del Litoral, especially to the head of the Facultad de Ingeniería y Ciencias Hídricas, Ing. Julio Theiler, and to Ing. Marta Pujol for their support during this period.

In Cochabamba (Bolivia), the field data collection was possible thanks to the support of the following persons and institutions, to whom I am deeply indebted: to the Rector of the Universidad Mayor de San Simón; the Head of the Facultad de Ciencias Agricolas y Pecuarias, Ing.Fernando Quitón, Ing. J. Amurrio and Ing. Espinosa; the staff of the Laboratorio de Suelos; Ing. J.C. Rocha, Ing. Pablo Lopez Antezana, and all the staff of the Laboratorio de Hidráulica; Ing. Roberto Mendez and all the staff of PROMIC; Ing. Luis C. Sanchez (CORDECO); Lic. Vilma Crespo (CISTEL), Ing. Alvaro Fernandez (GEOBOL), Ing. Carlos Rojas Ralde (PEIRAV); staff of the CABAS Project ; Ing. Gustavo Mendez (SEMAPA); SENAMHI and Empresa Misicuni. Two undergraduate students of agronomy, J. Torres and J. Carrion, helped during the field campaign. Special thanks to Hugo Miranda (Laboratory de Hidráulica) for his collaboration and good humour during the six months of fieldwork.
A Ramiro, Gladis, Rocio, Gabriel y Ramirin Iriarte, gracias por todos los domingos que disfrutamos en la PIL, poniendo a prueba nuestras habilidades para los deportes. Ustedes, al igual que Pablo y Mirna Lopez, nos ayudaron a sentir 'como a casa'.

At ITC, I would like to thank Dr. Carlos Valenzuela, who introduced me to the degradation problems arising in the Cochabamba valleys. The staff of the Soil Science Division; Dr. W.Elbersen, L. van Sleen, A. Farshad, E. Bergsma, R. Henneman and Dr. W. Siderius, supported this research in several ways. Dr. W. Siderius helped to translate of the summary and thesis title into Dutch. Staff of the Image Processing Laboratory , Gerard Reinink, Wan Bakx and Wim Bakker, sorted out software- and hardware-related issues. They also increased my hardisk quota proportionally to the growth of my files and converted my soft maps in real paper

prints. Thanks!!. Prof. Dr. P. Driessen (WAU-ITC) gave advice during different stages of the salinity and alkalinity data analyses and interpretation. Ir. Bart Kroll (ITC) helped to solve database-related problems. Dr. G. Epema (WAU) advised on the use of the radiometer as well as on the way to collect field reflectances. Mrs. Anneke Fermont (WAU) participated in the research through practical work on geostatistics and spectral unmixing. Dr. Jane Drummond introduced me to the 'fuzzy sets' world. Thanks Jane for your consistent interest in my research, and your friendship. I like the way you make difficult things look easy. I thank Dr. F. van der Meer for his advice on spectral unmixing and Roland Mora for his discussions and contribution on photo interpretation of the geomorphology of the study area. My colleague Jiang Bing contributed to the understanding of fuzzy modelling.

The staff of the Cartography Division; Dr. K. Sijmons, J.van der Worm, W. Feringa, H. Scholten, T. Mank and J.van der Steen, provided support and organized the production of the geopedologic maps. Thank you for your support during my five years at ITC!. Administrative and technical staff at ITC: Bert Riekerk, who always found a solution to my financial problems and Benno Masselink, Gerard Leppink, Michael Herdmann and R. Teekamp assisted in various ways. Cecil Wolters and Daniela Semeraro were always available for secretarial support. Thank you!. The ITC librarians, Marga and Carla, contributed to this research in an important way behind the scenes. Thanks for your efforts in getting all those 'impossible articles' in time. Ann Stewart tried to improve my English writing over the five years; thanks, Ann, for your friendship and availability.

The members of the jury, Prof. A. Antrop, Prof.Dr.Ir. K.J.Beek, Prof. W. De Breuck, Prof.Dr. L. Daels, Prof.Dr. M. De Dapper, Prof. K. Kerre, Dr. E. Kosters, Prof.Dr. J.L. van Genderen, Prof.Dr. E. van Ranst, Prof. C. Vernemmen and Prof.Dr. J.A. Zinck, are gratefully acknowledged for their valuable suggestions and time expended for reviewing the text.

Many friendships were forged during the five years. Wherever you are now, thank you Araceli Vargas, Soledad and Alfredo Martinez, Susana and Erasmo, Ivo Ricchetti, Lucia Luzi, Paola Napolitano, Fabio Fussi, Chris Schreuders, Daniel Somma and family, Julian and Sofia, Gabriel and Charo, S. Shakker, Lorena, Henry and Ana Maria Lopez, Marta Barrera, the van der Landen family, Asunción Saldaña, Rita and Eelco Nieuwenhuis for all the happy moments we shared. As you say, Rita, 'finita la comedia'!

Gracias por el soporte de toda mi familia en Argentina y Uruguay: Delia, Zulma, Cuca, Nanci, Ricar, Celia, Carlos y Susana. Last, but not least, my husband Sergio, who supported me along the way during these five years. His love, support and criticism helped me to complete this work. It has not been easy, but as M. Benedetti, the Uruguayan writer, says ***...'y en la calle codo a codo somos mucho mas que dos'....***

SUMMARY

In the Cochabamba valleys, central Bolivia, factors such as the introduction of large-scale irrigation, deforestation, population growth, drought periods and highly erosive precipitations led, over the past decades, to land degradation through salinization and alkalinization, accelerated soil erosion, flooding and torrential burying of agricultural lands. From the above degradation processes, land salinization and alkalinization and accelerated soil erosion were selected for analysis.

The core objective of this study is to identify and characterize indicators suitable to describe, map and monitor land degradation processes in the semiarid environment of the valleys. For this purpose, a synergistic approach combining data extracted from various types of remote sensing documents (aerial photographs, Landsat TM and JERS-1 SAR) and field observations, at multi-scale level, was used. To achieve the main goal, research focused on the following specific objectives:

1. Land degradation indicators:
   - detection and description of land degradation features
   - analysis and evaluation of the spectral discrimination of soil properties and surface degradation features
   - identification of land degradation indicators
   - investigation of the relationships between land degradation features, indicators, mechanisms and processes in selected landscape components
2. Land degradation processes:
   - delimitation and monitoring of the salinization-alkalinization process
   - assessment of soil susceptibility to erosion
3. Mapping land degradation processes and evaluating the research approach:
   - estimating the intensity, rate and spatial distribution of the land degradation processes
   - testing the relevance of the synergistic approach for maping and monitoring land degradation processes

The research method and techniques selected to handle the specific objectives are discussed in chapter three. The methodological approach is composed of four main steps: characterization of the geopedologic units and land degradation features; identification and measurement of land degradation indicators; design and implementation of exploratory models for monitoring and prediction; evaluation of the efficiency of the synergistic approach.

Chapter five highlights the importance of knowing the landscape origin and evolution over time for identifying land degradation factors and hazards. This facilitates the understanding of the mechanisms of action, location, extent and expansion trends of degradation phenomena. The tectonic and sedimentary history of the basins, the nature of the sediments and the spatial distribution of the geopedologic cover formations determine a differential susceptibility of the

three valleys (Central, Sacaba and Punata-Cliza) to specific land degradation processes. To frame the landscape and landform evolution and date the formation of badlands and other erosional features in the area, five buried soils located in different relief types were dated by radiocarbon determinations.

Remote sensing data provide an efficient way to identify, delineate and monitor soil surface features caused by salinity and/or alkalinity. The classification schemes based on the norms of the US Salinity Laboratory and the anion ratios developed by Russian soil scientists were applied and compared in chapter six. Fuzzy modelling of salt and sodium classes was carried out to improve the accuracy of spatial discrimination. Results achieved when working with different data sets (e.g. Landsat TM, Landsat TM+JERS-1 SAR and JERS-1 alone) and classification techniques (e.g. statistical pattern recognition and fuzzy classification) are compared. The salinity-alkalinity monitoring model considers the nature, magnitude and quality of the changes occurred specifically in the Punata-Cliza valley. It uses fuzzy sets and a rule-based system of if-then statements. Information on the possibility of actual changes to take place is incorporated as 'degrees of likelihood' of a certain event to occur.

Chapter seven concentrates on accelerated soil erosion by water in the Sacaba basin. Fuzzy knowledge-based exploratory models were designed to investigate the susceptibility of specific areas to erosion by incorporating expert knowledge on the soil properties and/or landscape elements assumed to control accelerated soil erosion. Fuzzy boundaries were applied to rank the landscape factors, used in modelling the likelihood of an area to be affected by different erosion degrees. Landscape elements such as vegetation cover percentage and rock fragment density were obtained from spectral unmixing of satellite data, using a linear mixture modelling technique. Although the model only provides qualitative estimations, it proved useful to explore indicator-cause-process relationships. In addition, it allows to assess the importance of the individual landscape elements related to soil erosion and select those which best predict soil erosion. The model considers the effect of rock fragments to protect the soil surface against raindrop impact and aggregate detachment. Seasonal variations in soil susceptibility to erosion because of changes in vegetation coverage are also taken into account.

Chapter eight evaluates the level of efficiency at which the various data sources and data processing techniques have performed in identifying, characterizing and discriminating specific surface indicators of land degradation. The spectral separability of the land degradation features was analyzed at plot and regional levels. At plot level, the synergy of the visible and near-infrared ranges was evaluated, while the advantage of combining the visible, infrared, thermal and microwave regions of the spectrum was assessed at regional scale. Detailed discrimination of type and intensity of the degradation processes requires increased synergy among remotely-sensed, field and laboratory data, especially in salinity-alkalinity studies.

RESUMEN

Deforestación, crecimiento de la población, introducción de sistemas de riego extensivos, prolongados períodos de sequía y el poder erosivo de las precipitaciones, entre otros factores, han ocasionado durante las últimas décadas una degradación progresiva de la tierra, a través de procesos de salinización y alcalinización, erosión de los suelos, inundación y pérdida de áreas agrícolas por efecto de las torrenteras en los Valles de Cochabamba, ubicados en la parte central de Bolivia. De los procesos mencionados, salinización, alcalinización y erosión de los suelos fueron seleccionaron para un análisis.

El objetivo principal de este estudio es la identificación y caracterización de indicadores adecuados para la descripción, mapeo y seguimiento de procesos de degradación de tierras en el ambiente semiárido de los Valles de Cochabamba. Para este propósito se utilizó un método sinergístico que combina datos extraídos de diversos tipos de imágenes teledeteccionadas (fotografías aéreas, Landsat TM y JERS-1 SAR) y observaciones de campo a diversas escalas. A fin de lograr este objetivo, la investigación se centra en los siguientes items:

1. Indicadores de degradación de las tierras:
   - detección y descripción de rasgos de degradación
   - análisis y evaluación de la discriminación espectral de las propiedades del suelo y rasgos superficiales de degradación de la tierra
   - identificación de indicadores de degradación del suelo
   - investigación de las relationes entre rasgos, indicadores, mecanismos y procesos de degradación de tierras, en componentes específicos del paisaje
2. Procesos de degradación de tierras:
   - delimitación y monitoreo de procesos de salinización-alcalinización
   - evaluación de la susceptibilidad del suelo a la erosión
3. Representación cartográfica de los procesos de degradación y evaluación del método de investigación:
   - estimación de la intensidad, proporción y distribución espacial de los procesos de degradación
   - evaluación de la relevancia del método sinergístico para la delimitación y monitoreo de los procesos de degradación.

En el capítulo tres se discuten el método de investigación y las técnicas seleccionadas para manipular los objetivos específicos. La metodología adoptada se compone de cuatro fases principales: caracterización de las unidades geopedológicas y los rasgos de degradación; identificación y medición de los indicadores de degradación; diseño e implementación de modelos exploratorios para el seguimiento y predicción; evaluación de la eficiencia del método sinergístico.

El capítulo cinco resalta la importancia relativa al conocimiento del origen y evolución del paisaje a través del tiempo para la identificación de factores de degradación, como así también predicción de su occurrencia. Esto facilita el entendimiento de los mecanismos de acción, localización, extensión y tendencias de expansión del fenómeno de la degradación de tierras. La historia tectónica y sedimentaria de las cuencas, la naturaleza de los depósitos y la distribución espacial de las formaciones geopedológicas determina una variabilidad en la susceptibilidad de los tres valles (Central, Sacaba y Punata-cliza) a procesos específicos de degradación del suelo. Utilizando el método del isótopo radioactivo del C-14 se dataron cinco suelos enterrados, ubicados en diferentes posiciones fisiográficas, a fin de formular la evolución del paisaje y su fisiografía, y estimar la formación de cárcavas y otros rasgos erosionales presentes en el área.

La teledetección es un medio eficiente para identificar, delinear y monitorear rasgos superficiales del suelo causados por salinidad y/o alcalinidad. En el capítulo seis se describe la aplicación y comparación efectuada entre los esquemas para la clasificación de la salinidad basados en las normas del Laboratorio de Salinidad de los E.U. (US Salinity Laboratory) y el de la proporción de aniones desarrollado por especialistas del suelo Rusos. Para mejorar la precisión de la discriminación espacial se aplicó un modelamiento 'fuzzy' de las clases de salinidad y sodicidad. También se compararon los resultados logrados a partir del uso de diferentes datos (p.e. Landsat TM, Landsat TM+JERS-1 SAR y solamente JERS-1SAR), técnicas de clasificación (p.e. reconocimiento estadístico de patrones y clasificación fuzzy). El modelo elaborado para el seguimiento de los procesos de salinización-alcalinización considera la naturaleza, magnitud y confiabilidad de los cambios ocurridos en el área del valle de Punata-Cliza. Se utilizan conjuntos 'fuzzy' y un sistema de normas basado en condiciones del tipo 'si'-'entonces'. La información relativa a la posibilidad de ocurrencia de cambios se incorpora como 'grados de posibilidad' de ocurrencia de un evento determinado.

El capítulo siete trata la erosión hídrica acelerada en la cuenca de Sacaba. Para investigar la susceptibilidad a la erosión de ciertas áreas se diseñaron modelos exploratorios 'fuzzy' basados en el conocimiento (fuzzy knowledge-based exploratory models). Los mismos incorporan conocimientos relativos a las propiedades del suelo y/o elementos del paisaje que se asume, controlan la erosión de los suelos. Los elementos del paisaje que se utilizaron en el modelamiento de la posibilidad de un área de ser afectadas por diferentes grados de erosión fueron categorizados usando límites graduales ('fuzzy boundaries'). Elementos del paisaje tales como el porcentage de cobertura vegetal y la densidad de fragmentos rocosos en superficie se obtuvieron a través de una separación espectral de los datos satelitales, utilizando una técnica de modelamiento linear de las mezclas espectrales (linear mixture modelling). Aunque el modelo provee solamente estimaciones cualitativas, se comprobó su utilidad para ezplorar las relaciones entre indicadores-causa-proceso. Por otra parte, el modelo permite evaluar la importancia de cada elemento del paisaje relacionado a la erosión del suelo, y seleccionar los más confiables para las tareas de predicción. El modelo cosidera además el efecto que ejercen los fragmentos rocosos en la protección de la superficie del suelo contra el impacto de las gotas de lluvia y la separación de los agregados. También se consideraron las variaciones estacionales

en la susceptibilidad a la erosión debido a cambios en la cobertura vegetal.

Finalmente, el capítulo ocho evalúa el nivel de eficiencia con que las diversas fuentes de datos y técnicas de procesamiento actuaron en la identificación, caracterización y discriminación de indicadores superficiales de procesos de degradación de tierra específicos. La separabilidad espectral de los rasgos de degradación fué analizada a escala local y regional. A nivel local se evaluó la sinergía de los rangos visible e infrarojo, mientras que la ventaja de la combinación de la regiones del espectro visible, infrarojo, termal y micro-ondas se evaluó a una escala regional. Se concluye que una discriminación detallada del tipo e intensidad de los procesos de degradación requiere una creciente sinergía entre sensores remotos, datos de campo y laboratorio, especialmente en estudios de salinidad-alcalinidad.

CONTENTS

TABLES

Pages Nº

FIGURES

Pages Nº

CHAPTER ONE:

INTRODUCTION

1.1 PROBLEM FORMULATION

Over the past decades, factors such as the introduction of large-scale irrigation, deforestation, population growth, drought periods and highly erosive precipitations have lead to land degradation through salinization and alkalinization, accelerated soil erosion, flooding and torrential burying of agricultural fields in the Cochabamba Valleys, central Bolivia.

The Cochabamba valleys comprise the Central, Sacaba and Punata-Cliza (figure 1.1). The tree basins have a total extension of 96,500 ha. The Punata-Cliza valley, also known as High Valley covers 45,500 ha, the Sacaba Valley comprises 10,000 ha, while the Central Valley has 41,000. Land degradation phenomena such as salinization, alkalinization, soil erosion and flash-floods affect 23% of the total area. Urban areas in constant growth cover approximately 7.2%, while 68% correspond to rural areas used mainly for agricultural activities (figure 1.2). About half of the agricultural lands is irrigated, but only 3.5% receives enough irrigation water. For 1978, the Integrated Water Resource Project (PIRHC), executed by GEOBOL (Bolivia Geological survey) and United Nations, estimated that 77,000 ha were suitable for agriculture. This area has been reduced to 69,000 ha in 1986 and 64,700 ha in 1994, mainly because of the salinization of agricultural land and urban expansion. According to the last National Census (Instituto Nacional de Estadística, 1992) the urban population duplicated in the period 1976-1992 while the rural population grew only by 20%. This resulted in land overcropping and overgrazing, with little consideration to sustainable land use.

The valleys are located at altitudes between 2500 and 3600 masl, and belong to the mesothermic interandean valleys. They originated from tectonic depressions filled in by Quaternary lacustrine, glacio-lacustrine and alluvio-lacustrine sediments. Large piedmonts, with torrential fans and glacis, border the depressions. The climate is semiarid with mean annual precipitation of 400 to 600 mm, 80% of which occurs from December to February. The mean annual temperature is 14º to 17ºC. The irregular rainfall conditions determine ephemeral streams of torrential regime.

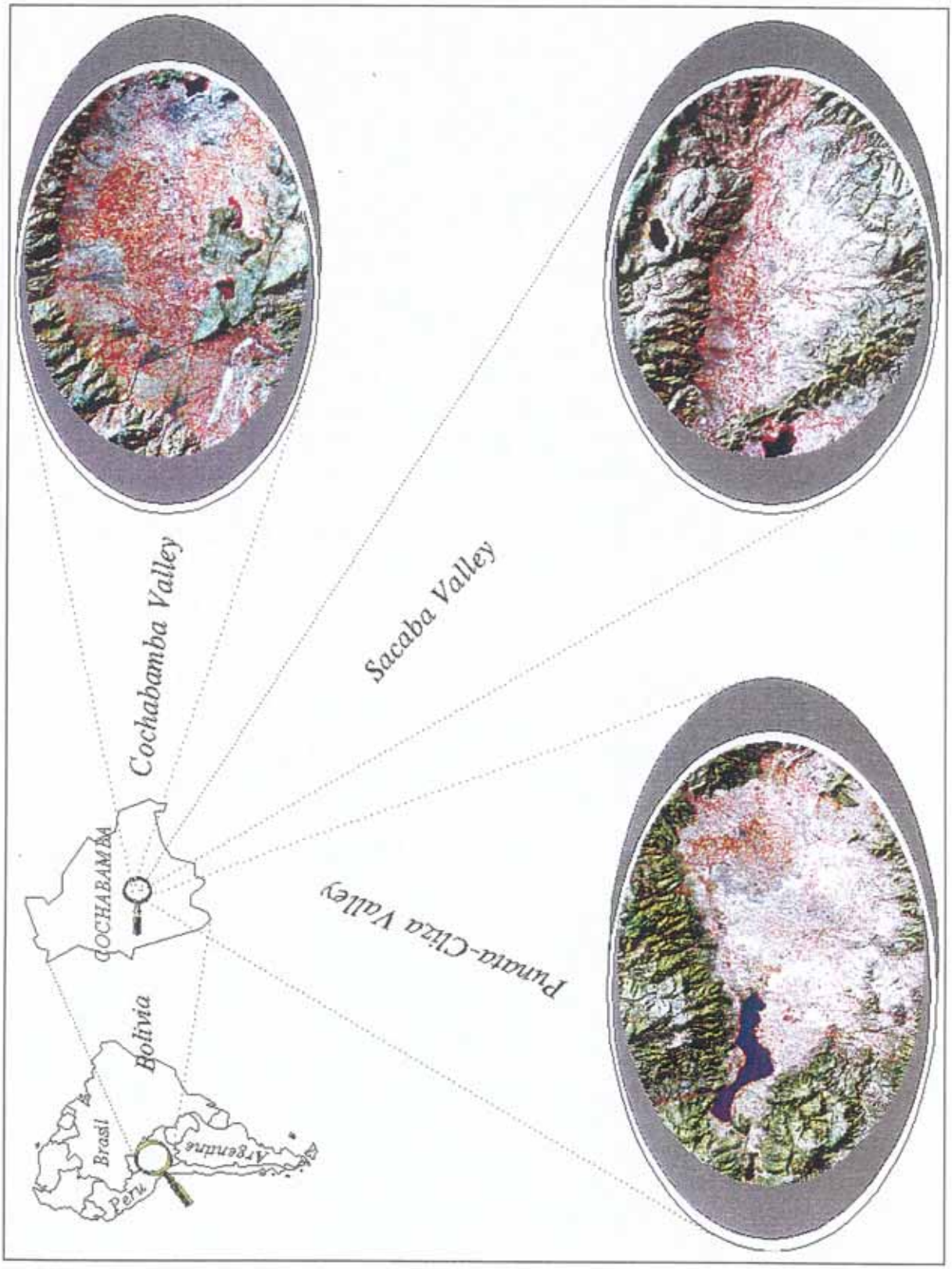

Fig. 1.1: Study area location

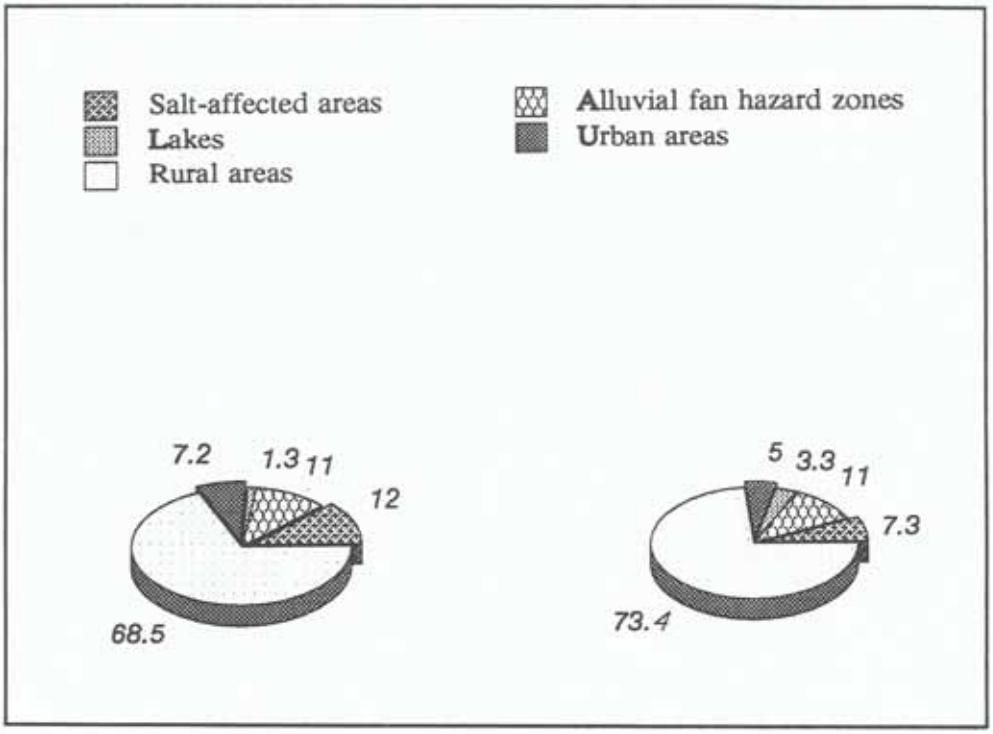

***Fig. 1.2:** Land cover in the valley areas (1986-1994)*

Severe erosion in the bordering mountains (e.g. the Tunari Cordillera) increases the flood hazard in the valley lowlands. For instance, about 30,000 hectares of fertile were damaged by torrential floods during the rainy season 1981-82, causing important economical losses. This situation repeated in the rainy period 1990-91, producing destruction of 7,000 hectares of agricultural land (CORDECO, 1991). Flooding and stream avulsion constitute a serious threat for urban settlements like Cochabamba, Vinto, Sipe-Sipe located in the piedmont and valley landscapes. Agricultural production is also affected by recurrent drought periods such as the extremely dry years of 1979 to 1982 and 1986 to 1989. During the rainy season 1989-1990 the Bolivian government had to work out an emergency plan against drought effects on the Cochabamba Department, because rainfall was as low as 255 mm. The aridification of the valleys revealed by increasing drought periods, followed by torrential precipitations which in turn cause flooding, landslides and debris flows towards the valley have not received the necessary attention in the past.

1.2 LAND DEGRADATION FACTORS

In the Cochabamba Valleys, natural and human causes are responsible of severe land degradation.

(1) Physical factors:

- Soil erosion

Water and wind erosion, causes substantial topsoil losses. Soils become shallower, badlands are extended and areas of productive land decrease. Subsurface processes such as tunneling and piping also contribute

to soil erosion.

- Climatic factors

During the rainy season, the Central Valley is affected by flush-flood erosion. Rushing streams transport high debris loads from the Tunari Cordillera. Streams dry up soon after the rains stop, spreading their sediment load over large fans. On the other hand, soil degradation by salinization is favored by the semiarid climate and severe drought periods.

- Lithology and geomorphic position

Clay sediments of lacustrine origin favor the formation saline-alkaline areas. Salinization is accentuated by the long-term use of brackish irrigation water, mainly in playas and flats landforms of alluvio-lacustrine origin.

(2) Factors resulting from human activity:

- Land overexploitation

In pre-Columbian times, intensive agricultural systems developed in Bolivia. The Incas were well-known for their sophisticated irrigation networks and for the storage and distribution of agricultural produce. The Incas were also aware of the importance of crop rotation and multiple cropping. Spanish colonizers introduced new crops and the traditional 'tajlla' or foot-plough was gradually replaced by animal traction and tractor at present. Demographic pressure also led indigenous population to exploit more marginal land, previously untouched or allowed to restore for long periods (Ellenberg, 1981). Additionally, the introduction of foreign livestock (cattle, sheeps, goats) not suitable for this region stimulated land degradation. Most of the farmers let their animals graze on communal land, because they are not used to produce cultivated forage crops. The result is overgrazing of almost all natural pastures.

- Deforestation

To feed the growing population, large portions of forest land were cleared for cultivation without sustainable landuse planning. Economic assessment does not consider the irreversible degradation of landscape components such as groundwater, soils and vegetation. Intensive deforestation in the upper watersheds causes severe problems in the lowlands, where most of the agricultural activities take place and the urban settlements are located.

- Land management practices

Inadequate land cultivation practices, such as tillage operations parallel to the slope, cause soil losses. Irrigation with brackish water and the lack of adequate drainage systems contribute to land salinization in the Punata-Cliza and Central Valleys. The most common water application practice is by flooding of the cultivated parcels ('lameado'), which causes the concentration of salts near to or on the soil surface and turns the land less productive. In the High Valley, roads acts as barriers obstructing the already poor

natural drainage and cause waterlogging.

(3) Factors derived from socio-economic context

- Excessive land parcelling

In 1953 started the agrarian reform in the Bolivian countryside. Vast landed estates or 'haciendas' were transferred to the Indian peasants, since the reform promoted landownership to the indigenous population. The dismembering of large holdings into small parcels was compounded by the native inheritance system. According to the second National Agricultural Census (INE, 1984), 46% of the land parcels are less than one hectare large, 37% have a surface of 1 to 3 ha, and only 16% are larger than 3 hectares.

- Lack of land use planning

Increasing public awareness about natural hazard calls for stronger land use control. A recent article entitle 'The suicide of Cochabamba', published by the local newspaper, Los Tiempos, remarks that 'the commercial parcelling above 2,750 m elevation will cause more debris flows, a movement of soil and stones from the highlands, which in conjunction with seasonal rainfall will create mass movements of millions of tons moving towards the Valley' (Sanz, 1994).
On lands not provided with irrigation water, farmers are constrained to dry farming. Good quality groundwater is usually more than 60 m deep and well excavation is very expensive. This situation makes land use planning difficult, since crops yields and consequently farmer's income greatly depend on climatic conditions.

1.3 RESEARCH OBJECTIVES

From the various soil degradation processes occurring in the area, land salinization and alkalinization and accelerated soil erosion were selected.
Salinization and alkalinization processes were studied in training areas located at the Punata-Cliza Valley. Rill and gully erosion was investigated in a training area located in the Sacaba Valley.

The main objective of this study was to identify and characterize indicators suitable to describe, map and monitor the land degradation processes in the semiarid environment of the valleys. A synergistic approach combining data extracted from various types of remote sensing documents and field observations, at multi scale level, was used for this purpose. To achieve this main goal, research focused on the following specific objectives:

(1) To identify the causes of land degradation
Understanding the landscape origin and evolution is important to infer causes and to delineate the spatial distribution of the land degradation phenomena. Therefore, a characterization of the main landscape components was carried out using ground-based data, laboratory determinations, geologic information and

correlation with past climatic changes.

(2) To investigate the relationships between land deterioration indicators, mechanisms, and processes in selected landscape components

Different physical, chemical and biological mechanisms act on degradation processes, determining specific land degradation features. These relationships were investigated using remote sensing techniques, field survey, soil geographic databases and process-oriented models, integrated in a GIS environment.

(3) To detect and assess land degradation features

Selected features included gullies, rills, tunneling, piping, crusting, sealing, surficial salt and sodium concentration and topsoil properties.

Statistical analysis was performed to evaluate the relative importance of the selected land degradation features.

(4) To analyze and evaluate spectral discrimination of soil properties and surface degradation features

Ground-based reflectance measurements, active JERS-1 and passive Landsat TM remote sensing data were correlated with field observation data to evaluate the spectral separability among land degradation indicators, in particular the possibility to discriminate type and abundance of certain surface components like salts and crusts. Correlation coefficients between ground-based radiometric measurements and surface degradation features were estimated.

(5) To determine the spatial distribution and monitor the salinization-alkalinization process

Systematic analysis of spatial and temporal changes of salt-affected areas was carried out to evaluate the usefulness of remote sensing techniques to detect and monitor this degradation process.

(6) To determine the soil susceptibility to erosion

Qualitative estimation and zonation of water erodibility was done using the K-USLE soil erodibilitiy coefficient.

(7) To assess the intensity, rate and spatial distribution of the land degradation processes

Qualitative evaluation of rate and intensity of degradation as well as spatial zonation of the different processes was done. Dynamic maps of salinization-alkalinization show extension trends of this phenomenon.

(8) To test the relevance of the synergistic approach

The results achieved by integrating active and passive remote sensing images and field data in a GIS environment, for identifying and assessing land degradation indicators representative of the processes acting in the study area, were evaluated.

CHAPTER TWO:

CONCEPTUAL FRAME AND RESEARCH APPROACH

2.1 BASIC CONCEPTS

2.1.1 Synergy and synergistic approach

Synergy (from Greek *synergos*, working together) is defined as '...the cooperative action of discrete agencies such that the total effect is greater than the sum of the two or more effects taken independently..' (Webster's Dictionary). The words 'synergy' and 'synergistic' are commonly used in the remote sensing literature (Lozano, 1988; Justice, 1991; Folving, 1994). However, only a few authors specify what synergy refers to in their work and, sometimes, its evocation does not imply more than using data from one sensor for a specific task (e.g. land cover classification).

In this research, the concept of synergy is applied in the sense that data of different nature (e.g. saline areas, land cover types) or accuracy (salt types and abundance) can be extracted from several sources such as field observations, laboratory analysis, remote sensing imagery, and integrated for further analysis.

Main trends in the study of land degradation combine in different ways and degrees ground data collection techniques at plot level, and remote sensing techniques at local and regional levels. Remote sensing techniques allow to obtain data over large areas of land in a short time. These data must be combined with field observations and measurements such as soil profile descriptions, characterization of surface components and radiometric measurements. However, field observations are very time-consuming and do not allow for synoptic land characterization. Table 2.1 shows in a schematic way the data sources to be used according to the scale and type of information needed. Data generated at plot level are three-dimensional, including internal and external features, but of small coverage. Local scale sources provide two-dimensional data about surface conditions, with a good resolution for the identification of land degradation features. At regional scale, satellite imagery is suitable for identifying and monitoring land degradation processes.

Table 2.1: Data sources

OBSERVATION SCALE	DATA SOURCE	DATA GENERATION
Plot level	Field observations and determinations	External features: soil surface conditions, reflectance measurements Internal features: topsoil properties
	Laboratory analysis	Internal features: soil components
Local level	Aerial photographs	External features: land degradation features, boundaries, surface dynamics
Regional level	Satellite imagery	External features: spatial distribution of land degradation processes; extrapolation and monitoring scale

The synergy of plot, local and regional scales, combining different data sources, was used in this study to characterize the land degradation processes occurring in the Cochabamba Valleys. The data were processed, analyzed and interpreted in a GIS environment to provide information about the nature, intensity and spatial distribution of the processes.

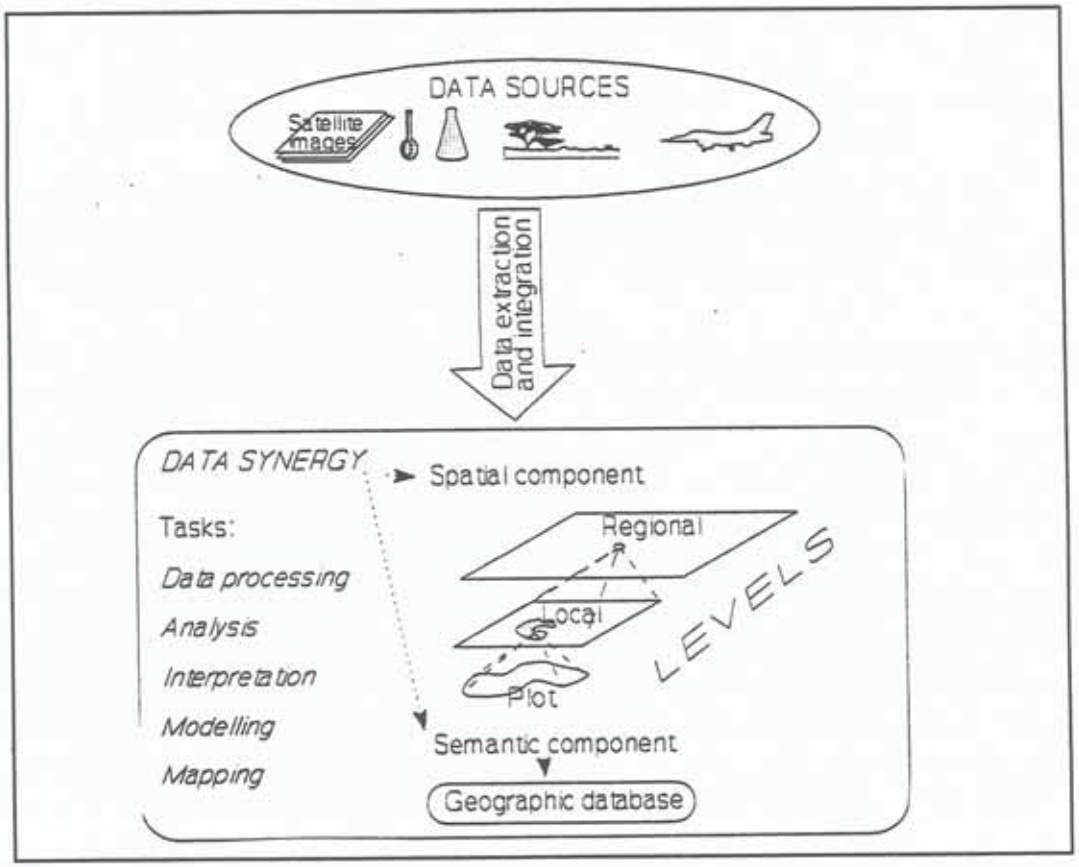

Fig. 2.1: The synergistic approach

2.1.2 Monitoring

Managing and planning the use of the natural resources is of practical importance and political relevance, since these resources provide the basis for our lives. In this context, comprehensive information on the spatial distribution and dynamics of land degradation processes is of permanent interest to environmental analysts and planners concerned with urban and rural developments. Detection and monitoring of degradation processes are essential to develop and control remedial programs.

Monitoring means 'to keep track of, regulate, or control a process' (Webster's Dictionary). Thus, monitoring can be seen as a management tool, which requires information about the status and evolution of the object under study. Additionally, qualitative aspects of information flow such as timing, coverage and validity are other important factors to be considered.

Putten (1991) mentions three principles involved in monitoring:

(1) Monitoring is based on a repetitive observation of the process to be analyzed. Repetitivity, or frequency of observation, is determined by a cost-efficiency factor and the speed of change of the phenomena to be observed.

(2) In monitoring, the emphasis is on timeliness, thus on the rapidity of information supply, including data collection, processing and communication.

(3) Monitoring provides factual data, not analytical information. Selection of suitable data implies the addition of values for analysis of the process under monitoring (e.g. salinization).

Based on the former, Townshend (1977) defined four types of monitoring systems to detect and follow spatial and temporal changes affecting diverse phenomena (figure 2.2)

The monitoring of land degradation processes is seen in a fourth dimensional space, the time interval or frequency of observation (e.g. t=0, t=1). The spatial unit of observation allows to detect and estimate the extent of the changes: for example, the surface area affected by salinization and/or alkalinization. The frequency of observation provides the rate of changes: for example, the speed of salinization.

2.1.3 Land degradation and desertification

(1) Definition

The lack of agreement about the concept of desertification has led to a confusion about its meaning. Additionally, the terms desert encroachment, aridization, desertization and desertification are often used more or less synonymously. The term 'desertification' was used first by Aubréville (1949), who included both soil and vegetation deterioration caused, at least partially, by human activities.

Desertification has been described either as a process or as a series of conditions or as the last phase of degradation. Desertification as a process in space and time refers to the expansion of desert-like conditions in arid,semiarid and some subhumid ecosystems, by the combined influence of human activities and climatic factors (Rapp, 1974; Dregne, 1976; UNCOD, 1977; Mabbutt, 1986).

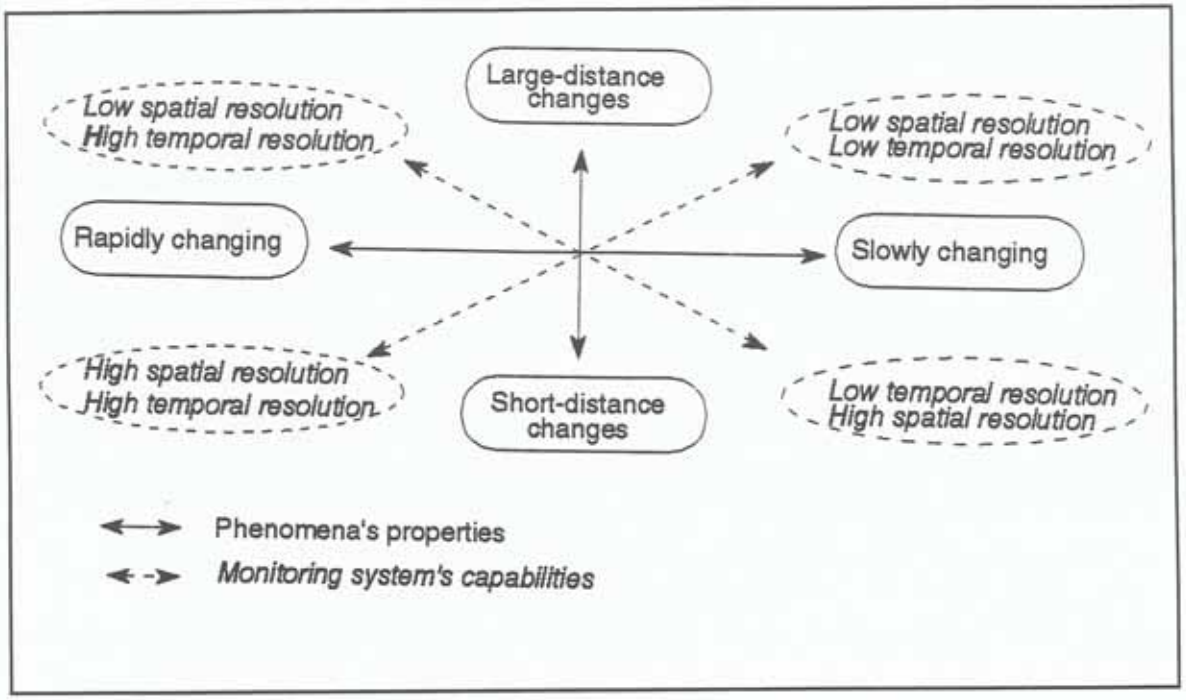

Fig. 2.2: Types of monitoring (modified from Townshend, 1977)

A desert status is achieved by series of conditions leading to reduced biological productivity and consequent decrease in plant biomass, crop yield, land capacity to sustain livestock and human well-being. When ecosystems lose their capability to revive or to repair themselves, desertification is seen as the last stage of degradation (Hare, 1985b).

The word desertification has been restricted to the degradation processes affecting drylands, i.e. the subhumid, semiarid, arid and the productive parts of the hyperarid climatic zones of low and variable rainfall, which are particularly susceptible to deterioration by excessive human exploitation (Mabbutt, 1984). To characterize deterioration processes outside the dry ecosystems, it is more adequate to use the term land degradation. Kust (1992) mentions that, in this context, 'land' includes soils, local water resources, land surface, vegetation and crops; the word 'degradation' denotes reduction of the resource potential by one or a combination of various processes acting on the land, including water or wind erosion and sedimentation, long-term reduction in amount and diversity of natural vegetation, salinization and alkalinization.

According to recent definition attempts, desertification is seen as land degradation in arid, semiarid and dry subhumid areas resulting from various factors, including climatic variations and human activities (UNCED, 1992). Thus both terms, land degradation and desertification, are integrated and desertification is considered space-specific. Also Grunblatt et al. (1992) consider desertification as a form of land degradation in semiarid and subhumid environments involving physical, biological, climatic and human influences altering the landscape.

(2) Causes

Desertification, revealed by drought, is caused by human activities in which the carrying capacity of land is exceeded; it proceeds by exacerbated natural or man-induced mechanisms and operates by intricate steps of vegetation and soil deterioration which result, in human terms, in an irreversible decrease or destruction of the biological potential of the land and its ability to support population (Mainguet, 1991). Thus aridization, the increasing dryness of the climate, does not lead by itself to desertification and must be seen rather as a precondition that reveals or intensifies this phenomenon.

Destructive human activities, or 'indirect causes', like overcultivation, overgrazing, deforestation, mismanagement of irrigated crop lands, together with physical processes, or 'direct causes', such as soil erosion, salinization and waterlogging, are recognized as the main causes of land degradation.
Causes are sometimes located far from the affected area. For instance, deforestation in upland areas causes flooding and siltation in lowlands, since the rainfall impact is not retarded by the water interception and retention capacity of the forest, and soils are eroded.

According to Kust (1992), there are three groups of causes: (1) human and physical factors of desertification; (2) basin, regional and local causes of desertification; and (3) main and derived causes of desertification. Recent research has emphasized the importance of studying local situations. This was not considered in the past decades, since there was a belief that the problem of desertification could be solved by a universal remedy (Mainguet, 1991).

(3) Processes and indicators

Processes are natural, either physical or biochemical such as wind and water deterioration actions, or man-induced like irrigation mismanagement. For two reasons it is important to focus desertification models on processes: (1) they lead to the formation of biogenic landscapes of desert character (Kust, 1992); (2) once processes are identified, it is possible to develop short-term remedial programs to reduce or control them (Mainguet, 1991).

The processes leading to land degradation and desertification can be detected and measured through indicators. The latter are measurable characteristics which provide information about the conditions being investigated, i.e. land degradation processes. Indicators can be physical, biological or socio-economic, or a combination of these. Common examples are changes in soil status, surface crusting, saline efflorescence, vegetation degradation, density of human settlements and deforestation. Indicators must be better defined to help determine the extent and rate of desertification. Also more suitable approaches to analyze desertification in terms of causes, processes and impacts must be implemented (figure 2.3).

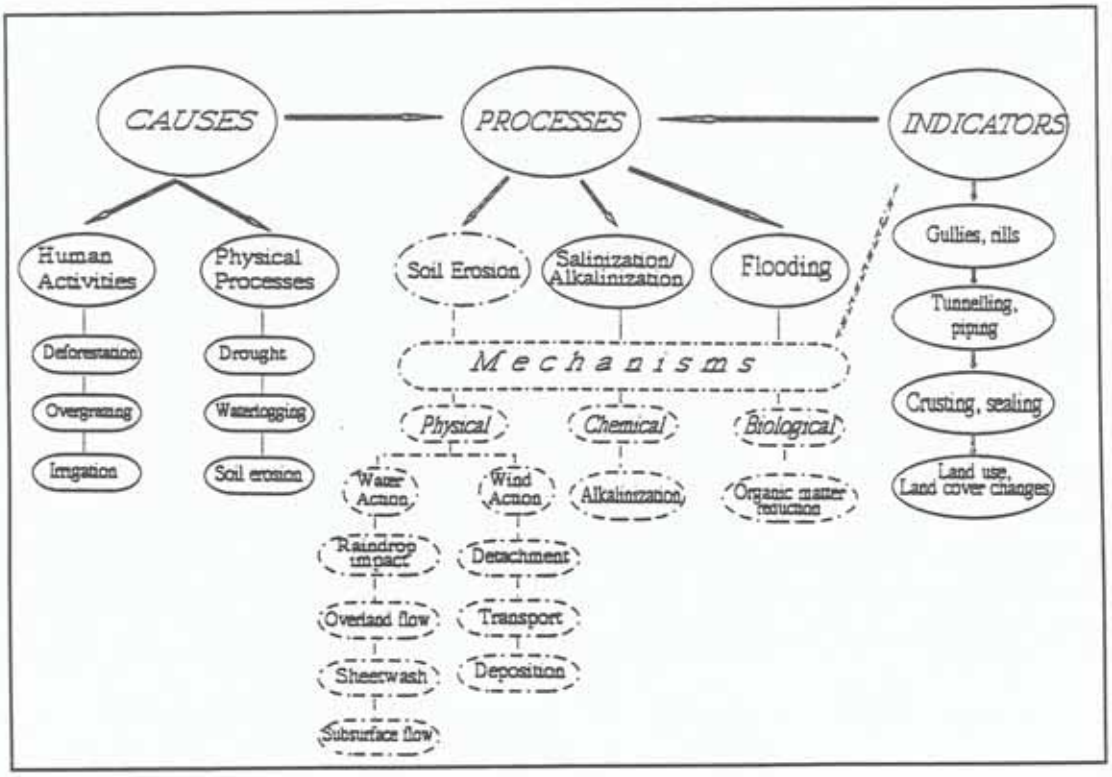

Fig. 2.3: *Relationship between causes, processes, mechanisms and indicators*

Climate, soils, geoforms, fauna, flora and water are the components of an ecosystem. Consideration of individual components gives the possibility to analyze them by their specific indicators and allows desertification and land degradation to be evaluated as complex series of relatively independent events, such as soil and vegetation degradation.

Soil deterioration is the most critical component of land degradation, especially of irreversible land degradation leading to desertification. Soil degradation is a consequence of depletive human activities and their interaction with natural environments, resulting in soil quality decline. Lal et al. (1990) distinguish three types of soil degradation: physical such as erosion and desertification by wind and water, chemical like alkalinization and acidification, and biological like decline in soil organic matter. Changes in soil properties help establish the rate of desertification, using present-time indicators such as deterioration of soil structure, crusting and salt content, rather than laboriously monitoring the phenomenon. However, the latter is indispensable for vegetation degradation.

The consideration of human influences in the characterization of degraded landscapes is of crucial importance. Cultural landscapes express the relative importance of both human and natural features (Olsson, 1985; Naveh, 1989). The way a landscape is used and managed can determine the initiation of degradation processes (OAS, 1991).

2.1.4 Soil erosion and degradation

Soil erosion is an aspect of landscape development. It can be defined as physical detachment, transport and deposition of soil particles. Detachment is the dislodging of soil particles from the soil mass by the erosive agents such as wind or water. Transportation is the displacement of sediments from their original location (Foster, 1982).

Processes responsible of soil deterioration are of three types: physical, chemical and biological (figure 2.4). Physical soil degradation encompasses soil erosion by wind and water. It involves the rearrangement of soil particles due to removal of finer particles which results in soil compaction, ablation of topsoil, damage to soil structure and changes in soil texture. Erosion is a joint result of the erosivity of the physical agents (i.e. wind, water) and the erodibility of the soil (Hudson, 1971).

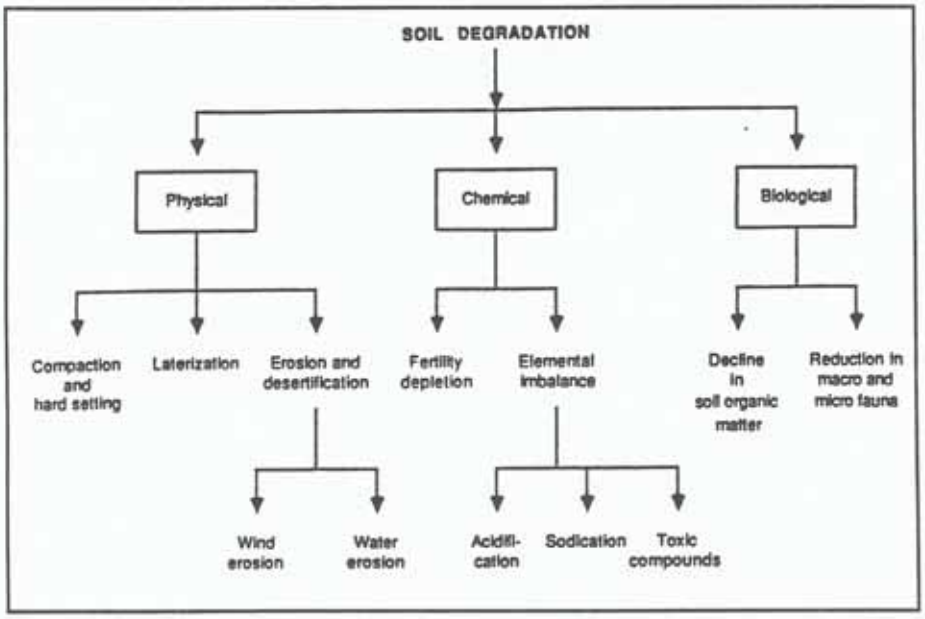

Fig. 2.4: Soil degradation types (after Lal, 1988)

(1) Erosivity

Erosivity expresses the ability of erosive agents, like water, to cause soil detachment and its transport (Lal et al., 1988), provided an initial input of kinetic energy from rainfall. Once separated from the main soil mass, soil particles are carried by runoff from one point to another. Both detachment and transport are linked to the rainfall characteristics but also to slope length and angle, surface roughness, plant cover and management practices (Mainguet, 1991). Erosivity depends on the amount and intensity of the rainstorm and the size of the raindrops.

Considering soil erosion by wind, erosivity is controlled by the force the flow exerts on the ground surface, which depends on the nature of the atmospheric flow itself and the surface roughness.

(2) Soil erodibility

Soil erodibility, or the soil susceptibility to erosional processes, has been studied primarily on agricultural soils exposed to rainsplash and sheetwash. Erodibility cannot neglect the importance of the biotic factors (i.e. vegetation), which affect the erosive forces, soil moisture conditions and soil physical and chemical properties. Erodibility is also dynamic, in that it may change through a storm or from season to season.

The soil erodibility concept was first incorporated in the Universal Soil Loss Equation, in which the K factor expresses the susceptibility of soils to sheetwash and rill erosion. Some shortcomings of this concept are:

(1) The concept lacks a precise definition, as it was developed from attempts to isolate individual soil properties such as soil structure and organic matter content, influencing the soil resistance to erosional processes. As a consequence, it evolved as a practical rather than a theoretical concept.

(2) Constraints and limitations on its application have not been widely established.

(3) Active erosional subprocess such as sheetwash, rainsplash and subsurface flow, have rarely been precisely identified. Proper definition of the erosive forces acting on the soil allows to identify the most appropriate soil indicators.

The use of soil erodibility to indicate soil's susceptibility to a particular erosional process, in process-oriented studies, will probably lead to considerable confusion. A distinction between the well-known soil erodibility K factor of the USLE and 'soil erodibility coefficients' expressing the susceptibility of a soil to a specific process, such as subsurface flow, is required (Bryan et al., 1989).

2.2 WATER EROSION

2.2.1 Conditions and flow types

Land is subject to water erosion as a natural mechanism of topographic shaping. However, erosion by water at a given site can be intensified by natural and man-induced conditions (figure 2.5). Water erosion acts through (1) raindrop impact and runoff at the topsoil (2) action throughout the depth of the soil profile.

Overland flow is usually analyzed as sheetflow or sheetwash, even if it concentrates in many small channels or rills (rill erosion). Erosion occurring between rills is interrill erosion. Both interrill and rill erosion are overland flow processes (Foster, 1982). Erosion occurring through channel flow is defined and analyzed as concentrated flow, gully or stream channel erosion (figure 2.6). Sometimes, distinction between channels and rills is difficult. By definition, rills become gullies or channels when they cannot be obliterated by usual tillage (Hutchinson et al.,1976).

Subsurface flow is controlled by the spatial heterogeneity of the permeable medium, especially when combined with transverse irregularities such as lenticular depositional structures. The basic requirement

for subsurface network development through piping or tunnelling is an irregular concentration of water in depressions or along zones of higher permeability (Jones, 1987). For example, concentrated flow along macropores can lead to tunnel erosion or, when macropores are not well developed, to piping.

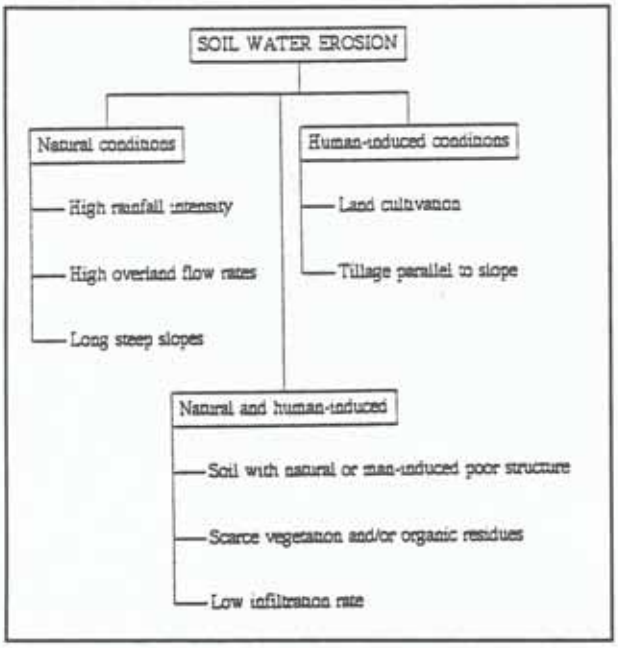

Fig. 2.5: Soil water erosion conditions

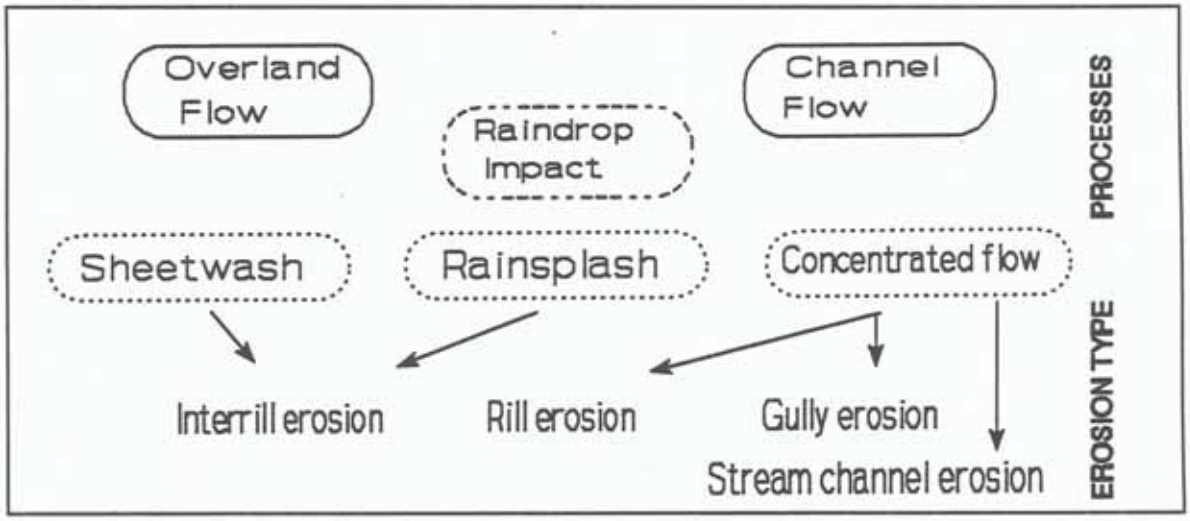

Fig. 2.6: Soil water erosion processes

2.2.2 Soil properties influencing erodibility

Agricultural and nonagricultural soils tend to differ in their susceptibility to erosion. Knowledge on soil

properties is essential to make qualitative and quantitative estimations of soil loss due to water (and wind) erosion mechanisms.

(1) Particle size distribution and clay mineralogy

Particle size distribution is one of the soil properties most frequently included to estimate soil erodibility from different soils around the world (Bennett, 1939; Barnett et al.,1966; Young et al.,1982; Meyer et al.,1984; Römkers, 1986). Increase in sand content leads to a decrease of aggregate stability and resistance to crusting, promoting sheet and rill erosion. Positive correlations between sand content and soil erodibility by splash have been found by several authors (Epstein et al., 1967; Wischmeier et al., 1969; Luk, 1977; Verhaegen, 1984; Martz, 1992). On the contrary, working on sandy loam soils from Africa, Obi et al. (1989) report a negative correlation between sand percentage and soil loss and conclude that the Wischmeier's nomograph overestimates the actual soil erodibility of sandy loam soils by a 30%.

The percentage of rock fragments greater than 2mm, plus the sand percentage is a good predictor to estimate interrill erodibility in sandy and loamy soils. High content of coarse fragments and sand favors infiltration; additionally, surface rock fragments may act as a mulch intercepting raindrops, or they may concentrate the runoff (Merzouk et al., 1991).

In soils varying from loam to loamy sand, high silt contents decrease soil erodibility as the silt fraction raises the soil cohesion and structural stability (Anderson, 1954; Bryan,1968a; Verhaegen, 1983; Martz, 1992). In contrast, the USLE equation assumes that the silt fraction increases runoff erosion (Wischmeier et al., 1971 and 1969).

Usually, a negative correlation between soil loss and clay content is reported (Luk, 1977; Meyer et al., 1984; Martz, 1992). Soils with more than 30 to 35% clay are generally coherent and form stable aggregates resistant to raindrop impact and splash erosion (Evans (1980). Furthermore, clay mineralogy has an important incidence on soil erodibility. El-Swafy et al. (1977) found that the slaking tendency of montmorillonite and the aggregation effect of kaolinite correlated with soil loss. These findings coincide with those of Trott et al. (1983), who showed that soils with kaolinite eroded less than those containing montmorillonite. The soil environment is important in determining how erodibility relates to clay types. In basic divalent cation-dominated soils, the swelling properties of 2:1 clays are minimized and aggregation is promoted. Conversely, in acid soils where monovalent cations are found and hydrogen dominates, the 2:1 clays are subject to more swelling and dispersion. In these soils, kaolinite in combination with relatively high organic matter and high levels of sesquioxides increases aggregate stability.

(2) Structure

Another parameter usually considered to predict erodibility is soil structure, which depends on soil pore space and the stability of the aggregates (Bennett, 1939; Wischmeier et al., 1969; Foster, 1987). The

degree of development of soil structure is an important factor governing soil susceptibility to erosion on rangelands (Rauzi et al.,1968). Soil structure also influences soil permeability and internal drainage.

(3) Porosity

If erodibility is studied in nonagricultural soils, attention to the soil and vegetation properties governing soil macroporosity is necessary. Flow in macropores can be as erosive as in rills. Small macropores, less than 1 cm wide, are adequate for initiation of tunnel erosion (Bryan et al., 1978).

(4) Aggregation

Two measures of aggregation, aggregate size distribution and aggregate stability, are important for estimating soil susceptibility to erosion, whether it refers to rainsplash mechanisms (Bryan, 1968 and 1974; Luk et al., 1977; Verhaegen, 1983) or rill and interril erosion types (Young and Onstad, 1982). In agricultural soils, the natural soil structure in the upper horizon is usually disturbed and replaced by an artificial structure of secondary and less stable aggregates.

Splash detachment and runoff depend on the resistance of the soil aggregates to dispersion and breakdown, and on the size of the water-stable aggregates. Aggregate sizes ranging from 0.25 to 0.5 mm and greater than 3 mm were found significant to explain soil loss (Bryan, 1968a; 1976; Yamamoto et al., 1978). For soils with textural extremes, an aggregate size parameter best estimates erodibility values (Römkens et al., 1986). Some authors report a positive correlation between water-stable aggregates and soil susceptibility to erosion, based on the fact that well-aggregated soils present larger surface area to raindrop impact (de Ploey et al., 1981; Martz, 1992). Others indicate a negative correlation between water-stable aggregates and soil erodibility, attributed to the increment of particle size with aggregation (Bryan, 1968a; Wischmeier et al., 1969; Luk et al., 1977 and 1979; Young, 1977).

(5) Bulk density

At higher bulk density, particle detachment decreases but runoff increases. Therefore, there is a positive correlation between bulk density and splash loss (Trott et al., 1983;McConnell, 1988; Martz, 1992).

(6) Moisture

Soils already wet at incoming rainfall will reach their final infiltration rate more quickly (Evans, 1980). When the soil is saturated, soil properties have minimal influence on the amount of material eroded. The moisture availability index and the soil moisture regime can be used as alternative diagnostic criteria to estimate rainfall erosivity risk, as related to land erodibility (Manrique, 1988).

(7) Shear strength

Shear strength is controlled by soil cohesion. Sheetwash erosion depends on coherent and non-coherent soil surface. Agricultural soils are commonly non-coherent after tillage. During storms, soils evolve into a coherent sealed or crusted surface cap. Infiltration usually declines, producing higher runoff and shear

stress, but shear strength of crusted surfaces increases, leading to reduced sheetwash entrainment (Bryan et al., 1989).

(8) Crusting

Crusting is a dynamic temporal soil property, changing in response to management or climatic influences. Climatic characteristics affect crust structure more than texture itself (Le Bissonais et al., 1993). Soils vary widely in susceptibility to crusting and in the rate at which crust develops. Epstein and Grant (1967) indicated that the erodibility of different soils may be related to the rate and extent of crust formation.

Crusting includes aggregate disruption under drop impact, redistribution and selective deposition of particles as filtration pavements, compaction and formation of a surface seal. The development of a surface seal decreases the infiltration rate, but splash and wash erosion also decrease because soil strength is reinforced (Bradford et al., 1987). Crusting enhances rill incision and is accompanied by a shift from interrill (sheetwash/rainsplash) to rill erosion. Most of the existing soil erosion equations do not incorporate crusting as a parameter which modifies infiltration. Physically-based models to handle the influence of crusting on infiltration, especially during the crop growing season, need to be developed (De Roo, 1993).

(9) Organic matter

Organic matter content changes slowly through time. Thus, it can be measured at almost any time throughout the year with no perceptible variation. A high negative correlation between soil loss and organic matter content, attributed to the influence of humus on the formation and maintenance of soil aggregates, is reported by Bryan (1968), Luk (1977), Meyer et al. (1984). However, under conditions of high organic content (e.g.>7.6%), the development of mutual electrostatic repulsion forces between soil particles may increase soil erodibility. Ekwue (1990) studied the influence of organic matter on splash detachment using soils with grass and peat treatments. For all studied soils there was a negative correlation between soil loss and organic matter content. However, the relationship between water-stable aggregates and soil loss by splash was positive for soils with peat treatments, while it was negative for soils under grass cover.

(10) Calcium carbonate

Calcareous soils, especially those having large amounts of $CaCO_3$ in aggregates smaller than 0.02 mm, possess an active form of calcium carbonate that leads to pore sealing, crust formation and decreasing infiltration rate. High erodibility of such soils has been reported from several Mediterranean areas (Gaiffi, 1990; Merzouk et al., 1991).

(11) Other chemical soil properties

Chemical soil properties like exchangeable calcium, sum of exchangeable bases and cation exchange capacity are indicated to be negatively correlated with interrill erodibility of soils with a wide range of

textures (Meyer et al., 1984). Also sesquioxides of iron and aluminum play an important role in decreasing soil susceptibility to erosion (Trott et al., 1983; Le Bissonnais et al., 1993).

2.2.3 Soil erodibility coefficients

Soil susceptibility to erosion can be estimated either by actual measurements of soil loss under controlled conditions on the field or in laboratory, or by the isolation of certain soil properties to establish erodibility indices. Assuming that all soils are erodible to some extent, an index of erodibility provides relative erodibility values.

Soil erodibility indices can usually be derived from common analytical data. They do not require very specialized equipment or professional expertise, which is advantageous for regional studies in developing countries. Since such coefficients can be applied to a large number of soils in a short time, they could be suitable for mapping soil erodibility in land use planning studies or for land degradation assessment. Even when researchers are aware of these advantages, none of the studies carried out over the last decades achieved an erodibility index simple to measure, reliable in operation and capable of universal application (Middleton, 1930; Bouyoucos, 1935; Anderson, 1954; Chorley, 1959; Wischmeier et al., 1971; Bergsma et al., 1981; Römkens et al., 1986; de Roo, 1993; etc.).

Examples of soil erodibility indices developed during the past 60 years were compiled (table 2.2). Most of them are based on properties controlling soil aggregation size and stability, water transmission and retention properties, raindrop impact, overland flow production and availability of erodible materials.

Table 2.2: Water soil erodibility indices

1) Index Name:	Dispersion ratio
Definition:	Percentage of silt and clay in a dispersed state divided by total silt plus clay.
Tested on:	"Erosive" silt loam,loam,sandy loam,silty clay and clay soils; and "non-erosive" clay and clay loam soils.
Country:	USA
Limits:	Erodible soils > 15% non-erodible soils < 15%
Erosion type:	no mention
Author:	Middleton, (1930)
2) Index Name:	Silica: sesquioxide ratio
Definition:	$SiO^2/R203$
Tested on:	Lateritic (highly clayey) soils.
Country:	Cuba
Limits:	Erodible soils > 9.03 Non - erodible soils < 0.52
Erosion type:	No mention
Author:	Bennett, (1926)
3) Index Name:	Clay ratio
Definition:	Silt plus sand content divided by clay content of soil sample.
Tested on:	Sandy loam,loam,silt loam,clay loam,silty clay and clay soils.
Country:	USA
Limits:	Not specified
Erosion type:	No mention
Author:	Bouyoucos, (1935)
4) Index Name:	Surface aggregation ratio

Continued

Definition:	Surface area of soil particles greater than 0.05 mm divided by aggregated silt plus clay.
Tested on:	Coarse and medium textured soils from volcanic and alluvial parent materials.
Country:	USA
Limits:	Not specified
Erosion type:	Watershed
Author:	Anderson, (1954).
5) Index Name:	**Modified clay ratio**
Definition:	Bouyoucos' clay ratio, adding organic matter to the binding fraction.
Tested on:	Brown earth and podzolic soils from limestone, shale and breccia parent materials.
Country:	England
Limits:	Not specified
Erosion type:	Sheet erosion
Author:	Bryan, (1968a)
6) Index Name:	**Modified surface aggregation ratio**
Definition:	Adds organic matter to the binding fraction of Anderson's surface aggregation ratio.
Tested on:	Brown earth and podzolic soils from limestone,shale and gritstone parent materials.
Country:	England
Limits:	Not specified
Erosion type:	Sheet erosion
Author:	Bryan, (1968a)
7a) Index Name:	**Percentage water-stable aggregates (WSA)**
Definition:	Percentage - weight of WSA > 3mm.
Tested on:	Brown earth and podzolic soils from limestone,shale and gritstone parent materials.

Continued

Country:	England
Limits:	Not specified
Erosion type:	Sheet erosion.
Author:	Bryan, (1968a)
7b) Index Name:	**Percentage water-stable aggregates (WSA)**
Definition:	Percentage - weight of WSA between 0.25 and 0.50 mm.
Tested on:	Latosols and regosols from ash and basalt colluvium parent materials.
Country:	Hawaii
Limits:	Not specified
Erosion type:	Splash erosion
Author:	Yamamoto et al., (1978)
7c) Index Name:	**Percentage water-stable aggregates (WSA)**
Definition:	Percentage - weight of WSA > 0.5mm.
Tested on:	Loamy sand, sandy loam, loam, silt loam, clay loam, sandy clay loam and clay soils. Gullied soils having silt loam, sand clay, loose sand textures.
Country:	Canada (Bryan) and USA (Woodburn et al.).
Limits:	Not specified
Erosion type:	Sheetwash (Bryan) and splash (Woodburn et al.)
Author:	Bryan, (1976); Woodburn et al.,(1956).
8) Index Name:	**Ratio of WSA < 0.25/MWD**
Definition:	Ratio of sum (percent) of aggregates smaller than 0.25mm to mean weight diameter in mm.
Tested on:	Latosols and regosols from ash and basalt colluvium parent materials.
Country:	Hawaii
Limits:	Not specified
Erosion type:	Splash erosion
Author:	Yamamoto et al., (1978)

Continued

9) Index Name:	Surf
Definition:	Surface area of aggregates larger than 0.25mm.
Tested on:	Latosols and regosols from ash and basalt colluvium parent materials.
Country:	Hawaii
Limits:	Not specified
Erosion type:	Splash erosion
Author:	Yamamoto et al., (1978)
10)Index Name:	**Sus/MWD ratio**
Definition:	Ratio of suspension percent to mean weight diameter in mm.
Tested on:	Latosols and regosols from ash and basalt colluvium parent materials.
Country:	Hawaii
Limits:	Not specified
Erosion type:	Splash erosion
Author:	Yamamoto et al., (1978)
11) Index Name:	**Erosion ratio**
Definition:	Obtained by dividing the dispersion ratio by the ratio of colloid (i.e. organic matter plus clay) to moisture equivalent.
Tested on:	"Erosive" silt loam,loam,sandy loam,silty clay and clay soils; and "non-erosive" clay and clay loam soils.
Country:	USA.
Limits:	Erodible soils > 10%. Non-erodible soils < 10%
Erosion type:	Not mentioned
Author:	Middleton, (1930)
12) Index Name:	**E (erodibility)**
Definition:	Ratio of a measure of dispersion of particles > 0.05mm (d), times an index of water retention capacity (h), to the amount of WSA > 0.25mm (a).(E = d*h/a)
Tested on:	Chernozems, sierozems, solonetz

Continued

Country:	Russia (Caucasian foothills)
Limits:	Not specified
Erosion type:	Not specified
Author:	Voznesensky et al., (1940)
13) Index Name:	**Chorley's erodibility index**
Definition:	One divided by mean shearing resistance times permeability. Mean shearing resistance obtained by ratio of density times range of grain size to soil moisture content.
Tested on:	Fine and medium soil textures
Country:	England
Limits:	Not specified
Erosion type:	Sheet erosion
Author:	Chorley, (1959)
14) Index Name:	**KE index**
Definition:	Average number of drops (kinetic energy) required to destroy a ped at Pf = 4.44.
Tested on:	Clay and sandy clay soils
Country:	Nigeria
Limits:	Stable soils: 0 - 0.4 Erodible soils > 0.4
Erosion type:	Rainsplash erosion
Author:	Bruce-Okine et al.,(1975)
15) Index Name:	**Water drop test**
Definition:	Percentage of aggregates destroyed by 15 drops without pre-wetting and 10 drops with 24 hours pre-wetting (15_{do} and 10_{d24})
Tested on:	Not mentioned
Country:	Spain
Limits:	Not specified
Erosion type:	Rainsplash erosion

Continued

Author:	Bergsma and Valenzuela, (1981)
16) Index Name:	**Mean soil loss**
Definition:	Predictive mean soil loss equation: MSL = 862 + 23.7 (Smectite + Vermiculite)+ (855Db + 135 (Al + Fe))+0.006 M Db: bulk density; M: from K - USLE factor.
Tested on:	Soil textural ranges from silty clay loam to loamy sand.
Country:	USA (California)
Limits:	Not specified
Erosion type:	Overland flow
Author:	Trott et al., (1983)
17) Index Name:	**S60 (Splash loss)**
Definition:	Predictive soil loss equation. Splash loss at 5 minutes sampling period, ending at time = 60 minutes. S_{60} = 23.35 + 3814.0 KE/soil shear strength - 0.28 (dispersed silt).
Tested on:	Soil textural ranges from sand to clay
Country:	USA
Limits:	Not specified
Erosion type:	Interrill erosion
Author:	Bradford et al.,(1987)
18) Index Name:	**Kr**
Definition:	Rill erodibility prediction equation. It incorporates organic matter, CEC, Aluminium percentage and SAR (sodium adsorption ratio) as soil properties, plus M parameter (from K - USLE factor).
Tested on:	Soil textural ranges from sand to clay
Country:	USA
Limits:	Not specified
Erosion type:	Rill erosion (e.g. concentrated flow)
Author:	Elliot et al., (1987)

Continued

19) Index Name:	Ki
Definition:	Interril erodibility prediction equation. It includes clay content, percentage of WSA < 0.25mm, water dispersable clay, Mg, Fe, Al, contents (meq/100g soil), and EC (electrical conductivity in saturated past). A differentiation is done for soils with clay percentage above and below 35%.
Tested on:	Soil textural ranges from sand to clay
Limits:	Not specified
Erosion type:	Interril erosion (rainsplash and overland flow)
Author:	Elliot et al., (1987)
20) Index Name:	SED (Suspended solids after five minutes)
Definition:	Based on aggregate stability. Cumulative percentage of suspended soils in water after five minutes.
Tested on:	Luvisols, colluvial soils and gravelly soils.
Country:	The Netherlands
Limits:	Not specified
Erosion type:	Rill and interrill
Author:	de Roo, (1993)
21) Index Name:	K - USLE
Definition:	It estimates soil erodibility based on a particle size parameter (M) organic matter percentage, a soil structure code, and the profile permeability class.
Tested on:	Wide range of soil texture. But it was designed to work on medium textured soils.
Country:	USA, and tested all over the world
Limits:	Not specified
Erosion type:	Rill and interrill
Author:	Wischmeier et al., (1971)
22) Index Name:	K - Römkens for surface soil erodibility

Continued

Definition:	Coefficient of soil erodibility for topsoil, based on the following multiple linear regression: K = 0.145 + (6.87.10_{-5} M) + 0.034 (structure)+ 0.038 (permeability)- 0.157 (O.carbon); were M is the particle size parameter of K - USLE factor.
Tested on:	Sandy loam, loam, silt loam
Country:	USA
Limits:	Not specified
Erosion type:	Rill and interrill
Author:	Römkens et al., (1977)
23) Index Name:	**K - Römkens for subsoil erodibility prediction**
Definition:	Soil erodibility coefficient for clayey subsoils. Based on multiple linear regression of the a textural parameter (M particle size parameter from K - USLE factor) and the percent of Fe_2O_3 plus Al_2O_3 extractable with citrate-dithionite-bicarbonate (CDB).
Tested on:	Clayey subsoils
Country:	USA
Limits:	Not specified
Erosion type:	Rill and interrill
Author:	Römkens et al., (1977)
24) Index Name:	**K - Römkens**
Definition:	Soil erodibility coefficient suitable for soils with textural extremes and well aggregated soils. It estimates soil erodibility values incorporating a geometric mean weight diameter (Dg.) of the primary soil particles to the K-value.
Tested on:	Wide range of soil textures
Country:	Not specified
Limits:	Not specified
Erosion type:	Raindrop impact and overland flow
Author:	Römkens et al., (1986)
25) Index Name:	**K - Martins**

Continued

Definition:	Modified K - USLE factor for Central European conditions. Incorporates the influence of cationic composition (Na and K) of the exchangeable complex and a parameter for stone coverage percent.
Tested on:	Luvisols, colluvial soils and gravelly soils
Country:	The Netherlands
Limits:	Not specified
Erosion type:	Rill and interrill
Author:	Martin, (1988)
26) Index Name:	**K - Young**
Definition:	It estimates soil erodibility based on the following parameters: an aggregate index (2.9mm), percentage of montmorillonite, silt plus very fine sand, bulk density and the dispersion ratio.
Tested on:	Loam sand, sandy loam, loam, clay loam, sandy clay loam soils
Country:	USA (Minnesota)
Limits:	Not specified
Erosion type:	Overland flow
Author:	Young et al., (1972)
27) Index Name:	**Relative erodibility index**
Definition:	Multiple regression model used as a relative erodibility index, and based on three soil variables: percentage of soil materials > 2mm plus sand percentage, electrical conductivity (EC 1:5) and $CaCO_3$ percentage of silt and clay size ("active" $CaCO_3$).
Tested on:	Sandy, loam, clay loam, silty clay and clayey soils
Country:	Morocco
Limits:	Not specified
Erosion type:	Interrill erosion
Author:	Merzouk et al., (1991)
28) Index Name:	**Standardized rainshowers**

Continued

Definition:	A small rainfall simulator measures runoff and soil loss generated by a standardized rainshower on a plot of 20% slopes and 0.0625 m^2 surface plot area.
Tested on:	Sandy, loamy sand, sandy loam, loess, clay loam and clayey soils.
Country:	The Netherlands
Limits:	Not specified
Erosion type:	Interrill
Author:	Kamphorst, (1987)
29) Index Name:	**Pinhole test**
Definition:	Distilled water is allowed to flow through a 1.0 mm diameter hole drilled through a compact sample.
Tested on:	Mainly clayey soils
Country:	Not specified
Limits:	The water becomes muddy and the hole rapidly erodes in dispersive clays. For non-dispersive clays the water is clear and there is no erosion.
Erosion type:	Rill and tunnel erosion
Country:	Not specified
Author:	Sherard et al., (1976)
30) Index name:	**Crumb test**
Definition:	A small clod of soil is placed in a beaker and submerged in water. If the soil clod is initially dry, it will often slake.
Tested on:	Clayey soils
Country:	Not specified
Limits:	In dispersive clays particles go into suspension in the quiet water, and the zone around the clod becomes cloudy.
Author:	Sherard et al., (1976)
31) Index name:	**Manipulation test**
Definition:	It rates soil coherence. The results indicate structural stability and provides an indication of the materials available for erosion.

Continued

32) Index name:	Rainfall acceptance test
Definition:	Volume of water infiltration in then minutes under splash without pounding.
33) Index name:	Soil loss test
Definition:	Amount of sediment eroded from a test plot 30x30 cm, with 9% slope. A small rainfall simulator is used.
34) Index name:	Rilling test
Definition:	A test of sensitivity of the soil surface to scour by concentrated flow.
35) Index name:	Shear vane test
Definition:	It measures shear strength of undisturbed soil surface against the pressure of a torvane.
Tested on:	Loamy sand to clayey soils
Country:	Spain, Thailand, Sri Lanka
Limits:	Seven individual test results (from 29 to 35) are ranked in two groups. Grouping is based on test's ability to provide information about erodible materials and overland flow production.
Erosion types:	Interrill and rill erosion
Author:	For 31 to 35: Bergsma, (1990)
36) Index name:	Raintest
Definition:	Relationship between kinetic energy of rainfall and soil loss.
Tested on:	Sandy soils.
Country:	Belgium.
Limits:	Not specified.
Erosion type:	Rainsplash and sheetwash erosion.
Author:	Gabriels et al., (1975)

2.3 SALINIZATION AND ALKALINIZATION

2.3.1 Causes

Salinization results from the accumulation of water-soluble salts such as chlorides, sulfates and carbonates of sodium, magnesium or calcium on the soil surface, in the subsoil and groundwater. Alkalinization or sodication involves an enrichment in sodium ions. Both land degradation processes are widespread and acute in soils under arid and semiarid climates and in coastal areas.

According to Szabolcs (1992), 'primary salinization' develops because of geologic, climatic and topographic factors but without human interference. Secondary salinization results from human activities, mainly irrigation (figure 2.7).

Geology is a primary cause of salinization/alkalinization processes in regions where the soil parent materials consist of marine deposits, paleolagoons, inland lake deposits, or salt accumulated in sediments (Mainguet 1991). Topography controls the groundwater depth. Lowlands such as closed depressions, flat areas adjacent to streams, river deltas and other low-lying areas near the sea are subjected to groundwater table fluctuations. Groundwater may rise because of overexploitation or inefficient drainage in irrigation schemes causing seawater intrusions in coastal regions (Sehgal et al., 1992).
In arid and semiarid regions, climate is a major factor contributing to salinization. As less rainfall is available, leaching of soluble salts is restricted. High evaporation rates tend to concentrate the salts in soils and surface waters (USDA, 1953).

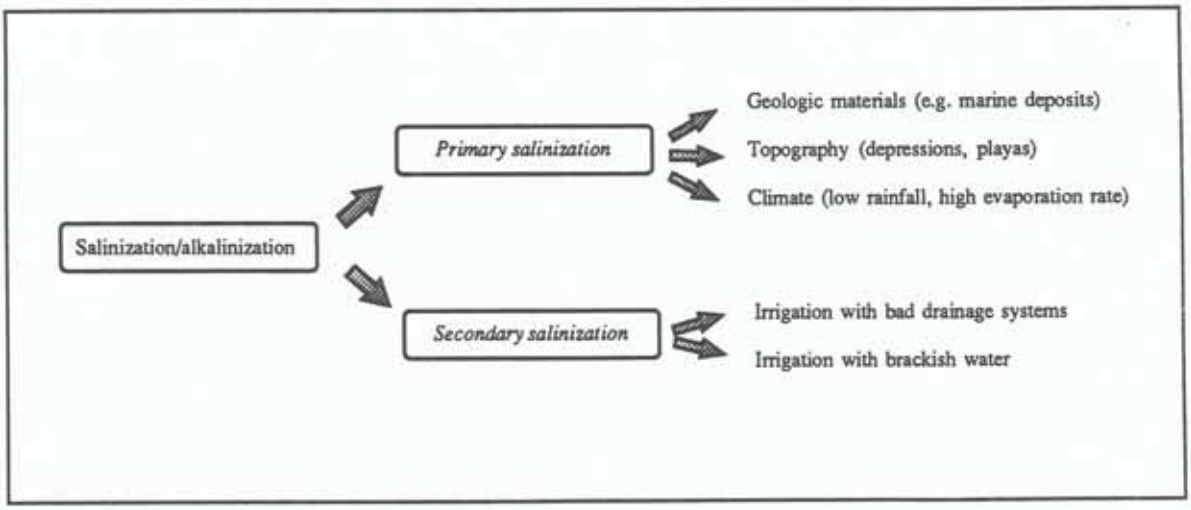

Fig. 2.7: Primary and secondary salinization and alkalinization causes

In the absence of runoff, the more soluble salts such as halite and chlorides concentrate on playa surfaces. Where more ephemeral conditions occur, the sodium salts are important.

In arid and semiarid regions, the main cause of secondary salinization is the application of improper methods of irrigation and drainage. One millon ha of lands has been lost in Central Asia because of erroneous irrigation practices (Rozanov, 1984). When bringing new land under irrigation, farmers and planners have frequently failed to recognize the need for establishing artificial drains to care for the additional water and soluble salts. Irrigation mismanagement may raise the groundwater table from considerable depths (10 or 20 m) to within a few meters (1 or 2 m) of the soil surface in a few years (Sehgal, 1992; Szabolcs, 1992). In addition, irrigation uses sometimes brackish water. Rivers traversing deserts and semideserts carry often high amount of soluble salts. In Arizona, for instance, the use of the Colorado river for irrigation purposes needed an expensive desalinization program (Sheridan, 1981).

Additional causes of secondary salinization include deforestation, overgrazing, changes of cultivation practices, depletion of fresh water and replacement by saline groundwater from deeper layers, and utilization of wood reserves for fuel in arid areas. Intensive deforestation turns forest into barelands, frequently changing the metabolism of compounds in soils and water. Salts are transported to the topsoil by the elevation of the groundwater table. Similar results are caused by overgrazing, where the original balance of compounds between natural plant cover and the soil may be altered (Szabolcs, 1992).

2.3.2 Salt-affected soils

Three types of salt-affected soils are distinguished: saline soils, saline-alkaline soils and alkaline or sodic soils (USA Salinity Laboratory, 1953). Table 2.3 shows the distinctive chemical and physical characteristics of salt-affected soils. More recently, Szabolcs (1988) distinguished five types of salt-affected soils, including saline soils, alkali soils, magnesium-rich soils, gypsiferous soils and acid sulphate soils (table 2.4).

Table 2.3: Chemical and physical parameters of salt-affected soils (modified from USDA Salinity Laboratory, 1953).

SALT-AFFECTED SOILS	CHEMICAL INDICATORS	PREDOMINANT ANIONS	PREDOMINANT CATIONS	OTHER PROPERTIES	MAIN EFFECTS ON SOIL PROFILE
Saline soils	• EC > 4dS/m • ESP < 15% • pH < 8.5	Chlorides, sulphates and sometimes nitrates. Small amounts of bicarbonates. Carbonates absent	Na: not more than half of the soluble cations. Ca and Mg: considerable amounts. K: not common. Sometimes gypsum and lime.	Generally flocculated; permeability equal or higher than that of similar non- saline soils. Presence of white crust on surface.	Higher osmotic pressure.
Alkaline (sodic) soils	• EC < 4dS/m • ESP > 15% • 8.5<pH<10	Chlorides, sulphates and bicarbonates. Carbonates: small amounts.	Na:dominant. K: sometimes (exch. and soluble) Ca and Mg: small amounts. At high ph and in the presence of carbonates Ca and Mg precipitate.	Organic matter dispersion and dissolution. Clay deflocculation. Columnar or prismatic structure.	Changes in structure. Decrease in permeability and porosity. Changes in soil biological activity. pH increases beyond 9 or 10
Saline-alkaline (sodic) Soils	• EC > 4dS/m • ESP > 15% • pH : variable	If excess of salts: appearance and properties similar to saline soils (i.e. pH<8.5, particles remain flocculated). If soluble salts are leached downwards: appearance and properties similar to sodic soils (ie. pH>8.5 and soil particles are dispersed)			Soils become unfavorable for the entry and movement of water and for tillage.

Table 2.4: Salt-affected soils and their electrolyte characteristics, environment and main effects (Szabolcs, 1988).

Ions causing salinity and/or alkalinity	Type of salt affected soil	Environment	Main effects
Sodium chloride and sulphate	Saline soils	Arid Semiarid	High osmotic pressure of soil solution
Sodium ions capable of alkaline hydrolysis	Alkali soils	Semiarid Semi humid Humid	Alkali pH Effect on water, physical soil properties
Magnesium ions	Magnesium soils	Semiarid Semihumid	Toxic effect, high osmotic pressure
Calcium ions (mainly gypsum)	Gypsiferous soils	Semiarid Arid	Acidic pH Toxic effect
Ferric and aluminum ions (mainly sulphate)	Acid sulfate soils	Sea-shores, lagoons with high sulfate contents	Strongly acid pH Toxic effect

In addition to the chemical and physical soil properties mentioned in table 2.3 and 2.4, diagnostic horizons are useful to identify salt-affected soils, including salic horizon with soluble salts, natric horizon with exchangeable sodium, gypsic and petrogypsic horizons, sulfuric horizon, calcic and petrocalcic horizons (Mougenot et al., 1994).

2.3.3 Effects of salts on soil properties

The accumulation of soluble salts produces changes in physical and chemical soil properties affecting in particular soil structure, permeability and chemical balance. Szabolcs (1992) proposes a method to monitor salinity and sodicity in irrigated areas, partly based on soil properties such as texture, structure, saturated and unsaturated water conductivity, exchangeable cations, pH and soluble salt contents. The detrimental effect of adsorbed sodium on the physical properties of soils results in low water infiltration rate, low permeability to water and gases, and poor soil structure. The degree to which the physical condition of the soil deteriorates in the presence of exchangeable sodium is a function of content and mineralogy of clay particles and the total electrolyte concentration of the soil solution (Frenkel et al., 1985).

(1) Mechanical soil properties

Flocculation is a process of sticking together colloidal particles in the form of loose, irregular clusters in which the original particles can be recognized. Flocculation values are influenced by the clay type and the composition of the exchange complex. Shainberg et al. (1981) investigated the effect of low electrolyte concentration on clay dispersion in a sodic soil. When high quality water (rainwater) is used for irrigation, an ESP value of 5% can be detrimental to the physical properties of soils. However, when high salinity water is used (> 3 meq/liter) damage to the physical properties of soils occurs at ESP equal or higher than 15%.

(2) Soil structure

Increasing exchangeable sodium promotes structural changes in the soil matrix through clay swelling and soil particle dispersion. Soils become unstable and compacted (Frenkel et al.,1985; Mainguet, 1991). The magnesium ion can also affect soil structure. In non-calcareous soils, exchangeable Mg stabilizes the structure and prevents clay dispersion (Alperovith et al., 1981).

(3) Crusting

Soil crusts result from two complementary mechanisms: physical dispersion caused by drop impact and chemical dispersion which depends on the ESP of the soil, the electrolyte concentration of the applied water and the clay mineralogy. At low concentration of Na and Mg in the exchange complex, the soil surface presents high susceptibility to sealing and crust formation (Kasman et al., 1983; Agassi et al., 1981).

(4) Hydraulic conductivity

The most severe effect of sodium ions on the physical properties of soils concerns hydraulic conductivity. In soils irrigated with sodic water, the filling of pores by dispersed clay particles is a major cause of reduced hydraulic conductivity (Frenkel et al., 1978; Shainberg et al., 1981).

(5) Infiltration

Water infiltration is more affected by the soil sodicity and the electrolyte concentration of irrigation water than the permeability of the underlying soil (Agassi et al., 1981). The combination of the mechanical impact of raindrops on the soil surface together with low salt concentration in infiltrating water can cause a severe decrease in infiltration and hydraulic conductivity of arid soils irrigated with saline-sodic water.

(6) Soil fertility

Mainly in sodic soils, the content of organic matter tends to drop or does not decompose satisfactorily. Additionally, an increase in the osmotic pressure restricts the availability of water to plants.

2.3.4 Surface features of salt-affected soils

Surface features common in saline areas are (Mabbut, 1986):

- Presence of dead trees, shrubs or colonization by salt-tolerant plants in previously vegetated areas.
- Saline efflorescence, crusting, cracking and puffy areas.
- Areal erosion by wind or water occurs on salt-affected areas (salt scalds). On the margin of the scalds, rills and gullies may form, while the breakdown of the puffy surfaces over the loose topsoil increases wind erosion.
- Salt accumulation and clay dispersion in the topsoil produce crusted surfaces, thus increasing runoff and leading to flooding of valley floors.
- Surface sealing increases surface salinization and hinders the establishment of natural vegetation on bare lands.
- The presence of moist horizons above perched saline water tables increases the capillary rise of salts to the soil surface.

2.4 SPECTRAL DISCRIMINATION OF SOIL PROPERTIES AND SURFACE FEATURES

Defined in simple terms, the soil is a system consisting of three phases: solid, liquid and gas (Hausenbuiller, 1972). The solid phase consists of a mixture of coarse primary minerals in the sand and silt fractions, organic fragments and fine materials such as clay minerals and humus.

The inclusion of rock fragments and follistic material and different surface roughness conditions determine a complex reflectance response from the soil surface, with supplementary spatial and temporal variation patterns at all scales. The goal of the remote sensing techniques is to exploit these patterns of energy interactions, in order to obtain the maximum information about the physico-chemical characteristics of soil surfaces.

Additionally, soil scientists try to extend these spatial measurements below the surface to describe the soil as a dynamic three dimensional body with spatially variable properties (Huete et al.,1991).

2.4.1 General soil reflectance spectra

Remote sensing measurements record electromagnetic radiation reflected and/or emitted by the soil surface.

Soil reflectance derives from the inherent spectral behaviour of the heterogeneous combination of the mineral, organic and liquid matter comprised in the soil surface layer (Stoner et al., 1981). The visible soil reflectance, or colour, is one of the most useful covariant soil properties used to identify and describe a particular soil material. In the past, soil reflectance measurements were confined to the visible portion of the spectrum, being determined in a semi-quantitative way by means of the Munsell colour notation (Baumgardner et al., 1985).

One of the early studies to quantify soil reflectance and determine differences between soil reflectance spectra was conducted by Condit (1970). Under laboratory conditions he measured the spectral reflectance of 160 soil samples, over the range of 0.32 to 1µm. From these results three general types of spectral soil curves were determined (figure 2.8). However, in these studies no attempts were made to quantitatively relate spectral shape to soil properties. Later, Stoner et al. (1981) presented five distinct soil reflectance curves, identified according to curve shape, the presence or absence of absorption bands, the predominance of soil organic matter and iron oxide composition, based on the measurement of 485 soil samples over the 0.52 to 2.32 µm wavelength range (figure 2.9).

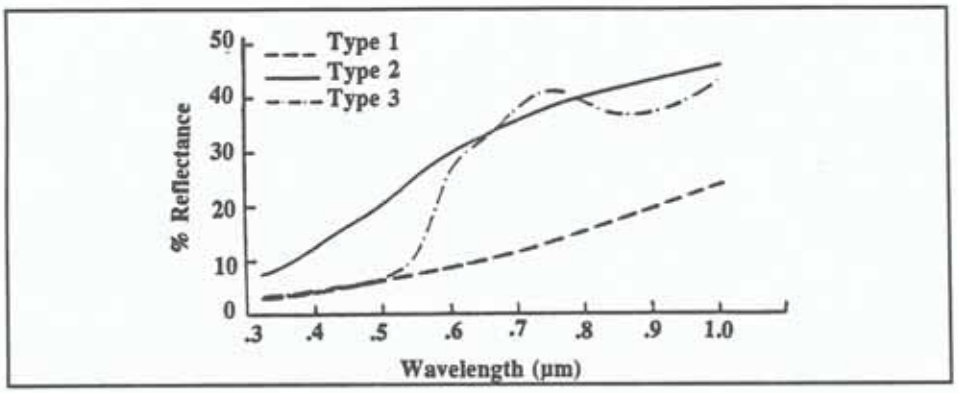

Fig. 2.8: *Soil spectral curve types defined by Condit (Baumgardner et al.,1985).*

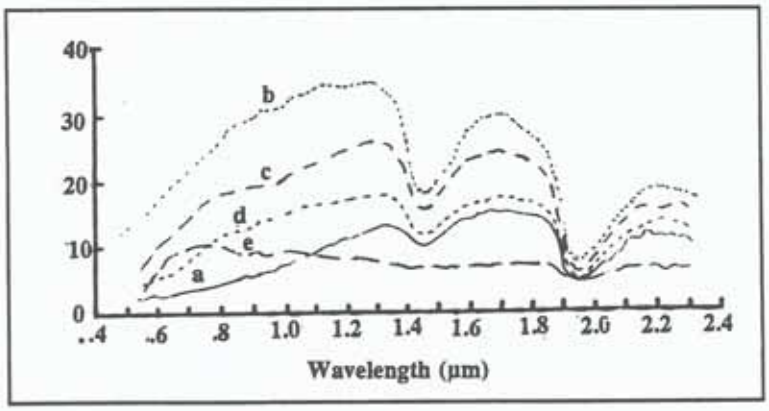

Fig. 2.9: *Representative reflectance spectra of surface samples from five mineral soils: (a) organic-dominated; (b) minimally altered; (c) iron-affected; (d) organic-affected; (e) iron-dominated (Stoner et al.,1981).*

The reflectance of 46 soil samples, over the range of 0.4 to 0.9µm, was measured using a field

spectroradiometer. Four characteristic basic curves, useful for reconstructing soil spectral signatures, were defined through spectral decomposition and mixture modelling techniques (Huete et al., 1991). The key curves represented soil brightness, red iron oxides, organic carbon, and reduced iron oxide (goethite). However, a better understanding of the relationships between the spectral reflectance of soils and soil properties, important for soil differentiation, is still required to fully utilize the capabilities of the present and future remote sensing systems (Coleman et al., 1993).

2.4.2 Reflectance of individual soil components

There are good correlations between soil reflectance and soil properties such as organic matter, soil moisture, particle size distribution, iron oxide content, colour, soil mineralogy, salts, and parent material (Bowers et al., 1965; Karmanov, 1981; Stoner et al., 1981; Latz et al., 1984; Coleman et al., 1987; Henderson et al., 1989; Escadafal, 1989; Epema, 1993).

(1) Soil moisture

Commonly, wet soils exhibit lower reflectance values than dry soils, resulting from a decrease in reflectance of the incident radiation in the visible region of the spectrum. Angström (1925) attributes this darkening effect of moisture in soils to the internal reflection within the thin water film covering soil particles. At higher water contents, the spectral curve does not change its shape but the reflectance decreases as moisture content increases (figure 2.10). The specific moisture-sensitive wavelength is 1.9 µm, as reported in experiments conducted under laboratory conditions, at six different soil moisture contents by Bowers et al. (1965). The middle infrared (2.08 to 2.35µm) is the key band to predict soil moisture (Coleman et al., 1987; Epema, 1993).

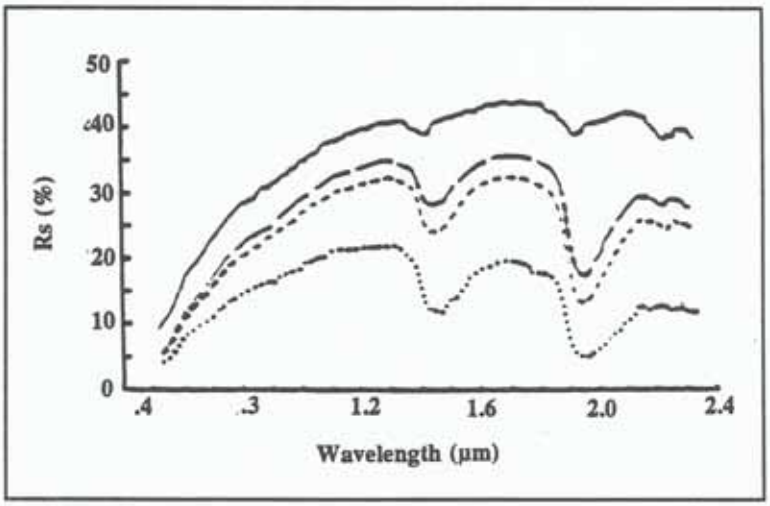

Fig. 2.10. Spectral (BRF) curves of a Typic Hapludalf soil at moisture tensions of ovendry (-); 15 bars (- -);0.3 bar (----) and 0.1 bar (....) (Baumgardner et al., 1985)

It is important to control soil moisture when soil reflectance studies are performed (Baumgardner et al.,

1985). Additionally, the sensitivity of spectral bands to moisture content were studied in combination with other factors influencing the reflectance such as roughness, texture, mineralogy and atmospheric conditions (Epema, 1993).

(2) Organic matter

The general effect of organic matter is the darkening of the soil. Organic matter contents higher than 2% dominate the mineral soil spectral properties in the visible region (Stoner et al., 1981). The decomposition state of the plant residues (i.e. fibric, hemic, sapric) alters the nonvisible reflectance in Histosols. Several studies have attempted to correlate wavelength regions with organic matter content (table 2.5).

Table 2.5: Relationship between organic matter content, wavelength range and sensor

WAVELENGTH RANGE (µm)	ORGANIC MATTER (%)	SENSOR	AUTHOR
0.72-0.80;1.5-1.80;1.00-1.4;0.4-0.58	0.75 to 6.20	airborne scanner	Al-Abbas et al. (1972)
0.76-0.90	1.97-2.32	multiband radiometer	Coleman et al. (1987)
0.4-0.9	0.46-7.9	spectroradiometer	Huete et al. (1991)
0.62; 0.56	1.1-5.6	spectrophotomer	Krishnan et al. (1980)
0.5-1.3	> 2.0	spectroradiometer	Stoner et al. (1981)
0.50-0.59;0.61-0.68	3.57	SPOT Xs	Agbu et al. (1990)
0.52-0.60;1.55-1.75;2.03-2.35;10.40-12.5	0.57-1.09	multiband radiometer	Coleman et al. (1991)

(3) Iron compounds

The secondary Fe oxides are the most important pigmenting agents in soils having low content of organic matter. More hydrated iron oxides (goethite, limonite) are yellowish while less hydrated compounds (hematite) are reddish. Iron compounds such as organo-iron, amorphous, weakly crystallized and nonsilicate irons have dissimilar effects on the visible spectral reflectance of soils. If all the nonsilicate iron is removed, the soil reflectances become practically identical, as controlled by the achromatic grey colour of clay minerals (Karmanov, 1981).

Curves of iron-affected soils have a similar sigmoidal shape because of the absorption in the shorter wavelengths. Typical hematite curves show an absorption extending to the 0.55 µm, while for goethite-shaped curves absorption is mainly produced in the blue band region (Escadafal et al., 1992). Indices developed to quantify the hematite content from soil colour demonstrate that Munsell colour notation is more correlated with the hematite content of soils than with either the hematite-goethite ratio or the total Fe oxide content (Torrent et al., 1983).

Iron oxides are best predicted using the blue (0.45-0.52μm), green (0.52-0.60μm), red (0.63-0.69μm) and thermal infrared (10.4-12.5μm) bands of the spectrum (Coleman et al., 1991). Iron oxide contents above 4% mask out the effects of high organic matter contents (Stoner et al., 1981).

(4) Mineralogy

Clay content and clay type indirectly affect soil reflectance because clay mineralogy is interrelated with organic matter, iron oxides and texture, which directly control soil reflectance. The organic-dominated curve reported by Stoner et al. (1981) is often associated with montmorillonitic clay, while iron-dominated curves are related to kandites (figure 2.9). Al-Abbas et al. (1972) could no establish a direct relationship between soil reflectance and clay content on the 0.4 to 2.6μm range because of high correlation between organic matter and clay content. In contrast, Coleman et al. (1991) reported the green, near-infrared, middle-infrared and thermal bands as best predictors of clay content in highly-weathered soils.

(5) Particle size distribution

In general, reflectance increases as particle size decreases (figure 2.11). Orlov (1966) found an increase in reflectance values for soil fractions less than 0.25 mm (fine sand and finer textures). An exponential increase in reflectance with decreasing particle size, on the basis of the behavior of textures varying from coarse silt to very coarse sand in the wavelength of 0.21 to 1.00μm, was reported by Bowers et al. (1965).

Additionally, surface roughness on a micro-scale may explain changes in reflectance as a function of particle diameter (Baumgardner et al., 1985). Coarse aggregates, having an irregular shape, form complex surfaces with a large number of inter-aggregate spaces. If incident energy falls on large irregularly-shaped aggregates, most of the incident flux is trapped, reducing the general reflectance (Escadafal, 1989).

(6) Soil colour

Color is a covariant soil property, providing indirect estimations of other parameters such as soil degradation, organic matter, carbonates and iron oxides. Colour can be quantitatively related to soil spectral reflectance in the visible domain. A linear relation between color expressed in red, green and blue coordinates, and reflectance values observed in the red, green and blue bands of the Landsat TM sensor was found by Escadafal et al. (1989). This simple relationship allows to compute, from data measured in the three first TM bands, surface parameters such as hue, intensity and saturation which are comparable to the Munsell color parameters (hue, value and chroma) observed in the field (Escadafal, 1994).

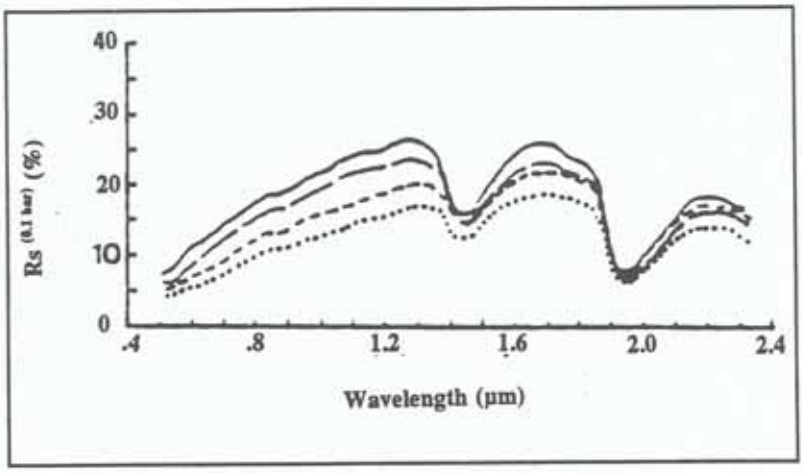

Fig. 2.11: Spectral curves of sandy soils. Fine sand (---); fine loamy sand (- - -); loamy sand (----); loamy coarse sand (···) (Baumgardner et al.,1985)

(7) Salts

Six spectral ranges characterize the salinity status of soils undergoing different salinization and alkalinization processes. These key bands are placed in the visible (0.55-0.77µm), near-infrared (0.9-1.03µm; 1.27-1.52µm) and middle-infrared (1.94-2.15µm;2.15-2.3µm; 2.33-2.4µm) (Csillag et al., 1993).

Ground observations and radiometric measurements show that the main factors affecting the reflectance are quantity and mineralogy of salts together with moisture, color and roughness. Salt- or sodium-influenced surface features are: crusts with or without low salt evidences, salt crusts (< 1 mm to 1 m thick), puffy structures containing soil aggregates and salt crystals (0.5 - 5 mm) derived from salty clays and sometimes from salt crusts, wind erosion of puffy structure horizons and gypsiferous sands (Mougenout et al., 1994).

2.4.3 Reflectance of surface material mixtures

Different surface components may have the same or similar spectral responses causing inconsistencies in their detection. For instance, organic matter, moisture and roughness behave similar in the visible and near-infrared: when these factors increase, reflectance decreases (Stoner et al., 1981). In addition, the reflectance recorded in an image pixel may be a mixture of different components such as soil, vegetation and rocks.

Several methods have been applied to overcome these problems, based on the combination of multitemporal, multi-sensor, multi-frequency or multi-scale remote sensing imagery, and the incorporation of ancillary data prior- and after-classification procedures. Spectral unmixing techniques such as linear mixing, artificial neural networks and fuzzy membership functions are usually applied to estimate ground cover proportions within one pixel.

The integration of multiple techniques contributes to object identification, characterization and differentiation. For instance, the principle of multitemporal observations lies in selecting the optimal period of time for accurate separation and mapping of surface features of interest. Verma et al. (1994) solved problems of spectral similarity between fallow sandy soils and salt-affected areas using images from different seasons and from different regions of the spectrum. This approach proved useful to map and monitor soil surfaces affected by salinity-alkalinity and waterlogging (Abdel-Hamid et al., 1991; Rao et al., 1991; El Badawi et al., 1992).

Spectral measurements taken in the visible and near-infrared provide information about soil roughness. The latter, however, is very difficult to separate from other intrinsic soil properties like color and moisture since several factors intervene simultaneously. Therefore, the visible, near-infrared and thermal ranges of the electromagnetic spectrum must be combined to improve the detection of soil moisture, waterlogging and salt-affected areas (Menenti et al., 1986; Epema, 1990a).
Topographic, geomorphic and other ancillary information has been largely used in soil erosion studies to differentiate soil materials, land use types, waterlogging areas and vegetation cover (Bocco et al., 1991; Brackman et al., 1992).

Spectral mixture analysis focuses on the dominant factors affecting spectral variations, such as mixture of surface materials within one pixel. Each ground-pixel-area is divided into different cover types (Smith et al., 1991). Thus, the spectral properties of a soil surface result from combining the individual reflectances of several components such as minerals, iron oxides, organic matter, water (Escadafal, 1994). Linear mixture modelling has been successfully applied to generate proportion maps of different surface materials including gypsum, halite, clastic sediments and water in a playa setting (Drake et al., 1994; White et al., 1993). The same approach was used to map land degradation and soil erosion hazard based on the computation of vegetation abundance and the identification of soil degradation levels in semiarid environments (Hill, 1993; Smith et al., 1991).

2.4.4 Equations for predicting soil properties from spectral signatures

Indices and quadratic or linear regression equations have been proposed to predict a variety of soil surface properties such as iron oxides, organic matter, gypsum, lime and particle size distribution, from ground-based measurements as well as from satellite data (Table 2.6). As an example, Mulders et al. (1987) elaborated thematic maps indicating gypsiferous, calcareous and clayey surfaces using different Landsat TM ratios (e.g. bands 5, 4, 3).

Table 2.6: Equations, indices and band ratios to predict soil properties

SOIL PROPERTY	EQUATION	SENSOR	AUTHOR
Sand content	$Y=90.87-22.51X_2+17.49X_3-127.41X_7$	Landsat TM	Coleman et al. (1993)
Silt content	$Y=17.64+34.72X_1+90.65X_2-63.35X_3+12.64X_7$	Portable multiband radiometer	Coleman et al. (1991)
Silt content	$Y=157.14-44.89X_1+9.95X_4+249.62X_7$	Landsat TM	Coleman et al. (1993)
Clay content	$Y=-482.68+69.02X_1-17.42X_3-17.91X_4-88.00X_5+459.98X_6$		
	$Y=43.09-28.79X_2+50.82X_5-42.63X_7+10.86X_8$	Multiband radiometer	Coleman et al. (1991)
	$\%clay=48.52091-0.11452X_{10}-0.17006X_{12}-0.16833X_5+0.36125X_7+0.10502X_1-0.28371X_6$	Multiband radiometer	Al-Abbas et al. (1972)
Organic matter content	$Y=1.11+2.90X_2-3.36X_6+1.84X_7-1.06X_8$	Multiband radiometer	Coleman et al. (1991)
	$Y=14.81-2.02X_1-0.59X_2+1.03X_3+0.53X_4-7.85X_6$	Landsat TM	Coleman et al. (1993)
	$\%O.M.=4.27924+0.0221X_8-0.2665X_{11}+0.170X_1-0.09893X_2-0.02911X_{10}-0.044034X_3$	Multiband radiometer	Al-Abbas et al. (1972)
	Organic matter index SO = R (750)/R (450) R: reflectance at specified wavelength	Radiometer	Courault et al., (1988)
Iron oxide content	Iron index RF= R(750)-R(900)	Radiometer	Cervelle et al. (1988)
	$Y=-281.38-5.26X_3-10.24X_4+466.36X_6-137.80X_7$	Landsat TM	Coleman et al. (1993)
	$Y=27.26-10.35X_1-36.80X_2+42.69X_3+11.69X_8$	Multiband radiometer	Coleman et al. (1991)
Soil minerals	Mineralization index: IM= TM1/TM2	Landsat TM	Escadafal (1989)
Iron oxides	Redness index RI=(TM3-TM2)/(TM3+TM2)	Landsat TM	Escadafal et al. (1991b)
Water content (at 0.1 bar tension)	Wetness R=0.03*TM1+0.20*TM2+0.31*TM3+0.16*TM4-0.68*TM5-061*TM7	Landsat TM	Crist (1985)
Soil color (Munsell chroma)	MSS5/MSS4 ratio	Landsat MSS	Escadafal et al. (1986)
Soil roughness	Related to image brightness (MSS4+MSS5)	Landsat MSS	Escadafal et al. (1986)
Quartz, carbonate and gypsum	MM7/MM4	Multiband radiometer	Epema (1991)
Gypsum content	TM5/TM7	Landsat TM	Mulders (1987)

Continued

	TM7-TM4/TM7+TM4	Landsat TM	Epema (1986b)
	TM7/TM4	Multiband radiometer	Epema (1990b)
Acid sulphates	TM5/TM7	Landsat TM	Amos et al. (1987)
	TM5/TM4	Multiband radiometer	Mougenot (1991)
Salt dominance	Low ratio of TM4/TM1	Multiband radiometer	Epema (1990a)
High moisture content	Low ratio of TM7/TM4	Multiband radiometer	Epema (1990a)

2.4.5 Applications of soil reflectance measurements

Natural resource scientists, especially soil scientists, utilize the soil spectral reflectances for purposes varying from soil survey, to soil degradation assessment, to soil database, to characterization of surface dynamics.

(1) Soil degradation assessment

In salt-affected soils, spatial distribution of salt contents is highly variable. Remote sensing data help identify and separate soil surface features caused by salt and sodium (Mougenot, 1991; Singh, 1994). By systematic visual interpretation of Landsat TM false color compositions, image elements such as dull white and bright white patches can be correlated with ground data to determine degrees of salinity-alkalinity (Rao et al., 1991; Verma et al., 1994). On this basis, only two or three degrees of salinity can be distinguished. For instance, Singh et al. (1983) report strong and medium salinity levels but fail in discriminating between moderately saline and non-saline soil surfaces. Underestimation of salt-affected areas is attributed to confusion with slightly-saline and non-saline surfaces. On bare soils, satellite observations permit to detect salts on the terrain surface, but direct and precise estimation of salt types and quantity is not yet possible. Ground validations are necessary to establish relationships between reflectances and salts in soils, inferred from surface features (Mougenout et al., 1994).

Remote sensing documents, satellite- or air-borne, are also useful for detecting eroded soils and monitoring erosion effects upon soil surfaces. Soil erosion classes can be discriminated and mapped by means of digital analysis techniques. Erosion severity can be related to variations in spectral reflectance (Mathews et al., 1973; Latz et al., 1984). Although individual gullies can generally not be identified, it is possible to extract information about the environmental factors that favor runoff and gullying. Indicators of land degradation, indirectly determined from land use, vegetation and geomorphology have to be checked in the field to establish relationships with soil erosion (King et al., 1994). For instance, gully erosion areas were identified and classified using visual interpretation of stereo SPOT data and multispectral classification of SPOT and TM data (Bocco et al., 1988).

(2) Soil survey

Since the 1970s, scientists have explored methods for incorporating satellite data into soil survey projects for delineating meaningful soil boundaries. Baumgardner et al. (1983) summarized the sources and uses of reflectance data from aerospace sensors (figure 2.12).

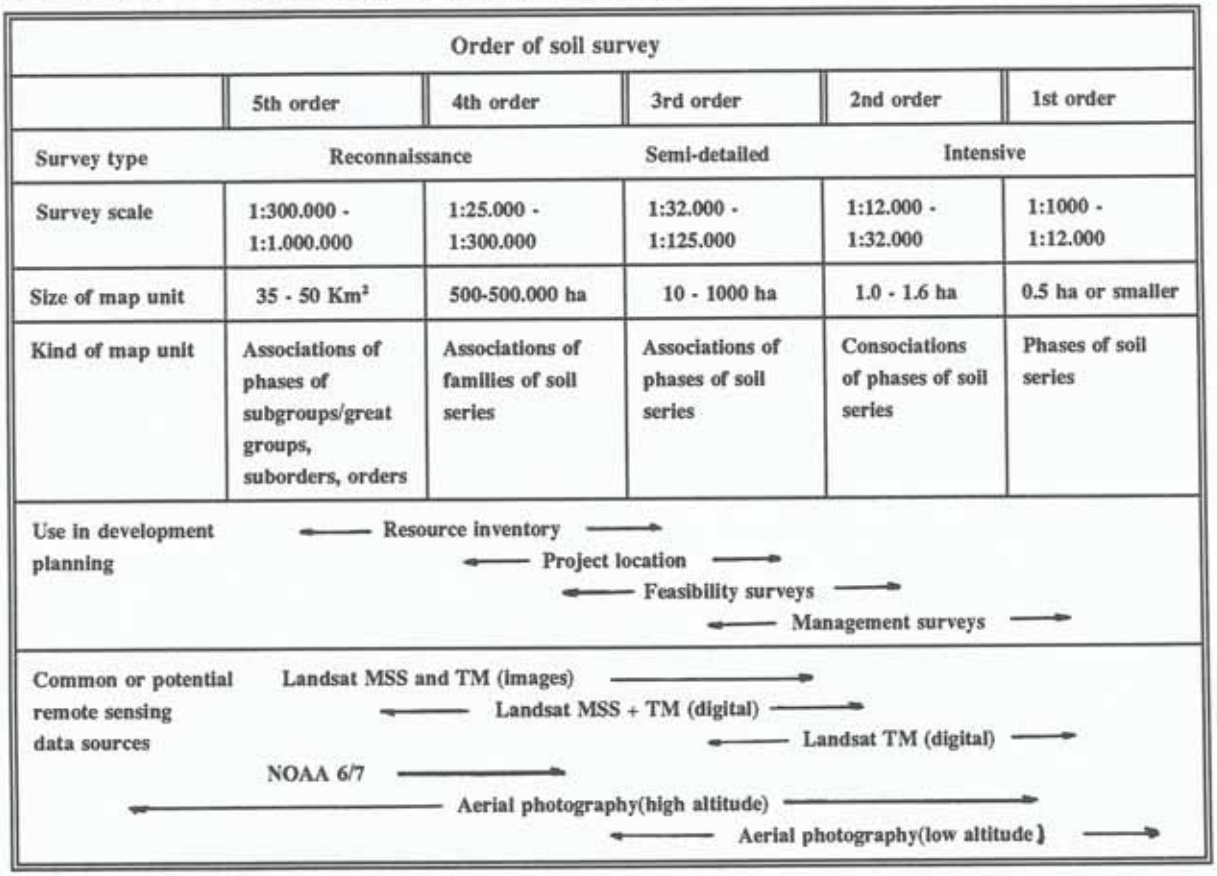

Fig. 2.12: Use of soil reflectance data in soil surveys (Baumgardner et al., 1985)

Studies involving the use of satellite multispectral data for differentiation of soil types and soil properties had so far limited success. Most of these studies have confined soil classification to the higher categories of the Soil Taxonomy (e.g. order, suborder). Landsat and SPOT data are useful for grouping soils in broad classes of drainage, surface colour or parent material (Cipra et al. 1980; Lee et al., 1988; Henderson et al., 1989; Agbu et al., 1990). However, none of these studies could reach the level of detail used in conventional soil classification.

(3) Dynamics of surface cover and landscape components

Landscape indicators are used to interpret remote sensing images for monitoring desertification processes, delineating landscape components and correlating them with depositional processes and landscape evolution (Alekseyeva et al., 1991; Filho and Zinck, 1994). Landscape features such as topography, drainage and vegetation help infer processes and phenomena not detectable on images by other means.

Specific soil surface features were identified by their roughness, related to the image brightness, and their Munsell chroma correlated to the MSS5/MSS4 ratio (Escadafal et al., 1986). Maps of soil surface conditions can be computed and used for further studies such as, for example, hydrological modelling or mapping desertification sensitivity (Escadafal, 1989). A variety of landforms of different origin and exhibiting variations in surface mineralogy, moisture content and topography can be detected by using Landsat TM data (Epema, 1993). Similarly changing factors such as moisture content can be monitored.

(4) Soil databases

Soil spectral reflectances can be used as a source for data generation in soil geographic databases. Maps of surface dynamics and soil properties, related to soil spectral reflectances, can be derived from satellite as well as ground-based measurements.

2.5 CONCLUSION

Desertification refers to processes leading to severe and irreversible land degradation, excluding rehabilitation in human time scale and within economic limits. It is spatially limited to arid, semiarid and dry subhumid areas. The term land degradation is applied if the desertification stage has not been reached and/or the region lies outside dry environments. The concept of land degradation was adopted for this study, since the Bolivian area does not present an irreversible stage of land deterioration.

Soil erodibility indices allow to characterize a large number of soils in a short time. Thus, they are suitable for mapping soil erodibility as, for example, a phase in land use planning and land degradation assessment. Even though researchers are aware of these advantages, none of the studies carried out in the last decades has achieved an erodibility index that is simple to measure, reliable in operation and capable of universal application. There is a need to reformulate the erodibility concept and establish a distinction between the general K-USLE soil erodibility factor and 'soil erodibility coefficients' expressing the susceptibility of a soil to a specific process.

Although salt-affected soils can be distinguished from non-saline soils, improvements are necessary to increase the accuracy in detecting and mapping slightly saline areas, salinity types and the effects of salinity on vegetation.

Most equations for predicting soil properties from remotely-sensed data are geographically dependent, regardless of whether they were developed from ground-based or satellite platforms. Thus, local correlations cannot be used for global data interpretation. Prior knowledge of the various band combinations that yield the best results is very valuable in generating prediction equations for different geographical regions using diverse platforms (e.g. spectroradiometers, airborne or satellite-borne sensors).

CHAPTER THREE:

METHOD AND TECHNIQUES

3.1 METHODOLOGICAL APPROACH

The methodological approach is composed of four main steps (figure 3.1):

(1) Characterization of geopedologic units and land degradation features
(2) Identification and measurement of land degradation indicators
(3) Design and implementation of exploratory models for monitoring and prediction
(4) Evaluation of the efficiency of the synergistic approach

The research comprises four stages, namely (1) data collection, (2) data processing, (3) data analysis and interpretation, and (4) prediction. The data collection phase includes a general inventory of the land units and their surface features, the selection of training areas and the capture of relevant data using several techniques such as photo interpretation, field determinations, soil laboratory analyses, ground-based radiometric measurements of surface reflectance, and the integration of multi-source, multi-temporal and multi-scale remote sensing data.

The data processing phase involves the determination of the geopedologic units, mapping of topsoil properties and characterization of land degradation indicators. A multi-purpose database is built up so that data can be easily retrieved for several thematic applications. Cartographic modelling encompasses point data interpolation and delineation of the soilscape units.

Data analysis and interpretation are supported by statistical and spatial analysis techniques. Descriptive and multivariate statistics are used, including simple and multiple regressions, correlations and one-way analysis of variance (ANOVA). Spatial analysis techniques are applied in a geographic information environment to integrate and compare data, and to derive new information.

Modelling and prediction are performed using fuzzy sets and knowledge-based systems. Data are retrieved and manipulated within a geographic information system. Maps depicting land degradation trends and hazard zonation are elaborated. The applicability and effectiveness of the synergistic approach for identifying, characterizing and mapping land degradation processes are evaluated.

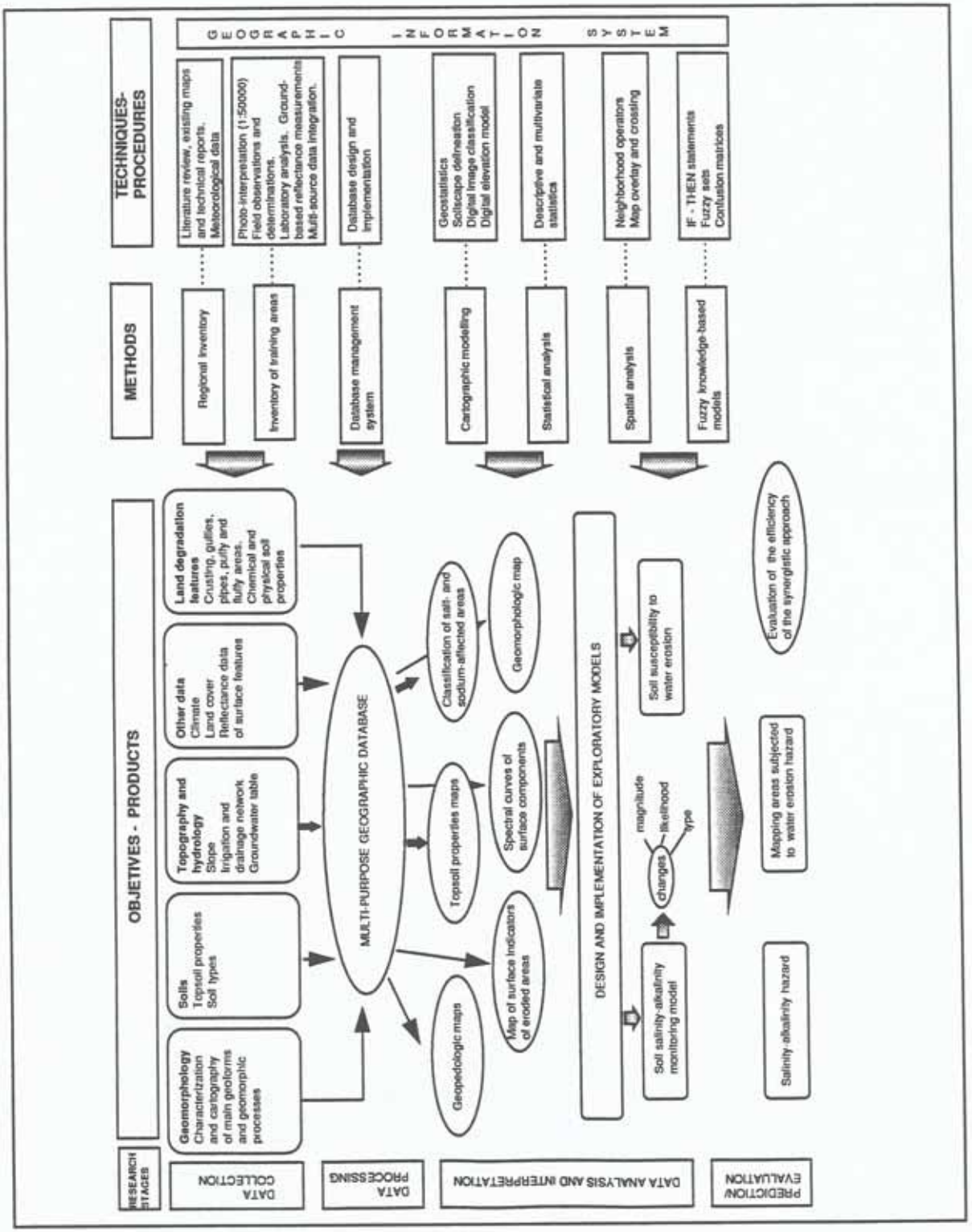

Fig. 3.1: The methodological approach

3.2 CHARACTERIZATION OF GEOPEDOLOGIC UNITS AND LAND DEGRADATION FEATURES

3.2.1 Delineation of the geomorphic units

A multi-level approach was used for data collection. Geomorphic characterization at regional level was performed by means of digital and visual interpretation of satellite images and visual interpretation of aerial photographs. Geomorphic units were delineated using a hierarchic classification system of geoforms comprising six categoric levels, each defined by a specific concept as indicated in table 3.1 (Zinck, 1988).

Three training areas affected by different land degradation processes were selected in piedmont and valley landscapes using a random-stratified sampling scheme. Stratification was based on the previously delineated geomorphic units, since soil spatial distribution and variability are controlled by, among others, the geomorphic factor. Ancillary data from existing soil observations, geological maps, technical reports and meteorological records were stored within a geographic information system for further analysis. A soil geographic database was built up to store and process the data gathered from several sources and at different spatial levels.

Table 3.1: Synopsis of the geoform classification system (Zinck, 1988)

LEVEL	CATEGORY	GENERIC CONCEPT	SHORT DEFINITION
6	Order	Geostructure	Large continental portion characterized by a broad geologic structure (e.g., cordillera, geosynclinal basin)
5	Suborder	Morphogenetic environment	Broad type of biophysical medium originated and controlled by a style of internal and/or external geodynamics (e.g., structural, depositional, erosional)
4	Group	Landscape	Large portion of land characterized by a repetition of similar relief types or an association of dissimilar relief types (e.g., valley, piedmont, mountain)
3	Subgroup	Relief/molding	• Relief as determined by a given combination of topography and geologic structure (e.g., cuesta, horst) • Molding as determined by specific morphoclimatic conditions or morphogenetic processes (e.g., glacis, terrace, delta)
2	Family	Substratum	• Lithology of hard rocks (e.g., gneiss, sandstone) • Facies of soft cover formations (e.g., periglacial, lacustrine, alluvial)
1	Subfamily	Landform	Conspicuous basic geoform type, characterized by an unique combination of geometry, dynamics and history (e.g., levee, dune, backslope, flat)

3.2.2 Soil characterization

Soil survey data were derived from three sources: (1) visual interpretation of aerial photographs and digital processing of Landsat TM images; (2) field observations and instrumental determinations of biophysical features, as well as observation of human activities; (3) laboratory analyses of mechanical, physical and chemical soil properties.

(1) Field observations

Field observations comprised the description of soil sites and surface dynamics, and reflectance measurements of the surface components. Point data were gathered from auger holes, minipits and some full pits. Modal profiles were described to check and improve the existing soil maps. Horizon depth and designation, structure, color, texture, stoniness, porosity and biological features were recorded according to the FAO guidelines for soil profile description (FAO, 1990). To account for soil spatial variability, a composite topsoil sampling scheme was adopted. Samples 5 cm deep, within a perimeter of 7 m from the central observation point, were collected for laboratory determinations, using a stratified-oriented sampling technique. The samples were taken at variable distances within selected geoform types exhibiting surface features related to salinization-alkalinization or water soil erosion (playas, lagunary flats, badland, dissected depositional glacis). The minipits were placed in the centre of bare plots, large about 90 by 90 m, to account for location errors caused by positional inaccuracies of the GPS and/or the geometric correction of the Landsat TM image.

A total of 267 soil samples was collected in the three valleys, covering an area of approximately 9000 ha in the Punata-Cliza valley and 1100 ha in the southern part of the Sacaba valley. Additional data about soil surface features such as crust color, texture and thickness, color and coverage percentage of surface rock fragments, and vegetation type and cover percentage were determined. Water erosion features were observed and recorded in relation to erosion type (gully, rills, overland flow) and degree (slight, moderate, severe). On ephemeral creek channels (quebradas), color, size, shape and percentage cover of stones were recorded. Stone pavements present in badlands were also described.

A Magellan GPS NAV 1000 PRO receiver was used to determine the spatial location of soil plots. Geographic coordinates (latitude and longitude) were recorded in three-dimensional (3D) mode of operation, using four satellites to obtain a position fix. Positional accuracy was checked using the Position Dilution of Precision (PDOP). The latter is a measurement of the possible errors related to the geometry of the satellites used for triangulating a position. In 3D operational mode, good accuracies are obtained when the PDOP is smaller than 6, implying field error locations between 30 and 100 meters. On average, PDOP between 2 and 4 were obtained. Five to ten measurements of individual soil plots were taken and averaged to reduce positional inaccuracies. Geographical coordinates were transformed to UTM projection, plotted on the topographic sheets at scale 1:50000 and stored in the database.

(2) Laboratory determinations

The following analyses were carried out: particle size distribution, bulk density, aggregate-size distribution, organic matter content, electrical conductivity, soil reaction (pH), soluble carbonates, bicarbonates, sulfates and chlorides. On 35 lagunary depression sites, sodium, magnesium and calcium contents were determined for SAR calculation. Because of the presence of rock fragments in the soil matrix, bulk density determinations were done on wax-coated clods instead of undisturbed cylinder samples. Table 3.2 summarizes the laboratory techniques implemented for soil determinations.

Table 3.2: Soil laboratory analyses

SOIL PROPERTY	UNITS	SAMPLES ANALYZED	LOCATION	TECHNIQUES
Bulk density	g/ cm^3	267	Punata-Cliza, Sacaba and Central Valleys	Wax-coated clods immersed in water
Particle size distribution (5 fractions:0.002.0.05,0.25,0.5,2 mm)	%	267	Punata-Cliza, Sacaba and Central Valleys	Bouyoucos and set of sieves
Aggregate-size distribution	%	25	Sacaba	Yoder -type wet sieving apparatus; aggregates size: 4,2,1,0.5mm
Organic carbon	%	267	Punata-Cliza, Sacaba and Central Valleys	Walkley -Black
pH		1000	Punata-Cliza, Sacaba and Central Valleys	soil- H_2O 1:2.5 by volume and paste, buffer solution (pH7.0), digital pH-meter
Electrical conductivity (EC)	dS /m	1000	Punata-Cliza, Sacaba and Central Valleys	soil- H_2O 1:2.5 by volume and paste,EC -meter
Carbonates and bicarbonates	meq /l	80	Punata-Cliza Valley	Titration with acid
Chlorides	meq /l	80	Punata-Cliza Valley	Titration with silver nitrate
Sulphates	meq /l	80	Punata-Cliza Valley	Titration
Sodium	meq /l	35	Punata-Cliza Valley	Flame Photometer
Calcium and magnesium	meq/l	35	Punata-Cliza Valley	Titration with versenate
Cation exchange capacity	meq /100g soil	5	Central Valley	Extract of ammonium acetate

To frame the landscape and landform evolution and date the formation of badlands and other erosional features in the area, five buried soils located in the dissected depositional glacis and lagunary depression relief types were sampled and described for ^{14}C determinations. Carbon-14 is useful to date materials directly or indirectly involved in the Earth's carbon cycle during the last 50000 years. Carbon dating determines the age of a sample in years, by measuring the concentration of carbon-14 remaining in the organic material, formerly living matter (Bates and Jackson, 1987). The ^{14}C age results from radioactive decay measurement. It closely approaches a Gaussian probability distribution with a well-defined standard deviation. However, variations in the atmospheric ^{14}C content due changes of the earth's magnetic field, known as long-term trends, or solar fluctuations, determining medium-term variations, complicate the conversion of conventional ages BP (i.e. years before AD 1950) into real calendar ages (AD/BC).

Determinations were carried out at the Laboratory for Isotope Research, University of Groningen. The resulting radiocarbon ages were calibrated to correct errors due to natural variations of the ^{14}C contents in the atmosphere, using the Seattle/Groningen method described by van der Plicht et al. (1989). The calibration points on the x-axis indicate the calendar age AD/BC, and those plotted on the y-axis indicate the years before the present (fig. 3.2). A cubic spline function is used to transform the ^{14}C age (BP, y-axis) into real calendar age (cal AD/BC, x-axis). The AD age is expressed as 1950 minus the years BP, and BC is equal to years before the present (BP) minus 1949 (van der Plicht et al, 1989).

Figure 3.2a illustrates the calibration of a ^{14}C age of 8740 ± 110 BP, obtained from a soil sample collected south of the Sacaba town, at approximately 8 m depth, in the distal part of a dissected depositional glacis. The graph shows the calibration curve, a spline function, connecting the calibration data points. The Gaussian probability distribution, corresponding to the ^{14}C age of 8740 ± 110 BP, is represented by the horizontal bars perpendicular to the y-axis. The calibrated calendar age (BC) is plotted along the horizontal x-axis.

Figure 3.2b shows the calendar axis probability distribution with levels corresponding to one and two confidence levels (dotted lines). The top dotted line indicates the date ranges covering a total probability of 68%: 7890-7690 and 7670-7630 cal BC. The bottom dotted line indicates the 2-σ range, meaning that there is a 95% probability that the true age lies in the area under the curve between 7980 and 7540 BC. Appendix II contains the results of applying the described calibration technique to the remaining four radiocarbon determinations.

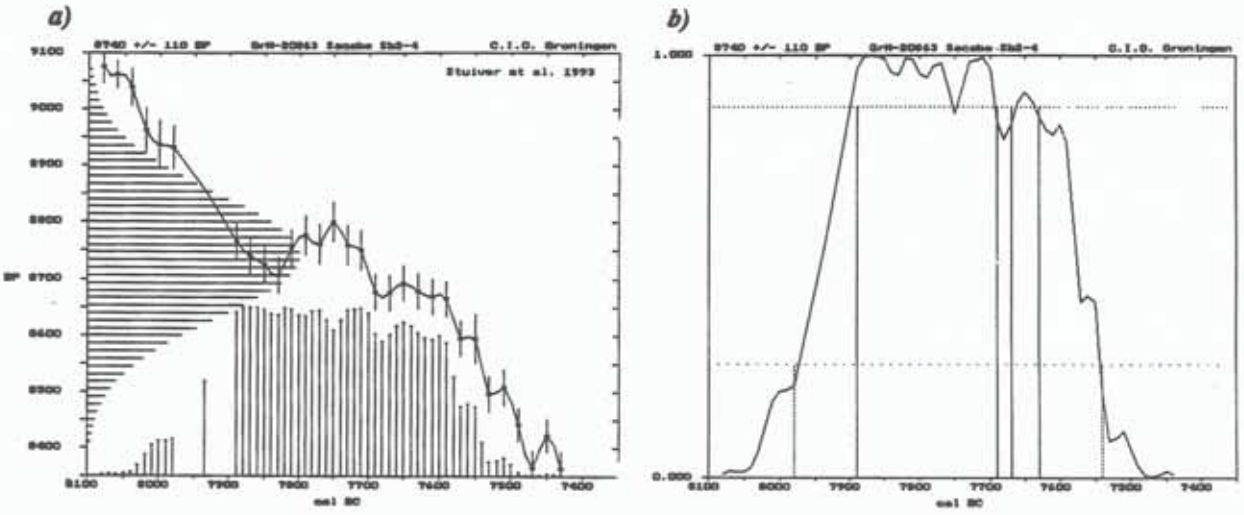

Fig. 3.2: Results of calibrating 8740±110 BP (soil sample Sb2). Figure a: shows the calibration curve, where the ^{14}C age is represented along the y-axis and the calibrated calendar age distribution is plotted along the x-axis. Figure b: indicates the calendar axis probability distribution with one and two confidence levels (dotted lines).

3.3 REFLECTANCE CONCEPTS AND MEASUREMENT DEVICES

Technologic developments over the last three decades have generated an array of new instruments, which scan a wide range of the electromagnetic spectrum and record quantitatively the intensity of energy radiating from a specific object. Thus, nowadays it is possible to measure soil reflectance in the laboratory or in-situ, and obtain spectral curves by plotting the intensity of reflectance in the ultraviolet, visible and infrared portions of the spectrum (Baumgardner et al., 1985).

3.3.1 Basic concepts related to reflectance

Radiant energy falling upon a surface is distributed through three different processes: reflection, absorption and transmission. In opaque material such as soils, transmittance is zero (Bowers et al., 1964). Thus, reflectance can be defined as the ratio of the reflected radiation to the total radiation falling upon a surface.

Soil reflectance measurements are usually reported as percent of the bidirectional reflectance factor (BRF) to correctly express the geometry of the spectral measurement. The bidirectional reflectance factor can be described as the ratio of the flux reflected by an object under specified conditions of irradiation and viewing to the flux reflected by an ideal, completely reflecting, perfectly diffusing surface, identically irradiated and viewed (Nicodemus et al., 1977). Commonly used ideal surfaces are magnesium oxide and barium sulphate plates.

3.3.2 Geometric considerations

Illumination conditions, viewing angles and sensor field of view are important geometric considerations influencing the measurements. The angular relationship between the source target and sensor can affect the reflectance measurement of the target. Therefore, most field observations are made at a sensor zenith angle of 0º, but at a variety of solar illumination angles. Laboratory observations consider a sensor zenith angle of 0º and illumination angles between 10º and 30º. For field measurements, a solar zenith angle less than 65º can be used to establish a field reference set (Epema , 1993).

The sensor field of view has to be wide enough to catch properly the geometric features of a target, since the signal received by the sensor is proportional to the square of the field of view. In field situations, a field of view of approximately 15º has been commonly used (Epema , 1993; Stoner et al.,1980).

3.3.3 Instruments

Instruments providing data about soil spectral properties can be laboratory instruments, ground-based instruments for in-situ measurements, low-altitude aircraft platforms and satellite-borne sensors.

(1) Laboratory and ground-based instruments

Multiband radiometers and spectroradiometers are used, differing by the way of gathering the energy. Spectroradiometers measure fluxes of energy in narrow and continuous spectral bands, operating over the range of 0.4 to 2.4µm . The reflectance data can be used to interpret different sets of broadband satellite data as for example Landsat TM and MSS, SPOT XS and NOAA AVHRR . Multiband radiometers contain several optical filters defining different spectral bands, selected to sample discrete portions of the spectrum. Generally, wavebands are compatible with Landsat MSS, Landsat TM or SPOT XS bands. These instruments present the disadvantage of having limited spectral range and resolution, and reflectance measurements compatible with certain satellite band passes are difficult to apply to others. For instance, Landsat MSS compatible data are difficult to apply to Landsat TM data

interpretations. The best correlation coefficients among spectral bands and soil properties are obtained when using ground-based sensors (Stoner et al., 1981; Coleman et al., 1991). In-situ measurements are not affected by atmospheric disturbances and provide higher spatial as well as spectral resolution when compared with operational space-borne sensors, such as the Landsat Thematic Mapper and SPOT.

In this research, ground-based reflectance measurements were carried out using the Cropscan multiband radiometer on soil surface plots sampled for laboratory determinations and on additional areas. The Cropscan radiometer has eight bands gathering reflected energy from the visible and near-infrared regions of the spectrum (table 3.3). Because reflectance values are obtained by nearly simultaneous inputs of voltages representing incident as well as reflected radiation, calibration plates are not needed. Instead, constants have to be generated through a calibration procedure carried out on a clear day and within two hours of the solar noon. The data acquired represent the average reflectance from the sampled area. The diameter of the field of view is one-half of the height over the surface being recorded. The altitude over the ground can be adapted to cover the surface component of interest. The field of view is equal to 180 degrees for the incident radiation and 28 degrees for the reflected radiation.

Sample plots of 90x90 m were disaggregated into 'basic surface components'. For instance, a selected soil plot was decomposed into percent coverage of stones, vegetation and crusted surface. The individual reflectance values of each surface component were recorded. Three samples per object were taken and averaged. The sensor zenith angle was equal to zero, and a solar zenith angle less than 65° was used for all field reference sets, as suggested by Epema (1993). Additional reflectance measurements were performed over badlands and seasonal creek channels (quebradas).

Table 3.3: Cropscan spectral band configurations

CHANNEL	CENTRE WAVELENGTH (nm)	BANDWIDTH (nm)	MINIMUM PEAK (%)
1	450	6.5	45
2	500	7.4	50
3	550	9.2	50
4	600	10.1	50
5	650	11.4	50
6	700	12.3	45
7	750	13.4	45
8	800	11.3	45

(2) Low-altitude aircraft and satellite-borne sensors

Air- and satellite-borne sensors are utilized since the 1970s to differentiate soil surface types and properties. They can be grouped either according to the energy source used to capture radiation from the surface cover, or the region of the spectrum recorded. Microwave remote sensors are referred to as active remote sensing systems, since they provide their own energy source and measure the amount of energy scattered back to the sensor. Passive remote sensors, optical and thermal, measure

radiation reflected by or emitted from the earth surface. This can be reflected sun energy or energy emitted by an object due to its own temperature.

Images from the Japanese Earth Resource Satellite (JERS-1) and the Landsat Thematic Mapper (TM) were selected to investigate the capabilities of active and passive satellite-borne sensors for identifying, characterizing and measuring the extent of selected soil degradation features. The main characteristics of these sensors are summarized in table 3.4.

Table 3.4: Main characteristics of active and passive satellite-borne sensors

TECHNICAL SPECIFICATIONS	LANDSAT THEMATIC MAPPER (µm)	JERS-1(cm)
Spectral bands	0.45 - 0.52 (1) 0.53 - 0.61 (2) 0.63 - 0.69 (3) 0.78 - 0.90 (4) 1.57 - 1.78 (5) 2.08 - 2.35 (7) 10.4 - 12.5 (6)	23, L-band HH polarization
Orbit type	sun-synchronous	sun-synchronous
Inclination	98.25°	98.5°
Nominal altitude (km)	705	570
Swath width (km)	185	75
Ground resolution (m)	30; 120 (thermal)	12.5
Radiometric resolution (bits)	8	16
Temporal resolution (days)	16	44
Incidence angle	---	35°
No. of looks	---	3

3.4 SOIL GEOGRAPHIC DATABASE

3.4.1 Soil database concept

A soil geographic database is a tool for storage, processing and display of soil data and information generated from multiple sources and observation levels. Within a geographic information system, a soil database facilitates the transformation of data into multi-purpose information, through the capabilities of data processing, automated interpretation and correlation.

Because geomorphology is a relevant soil forming factor and soil mapping criterion, the soil database uses geopedologic entries (Zinck and Valenzuela, 1990). As such, geoforms are considered as spatial and

temporal soil formation frames and as soil cartographic 'containers', classified according to the taxonomic system described in table 3.1.

The soil horizon is the basic unit of data capture. Horizon and substratum data are aggregated into observation profiles and modal pedons. Assemblages of similar contiguous pedons form polypedons, labelled according to a selected soil taxonomic classification system (USDA, 1992). On the landscape, the combination of a basic geomorphic unit with its associated polypedons results in a soilscape unit. Cartographically and taxonomically controlled soilscape units, as unique combinations of geomorphic polygons with their corresponding soil contents, result in soil map units
(SMU) (Zinck and Valenzuela, 1990).

3.4.2 Database design

A soil database comprises a set of components or tables, represented by one or more files. The structure of the database as well as the nature and number of files can vary according to specific purposes. The present database model comprises eight structural components (bold lower case letters in figure 3.3). The tables are created and stored in the Oracle relational database management system. The horizon table contains field observations and determinations, coded according to the FAO Guidelines for soil profile description (FAO, 1990). Soil physical and chemical laboratory data concerning the surface horizon were stored in a separate component, the laboratory table. The pedon table stores data related to geographic location, site and soil surface characteristics. Modal pedons are selected and stored in the polypedon table. Polypedons are labelled at family level according to the Soil Taxonomy (USDA, 1992). Since there is a many-to-many relationship between the soil map units and the polypedons because a SMU may have many polypedons and a polypedon may belong to many SMU, one combination entity matching both components has to be created (Zinck and Valenzuela, 1990). The soil composition table contains data related to the kind of soil map unit, polypedon names, percentage composition and inclusions. The geomorphic table contains the attributes used to delineate the geomorphic soil map units at the selected hierarchical levels. Soil surface reflectance data, recorded with the Cropscan multiband radiometer in its eight bands, are stored in the reflectance table. Data concerning the type and cover percentage of surface components present within each study plot are also included in this table.

The SMU code is the link between the semantic data stored in the Oracle relational database and the spatial data stored in the ILWIS (Integrated Land and Water Information System) geographic information system. By querying the soil database, different thematic tables can be obtained and exported to other software such as ILWIS, Statistica or Excel for further graphic and statistical processing. ILWIS has vector and raster data manipulation and analysis capabilities. Positional and tabular data can be linked by the 'tabcalc' tool (Gorte et al., 1990). A spatial modelling module provides analysis functions allowing for overlay, neighborhood and connectivity operations. A variety of vector functions, such as digitizing, cleaning, copying and merging of segments, and polygon to raster conversions can be executed using the vector module. Additional data import-export, image processing and output modules are included (ILWIS User's manual, 1993).

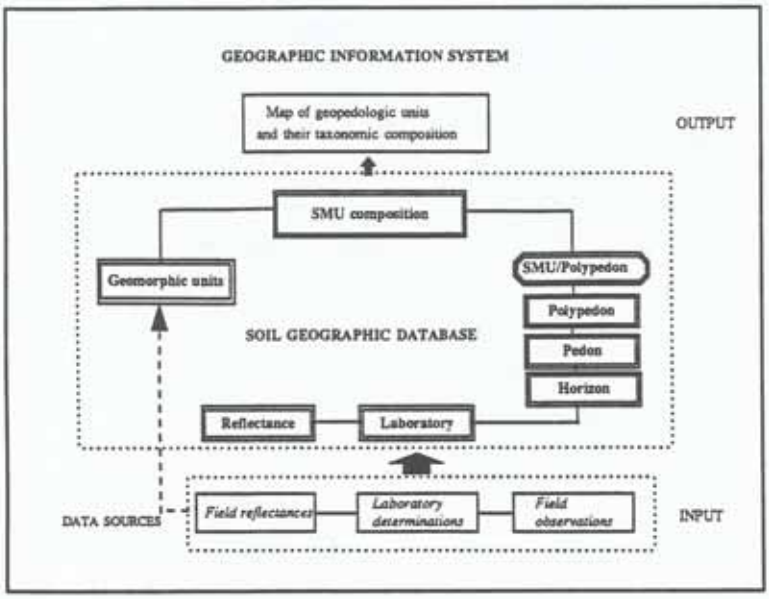

Fig. 3.3: Database design (bold lower case letters represent the structural components), (after Zinck and Valenzuela, 1990).

3.5 TECHNIQUES FOR DISCRIMINATING LAND DEGRADATION FEATURES FROM REMOTE SENSING DATA

Land degradation features must be properly identified and discriminated before they can be delineated. Discrimination is frequently obscured because of spectral mixtures caused by the combined reflectance of several components within one pixel, or due to a similar behaviour of different surface objects in the range of the spectrum considered. The multi-sensor and multi-frequency data fusion of Landsat TM and JERS-1 attempts to solve the spectral confusions. Passive remote sensors use the sun as a source of radiation. The sunlight illuminates the surface, interacts with it and reflects the energy towards the detector, which measures its intensity as a function of the wavelength. The radiation arriving at the surface is scattered by the material in all directions: some radiation penetrates, some is absorbed at the wavelength characteristic of the material and some is scattered in the direction of the detector, producing the spectral signature of the object (Kahle, 1982).

3.5.1 Preprocessing of raw satellite data

Several data transformation techniques were tested to improve the surface feature identification. Combination of data and thematic information from several sources required georeferencing to a common cartographic base. For this purpose, an image-to-map registration procedure was used. Well distributed control points were identified on the scenes and topographic sheets. A first-order polynomial transformation and nearest neighbourhood resampling method were selected to produce a geometrically corrected image set. Topographic sheets at 1:50000 scale and Universal Transversal Mercator projection were used as base maps. Check point coordinates were measured on the geometrically corrected image set and compared with the topographic sheets to evaluate the quality of the geometric correction. The root

mean square error resulting from the polynomial transformation was, in all cases, lower than one pixel.

The presence of speckle on the JERS-1 SAR scene increased the variance and hampered the visual and digital analysis. Speckle is defined as a form of multiplicative noise in the sense that the noise level (or standard deviation) increases with the magnitude of the radar backscattering (or the mean). The speckle presents a random distribution, which is assumed as non-Gaussian and asymmetrical (Lee, 1989). The statistical speckle model can be expressed as:

$$Se = \frac{\mu}{SD}$$

where Se : strength of speckle noise;
μ : mean value of the image;
SD: standard deviation of the image values.

Several studies have been carried out to evaluate the performance of different filtering techniques to reduce the speckle noise (Justusson , 1978; Frost, 1981; Durand et al., 1987; Mueller et al., 1989; Pan, 1990; K.Lee , 1990; Nezry et al., 1991; Metternicht , 1993). Quantitative and qualitative parameters are used to assess the efficiency of a filter in reducing the speckle without loosing features of interest. These include: visual inspection of edge-boundary retention, image smoothing, decrease of the image 'granular aspect', transformation of unimodal histograms representing different land cover types into multimodal ones, and computation of the speckle index defined as the ratio of the standard deviation to the mean of the selected image. A low speckle index indicates a good ability of the filter to reduce the noise on the image. To reach a compromise between fine details preservation and noise reduction, a lower limit threshold value has to be established. Lee (1988) suggested to take the noise standard deviation of the radar amplitude image as the lowest value for the SD/ μ ratio. The noise standard deviation of an amplitude image is defined by Durand (1987) as $0.523/\sqrt{N}$, where N is the number of looks used to process the image. Since the JERS-1 SAR data processing included three looks, the lower limit for speckle reduction was set at 0.30 ($0.523/\sqrt{3}$).

To separate the speckle noise from the thematic information, the gama maximum a-posteriori (MAP), sigma and median filters were tested on image subsets containing backscattered energy from surface features of interest, such as salt- and sodium-affected areas. The speckle index was selected as the quantitative parameter to evaluate filter performance, together with a visual assessment of the edge-boundary preservation and the decrease of the 'granular' aspect on the radar image. After qualitative and quantitative evaluations were performed, the more effective template, found to be the gamma MAP filter, was applied over the whole area of interest. Table 3.5 contains the speckle index values obtained after applying the pre-selected filters on the JERS-1 SAR subset. Figure 3.4 illustrates the procedure applied to selected the most suitable filter type, window size and number of iterations to reduce the speckle on the JERS-1 scene. Figures 3.5 shows the appearance of the raw JERS-1 scene, while figure 3.6 depicts the same area after the application of the gamma MAP filter. The gamma MAP filter has the ability to reduce the image speckle, while preserving linear and textural features of the surface cover. Texture preservation allows the separation of classes having similar spectral signature In the

visible and infrared ranges, but different roughness. The filtering process operates so as to separate the most homogeneous area containing the pixel to be filtered from the rest of the square moving window, once some heterogeneity is detected (Lopes et al., 1990).

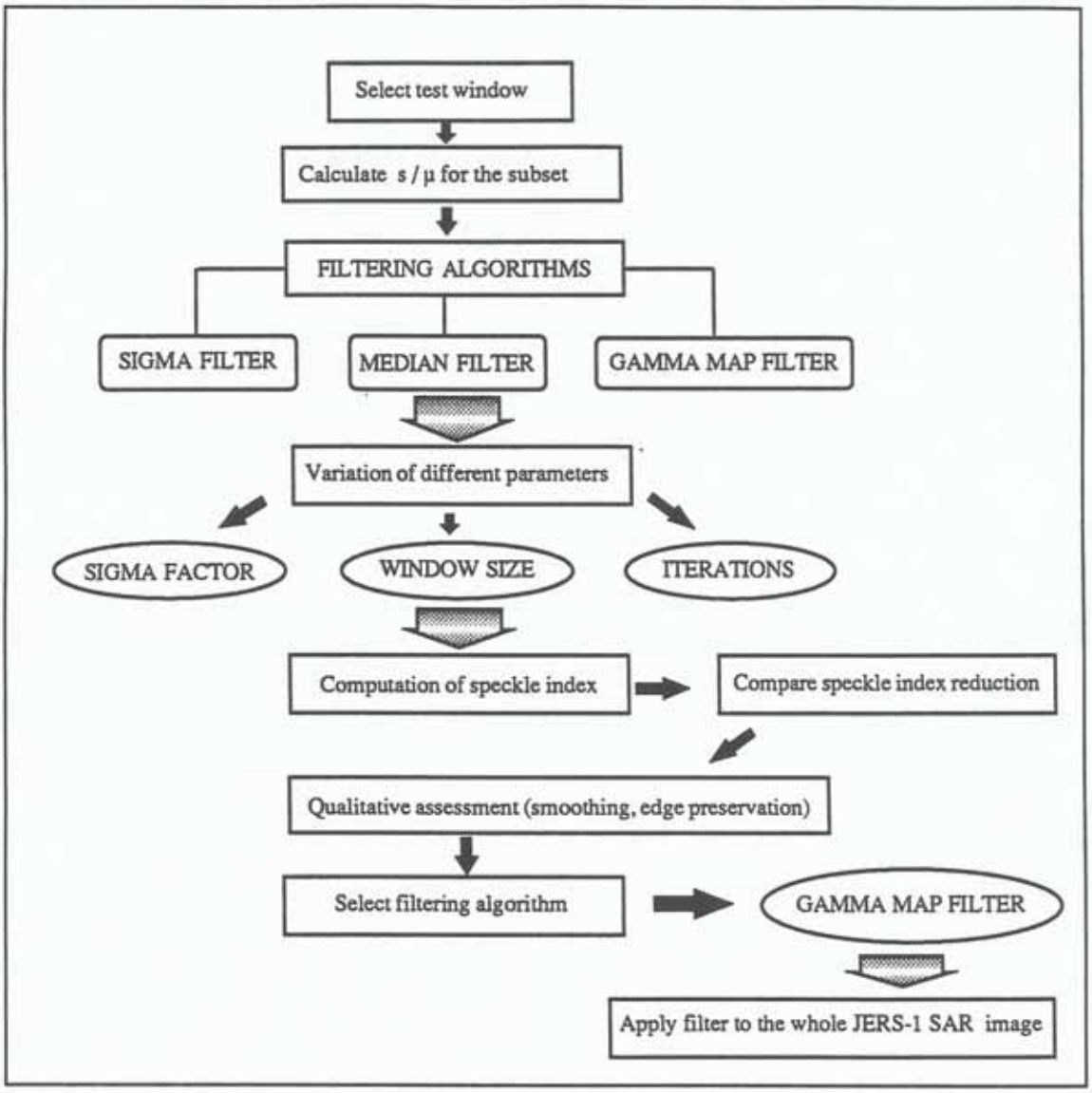

***Fig. 3.4:** The filtering process applied to the JERS-1 data*

Table 3.5: Results of the filtering procedure applied to the JERS-1 SAR subset.

FILTER TYPE	SIGMA /DAMP	No. OF ITERATIONS	WINDOW SIZE	SPECKLE INDEX
GAMMA MAP	- - - -	1	3x3	0.406
		2	3x3	0.375
		1	5x5	0.357
		2	5x5	0.329
		1	7x7	0.329
		3	3x3 -> 5x5(2)	0.324
		4	3x3(2) -> 5x5 (2)	0.318
		3	5x5(2) -> 7x7	0.303
		3	3x3-> 5x5-> 7x7	0.309
		2	3x3->5x5	0.344
FELEE	1 (damp)	1	3x3	0.406
		2	3x3-> 5x5	0.345
LEE	1.91 (sigma)	1	3x3	0.408
	2.45	1	3x3	0.38
	3	1	5x5	0.34
FROST	1 (damp)	1	5x5	0.36

Raw data speckle index = 0.53.

The damping constant specifies the extent of the damping effect of the adaptive filter. Large values for DAMP preserves sharp edges better, but reduces the smoothing effect (PCI Inc., 1994).

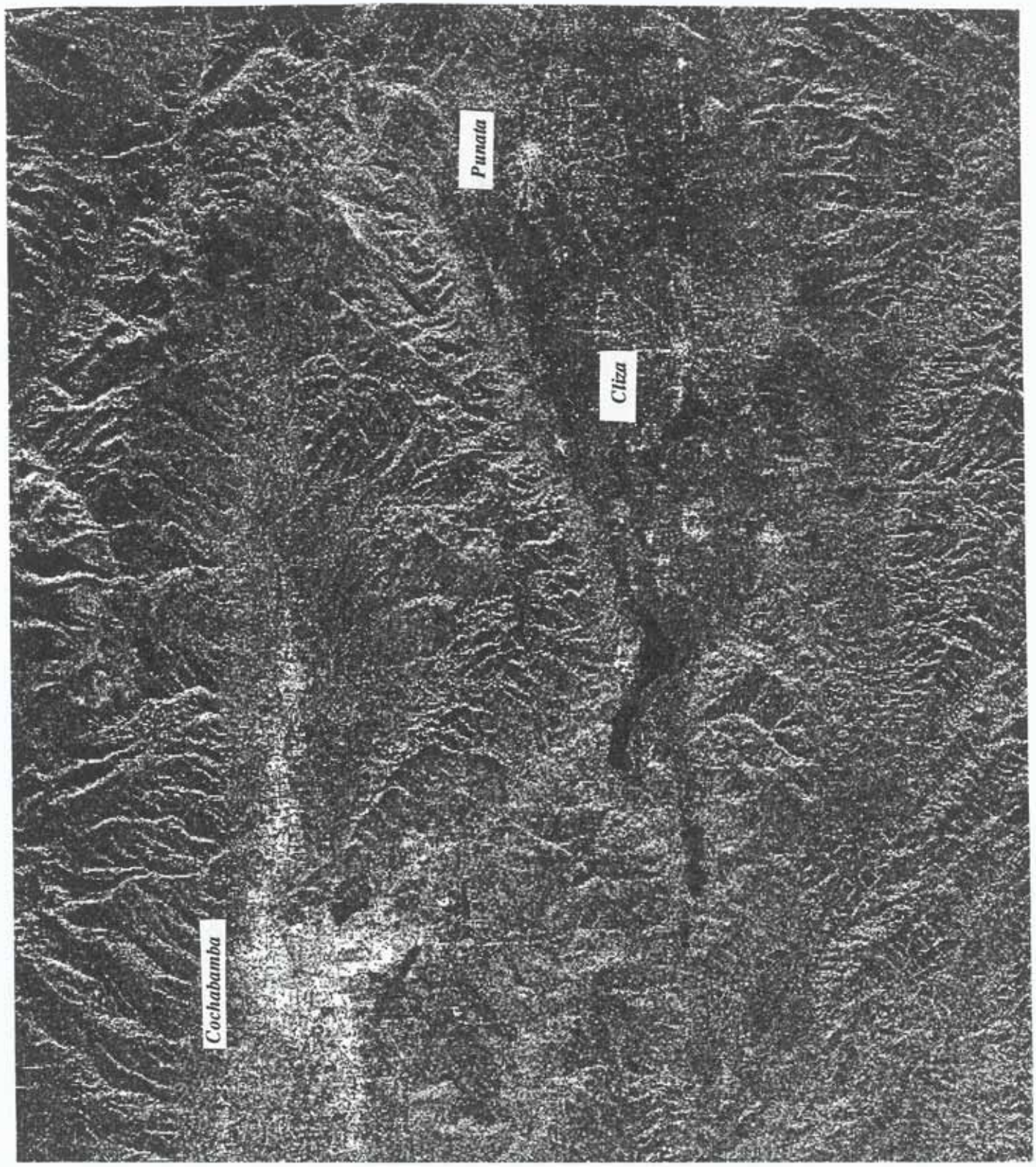

Fig. 3.5: The raw JERS-1 SAR data (Cochabamba, Sacaba and Punata-Cliza valleys).

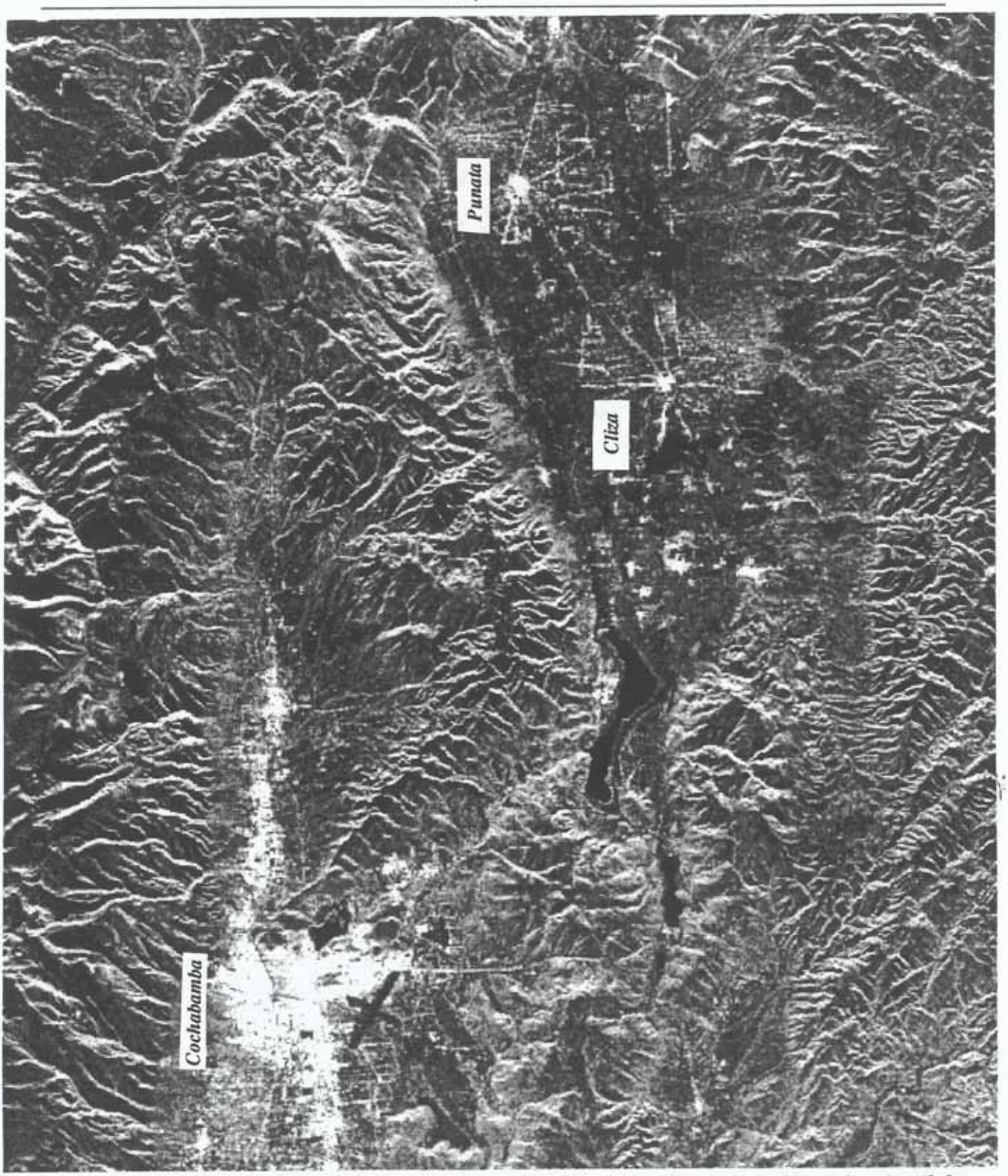

Fig. 3.6: JERS-1 SAR data after application of the gamma MAP filter,3 iterations, and variable window sizes (3x3->5x5->7x7).

The software ERDAS IMAGINE (ERDAS , 1994) and IDRISI (Clark University, 1995) were used for processing and analyzing the satellite images. They contain different modules to perform image rectification, interpretation and classification, as well as spatial modelling. Additional modules include a large variety of import-export options and tools to elaborate image maps. Vector and raster data can be handled. IDRISI provides also a decision support module to perform image labelling using fuzzy sets. The filtering process applied to the JERS-1 SAR image to reduce the speckle used the spatial filters available in the PCI software (PCI Inc., 1994).

3.5.2 Identification and delineation of land degradation features

There is a variety of methods to identify and map particular surface features, ranging from spectral indices to the design and inversion of physically-based models. Their applicability depends on the nature and accuracy of the information and on the availability of resources (i.e., sensor characteristics). Available techniques for mapping soil surface conditions, such as salinization-alkalinization or soil erosion, are based on the presence or absence of spectral absorption features related to a particular indicator of degradation, such as salt types, rock fragments, salt-tolerant vegetation. Simple identification and mapping of degradation features can be done by visual interpretation from color composite images. In contrast, digital information extraction relies on spectral and/or structural pattern recognition, which can be automated or supervised. Decision support systems allow to allocate ground pixels to given surface types by using, for example, classifiers based on statistical probability functions or fuzzy sets. In addition, techniques such as linear mixture modelling offer the possibility, not only to identify a certain cover type within a ground pixel, but also to estimate its proportion or abundance within that particular area. This research implements spectral mixture modelling, fuzzy modelling and statistical pattern recognition (maximum likelihood classifier) to identify and map land degradation features related to salinity-alkalinity and soil erosion processes. The results of applying different classifiers in the process of identification and labelling of salt- and sodium-affected areas are discussed in chapter 6. Chapter 7 examines the improvements obtained by applying spectral unmixing, instead of the classical maximum likelihood classifier, to delineate areas subjected to soil erosion. The basic concepts related to the mentioned decision support systems are described hereafter.

(1) Linear mixture modelling

Linear mixture modelling aims to map the respective abundance of the surface materials present within a particular pixel. This requires that several assumptions be satisfied: (1) the mixing of the surface components within one pixel is linear; this occurs when radiation interacts with only one material type on its path between the sun and the sensor, requiring the surface components to be distributed in patches large enough to allow such a unique interaction; (2) all the materials in the image have sufficient spectral contrast to allow their separation; (3) the surface components present within the image exist in a 'pure' state in at least one pixel, which can be properly identified and spatially located; such pure pixels are known as the end-members of a particular surface component (Smith et al., 1990a ; Drake et al., 1994).

Linear mixture modelling therefore assumes that the signal received at the satellite sensor depends on the proportion of individual surface components (soil, water, vegetation) present in a particular pixel and on the properties of the mixing process. Thus, spectral mixing may be modelled as a linear combination of pure components (end-members) such that:

$$Ri=\sum_{j}^{n} F_j \cdot RE_{ij} + \epsilon_i ; \sum F_j = 1$$

where Ri is the reflectance of the mixed pixel spectra in band i; $REij$ is the reflectance of the surface component j in band i; Fj denotes the proportion of the pixel area covered by the j ground cover type; and ε_i is the residual error in band i (Adams et al., 1985; Smith et al., 1990a; Hill, 1993).

Unmixing consists on estimating the proportion of the vector F, given an observation Ri. This process is done by inverting the linear mixing equation through a least-square regression, while constraining the sum of the F fractions (i.e., the proportion of the different components within one pixel) to a value of one. A unique solution is possible as long as the number of end-members, or surface components, is equal or less than the number of spectral bands used. End-members may be either extracted from the image data themselves, or derived from field spectral measurements, or still determined by choosing elements from laboratory spectral libraries. The spectral library should contain a set of spectra that fully characterize the scene components, avoiding to enter end-members not present in the scene.

The Spectral Image Processing System SIPS (CSES - CIRES,1992) used in this research, is a software developed to handle proportions of different cover types within one pixel. The program assumes that spectral mixing can be modeled as a linear combination of image components, or end-members. The SIPS unmix program contains three types of unmixing, namely unconstrained, partially constrained, and fully constrained (Smith and Adams, 1985). The unconstrained algorithm allows the resulting end-member abundances to take any value, including negative ones, regardless of whether or not the values are physically meaningful. In the constrained versions, the unmixing uses a constrained least-square algorithm. For partially constrained unmixing, constraints are set to avoid negative abundance values. In fully constrained unmixing, an additional constraint is included to obtain fractional abundances within a range of zero to one.

The spectral unmixing results in an abundance image for each selected end-member (surface component), providing the relative proportion of a surface feature at every pixel. Additionally, an error image and an image summing the surface component abundances at each pixel are calculated. The error image indicates how well the spectral variability was explained by the selected end-members, and is therefore used to validate the mixing model. The root mean square method is used to determine the error between the original mixed spectrum and the reconstructed one from the calculated abundances.

Results of applying linear mixture modelling to map surface indicators of accelerated soil erosion in the Sacaba valley are discussed in chapter 7.

(2) Classification using fuzzy sets

In the fuzzy sets approach, point data are not allocated to one specific class but given membership values for each of the classes being considered. Therefore, it is necessary to determine a membership function for each class. The function takes values between zero and one to measure the grade of membership , thus the possibility that a particular sample point belongs to a given class. Memberships close to one signify a high degree of similarity between an individual sample point and a cluster, while memberships close to zero imply little similarity. Common membership functions are sigmoidal, J-shaped or linear. A detailed description of the functions and the algorithms used for their computation are provided in chapter 6.

As with Boolean sets, logic operations are used to work with fuzzy sets, such as: intersection, union, complement, concentration, dilation and normalization (Zadeh, 1965). The final thematic map is obtained by fuzzy manipulation of the sets representing the classes of interest. The conceptual model and the results of applying either a fully fuzzy supervised classification or a fuzzy definition of class boundaries are presented and discussed in chapter 6.

(3) Statistical pattern recognition: the maximum likelihood classifier

Statistical pattern recognition techniques make use of probability functions associated with the patterns of particular classes. Probability functions can be estimated from a training set or accepted to be multivariate and normally distributed, implying that certain parameters such as the mean and standard deviation need to be estimated from that training set. For this reason, the method is called parametric. A well known parametric approach is the maximum likelihood classifier, which assumes a Gaussian distribution in a multi-spectral feature space. In contrast, if the form of the probability function is assumed to be unknown in advance, the approach is called non-parametric (Swain, 1978). The k-nearest neighbor, the parallelepiped or box classifier are examples of non-parametric classifiers.

The maximum likelihood methods for satellite image classification aim at assigning a 'most likely' class label C_i from a set of N classes $C1,C2$, ..., Cn , to a x feature vector in the image. A feature vector x is the vector ($x1,x2$,... xm). The vector components are pixel values in M spectral bands. The most likely class label Ci for a given feature vector x is the one with the highest posterior probability $P(Ci|x)$. So, all $P(Ci|x)$, $i \in [1...N]$ are computed, and the Ci with the highest value is selected. The calculation of $P(Ci|x)$ is usually based on the Bayes formula, which states:

$$P(Ci|x)=\frac{P(x|Ci)*P(Ci)}{P(x)}$$

where P(x|*Ci*) is the class probability density; P(*Ci*) is the prior probability of class *Ci*, and P(x) is the class independent feature probability density (Jensen, 1986; Mather , 1986; Gorte, 1994).
The results of applying a maximum likelihood classifier to discriminate and map salt- and sodium-affected surfaces in the Punata-Cliza valley, as well as soil erosion in the Sacaba valley, are presented and compared against fuzzy supervised classification and spectral mixture modelling in chapters 6 and 7.

3.6 MAPPING TOPSOIL PROPERTIES

Topsoil properties were mapped using geostatistical methods, based on the theory of regionalized variables (Matheron , 1963 and 1965). This theory takes into account both structural and random characteristics of spatially distributed values to provide quantitative tools for their description and optimal, unbiased estimation.

3.6.1 The semi-variogram

Central to the geostatistics is the semi-variogram, representing the spatial dependence of a certain soil property in a given area (McBratney and Webster, 1986). The semi-variogram helps understand the spatial variability of a soil property. It is also the basis of the kriging technique, which provides unbiased estimates of a variable throughout an area.

The semi-variance $\gamma(h)$ describes the spatially dependent component of the random function Z. It is defined as half the expected squared distance between sample values separated by a given distance h (Journel et al., 1978), such as:

$$\gamma(h)=E[Z(x)-Z(x+h)]^2$$

where h is the vector of separation between sample locations, or lag.

$$\gamma=\frac{1}{2N(h)}\sum_{i=1}^{N}[Z(x_i)-Z(x_i+h)]^2$$

The semi-variance at a given lag h is estimated as the average of the squared differences between all observations separated by the lag, where there are $N(h)$ pair of observations (Trangmar, 1985; Stein, 1993). The semi-variogram for a given direction is usually displayed as a plot of semi-variance values $\gamma(h)$ versus distance h (fig. 3.7)

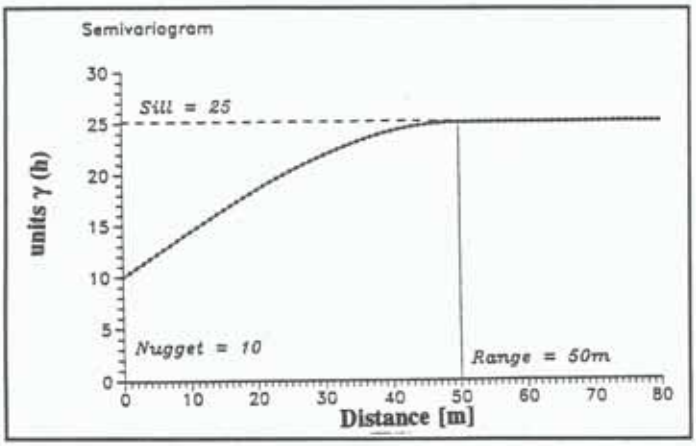

Fig. 3.7: Idealized semi-variogram.

The semi-variogram may adopt different shapes depending on the data and sampling interval used. In ideal situations, the semi-variance increases with the distance between sample location until a relatively constant value, the sill, is reached at certain separation distance known as the range of spatial dependence. The sill approximates the variance s^2 of the data set. Samples separated by a distance smaller than the range are said to be spatially dependant, while those separated by distances greater than the range are not spatially related because the semivariance equals s^2, implying random variations. The range defines the maximum radius from which neighbouring samples are drawn for interpolation by kriging (Trangmar, 1985). The semi-variogram may, however, increase continuously without showing a definite sill and range, indicating the presence of trend effects and non- stationarity (Burgess et al., 1980; Gajem et al., 1981; Yost et al., 1982). It is difficult to quantify the spatial relationship between samples at the sampling scale used, when no spatial structure can be defined in the semi-variogram .

When the separation between samples is zero the semi-variogram should pass through the origin. However, a non-zero variance is commonly observed when h tends to zero. This is known as the nugget effect, representing unexplained or random variance, often caused by measurement errors or variations at shorter distance than the selected sampling distance (Burgess and Webster, 1980). The nugget effect can be expressed as a percentage of the sill value to allow comparisons of the relative size of the nugget effect among soil properties (Yost et al., 1982a ; Burrough , 1983a). A nugget variance of 0% of the sill indicates neither measurement errors nor significant short-range variations. On the contrary, a nugget variance of 100% the sill expresses large point-to-point variations at short separation distance and indicates a total absence of spatial correlation at the selected sampling scale (Trangmar, 1985).

Concerning the size and statistical distribution of the sample set, Webster and Oliver (1992) state that variograms computed on the basis of less than 50 data points are of little value, and suggest at least 100 point observations. When the data set follows a non-normal distribution, the computed semi-variance is not reliable, requiring therefore some kind of transformation (logarithmic, square root) or the use of a technique known as robust estimation (Cressie et al., 1980; McBratney et al., 1981). The robust estimation is directly used to determine the semi- variograms of non-normally distributed

sample sets.

3.6.2 Interpolation methods

Interpolation techniques aim to provide precise estimation of a variable throughout an area on the basis of a given data set. The precision of the estimation of a property at any location largely depends on the amount of variation within the sample area, the size of the data set and the interpolation method used. There are several interpolation techniques useful to estimate the values of soil properties at unsampled locations. In this research, kriging and inverse square distance methods were used and, therefore, shortly described hereafter.

Kriging provides an unbiased estimation of regionalized variables at unsampled locations using the properties of the semi-variogram and the initial set of data values (Trangmar, 1985). The simplest form of kriging, adopted in this research, involves the estimation of point values through punctual kriging. Instead, block kriging is preferred for areal interpolation. The estimated variance of every kriged location depends only on the semi-variogram and the configuration of the data locations in relation to the kriged points and not on the observed values themselves (Burgess and Webster, 1980).

If the semi-variogram is not reliable, other interpolation techniques such as inverse square distance have to be used. Like for kriging, estimation of the interpolated locations is based on the values of the surrounding sample points and the assignment of weights to these points. When calculating a grid node, the weight given to a particular data point is proportional to the inverse of the distance, at the specified power, of the observation in relation to the grid node. The assigned weights are fractions and the sum of all the weights is equal to one. When an observation coincides with a grid node, the observation is given a weight of one, and all other observations are given a weight close to zero. In other words, the grid node is assigned the value of the coinciding observation (Surfer, 1993). The disadvantage of the inverse square distance respect to kriging is that it does not take into account spatial variability. But the advantage is that it can be used when only a small amount of data is available, where kriging does not show reliable semi- variograms .

3.6.3 Map production

Because soil distribution is strongly controlled by the geomorphic factor, interpolation between randomly distributed observation points was carried out only within individual landscape units. A masking procedure was used to extract the units of interest (Appendix I). Spatial and semantic point data within a particular unit were obtained by querying the soil database (fig. 3.8). The tabular data were analyzed to identify if the variables were or were not normally distributed. Since high coefficients of variation and skewness were observed (see table 2 and 3 in appendix I) and thus not all the properties were normally distributed, a robust estimation technique was adopted to build up the semi- variograms . Spherical, circular, exponential, Gaussian, linear and Bessel semi-variogram models are available. The conformity between the fitted model and the original data was expressed as the ratio between the square

sum of deviations and the total sum of squares (the ssd / sst ratio, tables 4 and 5 in appendix I). When the semi- variograms showed to be reliable, that is, exhibiting low ssd / sst values, not declining shape and sill values close to the variance, punctual kriging interpolation was used. Instead, the inverse square distance interpolation was applied when the landscape units presented unreliable semi-variograms .

Punctual kriging interpolation was possible only in the lagunary depressions of the Punata-Cliza valley, where reliable semi-variograms of the selected soil properties were obtained. This could be partly attributed to the higher number of point observations respect to the other landscape units (90 against 20 in the piedmont unit). The remaining units, including the southern piedmont of the Punata-Cliza valley as well as the valley and piedmont units south the Sacaba valley, were interpolated by the inverse square distance method, since only 42 point observations were collected in the lagunary depressions and 47 in the piedmont area of Sacaba (table 1, appendix I).

Grid files resulted from the application of kriging and inverse square distance interpolation techniques. Contour maps in vector format and coropleth maps in raster format were produced and imported in ILWIS for comparison with other rasterized data, in particular with satellite image classification data. Classify tables, containing user-defined soil property interval values, were built-up and used to produce maps expressing value ranges of each soil property (e.g., silt percentage ranges). The output values concerning the individual geomorphic units were merged in a map using the spatial modelling functions of ILWIS (fig. 3.8). Figure 3.9 shows the results of applying geostatistical interpolation to map the topsoil variations in silt and clay contents, respectively, of the Punata-Cliza valley. Appendix I contains the maps of the remaining analyzed topsoil properties.

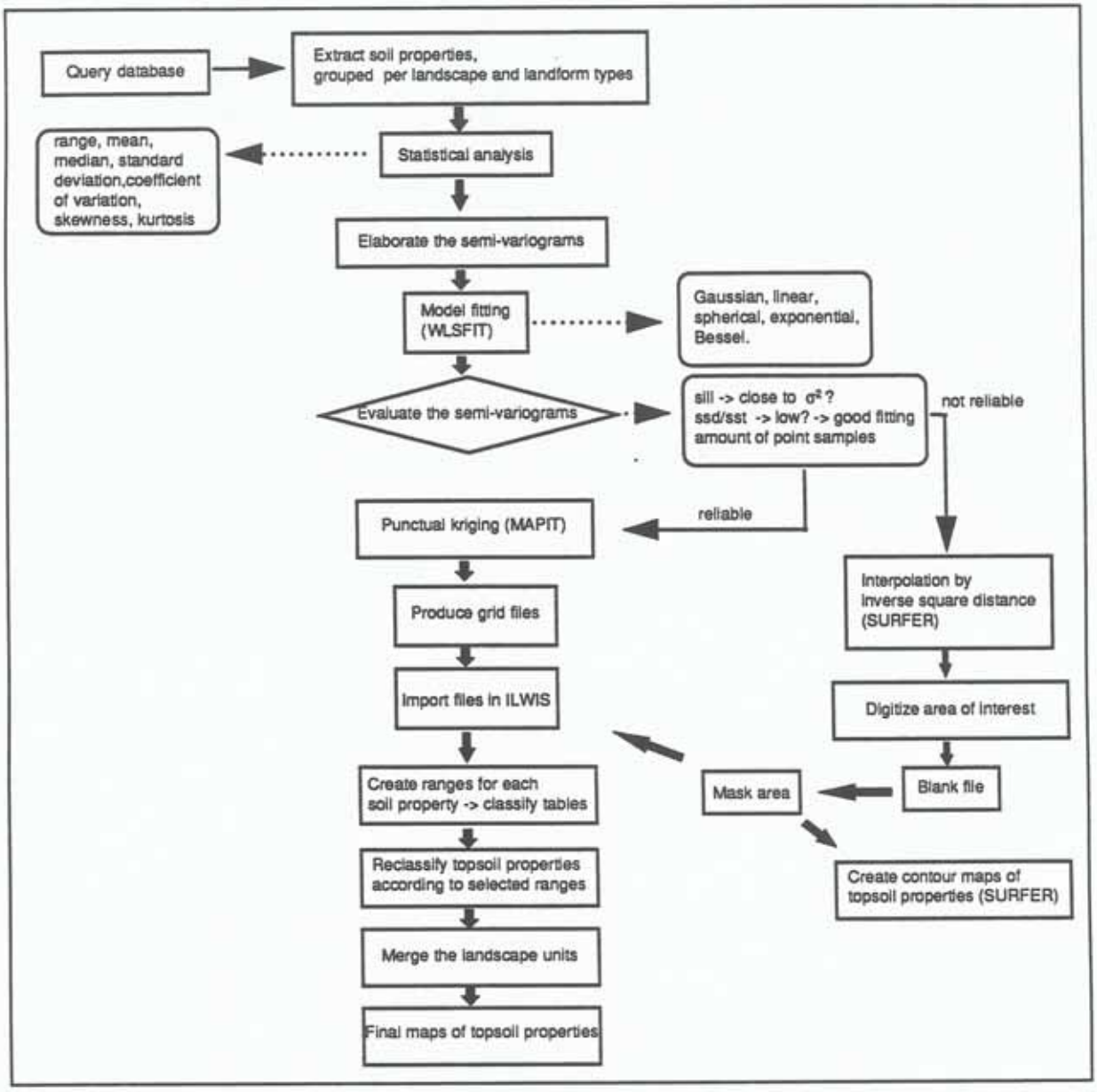

Fig. 3.8: Flowchart for creating the topsoil property maps.

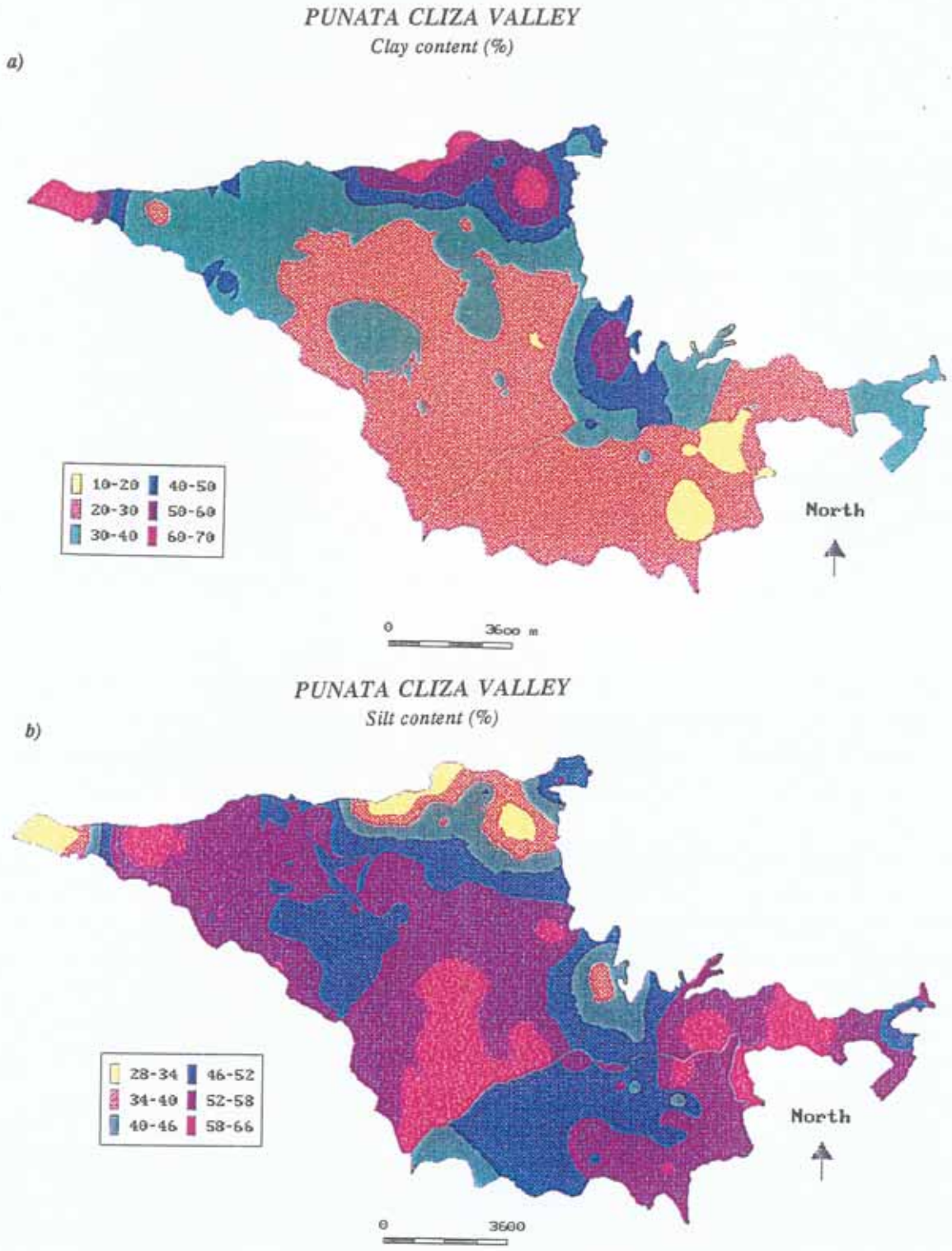

Fig. 3.9: Punctual kriging interpolation maps showing topsoil variations in clay percentages (a) and silt percentages (b) in the Punata-Cliza valley.

3.6.4 Analyzing the relation between soil properties and soil erodibility

A review of soil erodibility indices is presented in chapter 2. The USLE-K factor was used to compute soil susceptibility to erosion by water. Because of the lack of quantitative field estimations of soil erodibility, only qualitative comparisons were possible between observed erosion degrees and estimated erodibility values. Ancillary data such as field records, photo interpretation of erosional features and existing reports were used to evaluate the performance of the USLE soil erodibility coefficient. The STATISTICA software was used to carry out descriptive and multivariate statistics including correlation, regression analysis, analysis of variance and categorical data analysis (Statsoft , 1993).

Multiple regression techniques were implemented to investigate the effects of independent X variables on one dependent Y variable. According to the type of independent variable , two different kinds of multiple regression were used: (1) the standard multiple regression on numerical variables; (2) the analysis of variance (ANOVA), equivalent to a regression on only categorical or dummy variables (Wonnacott et al., 1990). The one-way-analysis of variance was used to analyze the relationship between topsoil properties and erosion type and degree. Diagrams were constructed to study the interactions between landscape position and erosion type, as well as between erosion degree and erosion type, and determine the variation of topsoil properties under different situations. The results are presented and discussed in chapter 7.

Stepwise regression was used to develop models predicting soil properties from the spectral reflectance and analyze the relationship between soil properties and soil erosion degrees. For instance, equations were derived to explain the relation between pH, electrical conductivity, sodium adsorption ratio and the reflectance values obtained with the Cropscan radiometer. These equations are presented and discussed in chapter 6.

Scatter diagrams and correlation coefficients were established to investigate the relationships between different soil variables. Data exploratory techniques such as skewness, kurtosis and normal probability plots were used to determine the type of data distribution and the need of data transformation via square root and logarithmic transformations (Webster et al., 1990).

3.7 DESIGN AND IMPLEMENTATION OF EXPLORATORY MODELS FOR MAPPING AND PREDICTION OF LAND DEGRADATION HAZARDS

Modelling uncertainty is caused by the inaccuracy of the data, inaccuracy of the interpolation methods and unreliability of the measurement tools. Also, some land degradation indicators, in particular certain soil properties, are not measurable. The values of variables such as the abundance of rock fragments on the soil surface or the strength of the soil structure, can only be approximated or evaluated using expert experience. A soil surveyor can describe the grade of the structure as weak, moderate or strong. The question is how to use and process such information.

Sometimes, the relations between the indicators of a certain process are not exactly known, or analytical models to express these relations are missing, or the data are insufficient for statistical analysis. In such cases, expert knowledge can be used to build empirical models. Therefore, fuzzy sets, fuzzy logic and multivariate statistical analysis were combined to determine the parameters, identify the factors and analyze the causes involved in each particular soil degradation phenomenon.

Compared with the conventional knowledge-based system, the application of the fuzzy set theory offers advantages in terms of: (a) the representation and processing of imprecise data in the form of fuzzy sets (e.g., a moderately saline class); (b) the representation and processing of vague knowledge in the form of linguistic rules with imprecise terms defined as fuzzy sets (e.g., the likelihood of an area to change from non-saline to moderately saline-alkaline class). The fuzzy logic approach to modelling land degradation processes allowed to work with imprecise knowledge about the relations between components of a degradation phenomenon and to build models based on qualitative information.

3.7.1 Fuzzy sets and certainty factors

(1) Membership grades

Crisp set theory is driven by a logic that permits a proposition to possess one out of two values: one (1) when the element belongs to the set, and zero (0) when it does not (fig.3.10). Applied to salinization, for example, an area might be saline or non-saline. This type of logic does not allow to represent vague concepts. In contrast, fuzzy sets introduce vagueness or uncertainty, by eliminating the sharp boundary separating members of a class from non-members. Uncertainty may exist because: (1) the set is not clearly defined (e.g., soil erodibility) and thus the membership to the set cannot be clearly determined; (2) the set is well-defined, but its membership is not (e.g., boundaries of salinity-alkalinity classes); (3) neither the set nor the membership is well defined (Drummond, 1991).

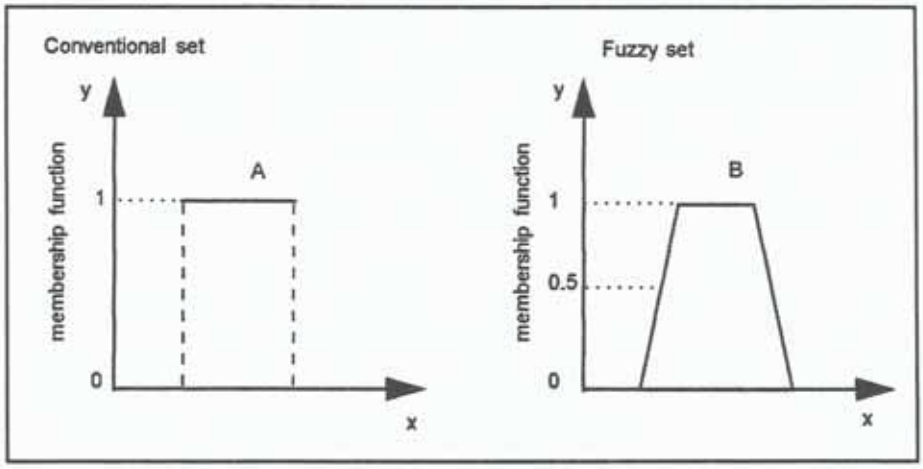

Fig. 3.10: Classical membership function and fuzzy set membership function.

A fuzzy set can be defined mathematically by assigning to each possible individual (e.g., EC values) in the universe of discourse (e.g., saline areas) a value representing its grade of membership in the fuzzy

set. This grade corresponds to the degree to which that individual is compatible with the concept represented by the fuzzy set. Thus, individuals may belong to the fuzzy set to a greater or lesser degree as indicated by a larger or smaller membership grade. The membership grades, also known as certainty factors or degrees of belief, are represented by values ranging in the interval between 0 and 1 (Klir and Folger , 1988).

(2) Certainty factors

Certainty factors are not probabilities. However, within a geographic information system environment, probability information may be manipulated as certainty factors. In the absence of probability information, alternatives including available expertise have to be used. Summarizing the assumptions inherent to the fuzzy set theory, Drummond (1991) includes: (1) an object from the universe of like objects is a member of a fuzzy set with a membership grade between 0 and 1; (2) the membership grade is determined by a membership function, which can be designed for each universe of like objects; (3) certainty factors for all possible outcomes need not to sum to 1.

States of a fuzzy variable may be represented by fuzzy sets with qualitative labels such as extremely high, very high, high, moderate, low, very low. Membership functions of the fuzzy sets corresponding to these labels may be drawn from a group of experts, using an appropriate method for scaling the expert perceptions and assessment. The shape of the fuzzy set membership function can be linear (trapezoidal or triangular) or nonlinear, as described and applied in chapter 6.

Expert knowledge, in the way of terms expressing degrees of likelihood for a certain fact, can be ranked and expressed as certainty factors within the range of 0 to 1. For instance, a soil surveyor can be asked, based on his experience, how likely it is that areas from the geopedologic unit 'lagunary depression' are saline. His answer could result in the statements reported in table 3.6.

Table 3.6: Relationship between certainty factors and verbal description of likelihood

VERBAL DESCRIPTION OF LIKELIHOOD	CERTAINTY FACTOR
absolutely likely	1.0
extremely likely	0.9
very likely	0.8
likely	0.6
neither likely nor unlikely	0.5
unlikely	0.4
very unlikely	0.2
extremely unlikely	0.1
absolutely unlikely	0.0

(3) Approximate reasoning

Very often, natural language is used for describing the knowledge about certain land degradation phenomenon. This knowledge can be represented by a set of linguistic rules of the form: 'IF ⟨premise⟩ THEN ⟨conclusion⟩'. The terms used in these rules ('low', 'moderate', 'high') are vague and imprecise, but can be defined in the form of fuzzy sets. The variables, which these terms take as their values, are called linguistic variables (Zadeh , 1975).

(4) Fuzzy set manipulations

Manipulations of membership grades include the union, intersection and complement of fuzzy sets (Zadeh , 1965). Considering an element x, its membership in the fuzzy set A U B, achieved by the union of A and B, is expressed by the following equation:

$\mu A \cup B(x) = \max [\mu A(x), \mu B(x)]$

Likewise, the membership grade of the element x in the fuzzy set $A \cap B$, achieved by the intersection of A and B, is expressed by the following equation:

$A \cap B(x) = \min [\mu A(x), \mu B(x)]$

Finally, if B is the complement of A then:

$\mu B(x) = 1 - \mu A(x)$

In addition of the above, fuzzy sets can be modified by special operations using linguistic terms, also called linguistic hedges, such as very, extremely, more or less, quite and so on. Operators such as concentration, dilation, normalization or intensification can be used to modify existing sets (e.g., steep slope) and produce others like very steep or more or less steep slope (Klir and Folger , 1988).

3.7.2 Fuzzy knowledge-based exploratory models

Exploration models do not have deterministic capabilities because they do not simulate and explain the

mechanisms involved in land degradation processes, but instead search cause-effect relationship on the basis of spatial coincidence of the degradation phenomenon and given landscape factors. They allow to reproduce the present spatial distribution of the degradation processes under study, as well as to predict their potential occurrence in areas where conditions are favourable (Vazquez-Selem and Zinck, 1994). The construction of a fuzzy knowledge-based exploratory model, required the following steps: (a) determination of the model structure; (b) formulation of fuzzy knowledge base; (c) selection of fuzzy knowledge processing methods; (d) calibration; (e) validation.

The model structure comprised the selection of the input and output variables, the number of sub-models and the connections between them. The process of the knowledge representation in the form of a knowledge base required the following steps: (1) definition of the rules; and (2) determination of the fuzzy sets used to describe the values of the model variables (e.g., 'moderately', 'slightly', 'strongly', etc.). The main problem in fuzzy modelling is to find an appropriate set of linguistic rules describing the phenomenon to be modelled. They can be taken directly from the expert experience, but sometimes the expert knowledge is too complex to be expressed in a limited set of rules. Additionally, the set of linguistic rules should be complete and provide a correct answer for every possible input value. Obviously, the formulation of these rules, as well as the definition of fuzzy sets, has a subjective character.

The fuzzy rules, the fuzzy sets and the data set are the main parts of the fuzzy knowledge-based model (fig. 3.11). Using membership functions and operators, the fuzzy knowledge was processed and output values corresponding to certain input values were computed. The input values could take a crisp (numerical) or fuzzy form (certainty factors). Linguistic terms were also allowed for the input (e.g., a moderately alkaline class, represented by the intersection of the fuzzy sets alkaline and non-alkaline). The output values were fuzzy sets which could be transformed into numerical values, by applying a membership function, or approximated to one of the linguistic terms defined for the output variable (e.g., saline, alkaline, saline-alkaline areas) by calculating the distance between fuzzy sets (see chapter 6).

During the calibration process, selected parameters were adjusted to improve the model performance. For example, the parameters determining the fuzzy set 'alkaline areas' were changed and class intervals shifted to find the best combination of parameter ranges. Finally, the model was validated by assessing the spatial coincidence between the results, in terms of extent and type of degradation processes, obtained by different methods of detection and mapping , including satellite image classification supported by field data , geostatistical interpolation of topsoil properties, and analysis of laboratory data. Chapters 6 and 7 present and discuss the results derived from the application of fuzzy knowledge-based exploratory models to the mapping and monitoring of land degradation processes.

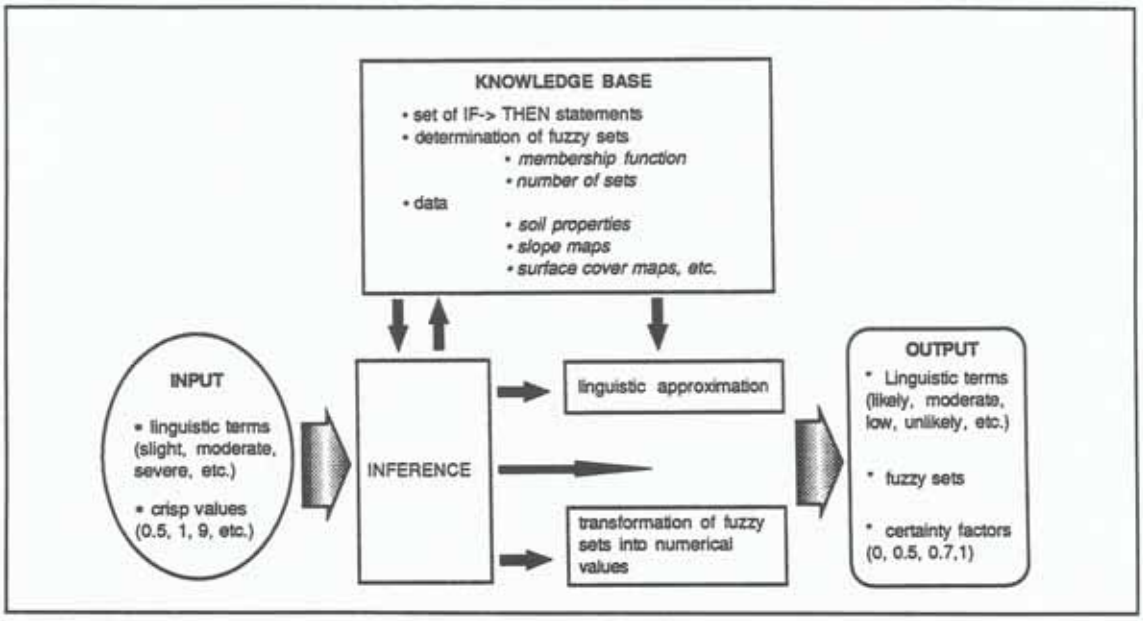

Fig. 3.11: Information flow in the fuzzy knowledge-based exploratory models

3.8 EVALUATION OF THE EFFICIENCY OF THE SYNERGISTIC APPROACH

Plot diagrams were built-up to compare and evaluate the results of integrating different data sources. X-axis represents the different sensors or a combination of sensors used to discriminate and map certain degradation features, while the accuracies obtained by using a particular sensors combination and/or classification technique are plotted on the Y-axis. Improvements derived from the synergy of data in different regions of the electromagnetic spectrum were compared: (a) synergy of visible, infrared and thermal data; (b) synergy of visible, infrared, thermal and microwave data; (c) microwave data alone. Advantages and disadvantages observed when using synergy of different data sources and scales were also assessed, concerning: (a) spectral data alone (satellite data and ground-based recordings); (b) spectral data and field observations; (c) spectral data, field observations and laboratory determinations.

Quality control concerning the accuracy and reliability of surface feature discrimination and mapping, using remotely sensed data, was carried out through confusion matrices. Class accuracy and reliability as well as overall accuracy measures were derived from these matrices, as described in chapter 6. The application of linear mixture modelling, to map proportions of different surface erosional features, provided an error image allowing to identify areas of less accurate location. Map readability was also assessed by comparing the portions of cartographic noise included in the various maps.

The degree of spatial coincidence of the same land degradation features, delineated using different approaches, was used as a qualitative measure to compare these approaches. Finally, certainty factors, expressed as degrees of likelihood, were used to test the reliability of the salinity-alkalinity

monitoring model implemented in the Punata-Cliza valley. Performance assessment results of the models and approaches implemented are presented and discussed through chapters 6, 7 and 8.

CHAPTER FOUR:

STUDY AREA CHARACTERIZATION

Bolivia comprises two broad geographic regions: the Andean and the Chaco-Amazonas regions (figure 4.1). The Andes form an imposing topographic and climatic barrier along the western border of South America. They block the transit of the wet air masses towards the west and create a climatic asymmetry between both sides of the cordillera, being the east side wet and the west side dry. The Andean region itself is subdivided into high Andes, puna or altiplano, dry valleys, subandean belts and 'yungas' (i.e. very humid subtropical areas with high internal relief).

The study area lies between 17°10' and 17°40'S and between 65°45' and 66°30'W, and belongs to the subregion of the dry valleys (figure 4.2). Two different morphologic environments compose the area: the cordillera and sedimentary basins, both formed during the Tertiary orogeny. The depressions of Cochabamba (Central Valley), Punata-Cliza (High Valley) and Sacaba of variable dimensions and located at different altitudes are grabens filled with Quaternary sediments. The basins have a regional east-west slope. Faulting caused an abrupt change in elevation of more than 1000 m between the mountain range and the basins. The Cordillera of Tunari, forming the northern limit of the Sacaba-Cochabamba basins, has an elevation ranging from 4000 to 5000 masl. Southwards the mountain range has lower elevations.

Along the northern boundary of the Cochabamba basin, the Tunari fault has a vertical displacement of 1500 to 2000 m, originating a piedmont area of steep alluvial fans on the mountain front.

4.1 GEOLOGY

The valleys are located in the eastern Andes, affected by intensive diastrophism related to the Andean orogenic cycle. The cordillera rocks are mainly Ordovician and Silurian shales, sandstones, siltstones, quartzites and phyllites, but also Permian and Cretaceous claystones, sandstones and marls, and Tertiary conglomerates occur in the west and southwest of the area. Glacial sediments and lakes are present in the summit areas of the cordillera. Table 4.1 summarizes the stratigraphic sequence of the study area.

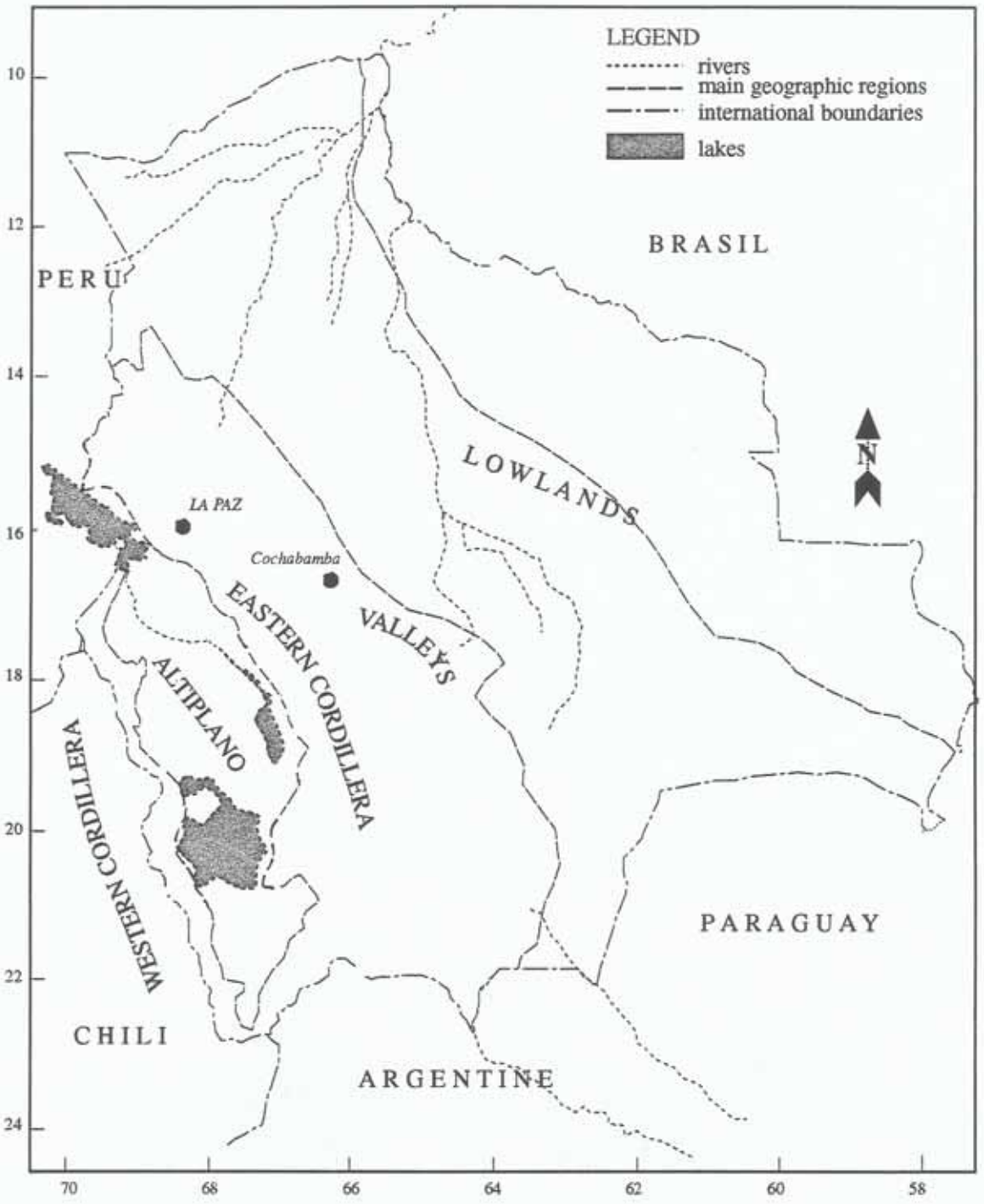

Fig. 4.1: Geographic regions of Bolivia

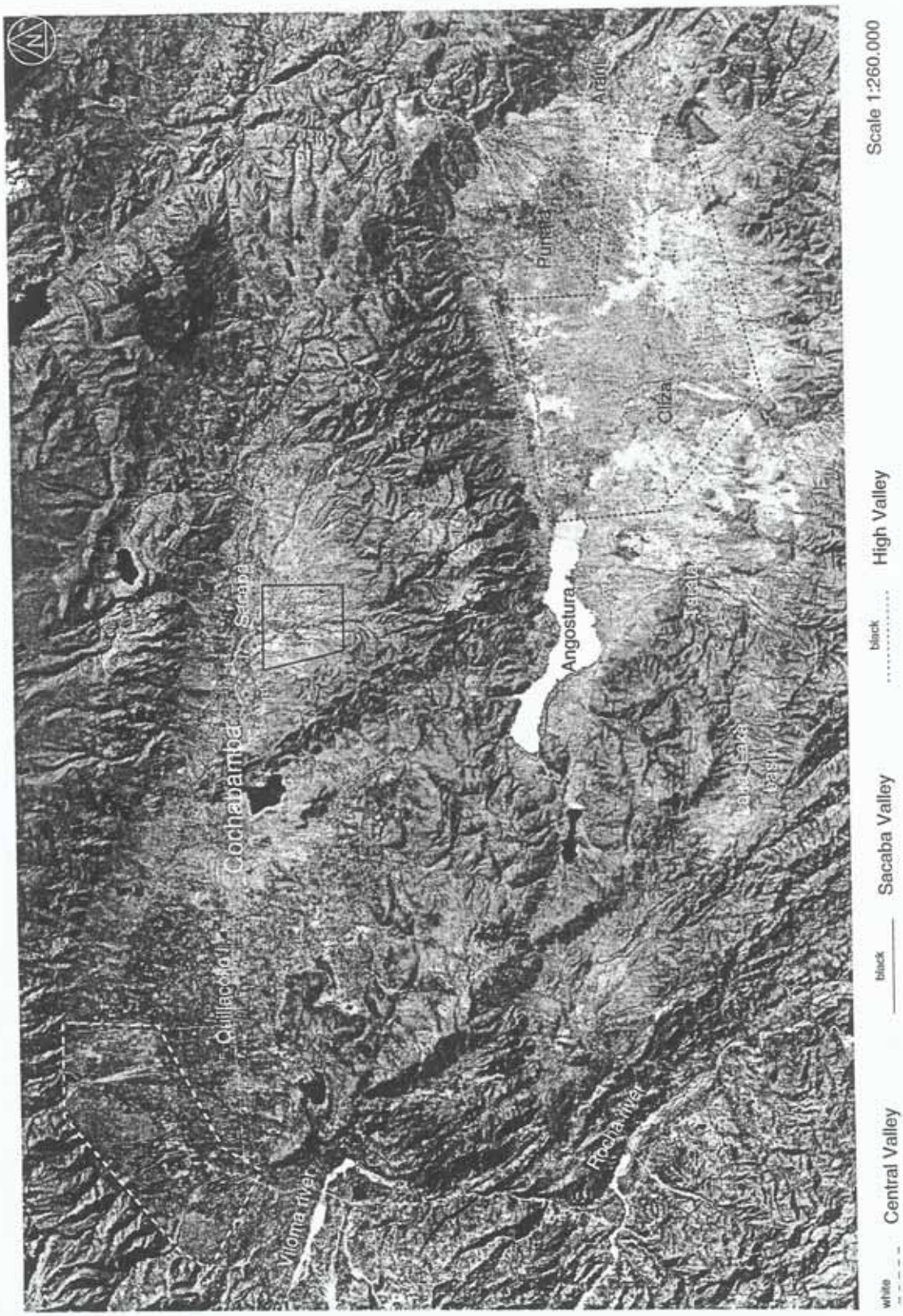

Fig. 4.2: Study area and sample areas

According to Lavenau (1986), the Cochabamba basins are half grabens, originated by a pull-apart mechanism during the occurrence of a strike-slip fault. The Paleozoic rocks bordering the depressions were affected by NW-SE foldings during the Hercynian and Andean orogenies. The Mesozoic and Cenozoic rocks of the western areas were affected by the Andean orogeny. The Tamborada river, which trenched a narrow valley in the Silurian shales, communicates the Cochabamba and the Punata-Cliza basins. Regional geology is dominated by Ordovician schists and quartzites. The core of the synclines contains rocks of Silurian age. In the western part, elongated Cretaceous and Tertiary rock outcrops, following the general NW-SE direction, occur.

Torrential alluvial sediments range from conglomerates to silt and clay, and predominate in the frontal part of the alluvial fans bordering the Paleozoic outcrops. Sediment sizes diminish gradually towards the centre of the basins and mix with silty-clayey sediments of lacustrine origin. Where coarse materials are absent, fine sediments can extent over variable depths from the terrain surface until the contact with the Paleozoic basement. According to geophysical determinations, the basement depth ranges from a few meters till 1000 m in the northern limit of the Cochabamba basin (Figure 4.3).

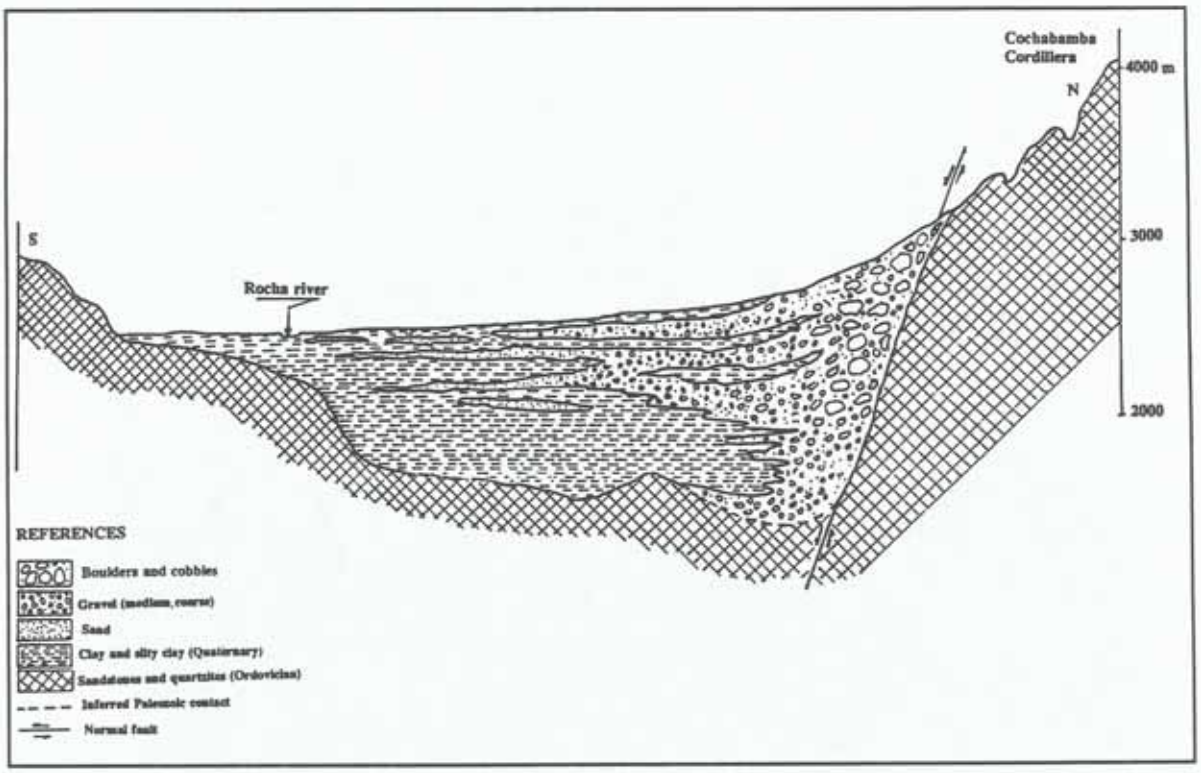

Fig. 4.3: Cross-section of the Cochabamba basin (Geobol, 1978)

Table 4.1: Stratigraphic sequence and hydrogeologic characteristics (modified from Geobol, 1978).

ERA	PERIOD	EPOCH		LITHOLOGY/ FACIES	PHYSICAL CHARACTERISTICS	HYDROGEOLOGIC CHARACTERISTICS
Cenozoic	Quaternary	Holocene		Colluvio-alluvial deposits	Angular rock fragments of variable size in a sandy-clayey matrix, occurring in chaotic accumulations which cover vast extents of the Cordillera sides.	High permeability. They sustain small springs of low salinity.
				Moraine deposits	Chaotic deposits of boulders and cobbles in a sandy-clayey matrix.	Variable permeability. Not important because of their short extent.
				Fluvial deposits	Coarse-grained materials formed by boulders, stones, gravels, sand and clay. They form alluvial fans and river-bed deposits.	Variable permeability, from low to very high. It is the basin water recharge zone.
		Pleistocene		Fluvio-lacustrine deposits	Mixed materials having characteristics of both alluvial and lacustrine origin. Fine clayey sands, medium to fine sands and gravels. Heterogeneous texture.	Moderate to low permeability, based on clay contents. Decreases towards the basin central part.
				Lacustrine	Fine materials (clay and sandy clay) with intercalations of peat and clayey layers containing animal and plant fossils.	Low to very low permeability.
	Tertiary	Paleocene (Morochata Formation)		Conglomerates	Poorly sorted red-violet clastic sediments, composed of fragments up to 20 cm diameter and occasional clayey layers. Polymictic conglomerates, in a red sandy-clayey matrix, are found at the base.	Moderate to low permeability
Mesozoic	Cretaceous	Maestrichtian-Danian (Santa Lucia Formation)		Clay,marls, calcareous sandstones	Clay and marls with violet-brown to greenish-brown gypsum veins. Calcareous reddish-yellow sandstones of fine and medium grain-size. Multicolor clay and marls.	Not important because of its reduced extent.
		Senonian-Maestrichtian (El Molino Formation)		Marls, limestones, oolitic limestones, compact limestones and calcareous sandstones	Multicolor marls intercalated with grayish-yellow limestones. Oolitic fossiliferous whitish-gray limestones. Hard and very hard compact dark-gray limestones. Calcareous yellowish-brown sandstones, fine to medium grained.	Overall low permeability. Locally higher because of dissolution effects.
Paleozoic	Silurian	Gotlandian	Uncia Formation	Shales	Friable shales, mainly dark-gray in fresh surface and brownish-reddish in altered surface. Plate exfoliation, with high mica content in the stratification planes.	Very low permeability.
			Cancañiri Formation	Clay-gritstones and quartzites	Glacio-marine sediments, grayish in fresh surface and reddish-brown in altered surface; sporadic intercalations of quartzitic dark-grey sandstones.	Not important because of their short extent.
	Ordovician	Caradocian	San Benito Formation	Quarzitic-sandstones	Micaceous quartzitic whitish-gray sandstones, fine to medium grained, disposed in layers of 0.20 to 0.80 m thickness. White quartzitic sandstones, stratified in layers of 0.80 to 1.5 m thickness.	High secondary permeability because of local fissures.

Continued

			Cuchu-Punata Formation	Siltstones and sandstones. Siltstones and shales	Greenish-gray siltstones, intercalated with sandstones of same color; medium to coarse grain-size, hard and compact sacaroidal aspect. Sporadic alternate with thin layers of micaceous quartzitic sandstones, of fine to medium grain-size and white color. Intercalations of brown shales and greenish-gray siltstones.	Very low permeability.

Well logs indicate a high vertical and lateral variability of the basin sediments, reflecting past intricate alluvial fan systems and lacustrine deltas. Sediments deposited in these environments show rhythmic, chaotic and torrential depositional structures. Interdigitated alluvial fans and stream migrations difficult the sediment correlation. Clayey materials dominate below 150 m depth, including small lenses of gravel and sand. Good examples of the Quaternary stratigraphic sequence are found in the distal part of the Central Valley fans and the central part of the Punata fan in the Punata-Cliza basin. Because of the organic materials mixed with the lacustrine sediments, clays are dark-colored. Well logs indicate that below 150 m depth the groundwater is strongly saline (Geobol, 1978).

4.2 GEOMORPHOLOGY

Landscape units are mountains, hillands, piedmonts and valleys.

4.2.1 Mountains

Mountains are of structural or structural-denudational origin, including Paleozoic quartzitic sandstones, shales and siltstones and some calcareous materials of Cretaceous age. The topography reflects past glacial erosion between 4.400 and 3.900 masl. Moraine deposits, U-shaped valleys, glacial lakes are present as relicts of Quaternary glaciations. From 3.900 to 2.800 masl, slopes are very steep and cause high runoff, soil erosion and deep river incisions in the highlands. Rounded summits of sandstones lithology can be differentiated from escarpments originated by the alternance of sandstone and clayey sandstone layers.

4.2.2 Piedmonts

The piedmonts present alluvial and colluvio-alluvial materials in the form of glacis and fans. The variety of relief types occurring in the piedmont landscape is described hereafter (table 4.2).

(1) Dissected depositional glacis composed of coalescent alluvial fans. They present a lenticular depositional structure reflecting paleo-rills. Materials are heterometric, including gravels, cobles and boulders in a fine-textured matrix. Typical erosional features such as gullies and rills are present.

(2) Old dissected fans of fluvio-glacial origin, characterized by chaotic depositional structures,

without selection and stratification. Boulders, sometimes several meters of diameter, are spread in a coarse-textured matrix (gravel, sand and silt) of high permeability. Most of these fans have been eroded, trenched or fossilized by recent alluvial fans. Representative examples are the Rio Llave and the Punata fans. Some fan remnants are found at higher elevations, uplifted by past tectonic activity.

(3) Recent colluvio-alluvial fans. They generally have small catchment areas and different textural gradients. Predominant material is gravelly sand. Some areas present stratifications of finer materials, mainly silty. Typical examples are found along the northern border of the Punata-Cliza and Central Valleys.

(4) Active alluvial fans. During the rainy season, they receive and transport heterometric sediment loads from the highlands. Two types can be identified: (1) deeply incised fans, in the way of canyons (*cañadones*), cutting through old fans (e.g. current fan of the Río Llave); (2) shallow alluvial fans characterized by intermittent streams due to their small catchment areas, the absence of deep incisions, materials just spread on the fan surface during the rainy season, shifting sedimentation channel, representing potential hazards for agricultural lands and settlements (e.g. Tacata and Viloma fans).

(5) Depositional glacis, formed by gently sloping coalescent fans of colluvio-alluvial origin. They predominate in the Central and Sacaba Valleys, where they form a transition between the lagunary depressions in the center of the valleys and the recent alluvial fans of the piedmont.

(6) Hills composed of marls, shales, siltstones and sandstones. They form isolated relief types within the piedmont landscape, characterized by the presence of gullies and rounded summits.

4.2.3 Valleys

Valleys are tectonic depressions (i.e. grabens) filled in by Quaternary sediments, deposited in lacustrine and alluvio-lacustrine environments. The terminal deposition, in the center of the valleys, is frequently of lagunary facies. The main relief types and landforms are playas, lagunary flats, badlands and river terraces.

(1) Playas are low-lying, slightly concave landforms originated from topographic depressions that contained lakes during the Pleistocene. They are typically underlaid by thick beds of clay and sandy-clayey materials, saline in the deeper zones, deposited during a lacustrine-lagunary phase. The inclusion of fossilized organic materials and the absence of gravelly lenses in the clayey matrix indicate a low-energy depositional environment. Playas are extensive in the lowest parts of the basins, have a flat topography and are affected by periodic floods. The soil surface becomes saline during the dry season.

(2) Lagunary flats are slightly sloping to level landforms of alluvio-lagunary origin. They occupy the rims of the large depressions at the bottom of the valleys, forming transitions between the playas and the alluvial fans or glacis. Lakes were present during the upper Quaternary, but because of climatic changes they were filled by rivers transporting and depositing high amounts of heterometric materials (gravels, sands, clays), with a gradation to finer materials towards the central parts of the basins. Lenses of gravel and coarse sand are frequently intercalated with the typical lagunary clayey depositions.

(3) Badlands result from the intensive dissection of the alluvio-lacustrine sediments, composed by lenses of heterometric materials (gravels, coarse sand) intercalated with layers of sandy, silty clay and clayey textures. Typical surface erosional features are gullies and rills, frequently initiated by underground pipes and tunnels.

(4) Alluvial terraces are located mainly along the Rocha river, in the Central and the Sacaba Valleys. It is no clear whether the Rocha river incised the alluvio-lacustrine sediments in response to neotectonic activity or climatic changes.

4.3 CLIMATE

Tectonism and river dissection have created an important relief energy with elevations ranging from 2500 to 5000 masl. These altitude differences in turn originate strong climatic variability. The bottom of the basins, between 2500 and 2800 masl, has a temperate semiarid climate, with mean annual temperatures of 14 to 17°C and mean annual precipitation of 400 to 600 mm. Figure 4.4 shows the annual precipitation record for a period of 48 years (1943-1991) at the Cochabamba Airport station. A three-years moving average rainfall reveals a tendency to increased inter-annual variability over time, causing more extreme dry years and subsequent higher rainfall periods. A longer climatic cycle of 12 years is also depicted. For Bolivia, Vacas (1990) identified a short climatic cycle of 3 to 5 years and a larger one of 12 years, as determined from correlation to sunspots activity. At higher altitude, temperature decreases and precipitation increases, with a gradual change towards more humid and colder climates. A thermic gradient of 0.8°C decrease is reported for each 100 m of increment in altitude, while rainfall increases approximately 100 mm each 250 m of increment in altitude (Geobol, 1978; CORDECO-SUBDESAL, 1993). The regional isohyet map exhibits an unbalanced rainfall distribution over the three valleys, with higher amounts of rain falling towards the western cordillera front (fig. 4.5).

The isolation of the area determines very special wind conditions. Prevailing winds during the wet summer months, from October till April, come from the northwest, north and northeast. During the dry season, from March to November, winds from southwest are more frequent (Graf, 1982). Wind speed increases with altitude. Data from the meteorological station AASANA, located at the Cochabamba airport, indicate mean monthly speeds from 1.5 km/h in May up to 5.9 km/h in October.

Table 4.2: Geomorphic units

LANDSCAPE	RELIEF TYPE	LITHOLOGY/ FACIES	LANDFORM	CODE
Piedmont	Dissected depositional glacis	Alluvial	Proximal	Pi111
			Central	Pi112
			Distal	Pi113
	Depositional glacis	Colluvio-alluvial	Proximal	Pi211
			Central	Pi212
			Distal	Pi213
	Swale	Alluvial	--	Pi31
	Active fans	Alluvial	Active channels	Pi411
			Inactive channels	Pi412
	Recent fans	Colluvial-alluvio	--	Pi51
	Old dissected fans	Glacio-alluvial	Proximal	Pi611
			Central	Pi612
			Distal	Pi613
	Hills	Quarzitic sandstones		Pi71
		Marls, limestones, sandstones		Pi72
Valley	Lagunary depressions	Alluvio-lagunary	Higher lagunary flats	Va111
			Middle lagunary flats	Va112
			Lower lagunary flats	Va113
			Badlands	Va115
		Lagunary	Playas	Va124
	Alluvial terraces	Alluvial	Higher alluvial terraces	Va211
			Lower alluvial terraces	Va212

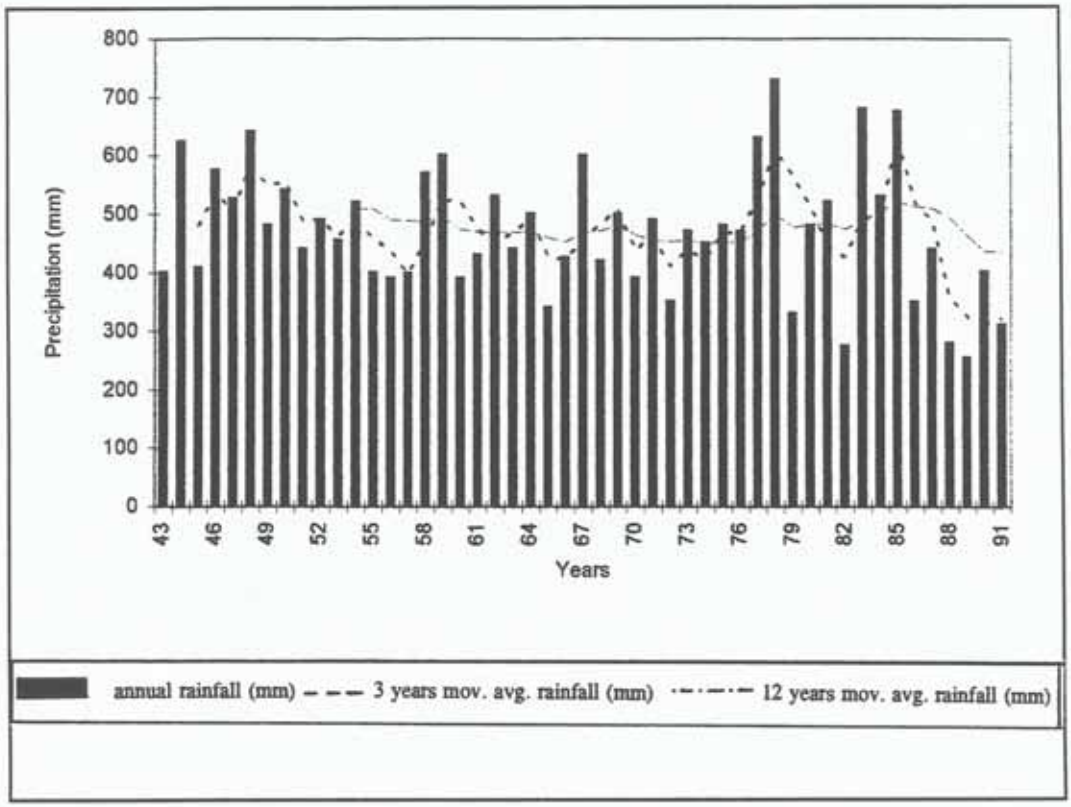

Fig. 4.4: Annual precipitation (1943-1991) at the Airport station, in the Cochabamba Valley (SENAMHI, National Service of Meteorology and Hydrology, Cochabamba)

The 80% of the total rainfall occurs from December to March, being occasional during winter time. April and October are considered transitional months (fig. 4.6). This causes a moisture deficit during eight to nine months per year (fig. 4.8). In areas subjected to salinization-alkalinization processes, salts tend to concentrate in the topsoil and the leaching of soluble salts is restricted because of the low rainfall. The highest amounts of precipitation are registered in January, the lowest in June and July.

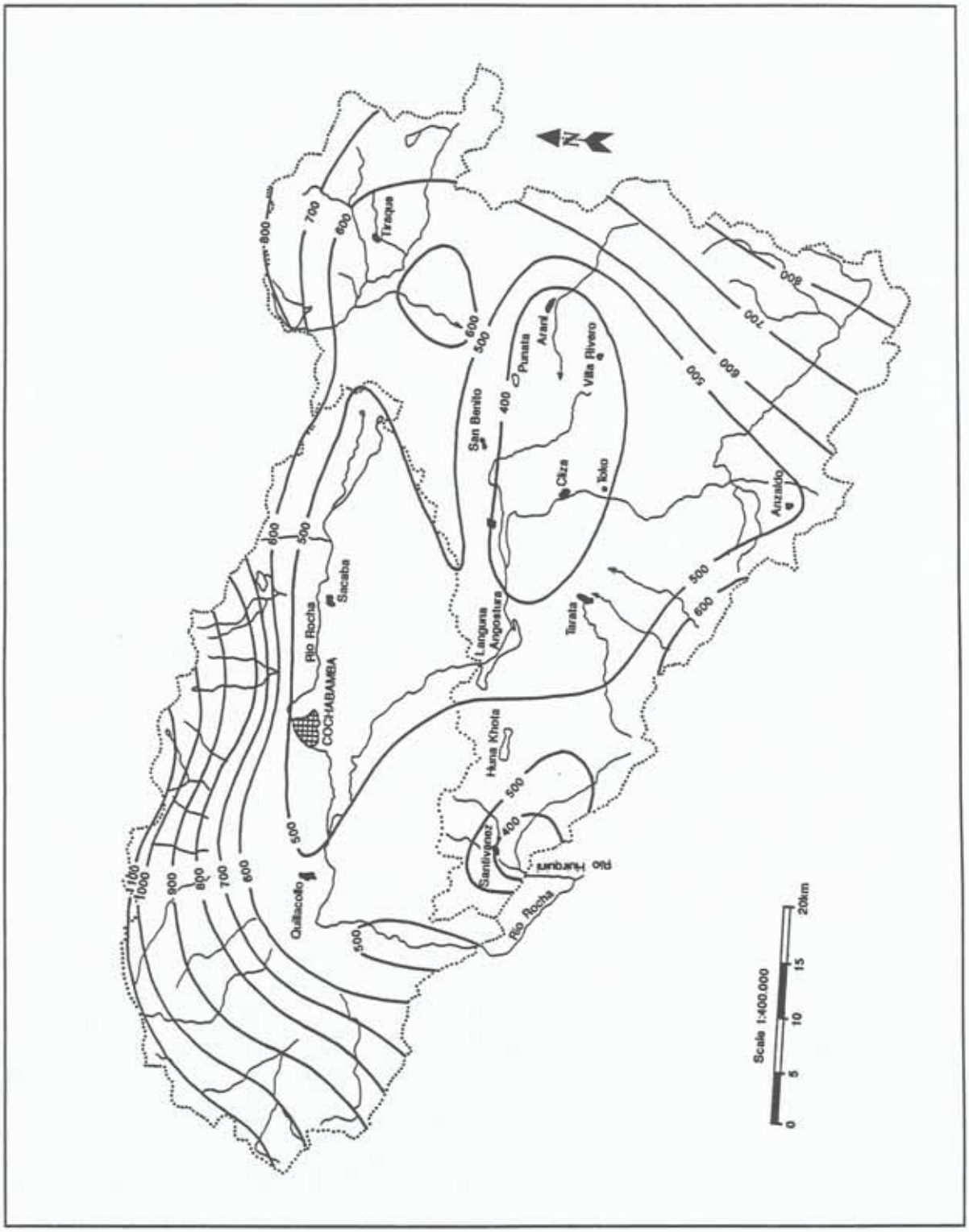

Fig. 4.5: Isohyet map in mm of rainfall of the Cochabamba valleys (Geobol, 1978)

Rainfall events are commonly of short duration. Half of the precipitations occurring in Cochabamba have a span of less than one hour. Highest intensities correspond to shortest rainfall durations. As example, figure 4.7 shows that a rainfall event of 48 mm/h intensity and ten minutes duration may occur within a period of 10 years. These are erosive events determining high runoff and low infiltration rates, responsibles in turn for the beginning of erosional processes such as gullies and rills in scarcely vegetated areas. In contrast, a rainfall of 64 mm/h intensity and 10 minutes duration has a return period of 100 years.

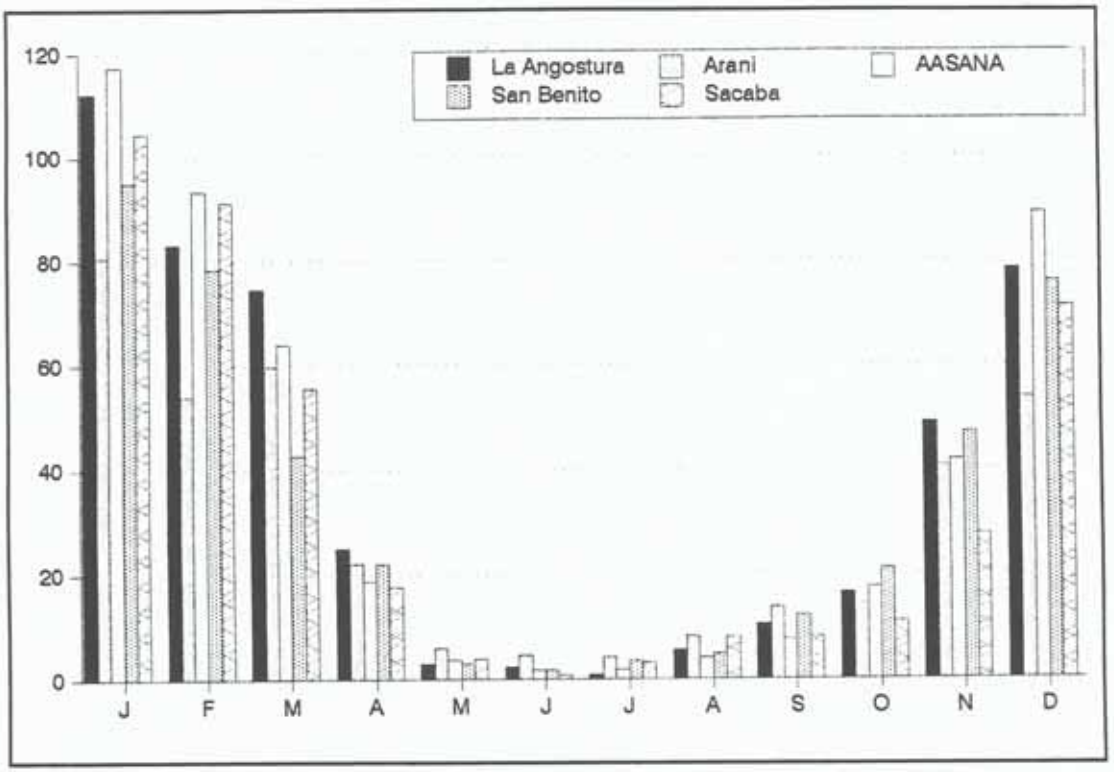

Fig. 4.6: Average monthly rainfall (SENAMHI, Cochabamba).

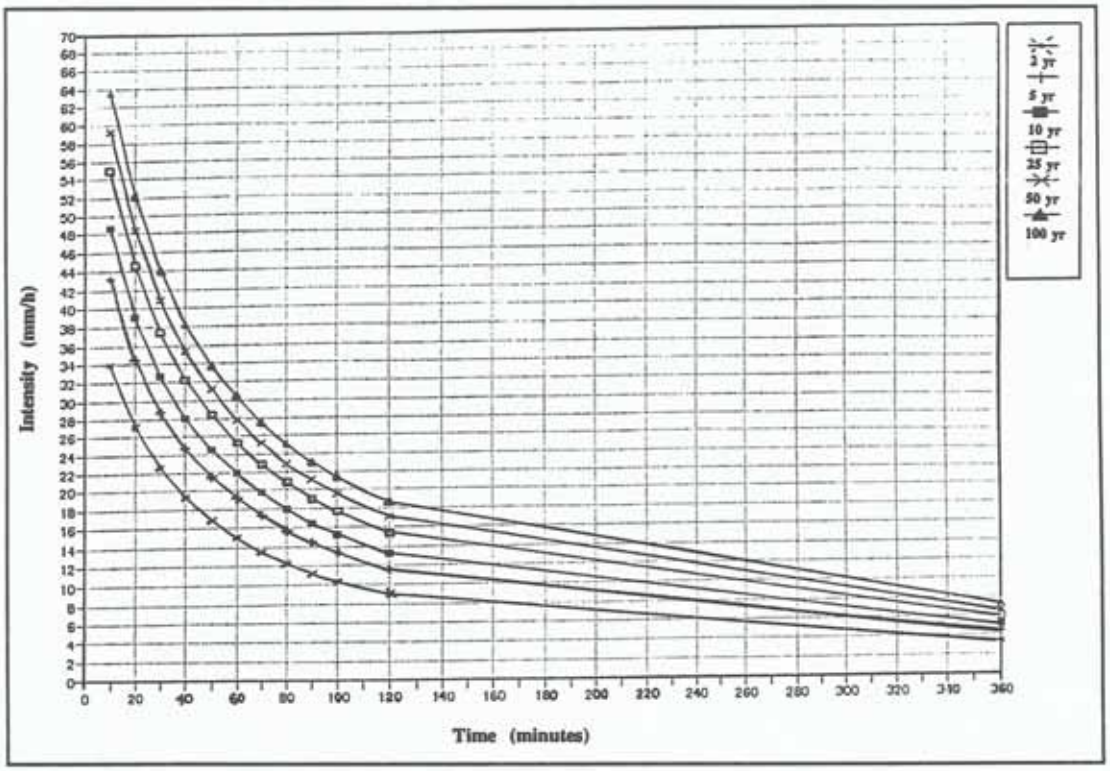

Fig. 4.7: Rainfall intensity-duration-frequency at the Cochabamba Airport station (CORDECO-SUBDESAL, 1993).

The main climatic characteristics for the valleys are reported in table 4.3. The values are averages of data recorded during 40 years (1950-1990) at the Cochabamba Airport meteorological station (2548 masl; 17°24'58'S, 56°10'28"W).

In accordance to Köppen's classification, the type of climate is mesothermic with dry winter in the valleys (Cw), steppic with dry winter at intermediate altitudes (Bsw) and high mountain polar at the highest elevations (EB).

Table 4.3: Meteorologic data at the Cochabamba Airport station (source: SENAMHI, 1950-1990).

Parameter	J	F	M	A	M	J	J	A	S	O	N	D
Predominant wind direction	NW	SE	SE	SE	SW	SW	SW	NW	N	N/SE	SE	SE
Wind speed (in km/h)	3.5	3.5	3.0	2.4	1.5	1.5	2.0	3.7	5.6	5.7	5.6	4.2
Number of days with wind speeds higher than 37 km/h	3	3	3	2	2	2	2	5	8	9	7	5
Number of days with a visibility lower than 2.000 m	1	1	1	0	0	0	0	1	1	0	0	1
Number of days with rainfall	17	15	11	5	2	1	1	2	3	5	8	14
Maximum rainfall in 24 hours	75.5	44.77	49.7	44.4	23	6.7	12.6	26.4	16.4	21	31.2	37.1
Average temperature	19	18.5	18.6	18	15.9	14	14	16	18.2	20.1	20.6	25.6
Average maximum temperature	24.5	24.3	25.1	25.6	25.2	24.1	24.1	25.1	26.1	27.3	27.2	25.6
Average minimum temperature	12.1	11.8	10.9	8.5	4.2	1.5	1.6	4.2	7.4	10	11.4	12.1

4.4 SOILS

According to climatic data and field observations, the soil moisture regime is aridic, since soils are commonly dry for more than six months (fig. 4.8). Exceptions are found in depressions and some flat areas where ustic and sometimes aquic regimes may be present, as evidenced in the field (mottling, shallow groundwater table). In the piedmont areas, the groundwater table ranges from 10 to 30 m depth, while in the valleys it can be found at a depth ranging from 2 to 8 m. Because of the regionally dominant aridic regime most of the soils classify as Aridisols or Entisols if diagnostic horizons are absent. The soil temperature regime is thermic because the average soil temperature is 16°C and the difference between the winter and summer soil temperatures is greater than 5°C (estimated from air temperature data). Buried Alfisols and Mollisols, correlated with past more humid climatic conditions, occur in the Sacaba and Central Valleys. Commonly, these soils present a loamy or silty loam sedimentary cover as consequence of recent alluvial depositions.

4.4.1 Punata-Cliza Valley

Soils on alluvial and colluvio-alluvial depositions in piedmont areas exhibit an overall low development. Entisols dominate on recent and actual fans. Glacis have more developed soils, mainly in their proximal and distal parts, where Haplargids are predominant. Calciorthids occur in the proximal part of the dissected depositional glacis, where fragments of the calcic horizon are brought up to the surface as consequence of ploughing (table 4.4).

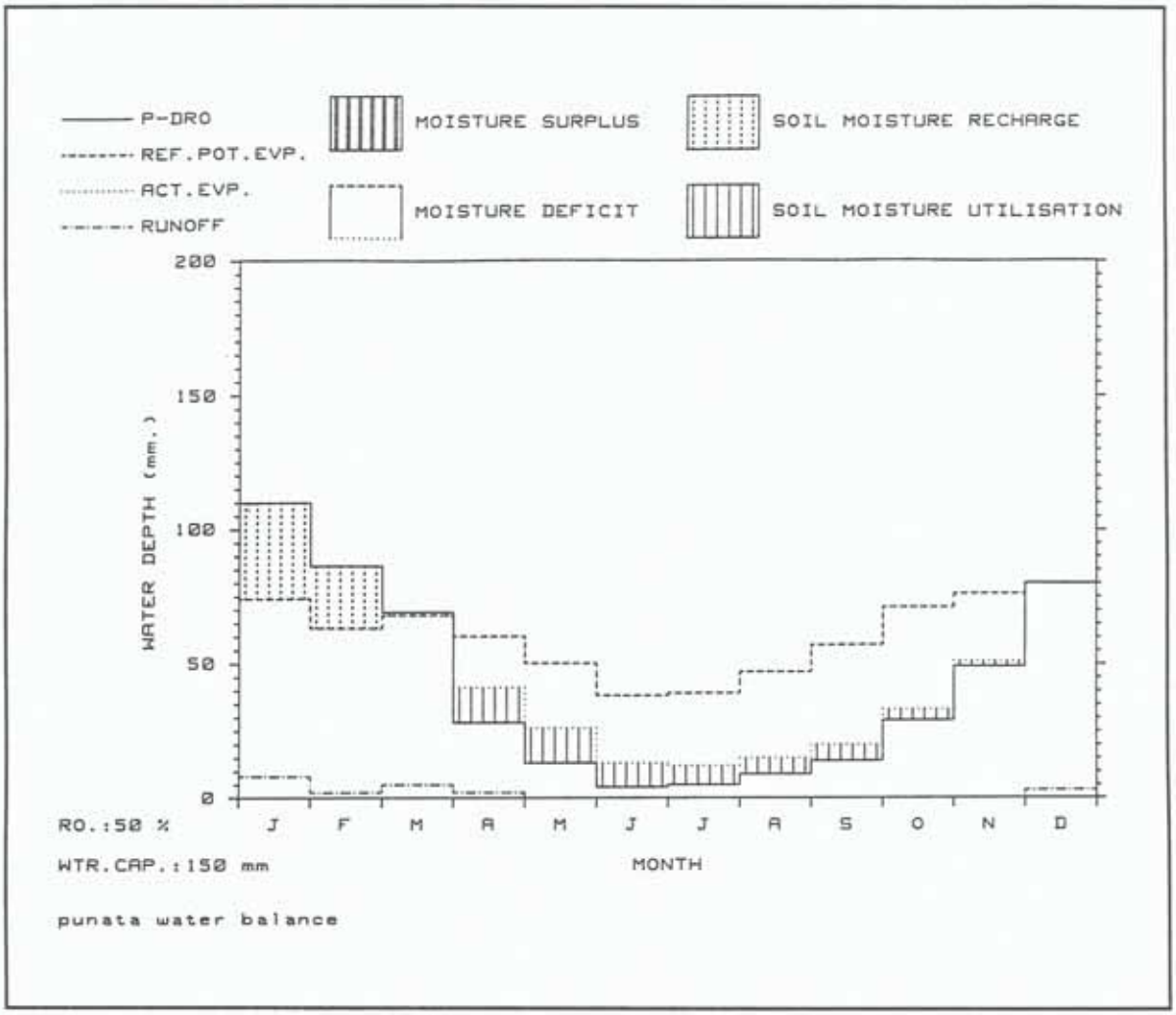

Fig. 4.8: Water balance at San Benito station (SENAMHI, Cochabamba)

Surface horizons of variable thickness have loam and silt loam textures and subangular blocky structure. Subsurface horizons are texturally more variable, ranging from silty clay loam to sandy loam, as reflection of different depositional facies.

Soils located on the distal parts of the glacis present a gradual increase in salt contents. However, most of the salt-affected areas correspond to depressions of lagunary origin (playas and lagunary flats). Surface horizons have clay, silty clay loam and silty clay textures and strong to moderate subangular blocky structure. Chlorides and sulphates of sodium and calcium are the predominant anions. Chemical analysis, climatic conditions and macromorphologic features observed in the field evidence that the main salt types migth be: thenardite (Na_2SO_4), mirabilite ($Na_2SO_4.10H_2O$), bloedite ($Na_2Mg(SO_4)2.4H_2O$), halite (NaCl) and soda ($NaCO_3$), as described in chapter 6. Electrical conductivity of the surface horizons reaches values as high as 80 dS/m and pH ranges from 6.5 to 10

(fig. 4.9). Therefore, most of the soils belong to the Natric Camborthids and Salorthids. Weak, puffy soil crusts of laminar structure, half centimeter thick, are common in these areas. Pulvulent materials, blown away by wind action once the crust is broken, are found below the soft crusts.

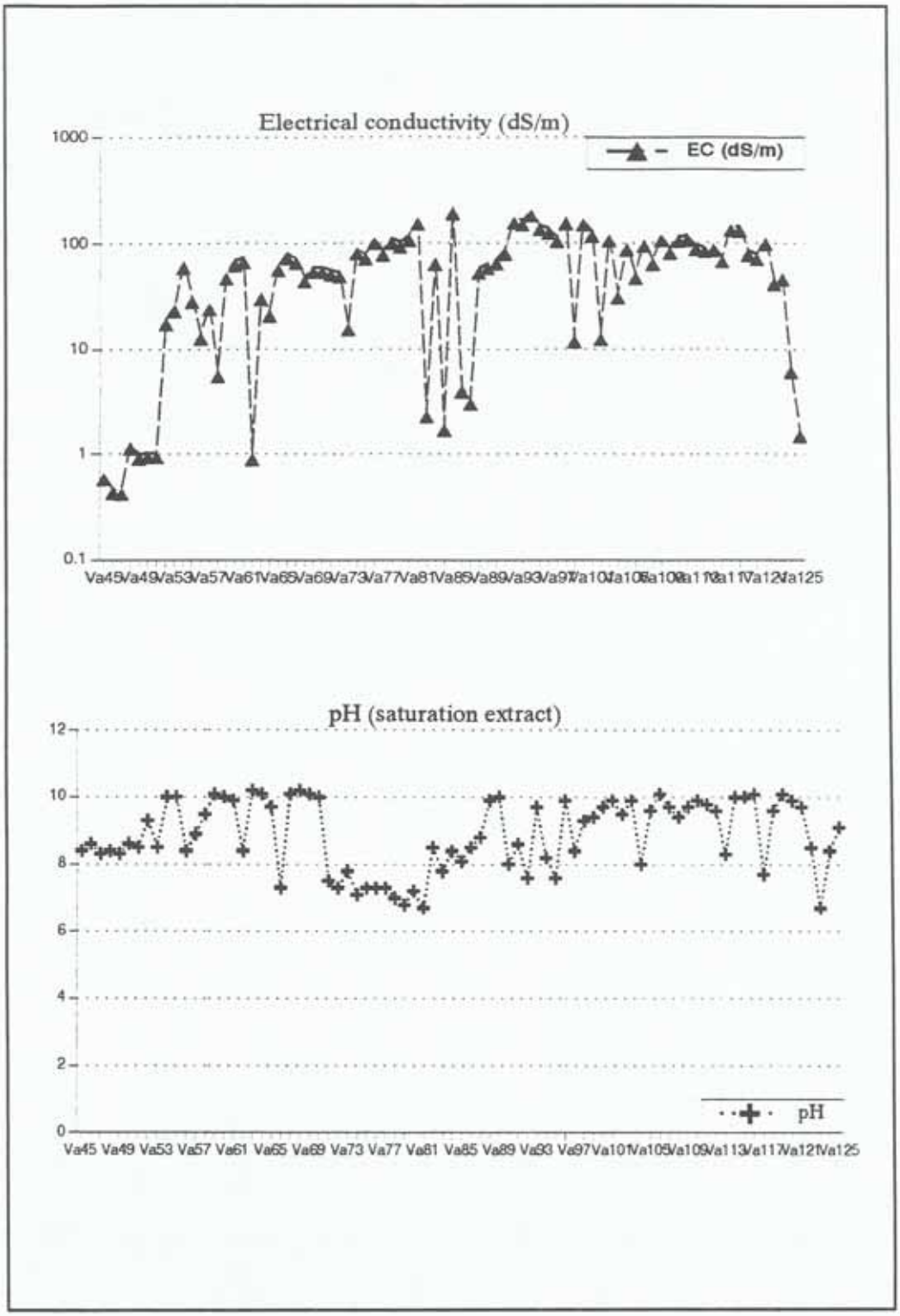

Fig. 4.9: Electrical conductivity (dS/m) and pH values from topsoils of lagunary depressions

Table 4.4: Geopedologic units of the Punata-Cliza Valley

GEOPEDOLOGIC UNIT	MAP UNIT TYPE	POLYPEDON		INCLUSIONS		PHASE
		NAME	% obs.	NAME	% obs.	
Pi111	Association	Typic Calciorthids Typic Camborthids	60 15	Typic Haplargids Fluventic Camborthids Ustic Torrifluvents Aridic Calciustolls (sc)	13 4 4 4	(sc):sedimentary cover
Pi112	Consociation	Typic Camborthids (ca) Ustochreptic Camborthids	70 30			(ca):calcareous
Pi113	Association	Ustalfic Haplargids Ustochreptic Camborthids	55 30	Typic Haplargids Ustic Torriorthents	10 5	
Pi213	Consociation	Ustochreptic Camborthids Typic Camborthids	80 20			
Pi 411	Miscellaneous land type	Mixed alluvial land	100			
Pi412	Consociation	Typic Torrifluvents Typic Torriorthents	80 20			
Pi51	Association	Ustic Torriorthents Typic Torrifluvents	50 40	Typic Torriorthents	10	
Pi611	Association	Typic Camborthids Typic Haplargids	50 30	Typic Ustochrepts Fluventic Ustochrepts	10 10	
Pi612	Consociation	Ustochreptic Camborthids (ca)	85	Ustochreptic Calciorthids	15	(ca): calcareous
Pi613	Consociation	Ustochreptic Camborthids	90	Typic Camborthids	10	
Pi71	Consociation	Lithic Torriorthents	90	Typic Torriorthents	10	
Pi72	Consociation	Typic Calciorthids Lithic Calciorthids	60 30	Lithic Torriorthents	10	
Va111	Association	Fluventic Camborthids Ustochreptic Camborthids	60 30	Ustalfic Haplargids Ustic Torrifluvents	5 5	
Va112	Association	Ustalfic Haplargids Ustochreptic Camborthids	50 35	Fluventic Camborthids Ustic Torrifluvents (sa)	10 5	(sa): saline
Va113	Association	Ustalfic Haplargids (saso) Ustochreptic Camborthids (sa)	60 20	Ustic Torrifluvents Natric Camborthids Fluventic Camborthids	10 8 2	(sa): saline (saso): saline-alkaline
Va124	Association	Typic Salorthids Natric Camborthids	40 35	Ustic Torrifluvents (saso) Aquic Haplargids (saso) Fluventic Camborthids Typic Natrargids Aquic Camborthids	8 7 5 2 3	(saso):saline-alkaline

4.4.2 Sacaba Valley

Piedmont areas present surface and subsurface erosional features such as gullies, rills and pipes. Soils are of loamy and silt loam textures and contain variable amounts of rock fragments. In the southern and southeastern parts of the basin, calcareous crusts occur within the profiles. Soil permeability is commonly high. The salt and organic matter contents are low. Depositional glacis have finer soil textures and include locally poorly drained areas. Higher salinity values, poor internal drainage, and dominant clay and clay loam textures characterize the soils originated from parent materials of alluvio-lacustrine origin.

Buried soils present evidence of depositions occurred in a lacustrine-lagunary environment, such as silty clay and silty clay loam textures, and horizontal root channels filled with manganese. Most of these soils classify as Mollisols and, in the presence of an argillic horizon, as Alfisols.

Badlands, characteristic of the lagunary depressions of the Sacaba Valley result from collapsed subsurface tunnels and pipes. The fine textured lacustrine sediments include isolated gravel channels, lenses and sheets which conduct subsurface water flow, causing the formation of tunnels and pipes. As a consequence of gradual enlargement, the roof of the underground conducts collapses. The evacuation of the collapsed material through channel incision originates a system of gullies developing into badlands. Lacustrine sediments are very erodible silty and loamy materials, with weakly developed pedogenic features. Predominant soils are Torrifluvents and Fluventic Camborthids (table 4.5).

4.4.3 Central Valley

In the piedmont, Argids occur on the surface, or as buried phases of the old dissected fans. Stoniness is a common feature on recent and actual fans. Depositional glacis under intensive agricultural activity possess buried Haplustolls in their proximal and central parts. The distal zone, a transition between landforms of lagunary origin and the piedmont area, has higher moisture contents. Therefore, soils from this unit were classified as Ustochrepts (table 4.6).

Salt-affected areas predominate in the southern and southwestern parts of the basin. Calcareous parent materials, lacustrine clays and irrigation with brackish water contribute to the extension of the salt-affected areas over time.

Table 4.5: Geopedologic units of the Sacaba Valley

GEOP. UNIT	MAP UNIT TYPE	POLYPEDON		INCLUSIONS		PHASE
		NAME	% obs.	NAME	% obs.	
Pi111	Association	Typic Camborthids Aridic Haplustolls	60 25	Ustalfic Haplargids Ustic Torriorthents	5 10	
Pi112	Association	Aridic Haplustolls (sc) Typic Camborthids Ustalfic Haplargids	50 20 15	Ustic Torrifluvents Aridic Haplustalfs (sc)	5 5	(sc): sedimentary cover
Pi113	Association	Ustochreptic Camborthids Torrifluventic Haplustolls (sc) Ustalfic Haplargids	50 20 15	Fluvaquentic Haplustolls Fluventic Camborthids Aridic Haplustalfs (sc)	5 5 5	(sc): sedimentary cover
Pi212	Association	Torrifluventic Haplustolls (sc) Aridic Haplustolls	55 30	Ustic Torriorthents Typic Ustifluvents	5 10	(sc): sedimentary cover
Pi213	Association	Ustochreptic Camborthids Aridic Haplustolls	60 30	Ustalfic Haplargids	10	
Pi 411	Miscellaneous land type	Mixed alluvial land	100			
Pi412	Consociation	Ustic Torriorthents	85	Ustic Torrifluvents	15	
Pi51	Consociation	Aridic Haplustolls	100			
Pi611	Consociation	Typic Haplustolls	85	Typic Ustochrepts Typic Ustorthents	10 5	
Pi612	Association	Ustochrepts Camborthids Ustalfic Haplargids				
Pi613	Association	Typic Ustochrepts Typic Ustorthents	60 30	Aridic Ustifluvents	10	
Pi 71	Consociation	Lithic torriorthents				
Va112	Association	Fluventic Camborthids (sc) Aridic Haplustolls (sc) Ustochreptic Camborthids (sc)	30 30 25	Ustic Torrifluvents Ustic Torriorthents	5 5	(sc): sedimentary cover
Va113	Association	Aridic Haplustolls (sc) Typic Camborthids Fluvaquentic Haplustolls	35 30 20	Ustic Torrifluvents Torrifluventic Haplustolls Natric Camborthids	5 5 5	(sc): sedimentary cover
Va115	Consociation	Fluventic Camborthids Typic Torrifluvents (sc)	50 25	Torrifluventic Haplustolls (sc) Aridic Haplustalfs (sc)	20 5	(sc): sedimentary cover
Va211	Consociation	Typic Ustochrepts	85	Aridic Ustifluvents	15	
Va212	Consociation	Typic Torrifluvents	90	Ustic Torrifluvents Typic Ustifluvents	5 5	

Table 4.6: Geopedologic units of the Central Valley.

GEOPEDOLOGIC UNIT	MAP UNIT TYPE	POLYPEDON		INCLUSIONS		PHASE
		NAME	% obs.	NAME	%obs.	
Pi211	Association	Torrifluventic Haplustolls (sc) Ustalfic Haplargids	45 30	Fluvaquentic Haplustolls (sc) Ustic Torrifluvents Ustic Torriorthents Typic Haplustolls Aquic Camborthids	10 5 4 4 2	(sc): sedimentary cover
Pi212	Association	Fluvaquentic Haplustolls (sc) Aquic Camborthids Torrifluventic Haplustolls	45 25 20	Ustalfic Haplargids Typic Haplustolls Aquic Torrifluvents	4 3 3	(sc): sedimentary cover
Pi213	Association	Fluventic Ustochrepts Ustalfic Haplargids Aquic Camborthids	45 25 20	Fluvaquentic Haplustolls Torrifluventic Haplustolls (sc) Ustochreptic Camborthids	5 2 3	(sc): sedimentary cover
Pi31	Association	Torrifluventic Haplustolls Aquic Camborthids	60 40			
Pi 411	Miscellaneous land type	Mixed alluvial land	100			
Pi412	Consociation	Ustic Torriorthents	90	Aridic Haplustolls	10	
Pi51	Association	Aridic Haplustolls Ustic Torriorthents	60 20	Ustochreptic Camborthids Torrifluventic Haplustolls	10 5	
Pi611	Association	Aridic Haplustolls Ustalfic Haplargids Ustochreptic Camborthids	60 20 15	Ustic Torriorthents	5	
Pi612	Association	Ustochreptic Camborthids Ustalfic Haplargids	60 25	Aridic Haplustolls	15	
Pi 71	Consociation	Lithic torriorthents				
Val12	Association	Fluvaquentic Haplustolls Aquic Camborthids	50 30	Natric Camborthids Ustic Torrifluvents	10 10	
Val13	Association	Aquic Camborthids Natric Camborthids Fluvaquentic Haplustolls	40 30 20	Typic Eutrochrepts Torrifluventic Haplustolls (sc)	5 5	
Val24	Association	Natric Camborthids Aquic Camborthids Typic Salorthids	40 35 25			

4.4.4 Soil correlation attempt

In spite of their common tectonic origin, the three basins have undergone a different evolution over time, resulting in significant geopedologic variations. For example, the dissected depositional glacis were only mapped in the southern part of the Punata-Cliza and the Sacaba Valleys. The undissected depositional glacis predominate in the northern piedmont of the Central and the Sacaba Valleys, but they are largely buried by recent alluvial fans in the Punata-Cliza Valley. Badlands are present in the Sacaba Valley and the lagunary flats dominate in the Punata-Cliza Valley. However, old dissected as

well as recent and actual fans were mapped in all three valleys.

Local differences in lithology and tectonics contribute to diversify the taxonomic composition of similar geomorphic units in the three valleys (table 4.7). For instance, Haplustolls are absent in the Punata-Cliza Valley, while they predominate as buried or exposed soils in the Central and Sacaba Valleys. The presence of Mollisols might reflect moister climatic conditions in the past. Their absence in the Punata-Cliza Valley could be related to the persistence of the lacustrine-lagunary conditions in this basin, as also hypothesized by Veicht (1992) and Geobol (1977). Orthids (Camborthids, Salorthids) are common in climatic conditions similar to the present ones. Topographic shape and location increase locally the availability of moisture with the occurrence, for example, of Aquic Camborthids or Aquic Haplargids in the playa positions. Depressions cause local waterlogging conditions, proper for the development of Natric Camborthids and Salorthids on lacustrine-lagunary clayey parent materials.

Table 4.7: Comparison of the geopedologic units occurring in the three Cochabamba valleys

GEOPEDOLOGIC UNITS	PUNATA-CLIZA	SACABA	CENTRAL	COMMON SOILS (*)
Pi71	Lithic Torriorthents	Not mapped	Not mapped	--
Pi72	Lithic Calciorthids Typic Calciorthids	Not mapped	Not mapped	--
Pi611	Typic Camborthids Typic Haplargids	Aridic Haplustolls	Aridic Haplustolls Ustalfic Haplargids Ustochreptic Camborthids	Camborthids Haplustolls Haplargids
Pi612	Ustochreptic Camborthids	Ustochreptic Camborthids Ustalfic Haplargids	Ustochreptic Camborthids Ustalfic Haplargids	Camborthids
Pi613	Ustochreptic Camborthids	Typic Ustochrepts Typic Ustorthents	Not mapped	--
Pi51	Typic Torrifluvents Ustic Torriorthents	Aridic Haplustolls	Aridic Haplustolls Ustic Torriorthents	Haplustolls Torriorthents
Pi412	Typic Torrifluvents Typic Torriorthents	Ustic Torriorthents	Ustic Torriorthents	Torriorthents
Pi31	Aquic Camborthids Torrifluventic Haplustolls	Not mapped	Not mapped	--
Pi211	Not mapped	Not mapped	Torrifluventic Haplustolls Ustalfic Haplargids	--
Pi212	Not mapped	Torrifluventic Haplustolls Aridic Haplustolls	Torrifluventic Haplustolls Fluvaquentic Haplustolls Aquic Camborthids	Haplustolls
Pi213	Ustochreptic Camborthids Typic Camborthids	Ustochreptic Camborthids Aridic Haplustolls	Fluvaquentic Ustochrepts Ustalfic Haplargids Aquic Camborthids	Camborthids
Pi111	Typic Calciorthids Typic Camborthids	Typic Camborthids Aridic Haplustolls	Not mapped	Camborthids
Pi112	Typic Camborthids	Aridic Haplustolls Typic Camborthids Ustalfic Haplargids	Not mapped	Camborthids
Pi113	Ustochreptic Camborthids Ustalfic Haplargids	Ustochreptic Camborthids Torrifluventic Haplustolls Ustalfic Haplargids	Not mapped	Camborthids Haplargids
Va211	Not mapped	Typic Ustochrepts	Not mapped	--

Continued

Va212	Not mapped	Typic Torrifluvents	Not mapped	--
Va111	Fluventic Camborthids Ustochreptic Camborthids	Not mapped	Not mapped	--
Va112	Ustalfic Haplargids Ustochreptic Camborthids	Fluventic Camborthids Ustochreptic Camborthids Aridic Haplustolls	Fluvaquentic Haplustolls Aquic Camborthids	Camborthids Haplustolls
Va113	Ustalfic Haplargids Ustochreptic Camborthids	Aridic Haplustolls Fluvaquentic Haplustolls Typic Camborthids	Aquic Camborthids Natric Camborthids Fluvaquentic Haplustolls	Camborthids Haplustolls
Va115	Not mapped	Fluventic Camborthids Typic Torrifluvents	Not mapped	--
Va124	Typic Salorthids Natric Camborthids Aquic Haplargids	Not mapped	Natric Camborthids Typic Salorthids Aquic Camborthids	Camborthids Salorthids

* Common soils=soils present at least in two of the three valleys

4.5 VEGETATION

Natural vegetation is mostly xeromorphic. According to Holdridge's life zone classification, the valleys belong to the subtropical lower montane thorn steppe ecosystem (Holdridge, 1947). Locust (*Prosopis juliflora*) and acacia (*Acacia macracantha* and *Acacia caven*) trees, as well as orko karalawa (*Carica lanceolata*) and cacti (*Opuntia, Echinocactus, Lovibia* and *Echinopsis*), are exceptionally preserved as parcel hedges by the farmers. Eucalyptus (*Eucalyptus globulus*), molle (*Schinus molle*) and ulala (*Cereus haenkeanus*) are common species in the flat areas.

The vegetation pattern varies according to the ecological conditions. On the mountain slopes, where the soil cover is very shallow and stony, sparsely distributed native grasses and shrubs are found. Steep slopes, rapid soil permeability and high infiltration rates prevent the establishment of denser vegetation and favor erosion processes.

On most of the alluvial fans, unfavorable to agriculture because of the high amount of rock fragments on the soil surface and within the soil matrix, there are xerophytic species including cactaceae and shrubs such as locust and molle trees. Some areas located on recent alluvial fans and depositional glacis, especially in the Central and Sacaba Valleys, are being increasingly used for agricultural purposes, previous destoning of the soil surface and matrix. Rainfed crops include corn (*Zea mayz*), wheat (*Triticum sativum*), alfalfa (*Medicago sativa*) and, to a lesser extent, beans (*Vicia faba*), peas (*Pisum sativum*), onions (*Alliumcepa*) and quinua (*Chinchona amygdalifolia).* Some of these crops are also produced in small-scale irrigation schemes.

Halophytic salt-tolerant perennial vegetation (*Chenopodium ambrosoides, Ch. mixdentatum, Portulaca floccosa, P. pilosa, Anoda parviflora, Chrysantelum sp. and Cydonon dactylon*) grows in patches on the vast salt-affected areas of the Punata-Cliza Valley, locally bordered by locust shrub hedges. The distribution of the halophytic vegetation is determined by the nature and degree of salinity: (a) highly tolerant species of the Chenopodiaceae and Aizoaceae grow in dispersed patches on soils severely affected

by salinity-alkalinity; (b) less-tolerant species, belonging to the Cyperaceae, Graminae and Plantaginaceae families, germinate after the rains and grow between the halophytic species.

4.6 HYDROLOGY

Most of the rivers and brooks have a torrential regime because of the climatic and geomorphic conditions. Streams are ephemeral and unstable, and carry large loads of sediments from the highlands during the rainy season. The catchment areas have variable extents. In the Central Valley, the larger drainage areas are located in the western part, belonging to the San Miguel, Llave, Viloma and Khayarani rivers. The Punata basin has its main catchment areas located in the southern part, including the Calicanto (Tarata), Siches-Cliza and Escalera rivers (Villa Rivero). Only the Wasa Mayu river (Punata) is located towards the northwest of the basin.

The drainage network is controlled by tectonics. Main faults along the northern mountain front, such as the Tunari fault, determine short-extent, highly torrential drainage patterns. On the contrary, towards the south of the Punata-Cliza basin, a gentler basement subsidence allowed the development of a more extensive and integrated drainage network. In the highlands the rivers have a dendritic distribution pattern, but all the drainage systems converge towards the central part of the basin. Figure 4.10 shows the topographic profile of the main rivers. The steep slopes are indicative of the non-equilibrium conditions of the drainage network.

The Rocha river, draining the Cochabamba-Sacaba basins is dry in winter time (dry season). During the rainy season, most of the water is diverted for irrigation purposes. In the lowlands, some short streams such as the Sulty river drain the lagunary depressions of the Punata-Cliza basin, originating local waterlogged areas.

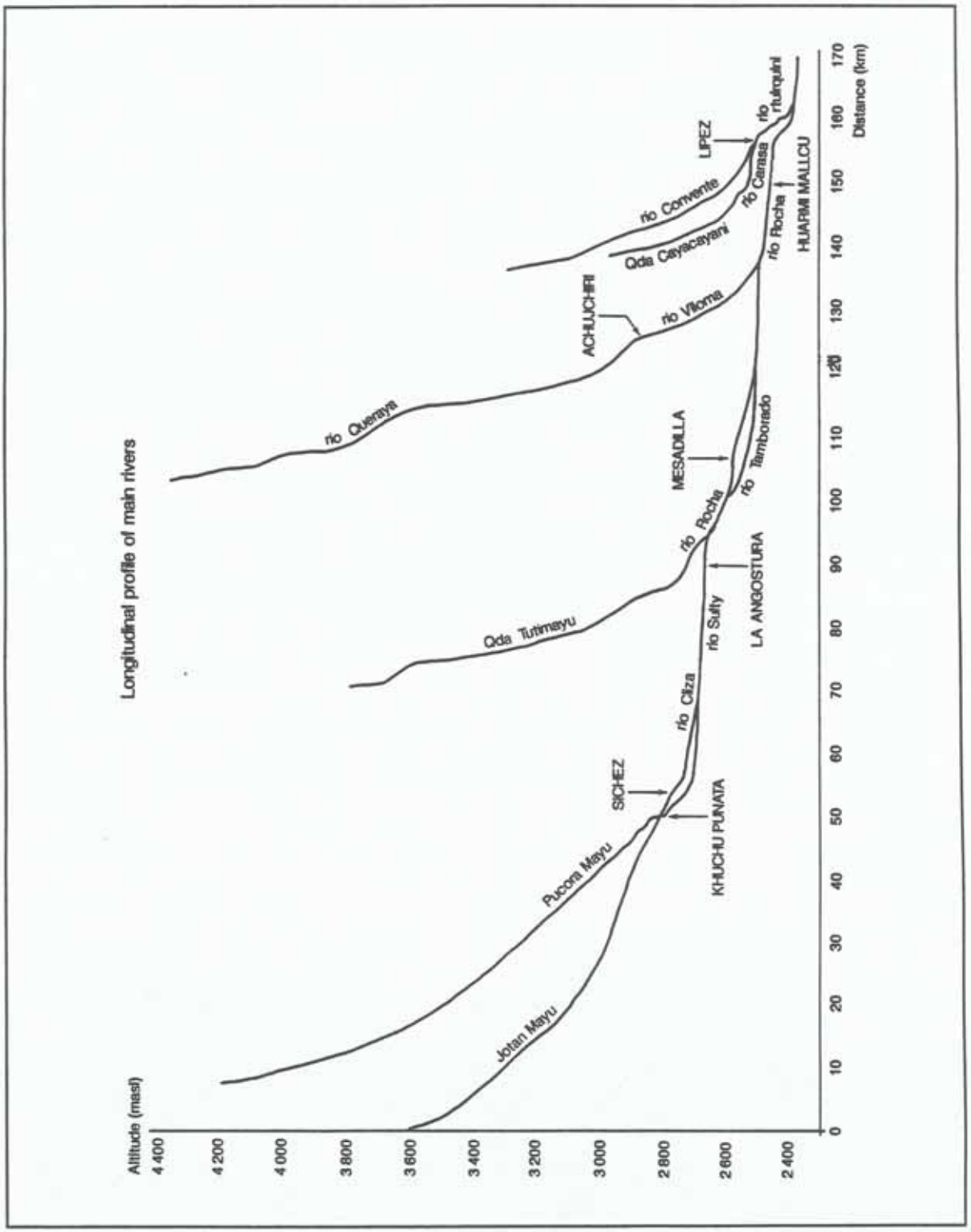

Fig. 4.10: Topographic profile of the main rivers

4.7 CONCLUSION

The semiarid conditions of the area control the landscape and soil degradation processes. The water balance shows a moisture deficit during eight to nine months per year, accompanied by high evaporation rates. Salts tend to concentrate in the topsoil and leaching of soluble salts is restricted because of the low rainfall. Because of the soil moisture deficit most of the soils classify as Aridisols or Entisols if diagnostic horizons are absent. Natric Camborthids and Salorthids dominate in flat landscape areas (playas and lagunary flats) of lacustrine-lagunary clayey parent materials.

Highly intensive, short-duration rainfall events are common in the area. They determine high runoff and low infiltration rates, causing the initiation of erosional processes such as rills in scarcely vegetated areas. Badlands result from the intensive dissection of the alluvio-lacustrine sediments. Typical surface erosional features are gullies and rills, frequently controlled by collapsed underground pipes and tunnels.

The 80% of the annual rainfall occurs from December to March, causing torrential water flows in rivers and brooks. Streams are ephemeral and unstable, and carry large loads of sediments from the highlands during the rainy season. Therefore, exceptional rainfall events are prone to originate stream avulsions, putting at risk agricultural lands and urban settlements in the piedmont areas.

CHAPTER FIVE:

LANDSCAPE ORIGIN AND EVOLUTION

Soil properties, ^{14}C dating of buried soils, pollen profiles, well logs stratigraphy, depositional facies and shape of the geomorphic units are used as indicators to reconstruct the origin and the long-term evolution of the Cochabamba, Sacaba and Punata-Cliza Valleys, in the context of regional tectonics, climatic oscillations and hydrologic changes occurred during the Tertiary and Quaternary periods.
The rate and degree of tectonic uplifts, folding and tilting, relative elevation above the base level, and structural control on drainage development are geologic-tectonic factors influencing landscape origin and evolution. Lithologic composition of the rock strata, the rates of rock weathering, and rock resistance to erosion control sediment availability in catchment areas and, hence, downstream fan development. The magnitude and frequency of storm events, the seasonality of rainfall and the evapotranspiration rates affect patterns of soil and vegetation cover, determining in turn the rates of surface runoff and sediment yield (Maizels, 1993).

Changes in the tectonic, climatic and hydrologic catchment parameters can be expected to cause spatial and temporal changes in the nature of the stream pattern itself, in the morphology and sedimentology of the channels, and in local and regional channel stability.

5.1 INDICATORS OF LANDSCAPE EVOLUTION

5.1.1 Paleosols

Paleosols are soils formed on past landscapes or formed under changing environmental conditions, notably climatic and associated vegetation changes (Ruhe, 1956; Yaalon, 1971; Catt, 1989; Bronger et al. 1989). Their position on the landscape, taxonomic classification and pedogenetic features can be used to interpret Quaternary landscape evolution due to climatic changes, especially those of the Holocene epoch.

Main factors influencing soil development are climate, organisms, relief, parent material and time (Jenny, 1941 and 1980). Changes in climate and organisms over time control soil development, whereas changes of the other factors might imply either destruction or burial of antecedent soils. Hence, many relict soil features result directly or indirectly from climatic changes. Relict soil properties are inherited from past periods when soil-forming conditions were sufficiently different from those of the present. The burial of soils decreases the possibility of continuing soil differentiation over time. As burial often results from depositions following rapid climatic deteriorations after each interglacial or interstadial, the episodes of soil formation can be linked to these single stages (Catt, 1989).

In some regions, it is possible to distinguish soil relict features developed during late Quaternary interglacials from those originated in climates warmer than the present, that is from the Tertiary or the early Quaternary. Locally, soils have been attributed to the Tertiary either by the presence of desiccation features, such as secondary carbonates (caliche) formed by evaporation from the soil surface, or by the occurrence of a continuous calcareous layer with burrows of terrestrial animals or plant root remnants. Landscape position is also used to recognize Pre-Quaternary soils, as the latter may occur in remarkable stratigraphic situations such as beneath major unconformities (e.g. along the Cretaceous-Tertiary boundary) or within terrestrial sedimentary sequences (Retallack, 1981). But the best estimate of time is done by direct dating (thermoluminescence or magnetostratigraphy).

During the interglacial stages, erosion and deposition were confined to specific areas, mainly glacial and periglacial land surfaces but also some alluvial and littoral zones and lakes (Semmel, 1989). During the colder periods, erosion, transport and deposition by ice, water and wind were more widespread than when the climate was warmer and land surfaces were stabilized by dense vegetation covers. During the warmer periods, strongly developed soils formed, with distinctive pedogenetic features such as rubification and thick Bt horizons. Colour is therefore a soil property that helps identify buried soils. Cambic horizons from the Holocene exhibit lower degree of rubification (10YR - 7.5 YR) than those of the interglacial stages having redder 7.5YR or 5YR colors (Catt, 1989). The process of rubification is attributed to the pedogenetic formation of iron oxides (e.g. hematite) in a strongly seasonal climate with hot, dry summers associated with the warmest periods of the Pleistocene and early Holocene. In Holocene soils, it is however important to distinguish red colors caused by the weathering of primary minerals from those inherited from red parent materials. Interglacial Bt horizons are often thicker than those formed during the Holocene, and may contain up to 1.5 times as much alluvial clay (Bullock, 1974; Catt, 1979). Many thin, weakly developed buried soils have been attributed to short periods of climatic amelioration (interstadials) within the major cold stages of the Quaternary.

Increased dryness causes the formation of calcrete crusts in arid and semiarid environments. Calcareous layers are another feature used to identify soils from the past. Three types of crust can be recognized: (1) weak crusts correlated with the last glacial age, including indurated crusts showing intergranular cementation, weakly developed petrocalcic horizons not more than 20 -30 cm thick, and very limited discontinuous, laminar calcrete layers; (2) completely cemented mature crusts, assigned to Rissian and early-to-mid Pleistocene ages, including massive petrocalcic horizons up to about 50 cm thick, secondary brecciation and recementation, and discontinuous laminar calcretes several millimeters in thickness; (3) ancient crusts, confined to early Quaternary surfaces and showing massive petrocalcic horizons 1 m or more thick and laminar calcretes several centimeters thick (Dumas, 1969 and 1977).

5.1.2 Alluvial fans

Alluvial fans are landscape features affected by autocyclic and allocyclic controls. Autocyclic controls refer to long-term fan aggradation, changes of catchment area and sediment availability. Allocyclic or

external controls refer to climatic changes such as rainfall seasonality and magnitude of storm events, or to tectonic effects like mountain uplift, basin subsidence, fan tilting and faulting. Tectonism influences fan slope, dissection and burial, and the dominant depositional process controls fan morphology. These external factors in turn influence the river transport capacity and sediment supply characteristics of the catchment areas.

Shape, location, dissection and morphology of alluvial fans can be used as indicators to explain Quaternary and Pre-Quaternary landscape evolution because they provide evidence of channel response to external and internal controls. Alluvial fans also show evidence of paleoclimatic oscillations (e.g. presence of buried soils), neotectonics and base level fluctuations.

5.1.3 Paleontological approach

Paleontological features, such as the presence of terrestrial molluscs and the nature of pollen, are used to explain past climatic changes. The type of sporomorphs present in a certain area can help explain past climatic and depositional environments. Knowledge about the living environment of ostracodes helps decifrate landscape characteristics over time. Their presence or absence in stratigraphic profiles can inform about the type of depositional environments (Breman, 1981).

5.2 DEVELOPMENT OF THE COCHABAMBA BASINS

5.2.1 Tectonics

There are two theories regarding the origin of the Cochabamba basins. According to Hoek et al. (1906), Troll (1929), Jordan (1967) and Alhfeld (1970, 1972), the basins are tectonic grabens, limited by normal faulting in the northern and southern parts and by reverse faulting on the western side. In contrast, Lavenau (1986) postulates a 'pull-apart' mechanism creating half-graben basins during the occurrence of strike-slip faults (fig. 5.1).

The basins are Miocene and Pliocene-Pleistocene age, related to ESE- trending strike-slip and normal faults. The fault systems cut across folded lower Paleozoic to Eocene rocks. Fault activity appears to have begun prior to the early Miocene (Kennan et al., 1995). According to K-Ar (potassium-argon) dating of tuffs in the Sacaba, Punata and neighboring Parotani basins, Kennan et al.(1995) concluded that the basins in the Cochabamba area are of different ages (fig. 5.2). The Parotani tuff suggests that sedimentation began in the early Miocene and not the Pliocene as previously considered by Lavenau et al.(1979). The sediments are folded and lie unconformable on Cretaceous and Paleozoic rocks, suggesting pre-early Miocene deformation. Gentle folding occurring in the Sacaba basin is probably related to a sinistral strike-slip movement of the Tunari fault and said to be younger than Pliocene.

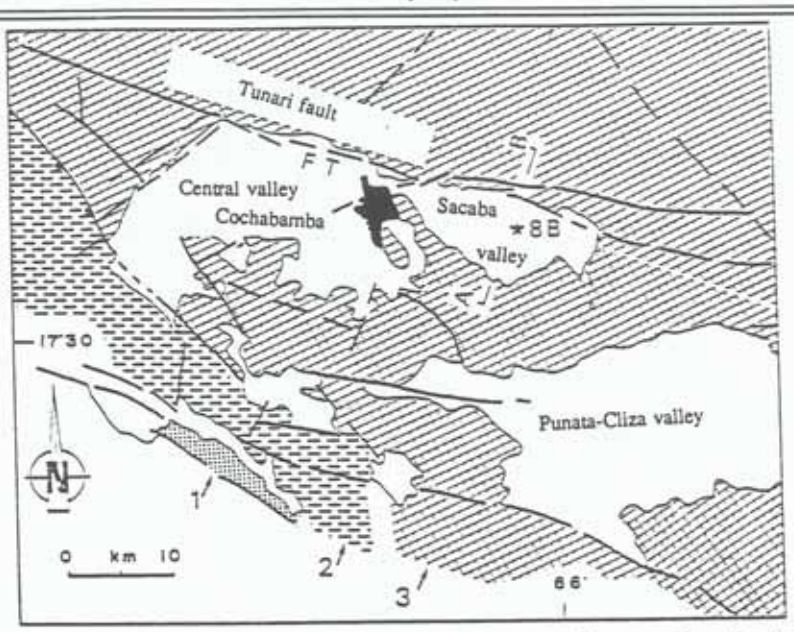

Diagram of predominant fault direction (N 41°)

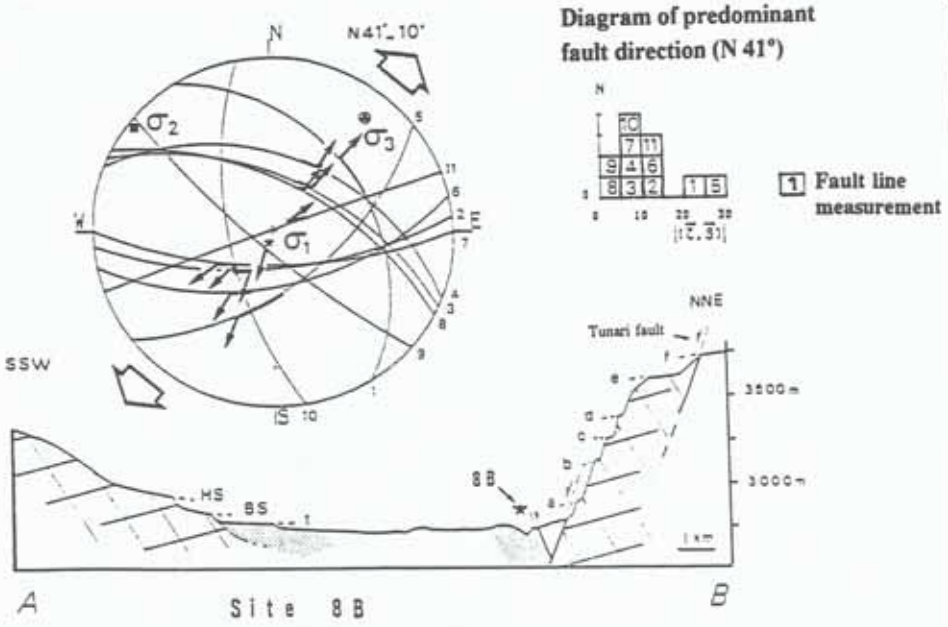

1 Fault line measurement

LEGEND

1. Cenozoic
2. Mesozoic
3. Paleozoic
Fault lines
AB: Cross section

a,b,c,d --: Six different erosion surfaces along the active Tunari fault
HS,BS,t: Three erosion surfaces, S. of Sacaba.
8B* : Site selected for faults measurements
O_1,O_2,O_3 : Direction of fault compression

Fig. 5.1: Half-graben origin of the Cochabamba basins (Lavenau, 1986)

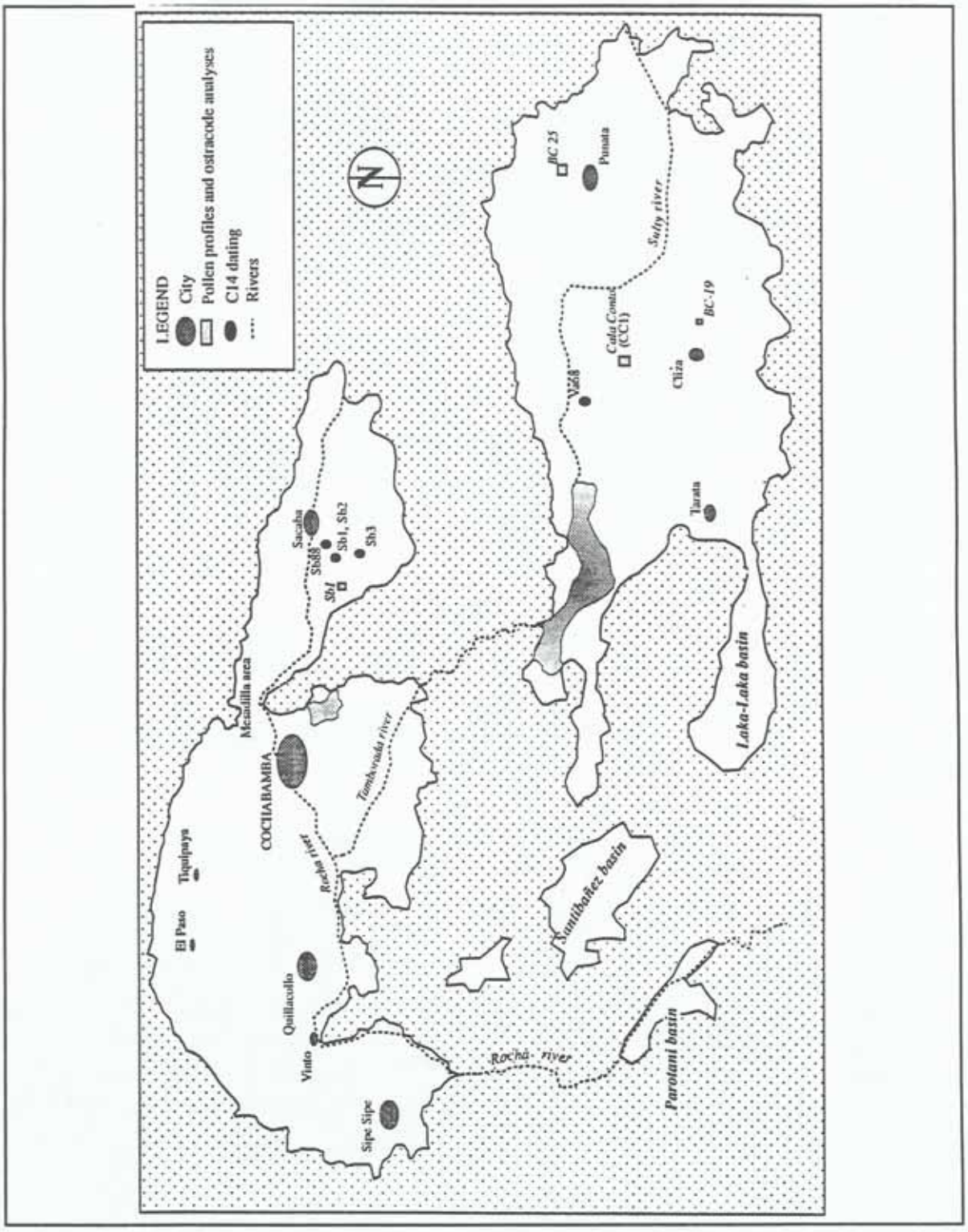

Fig. 5.2: Location of the basins and radiocarbon dating sites

Folding and faulting continued during the Quaternary. The Plio-Quaternary lacustrine and fluvio-lacustrine sediments of the Sacaba basin show evidence of compressed ENE-WSW to NNW-SSE tectonism. Faults cutting the lower Pleistocene valley fills near the Santibañez basin suggest that faulting probably continued around the western Cochabamba basin while the Sacaba basin fill onlaps the basin margins at the southeastern part and is unfaulted (Mancilla, 1979; Lavenau, 1986; Kennan et al., 1995).

Sequential faulting is also confirmed by the existence of at least three erosion surfaces located at 3700, 3400 and 2900 masl in the northern part of the Cochabamba and Sacaba basins (Veicht, 1992). Mancilla (1979) distinguishes two pediments in the northern part of the Sacaba basin. The upper one, located between 2800 and 2900 masl, is a non-continuous surface of reduced extent, while the lower, more continuous pediment dominates over the basin. The Tunari fault, which marks the northern border of the Cochabamba-Sacaba basins, shows evidence of activity during the Quaternary, with a strong uplift of the northern block. The fault is masked by several active alluvial fans. Mancilla (1979) mentions an echelon topography resulting from the adjustment to the Tunari fault activity in the northern part of the Sacaba basin, where it communicates with the Cochabamba basin. Red paleosols with calcareous crusts, buried by colluvio-alluvial sediments, characterize these echelon surfaces.

5.2.2 Quaternary glaciations and climatic oscillations

Several glaciations occurred in the Bolivian Andes cordillera during the early and middle Pleistocene, starting about 3.3 Ma ago with the Patapatani glaciation (table 5.1). Different authors hypothesize 3 to 5 glaciations, but clearly identifiable and agreed upon are only the last three glaciations called respectively Choqueyapu II, Choqueyapu I and Sorata. Radiocarbon dating has established an approximate age of 40000 BP for Choqueyapu I and 16000 BP for Choqueyapu II (Argollo, 1982). Mercer et al.(1977) and Seltzer (1990) also agree on a late Pleistocene glacial advance in Bolivia after 27000 BP and perhaps even later than 16000 BP. Several smaller glacial advances and retreats appear to have occurred between 12000 and 10000 BP. There is little evidence of renewed glacier activity during the early Holocene, but several periods of minor glacial pulsations occurred during the late Holocene as summarized in table 5.2.

In the Cochabamba basins, glacial phases are related to the formation of moraines in the mountains and fluvio-lacustrine or glacio-lacustrine sedimentation in the valleys. During the glacial retreats, lacustrine sediments predominate in the valleys. During the Pleistocene period, the basin bottoms were never glaciated but the Tunari range was. In the Cochabamba Cordillera, interstadial sediments were found below a moraine deposit of the Choqueyapu II period, dated from 30000 to 16000 years BP (Servant, 1978).

Table 5.1: Glaciations in Bolivia (modified from Veicht, 1992)

AGE	AUTHOR					DATE (Years BP)
	Troll (1935)	Dobrovolny (1962)	Servant(1977), Ballivian et al. (1978), Argollo (1982)	Lauer et al. (1986)	Servant et. al (1978)	
Upper Pleistocene	---	Choqueyapu II	Choqueyapu II	Chacabaya	Tauca	16000 - 11000
	moraines	Choqueyapu I	Choqueyapu I	Canlaya	Minchin	45000 - 40000
Middle Pleistocene	moraines	Milluni	Sorata	Charazani	Ballivian	--
Lower Pleistocene	---	---	Kaluyo	---	---	--
	---	Calvario	Calvario	---	---	1.6 Ma
	---	Patapatani	--	---	---	2.8-3.3 Ma

Table 5.2: Selected radiocarbon and palynological data from Bolivia and Peru.

PERIOD	CLIMATIC CHARACTERISTICS	LOCATION	TECHNIQUE USED FOR INTERPRETATION	AUTHOR
UPPER PLEISTOCENE				
Choqueyapu II Interstadial or interglacial ? Choqueyapu I or Sorata Interglacial	H4(0-55m): dry and cold H3(55-105m): humid and warm H22(105-135m): warmer and wetter H21(135-165): dry and cold H1 (165-260m): humid and warm	Punata-Cliza valley (2700 masl)	A pollen profile	Graf, (1982)
Late Pleistocene-Lower Holocene Upper Pleistocene C1: postglacial C2: interstadial C3: Choqueyapu II Interglacial Choqueyapu I	D (0-20m): warm C (65-150m): *C1*: cold and dry; *C2*: humid; *C3*: cold B (150-210m): warm A (210-250m): cold	Central Cordillera (Chacaltaya, Monte Blanco, Cumbre Yungas, approx. 4750 masl) Punata-Cliza (2600 masl)	Three pollen profiles (Central Cordillera) and well logs (Punata-Cliza valley)	Graf, (1977)
43000 - 24000/12000 BP	Colder and drier: apparent decrease of the east Andean forest	Laguna Junin	Pollen profile and radiocarbon dates	Hansen, (1984)
12500 - 10000 BP : Tauca episode prior 28000 BP: Minchin episode	Wet: 50% more rainfall than present Wet: 75% more rainfall than present	Peruvian-Bolivian Altiplano (3800 masl)	Geomorphic evidence and heat and water budget calculations	Hastenrath and Kutzbach,(1985)
  Interglacial Interglacial	Dry: absence of ostracodes Dry: dominance of *Heterocypris* Humid: abundance of *Limnocythere* Less humid: dominance of *Heterocypris* Humid: dominance of *Limnocythere*	Punata-Cliza and Sacaba valleys (2500 -2700 masl)	Presence of ostracodes (*Limnocythere and* *Heterocypris*) in two drill holes. *Limnocythere:* deep water *Heterocypris*: shallow water (lagunary)	Breman, (1981)
HOLOCENE				
10000 - 7500 BP 7500 - 5500 BP 5500- 3500 BP 3500 BP - present	Dry and cold Moderately humid and warmest period Warm and wet Quite humid high mountain steppe	Central Cordillera (Cotapampa, 4450 masl; Laguna Katantica, 4820 masl)	Two pollen profiles	Graf, (1981)
Postglacial: prior 7700 BP 7700 - 3650 BP 3650 BP	Humid Dry: decrease in precipitation Increased humidity	Titicaca lake (4000 masl)	Sedimentological and paleontological analysis Radiocarbon dating of carbonate sediments	Wirrmann et al., (1987)
7000-5000 BP 3900-1400 BP	Dry: the dense Amazonian forest in SE Bolivia disappeared	Amazonian forest , SE Bolivia		Servant et al., (1981)
8812 ± 45 BP	Glacier advance	Canuma valley, Apolobamba Cordillera, Bolivia	Radiocarbon dating of a buried soil	Lauer et al., (1986)
3560 ± 100 3470 ± 215	Glacier advance after 3560 BP Glacier advance after 3470 BP	Glacier Tulparaju, Glacier Ocshapalca Cordillera Blanca, Peru	Radiocarbon dating of a buried soil Radiocarbon dating of a buried soil	Röthlisberger, (1987)
2375 ± 35 BP	Glacier advance	Minas Raura, Cordillera Huayhuash, Peru	Radiocarbon dating of compressed peat	Clapperton, (1983)
1290 ± 85 BP (upper Holocene) 535 ± 105 BP	Glacier advance before 1300 BP and 500 BP	Nevado Huaytapallana, Peru	Radiocarbon dating of peats (bottom tier)	Seltzer, (1987)

Pollen analysis was used to reconstitute past climatic oscillations. Graf (1982) distinguishes four zones namely H1 (260-165m), H2 (165-105m), H3 (105-55m) and H4 (55-0m) in a pollen profile located in the Punata-Cliza valley (fig. 5.2, code CC1). Dry and cold H2 and H4 zones are attributed to the last two glacial stages. They could correspond to the Choqueyapu I and II glaciations or even to an earlier phase, the Sorata glaciation. Humid and warm interglacial conditions are reflected by the sporomorphs present in zones H1 and H3.

The analysis of another pollen profile (fig. 5.3), located in the proximal part of the Punata fan, reveals also the occurrence of four zones (Graf, 1977). The upper 20m represent the postglacial period, showing Holocene climatic fluctuations. It follows a zone representing the last glacial period, subdivided in cold and dry postglacial, warmer and humid interstadial and the cold glacial Choqueyapu II. The last interglacial corresponds to zone B and the Choqueyapu I glaciation to zone A.

Interglacials and insterstadials are reported as warm and humid periods, when pedogenesis occurred. The glacial advances were characterized by colder and dry conditions, with more sedimentation and frequent soil burial. The late Pleistocene was a moist and warm period (Servant, 1977; Graf, 1977; Hastenrath et al., 1985; Veicht, 1992). Based on the interpretation of the pollen profiles, Graf (1981) reports the early Holocene as dry and cold. These conditions are also supported by Lauer et al.(1986) on the basis of a glacial advance. In contrast to Graf's hypothesis, Wirrmann et al.(1987) assume humid conditions based on a higher stand of the Titicaca lake, caused by a precipitation increase (table 5.2). Additional disagreements regarding the climatic conditions during the middle and early part of the lower Holocene are shown in table 5.2. The interpretation of two pollen profiles located in the Central Cordillera of Bolivia allowed Graf (1981) to conclude that the middle and early parts of the lower Holocene were moderately humid and corresponded to the warmest postglacial period. In contrast, Wirrmann et al. (1987) and Servant et al. (1981) report dry conditions for the same period based on the low stand of the Titicaca lake and the diminution of the Amazonian forest in southeast Bolivia.

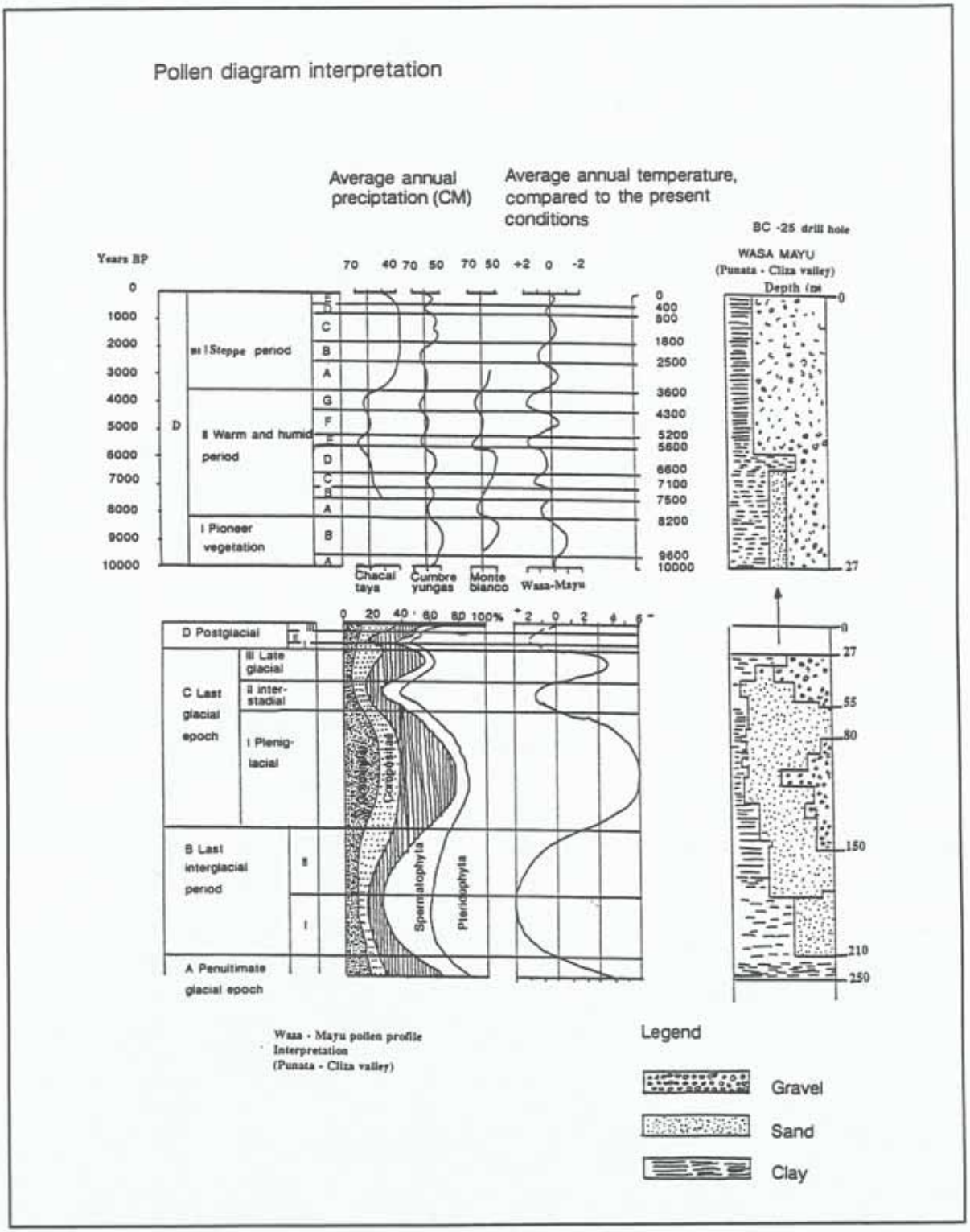

Fig. 5.3: Pollen profile BC-25 from the Punata-Cliza basin (after Graf, 1977).

5.2.3 Sedimentary stratigraphy and depositional conditions

(1) The Cochabamba basin

According to geophysical studies, the thickness of the Plio-Quaternary sediments in the Cochabamba basin is estimated in the range of about 900 to 1400 m (Geobol, 1970; Semapa, 1994). Four consecutive resistivity zones, correlated with different depositional materials, were identified: (1) the resistant Paleozoic substrate of shales and quartzite (500 Ωm, ohm/mm); (2) lacustrine deposits (5 - 50Ωm) less than 700 m thick, composed of fluvio-lacustrine and moraine sediments from the interglacial periods, whose resistivity decreases towards the southern part of the basin, reaching minimum values in clay deposits (2Ωm); (3) alluvial deposits less than 650 m thick, composed of heterometric gravels and cobbles with resistances around 150 Ωm but decreasing in southern direction ; (4) a top layer 20 to 50 m thick, of heterogeneous composition and variable resistivity.

Materials in the southern part of the Cochabamba valley (Vinto and Sipe-Sipe) are coarser than in its eastern part. There is also a decrease in the thickness of the Plio-Quaternary sediments. Only towards the southwestern part, in the region of the Kollpamayu brook, thick layers of fine sediments predominate as indicated by the geophysical profiles carried out by Geobol (1977) and Semapa (1994). These fine sediments are the weathering products from the Cretaceous-Tertiary rock outcrops present in the zone. A substratum dorsal arises in the vicinity of Vinto, which might have limited the extension of the former lake towards the northwest. On this basis, Veicht (1992) hypothesized that lacustrine conditions never existed in the western part of the Cochabamba basin.

The piedmont stratigraphy of the Cochabamba basin includes heterometric glacio-fluvial sediments interdigitating with finer lacustrine sediments in the deeper zones (fig. 4.3). The wedge-shaped depositional layers, with the thickest part closer to the mountain front and the thinnest part away from it, suggest a major uplift of the mountain range prior to or during the initial fan deposition (Lece, 1990). Most of the old fans located on the northern belt are buried by recent alluvial fans and depositional glacis, indicating continued uplift over time. In contrast, such old fans predominate along the western and northwestern fringe of the basin, suggesting decreased tectonic activity in this area respect to the northern faulted block. Some fans, such as the Llave fan, have deep stream trenches exhibiting representative stratigraphic sequences of the upper Quaternary. Thick layers of heterogeneous, chaotic material, including large boulders (4-5m diameter), cobbles and gravels within a sandy and silty matrix indicate a glacio-fluvial origin, in connection with the Pleistocene glaciations of the Tunari Cordillera (fig. 5.5). Red buried soils are locally intercalated with the fan deposits.

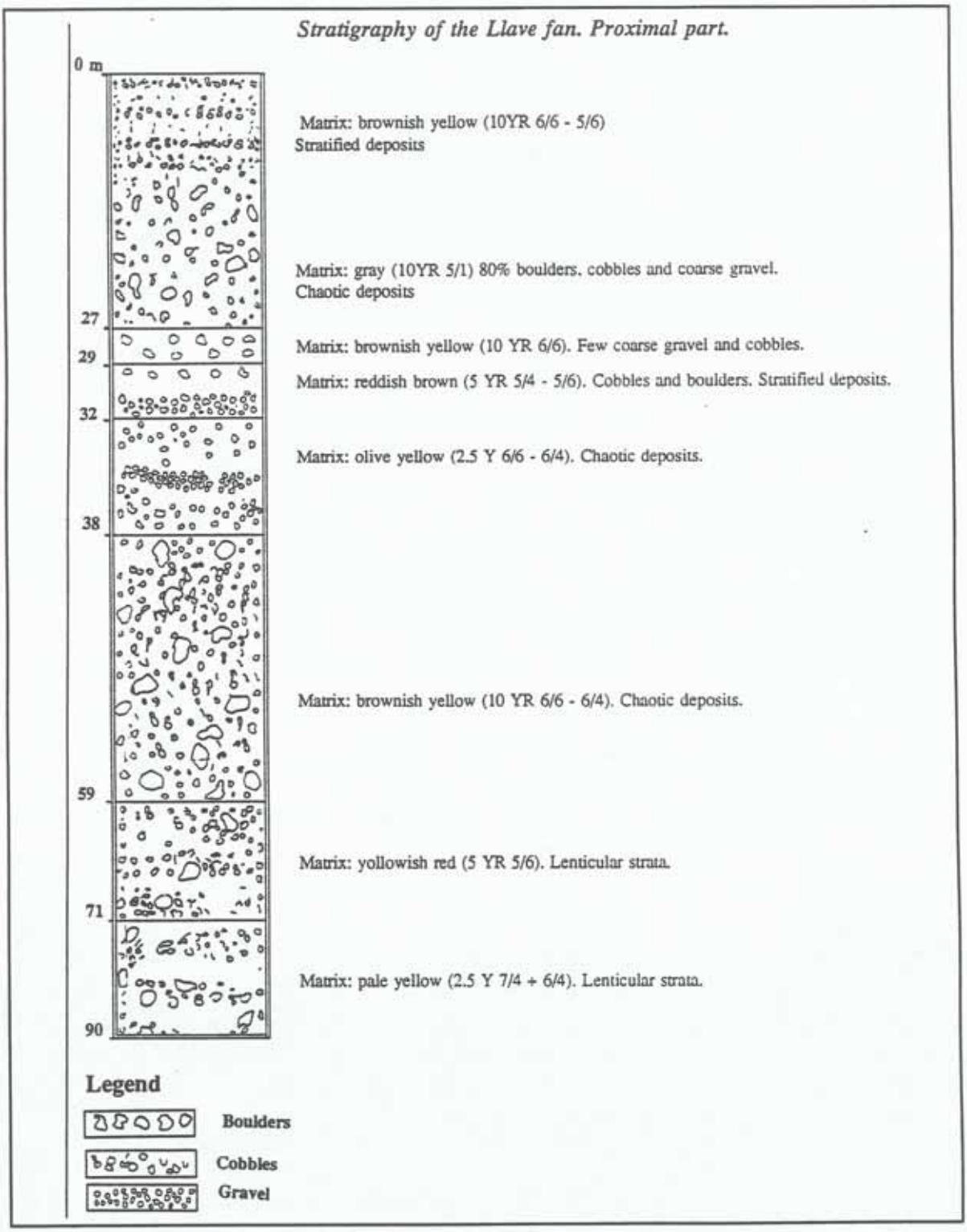

Fig. 5.4: Simplified stratigraphy of the proximal part of the Llave fan (Cochabamba valley).

(2) The Sacaba basin

In general, the Plio-Quaternary stratigraphy of the Sacaba basin is similar to that of the Cochabamba basin (Geobol, 1977; Semapa, 1994). The stratigraphic sequence, from the bottom to the top is as follows (fig. 5.5):

Unit 1: a transitional zone between the Paleozoic basement and the Quaternary sediments, composed of silty clayey, loamy and gravelly silt lacustrine deposits, mixed with alluvial and moraine materials in the base.

Unit 2: fluvio-lacustrine sediments overlying the transitional unit 1, including two subunits: (2a) clayey sediments without gravel lenses (also occurring in the southern part of the Cochabamba basin); (2b) lagunary sediments consisting of a silty matrix with gravelly sand lenses.

Unit 3: alluvial and colluvio-alluvial deposits of recent and presently active alluvial fans located near the mountain front, composed of heterometric gravels and cobbles in a sandy or sandy-clayey matrix, and lying in tectonic discordance on the underlying unit 2b (Semapa, 1994).

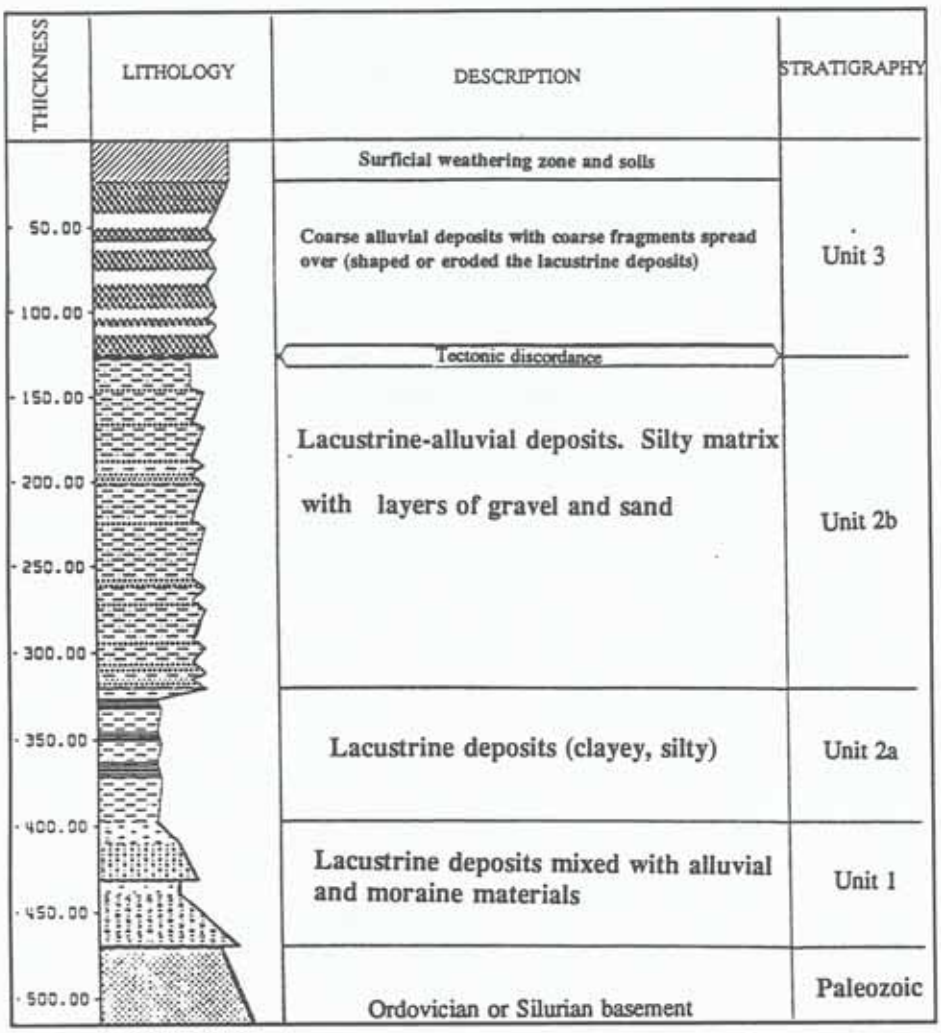

Fig. 5.5: Stratigraphic section of the Quaternary deposits in the Sacaba valley (Semapa, 1994)

Local stratigraphies might be slightly different from the general sequence. For example, the drill Sb1 located southwest of Sacaba (fig. 5.6) presents a sequence of lagunary and alluvial facies overlying clayey lacustrine sediments. In the southern part of the Sacaba valley, a silty clay top layer overlying glacis deposits is a loess-like material which might have deposited in a shallower lagunary environment (from Sb3 to Sb4 in figure 5.6).

Geophysical studies confirmed the existence of a connection between both basins, filled with Quaternary sediments. However, the lithologic sequences are slightly different, in particular the depth to the ostracode-rich lacustrine sediments which are nearer to the surface in the Sacaba basin (Geobol, 1977). This suggests an earlier desiccation of the latter, resulting from either tectonics or a climatic change causing deep dissection in the Mesadilla area, which connects the Cochabamba and Sacaba basins (fig. 5.2).

Breman (1981) analyzed three drilling cores from the Quaternary sediments filling the Punata-Cliza and Sacaba valleys to identify ostracodes (fig. 5.2). He found two genera: *Limnocythere*, whose representatives live on the bottom of fresh or brackish water lakes, and *Heterocypris*, a genus characteristic of shallow lagunary environments. Limnocythere dominates in the Punata-Cliza basin, while both species are present in the Sacaba basin with Heterocypris increasing upwards. Ostracode variations reflect variations of the lake level. An increase of Heterocypris, proper of lagunary conditions, correlates with low water stands and dry climatic conditions, whereas a predominance of Limnocythere relates to a rising lake level due to precipitation increase. This suggests that lacustrine conditions persisted in the Punata-Cliza valley longer than in the Sacaba basin, where shallow lagunary conditions predominated.

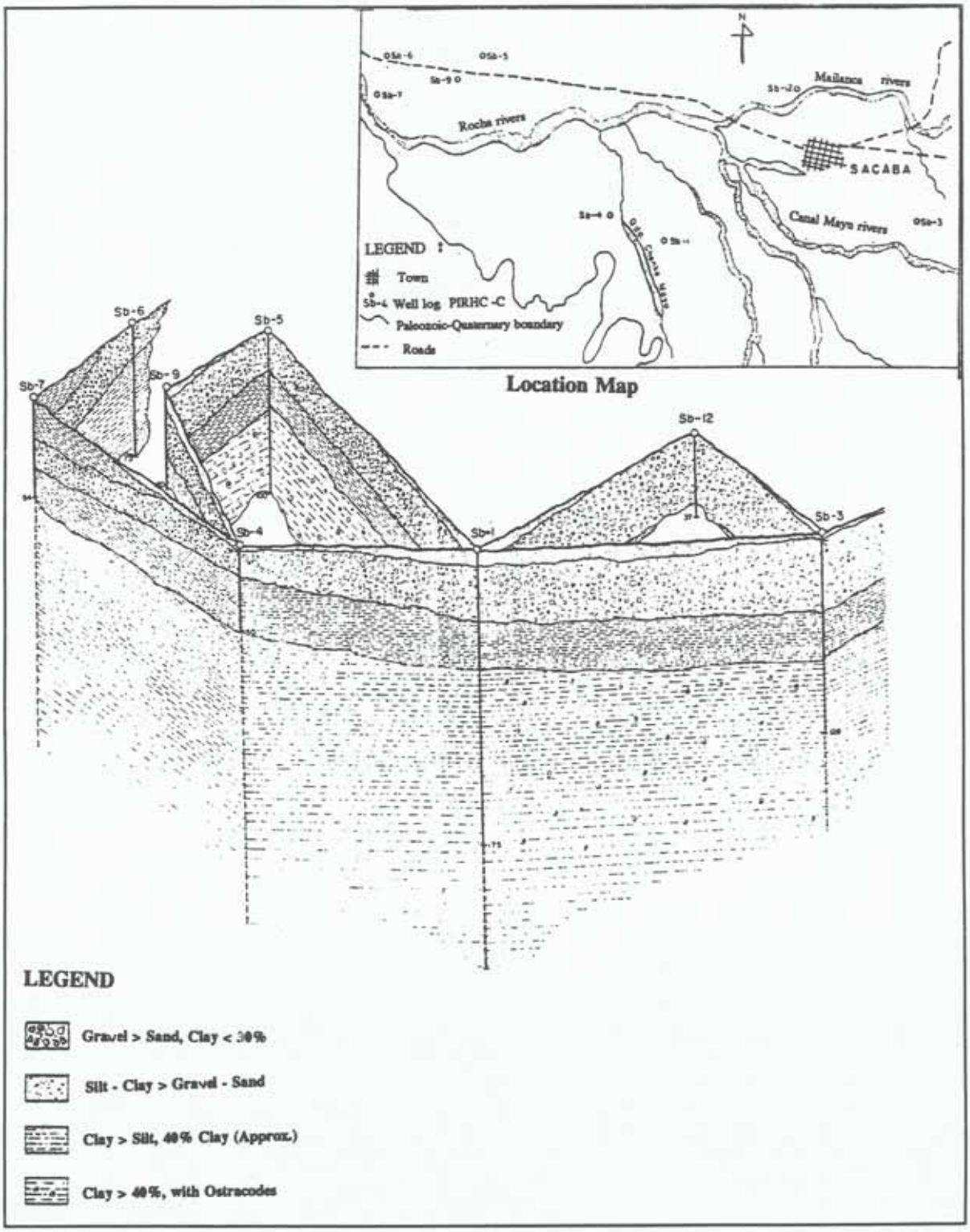

Fig. 5.6: Isometric diagram of the southern and central parts of the Sacaba basin (Mancilla, 1979).

(3) The Punata-Cliza basin

Geophysical studies were also carried out in the Punata-Cliza basin (Geobol, 1977). Low resistivity values were found along the Sulty river in western direction towards the Angostura area, related to the clayey sediments of the playa zone.

The isometric diagram of the northeastern part of the valley shows actual depositions on the left proximal part of the Punata fan and thick recent depositions on the proximal and central parts (fig. 5.7) . The distal part of the glacio-fluvial fan is composed of gravels within a 20 to 40% clay matrix, subsequently buried by lacustrine-lagunary sediments containing more than 40% clay. Inverse sediment sequences can be found because of base level fluctuations of the former lake. The 270 m deep stratigraphic profile of the well log BC-25 (Geobol, 1977), crossing the proximal part of the Punata fan, shows a 100 to 150 m thick fluvio-glacial deposit overlying lacustrine clays. There is no evidence of large boulders as in the Llave fan. Two more recent alluvial sequences, corresponding to Quaternary climatic fluctuations, can be identified (Geobol, 1977; Mancilla, 1979).

The Tarata fan evolved similarly to the Punata fan. The isometric diagram exhibits a sequence of thick lenses of gravel and sand in a 20% clay matrix, overlying lacustrine clays. The alluvial deposits, in turn, were buried by a subsequent rise of the lake level (fig. 5.8, well log BC-13).
Sandy and gravelly alluvial facies characterize the glacis overlying the ostracode-rich clayey lacustrine sediments in the southern part of the basin (fig. 5.8). The top layer of the drill located near Cliza (BC-19) has an alluvio-lagunary facies, whereas the stratigraphy of the proximal part of the Punata fan (BC-25) exhibits a depositional sequence of fluvio-glacial and alluvial facies (figures 5.7 and 5.8).

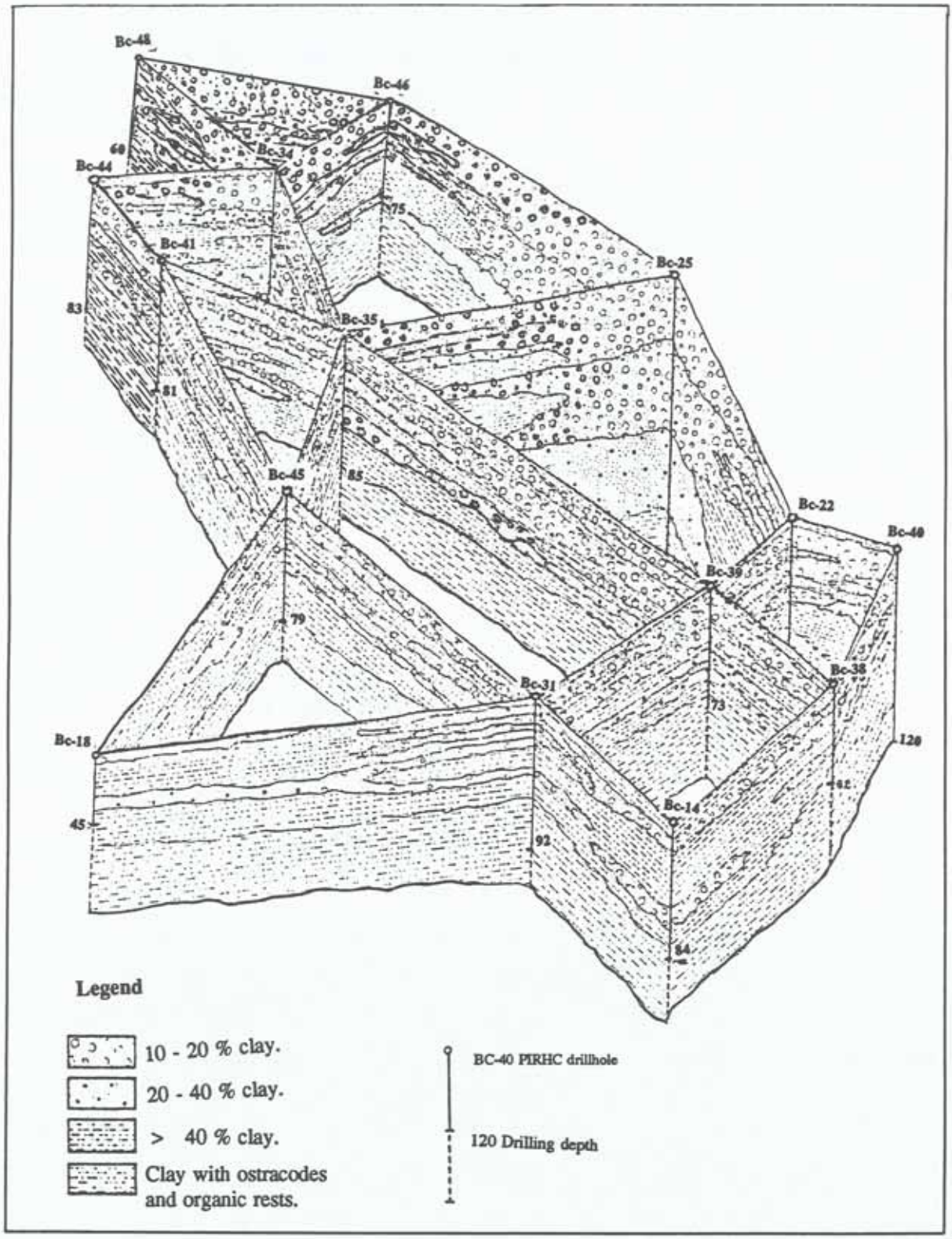

Fig. 5.7: Isometric diagram of the NE part of the Punata-Cliza Valley (Geobol, 1977)

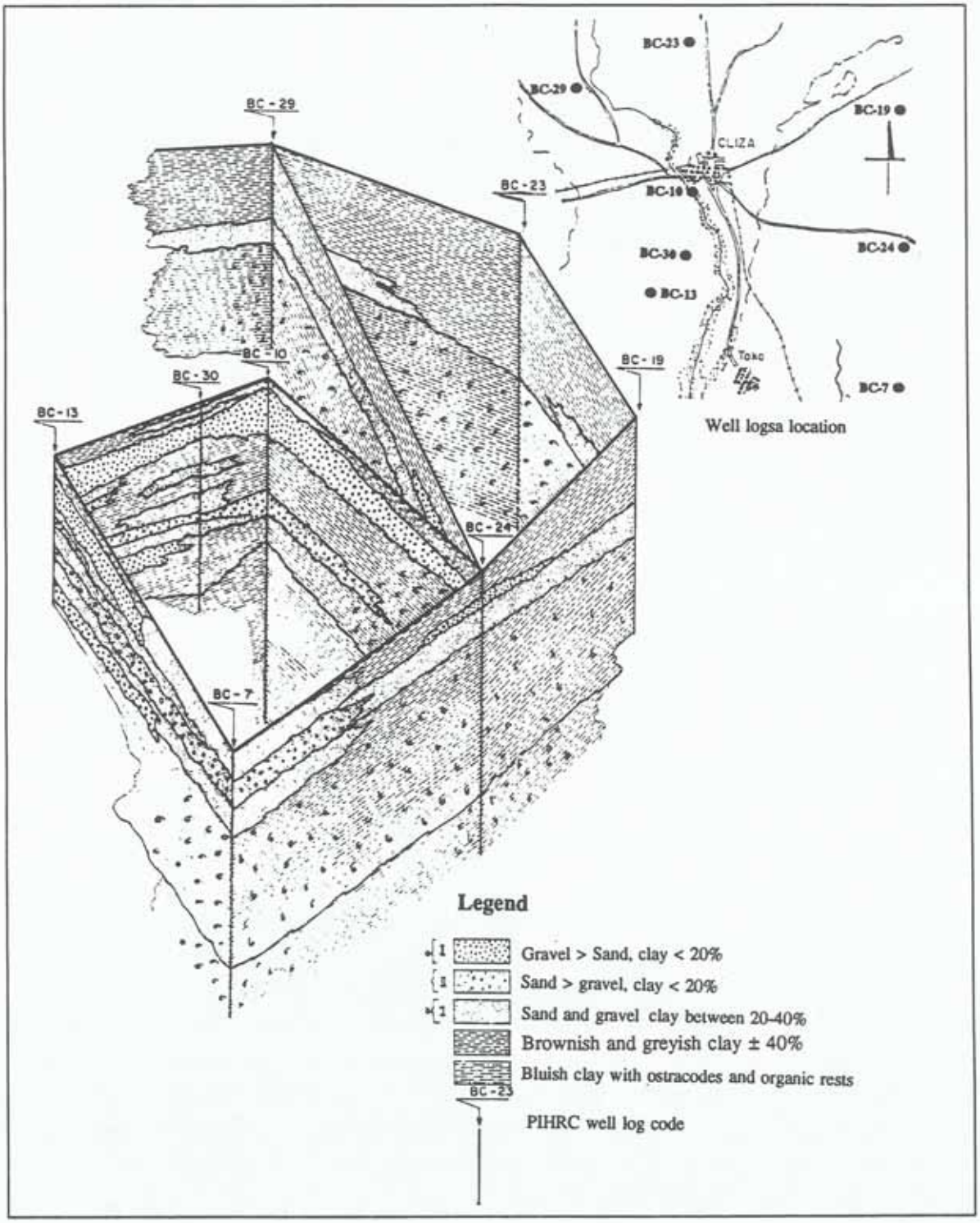

Fig. 5.8: Isometric diagram of a glacis in the southern part of the Punata-Cliza valley (Jordan, 1977)

A pollen profile from the lagunary flat of the Punata-Cliza Valley, in the vicinity of Cala Conto (fig. 5.2, code CC1), suggests slow siltation of the former lake due to the presence of vegetation indicative of locally humid conditions and the absence of ostracodes in the silty clayey deposits from 65 m upwards (Graf, 1982). It is also hypothesized that the silty clay deposits could be loess-like material, deposited in a shallow lagunary environment. The upper 55 m are poor in pollen from the local vegetation such as Gramineae, but rich in sporomorphs transported over long distances. Since local pioneer vegetation (e.g. Chenopodiaceae and Amaranthaceae) dominate in the uppermost pollen zone, Graf (1982) concluded on a dry and cold steppe climate prevailing during the lower Holocene. A second pollen profile (BC-25), located in the proximal part of the Punata fan (fig. 5.2) shows that lacustrine conditions dominated the Punata-Cliza basin during the penultimate glacial period and that the lake started retreating during the last glaciation around 16000 BP (Graf, 1977).

(4) Correlation of paleoenvironments

The bottom of the depositional sequence in the central parts of the three valleys is composed of lacustrine clays with inclusions of ostracodes, tuffs and charcoal, in contact with the Paleozoic basement. The presence of 2.2 Ma-old folded tuffs in the Sacaba basin (Kennan et al., 1995) and the identification of Pliocene Glyptodont fossils in the lacustrine clays bestow a Pliocene-lower Pleistocene age to the early lacustrine sediments (Mancilla, 1979; Marshall et al., 1992).

Correlation of the core drills studied by Breman (1981) with past climatic changes suggests that lagunary conditions dominated in the Sacaba basin during the last glaciation. Similar conditions can be hypothesized for the Cochabamba basin in the late Pleistocene, based on the finding of a human fossil, dated 13200 BP, within fine silty loam lagunary sediments in the southern flat area of Laguna Pampa (UMSS-ORSTOM, 1981). A different situation occurred in the Punata-Cliza valley, where pollen profiles suggest that the valley was drained after the last glaciation called Choqueyapu II (Graf, 1977 and 1982).

The stratigraphy of the well logs located in the Punata fan shows evidence of lake retreat (fig. 5.7). During the Choqueyapu II period, the lake retreated allowing the deposition of glacio-fluvial sediments relatively far from the mountain front. Lacustrine conditions remained only in the center of the basin. Unlike the Cochabamba basin (fig. 4.3), glacio-fluvial deposits are not in contact with the Paleozoic basement but overlay lacustrine clays, and the depositional layers are thinner than those of the Llave fan. Subsequently, the lake rose again burying the distal part of the Punata fan, as shown in the stratigraphy of the BC-18 well log (fig. 5.7). This wetter period could correspond to the late Pleistocene, coinciding with an estimated 50% rainfall increase in the Altiplano around 12500-11000 BP (Hastenrath et al., 1985). Assuming the hypothesis supported by Servant (1981) and Wirrmann et al.(1987) on dry middle Holocene conditions and drainage through the Tamborada river, a postglacial desiccation of the former Punata-Cliza lake is very likely (Graf, 1983; Veicht, 1992).

5.2.4 Organization of the drainage network

The tectonics greatly controls the overall organization of the drainage network in the three basins. But, local drainage patterns are more influenced by lithology and topography. The northern mountain front and the southern part of the basins have a dendritic drainage network revealing uniform rock composition. Centripetal drainage characterizes the lowlands of the valleys.

The former lakes of Sacaba and Cochabamba valleys have been drained by the Rocha river, whose position was controlled by the activity of the alluvial fans formed along the northern mountain front. South of Vinto, the alluvial deposits from the highlands of the western part of the Cochabamba basin displaced the Rocha river towards the east side. The Vinto fault probably started its tectonic activity during the Pliocene, draining part of the former lake of Cochabamba (Veicht, 1992). Tectonism and/or Quaternary climatic oscillations caused intensive linear erosion of the Rocha river and its tributaries.

In the Laba-Laba Alta area of the southern Sacaba basin, alluvial terraces located 10 to 12 m higher than the present river base level, testimony of past intensive dissection. Many brooks and ephemeral streams such as the Loro Mayu, Canal Mayu and Crespo Mayu, draining south and southeast of the Sacaba basin, evidence past intensive dissectional power leading to the excavation of deep vertical bed walls as high as 9 to 10 meters (figure 5.9).

The Tamborada river established communication between the Cochabamba and the Punata-Cliza basins after the last glaciation. Neotectonic events helped the Tamborada river dissect the Silurian shales and sandstones in the Angostura area. Many other waterways show adjustments to tectonic activity during the Quaternary (Semapa, 1994; Mancilla, 1977)

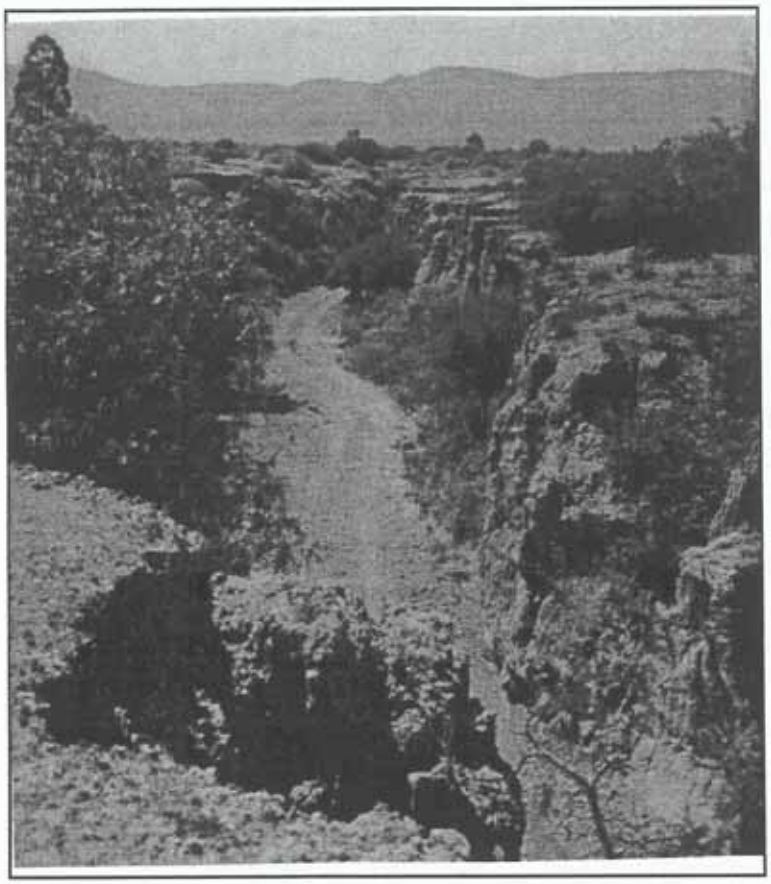

Fig. 5.9: Evidence of past intense erosional energy of presently ephemeral streams. Canal Mayu river, south of Sacaba.

5.3 GEOMORPHIC UNITS AND LANDSCAPE EVOLUTION

Geoforms such as alluvial fans, glacis and lagunary flats provide evidence of sedimentary sequences in the geological record. Their location and dynamics reflect the relationship between sediment generation and transport capacity. High sediment supply may be related to climatic changes or tectonic uplift and renewed erosion.

5.3.1 The alluvial fans and glacis

Three fan generations, namely old dissected, recent and presently active fans, of different age and origin were identified in the piedmont landscape. The oldest fans are located closer to the mountain front and some remnants are preserved at higher elevations. They were exposed to different processes over time, resulting in polygenic fans (e.g. the trenched Llave fan). Recent fans are located along active fault lines. Actual fans are either distally aggrading or overlap recent and old fans along the mountain front (fig 5.10).

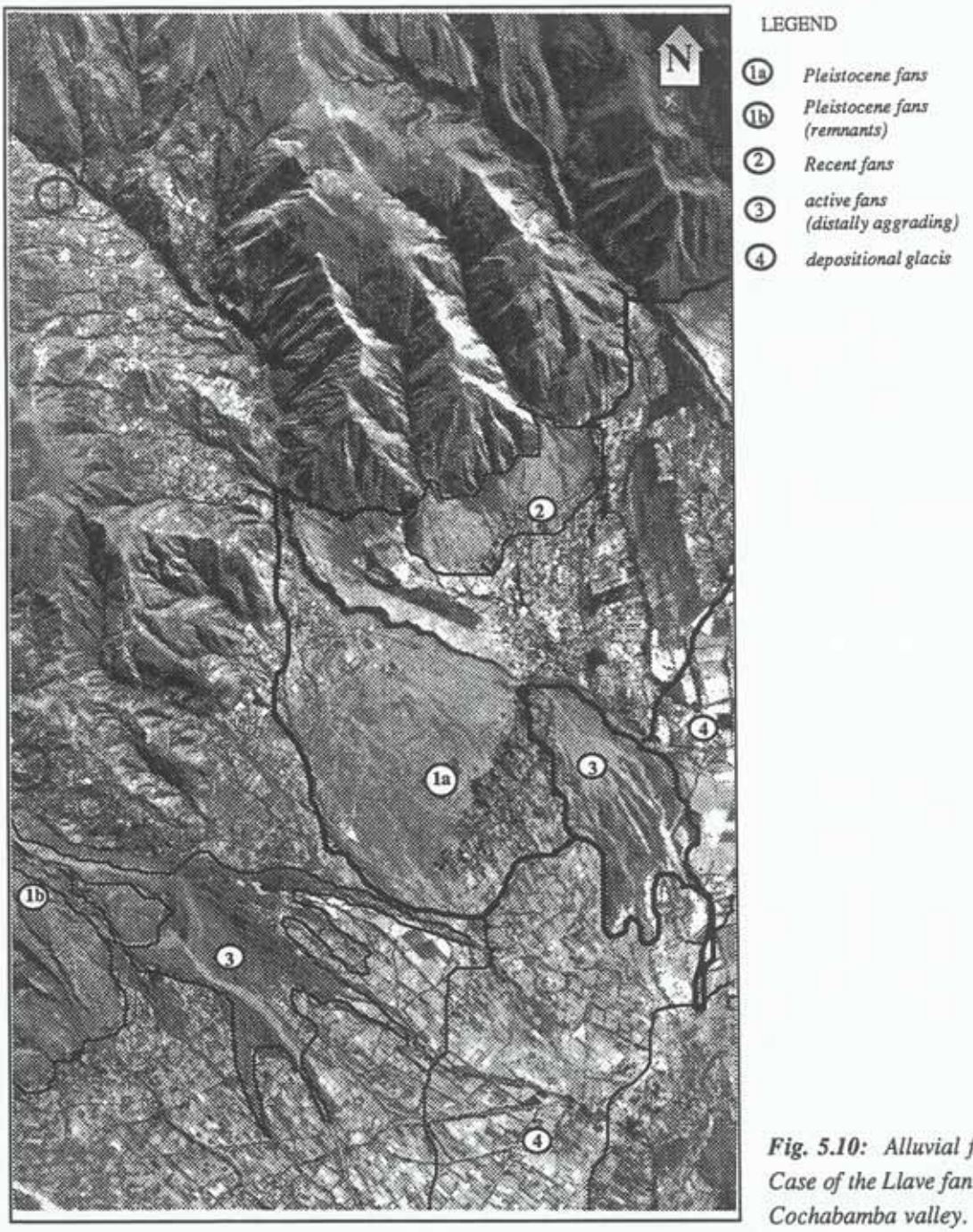

Fig. 5.10: Alluvial fan generations. Case of the Llave fan, NW part of the Cochabamba valley.

(1) The old dissected fans

The Llave fan, located in the northwestern part of the Cochabamba valley, is characterized by a deep and permanent fanhead trenching of about 90 m depth. The strongly sloping proximal part is inactive, receiving no further deposits. The fan channel slope is less than that of the fan surface, which ranges from 7 to 10% slope gradient; the two longitudinal profiles converge towards an intersection part where the

channel emerges onto the fan surface, burying its distal part and spreading the sediments throughout. Aerial photographs show evidence of channel migration of these active fans (fig. 5.10). Deep fanhead incision, where the youngest deposits are located down-fan, is mainly related to a reduced rate of tectonic uplift or climatic changes inducing accelerated stream incision (Bull, 1961).

Old dissected fans and some erosional surfaces located at higher elevations (3700, 3400, 2900 masl) in the Cochabamba and Sacaba basins are reported to possess well developed red buried Alfisols, with calcrete crust in their subsoil and glacial parent material (Mancilla, 1979; Guamán 1993). Their yellowish red (5YR 5/6) colour is redder, more rubefied than that of Holocene soils. The presence of calcium carbonate crusts and nodules suggests alternation of wet and dry periods. Such soils might have developed under warmer and moister conditions than the present ones. In the Andes, the late glacial-lower Holocene, between 15000 and 8000 BP, is considered the last favorable period for their formation (Servant, 1977; Graf, 1981; Veicht, 1992). Aridity increased during the lower Holocene, as proved by the lower standing of the Titicaca lake (Wirrmann et al., 1987). These soils might therefore be placed within the late Pleistocene, developed from fluvio-glacial sediments of the last glaciation, identified by Veicht (1992) to be Choqueyapu II. This allows also to conclude that old dissected fans of glacio-fluvial origin are mostly of late Pleistocene age. But some older fans, such as the Payrumani fan, are in stratigraphic contact with Choqueyapu I moraine deposits from the penultimate glaciation.

Similarly, the Punata fan in the northeastern part of the Punata-Cliza basin is also of glacio-fluvial origin (fig. 5.11). Its upper catchment area was in contact with moraine sediments identified on the Tiraque, Pucara and La Villa highlands. Well log stratigraphy, soil development and terrain surface features show evidence of an evolution over time different from that of the Llave fan. The Punata fan has no deep fanhead trenching, the slope gradient ranges from 2 to 1% in its proximal part, decreasing to less than 1% in the central and distal areas, and it is fossilized by actual and recent fans. The river channel is braided, shallow and wide. Hooke (1967) suggests that such a channel type results from intrinsic causes, related to short-term random variations in the process-form relationships within the fan environment. Fan aggradation can be caused by climatically controlled increases in sediment production, followed by fan trenching when sediment supply is depleted (Eckis, 1928; Bull, 1964a and 1964b).

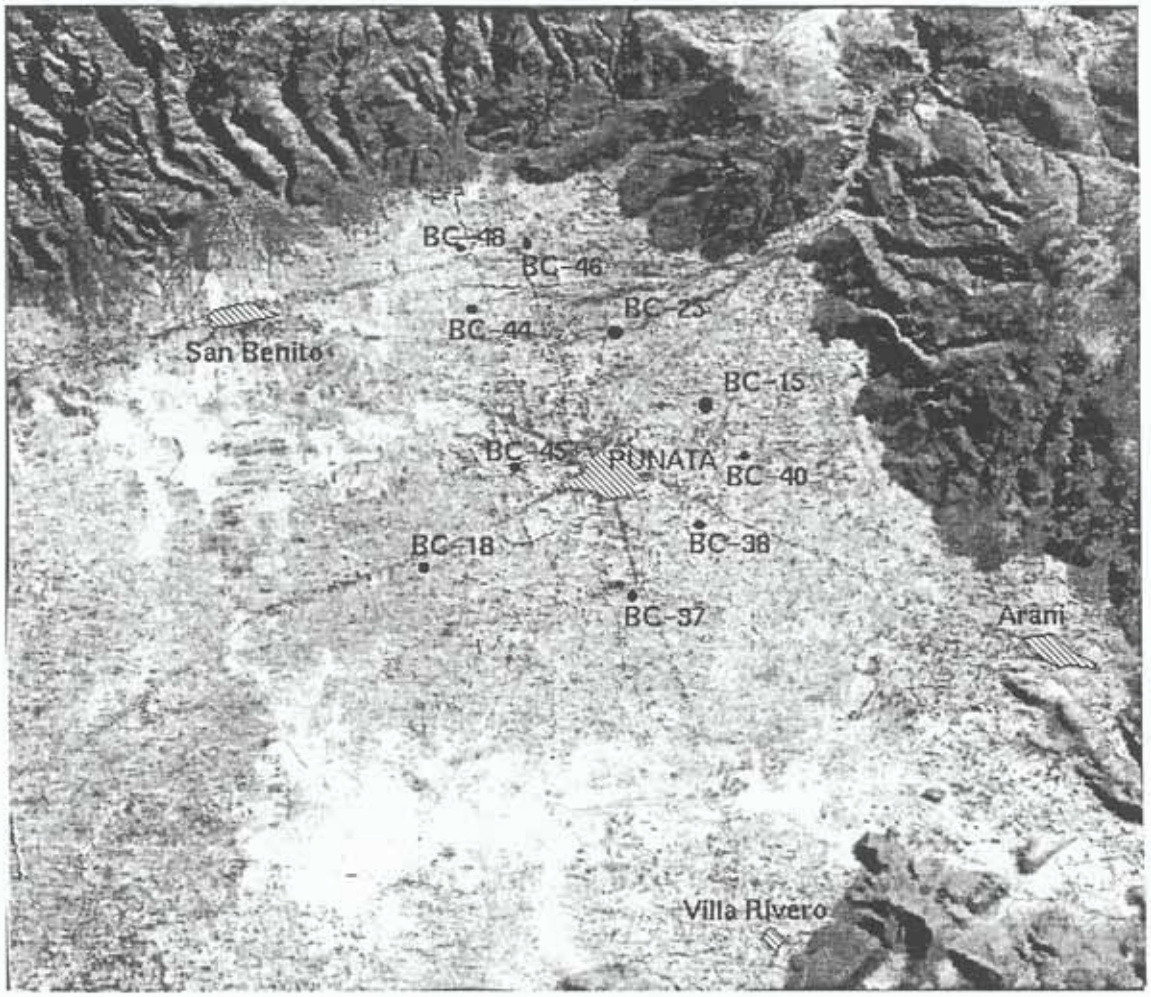

Fig. 5.11: The fossilized fluvio-glacial Punata fan located in the NE part of the Punata-Cliza valley; labels (e.g. BC-18) identify drill holes of Geobol (1977).

(2) The depositional glacis

Very gently sloping depositional glacis, with slope gradients ranging from 1 to 2%, overlap the distal sections of the glacio-fluvial fans, as is the case in the western and northwestern part of the Cochabamba valley (fig. 5.10). Otherwise, glacis deposits ranging from 2 to 3% slope gradient fringe directly the mountain front, as in the Tiquipaya area and the northern part of the Punata and Sacaba valleys. In general, there is a transitional gradation from coarser to finer materials as depositions occur further from the mountain front.

(3) The recent alluvial fans

Undulating recent fans of colluvio-alluvial origin predominate in the northern part of the three valleys, burying older fans and depositional glacis. Tectonic factors control their shape, steep gradient (5 to 8%) and location along the fault lines, suggesting an intermittent pulsed uplift of the mountain front.

Backfilling could imply early faulting along the mountain front, followed by later excess of sediments, perhaps because of climatic fluctuations as found by Harvey (1990) on Quaternary Spanish fans.

(4) The active fans

The location and shape of the presently active fans are directly related to the size and the geologic materials of the catchment areas. The current fan of the Llave river is distally aggrading, has 2 to 3% slope gradient (fig. 5.10), presents features of channel migration and is mainly composed of gravels and boulders of Ordovician quartzitic sandstones. The active fans in the western part of the Cochabamba basin, with catchment areas on Cretaceous sandstones, shales, marls, limestones and conglomerates, have wide and shallow stream channels. Active fans, aggrading near to the mountain front have steeper slope gradients ranging from 8 to 13%.

5.3.2 The lagunary depressions

(1) The margins

The margins of the lagunary flats are almost level surfaces with slope gradients less than 1.5%. They fringe the gently sloping piedmont glacis of alluvial origin. Agricultural activities are common as soils have less rock fragments and overall finer textures than the surrounding piedmont units.

Heterometric lenses, of variable thickness and length, characterize the transition from the piedmont relief types towards the lagunary depressions. Subsurface flow occurs within these discontinuous layers of high permeability, overlaid by sequences of silt and silty clay lagunary materials. Erosion pipes and tunnels develop in the gravel and coarse sandy materials of the lenses and communicate with streams and minor ephemeral brooks such as the Crespo Mayu, Canal Mayu and Loro Mayu in the southern part of the Sacaba basin. The collapse of the tunnel roofs originates severe gully erosion in the distal part of the dissected depositional glacis. Gullies develop in particular by regressive erosion from areas of intersection between tunnels and ephemeral streams (fig. 5.12).

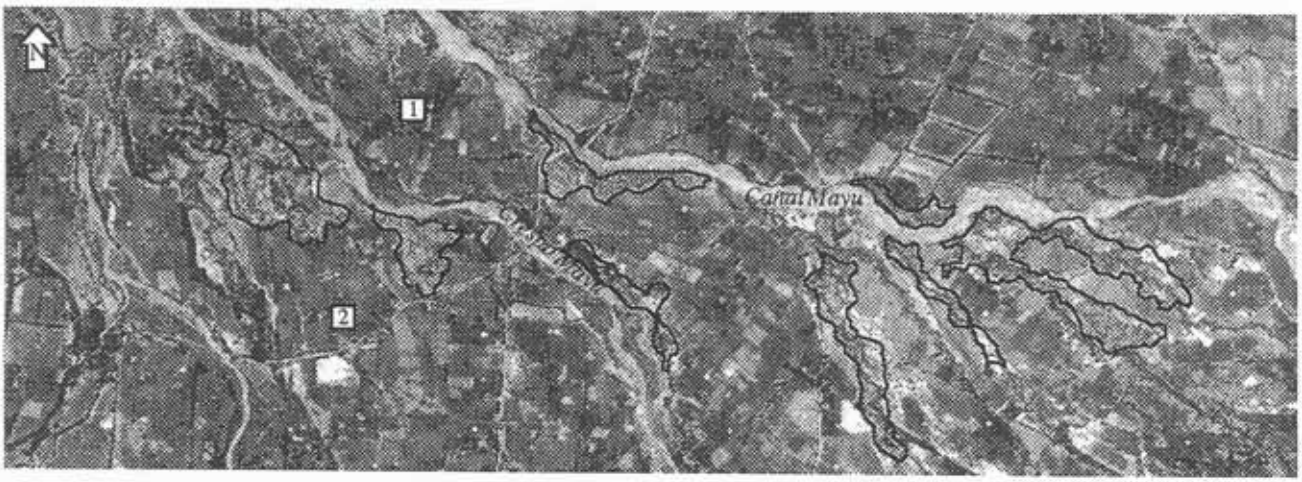

REFERENCES:

Tusca Pujio (1),
Banda Pampa Miraflores (2) .... Communities
Crespo Mayu ..... Ephemeral streams

zone of severe gully erosion

Fig. 5.12: Severe gully erosion in areas adjacent to ephemeral streams.

(2) The central areas

The central parts of the lagunary flats are level to slightly concave surfaces with slope gradients less than 1%. They are composed of clearly stratified materials showing successive aggradation cycles (fig. 5.13). The depositional sequence of a 4 m wall in the badlands of Sacaba, indicated in figure 5.13, has a yellowish brown (10YR 6/4) color throughout. The sedimentary joints are clearly visible. The cross-section is composed of the following layers:

A: 0.7 m of a coarse loamy sand layer;
B: a massive, 2 m thick fine-textured layer. A lithologic discontinuity marks the change to the underlying unit;
C: a silty clay layer, from 1.9 to 2.5 m depth, showing polyhedral erosional features;
D: a fine silty deposit 1 m thick;
E: a coarse loamy layer with discontinuous subangular gravel lenses.

In general, the sediment sequence evidences a low-energy depositional environment. The presence of gravelly layers suggests sub-lacustrine delta penetrations or fluvial activity during low water levels. Loess-like silty clay layers occur frequently in areas where badlands develop (fig. 5.6). Soils are mainly weakly developed loam and silty loam Orthents and Fluvents. The combination of erodible soil textures

with high-intensity and short-duration rainfall events, occurring during the wet season, determines the initiation of surface erosion processes. The combined action of subsurface (piping and tunnelling) and surface processes (overland flow and concentrated runoff) causes the formation of badlands in the lagunary depressions of the Sacaba valley.

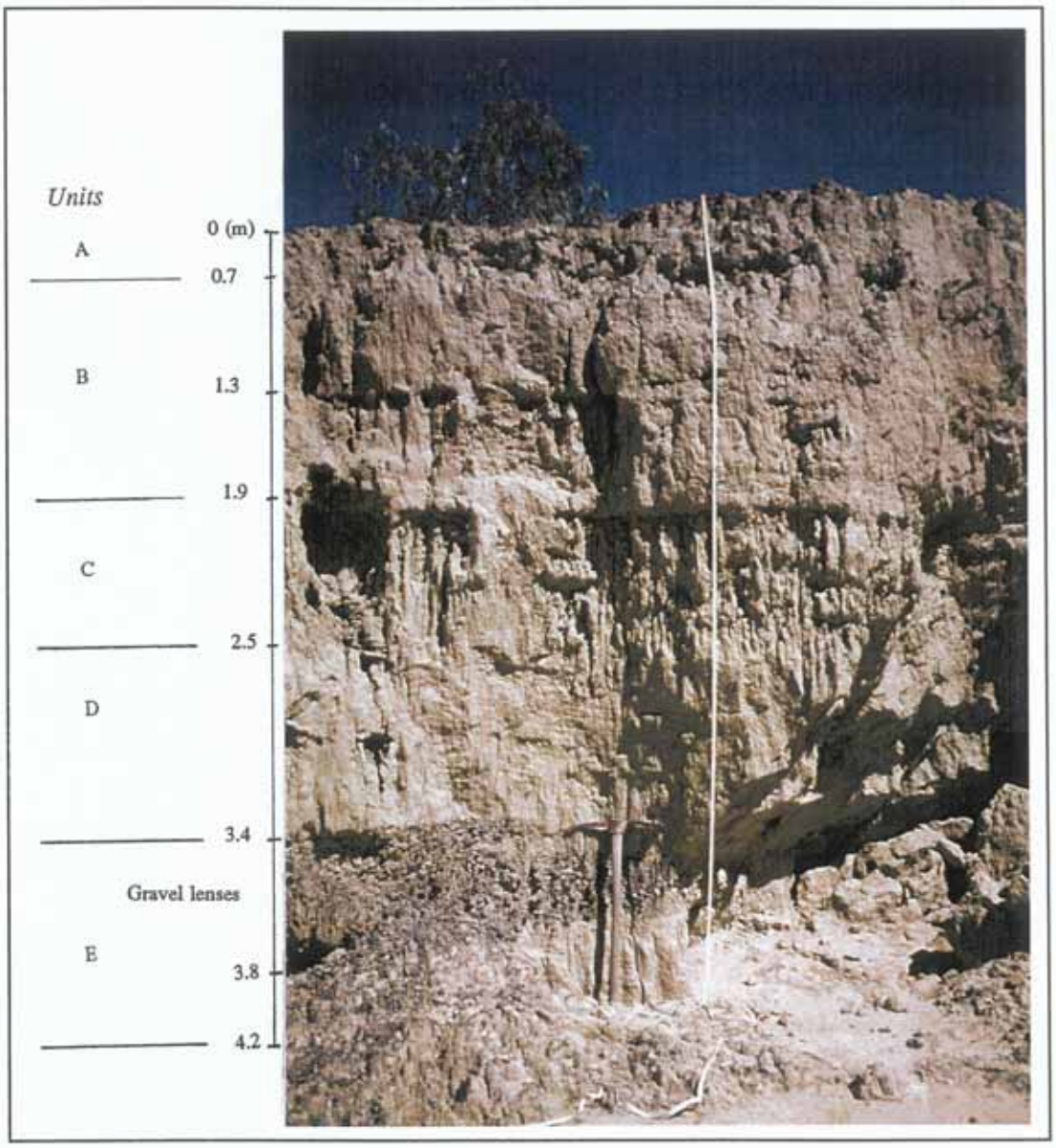

Fig. 5.13: Stratigraphic section of a wall in the badlands of Sacaba.

5.4 SOILS AS INDICATORS OF LANDSCAPE AGE

Soil relict features and radiocarbon dating were used to estimate the age of the soils developed on the

piedmont and valley landscapes. Decomposed soil organic matter of five buried soils was dated. Four soils were located in the Sacaba basin, in distal and central positions of dissected depositional glacis and on lagunary flats, one in a playa position in the Punata-Cliza valley (fig. 5.2). The classified polypedons have a thermic temperature regime and mixed mineralogy families. Semiarid climatic conditions prevail at present in the three valleys. Annex 1 contains the profile descriptions and chemical analyses of the radiocarbon-dated soils. Table 5.3 summarizes the radiocarbon dating results at two confidence intervals.

Table 5.3: Summary of radiocarbon dated soil samples, calibrated by the Seattle /Groningen method (Stuiver et al., 1993)

SOIL SAMPLE	LANDSCAPE POSITION	^{14}C years BP	1σ CONFIDENCE INTERVAL (68.3%)	2σ CONFIDENCE INTERVAL (95.4%)
Sb3	dissected depositional glacis (Kererani area, Sacaba)	1340 ± 40	658 - 710 AD 746 - 762 AD	650 - 772 AD
Sb1	dissected depositional glacis (Canal Mayu, Sacaba)	2130 ± 40	192 - 96 BC 80 - 70 BC	354 - 304 BC 206 - 38 BC
Sb2	dissected depositional glacis (Canal Mayu, Sacaba)	8740 ± 110	7890 - 7690 BC 7670 - 7630 BC	7980 - 7540 BC
Sb88	lagunary flat (near Sacaba cemetery)	1740 ± 40	252 - 300 AD 314 - 346 AD 354 - 378 AD	234 - 406 AD
Va68	playa (Tolata area, Punata-Cliza valley)	660 ± 110	1268 - 1420 AD	1060 - 1080 AD 1160 - 1470 AD

5.4.1 The soils of the glacis

Buried A horizons or full profiles are common in glacis positions. On a dissected depositional glacis in the south of the Sacaba basin three soil samples were collected for radiocarbon dating (fig. 5.2).

(1) The central part of the dissected depositional glacis

(a) The Sb3 profile

The Sb3 soil profile is located at 2740 masl in the Kererani area, in the central part of a piedmont glacis characterized by a gently undulating topography and complex slope form with 2 to 4% gradient towards the north. The groundwater table is very deep (about 16 m) and soils are well drained. Variable percentages of rounded and subangular gravels are present on the terrain surface and in the matrix of the alluvial parent material originated from shales, sandstones and siltstones. Slight sheet and rill erosion features are observed in the site surrounding the soil profile location. Molle and eucalyptus are the natural vegetation while maize, barley, beans and wheat are commonly cultivated rainfed crops.

The dated Sb3 profile presents the following horizon sequence:
(1) The cover soil: a 70 cm thick, yellowish brown silt loam alluvial deposit from which a fine loamy Ustochreptic Camborthid, with an ochric epipedon and a cambic horizon, developed. The cambic horizon has a yellowish brown silt loam texture and a moderate medium subangular blocky structure.
(2) The buried soil: a dark grayish clay loam material (Sb3), including two horizons:

2Ab: the buried A horizon (70-88 cm), collected for radiocarbon dating, has many medium rounded gravels within a clay loam matrix, with moderate medium subangular blocks. The soil reaction is neutral and the electrical conductivity very low (0.1 dS/m). Except for the thickness, the horizon meets the requirements of a mollic epipedon: very dark gray (10YR 3/1) color, organic carbon content of 0.88% and base saturation above 50%. The boundary to the underlying C layer is clear and smooth.

3Cb: a structureless brown C layer, where gravels of different sizes dominate in a sandy loam matrix.

Radiocarbon dating conferred an age of 1340 ± 40 BP (upper Holocene) to the buried A horizon.

(b) The Sb31 profile

The Sb31 profile (fig. 5.14) is also located in the central part of a dissected depositional glacis, at 2740 m elevation, on a gentle slope towards the northwest (2-3% slope gradient). Rainfed crops are maize and wheat, and the natural vegetation includes molle schinus and locust trees. The soil profile is composed of the following sequence of horizons.

(1) The cover soil is a fine loamy Typic Camborthid, composed of two horizons:

A: a 34 cm thick, brown (10YR 4/3) silt loam to sandy loam ochric horizon of subangular structure.

2Bw: a 43 cm thick, dark yellowish brown (10YR 3/3) silty clay loam cambic horizon of medium prismatic structure.

(2) The first buried Haplustoll:

3Ab: a 40 cm thick, very dark yellowish brown (10YR 3/2) clay loam mollic horizon.
This A horizon is followed by a pale brown (10YR 7/3) sandy loam C layer, of strong effervescence to hydrochloric acid and alkaline reaction. An indurated calcic layer was observed from 1.55 to 1.69 m. The bottom of this sequence presents oxido-reduction features, including Mn nodules.

(3) The second buried Haplustoll starts at 2 m depth with a mollic horizon including abundant rock fragments in the soil matrix.

(2) The distal part of the dissected depositional glacis

The Sb1 and Sb2 profiles were sampled closer to the Sacaba town, 1100 m north of the Sb3 location,

in the exposed channel wall of the Canal Mayu river, an ephemeral stream crossing the distal part of a dissected depositional glacis south of Sacaba. The Sb1 profile was sampled 97 cm below the terrain surface in the top layer of the depositional section, while the Sb2 profile was sampled at the bottom of the section, seven meters from the surface (figure 5.15).

(a) The site and the depositional section

The site lies at 2710 masl, in a transitional area between the piedmont and the valley landscapes. Badlands are frequent, resulting from piping and tunneling in texturally contrasted alluvial sediments and from the collapse of tunnel roofs evolving into gullies (fig. 5.12). A very gently sloping (0.5 to 1.5%) topography characterizes the distal part of the glacis. The groundwater table is at more than 10 m depth. Agricultural activity is limited to the areas without severe gully erosion.

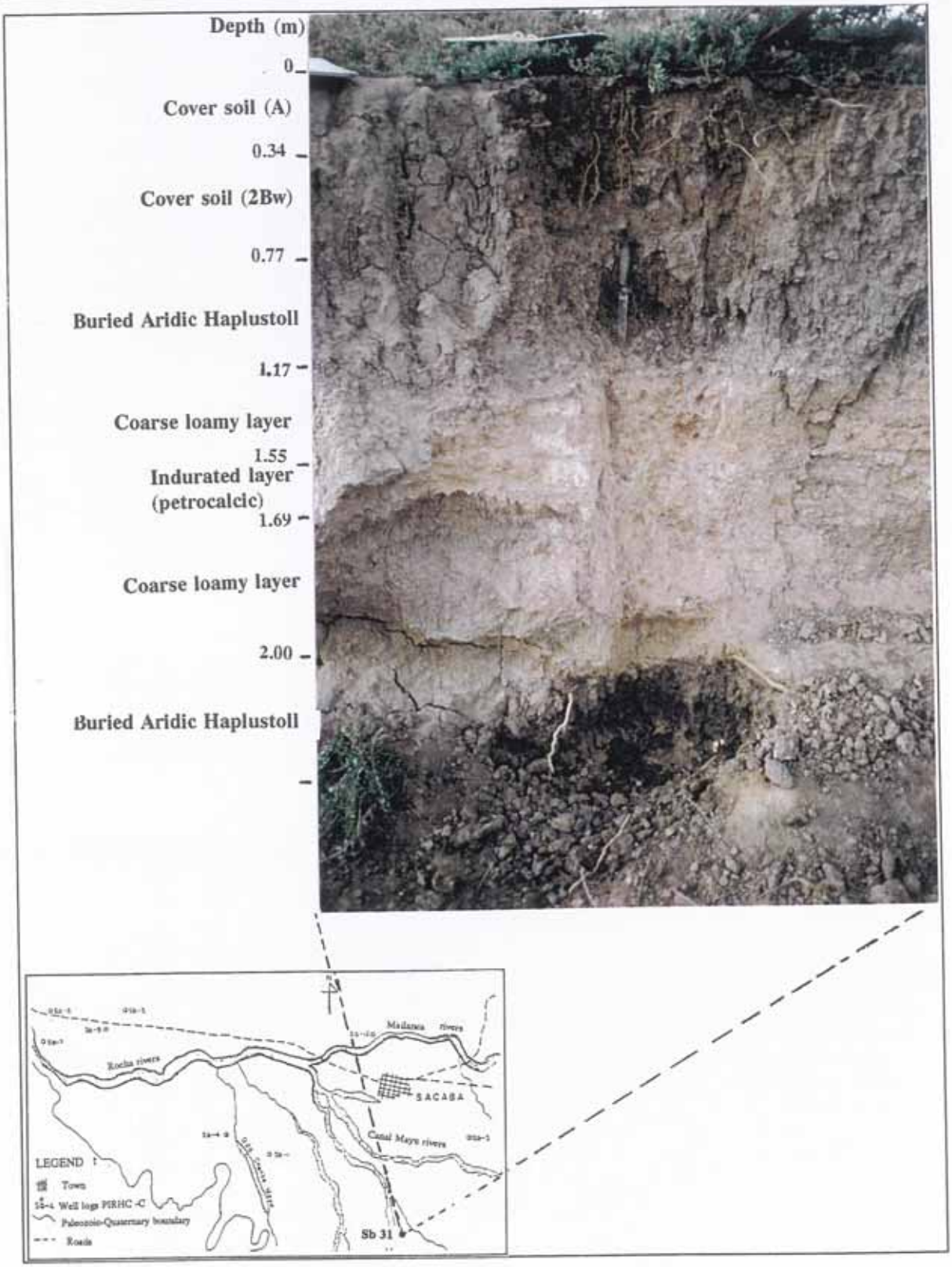

Fig. 5.14: Buried Mollisols on a dissected depositional glacis of the Sacaba valley.

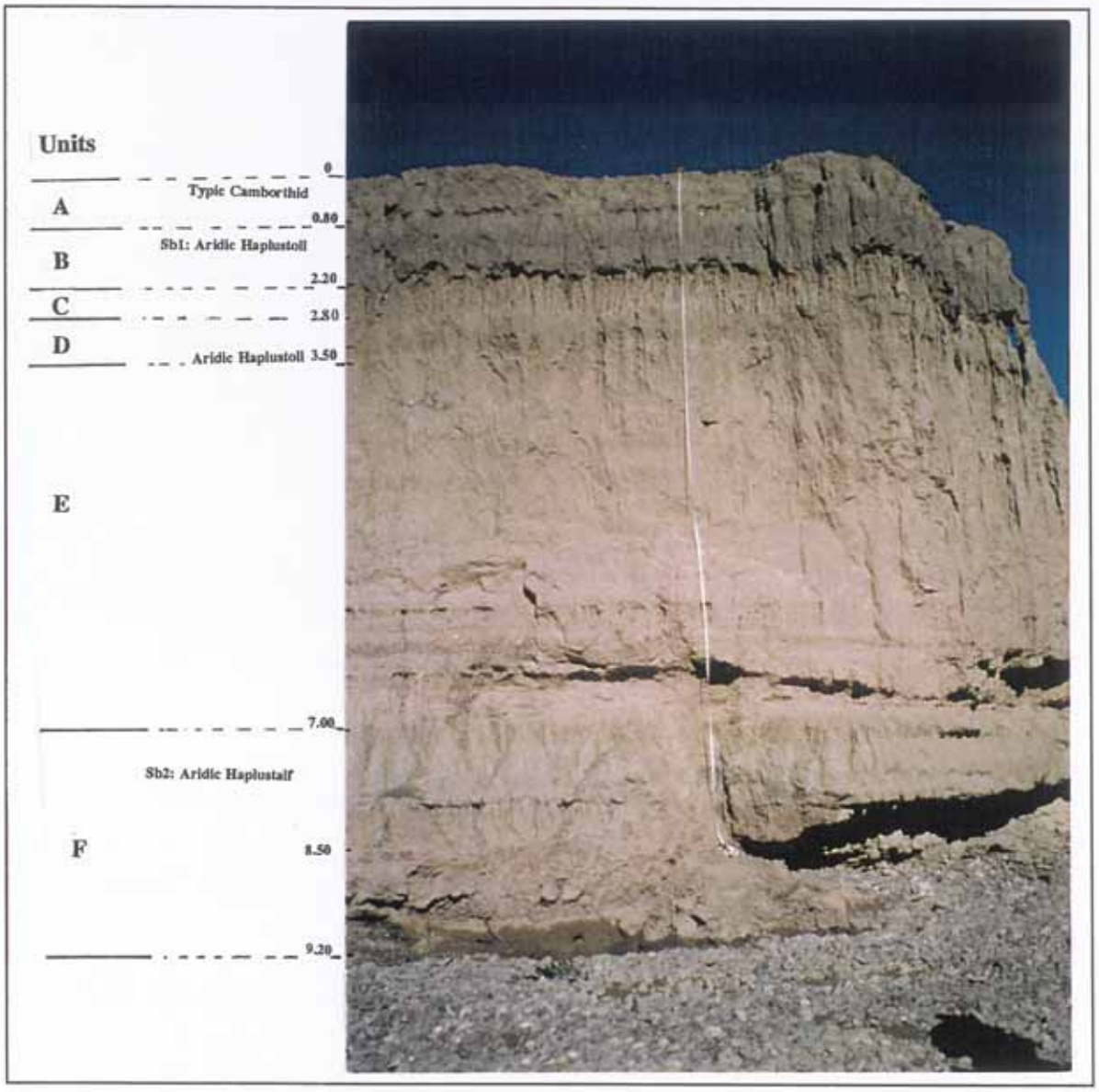

Fig. 5.15: Stratigraphy of the Canal Mayu river wall

Figure 5.15 represents the depositional section of the exposed Canal Mayu river wall, composed of the following main units:

A: A 24 cm yellowish brown silt loam sedimentary cover, similar to the one covering the buried Sb3 profile, overlies discontinuously a pale olive and yellowish brown loamy sand deposit. Together, these two top layers, approximately 70 to 80 cm thick, form a Typic Camborthid.

B: The first buried profile (Sb1) is a fine silty, dark yellowish brown soil which starts at 70 -80 cm from the soil surface and extends down to 2.2 m depth.

C: A yellowish brown silt loam deposit, about 60 cm thick, separates the Sb1 profile from a second buried soil. Wall erosion enhances the presence of vertical polyhedrons developed in the fine-textured material of unit C.

D: The second buried soil starts approximately at 2.8 m from the soil surface and is about 50 cm thick. This soil profile could not be described and sampled because of poor accessibility. The material is brown color and has external characteristics similar to those of the Sb1 buried soil. A diffuse smooth boundary makes the transition towards unit E.

E: The central part of the section is a set of yellowish brown layers, about 3.5 m thick. Few discontinuous thin gravel lenses are present within the fine-textured matrix and some roughly sculptured large polyhedrons are visible along the channel wall. The bottom of unit E is a light yellowish brown, silt loam material, overlying a buried soil.

F: The third buried profile (Sb2) is a brown to dark grayish brown, silty clay loam and clay loam material, located at the bottom of the depositional sequence, approximately at seven meters from the soil surface.

(b) The Sb1 profile

The layer sequence of the Sb1 profile is as follows:

(1) The cover soil: a 70 cm thick yellowish brown sedimentary cover, from which a loamy Typic Camborthid developed. Textures range from silt loam in the A horizon to a structureless sandy loam in the 2C layer.

(2) The buried Sb1 soil includes the following sequence of horizons:

3Ab: a 56 cm thick, brown to dark grayish brown mollic horizon with silty clay loam texture, prismatic structure breaking into coarse subangular blocks and fine horizontal pores. Clay and organic carbon contents increase with depth, in particular between 97 and 126 cm. Therefore, the lower part of the A horizon was sampled for radiocarbon dating. The contact with the underlying B horizon is clear and smooth.

3Bwb: a 36 cm thick, dark brown to dark yellowish brown, silt loam cambic B horizon with subangular blocky structure, high base saturation, organic carbon content decreasing with depth, and gradual smooth lower boundary.

4Cb: a brown silt loam horizon, with fine and medium gravel and coarse subangular blocky structure.

The soil meets the requirements for mollic epipedon and cambic horizon, classifying therefore as a fine silty Aridic Haplustoll, fossilized by a loamy Typic Camborthid. The radiocarbon dating allocates an age of 2130 ± 40 BP (upper Holocene) to the A horizon.

(c) The Sb2 profile

The Sb2 soil profile starts at 7 m below the soil surface. The section lying between the bottom of the Sb1 and the top of the Sb2 profiles (units C, D, E in fig. 5.15) could not be described due to inaccessibility of the river wall. The bottom of unit E is a 50 cm thick, yellowish brown silt loam to loam

layer. The contact with the underlying Sb2 buried soil is clear and smooth.

The buried Sb2 profile is a fine loamy Aridic Haplustalf, composed of the following horizons:

Ab: a 1.13 m thick, brown (10YR 4/3) to dark grayish brown (10YR 3/2), silty clay loam horizon with subangular blocks and low organic carbon content (0.2%). A clear smooth boundary indicates the transition towards the underlying horizon. The lower 45 cm were sampled for radiocarbon dating because of higher organic carbon content.

Btb: a 40 cm thick, brown (7.5 YR 3/4) clay loam Bt horizon. Broken clay cutans are present on the pedfaces and in root channels. The organic carbon content (0.02%) is very low and the soil reaction is neutral.

Cb: a yellowish brown (10YR 5/6) loamy to sandy clay loam layer with subangular blocks, extending from 9 m depth down to the base of the riverbed wall.

Radiocarbon dating bestows an age of 8740 ± 100 BP (lower Holocene) to the lower part of the A horizon, in the transition towards the argillic horizon.

The color, thickness and stratigraphic position of the two buried Mollisols illustrated in figure 5.14 are similar to the sequence of units B (first buried Mollisol), C (representing a period of renewed aggradation) and D (second buried Mollisol) of the Canal Mayu wall, illustrated in figure 5.15.

5.4.2 The soils of the lagunary depressions

Lagunary depressions occupy the center of the Punata-Cliza and Sacaba valleys as well as the south-central part of the Cochabamba basin. Lagunary flats are common to the three valleys, while playas are found in the Cochabamba and Punata-Cliza valleys. Lagunary deposits are susceptible to gully erosion, but extensive badlands exist only in the central part of the Sacaba valley. Two soil profiles, one located in a lagunary flat of the Sacaba valley (Sb88) and another in a playa of the Punata-Cliza valley (Va68), were described and dated.

(1) Lagunary flats

The soil profile Sb88 is located 100 m west of the Sacaba cemetery, at 2700 masl, in a site characterized by flat topography, absence of surface rock fragments, deep groundwater table and natural grass cover. The horizon sequence is as follows:

(1) The cover soil is a thin (15 cm), lithologically discontinuous, pale brown silt loam layer of neutral to slightly acid soil reaction and relatively high organic carbon content (0.9%).

(2) The buried Sb88 soil profile includes the following horizons.

2A: a 47 cm thick, brown (10YR 3.5/3) silty clay loam horizon of neutral reaction and 0.57% organic carbon content. Undecomposed plant remains were found in the soil matrix.

2Bw: a 22 cm thick, yellowish brown (10YR 4/3) silt loam cambic horizon of moderate subangular blocky structure, slightly alkaline reaction and low organic carbon content (0.44%). The transition to the underlying C layer, belonging to a different aggradational cycle, is gradual and

irregular.

3C: a gravelly C layer having a coarse loam matrix and yellowish brown (10YR 4/4) colour, from 1.44 m downwards.

The presence of a cambic horizon and ochric epipedon labels the soil as a fine silty Fluventic Camborthid. The A horizon is transitional towards a mollic epipedon, as the requirements for color, thickness, texture, base saturation and structure are fulfilled, but organic matter content is low. A sample of the cambic horizon, taken at 84 cm depth, provides a radiocarbon age of 1740 ± 40 BP.

(2) Playas

Playas are characterized by fine clayey lacustrine materials grading into lagunary facies at the top of the depositional sequence. Graf (1982) and Geobol (1977) mention such an upwards transition from lacustrine to lagunary conditions. Rock fragments are absent on the soil surface as well as within the profile. Unlike the sites described previously, the groundwater table is at shallow depth and generally brackish. As a consequence, soluble salts migrate upwards during the dry season and accumulate in the topsoil. Soils are moderately to poorly drained because of the low permeability of the parent material and the slightly concave topography of the position. Salt-tolerant vegetation covers the site surrounding the soil profile Va68, located 1 km south of Tolata at 2700 masl. Puffy crusts overlay a layer of pulverulent material at the soil surface. Crusts are frequently destroyed by cattle trampling and the fluffy material is exposed to eolian deflation. Figure 5.16 illustrates the general stratigraphy of the Va68 setting.

The profile is a stratified sequence of four consecutive soil layers, separated by lithological discontinuity surfaces which reflect a stepwise aggradational process. The layer sequence is as follows:

(1) The cover soil is a 44 cm thick layer having a fine silty to loamy texture, light yellowish brown colour, fine platy structure and horizontally stratified distribution of materials of variable color and texture. An abrupt smooth boundary indicates the contact with the buried soil.

(2) The buried Va68 soil profile includes the following horizons:

2BAb: a 46 cm thick, light brownish gray (2.5Y 4/2), very fine clayey transitional B horizon, with strong subangular blocks. Broken clay skins cover the root channels. Undecomposed organic rests are frequent. This layer gradually changes in depth to a coarser material with fine loamy texture, olive brown color and common manganese mottling.

3Btgb: a 37 cm thick, light yellowish brown, fine clayey to fine loamy layer with common reduction features and patchy thin clay skins in root channels.

4BCb: at the bottom of the sequence, at 127 cm depth, a fourth depositional layer occurs with coarse loamy texture, light yellowish brown color and many distinct Fe and Mn mottling in the soil matrix.

All soil horizons have very alkaline reaction and high electrical conductivity. Organic carbon is everywhere lower than 0.6% and the calcium carbonate content decreases with depth. The pedon meets the requirements for an ochric epipedon and argillic horizon. Being poorly drained, the soil classifies as

clayey Aquic Haplargid. Radiocarbon dating bestows an age of 660 ± 110 BP to the BA horizon, buried between 44 and 90 cm depth.

5.4.3 Paleoenvironmental reconstitution and paleopedology

An attempt to reconstitute the paleoenvironmental conditions prevailing during the Holocene in the three basins was carried out on the basis of the five soil dating results. Table 5.4 summarizes the main physical characteristics and age data of the selected profiles.

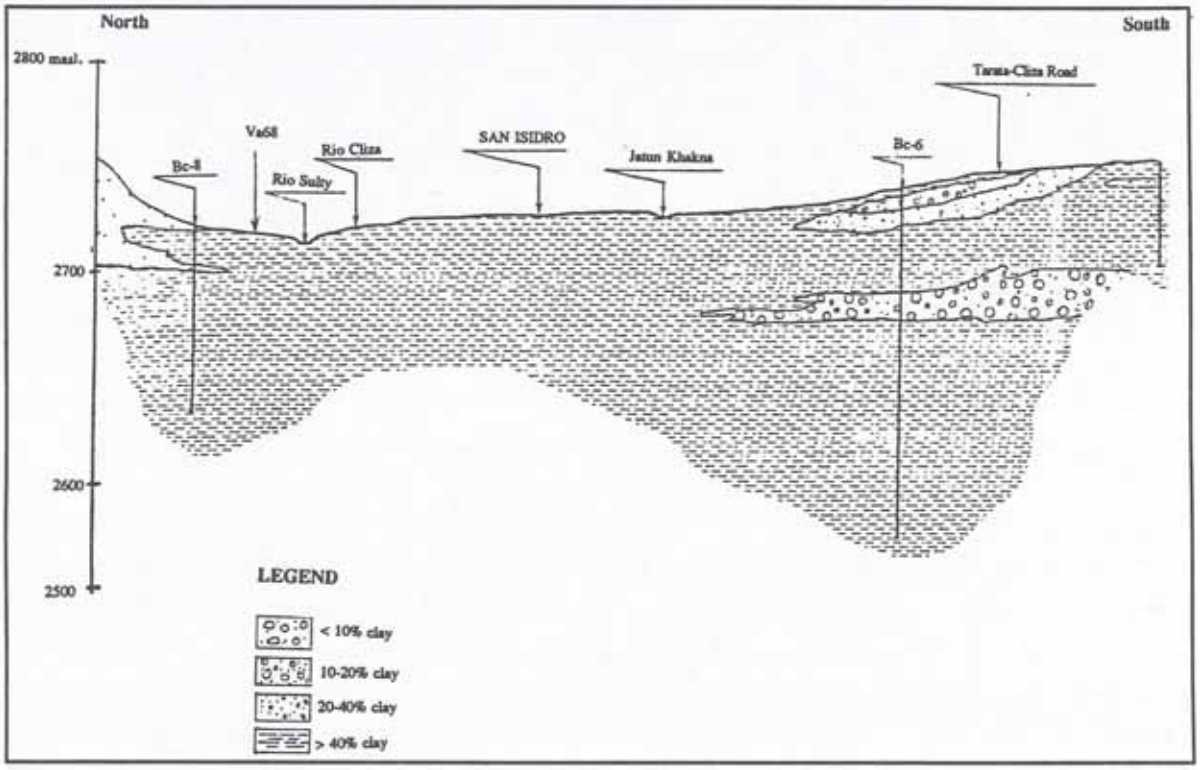

Fig. 5.16: Cross-section of the Punata-Cliza valley (Va68= ^{14}C dated soil sample).

Table 5.4: Some properties of the radiocarbon-dated soil horizons.

Code	Depth buried	Sampled horizon						
	soil (m)	Desig.	depth (m)	texture (1)	Color (moist) (2)	Horizon type	Age (BP)	Soil sequence
Sb3	0.71	2Ab	0.71 - 0.88	Fine loamy	VDG (10YR 3/1)	ochric->mollic	1340 ±40	Camborthid/Camborthid->Haplustoll
Sb1	0.7	3A2b	0.97 - 1.26	Sicl	VDG (10YR 3/2)	mollic	2130 ± 40	Camborthid/Haplustoll
Sb88	0.15	2Bw2	0.84 - 1.44	Sil/Sicl	B (10YR 4/3)	cambic	1740 ± 40	Camborthid->Haplustoll
Sb2	7.5	A2b	8.18 - 8.63	Sicl	VDG (10YR 3/2)	ochric	8740 ± 100	Haplustalf
Va68	0.44	2BAb	0.44 - 0.54	Clay	DGB (2.5Y 4/2)	argillic	660 ± 110	Haplargid

(1) Texture code:
Sicl: silty clay loam
Sil: silt loam

(2) Color code:
VDG: very dark gray
B: brown
DGB: dark gray brown

(1) The depositional sequence of the piedmont glacis and lagunary flats

The bottom of the Canal Mayu river sequence corresponds to a 1.5 m thick Alfisol (Sb2) dated 8740 BP, which required moister conditions than the present ones for clay illuviation and formation of the thick argillic horizon. Since the A horizon was dated, pedogenesis must have started quite earlier, perhaps immediately after the last glacial period (Choqueyapu II). The bottom of the exposed stratigraphic sequence could therefore be late Pleistocene-lower Holocene, characterized by moist climatic conditions.

The central part of the sequence contains a 3.5 to 4 m thick, loess-like fine-textured material (unit E from figure 5.15), with irregular and discontinuous gravel lenses and sheets at the base of the unit, which might reflect either drier conditions or marked seasonal rainfall fluctuations, with high-energy rainfall events capable to detach and transport coarse sediment loads. A rhythmic depositional structure prevails in the unit, characterized by cyclic aggradation of fine-textured materials, which would relate to climatic fluctuations. The thickness and composition of the deposit indicate an overall low-energy depositional environment, with intrusions of coarse materials laid down either in subaquatic deltas or subaeric splay conditions. Upwards diminution in size and amount of the gravel lenses highlights a transition towards lagunary-like conditions.

Subsequent lake desiccation allowing soil development under moist conditions would be reflected in the 0.7 m thick unit D (fig. 5.15). This soil, with dark color mollic features, could not be sampled. A 60 cm thick, fine-textured yellowish brown C layer represents a renewed low-energy aggradational period, separating the buried Mollisol of Unit D from the buried Mollisol of Unit B (2130 BP). Thus, during the upper Holocene, conditions favorable to the formation of Mollisols have alternated with lagunary or (drier) loess-like depositional conditions.

Correlating the former conclusion, derived from profile Sb1, with the results provided by the other dated

profiles (Sb3 and Sb88), occurring in approximately similar environments, it can be inferred that conditions favoring the development of Mollisol-like pedogenetic features reigned between 1340 and 2130 BP (table 5.4). Profiles Sb3 (1340 BP) and Sb1 (2130 BP) are located on the same dissected depositional glacis, at similar slope position, and buried by a sedimentary cover of similar texture and thickness. The buried soil Sb88, located in a lagunary flat at lower elevation than Sb1, is closer to the surface and covered by a thinner sedimentary cover of however similar coarse texture.

After 1340 BP, aridity increased and present-like conditions prevailed. Camborthids are now developing on top of the buried Mollisols, from coarse-textured, more torrential alluvial cover formations. The soil survey carried out in the three basins did not reveal the occurrence of exposed Mollisols under the present semiarid conditions. All mapped Mollisols are buried by coarse deposits of variable thickness.

In conclusion, radiocarbon datings, summarized in table 5.4, suggest moister conditions than the present ones, suitable for the development of steppe or grassland vegetation, a type of cover generally associated with Mollisols, between 1340 and 2130 BP. Since the dated materials belong to A horizons, the obtained dates are good approximations of the burial dates, indicating antecedent moister conditions from the middle Holocene to the early part of the upper Holocene, when Mollisols developed. Since then, aridity increased towards present-like conditions.

The 4 m thick loess-like deposit, separating the middle-upper Holocene Mollisols from the lower Holocene Alfisol, might correlate to the middle Holocene period, with increased dryness or marked seasonal torrential rainfall fluctuations to allow sediment aggradation to dominate over soil formation (fig. 5.17).

The hypothesis about a humid period during the postglacial and lower Holocene time, favouring the development of Alfisols, followed by a dry period during the middle Holocene when aggradational processes dominated and returning towards increased humidity, suitable for the development of mollic and calcic horizons, during the transition from middle to upper Holocene, agrees with the findings concerning the Holocene climatic fluctuations in the Titicaca lake (Wirmann et al., 1987), but diverges partially from other regional attempts of paleoenvironmental reconstitution in Bolivia (Graf, 1981).

(2) Pedogenetic features of the Punata-Cliza valley

Genetic features related to Mollisols were also observed in the Punata-Cliza valley. Table 5.5 summarizes some of the field observations and their landscape position. The Haplargids mapped on the distal parts of the dissected depositional glacis and on the lower lagunary flats meet the color, structure and thickness requirements for mollic horizons, but exhibit higher clay illuviation (clay skins on pedfaces and in root channels) than the Mollisols recognized in the Sacaba and Cochabamba valleys. This might be related to longer persistence of lacustrine or lagunary conditions in the Punata-Cliza valley, where mainly fine-textured materials deposited.

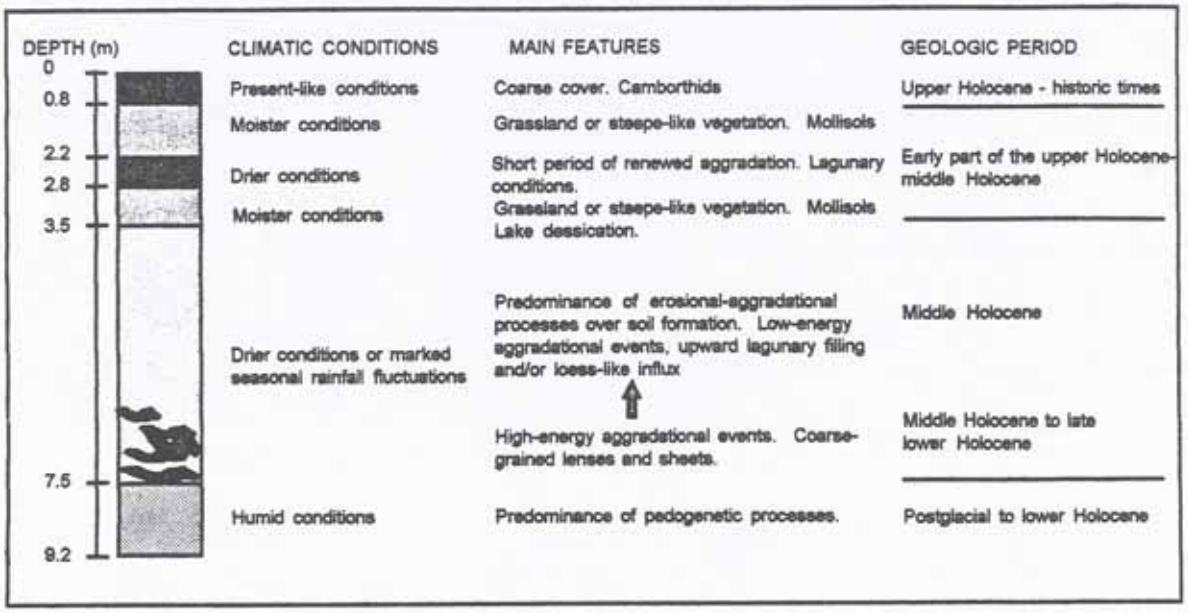

Fig. 5.17: Generalized paleoenvironmental reconstitution of the Holocene period in the Cochabamba valleys (extrapolated from the Sacaba valley sites).

Haplargids might be contemporaneous to or even younger than the Haplustolls identified in the other valleys, because the local soil forming factors such as slightly concave depressional topography, clay-rich parent materials and the abundance of salts, accelerate certain pedogenetic processes, in particular clay illuviation and neoformation. Radiocarbon dating of an Aquic Haplargid from a playa position (Va68) indicates development of an argillic horizon in a relatively short period (660 BP), favored by local moist conditions which would induce in-situ clay formation as well as faster illuviation to the lower horizons.

The absence of well developed Mollisols in the Punata-Cliza valley might also be attributed to the persistence of lagunary-like conditions in the lower parts of the basin when Mollisols formed in the already drained Sacaba and Cochabamba basins. However, lagunary-like conditions would not extend to the piedmont areas of the basin (Pi111 and Pi112 in table 5.5), as mollic features were identified on the dissected depositional glacis south of the Punata-Cliza basin. But intensive decarbonation led to high concentration of secondary carbonates in filaments, nodules and pendants, as dominant pedogenetic features.

Table 5.5: Genetic features related to formation of mollic horizons in the Punata-Cliza valley.

PEDON	MAP UNIT (1)	HORIZON (cm) thickness	depth	MOIST COLOR (*)	DRY COLOR (*)	TEXTURE	DIAGNOSTIC HORIZON	TAXONOMIC CLASSIFICATION
	PIEDMONT							
Va05	Pi111	18	22	DB 10YR 3/3	PB 10YR 6/3	Silt loam	Cambic	Typic Camborthid
Va01	Pi111	20	24	DB 75YR 3/3	B 75YR 5/4	Silt loam	Calcic	Typic Calciorthid
Va04	Pi111	20	32	DB 75YR 3/3	B 75YR 4/2	Clay loam	Argillic	Typic Haplargid
Va08	Pi111	60	60	DB 75YR 3/3	B 75YR 4/4	Silty clay loam	Mollic/Calcic	Aridic Calciustoll
Va01	Pi111	36	77	DB 75YR 3/3	B 75YR 5.5/4	Silt loam	Calcic	Typic Calciorthid
Va03	Pi111	19	92	DB 75YR 3/2	DYB 10YR 4/4	Sandy clay loam	Cambic	Fluventic Camborthid
Va23	Pi112	?	48	DYB 10YR 3/3	not recorded	Silt loam	Cambic	Ustochreptic Camborthid
Va15	Pi112	?	52	DB 75YR 3/3	DYB 10YR 4/4	Silty clay loam	Cambic	Ustochreptic Camborthid
Va35	Pi113	59	33	DB 75YR 3/3	not recorded	Silty clay loam	Argillic	Typic Haplargid
Va24	Pi113	?	43	DB 75YR 3/3	B 75YR 4/2	Clay loam	Argillic	Typic Haplargid
Va21	Pi113	30	50	DYB 10YR 3/3	not recorded	Silty clay loam	Argillic	Ustalfic Haplargid
Va26	Pi113	58	58	DB 75YR 3/3	B 7.5YR 4/3	Clay loam	Argillic	Typic Haplargid
	VALLEY							
Va106	Va113	16	35	DB 75YR 3/3	B 75YR 4/3	Silt loam	Argillic	Ustalfic Haplargid
Va66	Va124	10	19	DYB 10YR 3/3	B 10YR 5/3	Silty clay loam	Argillic	Ustalfic Haplargid
Va112	Va124	7	40	DB 75YR 3/3	not recorded	Silt loam	Salic	Typic Salorthid
Va113	Va124	?	47	DYB 10YR 3/3	not recorded	Silt clay loam	Salic	Typic Salorthid
Va57	Va124	?	50	DB 10YR 3/3	DYB 10YR 3/6	Silty clay loam	Cambic	Natric Camborthid
Va69	Va124	?	50	VDGB 10YR 3/2	B 10YR 5/3	Clay loam	Cambic	Natric Camborthid
Va67	Va124	?	55	VDGB 10YR 3/2	GB 10YR 5/2	Clay loam	Argillic	Aquic Haplargid

(*) COLOR CODES:
PB: pale brown
B: brown
DYB: dark yellowish brown
GB: grayish brown
VDGB: very dark grayish brown
DB: dark brown

(1) UNIT CODES:
Pi111: dissected depositional glacis (proximal part)
Pi112: dissected depositional glacis (central part)
Pi113: dissected depositional glacis (distal part)
Va113: lower lagunary flat
Va124: playa

(3) Soil-landscape correlation

Table 5.6 summarizes the general relationships between soil distribution and landscapes in the three valleys. Entisols and weakly developed Aridisols dominate on the active and recent fans, while Argids and Orthids developed mainly from the lacustrine-lagunary deposits. Buried Mollisols are widespread on the depositional glacis and lagunary flats of the Cochabamba and Sacaba valleys, while Alfisols were identified in the bottom tiers of alluvio-lagunary depositional sequences and of old fluvio-glacial fans.

Table 5.6: Correlation between soils and landscape.

FACIES	SOIL CHARACTERISTICS	RELIEF TYPE AND AGE
Colluvio-alluvial	Angular gravels in sandy matrix, low clay contents. Predominance of Entisols and Aridisols.	Active fans: late upper Holocene Recent fans: upper Holocene
Lacustrine-lagunary	Clay and silty-clay soil textures, abundance of horizontal root channels filled with manganese. Argids and Orthids	Lagunary flats: middle to upper Holocene
Alluvial	Clay loam and loam textures. Gravelly loam and silty loam sedimentary covers. Predominance of buried Mollisols.	Depositional glacis: middle Holocene
Alluvio-lagunary	Fine textures, fossilized red Alfisols	Depositional glacis: lower Holocene
Glacio-fluvial	Boulders, stones and gravels in sandy and silty matrix. High degree of weathering of some stones. Several buried sequences of red and brownish soils were recognized (Alfisols ?)	Old dissected fans: late Pleistocene.

5.5 SYNOPSIS OF THE MAIN BASIN FORMATION EVENTS

On the basis of geologic, geomorphic, palynological, geophysical and soil data it is possible to establish the following chronology of the main paleogeographic events occurred in the Cochabamba basins.

5.5.1 Miocene

During the early Miocene, isolated half-graben basins formed in the Eastern Cordillera as a consequence of major strike-slip faults associated with the Tertiary Andean orogeny. The differential uplift was more pronounced along the northern border of the basins.

5.5.2 Pliocene

The tectonic depressions were occupied by Pliocene lakes, where silty and clayey lacustrine and fluvio-lacustrine sediments accumulated. The Pliocene sediments present evidence of folding in the Sacaba basin, while faulting affects lacustrine sediments located in the western part of the Cochabamba basin, suggesting therefore a continued tectonic activity during the Tertiary. Erosion surfaces, located at different elevations in the mountains, developed during periods of minor tectonic activity. Coarse alluvial sediments deposited near the northern mountain front of the Cochabamba and Sacaba basins, in contact with the Paleozoic basement. Their short longitudinal extent is explained by the existence of lakes, which decreased the stream transport capacity and induced accelerated deposition as fans or deltas. Geophysical studies suggest an earlier lake retreat in the Sacaba basin, draining into the Cochabamba lake through the Mesadilla area which connects both basins. As a consequence, shallow-water, lagunary-like conditions predominated in the Sacaba basin since the late Pliocene.

5.5.3 Pleistocene

The lower and middle Pleistocene is not well documented in the region. Two main glaciations belonging to the upper Pleistocene were recognized and labelled as Choqueyapu I and II. Moraine sediments from these two glacial stages have been identified in the northern and northwestern parts of the Cochabamba and Sacaba basins, and the northeastern part of the Punata-Cliza valley (Veicht, 1992). Glacial erosion in the mountains caused aggradation of the glacio-fluvial fans in the piedmont. Different depositional-dissectional sequences occurred because of the climatic oscillations between glacial, interglacial and interstadial periods. During the warmer and wetter periods, red Alfisols developed, now buried at different depths within the Pleistocenic fluvio-glacial fans.

5.5.4 Lower and middle Holocene

The Pleistocene fans were dissected by younger fans or buried by depositional glacis. The development of Mollisols, presently buried by coarse textured sedimentary covers, on the top of the depositional glacis, reflects increased moisture conditions. Dated Mollisols, occurring at shallow depths (10-100 cm) in the glacis of the Sacaba basin, are of upper Holocene. More deeply buried Mollisols could not be dated, but are assumed to correlate with the middle Holocene.

Climatic oscillations or neotectonic activity might have caused new obstruction in the Mesadilla area which connects the Sacaba and Cochabamba basins creating recurrently local lacustrine-lagunary conditions. This is hypothesized from the isometric diagrams and the lithologic sequence in the southern part of Sacaba (e.g. Canal Mayu wall, fig. 5.15), where Haplustalfs from the early part of the lower Holocene are topped by about four meters of a fine-textured deposit, intercalated with laterally extensive gravel sheets and isolated gravelly coarse sand channel fills of alluvial origin, specially frequent in the bottom layer of the deposit. Later, linear erosion by the Rocha river in the lacustrine and alluvial sediments would have re-opened the inter-basin closure.

Loess-like sediments characterize the surface materials of the badlands formed in the lagunary depressions of the Sacaba basin. Buried Mollisols of middle and upper Holocene, occurring south of Sacaba town, were not observed in the badland areas. It is thus presumed that shallow lagunary conditions remained for a longer period in the lowest parts of the basin, hindering soil development.

Neotectonics and the lithologic composition of the mountains separating the Punata-Cliza and Cochabamba basins have facilitated the incision of the Tamborada river, allowing both basins to communicate and contributing to a progressive desiccation of the Punata-Cliza valley. Calcic and argillic horizons, requiring moist soil conditions to allow downwards clay and carbonate migrations, developed on the southern piedmont at the time Mollisols formed on the piedmont glacis of the Cochabamba and Sacaba valleys. The absence of well developed Mollisols in the lagunary depressions might indicate the prevalence of lagunary-like conditions in the center of the basin. Radiocarbon-dating of an Aquic Haplargid from a playa area indicates that an argillic horizon might form in a relatively short period (660 BP), favored by

locally moister soil conditions, clayey-rich parent materials and the abundance of salts.

Climatic conditions moister than at present reigned in the three valleys during the later part of the middle Holocene, allowing the development of mollic, argillic and calcic horizons, under the influence of diverse parent materials and topographic positions.

5.5.5 Upper Holocene

Recent and actual fans of upper Holocene age buried locally the glacis and old fans. Their shape and location are related to the size and the geologic materials of the catchment areas. Recent fans predominate along fault lines in the northern fringes of the three valleys. Their shape and steep gradient suggest an intermittent pulsed uplift of the mountain front during the Holocene. Torriorthents and Camborthids developed on their surfaces under present-like climatic conditions. In the center of the basins, lagunary conditions persisted until recent times, as evidenced by the word Cochabamba which originates from indigenous words 'khocha' meaning lake and 'pampa' meaning plain.

5.6 CONCLUSIONS

This chapter intends to highlight the importance of knowing the landscape origin and evolution over time for identifying land degradation factors and hazards. This facilitates the understanding of the mechanisms of action, location, extent and expansion trends of degradation phenomena. The tectonic and sedimentary history of the basins, the nature of the sediments and the spatial distribution of the geopedologic cover formations determine a differential susceptibility of the three valleys to specific land degradation processes.

In the Cochabamba valley, stream avulsion is the main environmental hazard. The moraine deposits from the last glacial periods, located in the northern parts of the Cochabamba and Sacaba valleys, constitute a permanent threat to urban settlements and agricultural lands in the lowlands. The heterometric, poorly sorted, highly unstable moraine deposits are a source of material available for stream avulsion, especially under exceptional situations such as earthquakes or extraordinary rainfall events. The direct connection between moraine deposits and some presently active fan channels, such as the Pairumani, Largon Mayu and Taquiña, aggravates the situation, transforming their areas of influence in hazardous zones, prone to channel avulsion.

In the Sacaba valley, badlands develop through gully formation from collapsing of subsurficial tunnels and pipes. The presence of lenticular gravel and coarse sand depositional structures, the Quaternary lake level fluctuations, and the erodibility of the silty and sandy clay lagunary materials are among the factors controlling the initiation of the erosional processes in the Sacaba area. Soil erosion features such as gullies, tunnels and pipes, occurring in the distal parts of the dissected depositional glacis located south of Sacaba, are originated mainly by subsurface flow. The highly permeable gravel lenses and sheets cause an irregular and preferential concentration of the water movement, originating a subsurface network

through tunnelling and piping. The collapse of the tunnels and pipes causes gullies from which badlands develop. On the other hand, the easily erodible sandy clay, silt loam and loamy lagunary materials do not allow the development of well structured soils and favor surface sealing and crusting. Intensive seasonal rainfalls cause overland flow and concentrated runoff with the initiation of rill and interrill erosion. The combined action of subsurface (piping, tunnelling) and surface erosional processes determines the formation of badlands in the lagunary depressions of the Sacaba valley.

In the Punata-Cliza valley, topsoil degradation dominates because of surface crusting and salt concentration. The lagunary depressions of the valley are characterized by thick clayey and sandy clay lacustrine sequences, with abundant ostracodes and organic materials in the deepest zones. The rainwater percolates through the subsurface alluvio-lacustrine and lacustrine deposits, increasing its salt concentration with depth. Jordan (1977) mentions groundwater from lacustrine deposits having high Cl^- and Na^+. Dissolved salts concentrate in the surface layers as a result of capillary rise from the groundwater table.

CHAPTER SIX:

SALINIZATION-ALKALINIZATION

6.1 CAUSES OF SALINIZATION-ALKALINIZATION

Salt-affected soils form under the dominating influence of different ions in solid or liquid phases which alter the physical, chemical and biological properties of the soils. Water-soluble salts and compounds determine the processes leading to the formation of different types of salt-affected soils as seen in 2.3.1. Salt types are closely related to the environmental condition, and generally mixed under field conditions, in spite of the dominant occurrence of one or another. Several causes, such as biological activity, surface- or groundwater fluctuations and mineral weathering, among others, intervene in salt formation. The chemical compounds of the salts lead to the development of different types of salt-affected soils (Szabolcs, 1989). In the Punata-Cliza valley, the occurrence of saline-alkaline areas results from natural processes and the combined influence of human activities.

6.1.1 Natural causes

(1) Geology

Primary salinization develops because of geologic, topographic, climatic and hydrologic factors.
The dominant basin lithology consists of fine clay and silty clay lacustrine-lagunary sediments, intercalated with lenses and sheets of gravelly and sandy alluvial materials. This originates low internal drainage in general but also local zones of variable permeability. Sequential depositions of coarser sediments of alluvial and alluvio-lacustrine origin allowed the development of groundwater tables at variable depths. In the catchment areas, the lithology is mainly gneiss, sandstones, quartzitic sandstones, claystones, shales and calcareous sandstones intercalated with marls of Paleozoic age (San Benito and Cuchupunata formations).

In most of the flat basin areas, deep bluish lacustrine clays constitute a thick layer in contact with the Paleozoic basement. They are enriched with ostracodes and undecomposed organic rests. According to chemical analyses of the groundwater from well logs located in the playas, salinity levels increase with depth (Cordeco-Subdesal, 1993).

(2) Topography

Flat areas with slope gradient less than 1% dominate towards the center of the basin, causing a very slow surface drainage. As a consequence, topographic depressions are temporally water-logged. This is the

case in Arce Pampa, Crespo Pampa, Laguna Carmen, Tolata Chico, Ticani Pampa, Tejar, Estancia Champa, South of Baco Pampa, San Isidro Pampa and Lequinas (fig. 6.1). Natural drainage through the Sulty, Cliza and Kory Mayu rivers is discontinuous. The Sulty river, the main collector traversing the basin, has a gradient 0.5% southward and 0.1% westward. The building of the Angostura dam originated an elevation of the Sulty river base level, locally silting up the riverbed and diminishing the drainage.

(3) Climate

Because of the moisture surplus occurring during the rainy season, soluble salts translocate downwards the soil profile. However, shortage of water and high evapotranspiration rates during the dry season cause upwards migration of salts due to capillary rise.

Rainwater plays an important role in the salinization-alkalinization process. The rainwater falling onto the basin is enriched with CO_2, which dissolves in the water to form carbonic acid. The carbonic acid induces chemical weathering as it percolates through the Quaternary sediments filling the basin or infiltrates the diaclases of the Paleozoic formations (Zubieta, 1977). The less resistant minerals such as carbonate concretions and halite crystals are dissolved first. As the percolation continues through subsurface flow in the alluvial and lacustrine-lagunary sediments, the salt content of the water increases. The moisture deficit of the dry season originates the rise of the groundwater table by capillary movement. As a consequence, water evaporates and salts accumulate on the soil surface, forming salt efflorescences, puffy crusts and fluffy cover layers.

(4) Hydrology

Salt efflorescences are controlled by the hydrological regime of the basin. Salts are mobilized either by surface flow or rising groundwater. In the colluvio-alluvial fans, the salt concentration of the groundwater is low because the contact time for the rainwater percolating through these materials is limited due to the high permeability of the sediments. In the distal part of the fans, in the transition areas between the piedmont and the lagunary flats, the groundwater movement is considerably slower and there is enough time for ionic exchange reactions to take place. Al, Ca and Mg ions are mobilized from the hydrous silicates of the clay matrix, and K, Mg and Fe ions are available from the clastic rocks. As the water percolates through the transition zone towards the lacustrine sediments of the basin floor, the salt concentration increases. In the center of the playas, the groundwater flow is slow, downward percolation is limited, and the reaction of the water with the lagunary-lacustrine clays lasts for longer periods allowing the dissolution of the salts.

Jordan (1977) reports that 61% of the groundwater from the lacustrine zones are rich in chlorides of Na, Ca and Mg; 11% are sodium bicarbonate enriched and have lower inclusions of Ca, Mg, Cl and SO_4 ions. Only 1% of the groundwater is mainly magnesium bicarbonate enriched. Water quality varies also spatially. Waters from the Cliza river are rich in bicarbonates of sodium, calcium and magnesium, whereas magnesium and calcium chlorides predominate in the vicinity of Tolata, south of the Angostura dam.

The groundwater table is at shallow depth in the center of the basin, standing at 1 to 3 m below the surface. This favors upward migration of salts during the dry season, in particular along the depressions of the Sulty and the Cliza rivers.

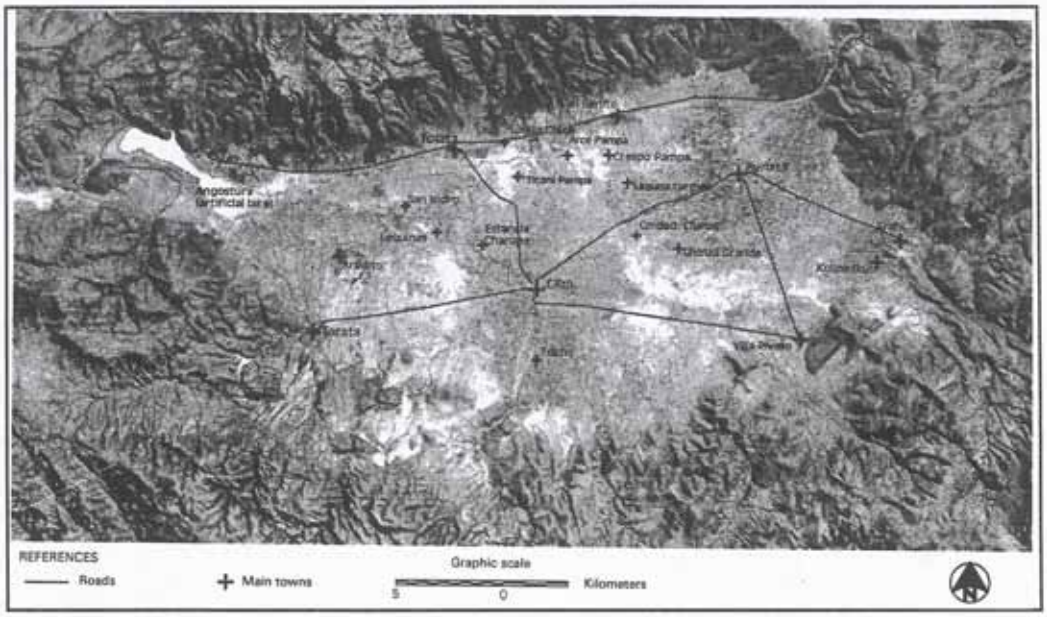

Fig. 6.1: *Lagunary depressions of the Punata-Cliza valley affected by temporal waterlogging.*

6.1.2 Human influences

Secondary salinity arises because of infrastructure construction and irrigation mismanagement. The Angostura dam, built in the mid 1960s, occupies the northwestern sector of the basin and impedes the natural drainage through the Tamborada river. As a consequence, the water table rose in the surrounding areas up to 1 or 2 meters from the surface, as well as the base level of the Cliza and Sulty rivers which discharge into the reservoir. Almost all the ground and surface waters from the Punata-Cliza basin end up in the Angostura artificial lake, thus increasing its salinity. This has markedly reduced its value as a source of irrigation water. Salts intrusion occurs mainly at the beginning of the rainy season when the first showers wash out the saline crusts from the riverbeds and playas. Additionally, the construction of roads in the areas of Villa Rivero-Cliza, without adequate culverts, blocks the already poor surface drainage towards the Sulty river.

Irrigation practices, in particular the 'lameado' technique, and the use of saline-alkaline water accentuate the salinization process. For instance, waters from glacial lakes such as the Juntutuyo and Parcko Khocha are highly saline-alkaline and rate C4, C3, S4 and S3 according to the USDA classification scheme. Nevertheless, they are being used for irrigation purposes in the area of Arani. When bringing new

agricultural lands under irrigation, farmers frequently omit to provide the necessary artificial drainage to carry off the additional water and soluble salts. This has resulted in a rising water table and increased salt concentration in waters and soils.

6.2 NATURE AND SPATIAL DISTRIBUTION OF THE SALTS

The effects of water-soluble salts on soil properties depend on environmental conditions as well as on the types of ion causing salinity and/or alkalinity. The salt ionic composition originates diverse terrain surface features such as saline efflorescences, puffy crusts and fluffy consistence. The Punata-Cliza valley, where these features are common, was selected to investigate the effects of salinization and alkalinization on land degradation.

6.2.1 Chemical composition of the salt-affected topsoils

Ninety five soil surface samples were collected from lagunary flats and playas, following the sampling scheme described in chapter three. The soil analysis techniques described in Richards (1954) were used to determine the amounts of Na^+, Ca^{2+}, Mg^{2+}, CO_3^{2-},HCO_3^-,Cl^- and SO_4^{2-} ions present in the saturation extracts. Table 6.1 presents the results of these analyses and indicates the main salts influencing the development of salt-affected areas.

Table 6.1: Chemical composition of salt-affected topsoils of the playas and lagunary flats

LANDSCAPE	RELIEF TYPE	LANDFORM	PEDON	pH	ECe	Na	Ca	Mg	Cl	SO4	CO3	HCO3	Predominance of
Piedmont	Depositional glacis	Distal	Va66	8.5	3.96	6.00	13.00	35.00	15	35	.5	3	SO4 > Cl
			Va67	8.8	3.00				15	9.5	.5	8	SO4 > Cl
Valley	Lagunary depressions	Higher lagunary flats	Va33	8.30	0.22				1.8	.9	0	3.2	HCO3 > Cl
			Va34	7.70	0.10				.9	1	0	1	HCO3 = SO4 = Cl
			Va37	7.90	0.27				.5	.6	0	1.6	HCO3
			Va38	8.40	0.16				.7	2.5	0	2.4	HCO3=SO4
			Va39	8.60	0.18				.5	.1	0	1.6	HCO3 > Cl
			Va40	8.10	0.24				5	8.1	0	2	SO4 > Cl > HCO3
			Va41	8.30	0.15				.4	.2	0	2.7	HCO3
			Va42	7.85	0.14				.5	1.5	0	1.4	HCO3 = SO4
			Va43	7.90	0.12				.4	.5	0	1.2	HCO3 > SO4
			Va44	8.00	0.09				.4	.5	0	1.2	HCO3 > SO4
			Va46	8.6	.43				.5	.5	.5	5.5	HCO3 > SO4=Cl=CO3
			Va47	8.3	.42				.37	.9	.2	3.8	HCO3 > SO4
			Va48	8.4	1.13				.75	4.5	.5	6.5	HCO3 > SO4
			Va61	8.5	.94				.87	1.5	.5	8	HCO3 > SO4
			Va64	10.1	20.35				75	123	166	59	CO3 > SO4
		Medium lagunary flats	Va60	8.00	63.94				3500	320	0	15	Cl > SO4
		Lower lagunary flats	Va29	8.10	0.14				.2	2	0	.5	SO4 > HCO3
			Va30	8.20	0.22				2.3	.1	.5	2.5	HCO3 = Cl
			Va31	8.60	0.33				6.2	2	0	3.5	Cl > HCO3
			Va32	8.40	0.13				.5	.1	.5	3	HCO3 > Cl=CO3
			Va45	8.4	.58				1	1	.5	3	HCO3 > Cl=SO4
			Va49	8.3	.91				1.5	1.5	.5	6.5	HCO3 > Cl=SO4
			Va50	8.6	.84				.75	.5	2.75	7	HCO3 > CO3
			Va62	8.4	.89				5	.7	.5	3.5	Cl > HCO3
			Va60	7.2	106.86				1300	873	0	2	Cl > SO4
			Va88	9.9	52.71				350	175	104	3.5	Cl > SO4
			Va89	10.00	58.6	1.50	4.00	1520.00	550	800	170	1	SO4 > Cl
			Va91	8.6	78.95	30.00	34.00	350.00	290	130	.5	9	Cl > SO4
			Va104	8.00	30.35				350	214	0	10	Cl > SO4
			Va105	9.6	87.29	1.50	4.50	1800.00	900	750	80	40	Cl > SO4
			Va106	10.1	46.92	2.50	14.50	869.00	175	300	280	110	SO4 > CO3
			Va116	10.1	66.38				200	840	520	105	SO4 > CO3
			Va123	8.7	45.48				550	100	0	3.5	Cl > SO4
			Va124	8.4	5.17				50	18	0	5	Cl > SO4
			Va125	9.1	1.5				2.5	6	.15	7.5	HCO3 > SO4
		Playas	Va62	9.3	17.38				85.5	95.5	10	14	SO4 > Cl
			Va63	8.5	23.13	3.00	12.00	190.00	150	95	.5	11.5	Cl > SO4
			Va64	10.00	89.6				550	253	240	40	Cl > SO4
			Va65	10.02	28.36	4.00	0.50	560.00	75	225	210	55	SO4 > CO3
			Va54	8.4	12.67	8.00	2.00	150.00	105	60	0	5	Cl > SO4
			Va57	8.9	23.9				115	206	1	14	SO4 > Cl
			Va58	9.5	8.56				20	23	14	10.5	SO4 > Cl
			Va59	10.1	46.28	3.00	2.00	1000.00	250	295	430	120	CO3 > Cl
			Va60	10.00	62.16				250	400	520	200	CO3 > SO4
			Va61	9.9	65.83	3.00	0.50	1660.00	300	560	520	180	SO4 > CO3
			Va63	10.2	29.24				160	180	82	2.28	SO4 > Cl
			Va65	9.7	55.82	2.00	2.50	750.00	400	300	50	0	Cl > SO4
			Va66	7.3	73.00				900	459	0	2	Cl > SO4
			Va67	10.1	68.94				500	690	26	50	SO4 > Cl
			Va68	10.2	43.81	2.00	3.50	1300.00	360	770	145	25	SO4 > Cl
			Va69	10.1	54.15	1.50	2.00	775.00	375	665	300	81	SO4 > Cl
			Va70	10.00	53.93				360	630	170	100	SO4 > Cl
			Va71	7.5	56.93				485	460	0	5	Cl > SO4
			Va72	7.3	48.37				550	370	0	4.5	Cl > SO4
			Va73	7.8	15.34				150	60	0	4	Cl > SO4
			Va74	7.1	79.5				530	964	0	2.5	SO4 > Cl
			Va75	7.3	70.72	81.00	1020.00	620.00	880	815	0	2.5	Cl > SO4
			Va76	7.3	99.66	0.30	0.30	1670.00	1365	550	0	2	Cl > SO4
			Va77	7.3	77.17	74.00	127.00	1220.00	1300	110	0	2	Cl > SO4
			Va78	7.00	99.97	97.50	513.50	915.00	1000	490	0	2	Cl > SO4
			Va79	6.8	92.74				1300	550	0	1.5	Cl > SO4
			Va81	6.7	150.89	26.50	564.00	1900.00	2200	270	0	2	Cl > SO4
			Va82	8.5	2.27				15	7	0	2	Cl > SO4
			Va83	7.8	63.06				715	550	0	5	Cl > SO4
			Va84	8.4	1.7				15	1	0	2	Cl > HCO3
			Va85	8.1	189.92				4670	1343	1	.5	Cl > SO4
			Va92	7.6	154.00	37.00	206.00	1850.00	2150	85	0	5	Cl > SO4
			Va93	9.7	150.67				2850	612.5	134	8	Cl > SO4
			Va94	8.2	181.00	29.00	74.00	3060.00	3000	114	2	4	Cl > SO4
			Va95	7.5	133.99				2000	105.5	0	2.5	Cl > SO4
			Va96	9.9	124.32	2.00	2.50	3060.00	1650	1320	94	0	Cl > SO4
			Va97	8.4	104.52				1400	1110	.5	3.5	Cl > SO4
			Va98	9.3	152.78				2400	1580	49	17	Cl > SO4
			Va99	9.4	11.75	3.00	2.00	3200.00	1850	1288	45	22	Cl > SO4
			Va100	9.7	147.78	0.50	2.50	4600.00	1300	2560	728	222	SO4 > Cl
			Va101	9.9	117.31				750	2750	462	136	SO4 > Cl
			Va102	9.5	12.23				100	80	10	10	Cl > SO4
			Va103	9.9	105.5	1.00	9.00	2560.00	1150	1100	280	40	Cl > SO4
			Va107	9.7	93.29	1.00	2.00	2120.00	1100	620	360	40	Cl > SO4
			Va108	9.4	63.16				775	80	60	7.5	Cl > SO4
			Va109	9.7	105.6				1300	1180	860	196	Cl > SO4
			Va110	9.9	80.00	5.00	0.50	2450.00	400	1600	320	120	SO4 > Cl
			Va111	9.8	104.3				1400	910	340	40	Cl > SO4
			Va112	9.6	106.52	1.00	0.50	3200.00	1350	1565	250	40	SO4 > Cl
			Va113	8.3	87.04				1370	250	0	10	Cl > SO4
			Va114	10.00	82.84				1200	405	325	30	Cl > SO4
			Va115	10.00	85.62	2.00	0.30	1400.00	750	232	200	250	Cl > HCO3
			Va117	7.7	131.1	224.00	151.00	940.00	50	1280	0	10	SO4 > Cl
			Va118	9.6	129.49	1.50	16.50	1300.00	75	1233	1	9	SO4 > Cl
			Va119	10.1	77.5	1.00	2.50	6.25	500	320	0	0	Cl > SO4
			Va120	9.9	79.61	0.75	0.70	730.00	400	317	0	0	Cl > SO4
			Va121	9.7	98.97				1200	102	190	32.5	Cl > SO4
			Va122	8.5	41.36	0.30	0.30	540.00	437	135	0	11	Cl > SO4

ECe in dS/m; ions in meq/l

Salt-affected soils vary according to their chemical composition. In the processes of salinization, the various salts accumulate in a proportion inverse to their solubility. In non-saline or slightly saline soils, Ca^{2+}, Mg^{2+} and HCO_3^- predominate in the soil solution. As salinity increases, the more soluble salts become dominant. Strongly saline soils contain large quantities of NaCl and Na_2SO_4. Sodium salts capable of alkaline hydrolysis, such as Na_2CO_3 and $NaHCO_3$, dominate in alkaline soil-forming processes. The main characteristics of the salt compounds present in the Punata-Cliza area are described hereafter:

(1) Carbonates

Carbonates exert different effects on the soils, depending on the cation the carbonate is bound to, the amount accumulated in the soil and the solubility.

(a) Calcium carbonate

Calcium carbonate may occur as a pure chemical but is also found as a calcium-magnesium mixture. It has very low solubility in water, which depends on the CO_2 concentration and the pH of the solution. A saturated aqueous solution of calcium carbonate has a pH of 8.3 to 8.4. The interaction between the three factors namely CO_2 concentration, pH and calcium concentration is expressed by the graph of figure 6.2.

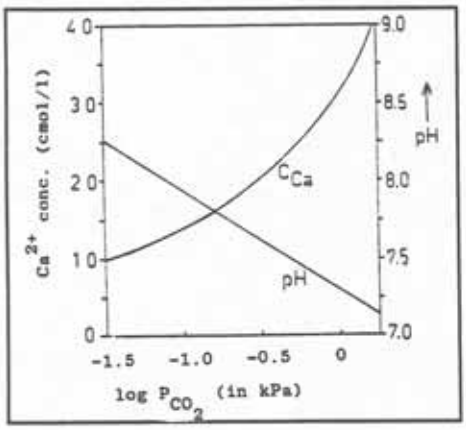

Fig.6.2: Solubility of calcite and resulting pH values in water at different CO_2 pressures

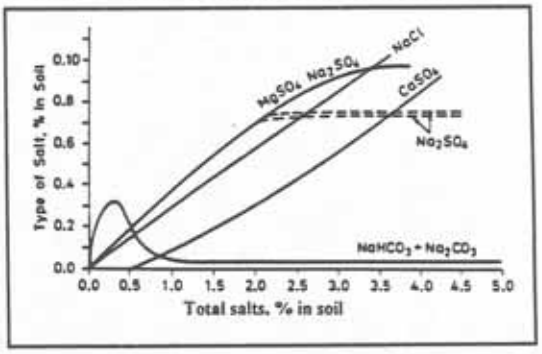

Fig. 6.3: Relationship between the degree of alkalinization of the soil and the acumulation of alkaline salts (Kovda, 1947)

The precipitation/dissolution equilibrium of carbonates in the soil is governed by two factors: the CO_2 pressure of the soil atmosphere and the concentrations of dissolved ions in the soil moisture solution (Driessen et al., 1991). The equilibria can be represented as follows:

$$CO_2 + H_2O \rightarrow H_2CO_3$$
$$CaCO_3 + H_2CO_3 \rightarrow Ca(HCO_3)_2$$

An increase in the carbon dioxide of the soil air leads to a decrease in the soil pH, thus increasing the solubility of calcium carbonate. Precipitation occurs if the CO_2 pressure lowers and the pH increases.

(b) Magnesium carbonate

Magnesium carbonate occurs in soils in the form of magnesite ($MgCO_3$). A saturated solution of magnesium carbonate has a pH around 10. Its formation results from the chemical decomposition of crystalline rocks. It might be toxic, especially when the ratio Ca:Mg is unbalanced.

(c) Sodium carbonate

Sodium carbonate is a highly soluble compound which, as a result of alkaline hydrolysis, reaches pH values between 9 and 11. But the formation of bicarbonates reduces soil alkalinity regardless of the anion bound, as it was observed in soils belonging to the lagunary flats in the surroundings of Cliza and Arce Pampa (samples Va29 to Va52 and Va71 to Va81 from table 6.1), where the soil reaction is ≤ 8.5. The transformation of carbonate into bicarbonate is a reversible process, and a decrease in carbon dioxide causes the formation of carbonate from bicarbonate. This occurs where the activity of micro-organisms is weak and the content of organic matter low, as reported in the playas and lower lagunary flats. Accumulation of $NaCO_3$ occurs from sodium carbonate and bicarbonate. The absence of calcium sulphate compounds allows the formation of soda-saline soils.

Sodium carbonate can develop under different processes and conditions, in particular biological reduction, chemical weathering due to the interaction of silicates and water containing CO_2, fine clayey texture, and the interaction between NaCl or Na_2SO_4 and calcium carbonate (Szabolcs, 1989). When the soil reaches a total salt concentration of 0.3 to 0.5 %, Na_2CO_3 precipitates in preference to the other salts, as illustrated in figure 6.3 (Kovda, 1947; Szabolcs, 1989).

Soda formation in the Punata-Cliza valley may be attributed to one of the following processes or a combination of these:

- The interaction of silicates (feldspars, quartz, mica, clay minerals) and carbon dioxide. During this process bicarbonates of Ca, Mg, Na and K are formed. Upon evaporation of the resulting solutions, Ca and Mg carbonates precipitate, while $NaHCO_3$ gradually loses CO_2 and is transformed into Na_2CO_3.

- The action of NaCl or Na_2SO_4 on $CaCO_3$ (Hilgard, 1906; Szabolcs, 1989). The following reactions are produced:

$$2NaCl + CaCO_3 \rightleftharpoons Na_2CO_3 + CaCl_2$$

$$Na_2SO_4 + CaCO_3 \rightleftharpoons Na_2CO_3 + CaSO_4$$

Chemical analyses show that Na-sulphates and chlorides predominate in the salt-affected areas. $CaCO_3$ is present in the groundwater from the Punata fan and the south and southwestern parts of the valley, as reported by Jordan (1977).

- Biological reduction of sulfates. In reduced anaerobic conditions, soda formation could occur as consequence of biological reduction of sulfates in the soil (Szabolcs, 1979). In presence of high clay content and relatively low salt concentration, sodium carbonate forms by exchange reactions in the colloid

fraction (Gedroitz, 1955; Szabolcs, 1989). This process might occur in the areas bordering the Angostura dam, previously covered by water and subject to waterlogging.

(2) Sulphates

The chemical composition of the soluble salts from the Punata-Cliza valley shows the presence of magnesium and sodium sulphates.

(a) Magnesium sulphate

Magnesium sulphate is a highly soluble and mobile salt which precipitates in the form of epsomite ($MgSO_4.7H_2O$). Epsomite never accumulates in soils in a pure form, but is always found together with other readily soluble salts, such as sodium sulphate, sodium chloride and magnesium chloride (Szabolcs, 1989). As the concentration of sodium sulphate increases, the saturation of magnesium sulphate decreases.

(b) Sodium sulphate

Sodium sulphate is also a highly soluble and mobile salt, which crystallizes in different ways according to temperature . Under relatively low temperature, it precipitates in the form of needle-shaped mirabilite ($Na_2SO_4.10H_20$), which dehydrates and turns into white powdery thenardite (Na_2SO_4) when temperature increases. In the Na_2SO_4-H_2O system, the stable phases are mirabilite, also known as Glauber's salt, thenardite and heptahydrite, the latter not definitely identified in nature. The solubility of mirabilite and thenardite is reduced by the addition of NaCl. Figure 6.4 shows that the mirabilite-thenardite transition point is lowered from 32o to 17.9oC in a NaCl-saturated solution (Braitsh, 1962).

(3) Chlorides

Together with sulphates, chlorides are the main compounds responsible for the formation of saline soils. They are highly soluble and may be highly toxic (Szabolcs, 1989). Calcium chloride (CaCl) is rarely present in soils because it commonly reacts with $NaSO_4$ and Na_2CO_3. As a consequence, the calcium precipitates in the form of $CaSO_4$ or $CaCO_3$. Instead, the highly soluble and toxic sodium chloride (NaCl), together with sodium and magnesium sulphate, is the most common component of saline soils.

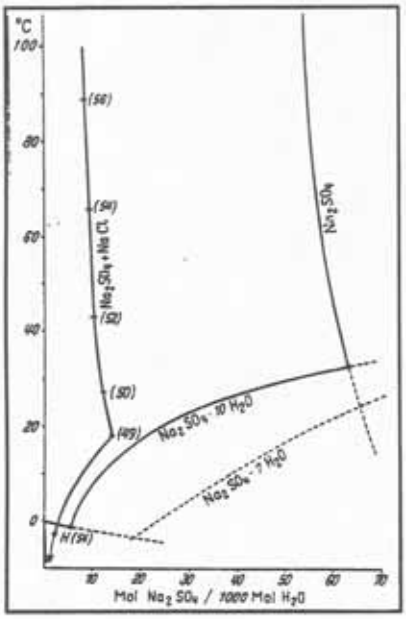

Fig. 6.4: The system Na_2SO_4-H_2O, in the absence of NaCl (right-hand curve) and at saturation with respect to NaCl (left-hand curve) (Braitsh, 1962)

6.2.2 Anion distribution on the landscape

From the anion percentage composition of the samples collected in the Punata-Cliza valley, four main categories of dominating salts were identified and correlated with different landscape positions (table 6.2).

(1) Carbonate dominated topsoils

Carbonate and bicarbonate anions, together with lower amounts of sulphates and few chlorides, dominate in the topsoils of the higher lagunary flats of alluvio-lagunary origin (fig. 6.24). They are also representative of the transitional areas from higher to lower lagunary flats and of the playas. Salinity-alkalinity values are low because of the low salt concentration (up to 0.3% by sum of anions). ECe is usually less than 1 dS/m and pH less or equal to 8.5. Anion composition is as follows: carbonates + bicarbonates >> sulphates > chlorides.

(2) Sulphate-carbonate dominated topsoils

A second category is composed of about 40% sulphates and variable amounts of chlorides, carbonates and bicarbonates. Up to 8% salt concentration is found in these soils, which dominate in the lower lagunary flats and playas (fig. 6.5). These are highly saline-alkaline areas, with average pH values higher than 8.5 and ECe values above 30 dS/m. Anion compositions is: sulphates > carbonates + bicarbonates > chlorides.

(3) Chloride dominated topsoils

Chlorides, accompanied by sulphates and small amounts of carbonates and bicarbonates, dominate in the playa areas affected by high salt concentrations (8 to 15%). These topsoils are very saline and non to slightly alkaline, with pH values lower than 8.5 in the absence of free carbonates and bicarbonates. On average, electrical conductivity values are above 60 dS/m. The ionic composition is: chlorides >>

sulphates > carbonates + bicarbonates.

(4) Chloride-sulphate dominated topsoils

The fourth category predominates in the playas and is composed of variable amounts of chlorides and sulphates with small proportions of carbonates and bicarbonates. These topsoils are saline-alkaline, with ECe ranging from 60 to 130 dS/m and pH values above 9. The ionic composition is: chlorides = sulphates >> carbonates + bicarbonates.

Table 6.2: Relative dominance of salts according to landscape positions (% anions). Averaged ranges of laboratory data.

CATEGORY	(a) CARBONATE DOMINATED	(b) SULPHATE-CARBONATE DOMINATED	(c) CHLORIDE-DOMINATED	(d) CHLORIDE-SULPHATE DOMINATED
Carbonates and bicarbonates	60 - 70	40	0 - 10	20
Chlorides	around 10	20	50 - 60	10 - 40
Sulphates	15 - 20	40	40	10 - 40
Predominate on	higher lagunary flats	lower lagunary flats and playas	playas	playas

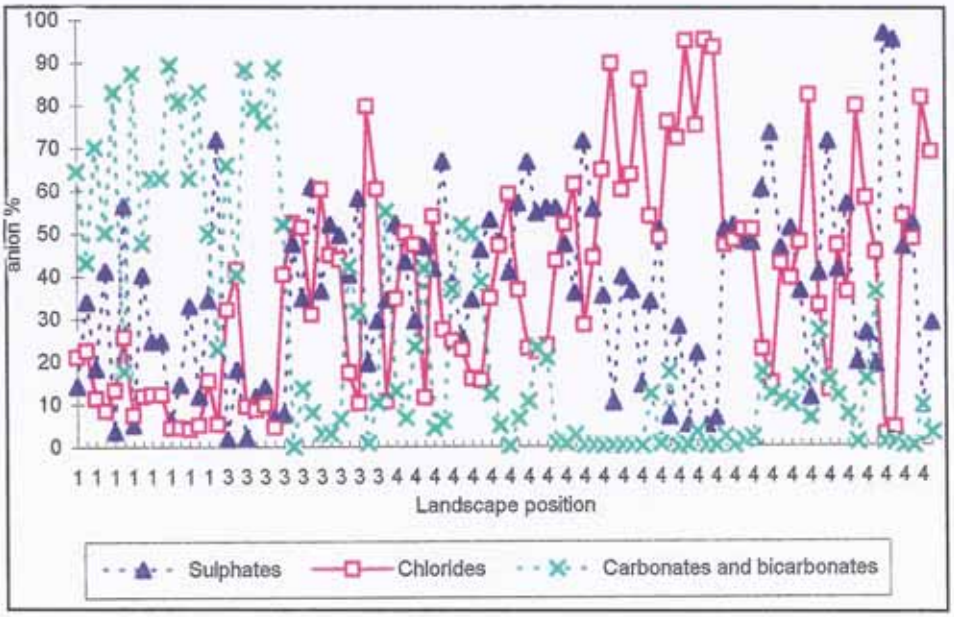

Fig. 6.5: Percentage anion composition of sampled topsoils on different landscape positions: (1) higher lagunary flats, (3) lower lagunary flats, (4) playas.

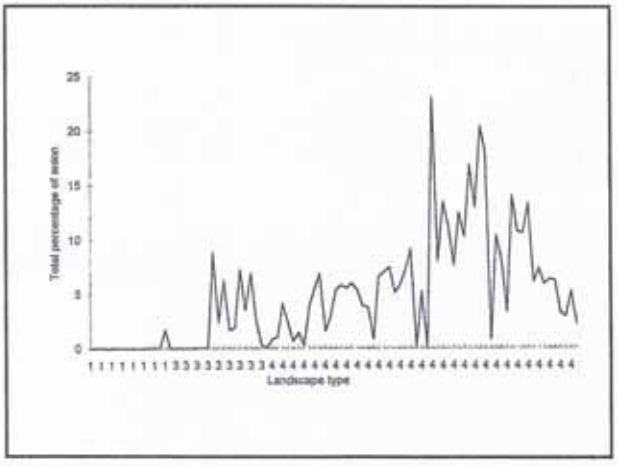

Fig. 6.6: Total anion amount of the sampled topsoils on different landscape positions: (1) higher lagunary flats, (3) lower lagunary flats, (4) playas.

The predominance of carbonates and bicarbonates over the other anions in the higher lagunary flats might be attributed to the alluvial deposits these flats received from the carbonate-rich materials occurring in the southern part of the Punata-Cliza valley. Carbonates tend to diminish towards the center of the valley, being replaced by sulphates in the lower lagunary flats and by similar proportions of chlorides and sulphates in the lacustrine-lagunary playas. Greatest salt concentrations occur in the playas, with values as high as 20% in the topsoils sampled (fig. 6.6). Instead, the higher lagunary flats register the lowest salt concentrations, with values ranging from 0.01 to 0.5%.

6.2.3 Morphology of salt-affected terrain surfaces

Salt-affected terrain surfaces vary in color, consistence and micro-topography according to the texture of the soil material, the type and concentration of salts, and the moisture content. Three main types were identified in the field: puffy soil surfaces, glassy salts crusts and structureless crusts.

(1) Puffy soil surface

Puffy material is a mixture of soil aggregates and salts of different crystal forms containing mainly sodium sulphates. Puffed surface layers are common on Camborthids with saline phases and Salorthids found throughout the area (fig. 6.7). They occur on the playas, which are transitional areas between the piedmont and the lagunary depressions. The mixtures of soil particles and sulphates forming the puffed surface layer of the Natric Camborthids and the Salorthids may correspond to a Na_2SO_4-H_2O system, with or without the presence of NaCl salts (Braitsch, 1962; Driessen et al., 1991).

The morphology of the salts in the puffy layers of the playas and lower lagunary flats changes with temperature fluctuations. The needle-shaped crystals push the soil aggregates apart when they form, creating a fluffy salt-soil mixture at the surface (Janitzky, 1957; Driessen et al., 1991).

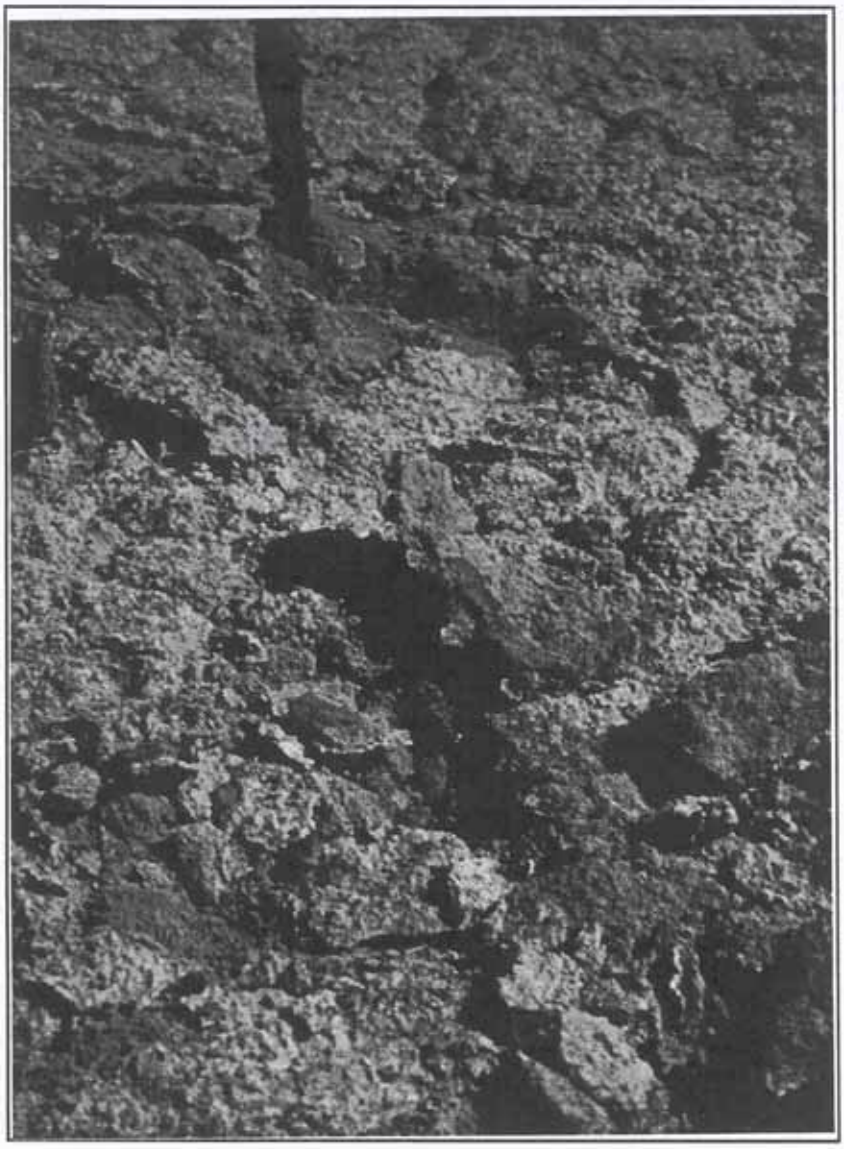

Fig. 6.7: Puffed surface layer occurring in playas and lagunary depressions.

(2) Glassy salt crust

Glassy salt crusts are rich in sodium and magnesium (e.g. soil samples Va75, Va77 and Va78 in table 6.1). The crust consists mostly of chlorides or equal proportions of sulphates and chlorides. The morphology of the crust and its chemical composition suggest the presence of bloedite [$Na_2Mg(SO_4)_2.4H_2O$] (Braitsh, 1962; Driessen et al., 1973).

The dominance of hygroscopic salts, such as $CaCl_2$ or $MgCl_2$, causes the absorption of atmospheric moisture, keeping the soil surface moist and making it dark-coloured. The soil surface is dark-coloured in the morning as a result of moisture absorption during the night. The dark colour vanishes in the course of the day when the temperature rises and air humidity drops to low values. This situation was observed in some playa areas located in the southern part of the basin.

(3) Structureless crust

The third type consists of a loosely structured crust, including needle-shaped crystals such as thenardite and/or mirabilite (fig. 6.8). These are crystals of sodium, magnesium and calcium compounds. Sulphate content may be as high as 96% (fig. 6.9). Such crusts were found in places with shallow saline groundwater table and close to the Sulty river and irrigation canals. They are common in the southeastern part of the basin (Kollpa Bajo), in the central areas occupied by playas and lower lagunary flats (fig. 6.1).

Fig. 6.8: Fluffy, structureless saline surface

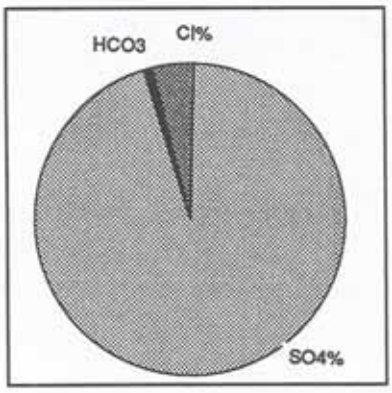

Fig. 6.9: Ionic composition of a fluffy surface layer.

Under natural conditions, soluble salts concentrate in the topsoil and on the terrain surface because of the water capillary rise. The top horizons of saline soils accumulate greater amounts of soluble salts, such as NaCl, Na_2SO_4 and $NaCO_3$, than the lower horizons. For instance, salt concentrations ranging from 100 to 400 gr/l can be found in the top horizons, while 20 to 50 gr/l occur in the lower ones (Szabolcs, 1989). Salt-affected soils formed under the influence of neutral sodium salts do not always

contain enough quantity of soluble salts to cause salt efflorescences on the surface.

In general, the formation of salt crusts hinders evaporation and hence the drying of the underlying soil material, which has been moistened during the previous wet summer period. Low-lying local areas of slightly concave topography and slow permeability remain moist throughout the dry winter months, while the surrounding soils dry, shrink and commonly crack even if the water table is high (Driessen et al., 1973). Because of the low permeability, excess soluble salts are not leached during the relatively moist summer. The salt content increases every dry season, because the actual evapotranspiration (211 mm) from April to November exceeds the precipitation (153 mm) and causes upward migration of brackish water by capillary rise, even at low soil permeability (fig. 4.8). Rain falling during the summer time, from December till middle March, is only partly available for leaching because the precipitations are intensive and of short duration. In areas of low infiltration, the water runs off and stores in water-logged local depressions.

Spatial and temporal variations in groundwater depth and soil temperature make certain salts accumulate faster than others, causing changes in the aspect of the surface layers. The formation of salt efflorescences is enhanced by alternating wet and dry seasons. The solubility of most salts increases in the temperate dry season, when there is upward migration of brackish groundwater to the soil surface, and decreases in the wet season when salts are leached or washed from the surface by surplus rainfall. This could explain the extremely high Na concentrations in the upper layers during the core of the dry season, when the sampling was carried out. The highly soluble sodium salts, such as NaCl and Na_2SO_4, move through capillary fluctuations of the groundwater.

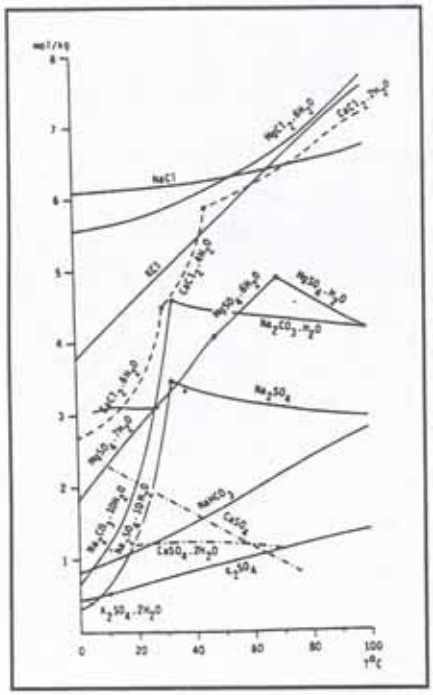

Fig. 6.10: *The solubility of common salts in Solonchaks, expressed in mole anhydrous salt per kg H_2O, as a function of the soil temperature (Braitsh, 1962).*

Figure 6.11 presents the stability diagram of salt minerals in a NaCl-saturated Na_2SO_4-$MgCl_2$-H_2O system. The diagram demonstrates that diurnal or seasonal temperature fluctuations alone may induce mineralogical transformations. Taking into account the local temperature regime (fig. 6.12), the basic chemical constituents of the salts identified in the area (table 6.1) and the macro-morphologic features observed in the field, the following minerals might be expected to occur in the salt-affected areas of the Punata-Cliza basin: halite (NaCl), mirabilite ($Na_2SO_4.10H_2O$), thenardite (Na_2SO_4), bloedite ($Na_2Mg(SO_4)_3.4H_2O$) and epsomite ($MgSO_4.7H_2O$).

Halite is the major salt mineral in the soil surface. Nevertheless, the concentrations of major cations and anions in the saturation extracts of several samples show that other minerals, in particular sulphate salts, can coexist together with sodium chloride. For instance, the sample Va105 (table 6.1) has the following ionic concentrations: Na 1800 meq/l, Mg 5 meq/l, Ca 2meq/l, CO_3 80 meq/l, HCO_3 40 meq/l, Cl 900 meq/l and SO_4 750 meq/l. Assuming all chloride ions are in the form of halite, 900 meq/l of Na remain to form some kind of sulphate salt.

According to chemical analyses, observed soil surface features and soil temperature, a glass salt crust consisting mainly of platy bloedite crystals sealing the underlying soil surface may be expected to occur at some locations north of Villa Rivero. The soil sample Va117 (table 6.1) collected in this area has enough Na^+, Mg^{2+} and SO_4^{2-} to form bloedite.

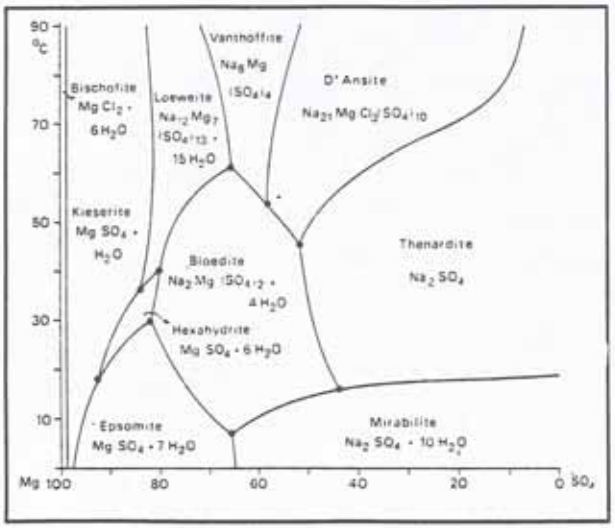

Fig. 6.11: *Stability diagram of minerals in a NaCl-saturated Na_2SO_4-$MgCl_2$-H_2O system (from Braitsch, 1962).*

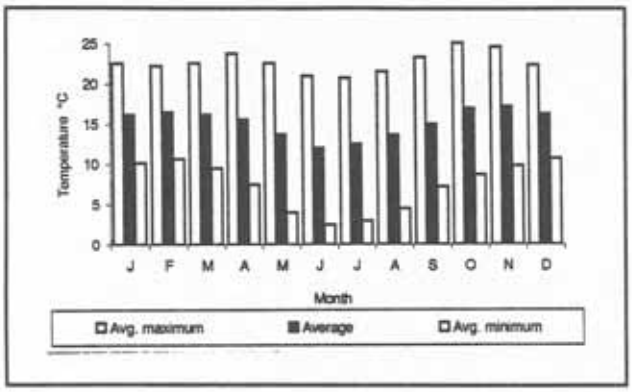

Fig. 6.12: *Average daily, minimum and maximum monthly temperatures in the Punata-Cliza valley (SENAMHI, Cochabamba, 25 years records).*

6.3 CLASSIFICATION OF THE SALINE-ALKALINE SOILS

6.3.1 General classification criteria

Saline soils contain high amounts of water-soluble salts, producing harmful effects on crops. Determination of a salt percentage limit for saline and non-saline soils is very difficult since some crops are more tolerant than others to the effects of high salt contents (Driessen, 1993). Furthermore, not all salts are equally harmful: sodium salts, for instance, are more so than calcium and magnesium salts (fig. 6.13).

NaCl	Na_2SO_4	Na_2CO_3	$NaHCO_3$
$MgCl_2$	$MgSO_4$	$MgCO_3$	$Mg(HCO_3)_2$
$CaCl_2$	$CaSO_4$	$CaCO_3$	$Ca(HCO_3)_2$

Fig. 6.13: *Harmful (above the line) and harmless (below the line) salts. (Plyusnin, 1964)*

(1) Classification per anion ratios

Russian soil scientists developed a system to classify salt-affected soils on the basis of salt types, in terms of chloride, sulphate and carbonate anion ratios present in the saturation extract. Saline soils are divided in sulphate soils, chloride-sulphate soils, sulphate-chloride soils and chloride soils according to the Cl/SO4 ratio (table 6.3). Predominance of sulphates over chlorides results in lower anion ratios. Five times more sulphates than chlorides to equal proportion of both anions are present in chloride-sulphate soils.

Table 6.3: Classification of saline soils based on anion ratios (Plyusnin, 1964).

SOIL TYPE	RATIO	Plyusnin	Rosanov	Sadovnikov
Sulphate soils	Cl/SO_4	< 0.5	< 0.2	< 0.2
Chloride-sulphate soils	Cl/SO_4	0.5 - 1.0	0.2 - 1.0	0.2 - 1.0
Sulphate-chloride soils	Cl/SO_4	1.0 - 5.0	1.0 - 2.0	1.0 - 5.0
Chloride soils	Cl/SO_4	> 5.0	> 2.0	> 5.0
Soda soils	CO_3/SO_4			< 0.05
Sulphate-soda soils	CO_3/SO_4			0.05 - 0.16
Soda-sulphate soils	CO_3/SO_4			> 0.16

Sulphate-type soils usually contain Na_2SO_4, $MgSO_4$ and $CaSO_4$. These soils have about five times more sulphate than chloride anions, are not alkaline and contain the least toxic soluble salts. Chloride-sulphate soils are characterized by the predominance of sulphates over chlorides. These are saline, non to slightly alkaline soils, with salt contents between 2 and 5%. Sulphate-chloride soils possess varying proportions of chlorides and sulphates, being chlorides predominant in proportions up to five times the chloride content. They are referred to as saline-alkaline soils, with large quantities of soluble salts in the top horizons (3 to 5%). Chloride soils contain great amounts of NaCl and $MgCl_2$, and chloride anions largely dominate over sulphates.

Saline soils containing salt compounds capable of alkaline hydrolysis classify as soda soils, sulphate-soda soils and soda-sulphate soils on the basis of their CO_3 to SO_4 ratio. Sulphate-soda soils can be referred to as saline-alkaline, sulphate-rich soils. Bicarbonates are present in proportions between 0.1 and 0.15%, being the pH between 8.7 and 9.5. The presence of Na_2CO_3 derives in high alkalinity, being the salinity comparatively lower. Soda soils do not contain great amounts of soluble salts (less than 1.5%), being therefore classified as alkaline, non to slightly saline soils. Common salt types are carbonates, bicarbonates and sulphates of sodium with pH values ranging from 9.5 to 12 (Szabolcs, 1989).

The World Reference Base for Soil Resources also follows an approach based upon anion assemblages, distinguishing six facies of salt-affected soils (Spaargaren, 1994):

1. Chloride soils
    a. Acid chloride soils, where $Cl >> SO_4 > HCO_3$, and $Na >> Ca$.
    b. Neutral chloride-sulphate soils, having nearly neutral pH
2. Sulphate soils
    c. Neutral sulphate soils, with nearly neutral pH, $Na >> Ca$, and $SO_4 >> HCO_3 > Cl$
    d. Acid sulphate soils, with very low pH (less than 3.5)
3. Carbonate soils
    e. Alkaline bicarbonate-sulphate soils, where $pH > 8.5$, $HCO_3 > SO_4 >> Cl$, and $Na > Ca$.
    f. Strongly alkaline soils, where $pH > 10$, HCO_3 and $CO_3 >> SO_4 >> Cl$, and $Na >> Ca$.

(2) Classification per total salt and exchangeable sodium contents

On the other hand, the classification system developed by the USDA Soil Salinity Laboratory (1954) makes no distinction between salt types and considers only the total salt level estimated from the electrical conductivity of the saturation extract (ECe), expressed in dS/m at 25°C temperature, and the exchangeable sodium percent (ESP) or sodium adsorption ratio (SAR) to classify among saline, saline-alkaline and alkaline soils (table 6.4).

Table 6.4: Classification of saline and/or alkaline soils based on ECe, ESP or SAR or pH.

SOIL TYPE	SOIL PROPERTY			
	SAR	ESP	pH	EC (dS/m)
Non saline, non alkaline	< 13	< 15	< 8.5	< 4
Saline	< 13	< 15	< 8.5	> 4
Alkaline	> 13	> 15	> 8.5	< 4
Saline-alkaline	> 13	> 15	> 8.5	> 4

6.3.2 Estimation of the sodium adsorption ratio (SAR)

The purpose is not only to differentiate saline, alkaline and saline-alkaline soil surfaces, but also to estimate the degree of salinity-alkalinity. In a first attempt, salinity-alkalinity classes were determined using reference values of SAR (<13, 13 - 26 and > 26) and ECe (0, 4, 8, 16, 32, 64 and >64 dS/m). These parameters showed to have great dispersion, since electrical conductivity ranged from 0.3 to 140 dS/m and SAR from 6 to 3900. Two additional problems arose: (a) only 33 out of the 95 samples selected for salinity studies had the necessary laboratory determinations to calculate SAR; (b) 90% of the SAR values were above 30.

(1) Simple regressions

Simple regressions between the sodium adsorption ratio values and the pH, cation and anion values were established with the purpose of predicting missing SAR values from existing ones to allow for soil classification at all observation points. Table 6.5 shows the correlation matrix among SAR, pH, chlorides, sulphates, carbonates, bicarbonates, sodium, calcium and magnesium values. Highest positive correlations concern SAR-sulphates (0.70) and SAR-sodium (0.77). Calcium and magnesium exhibit low negative correlations. The correlation with soil reaction values is low (0.29). Table 6.6 shows the correlation matrix obtained after the pH, cation and anion values were logarithmically transformed and regressed against SAR values. Correlations between SAR and pH, calcium and magnesium improved after this transformation.

Table 6.5: Correlation matrix of SAR, pH, cations and anions

Variable	pH	Cl	SO_4	CO_3	HCO_3	Na	Ca	Mg	SAR
pH	1	-0.38	0.29	0.57	0.46	0.15	-0.58	-0.65	0.29
Cl		1	0.11	-0.1	-0.14	0.66	0	0.25	0.3
SO_4			1	0.52	0.32	0.73	0.05	-0.06	0.7
CO_3				1	0.8	0.5	-0.3	-0.29	0.54
HCO_3					1	0.33	-0.23	-0.24	0.39
Na						1	-0.15	-0.12	0.77
Ca							1	0.48	-0.34
Mg								1	-0.32
SAR									1

Table 6.6: Correlation matrix of SAR, pH, cations and anions logarithmically transformed.

Variable	log pH	log Cl	log SO_4	log CO_3	log HCO_3	log Na	log Ca	log Mg	SAR
log pH	1	-0.22	0.35	0.92	0.77	0.18	-0.64	-0.69	0.32
log Cl		1	0.26	-0.03	-0.08	0.75	-0.02	0.13	0.41
log SO_4			1	0.42	0.36	0.69	-0.26	-0.18	0.58
log CO_3				1	0.77	0.33	-0.55	-0.57	0.41
log HCO_3					1	0.29	-0.45	-0.59	0.39
log Na						1	-0.17	-0.1	0.58
log Ca							1	0.82	-0.64
log Mg								1	-0.59
SAR									1

The soil reaction (pH) is more correlated to carbonate than to SAR values (tables 6.5 and 6.6). A logarithmic transformation and regression of CO_3 against the pH provides the best correlation (r), equal to 0.9 (fig. 6.14). In fact, the correlation is between soil reaction and free carbonates. High pH values

occur when the bicarbonate plus carbonate content is higher than the Ca^{2+} and Mg^{2+} content in solution, that is when there is a 'residual alkalinity' (van Reeuwijk, 1988). The presence of calcium and magnesium induces carbonates to precipitate because of the low solubility of $MgCO_3$ and $CaCO_3$. Excess bicarbonate is in practice always sodium bicarbonate which is eventually transformed in Na_2CO_3, because the sodium ions dominate in the intermicellar solutions as a result of the poor solubility of calcium carbonate (Szabolcs, 1989; Driessen et al., 1991).

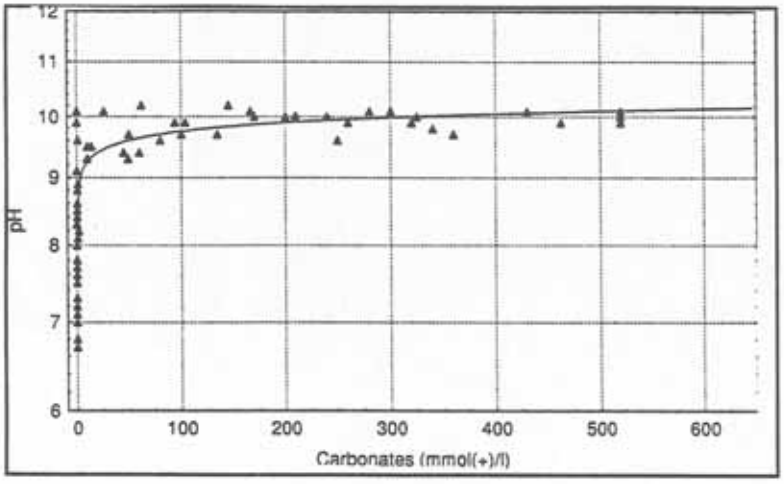

Fig. 6.14: *Logarithmic regression of carbonates against pH (r=0.9 and r^2=0.79).*

Scatterplots 6.15a to 6.15g show the best correlations and fit curves obtained by simple regression of SAR values against the selected variables. Table 6.7 resumes the correlations between SAR values and pH, cation and anion values using arithmetic and logarithmically transformed values. The r^2 coefficient of determination indicates the SAR variability explained by the use of a certain variable. For example, simple linear regression of the sulphates can explain about 48% of the SAR variability. Instead, the pH accounts for only 8% of this variability.

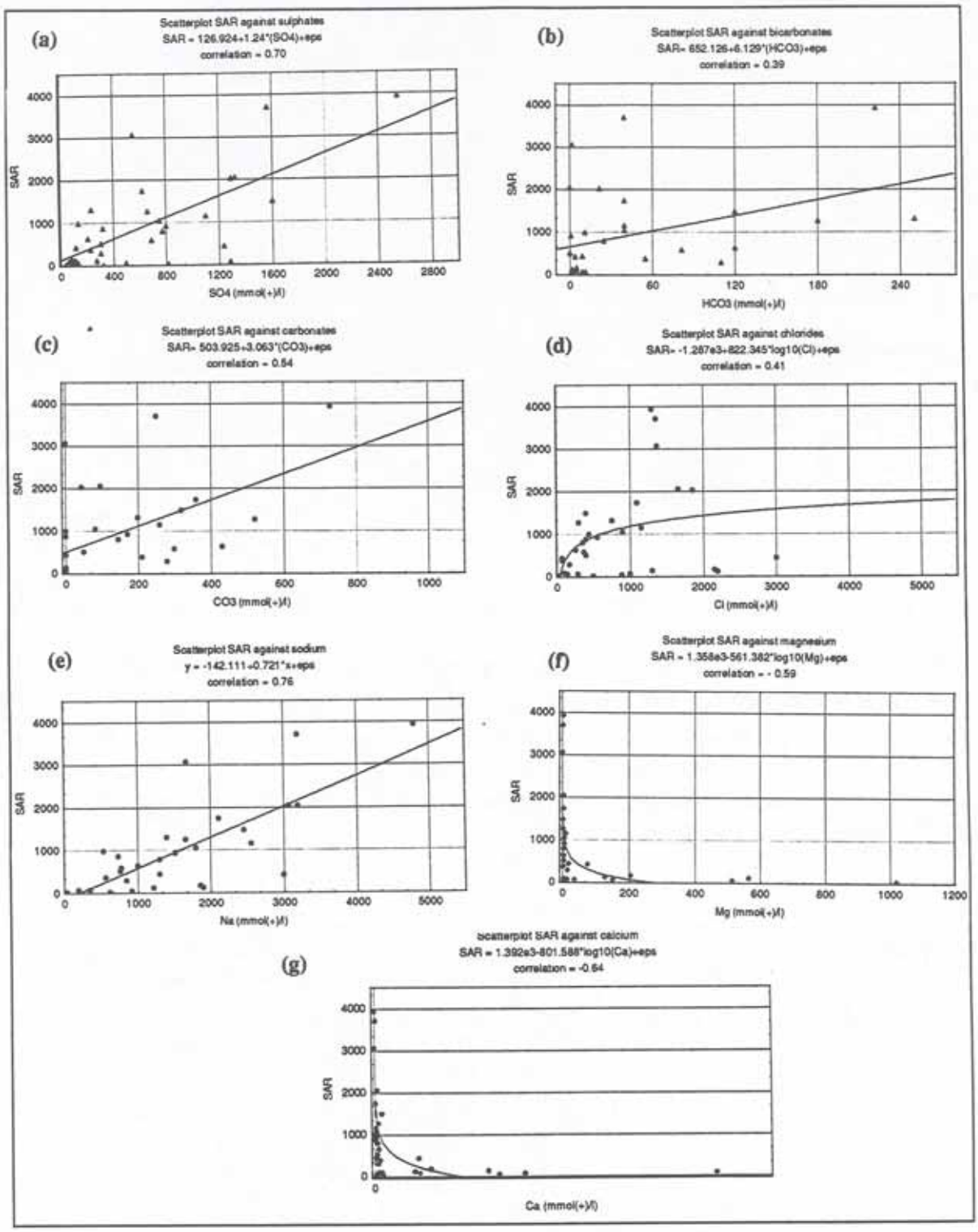

Fig. 6.15: Scatterplots of SAR values against (a) sulphates; (b) bicarbonates; (c) carbonates; (d) chlorides; (e) sodium; (f) magnesium; (g) calcium.

Table 6.7: Correlation coefficients and r^2 values between SAR and pH, cations and anions.

VARIABLE	r	r^2	F-TEST	p-VALUE <
pH	0.29	0.08	2.79	0.10
Cl	0.30	0.09	2.97	0.09
SO4	0.69	0.48	29.18	0.00
CO3	0.54	0.29	12.71	0.00
HCO3	0.39	0.15	5.63	0.02
Na	0.77	0.59	44.44	0.00
Ca	0.34	0.11	4.00	0.05
Mg	0.32	0.10	3.53	0.07

** significance at the 0.05 level

Table 6.8: Regression equations computed to predict missing SAR values

REGRESSION EQUATION	r	r2	d.f.	F-test	p-value <
1. SAR= -2104.12+297.61*(pH)	0.664	0.44	1, 25	19.74	0.0002
2. SAR= -4961.363+ 5823.02*log(pH)	0.659	0.43	1, 25	19.21	0.0002
3. SAR= -217.476+0.385*(Cl)+0.257*(SO_4)+1.286*(CO_3)+3.203*(HCO_3)	0.77	0.6	4, 28	10.51	0.00002
4. SAR= -3285.29+44.68*log(CO_3)+304.89*log(HCO_3)+ 835.20*log(SO_4)+ 625.03*log(Cl)	0.69	0.48	4, 24	5.49	0.0028
5. SAR= -2005.265+228.564*(pH)+0.6529*(CO_3)+ 1.508*(HCO_3)+ 0.313*(Cl)+0.314*(SO_4)	0.80	0.64	5, 21	7.53	0.00035
6. SAR= -2607.81+0.45*(Cl)+0.91*(SO_4)+1.01*(CO_3)+1.09*(HCO_3)+ 2513.94*log(pH)	0.78	0.61	5, 27	8.49	0.00006

From particular relationships between SAR and the selected variables, six regression models were established to estimate the missing SAR values (table 6.8). Box and whisker plots were used to identify outliers having extreme values to be excluded from the regression analysis (fig. 6.16). The simple regression of SAR against pH values (1) explains 44% of the SAR variability (fig. 6.17), while the regression of SAR against logarithmically transformed pH values (2) explains 43% of the SAR variability. Figure 6.18 compares the results predicted by both regression equations with the 33 observed SAR values. In general, both equations fail in predicting extreme SAR values and reduce the range of the natural variability. Equation (1) works slightly better than (2).

SAR values predicted from the simple regression against pH values were plotted on a histogram to analyze their frequency distribution. Figure 6.19 shows the multi-modal histogram, negatively skewed with a leptokurtic distribution. Most of the forecasted SAR values were higher than 30, and the class 13-26 remained empty. Such an unbalanced SAR value distribution would not provide a good basis for satellite classification of salt-affected areas.

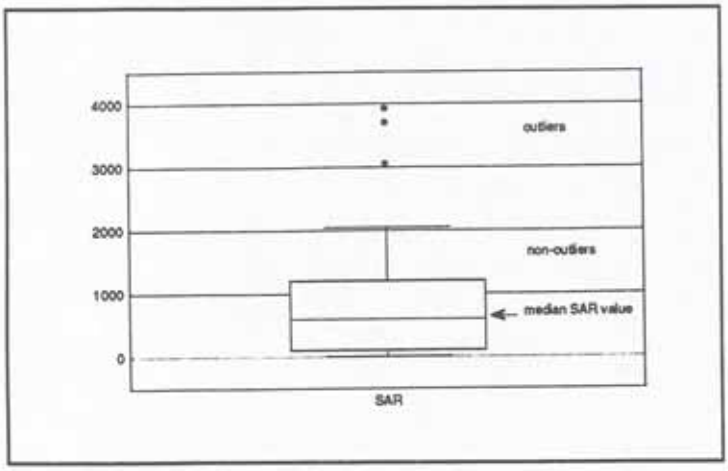

Fig. 6.16: Box and whiskers plot of the SAR values.

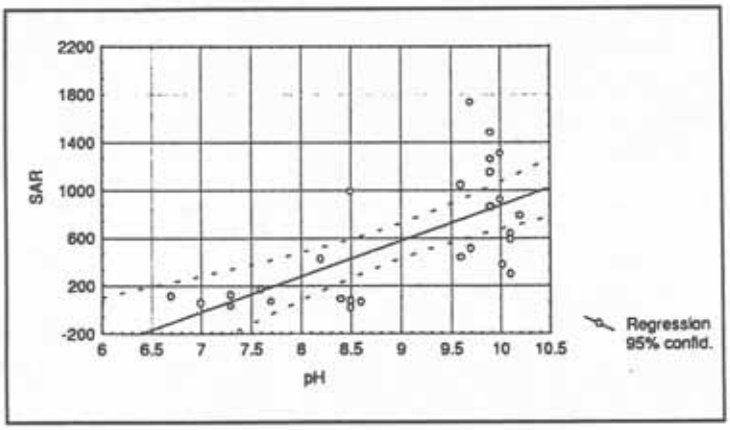

Fig. 6.17: Simple linear regression of SAR against pH values.

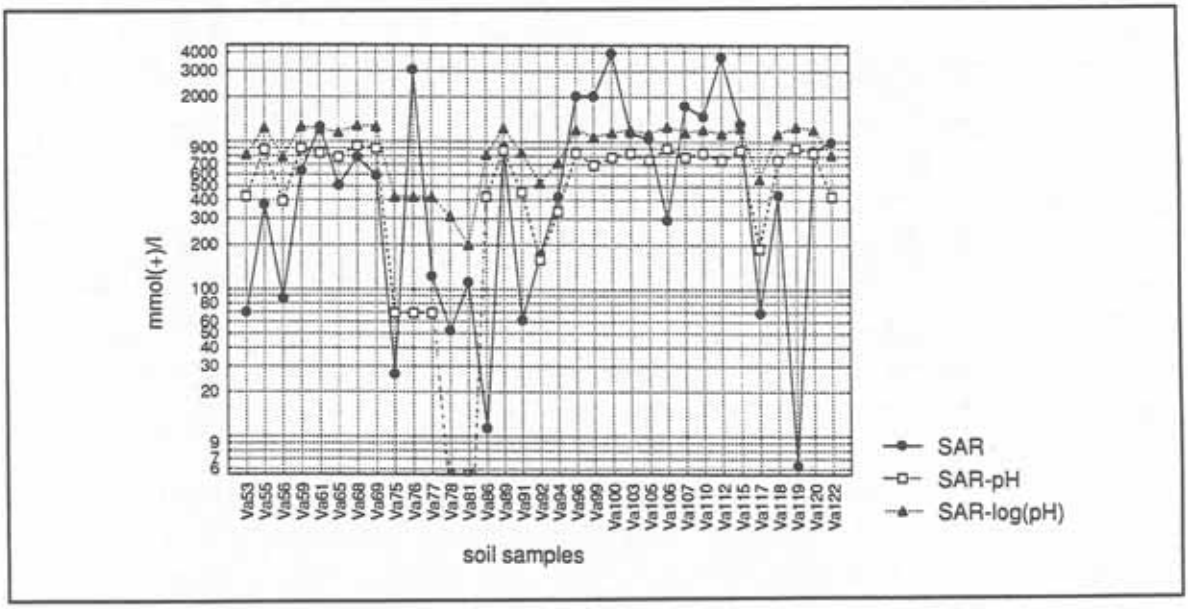

Fig. 6.18: Line plot of observed and predicted SAR values using pH(1) and log(pH) values(2).

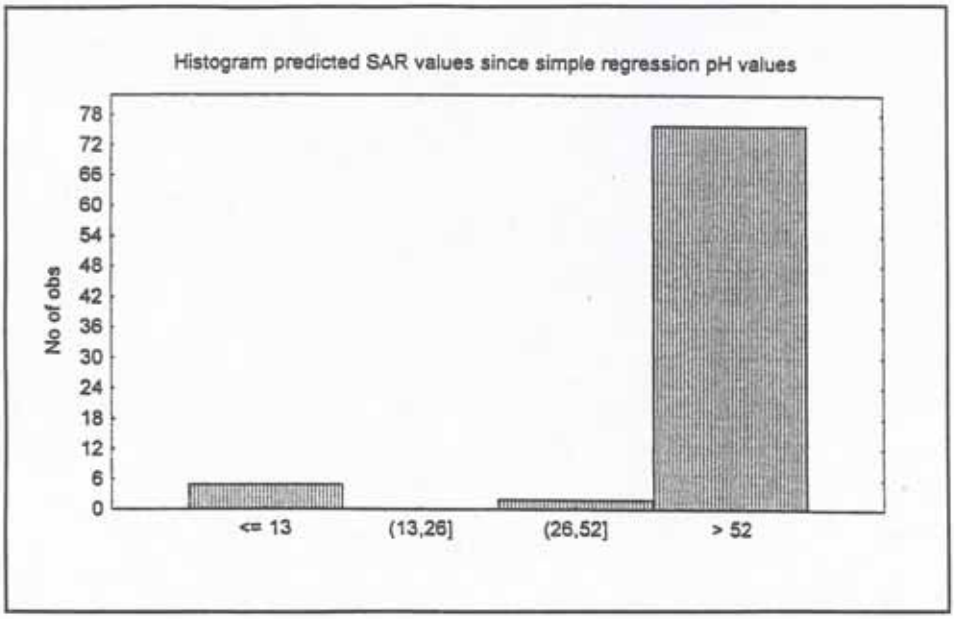

Fig. 6.19: Histogram of predicted SAR values.

(2) Multiple regressions

Multiple regression of SAR against the chloride, sulphate, carbonate and bicarbonate variables (3) gives an overall positive correlation of 0.77 and a coefficient of determination explaining 60% of the variance. After log transformation of the anion values, the r^2 coefficient drops to 0.48 and the overall correlation to 0.69. Figure 6.20 shows the relative poor performance of the multiple linear regression of the anions and their log transforms in predicting SAR values. As in the case of equations (1) and (2), extreme values and in particular extreme low values are not properly estimated. Multiple regression of SAR against a combination of anion and pH values provides somewhat better results. Equations (5) and (6) coincide in the estimation of the higher values, but are less successful in predicting values below 30 (fig. 6.21).

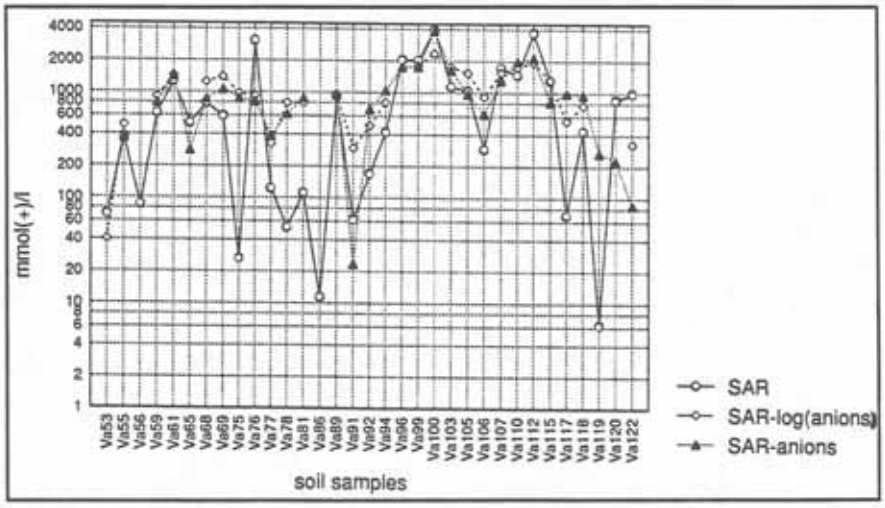

Fig. 6.20: Line plot of observed and predicted SAR values obtained by multiple regression against anions (3) and their log transforms (4).

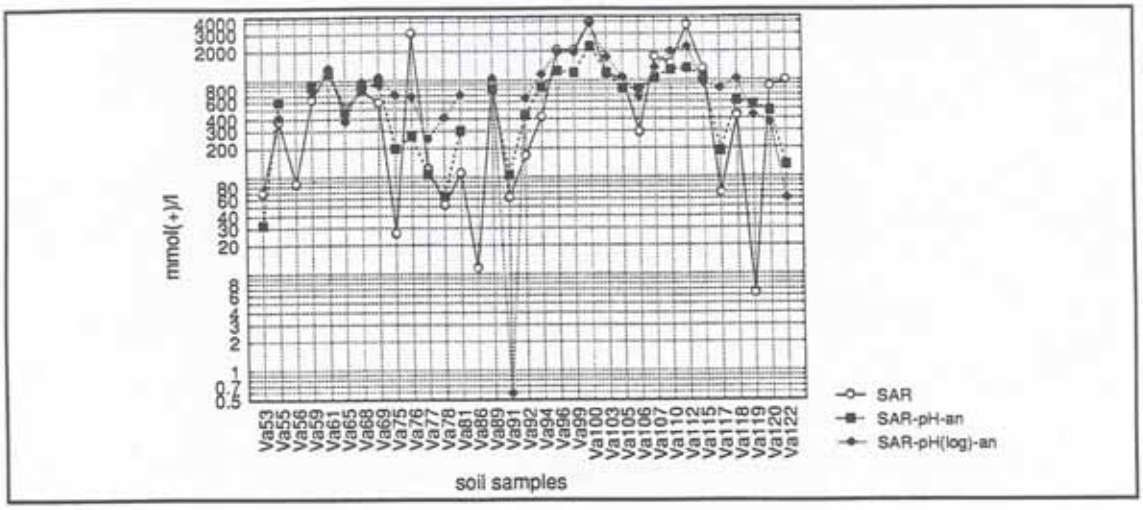

Fig. 6.21: Line plot of observed and predicted SAR values obtained by multiple regression against pH+anions (5) and against log transformed pH+anions (6).

Table 6.8 compares the results of the F-test, commonly used to test how well the regression line fits the data. In equation (1), the part of the SAR variation explained by the fitted line is significantly greater than the part that the line left unexplained, compared to the F-tests of equations (2) to (6). The larger the F values, the greater the variance explained by the regression. Hence, equation (1) would perform best as predictor of the missing SAR values.

6.3.3 Determination of salinity-alkalinity classes

(1) Using ECe and pH values

An approach based on ECe and pH values was tried out to determine salinity-alkalinity levels. Salinity classes were established using the ECe ranges previously mentioned. Alkalinity divisions were determined as proposed by Schroeder (1984) and illustrated in figure 6.22.

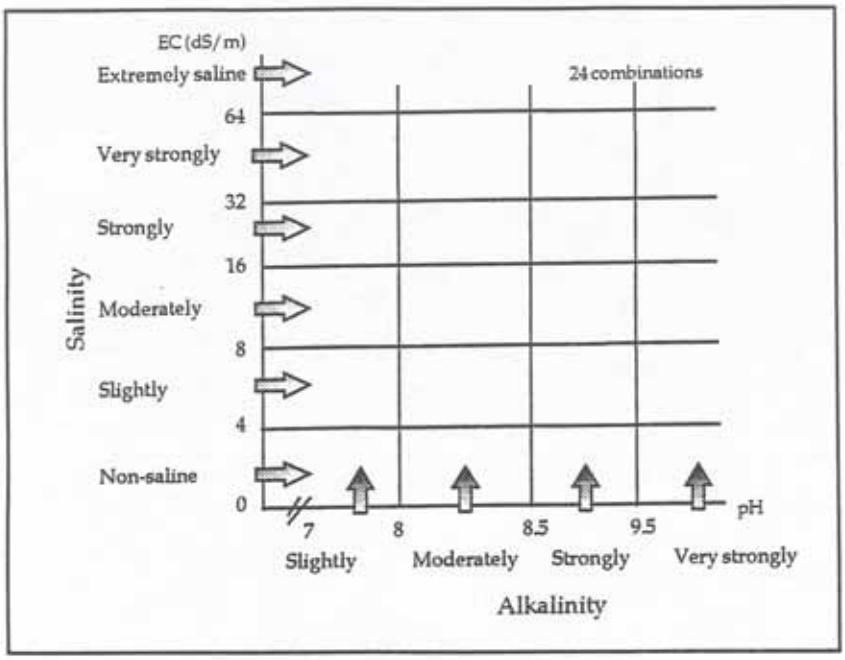

Fig. 6.22: Classification scheme to estimate levels of salinity-alkalinity.

(2) Using anion ratios

The soluble salts of the samples from the Punata-Cliza valley consist mainly of a mixture of sodium sulphate and chloride, with different Cl/SO_4 and CO_3/SO_4 ratios (fig. 6.23). The Cl/SO_4 ratio has greater variability and higher median values than the CO_3/SO_4 ratio. None of the samples register values equal to zero, which means higher proportions of chlorides than sulphates in all collected soil samples. The highest Cl/SO_4 ratios were computed in areas where the CO_3/SO_4 ratio is lowest, commonly zero. Both ratios reach similar values, in the range of 0.5 to 2, in the playas south of Tolata.

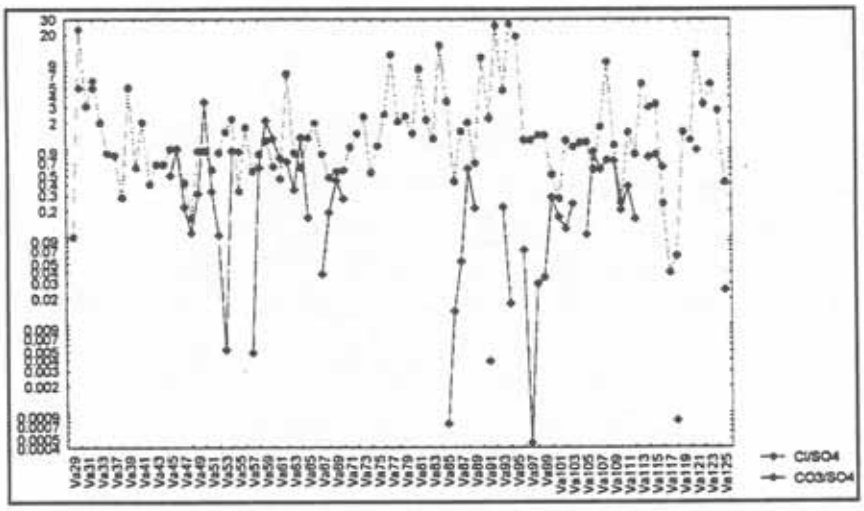

Fig. 6.23: Plot of the Cl/SO_4 and CO_3/SO_4 ratios from the collected samples.

On the basis of the anion ratios, 4% of the analyzed soil samples were found to belong to the sulphate type, 35% to the chloride-sulphate type, 46% to the sulphate-chloride type and 15% to the chloride type (fig. 6.24).

By ranking the CO_3/SO_4 ratio, Sadovnikov determined different alkaline soil types (Driessen et al., 1991). But class boundaries established by Sadovnikov did not show suitable for the Punata-Cliza valley. Therefore, these ranks were modified and two new boundaries (i.e. 0.005, 0.15) were introduced. According to this adjustment, 46% of the soil samples could be considered soda soils, 14% sulphate-soda soils and 40% soda-sulphate soils.

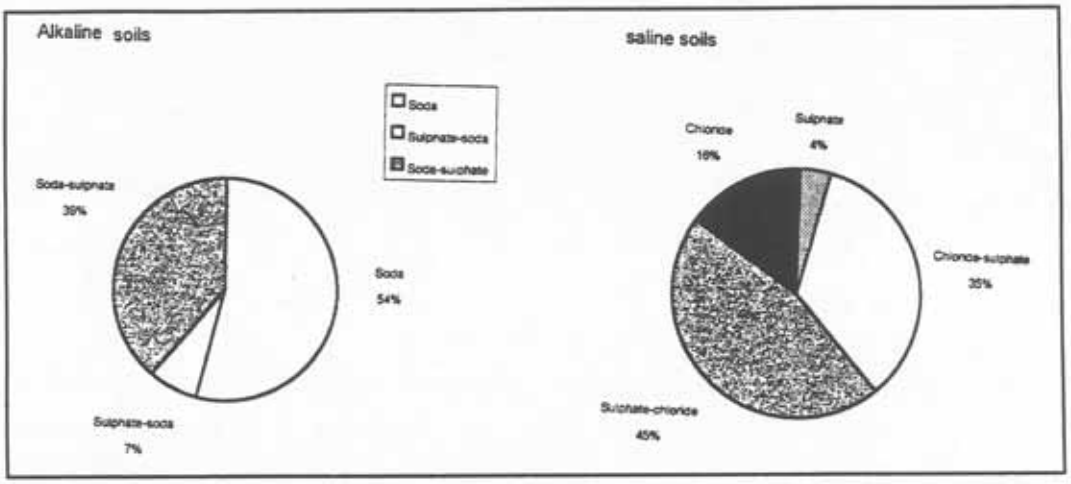

Fig. 6.24: Saline and alkaline soils classified on the basis of anion ratios.

6.4 FIELD REFLECTANCES

Soil reflectance is a property which derives from the spectral behavior of a combination of mineral, organic and fluid matter in mineral soils (Stoner et al., 1981). The relative contributions of soil properties such as organic matter, soil moisture, particle size distribution, soil structure, iron oxide content, soil mineralogy, salt types and contents, soil color, surface morphology and surface cover, have been well documented (Bowers and Hank, 1965; Baumgardner et al., 1970; Stoner et al., 1981; Mougenot et al., 1993; Coleman et al., 1993).

Main factors causing reflectance changes of surface features in the Punata-Cliza valley include: surface morphology (puffy saline crusts and fluffy surface layers), soil roughness, soil texture, soil colour and salt-tolerant vegetation cover. The effects of soil moisture on reflectance were not investigated because the field conditions were dry during the data collection period.

Field reflectance data were collected using the Cropscan multiband radiometer, which contains eight bands located in the visible and near-infrared regions of the spectrum, in the range between 450 and 800nm. The procedure followed for data gathering is explained in chapter 3. Data were analyzed to identify and explain the effect of surface characteristics on the reflectance in the visible and near-infrared wavelengths. The information obtained was further used to interpret surface features on a Landsat TM scene, specially to understand and solve labelling confusions due to spectral similarity of surface features.

The parameters used by the USDA Soil Salinity Laboratory (Richards, 1954) to identify saline and alkaline areas, namely the sodium adsorption ratio (SAR), soil reaction and electrical conductivity, were statistically regressed against the Cropscan band values to determine the wave bands which are specific to different salinity and alkalinity ranges.

6.4.1 Estimation of salinity-alkalinity variables using soil spectral properties

Soil samples were collected from the upper 5 cm of the surface horizons for laboratory determination of the soil reaction, electrical conductivity (saturated paste) and the exchangeable cations for SAR calculations. All spectral data were recorded within the same month of soil data collection. No variations in the climatic conditions occurred during that period. The Cropscan multiband radiometer collected the data in the blue (450-500nm), green (550-600nm), red (650-700nm) and near-infrared (750-800nm) wavelengths.

Stepwise regressions were used to develop linear equations predicting SAR, pH and EC values from the spectral reflectance data. The regression procedure adds one variable (e.g. waveband) in each step and the reduction in residual variance is noted. When enough regressors have been added so that no further significant reduction is possible, the calculation stops (Wonnacott et al., 1990).

(1) Estimation of sodium adsorption ratio (SAR) ranges

Several SAR ranges were identified to have high correlation with the ground-based reflectance data. Table 6.9 shows the results from a stepwise regression analysis to select the best band combination for predicting SAR ranges. By computing several possible linear regression equations for various ranges, considering the amount of variability explained and using the F-tests of the resulting equations, the best subset of SAR ranges was selected (table 6.10).

The regression analysis indicates a positive correlation between all SAR values and the Cropscan bands. The relationship is higher for the blue (450 - 500 nm) and near-infrared (750nm) wavelengths. Conversely, the SAR values correlate poorly with the red and green spectral bands. A coefficient of determination above 43% and an F-test ≥ 20 were used as threshold values to select the SAR ranges best predicted from the spectral data. The highest correlation and F-test values between spectral bands and SAR values occur in the following ranges: 0-27, 27-300, 300-700, 700-900, 900-1200, 1200-2400 and values greater than 2400. These are therefore the optimum ranges for determining soil alkalinity degrees

from spectral soil data.

The most effective spectral bands to predict SAR values smaller than 27 and greater than 2400 are in the blue and green regions of the spectrum, accounting for 98% and 77% of the SAR variability, respectively. The blue, green and red explain 67% of the variation when SAR values fluctuate between 27 and 300. The near-infrared band is useful to predict SAR values ranging from 300 to 700. Instead, the red band explains 85% of the SAR variability when it falls between 700 and 900. The most important wave bands for predicting sodium adsorption ratio values in the class 900 to 1200 are the blue, green and near-infrared, accounting for 95% of the variability. The near-infrared and blue wave bands are the best to predict SAR ranges between 1200 and 2400.

Table 6.9: Stepwise regression for determining the best combination of spectral bands for predicting SAR ranges

SAR RANGE	SELECTED BANDS (nm)	MODEL CORRELATION	EXPLAINED SAR VARIABILITY (%)	F-TEST
0 - 27	500*, 600*	0.99	98	148
27 - 100	750*, 600	0.37	14	2.58
27 - 200	550*, 650*	0.50	26	8.11
27 - 300	450*,750*,650*,550*,700*	0.86	74	28
27 - 400	750*, 550*, 450	0.62	38	11
300 - 500	750	0.31	10	2.02
300 - 600	800*, 750*	0.69	48	16.62
300 - 700	800*, 750	0.71	51	23.9
300 - 800	800*, 450	0.57	32	12.08
300 - 900	800*, 550*, 700*	0.49	24	6.14
700 - 1000	800*	0.74	56	21
700 - 1100	650*, 600*, 800	0.65	43	5
700 - 900	600*, 650*	0.92	85	29.12
900 - 1200	800*, 500*, 450*	0.97	95	51.24
1200 - 1500	500*, 450*, 800*, 650*	0.67	45	4.12
1200 - 1800	450*, 750*	0.60	36	8.18
1200 - 2000	450*, 750*	0.60	36	8.18
1200 - 2400	450*, 750*	0.66	43	20
1200 - 3000	450*, 750*	0.66	43	20
> 2400	500*, 600*, 450*	0.87	77	23.85

(*) significant at the 0.05 alpha level

Table 6.10: Multiple linear regression equations for estimating sodium adsorption ratio ranges from spectral reflectance data

SAR RANGE	REGRESSION EQUATION	r^2	F-TEST
< 27	SAR = 23.843-7.01(B500)+3.898(B600)	0.98	148.61
27 - 300	SAR = -8.159+23.8(B450)+23.05(B750)-37.85(B550)-4.393(B700)	0.67	25.706
300 - 700	SAR = 214.58+14.052(B800)-8.77(B750)	0.51	23.93
700 - 900	SAR = 849.30-19.785(B600)+18.099(B650)	0.85	29.13
900 - 1200	SAR = 915.126+8.169(B800)-47.962(B500)+42.463(B450)	0.95	51.24
1200 - 2400	SAR = 2157.274+32.518(B450)-26.375(B750)	0.435	20.382
> 2400	SAR = 3431.871+667.396(B500)-165.451(B600)-464.143(B450)	0.77	23.859

(2) Estimation of pH ranges

The results of the stepwise multiple regression indicate useful spectral ranges to estimate pH values from reflectance data at pH < 7.5, between 8.5 and 9 and greater than 9 (table 6.11). There is an overall positive correlation between pH and the visible and near-infrared ranges, but the highest correlations are in the near-infrared range, while the lowest occur in the blue range of the spectrum. Near-infrared bands are highly significant to explain variabilities when the pH is neutral (e.g. < 7.5). Strongly alkaline soil reactions are best predicted using all the visible and near-infrared bands of the Cropscan multiband radiometer. Moderately alkaline classes (pH 7.5 to 8.5) have the lowest correlation with spectral reflectance data, where the visible blue and red bands explain only 28% of the pH variability.

Table 6.11: Stepwise regression for determining the best combination of spectral bands for predicting pH ranges

pH RANGE	SELECTED BANDS (nm)	EXPLAINED pH VARIABILITY (%)	F-TEST
< 7.5	800*, 750*, 700	64	4.7
7.5 - 8.5	450, 600, 650	28	14.28
8.5 - 9.0	750*, 700*, 500	93	20
8.5 - 9.5	650*, 800, 750	48	3.94
9.0 - 9.5	550	29	3.03
9.0 - 10	550*, 700, 750, 600, 450	58	7.79
> 9.0	550*, 450*, 650*, 700*, 750*	59	11.68

(*) significant at the 0.05 alpha level

(3) Estimation of electrical conductivity ranges

There was a low positive relation between electrical conductivity and the blue and green wavelengths (450 to 550 nm), while the opposite occurred between the red and near-infrared bands (600 to 800nm) and all EC values taken at once. Table 6.12 shows the results from a stepwise regression analysis to select the best spectral bands for predicting useful ECe ranges.

Table 6.12: Stepwise regression for determining the best combination of spectral bands for predicting EC ranges.

EC RANGE (dS/m)	SPECTRAL BANDS (nm)	MODEL CORRELATION	EXPLAINED EC VARIABILITY (%)	F-TEST
< 4	750*	0.96	92	60
4 - 12	450*, 750	1.00	100	17428
>= 8	750*, 500*, 550*, 700	0.59	35	9.43
8 - 32	700*, 550*, 650	0.87	76	9
> 32	750*, 550*, 650	0.66	44	14
12 - 32	650*, 800*, 450*, 550*, 700*	0.97	94	27

(*) significant at the 0.05 alpha level

By computing several possible linear regression equations, considering the amount of variability explained and using the F-tests to evaluate how well the regression lines fitted the data, the best EC ranges expressed in dS/m are: < 4, 4 to 12, 12 to 32, and > 32 (table 6.13). Threshold values of $r^2 \geq 43$ and F-test ≥ 14 were selected. Electrical conductivities lower than 4 dS/m are best estimated using the near-infrared bands, while values comprised between 4 and 12 dS/m require the addition of the blue band. The blue, red and near-infrared bands are necessary to estimate EC values from 12 to 32 dS/m. Very saline soils (EC > 32 dS/m) can be isolated using the blue, green and near-infrared ranges of the spectrum, but with relatively low EC variability explained.

Table 6.13: Multiple linear regression equations for estimating EC ranges from spectral reflectance data

EC RANGES (dS/m)	REGRESSION EQUATION	r^2	F-TEST
< 4	EC = -4.621+0.178(B750)	0.92	60.24
4 - 12	EC = -0.505+0.173(B450)+0.077(B750)	0.99	17428
12 - 32	EC = -84.237+9.51(B700)-13.703(B650)+10.148(B800)-6.212(B750) + 2.477(B450)	0.92	12.39
> 32	EC = 111.531-3.677(B750)+10.37(B550)-9.65(B450)	0.43	14.34

6.4.2 Factors causing reflectance changes of surface features

(1) Surface morphology and terrain roughness

The reflectance of surface components is affected by changes in terrain roughness (fig. 6.25). Reflectance values of four soil surface features, namely (a) 'mullido' crust, (b) cloddy 'mullido' crust, (c) ploughed

field and (d) clods, were recorded in the field for comparison. These are non-saline surface components, where variations in roughness are caused by land management practices. 'Mullido' crusts form after fields have been harvested. Parcels are ploughed and clods destroyed to form a smooth artificial sealing cover, which prevents soil moisture losses during the dry season (fig. 6.26). The four observed surface features might coexist in a parcel at the moment of the satellite pass.

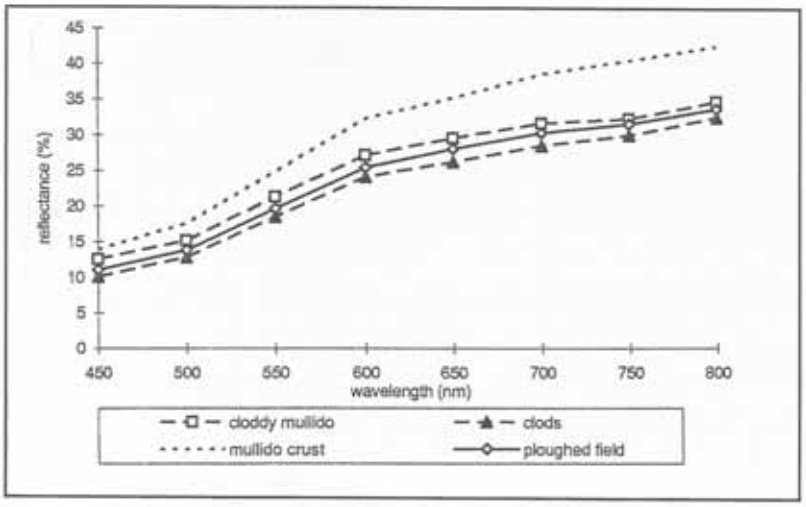

Fig. 6.25: Non-saline surface components affected by variations in surface roughness.

Fig. 6.26: Process leading to the formation of the 'mullido' crust (artificial sealing).

The smooth 'mullido' crust exhibits notoriously higher reflectance. As surface roughness increases, the reflectance tends to decrease. The reflectance sequence in the visible and near-infrared wave bands can be summarized as follows: smooth 'mullido' crusts >> smooth crusts with scarce clods (cloddy mullido) > ploughed field > clods. The size of the secondary aggregates (clods) varies, being greater in ploughed fields without further management. As sunlight falls on the large, irregularly shaped clods, most of the incident energy penetrates into light traps and is completely extinguished there.

Salts also cause variations in surface roughness. Figure 6.27 illustrates the influence of different salt types on the reflectance of crusted surfaces. Salt mineralogy produces distinctive macromorphological features at the soil surface. For example, puffy crusts form because of the abundance of sodium sulphates, while smooth salty crusts are due to the presence of chlorides (Driessen et al., 1973; Eghbal et al., 1989). In general, salty crusts are smoother than non-saline, commonly cultivated surfaces, and have an overall higher reflectance in the visible and near-infrared wave bands. Cracks, commonly present in silt- and clay-rich non-saline crusts, lower the overall crust reflectance because sunlight is trapped between the cracks. Similarly, reflectance decreases as roughness increases because of ploughing. The reflectance sequence is: smooth salty crust (chlorides) > puffy crust (sodium sulphate) = non-saline crust > bare soil without crust > non saline crust with cracks > ploughed fields with large clods.

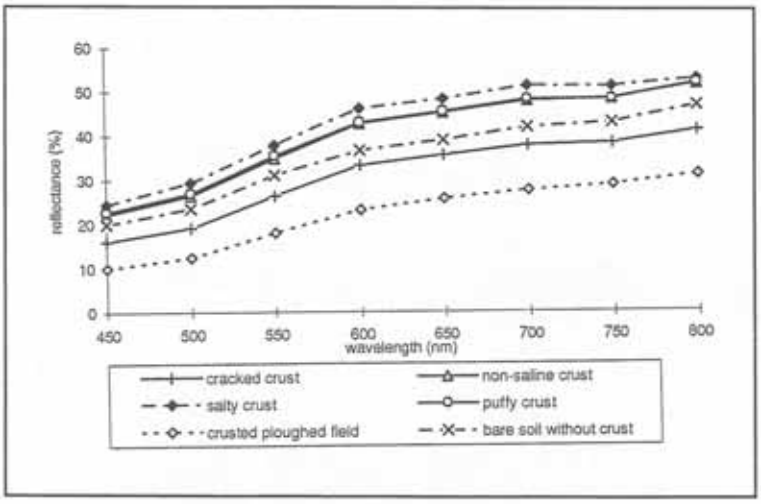

Fig. 6.27: Variations in reflectance of surface features because of different salt mineralogy and land management practices.

(2) Soil surface texture

Reflectance in the visible and near-infrared bands reveals information only of the first millimeters of the top horizon of bare soils (e.g. crusts). Under field conditions, bright crusts form usually because of silt-rich soil materials of alluvial or lacustrine origin. Figure 6.28 shows distinctive reflectance values attributed to textural changes in bright crusts. Variations in reflectance and curve shape are clearly dependant on silt contents. Silt loam and silty clay loam textures, with silt contents above 50%, generate different curve shapes and higher reflectances than silty clay and clay textures with lower silt contents. There is a positive correlation between silt content and reflectance, especially in the red and near-infrared

wave bands. Reflectance decreases in the following way: silt loam > silty clay loam > silty clay and clay with similar proportions of silt.

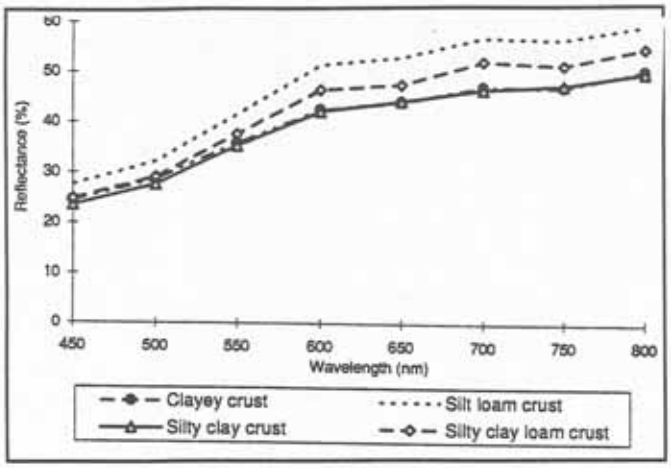

Fig. 6.28: *Influence of silt content on the reflectance of non-saline bright crusts.*

When non-saline crusts are dull, the influence of the silt content on the reflectance values is blurred in the blue range (fig. 6.29). Comparatively, the spectral range of 600- 800nm (red to near-infrared) offers a clear discrimination among soil textures. According to Stoner (1979), the silt content explains the variation in reflectance in this range. Silty clay textures have the highest reflectance, which could be attributed to a synergistic effect of silt and clay soil particles. The remaining soil textures have reflectance values proportional to the silt content. In general, the reflectance sequence of dull crusts is as follows: silty clay > silt loam > loam > clay.

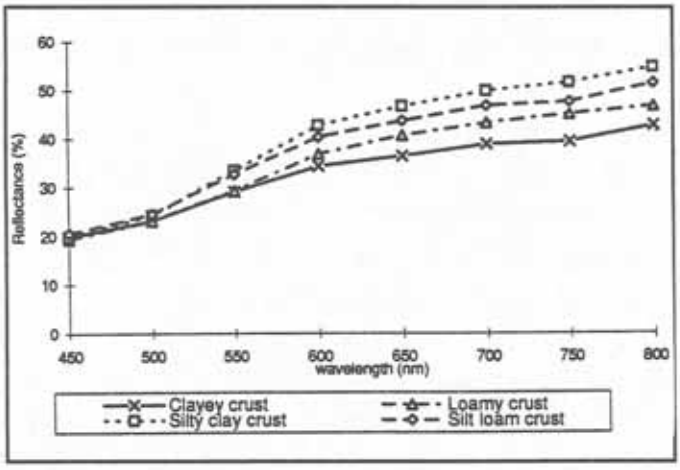

Fig. 6.29: *Influence of silt content on the reflectance of non-saline dull crusts.*

Particle size distribution in itself causes micro-scale surface roughness which explains changes in reflectance (fig. 6.30). Orlov (1966) attributes the occurrence of higher reflectances to the presence of fine particles filling the pore space more completely and providing more even surfaces. Coarse particles like sand form complex surfaces with large inter-particle spaces, trapping the sun energy. In general, the

reflectance decreases in the following sequence: clay > silty clay > loam > sandy loam.

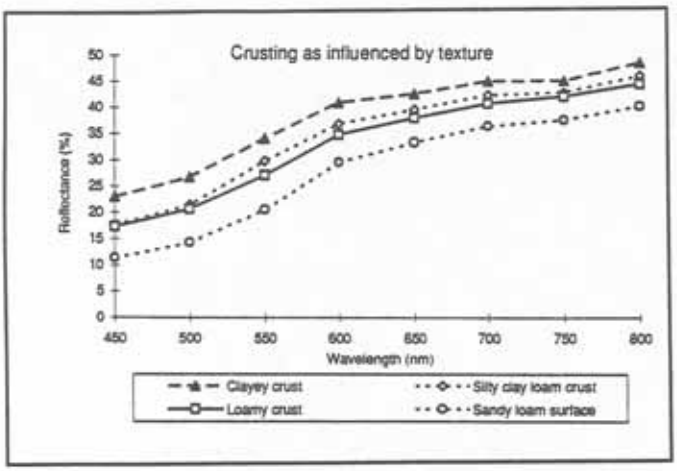

Fig. 6.30: *Influence of the particle size distribution on the reflectance of non-saline surfaces through changes in surface roughness at micro-scale.*

(3) Crust color

The Munsell hue refers to the dominant wavelength, while chroma is related to the saturation of a color and the value is the overall brightness ranging from 0 (black) to 10 (white). The predominant surface colors of the studied soils are yellowish, brownish and yellowish red (10YR, 7.5 YR, 2.5YR). Very pale brown (10YR 7/3) gives overall higher reflectance than the light brownish gray (10YR 7/2) in the green, red and near-infrared regions of the spectrum. For soils with constant hue and increasing chroma or value, reflectance variations in the red and near-infrared bands (600 - 800 nm) are more notorious than in the blue (450-500nm) or green (500-600nm) bands (fig. 6.31). The blue region reacts very little to alterations in color chroma. Differences in one point of color value or chroma causes changes in soil reflectance. However, the color chroma seems to control more the overall reflectance behaviour of the crusts than the color value.

Similar results are reported by Escadafal et al. (1989) and Escadafal (1993), who found that chroma variations correlated to a red: green ratio. For instance, as the chroma increased, higher reflectances were observed in the red bands, whereas reflectance increments were slightly lower in the green band. Similar conclusions were obtained by Salmon-Drexler (1977) but related to the variations in color value.

The overall shape of the curve is sigmoidal, showing an absorption of the radiation in the blue-green region of the spectrum and high reflectance in the red-near-infrared wavelengths (600-800nm), regardless of the variations in either color value or chroma. This shape is related to the yellowish red and reddish colors, where light reflection in the 600-700 nm increases as the color hue becomes redder. Yellowish red colors are related to proportionally high reflectances in the 550-700 nm range and high absorption in the blue region (450 - 500 nm). The more pronounced the curve, the more vivid the color (Escadafal, 1993 and 1994).

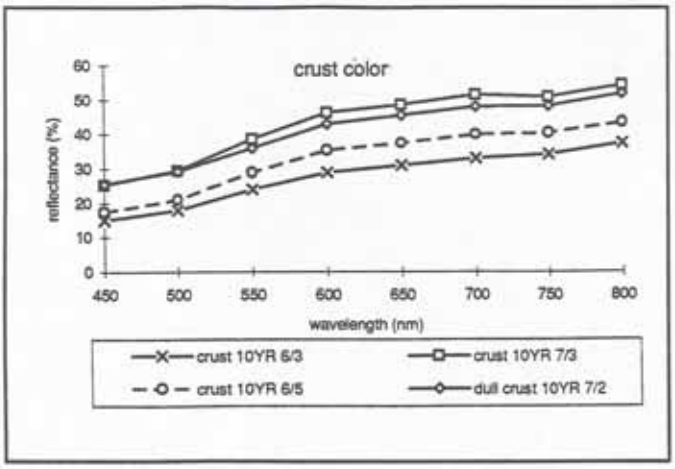

Fig. 6.31: Influence of color on the reflectance of non-saline crusts.

(4) Salt-tolerant vegetation

Halophytic salt-tolerant vegetation such as Cynodon dactilon and Chenopodiaceae is common on strongly saline and alkaline areas. Trees like locust and molle, shrubs and grasses grow on slightly saline and/or alkaline areas. Shrubs are rich in chlorophyll and have comparatively larger leaves than the salt-tolerant vegetation. Shrubs behave as 'green plants', showing high absorption in the green range, around 550 nm, and maximum reflectance in the near-infrared region.

Spectral data were collected using the Cropscan multiband radiometer and plotted in figure 6.32. The curve of the shrub cover shows a strong absorption in the visible caused by the leaf pigments, such as chlorophyll and carotene. These pigments absorb energy in the 450 nm wavelength and chlorophyll has an additional absorption feature around 650nm (Gates et al., 1965). There is a small reflectance peak in the green range (550 - 600 nm) and a high reflectance in the near-infrared. The spectral curve of salt-tolerant Chenopodiaceae follows a trend comparable to chlorophyll-rich vegetation, with strong absorption in the visible range and higher reflection in the near-infrared region of the spectrum. Cynodon dactilon, a salt-tolerant grass species, has a different spectral curve, monotonically increasing throughout the visible and near-infrared wave bands, which indicates lower chlorophyll content.

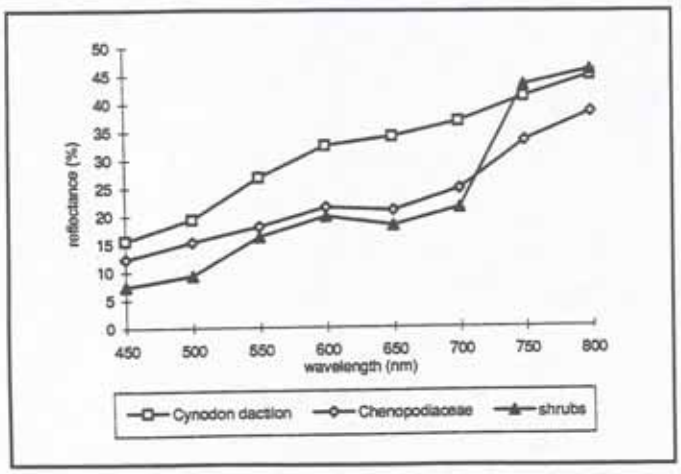

Fig. 6.32: Reflectance curves of local vegetation cover types

In figure 6.33, the spectral curves of yellowish and green semiarid grasses and a typical bare soil curve are compared to the salt-tolerant vegetation curves. Except for Chenopodiaceae, the curve shapes are similar. The higher overall reflectance corresponds to the bare soil surface, followed by the salt-tolerant Cynodon dactilon. Both reflectance curves become close in the near-infrared range (750 - 800 nm).

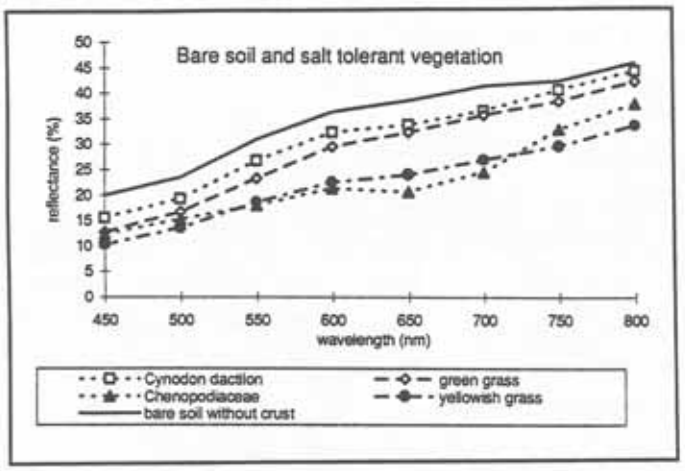

Fig. 6.33: Spectral curves of bare soil and salt-tolerant vegetation covers

(5) Mixtures of surface elements under field conditions

(a) Mixtures of soil properties

Under field conditions, the actual reflectance of a soil surface is determined not just by one single variable but a combination of properties including soil texture, organic matter content, salt type and surface roughness. Figure 6.34 illustrates the reflectance behaviour of a silt loam crust influenced by variations in surface roughness due to variable silt contents, salt types and organic matter contents.

Spectral confusions occur between salty and bright crusts in the blue and green regions of the spectrum (450 to 550nm). Surface brightness due to high silt content causes higher reflectance than a puffy or smooth salty crust. The non-saline crusts have lower reflectance and slightly different curve shape than

the salty crusts. The puffy, sodium sulphate-rich crust seems to respond more to the influence of silt than salt contents, because the curve shape and levels of reflectance are similar to those of the bright silt loam crust.

A clear diminution in reflectance is observed as the crusts become non-saline (e.g. silt loam dull crust). The lowest reflectance corresponds to non-saline crusts with slightly different silt, clay and organic matter contents. The soil sample having higher organic matter percentage and lower silt and clay contents exhibits the lowest reflectance. This is in agreement with conclusions reached elsewhere. For instance, Matthews et al.(1973) found that organic matter highly correlated with the 500 - 1000 nm range. Similarly, Stoner et al.(1981) showed that organic matter is an important variable explaining reflectance differences in the 520 - 1750 nm region.

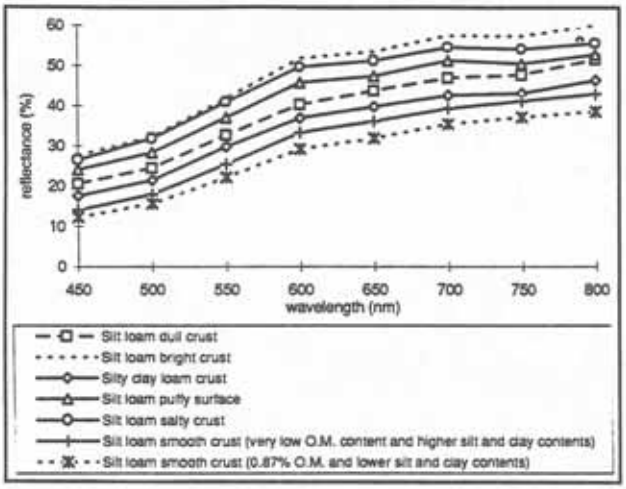

***Fig. 6.34:** Influence of mixtures of soil properties under field conditions on the reflectance of crusts.*

(b) Mixtures of vegetation and soil properties

Under field conditions, pure spectral plots of the surface components are difficult to isolate, specially when working with satellite remote sensing data. Therefore, the reflectance of mixed situations was recorded, including: (a) a pure plot of Halophytic Chenopodiacea; (b) a mixture of salt-tolerant species; (c) a mixture of salt-tolerant vegetation and saline puffy crust; (d) a mixture of salt-tolerant vegetation and smooth crust; and (e) mixed saline and non-saline vegetation.

The contribution of vegetation is practically negligible in the spectral curves representing the mixtures between salt-tolerant species and crusts, where the higher reflectance corresponds to the smooth saline crust. The spectral plots representing mixtures of salt-tolerant vegetation and non-saline species overlap with that of the pure Chenopodiaceae in the range of 550-800 nm. From 450 to 550nm, the influence of the background crust reflectance seems more evident. Vegetation, however, lowers the overall reflectance of the saline crusts. Thus, spectral confusion among classes representing different salinity degrees can be

expected to occur in areas partially covered by salt-tolerant vegetation.

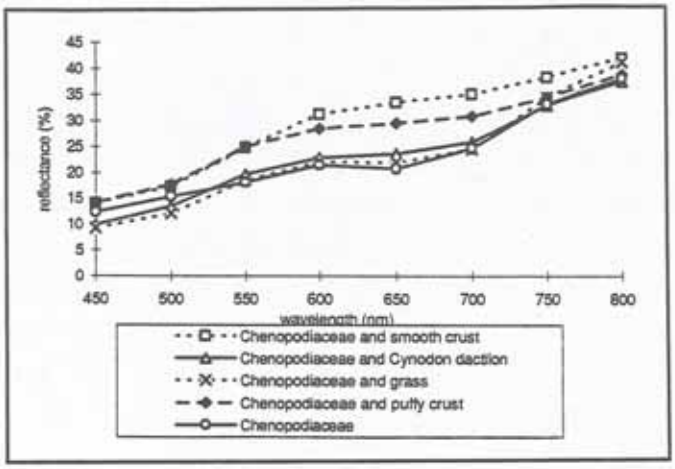

Fig. 6.35: Spectral mixtures between vegetation and saline crusts.

(6) Curve shape of bare soil surfaces

The spectral curves of the investigated soil surface features have similar shapes. They all have a uniform, moderate to steep slope in the 450 - 500 nm range. A change in the curve slope commonly occurs at 500 nm, registering the range 500-600 nm the steepest slope. At 600 nm there is a notorious change towards a gentle, sometimes almost flat slope.

The overall shape can be related to a sigmoidal curve, which has been reported by several authors working with soils having low organic matter and iron oxide contents and higher sand and silt than clay percentages (Condit, 1970; Stoner et al., 1981; Escadafal, 1992 and 1994). Condit (1970) described variations in curve shape and identified three main types (fig. 2.8). His 'type 2' curve correlates fairly well with those shown in figures 6.25 to 6.31 and 6.35. Although Condit does not relate the curve shape to specific soil components, the curve clearly predominates in loamy and coarse loamy soils with low organic matter contents. Also Huete et al. (1991) and Escadafal (1992) relate this kind of curve to soils having very low organic matter and iron oxide contents, yellowish red colors and loamy textures. Stoner et al. (1981) mention it as characteristic of 'minimally altered soils' (fig. 2.9), that is, low in iron oxide and organic matter contents with good drainage. It is difficult to relate variations in shape and reflectance of spectral curves to a given soil component alone, because measurements are carried out in field conditions where soil properties commonly interact. The clear and generalized inflection observed at 600 nm might be related to the fact that most of the studied soils are yellowish red, absorbing therefore energy in the blue-green range and reflecting more in the red part of the spectrum. In addition, higher silt and sand contents may sharpen the inflection at 600 nm. The opposite occurs with increasing clay contents which seem to flatten the curve shape, as shown by the clay and silty clay curves of figure 6.28.
In conclusion, the curve shape of the soil spectra studied in the Punata-Cliza valley depends mainly on the soil color, the percentage of silt and sand, and the organic matter content. The specific influence of these factors could not be established because measurements under controlled conditions are lacking.

Surface roughness and morphology affect mainly the reflectance percentage in the range from 450 to 800 nm, without major changes in the curve shape.

6.4.3 Conclusion

The estimation of sodium adsorption ratio, electrical conductivity and soil reaction ranges of soil surface materials, using ground reflectance spectra, is possible as indicated by the high r^2 values and F-tests that resulted from the data set. The established regression equations, however, are geographically dependent and may not be applicable to other areas.

Best SAR ranges predicted from visible and near-infrared wave bands were: < 27, 300, 700, 900, 1200, 2400 and greater than 2400. Positive correlations, higher for the blue and near-infrared bands, relate the SAR values with the wavelengths of 450-800nm. Also positive relationships, highest in the near-infrared range, were found between pH values and the spectral bands. Reliable pH ranges predicted from reflectance data are: <7.5, 8.5, 9 and > 9. The moderate alkaline soil class, with pH between 7.5 and 8.5, has the lowest r^2 coefficient (0.28). Thus, the possibility of discriminating moderately alkaline areas in the visible and near-infrared bands of satellite images might be poor. Electrical conductivity and the spectral bands have a positive relation in the blue and green wavelengths, while negative correlations occur with the red and near-infrared bands.

Main factors causing reflectance changes of surface features were identified to be: (1) surface morphology and roughness, (2) topsoil texture, (3) crust color and (4) salt-tolerant vegetation.
Changes in surface morphology are caused by management practices leading to the formation of crusts or ploughed fields with coarse clods, and by salt types producing puffy, smooth or fluffy surface features. Non-saline crusts have lower reflectance and slightly different curve shape than salty crusts. Soil textures, especially when high in silt contents, produce variations in reflectance and spectral curve shape. Surface roughness at a micro-scale also explains changes in reflectance as a function of soil particle diameter. In general, reflectance decreases with increasing size of the particles. For instance, a sandy loam texture has lower reflectance than clayey textures. Surface reflectance is also sensitive to variations in color chroma and value.

An overall sigmoidal curve shape was observed for bare soil surfaces. Soil color, the percentage of silt and sand, and the organic matter content might be the main factors controlling the curve shape. Their specific influence could not be established because measurements under controlled conditions are lacking.

Salt-tolerant vegetation decreases the overall reflectance of saline crusts. Therefore, spectral confusion among classes representing different salinity degrees might occur in areas partially covered by halophytic vegetation such as Cynodon dactilon and Chenopodiaceae. Confusions between different surface components, due to spectral similarity and/or their mixture under field conditions where pure spectral plots are difficult to isolate, can be expected to occur when working on spatial discrimination of salt- and

sodium-affected areas from space borne satellites.

6.5 SPATIAL DISCRIMINATION OF SALT AND SODIUM AFFECTED AREAS FROM SPACE-BORNE SATELLITES

An integrated approach, combining digital image classification with field observations and laboratory data was implemented to map the saline-alkaline areas of the Punata-Cliza valley. The data set consisted of 95 georeferenced composite topsoil samples of 5 cm depth, collected from a surface area of about 9.000 ha concurrently with the acquisition of a seven-band-Landsat TM scene and a JERS-1 SAR scene. Data collection followed a stratified-oriented sampling technique (chapter 3), and took place during the dry season when salt surface features were enhanced by high evaporation rates and scarce vegetation cover. Soil saturation extracts were prepared to determine ion types and contents, electrical conductivity and soil reaction (pH). These and other ancillary data such as ground cover type and percentage, soil particle size distribution, organic matter content, crust types and colors were stored in a geographic database.

6.5.1 Mapping salinity and alkalinity based on pH and EC

Several approaches were designed and implemented to map saline and alkaline areas, using different regions of the spectrum (visible, infrared, thermal, microwaves), different classification schemes (statistical pattern recognition and fuzzy sets) and different soil parameters defining the information classes (pH, electrical conductivity, chloride to sulphate ratio, and carbonate to sulphate ratio).

(1) Using Landsat Thematic Mapper

(a) The method

To identify and map salt-dependent features, salinity-alkalinity classes were established as described under point 6.3.1. Twenty four information classes resulted from the combination of EC and pH ranges (fig.6.22). Calcareous areas could be easily discriminated on the selected sub-scene by visual interpretation because of their well-defined landscape position, namely the proximal and central parts of the southern piedmont glacis. To reduce sources of spectral confusion with salt-dependent features in playas and other low-lying flats, a mask was created to classify these areas separately. The same labelling procedure was applied and the calcareous areas were merged with the other classes in the post-classification phase.

Image classification involved supervised training, signature evaluation, selection of best band combination and pixel labelling using a maximum likelihood classifier (fig. 6.36). During the training phase, representative samples of individual classes were selected from the soil database. A neighborhood operator, with spatial and spectral user-defined constraints, was used to determine spectrally homogeneous objects constituting the training set.

Descriptive class statistics, including mean, standard deviation and covariance matrix, and separability

among classes of interest were evaluated. The transformed divergence was chosen to evaluate the separability among spectral classes and select the best band combination to be used for pixel labelling. Usually transformed divergence is scaled between 0 and 2000. A divergence of zero indicates that the classes are inseparable. For TD_{ij} >= 1600 good separability of classes i and j can be expected (Richards, 1986).

The post-classification procedure involved class merging, an iterative majority filtering to remove small patches. A confusion matrix was used to evaluate classification performance, where class reliability as well as accuracy were computed. The overall accuracy of the classification is obtained by dividing the total correctly classified pixels (i.e. the sum of the main diagonal) by the total number of pixels in the error matrix. In addition, accuracies of individual classes can be computed in a similar way, by dividing the total number of correctly classified pixels in a particular class by the total number of pixels labelled in that class. The result expresses the probability that a pixel classified on the image is in reality representative of the same class on the ground, and is know as the class accuracy or user's accuracy (Congalton, 1991). Class reliability, also known as producer's accuracy, indicates the probability of correct classification of a reference data. It is obtained by rationing the total number of correct pixels in a particular class to the total number of pixels composing that class, as derived from the reference data (i.e. column totals).

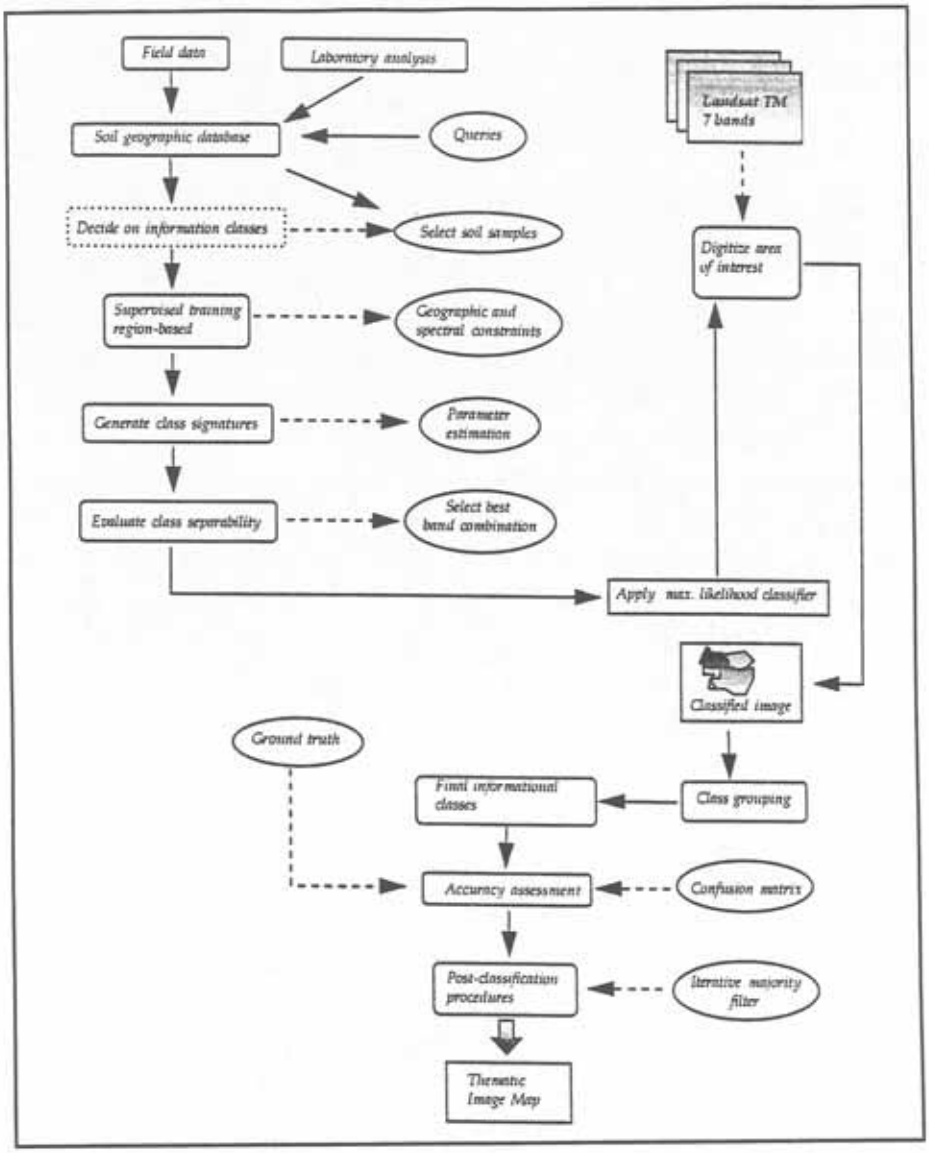

***Fig. 6.36:** The classification model*

(b) Data interpretation

After several trials, taking an increasing number of bands at a time, the transformed divergence analysis showed that six combined Landsat TM bands (1, 2, 4, 5, 6 and 7) provided the highest separability between salt- and sodium-affected soil classes (table 6.14). An average class separability of 1959 was obtained working with the six best bands.

Table 6.14: Results of the transformed divergence analysis to select the best band combination

No. OF BANDS	BEST AVERAGE SEPARABILITY	BAND COMBINATION
7	1934	1 2 3 4 5 6 7
6	1959	1 2 4 5 6 7
5	1957	1 2 4 6 7
4	1947	2 4 6 7
3	1919	2 6 7
2	1854	2 6
1	1669	2

Class grouping and neighborhood analysis allowed to compress the classification data into nine information classes (table 6.15). Two classes, namely strongly and slightly calcareous, were added (fig. 6.37).

Table 6.15: Final information classes and their dominant geomorphic units

CLASS NAME	DOMINANT GEOMORPHIC UNIT	pH RANGE	EC RANGE
1. Non- to slightly saline-alkaline	Higher lagunary flats	7 - 8	0 - 8
2. Moderately and strongly saline-alkaline	Middle and lower lagunary flats	8.1 - 9.5	8.1 - 32
3. Very strongly saline-alkaline	Playas	> 9.5	> 32
4. Moderately and strongly saline, slightly alkaline	Middle and lower lagunary flats	7.0 - 8.0	8.1 - 32
5. Very strongly saline, slightly alkaline	Playas	7.0 - 8.0	> 32
6. Very strongly saline, moderately and strongly alkaline	Playas	8.1 - 9.5	> 32
7. Moderately alkaline, non- to slightly saline	Middle lagunary flats and piedmont glacis (distal)	8.1 - 8.5	0 - 8
8. Very strongly alkaline, moderately and strongly saline	Playas	> 9.5	8.1 - 32
9. Strongly alkaline, non- to slightly saline	Playas	> 9.5	0 - 8

The incorporation of the thermal band 6 (10.4-12.5μm) was decisive for salt and sodium detection. This was attributed to the predominance of sulphates and chlorides together with small amounts of carbonates of sodium and calcium in the study area. Carbonates are characteristic of sodium-affected soils and present absorption features in the thermal range (between 11 and 12μm) due to internal vibrations of the CO_3^{2-} group. Sulphate anions have an absorption band near 10.2μm caused by overtones or combination tones of internal vibrations of constitutional water molecules (Siegal et al., 1980; Mulders, 1987). Carbonate absorption features are also reported at 2.34μm wavelength, comprised in the range of Landsat TM band 7 (Siegal et al., 1980). Middle-infrared bands, reflecting water and OH^- absorption, allow to differentiate between chlorides (as halites) and sulphates when both are dry. Band 5 (1.50-1.73μm) is one of the absorption bands for soil surface features containing $CaSO_4.H_2O$ (Mulders, 1987). Additionally,

this band is sensitive to variations in clay content (Beck et al., 1976).

Sodium carbonates predominate in some areas. No previous reports about the behavior of this salt type were found except by Csillag et al. (1993), who carried out spectral band selection for the characterization of soil salinity in areas dominated by Na_2CO_3. The visible (0.55-0.77µm) and near-infrared (0.9-1.3µm) ranges generated good results for salinity studies. No correlation between salt types and absorption bands was performed. The statistical selection of bands TM2 and TM4 could be explained by the presence of sodium carbonate. But such a hypothesis would have to be confirmed by more detailed studies about the behavior of anions in the visible and near-infrared regions of the spectrum. Furthermore, wavelength ranges between 0.52-0.60µm (TM2) and 0.76-0.90µm (TM4) are sensitive to variations in silt-sized soil particles and organic matter contents (Coleman et al.,1987 and 1990a; Stoner, 1979).

Although the overall accuracy was slightly low (64%), class accuracies of 100% were obtained for classes 2 and 8 (table 6.16). No omission errors were computed for classes 1, 4 and 8. Class 6 had the lowest accuracy and reliability (33%). Samples belonging to this class were labelled as class 5. Additionally, samples from classes 3 and 5 were erroneously included. Non-affected and slightly affected areas could not be separated. The association of different levels of salinity and alkalinity in one single class (e.g. classes 6 and 7), as well as alkalinity alone (e.g. class 9), generate lower classification accuracy.

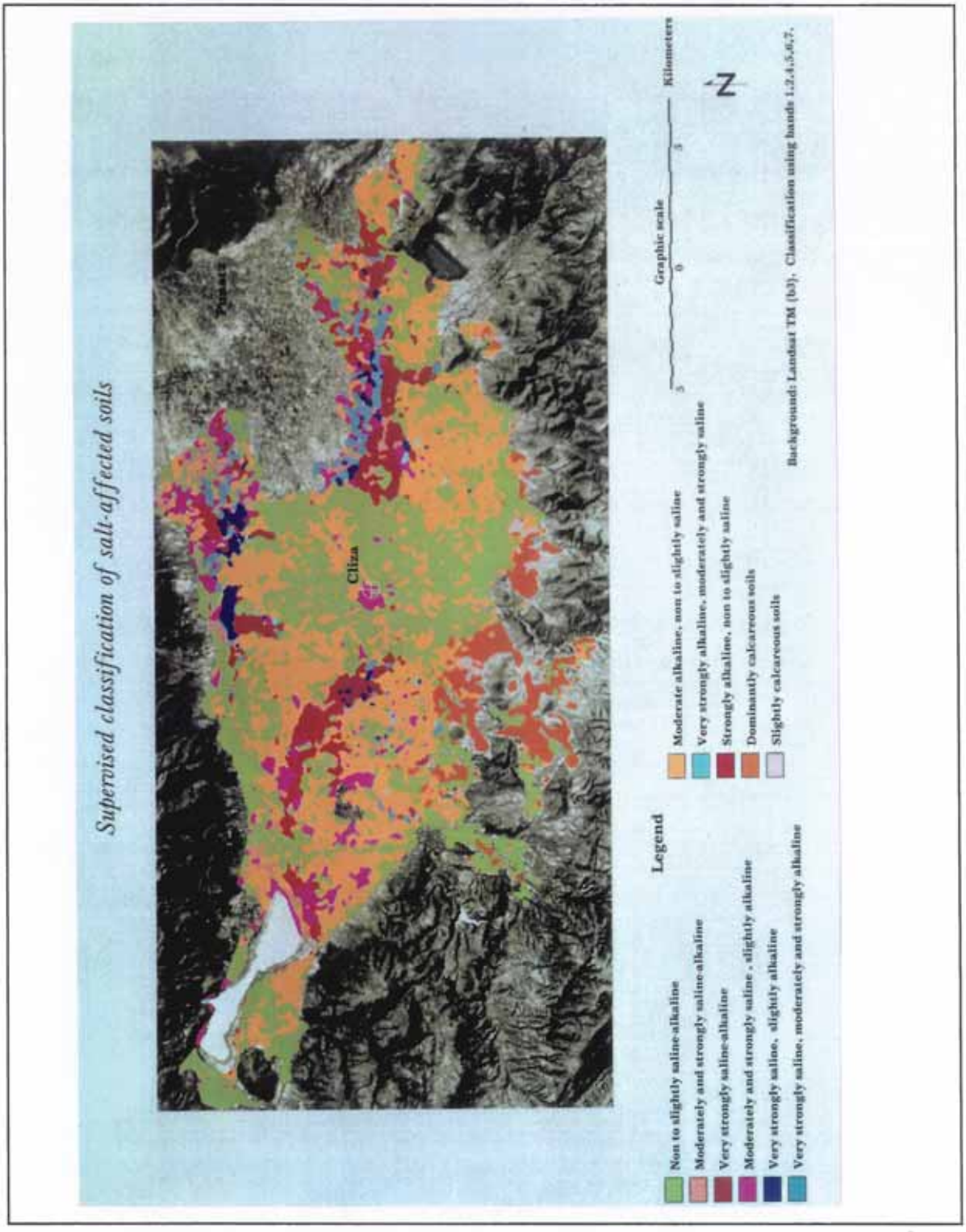

Fig. 6.37: *Spatial discrimination of salt- and sodium-affected soils using Landsat TM data.*

Table 6.16: Confusion matrix, reliability and accuracy of classified Landsat TM data.

CLASSIFIED DATA	REFERENCE DATA										
	1	2	3	4	5	6	7	8	9	TOTAL	ACC.%
1	18						9			27	66
2		18								18	100
3		9	135		18		9			171	79
4			36	27						63	43
5					45	18				63	70
6			9		9	9				27	33
7			9		18		27		18	72	38
8								18		18	100
9			9						9	18	50
TOTAL	18	27	189	27	90	27	45	18	27	468	
REL.%	100	67	71	100	50	33	60	100	33		

ACC.% = class accuracy %; REL.%= class reliability %

Clayey and silty topsoil textures were a source of spectral confusion between slightly, moderately and strongly alkaline areas (fig. 6.38). Clay-sized particles, causing overall high reflectance, masked the effect of different salt contents. This is accentuated by the fact that sodium chloride, spectrally featureless in the visible and near-infrared regions of the spectrum, is the dominant salt type in classes 5 and 6. Thus, soil texture causes important variations in the reflectance percentage, which could explain the inclusion of bands 1, 2 and 4 in the statistical band selection carried out with transformed divergence analysis.

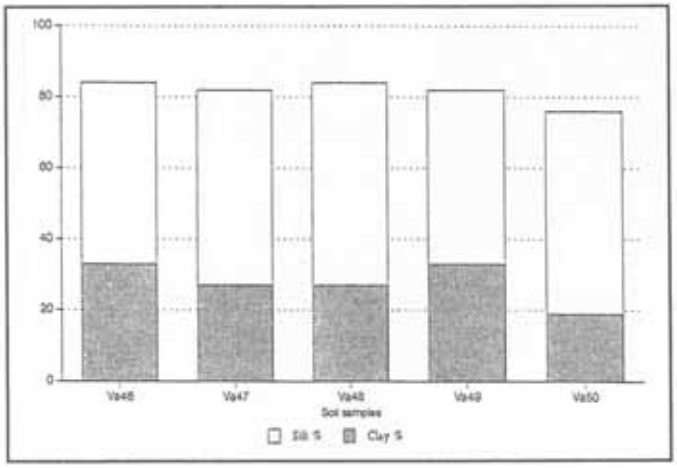

Fig. 6.38: Soil texture as a source of spectral confusion between salinity degrees (Va47, Va48, Va49 'moderately alkaline, non to sligthly saline'; Va46 and Va50 'Strongly alkaline, non to slightly saline').

The color and roughness of the soil crusts also influenced surface reflectance, thus masking the effect of the salt content. Figure 6.39 shows the influence of surface roughness and crust color on the visible and near-infrared regions of the spectrum (450 - 800 nm), as recorded from ground based-measurements. The selected soil sample pertains to class 5 (very strongly saline and slightly alkaline). A decrease of two chroma units (from 10YR 6/5 to 10YR 6/3) causes a reflectance reduction in all bands. A saline crust has higher reflectance than a non-saline soil surface. However, alteration of the saline crust through breaking increases the surface roughness, which causes a reflectance decrease at similar salt contents. The shape of the spectral curve does not change, but the overall reflectance does.

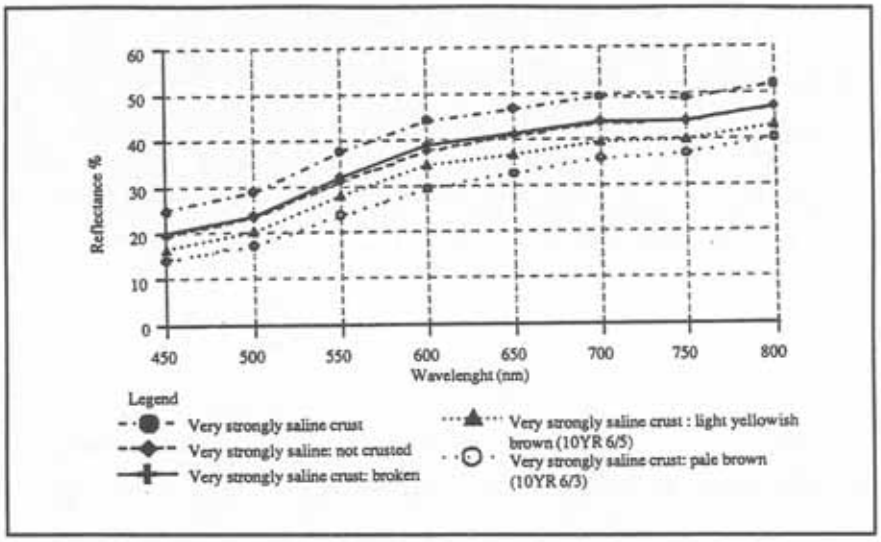

***Fig. 6.39:** Influence of colour and roughness on the reflectance of saline crusts. Data recorded by a ground-based radiometer.*

Because they are generally smoother than non-saline surfaces, crusted saline surfaces have higher reflectance. Salt-tolerant plants, considered good indicators to separate saline-alkaline areas from non-affected ones, caused spectral confusion between salinity-alkalinity classes. Very strongly saline-alkaline areas (eg. class 3) were mistakenly labelled as class 4, because they had the same herbaceous cover (*Cynodon dactilon*).

(2) Using fuzzy modelling and satellite data fusion

Data from the microwave region of the spectrum were merged with the visible, near, middle and thermal infrared ranges to improve the detection and mapping of different salinity-alkalinity degrees. The aim was to evaluate if the L-band could help distinguish variable surface roughness and penetrate through the salt-tolerant vegetation layer to resolve the spectral confusion caused by clayey and silty topsoil textures and vegetation. The Japanese JERS-1 SAR (L-band) and the seven bands of Landsat Thematic Mapper were used for this purpose. In chapter three, the procedure to reduce the speckle noise in the radar satellite

image and the geometric correction procedure are described.

As a radar image records the amount of energy backscattered from a surface, the returned energy depends upon the roughness of the surface. The apparent roughness of a surface is a function of the radar wavelength, incidence angle and polarization. A surface is said to be rough in the radar sense, if its structure or shape has dimensions which are an appreciable fraction of the incident radar wavelength. One qualitative measure of roughness is the Rayleigh criterion which considers a surface as rough if:

$$h > (\lambda/8*\cos\theta)$$

where: h: mean height of the surface

λ: wavelength of radar (e.g. L-band 23 cm)

θ: incidence angle (e.g. for JERS-1 is 35°)

For the JERS-1 SAR sensor, any ground surface with height differences greater than 3.5 cm is considered rough.

Another crucial step is the correct determination of information classes. Transitional class boundaries, derived from continuous salinity classes which intergrade gradually, were thought to provide better results. Information categories were therefore determined by fuzzy modelling of the pH and electrical conductivity values.

(a) The method

A bell-shaped membership function was chosen to model the pH and ECe classes (Dombis, 1990; Bing et al., 1995). The membership function is written as:

$$\mu A(x) = [(1-\upsilon)^{\lambda-1}(x-a)^{\lambda}]/[(1-\upsilon)^{\lambda-1}(x-a)^{\lambda} + \upsilon^{\lambda-1}(b-x)^{\lambda}] \qquad x \in [a,b] \quad (1)$$

$$\mu A(x) = [(1-\upsilon)^{\lambda-1}(c-x)^{\lambda}]/[(1-\upsilon)^{\lambda-1}(c-x)^{\lambda} + \upsilon^{\lambda-1}(x-b)^{\lambda}] \qquad x \in [b,c] \quad (2)$$

where equations (1) and (2) represent the monotonically increasing and decreasing parts. Dombi's membership function is optimal because there are two parameters, λ and υ, to modify the inflection and sharpness of the membership curves respectively. In this case, an inflection of 3.0 and sharpness of 0.7 were judged to best model the categories, after having tried 0.6, 0.7 and 0.8 sharpness values. The standard points, having a membership equal to 1, and the typical points representing the limits of the classes were selected according to the values shown in table 6.17.

Table 6.17: Standard and typical points characterizing salinity and alkalinity classes.

INFORMATION CATEGORY	STANDARD POINTS	TYPICAL POINTS
Non-saline	0 dS/m	5 dS/m
Moderately saline	8 dS/m	2, 20 dS/m
Strongly saline	32 dS/m	15, 91 dS/m
Very strongly saline	128 dS/m	52 dS/m
Non-alkaline	7*	8*
Moderately alkaline	8.5*	7.5, 9.5*
Strongly alkaline	10*	9*

* pH values

There is an overlap between class boundaries to avoid values with no membership (fig. 6.40). Where classes overlap, a soil sample belongs to the fuzzy set where its membership grade is the highest. For instance, a sample non-alkaline to a degree of 0.14 and moderately alkaline to a degree of 0.003 would be labelled as non-alkaline.

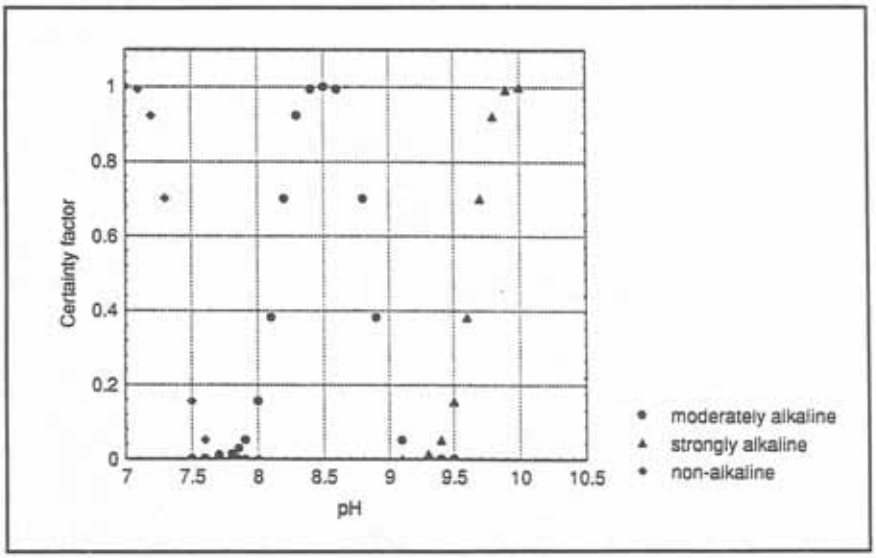

***Fig. 6.40:** Membership function for pH ranges, with an inflection of 3 and sharpness equal to 0.7*

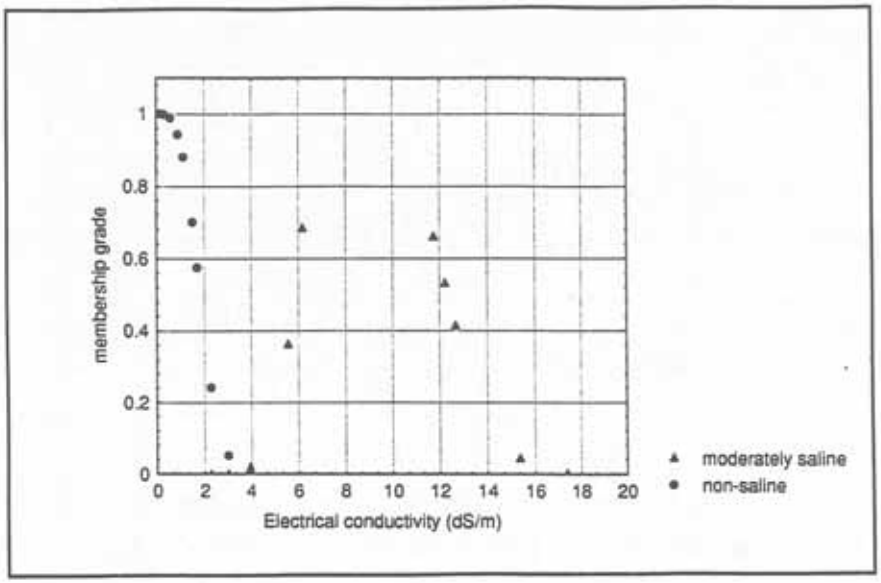

Fig. 6.41: Membership function of (a) non-saline and (b) moderately saline categories.

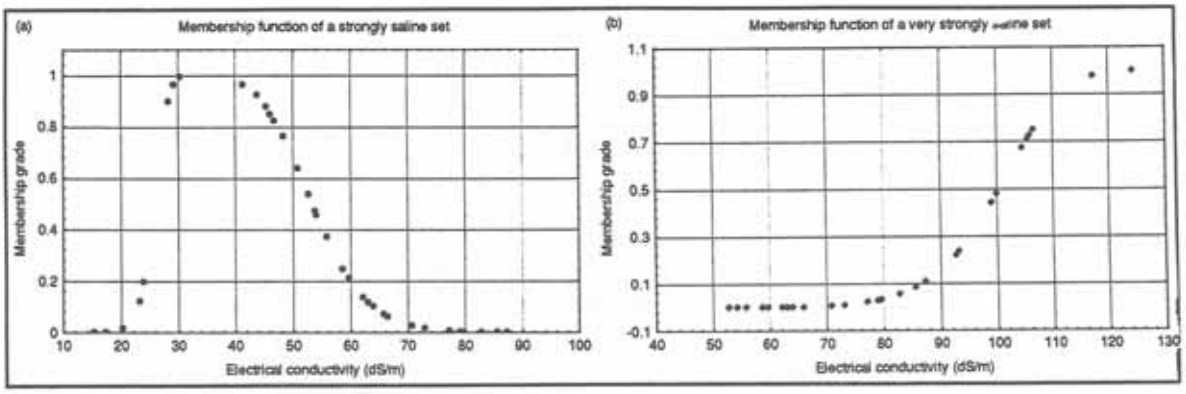

Fig. 6.42: Membership function of (a) strongly saline and (b) very strongly saline categories.

To obtain the final information categories, the salinity and alkalinity classes depicted in figures 6.40, 6.41 and 6.42 were combined by using the fuzzy set manipulation procedure developed by Zadeh (1965). Ten categories were obtained by intersection of the fuzzy sets of salinity and alkalinity classes, as described in table 6.18. Membership grade of a soil sample *(x)* to the final categories is resolved by:

$$\mu_{A\cap B}(x) = \min[\mu_A(x), \mu_B(x)]$$

If, for instance, a soil sample is non-saline to a degree of 0.7 and non-alkaline to a degree of 0.4, its membership grade to the category 'non-saline-alkaline' will be 0.4.

Table 6.18: Final fuzzy information classes

CODE	CATEGORIES	INTERSECTION OF FUZZY SETS
1	Non saline-alkaline	Non-saline *and* non-alkaline
2	Moderately alkaline, non-saline	Moderately alkaline *and* non-saline
3	Moderately saline-alkaline	Moderately saline *and* moderately alkaline
4	Moderately saline, strongly alkaline	Moderately saline *and* strongly alkaline
5	Strongly saline, non-alkaline	Strongly saline *and* non-alkaline
6	Strongly saline, moderately alkaline	Strongly saline *and* moderately alkaline
7	Strongly saline-alkaline	Strongly saline *and* strongly alkaline
8	Very strongly saline, non-alkaline	Very strongly saline *and* non-alkaline
9	Very strongly saline, moderately alkaline	Very strongly saline *and* moderately alkaline
10	Very strongly saline, strongly alkaline	Very strongly saline *and* strongly alkaline

Fuzzy sets were not normalized, that is, some sets did not have elements with membership grade of 1. One half of the soil samples composing the different sets were used to train the classifier. Samples having the highest membership grade were chosen for this purpose.

Spectral classes were established using a neighborhood operator with spatial and spectral constraints. The procedures described under 6.5.1 (1) for class signature evaluation, selection of the best band combination, pattern recognition and accuracy evaluation were followed.

(b) Data interpretation

On the basis of the transformed divergence analysis, the combination of Landsat TM bands 1,2,4,5,6,7 and JERS-1 SAR (identified as 8) provided the highest average separability between spectral classes. The maximum likelihood classifier was therefore implemented taking that set of bands. The radar scene contains an important amount of information for the classes of interest, since it was kept as one of the best bands when taking a combination of two or more bands at a time (table 6.19).

Table 6.19: Results of transformed divergence analysis of Landsat TM and JERS-1 data set

No. OF BANDS	BEST AVERAGE SEPARABILITY	BEST BAND COMBINATION
8	1989	1 2 3 4 5 6 7 8
7	1992	1 2 4 5 6 7 8
6	1991	2 4 5 6 7 8
5	1988	2 4 5 6 8
4	1979	2 5 6 8
3	1947	2 6 8
2	1881	2 8
1	1706	2

Figure 6.43 shows the results of applying fuzzy modelling of saline and alkaline classes to the merged Landsat TM and JERS-1 SAR data set. Overall accuracy was equal to 75% and average class reliability and accuracy achieved values of 75 and 77.5% respectively (table 6.20). However, the classifier could not distinguish between moderately saline-alkaline areas and moderately saline-strongly alkaline areas. This could be due to two reasons. First, the samples belonging to these categories have low membership grades (below 0.2 in the case of the moderately saline-strongly alkaline set and below 0.68 for the moderately saline-alkaline set); thus these sets are poorly represented. The above classes are also difficult to identify because of the spectral confusion caused by similar topsoil textures and the absence of specific external features, such as different surface roughness, in the alkalinity classes. Regardless of the alkalinity degree, samples from classes 3 and 4, for instance, were labelled as class 7. The common feature among these soil samples is their silt content above 40%. Stoner (1979) found silt content to contribute significantly to explain reflectance differences in the 520-620mm range, i.e. the Landsat TM band 2 which together with the JERS-1 data forms the best band combination when taking two bands at a time.

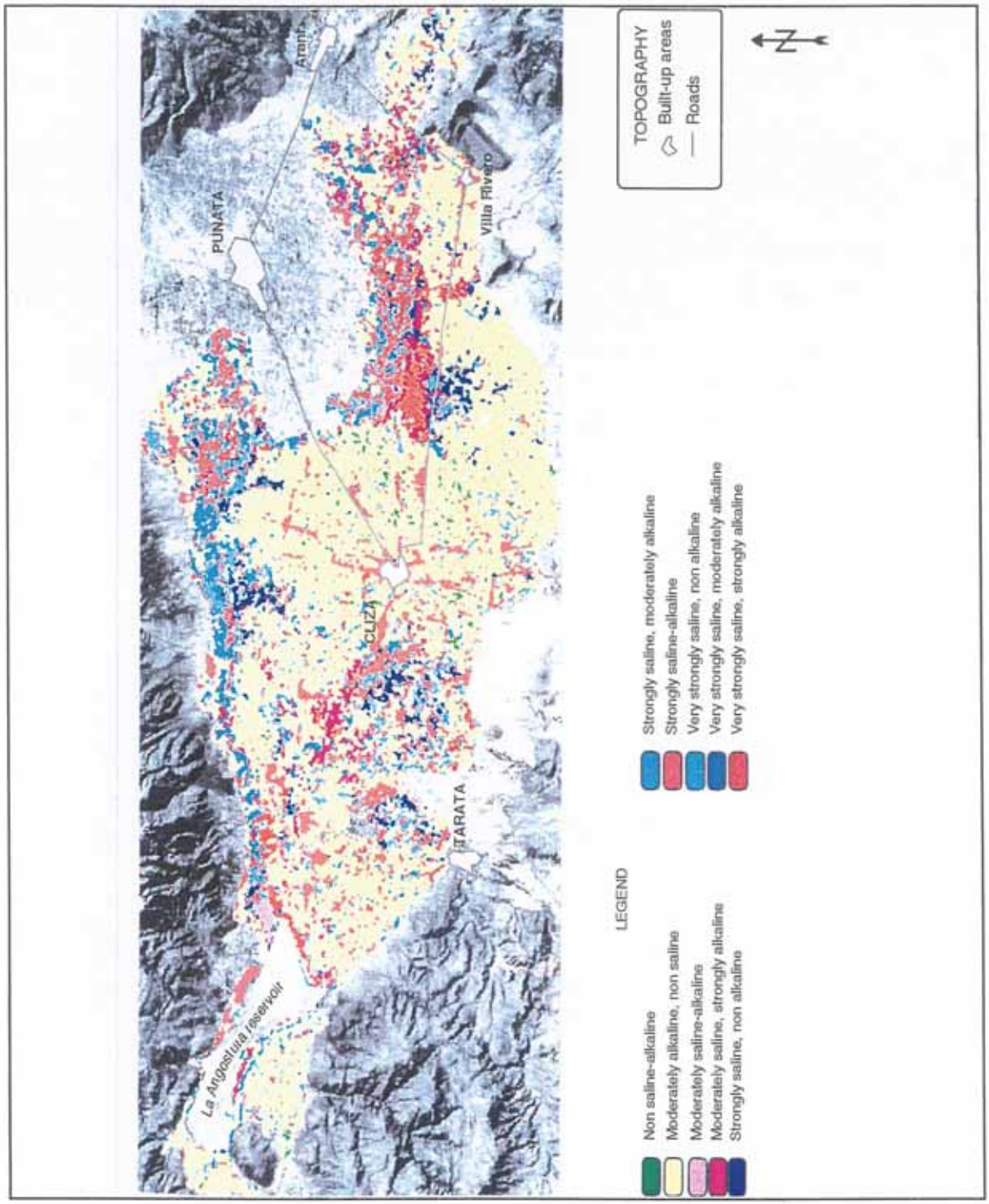

Fig. 6.43: *Spatial discrimination of salt- and sodium-affected areas after fusion of JERS-1 and Landsat TM data sets.*

Table 6.20: Confusion matrix of Landsat TM and JERS-1 data set

CLASSIFIED DATA	REFERENCE DATA											
	1	2	3	4	5	6	7	8	9	10	TOTAL	ACC.%
1	10										10	100
2		130					10				140	93
3		10	20								30	67
4				20				10			30	67
5					20		10				30	67
6						20					20	100
7		10	20	20			80	10		10	150	53
8					10			50			60	83
9						10			20		30	67
10							20			70	90	78
TOTAL	10	150	40	40	30	30	120	70	20	80	590	
REL.%	100	87	50	50	67	67	67	71	100	88		

ACC.%= accuracy %; REL.%=reliability %

In conclusion, classes containing the qualitative term 'moderate' were poorly identified, regardless of the data set and the modelling of information categories. Very strongly saline categories, with different alkalinity degrees, performed best. The inclusion of radar image data and fuzzy modelling improved the distinction of these classes. Overall accuracy improved by as much as 11%, with respect to the classification obtained from the Landsat Thematic Mapper data set.

(3) Using supervised fuzzy classification of JERS-1 data

(a) The method

To explore potential improvements in discriminating saline and alkaline areas, a fully fuzzy classification approach was attempted. Classes were determined using the ranges established by the US Salinity Staff (1954) for saline, saline-alkaline and alkaline areas. The following rules define the four information categories considered:

(a) 'Non-affected soils' if EC <= 4 dS/m and pH < 8.5.
(b) 'Alkaline areas' if EC <=4 dS/m and pH >= 8.5.
(c) 'Saline areas' if EC > 4 dS/m and pH < 8.5
(d) 'Saline-alkaline areas' if EC > 4 dS/m and pH >= 8.5.

Four fuzzy sets, namely 'non-alkaline', 'alkaline', 'saline' and 'non-saline' are necessary to characterize these categories.

A bell-shaped model (Dombi, 1990), with inflection equal to 3 and sharpness of 0.7, was used to build up the functions. Figure 6.44 illustrates the fuzzy membership function obtained for the soil reaction (pH). A pH value of 7 has a membership degree of 1 in the fuzzy set 'non-alkaline', while a pH equal to 10 has a certainty factor of zero in that same set but of 1 in the fuzzy set 'alkaline'. Figure 6.45 depicts the membership function of the electrical conductivity. Soil samples with an EC value of zero belong to the fuzzy set 'non-saline' soils to a degree of 1. Instead, when a sample has an electrical conductivity greater than 4, it belongs to the set 'saline' soils.

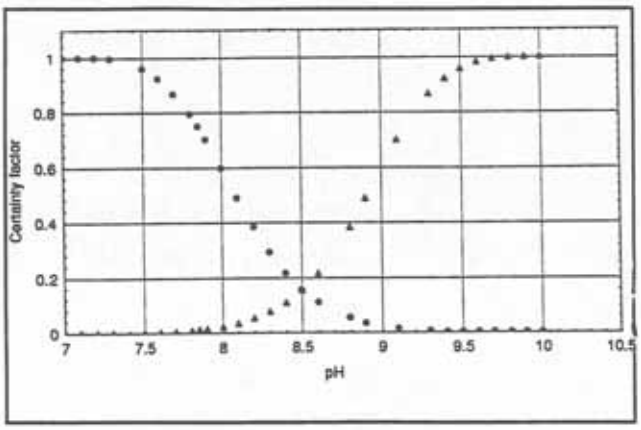

Fig. 6.44: *Membership function of the fuzzy sets 'non-alkaline' with pH values less than 8.5 and 'alkaline' with pH values equal to or above 8.5.*

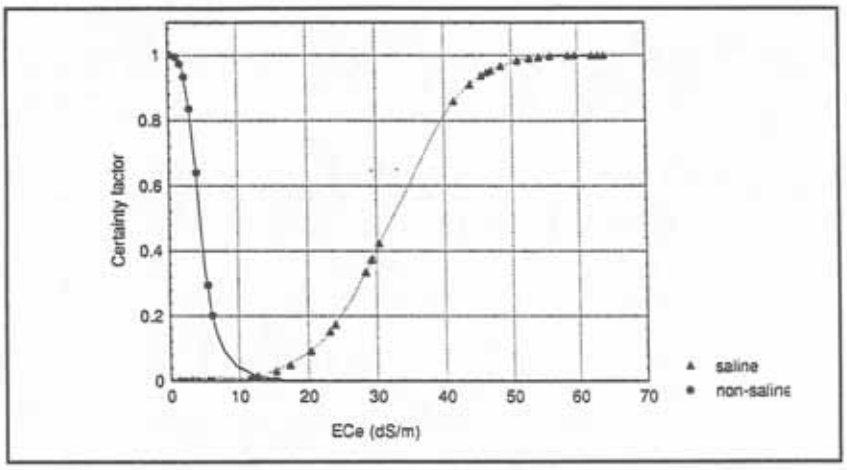

Fig. 6.45: *Membership function of the fuzzy sets 'saline' and 'non-saline' soils.*

The membership grades of the soil data to the four different fuzzy sets were computed. As a result, a soil sample may belong to the fuzzy set 'alkaline' or 'non-alkaline' and to the set 'saline' or 'non-saline' (fig. 6.46).

Afterwards, the spectral signatures of the soil samples belonging to the different sets were extracted using a neighborhood-based operator. The 95 georeferenced backscattering values were allocated to the four categories according to their fuzzy set membership (fig. 6.47).

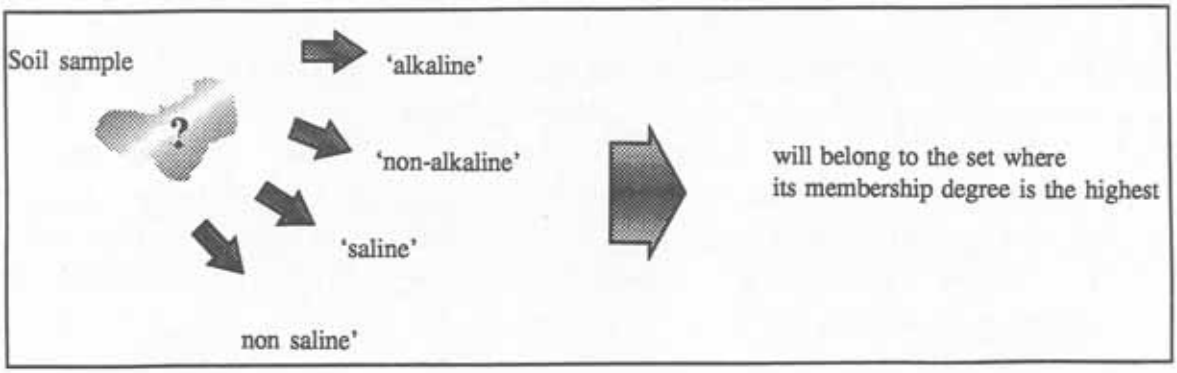

Fig. 6.46: *The membership grades of an hypothetical soil sample.*

The median value of each class was taken as standard point, with a membership degree of 1 to the set under consideration. Other fuzzy classification models take the mean value of a cluster as the standard point (Foody, 1994; Wang, 1990; Key et al., 1989). The median is preferable to the mean as the latter is very sensitive to extreme scores or measurements (fig. 6.47). Histogram tails were taken as the typical points, having a membership grade of zero in a particular class.

The user has also to define the type of membership function (eg. linear, sigmoidal) to be used for fuzzy modelling of the layers. A sigmoidal function was selected, such as:

$$\mu=\cos^2\alpha,$$

where, in the case of a monotonically increasing function,

$\alpha= (x-a)/(b-a)*pi/2$ *for* $x < b$ (1)

and $1[(c-x)/(c-b)*pi/2]$ *for* $x > b$ (2)

being *a* and *c* the typical points and *b* the standard point (IDRISI for Windows user's guide, 1995). Table 6.21 contains the standard and typical points selected for each class.

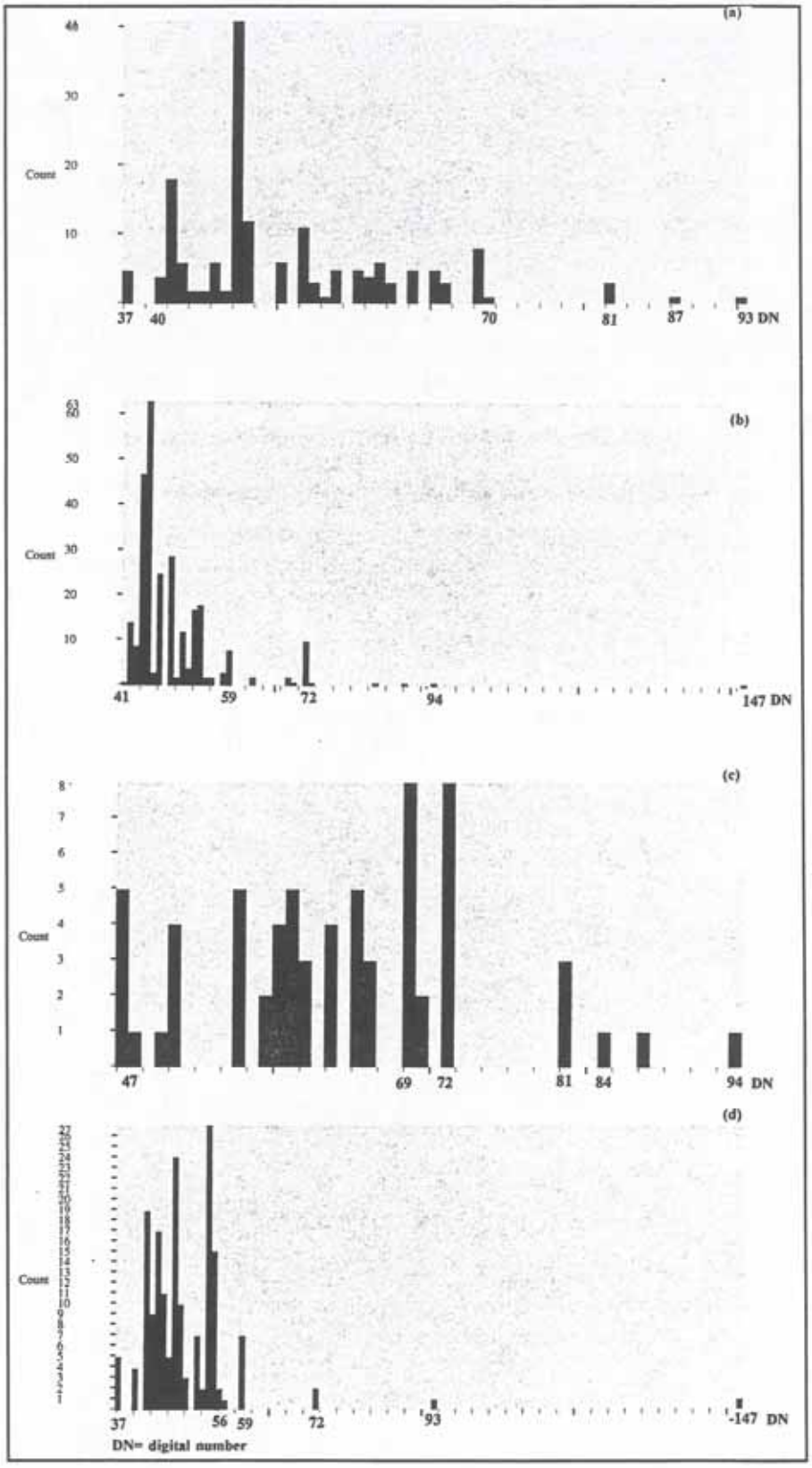

Fig. 6.47: Histograms of the four data classes: (a) 'non-alkaline' set; (b) 'alkaline' set; (c) 'non-saline' set; (d) 'saline' set.

Table 6.21: Typical and standard points characterizing the membership functions

CLASS	TYPICAL POINTS	STANDARD POINT
Non-alkaline	36, 94	47
Alkaline	40, 74	45
Non-saline	46, 95	69-72
Saline	36, 73	53

A fuzzy overlay model was used to classify the satellite image (fig. 6.48). Such a model is useful for natural resource applications (Drummond, 1991; Giang et al. 1995). Individual layers are created for each of the classes under consideration and processed using the fuzzy operators developed by Zadeh (1965) to produce one final map. Layers can be combined through user-defined rules of the type if-then statement. The following rules were established:

1. IF 'non-alkaline' AND 'non-saline', THEN 'non-affected areas'
2. IF 'alkaline' AND 'non-saline', THEN 'alkaline areas'
3. IF 'non-alkaline' AND 'saline', THEN 'saline areas'
4. IF 'alkaline' AND 'saline', THEN 'saline-alkaline areas'

The membership grade of a pixel *(x)* to the new categories (e.g. non-affected areas, etc.) is computed using a minimum operator:

$$\mu_{non\text{-}affected}(x) = \text{MIN}\,[\mu_{non\text{-}alkaline}(x), \mu_{non\text{-}saline}(x)] \qquad (3)$$

In other words, the membership grade of a pixel(x) in the fuzzy set 'non-affected areas' is the smallest of its membership grades in the sets 'non-alkaline' and 'non saline'. Membership grades to the other sets are computed in the same way, using the minimum operator (Zadeh, 1965; Negoita, 1985; Klir and Folger, 1988).

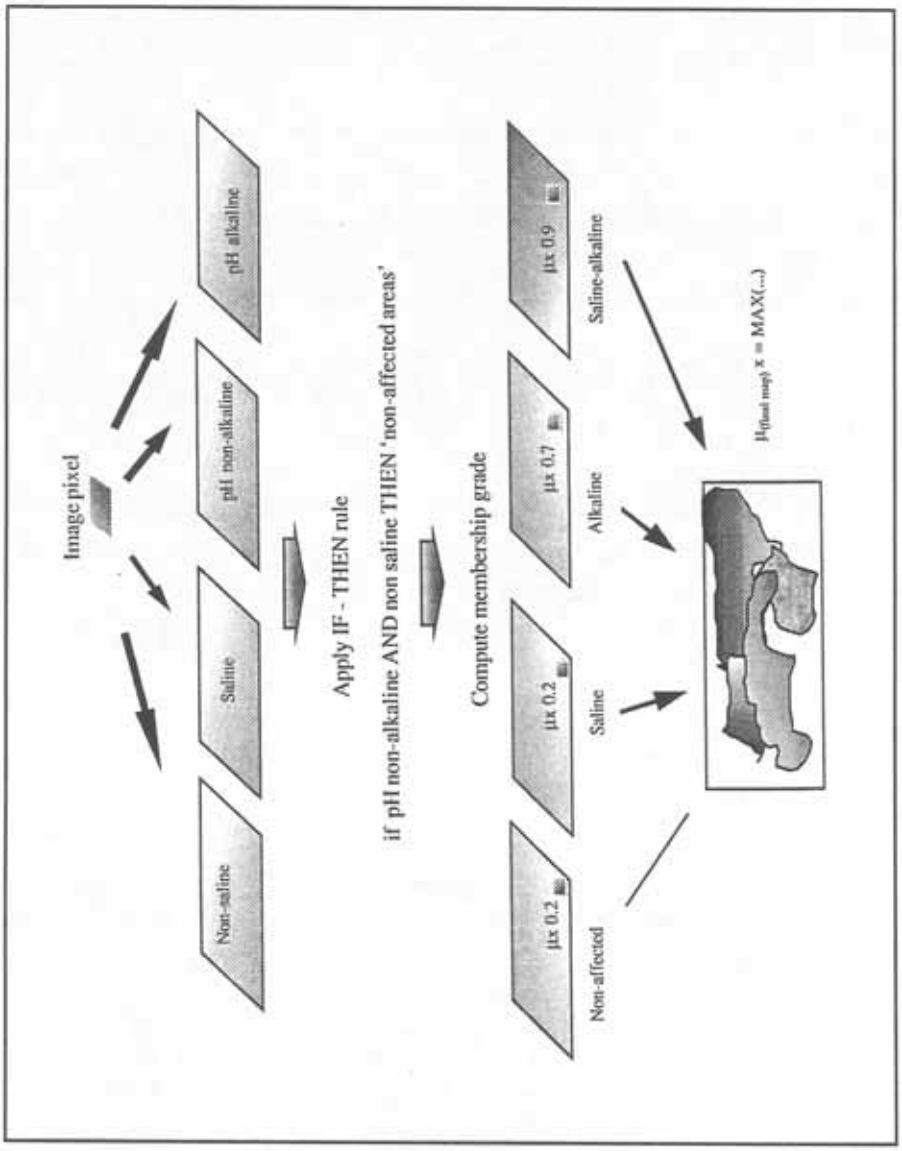

Fig. 6.48: The fuzzy overlay model

Each pixel has attached to it a group of membership grades to indicate the extent to which the pixel belongs to different classes. Pixels with class mixture or in transitional conditions can now be described. For example, if a ground cell contains two classes such as 'saline areas' and 'saline-alkaline areas', it has two membership grades indicating the extent to which the pixel is associated with the two classes. The closer the value of $f_{'non\text{-}affected'}(x)$, which represents the membership grade of (x) to the 'non-affected' set, is to 1, the more the pixel belongs to that class.

The union of the classes provides the final map. A pixel will take the label of the group in which it has the highest certainty factor. This is implemented by using a maximum operator:

$\mu_{\text{'final map'}}(x) = \text{MAX}\ [\mu_{\text{'non-affected'}}, \mu_{\text{'alkaline'}}, \mu_{\text{'saline'}}, \mu_{\text{'saline-alkaline'}}]$ (4)

The membership grade of a pixel (x) in the output map is either its membership grade in 'alkaline' or 'saline' or 'saline-alkaline' or 'non-affected', whichever has the largest value. To identify the class to which the highest membership grade belongs, the following rule is applied:

Class=IF(class='non-affected',1,IF(class='alkaline',2,IF(class='saline',3,IF(class='saline-alkaline',4))))(5)

The combination of equations (4) and (5) allows to know the pixel labelling and its membership grade to a particular category.

The amount of layers may be a drawback in modelling. For instance, the combination of four salinity-alkalinity classes and one satellite band generates a 4-layer output. But if the number of bands increases to 6, 24-output layers will be created. Since the JERS-1 SAR satellite has only one band, four layers were produced.

(b) Data interpretation

Table 6.22 is the confusion matrix computed from the fuzzy classification of the JERS-1 SAR scene presented in figure 6.49. Soil sites belonging to the saline category were 100% identified and the accuracy of areas classified as saline against the ground-truth is also high (88%). The poorest performance corresponds to the proper identification of alkaline and saline-alkaline areas. They were spread over all the information categories, specially that of the non-affected areas. The reason of the failure may be strongly related to the roughness of the soil surface, which the radar backscattering heavily depends on.

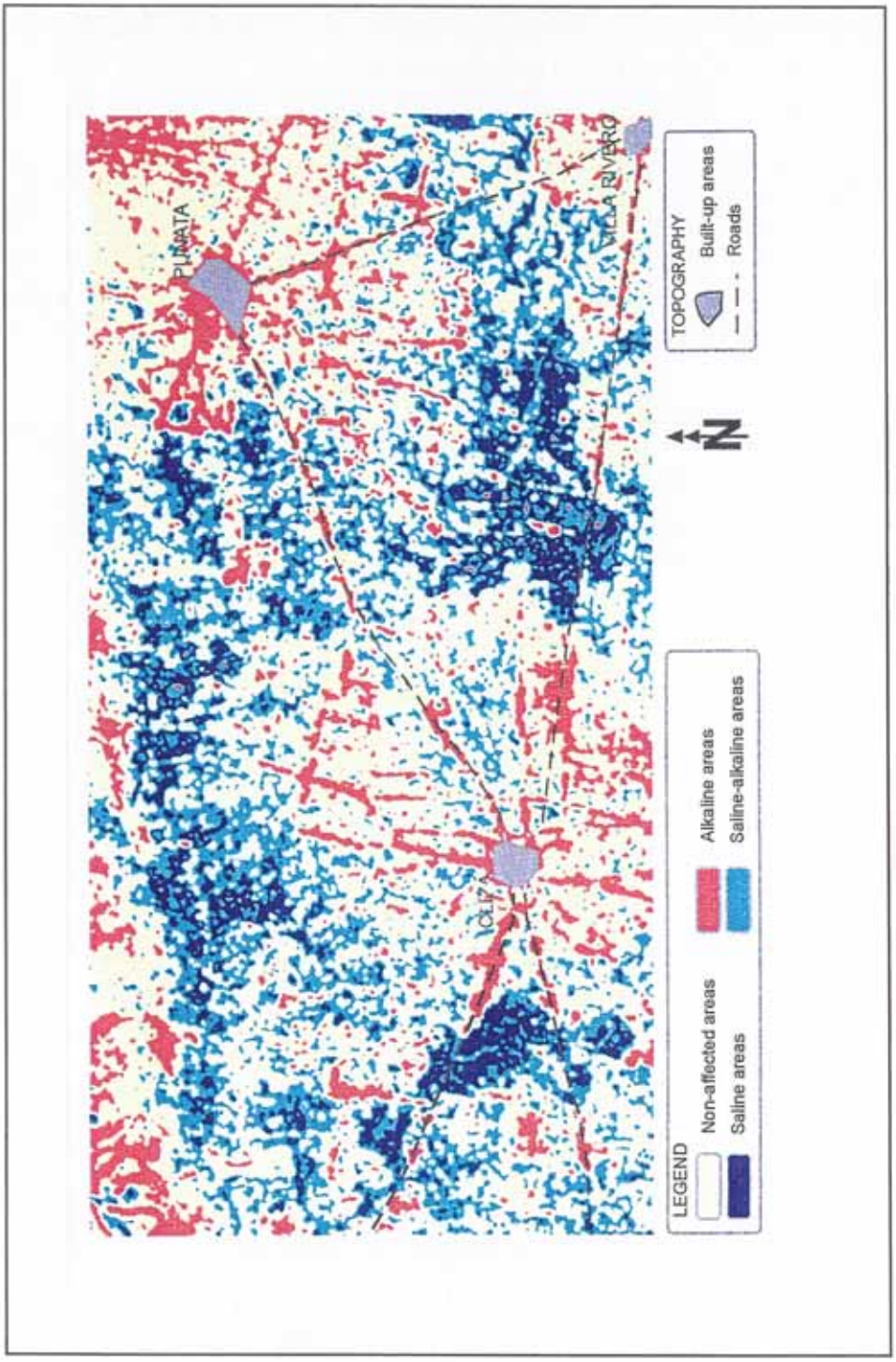

Fig. 6.49: Spatial discrimination of salt- and sodium-affected areas using a fuzzy supervised classification of JERS-1 data.

For the JERS-1 SAR, a surface is considered rough when its height difference is greater than 3.5 cm. Surfaces exposed to cultivation or maintained fallow during the dry season, when the image was collected, have clods of variable sizes as a result of ploughing either by tractor or animal traction. Such 'rough' surfaces directly influence the radar backscattering and mask the effect of other soil properties such as salt type and degree or soil particle size.

During the field campaign, it was observed that farmers cultivate land parcels with pH values up to 9, belonging thus to alkaline areas. The statistical analysis between radar signal and pH showed a low negative correlation (r=-0.19). Thus, when pH increases, the backscattering decreases because the surface is smoother, since the land becomes unsuitable for cultivation.

Table 6.22: Confusion matrix of the fuzzy supervised classification

CLASSIFIED DATA	REFERENCE DATA					
	Non-affected	Alkaline	Saline	Saline-alkaline	TOTAL	ACC.%
Non-affected	180	40		50	270	67
Alkaline		10		10	20	50
Saline		10	220	20	250	88
Saline-alkaline	10	10		220	240	92
TOTAL	190	70	220	300	780	
REL.%	95	14	100	73		

Overall accuracy: 80.7; average reliability: 70; average accuracy: 74

Soil roughness explains also the good discrimination of saline areas. Saline topsoils are generally smoother than non-saline ones, having therefore lower backscattering values as less energy returns to the radar antenna and, as a consequence, darker colors on the scene.

Electrical conductivity also correlates negatively with the radar backscattering signal (r=-0.47). Thus, as the electrical conductivity increases, the energy returned to the antenna decreases. Additionally, as the land parcels become more salinized, cultivation practices diminish and the clods produced by ploughing disappear.

Table 6.23 reflects the correlation between radar backscattering and several soil properties. The highest negative relationship is between radar backscattering and electrical conductivity, followed by pH, clay and coarse sand. Fine sand and silty particle sizes have a weak positive correlation with the radar backscattering. Thus as their content increases, the radar signal becomes brighter on the scene. A multiple regression of these variables against the radar backscattering showed a low coefficient of determination (r^2=0.27).

Table 6.23: Correlations between JERS-1 SAR backscattering signal and soil properties

VARIABLE	ECe	pH	Clay	Silt	Fine sand	Coarse sand
Radar backscattering	-0.47	-0.19	-0.10	0.06	0.11	-0.06

(4) Evaluation of the classification performance

(a) Causes of spectral confusion

Soil texture seems to have a low influence on images collected by active sensors, unlike the passive satellite sensors. Radar backscattering is mostly affected by the roughness of the surface, produced by land cultivation. This is the main factor causing erroneous allocation of alkaline and saline-alkaline soils to non-affected areas. Except for alkaline areas, the fuzzy supervised classification of the JERS-1 SAR data provided reliable results.

Main causes of spectral confusion, masking the real variability of salinity-alkalinity degrees, were: (1) the type and abundance of the vegetation cover, which control the reflectance values when the soil surface is not bare; (2) the topsoil textures, as high amounts of silt plus clay hinder the effects of variable salt and sodium contents; (3) the mixture of topsoil properties under field conditions, where salt, particle size and crusting mutually interfere. These findings reinforce previous conclusions derived from ground-based measurements of soil properties when determining best band combinations to predict moderately alkaline soils (pH 8-9). Very low coefficients of determination resulted from the prediction models developed for that range of soil reaction.

(b) Data fusion

Except for the 'moderately and strongly saline-alkaline' and for the 'moderately and strongly saline classes, the probability of ground data to be correctly labelled improved by as much as 49% after merging Landsat TM and JERS-1 data (fig. 6.50). Strongly and moderately saline classes possess distinctive surface features such as puffy crusts and saline efflorescences, which can be discriminated already from the visible and infrared data. The very strongly saline and moderately alkaline class strongly benefited from the radar inclusion.

After comparing the different techniques applied to map saline and alkaline areas, it can be concluded that moderate salinity and/or alkalinity classes are difficult to discriminate, regardless of the data set and modelling approach used.

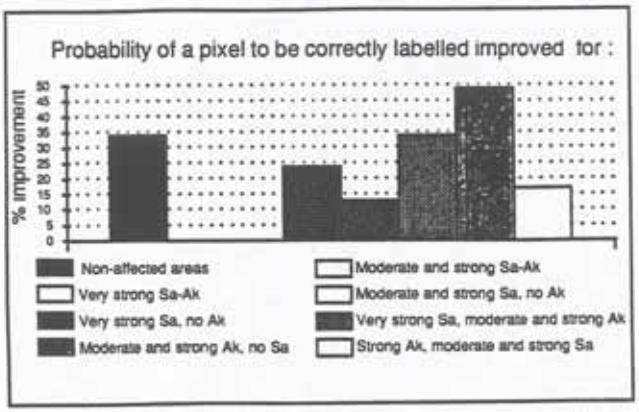

Fig. 6.50: Improvement on class discrimination achieved by merging Landsat TM and JERS-1 data.

(c) Class discrimination versus sensor performance

Supervised fuzzy classification of JERS-1 SAR data is the most effective approach to discriminate saline and saline-alkaline areas (fig. 6.51). On the other hand, the fusion of visible, infrared and microwave data is suitable to map areas non-affected by salinity-alkalinity and discriminate alkaline soil surfaces, at a level of accuracy remarkably superior to the accuracy achieved by Landsat TM and JERS-1 separately (35 to 40% accuracy increase).

In general, lower class reliability and accuracy were obtained when working with Landsat Thematic Mapper and crisp class boundary definition. The highest accuracies are provided by full supervised fuzzy classification, including not only fuzzy class boundary definition, but also pixel allocation to given classes. Landsat TM and JERS-1 data fusion and the fuzzy modelling of information categories provided the highest class reliability and accuracy (fig. 6.52).

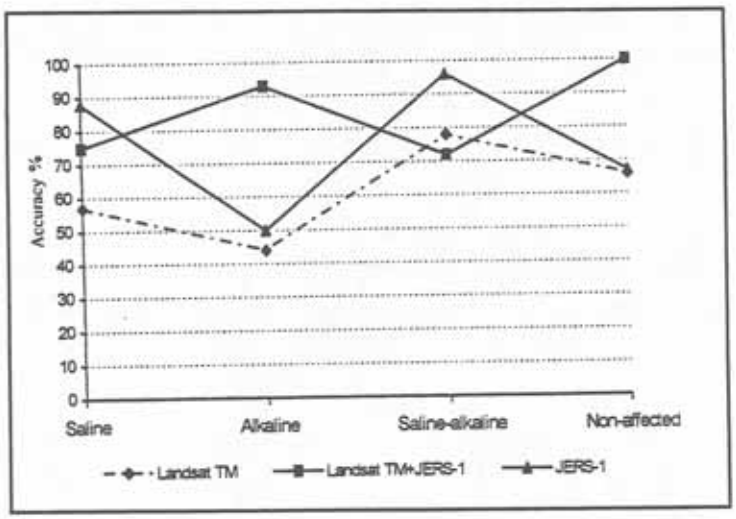

Fig. 6.51: Class discrimination vs. sensor performance

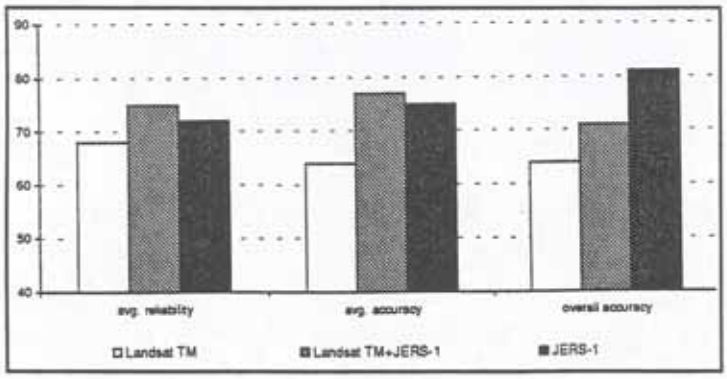

Fig. 6.52: Comparison of class reliability and accuracy achieved by the different approaches.

(d) Map quality and readability

Comparison of figures 6.37, 6.43 and 6.49 shows that classification improvements, generating higher class accuracy and reliability, not increase map readability. The map of salt- and sodium-affected areas, obtained by fully supervised fuzzy classification (fig. 6.49), showed to be accurate but is of poor readability. The saline and saline-alkaline soils are distributed in three main areas, including southwest of Cliza, between Cliza and Arani and west of San Benito. The alkaline areas constitute small noisy patches, spread all over the lagunary flats and playas, and create confusion with roads, built-up areas and ditches. The application of an iterative majority filter, commonly used as a post-classification procedure to eliminate or reduce noisy features and improve map readability, would imply alkaline areas to disappear and be replaced by one of the other more homogeneous groups (non-affected areas, saline areas).

The map depicting salt and sodium distribution, obtained by fusion of Landsat TM and JERS-1 data (fig. 6.43), coincide with figure 6.37 in locating degraded areas in the playas between Cliza and Arani, the area southwest of Cliza, and the playas and lagunary flats of the Angostura-Tolata-San Benito area. A majority filter with a 3 by 3 window size was applied as post-classification procedure to reduce the image noisy aspect. However, subsequent iterations or the use of larger window sizes would imply the disappearance of non saline-alkaline areas and the areal reduction of other classes to the benefit of the dominant ones, in particular the moderately alkaline, non saline class.

The salt- and sodium-affected areas, mapped by using statistical pattern recognition and Landsat TM data (fig. 6.37), have slightly lower accuracy but comparatively the best map readability. The map highlights correctly the position of the most degraded areas on the landscape, as the two previous maps also do, but the classes are more homogeneously displayed. The classification procedure implemented here provided more uniform, relatively large patches. Therefore, the majority filter could be applied with larger window sizes, without prejudicing the classes corresponding to relatively smaller clusters.

Comparing figures 6.37 and 6.43, it results that non to slightly saline-alkaline areas and moderately alkaline, non to slightly saline areas, mapped as predominant classes in the higher lagunary flats and dissected glacis (fig. 6.37), are replaced by the moderately alkaline, non-saline group in the same

landscape position (fig. 6.43). This might be partly attributed to the limits imposed as class boundaries and to the selected boundary type, crisp or fuzzy. In fact, non to slightly saline-alkaline areas on figure 6.37 overlap with the boundaries imposed to the moderately alkaline-non saline fuzzy set on figure 6.43.

(5) Relationship between landscape positions and salinity-alkalinity degrees

Salt- and sodium-affected areas mapped using different sensors and classification techniques (figs. 6.37, 6.43 and 6.49) were confronted with the map of the geopedologic units and the laboratory data (section 6.2.2) to evaluate their spatial distribution. Non to slightly saline-alkaline areas correspond to the higher lagunary flats in the southern part of the valley, where coarser carbonate-rich alluvial deposits overlay lacustrine materials. The predominance of free carbonates and bicarbonates over chlorides and sulphates causes the pH values to be less than 8.5. This boundary was adopted to discriminate non-alkaline classes from satellite image.

The most degraded areas, represented by classes labelled as very strongly saline-alkaline, very strongly saline and slightly alkaline, very strongly alkaline and moderately saline, and strongly alkaline are located on the playas, which occupy the lowest landscape positions and have fine soil textures. Clear degradation features such as puffy structureless crusts, saline efflorescences and halophytic vegetation, are common. The highest salt concentrations occur in these areas, with values as high as 20%.

Most of the moderately and strongly saline, slightly alkaline areas were mapped on the lower lagunary flats, a transitional zone between the pure lagunary and the mixed alluvio-lagunary deposits. Up to 8% salt concentration was found in soil samples located in this unit, where ECe values are above 30dS/m and pH > 8.5. Soluble salts such as sulphates and chlorides predominate in this unit.

Moderately alkaline, non to slightly saline areas predominate on the middle lagunary flats, the borders of the high lagunary flats and the distal parts of the piedmont glacis, originated by alluvial deposits coming from the erosion of claystones, shales and calcareous sandstones of the surrounding mountains (San Benito and Cuchupunata formations).

In conclusion, the parent materials, the topographic positions and the dry climate, which reduces leaching and causes the migration of soluble salts towards the surface horizons, are the main factors controlling the spatial distribution of salt- and sodium-affected areas. The most degraded areas are located on playas. Non to slightly saline-alkaline areas coincide with the higher lagunary flats (fig. 6.53). Middle and higher lagunary flats are exposed to future salt expansion.

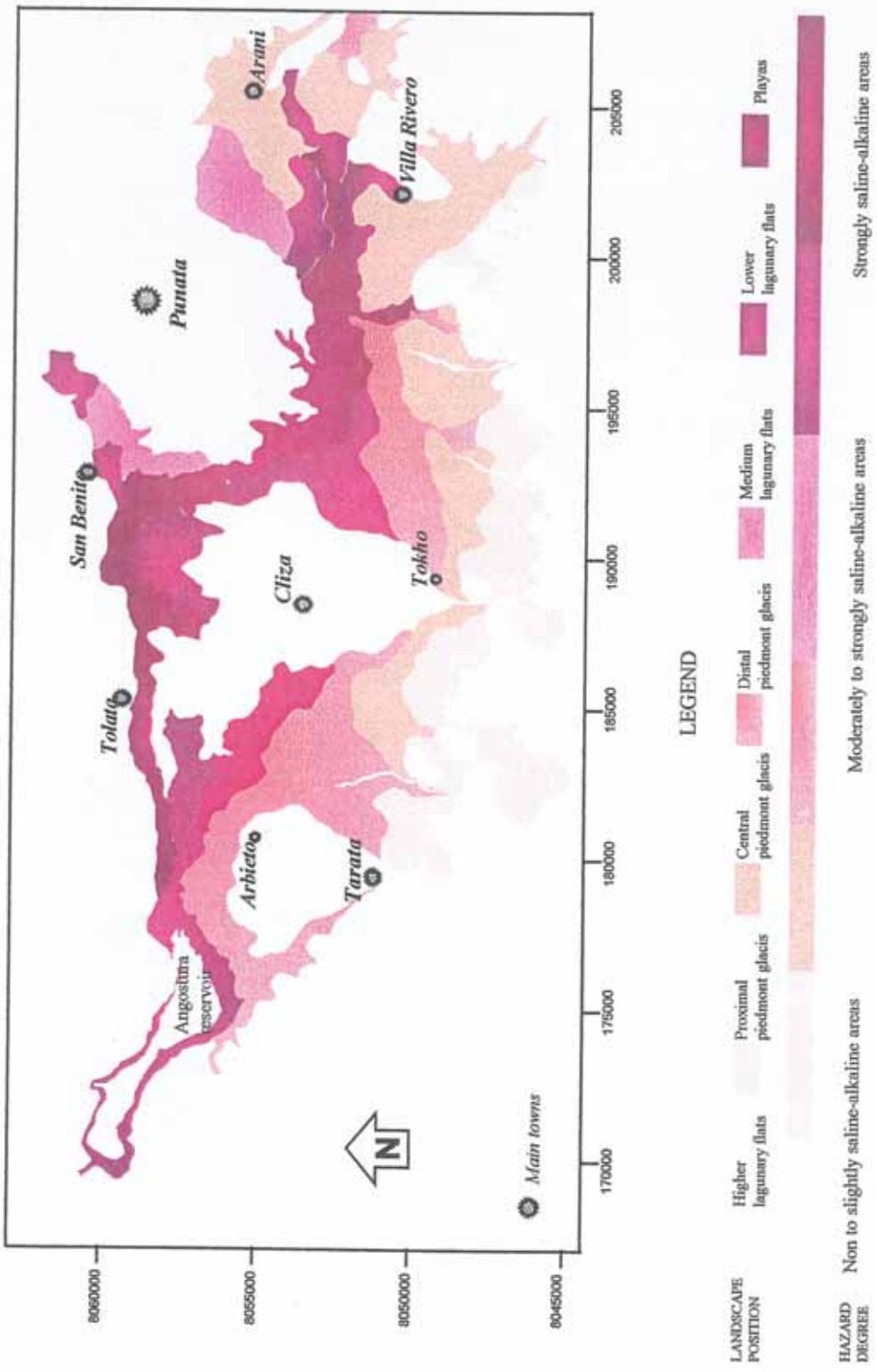

Fig. 6.53: Salinity-alkalinity degraded areas in the Punata-Cliza valley.

6.5.2 Mapping salinity-alkalinity based on anion ratios

Since not all salts are equally harmful, it is important to analyze the salt-type distribution on the landscape. For this purpose, the classification of saline soils based on anion ratios was applied to the Punata-Cliza valley. The ninety-five soil samples were allocated to anion ratio classes. Since two different ratios define sulphate-chloride and soda soils, a given soil sample may simultaneously be sulphate-type and soda-like if its Cl/SO_4 ratio is less than 0.2 and its CO_3/SO_4 ratio less than 0.005.

Table 6.24: Information classes to recognize different salt types

INFORMATION CLASSES	RATIO	BOUNDARIES
Sulphate soils	Cl/SO_4	< 0.2
Chloride-sulphate soils	Cl/SO_4	0.2 - 1.0
Sulphate-chloride soils	Cl/SO_4	1.0 - 5.0
Chloride soils	Cl/SO_4	> 5.0
Soda soils	CO_3/SO_4	< 0.005
Sulphate-soda soils	CO_3/SO_4	0.005 - 0.15
Soda-sulphate soils	CO_3/SO_4	> 0.15

(1) Using crisp class boundaries and statistical pattern recognition

The data set consisting of 95 georeferenced composite topsoil samples was partly used to train the classifier and to evaluate the classification results. The procedure previously mentioned, using a neighborhood-based operator to locate topsoil samples representative of selected classes, was followed to train the classifier, evaluate signatures and select the best band combination to label the image. One-third of the field data set was used to determine spectral class signatures, while the remaining data were used to evaluate the classification accuracy and reliability. The maximum likelihood classifier, without prior probabilities, was implemented for class allocation.

Using the transformed divergence analysis, the average separability between categories and the best band combinations taking seven, six, five, four, three and two bands at a time, were determined for the sulphate-chloride and soda soils, respectively (tables 6.25 and 6.26).

Table 6.25: Transformed divergence analysis to evaluate the separability between sulphate, sulphate-chloride, chloride-sulphate and chloride soils.

No. OF BANDS	BEST AVERAGE SEPARABILITY	BAND COMBINATION
7	1947	1 2 3 4 5 6 7
6	1968	1 2 4 5 6 7
5	1967	1 2 4 6 7
4	1657	2 4 6 7
3	1922	1 4 7
2	1846	2 4

Table 6.26 : Transformed divergence analysis to evaluate the separability between soda, soda-sulphate and sulphate-soda soils

No. OF BANDS	AVERAGE SEPARABILITY	BAND COMBINATION
7	1968	1 2 3 4 5 6 7
6	1982	1 2 4 5 6 7
5	1979	1 2 4 6 7
4	1973	2 4 6 7
3	1945	2 4 7
2	1886	2 4

In both cases, the best average separability between spectral classes resulted from the combination of bands 1,2,4,5,6,7 of the Landsat Thematic Mapper. Spectral classes were grouped and re-coded to the final information classes. Confusion matrices were built up to evaluate the results (tables 6.27 and 6.28). Figures 6.54 and 6.57 show the spatial distribution of the chloride-sulphate and soda-sulphate soils.

Table 6.27: Confusion matrix of sulphate-chloride soils using a maximum likelihood classifier.

CLASSIFIED DATA	REFERENCE DATA				TOTAL	ACC.%
	Sulphate	Chloride-sulphate	Sulphate-chloride	Chloride		
Sulphate	10	60	40	10	120	8
Chloride-sulphate		130	80	20	230	56
Sulphate-chloride		30	140	20	190	74
Chloride	10		40	50	100	50
TOTAL	20	220	300	100	640	
REL.%	50	56	47	50		51

REL.%= class reliability; ACC.%= class accuracy

Class accuracy and reliability are low (table 6.27). Sulphate soils are overestimated because ground data corresponding to other classes were mistakenly labelled to this class, generating a high error of commission. The confusion occurs because the chemical composition of chlorides such as NaCl cannot

induce light absorption in the visible and near to thermal infrared bands (Hunt et al., 1972). The absorption features of the sulphates dominate, determining the inclusion of chloride-sulphate, sulphate-chloride and chloride soils as sulphate soils, even with low contents of sulphate anions in the soil samples.

Table 6.28: Confusion matrix of the soda-sulphate soils using a maximum likelihood classifier.

CLASSIFIED DATA	REFERENCE DATA			TOTAL	ACC.%
	Soda	Sulphate-soda	Soda-sulphate		
Soda	230	10	60	300	77
Sulphate-soda	30	70	50	150	47
Soda-sulphate	40	0	140	180	78
Total	300	80	250	630	
REL.%	77	88	56		70

REL.%= class reliability; ACC.%= class accuracy

Discrimination between soda, sulphate-soda and soda-sulphate soils is better than between sulphate and chloride soils (table 6.28). The lowest class accuracy concerns the sulphate-soda soils. Since this class includes mixtures of both anions, soil surfaces located at the edge of either soda (predominance of sulphates) or sulphate-soda (predominance of carbonates) information classes, are labelled as sulphate-soda soils. The carbonates have specific absorption features in two spectral ranges, at 2.34μm (TM7) and between 11 and 12μm (TM6). The sulphates, instead, have only one absorption band near 10.2μm.

Bands TM2 and TM4 contain information important to discriminate among the classes of interest, since the combination scored the best when taking two bands at a time in the transformed divergence analysis. Bands 2 and 4 coincide with the region of the spectrum identified by Csillag et al. (1993) as particularly useful to characterize the salinity status of soda-rich soils. The highest class accuracy, reflecting the probability that a pixel classified on the image is in reality representative of that category on the ground, concerns the soda-sulphate soils, which contain more carbonate than sulphate anions.

Differentiation between sulphate, sulphate-chloride and chloride soils is the least effective. Similar soda, sulphate-soda and soda-sulphate soils could not be completely isolated. This could be attributed not only to a poor spectral separability of the classes but also to an erroneous determination of the information class boundaries. Therefore, a second approach was attempted to improve the discrimination of soil surfaces affected by different types of salinity. It assumes that natural boundaries between salinity categories are not sharp but transitional. Fuzzy sets are used to account for these intergrading class boundaries. Class membership functions, defining the degree of belonging of a soil sample x in class A, are built up.

(2) Using fuzzy sets to model information categories

Fuzzy sets admit the possibility of partial membership of a soil sample to more than one category. The degree of membership is assessed by values which vary between zero and one. A value close to one

denotes a high degree of similarity between the sample point and a cluster representing the class of interest, while a value close to zero implies little similarity.

Fuzzy sets were used to determine gradual class boundaries between salinity types. Certainty factors were considered similar, but not equal, to probabilities. The membership grades of the soil samples constituting the training set were used as a possibility to find the category of interest on the field. The possibility refers to the value of the membership function associated with a certain value of x, the soil sample, and is not derived from a probability distribution function.

a) The method

To avoid erroneous conclusions about classification performance, the same 95 georeferenced soil data set and information classes as the ones used for determining crisp class boundaries, served as basis for fuzzy modelling.

The first step was to create the membership functions of the information classes. Class boundaries were defined between the values having zero certainty factor and the typical values (standard points) having a membership grade of 1. The median value of each class was taken as its standard point. For example, the chloride-sulphate class has a Cl/SO_4 ratio between 0.2 and 1. All soil samples falling within this range were taken into account to calculate the median. Class overlap allows to avoid class boundaries with membership grades equal to zero. Soil samples located within the overlap zone belong to the class where they have the highest membership grade. For categories such as soda and sulphate soils, samples with a ratio equal to zero have a certainty factor equal to 1.

The shape of the membership function determines how the transition between 0 and 1 takes place. There are several suitable functions such as triangular, trapezoidal, bell-shaped or sigmoidal. The triangular membership function was adopted for this exercise. To build up such a function, three points (a_1,a_2,a_3) are selected. The membership function is defined as:

$$\mu_A(x)= \begin{cases} 0, & x < a_1 \\ (x - a_1)/(a_2-a_1), & a_1 \leq x \leq a_2 \\ (a_3 - x)/(a_3 - a_2) & a_2 < x \leq a_3 \\ 0, & x > a_3 \end{cases}$$

where $\mu_A(x)$ represents the membership grade of x in A; a_1, a_3 are the class boundaries and a_2 is the standard point with a membership grade equal to 1 (Binj et al., 1995; Dombi, 1990). Table 6.29 indicates the membership grades and anion ratios of samples selected to identify soda, soda-sulphate and sulphate-soda soils. The same procedure was followed to calculate the membership grades of the samples used as training set to classify sulphate, chloride-sulphate and sulphate-chloride soils.

Table 6.29: Certainty factor (CF) of soil samples constituting the training set, as a function of their CO_3/SO_4 ratio.

SODA SOILS		SULPHATE-SODA SOILS		SODA-SULPHATE SOILS	
Ratio	CF	Ratio	CF	Ratio	CF
0	1	0.003	0	0.10	0
0.001	0.816	0.005	0.06	0.15	0.05
0.005	0	0.01	0.219	0.17	0.07
		0.03	0.84	0.20	0.1
		0.10	0.435	0.22	0.12
		0.11	0.348	0.29	0.19
		0.13	0.174	0.37	0.27
		0.15	0	0.58	0.48
				.61	0.51
				0.71	0.61
				0.73	0.63
				0.75	0.65
				0.79	0.69
				0.86	0.76
				0.98	0.88
				> 1.1	1.0

The extent to which a certain soil sample is associated to a class (i.e. its membership grade) was used as a certainty level to find areas on the image similar to those represented by the sample. This assumption was implemented using the certainty factors as prior probabilities in the maximum likelihood classifier. The classification is based on the probability density function from which the posterior probability of the class membership is derived as follows:

$$P(Ci \mid x) = P_i p(X \mid i) / \sum P_i p(X \mid j)$$

where $P(Ci \mid x)$ is the posterior probability of pixel X to belong to class Ci, $p(X \mid i)$ is the probability density function for pixel X as a member of class i, Pi is the a-priori probability for class i, and c the total number of classes. The prior probability to find a given class was replaced by the certainty factors computed for the samples representing that class (CF values from table 6.29).

The maximum likelihood classifier, with the prior probabilities computed for the samples composing the training set, was applied to the Landsat TM set represented by bands 1,2,4,5,6,7. The results of the classification were evaluated using confusion matrices. Figure 6.55 displays the spatial distribution of the chloride-sulphate soils, while figure 6.57 displays that of the soda-sulphate soils.

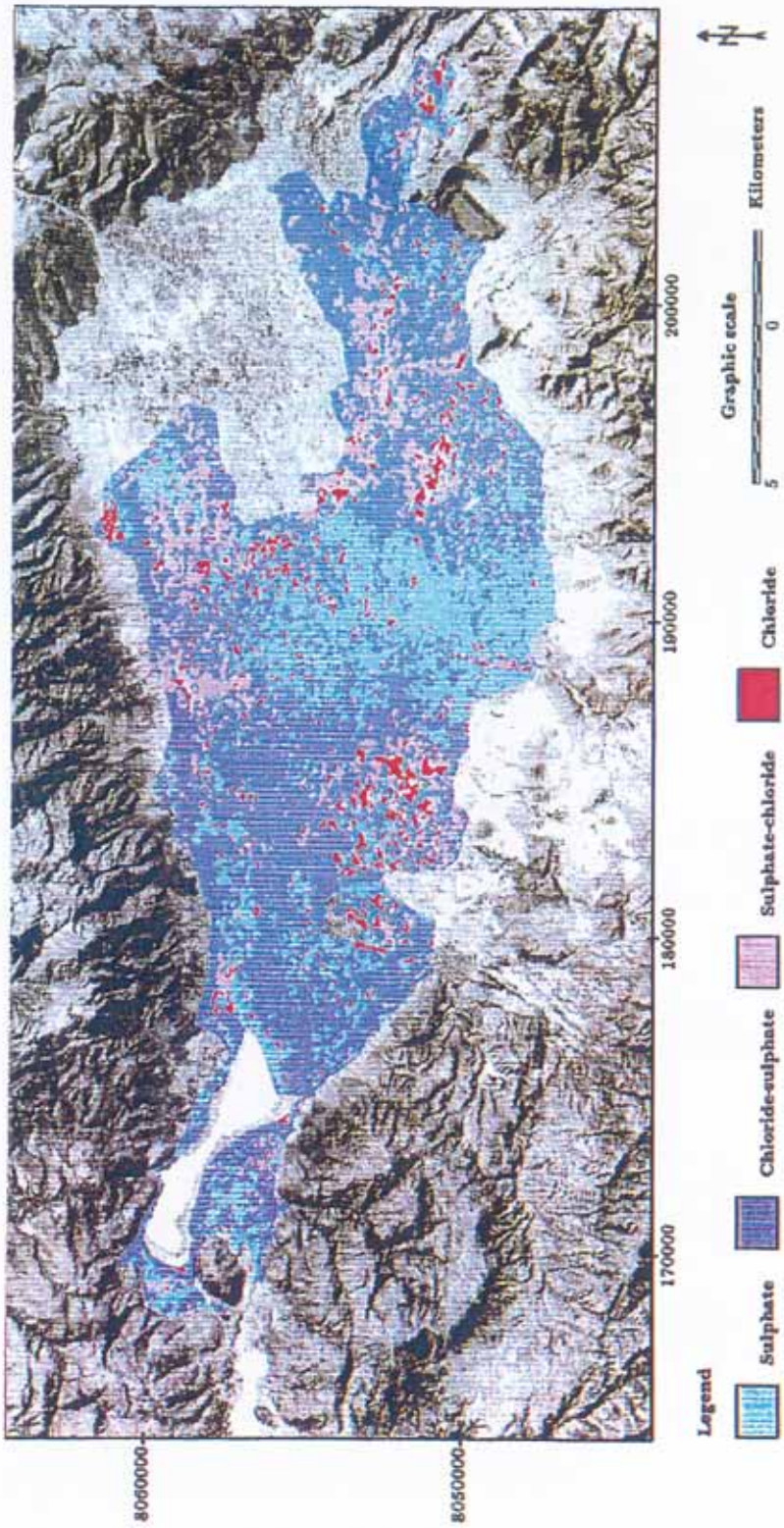

Fig. 6.54: Spatial distribution of sulphate-chloride soils using a maximum likelihood classifier without prior probabilities and crisp class boundaries.

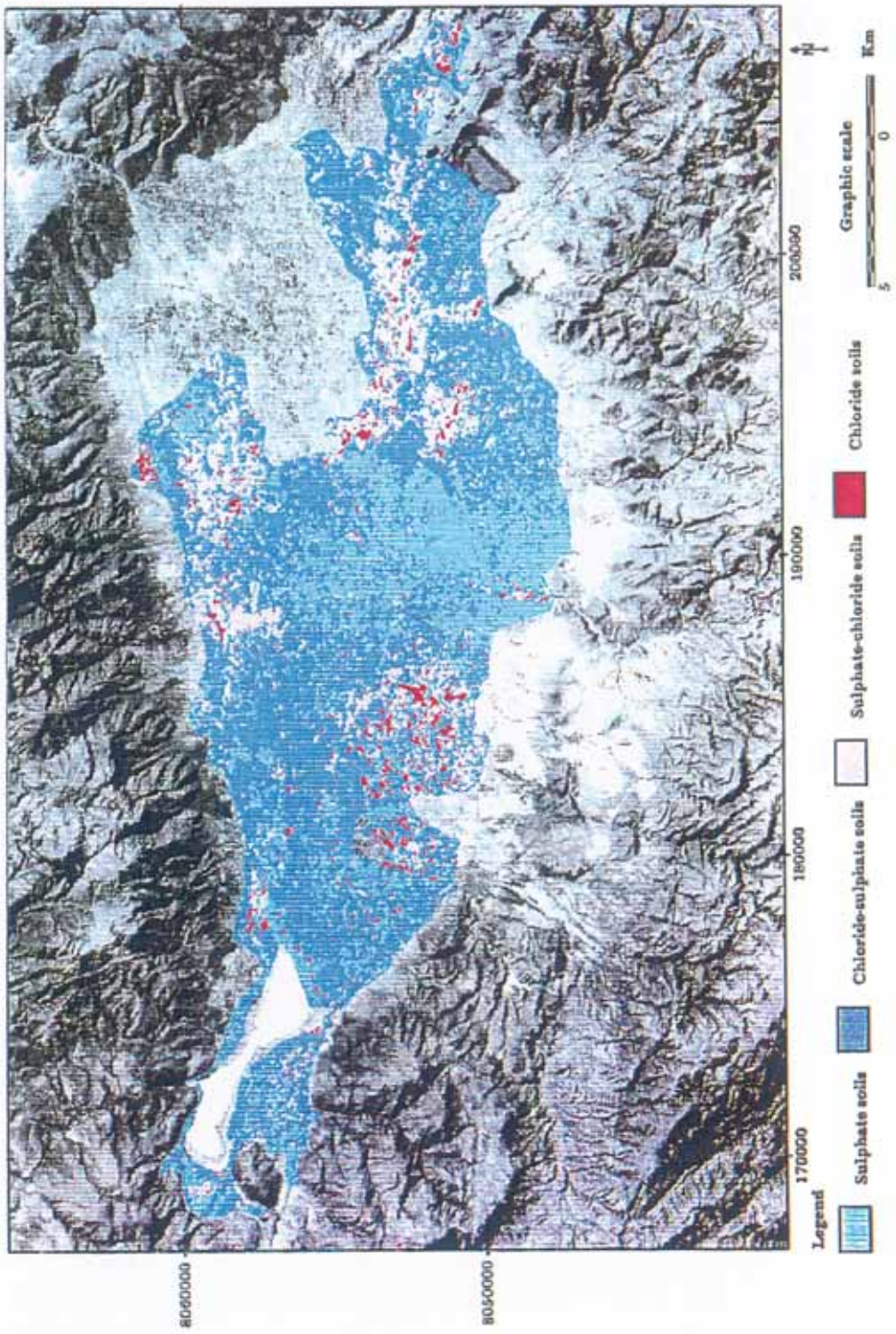

Fig. 6.55: Spatial distribution of sulphate-chloride soils using a maximum likelihood classifier with prior probabilities and fuzzy modelling of information classes.

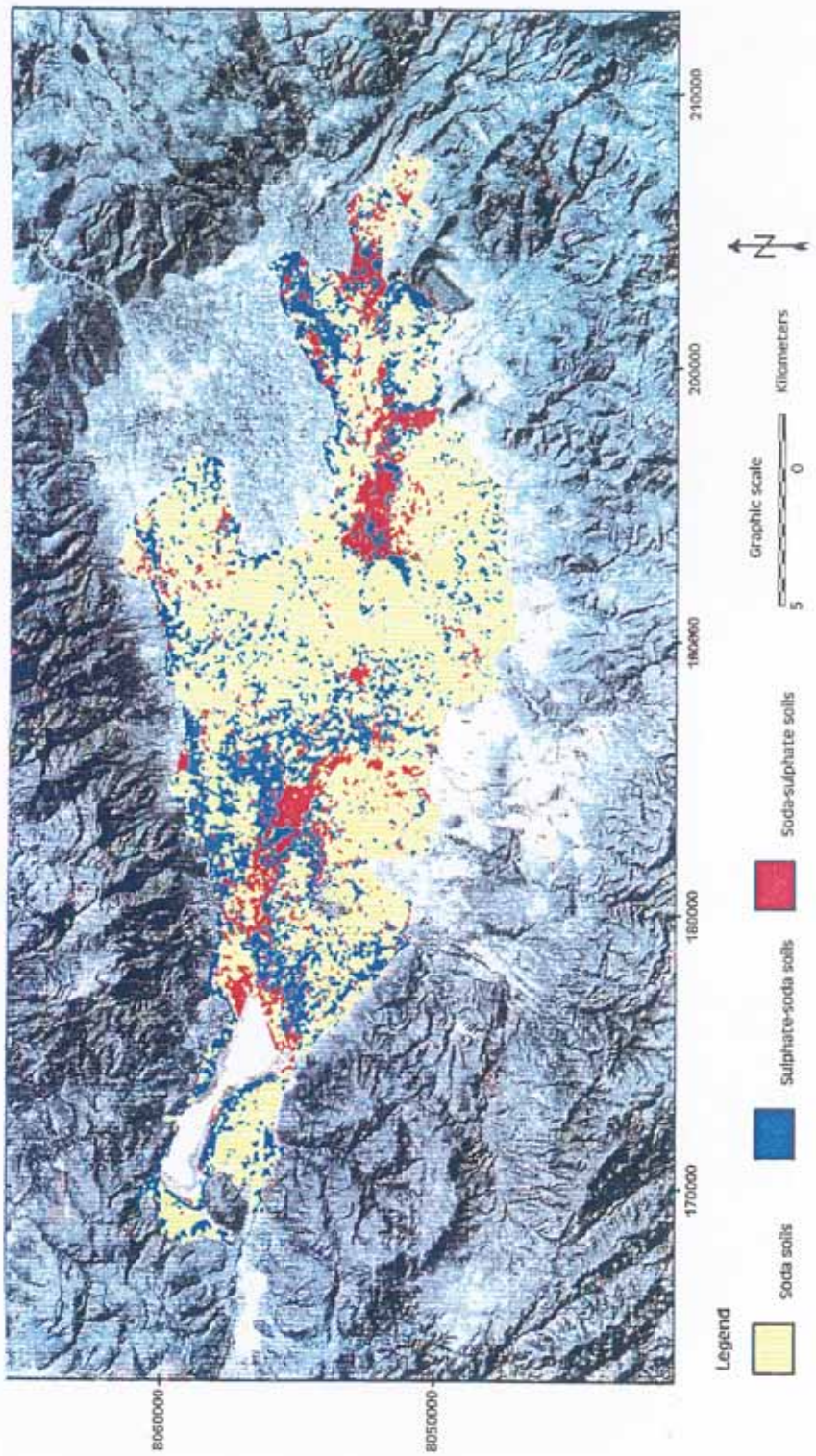

Fig. 6.56: Spatial distribution of soda-sulphate soils, using a maximum likelihood classifier without prior probabilities and crisp class boundaries.

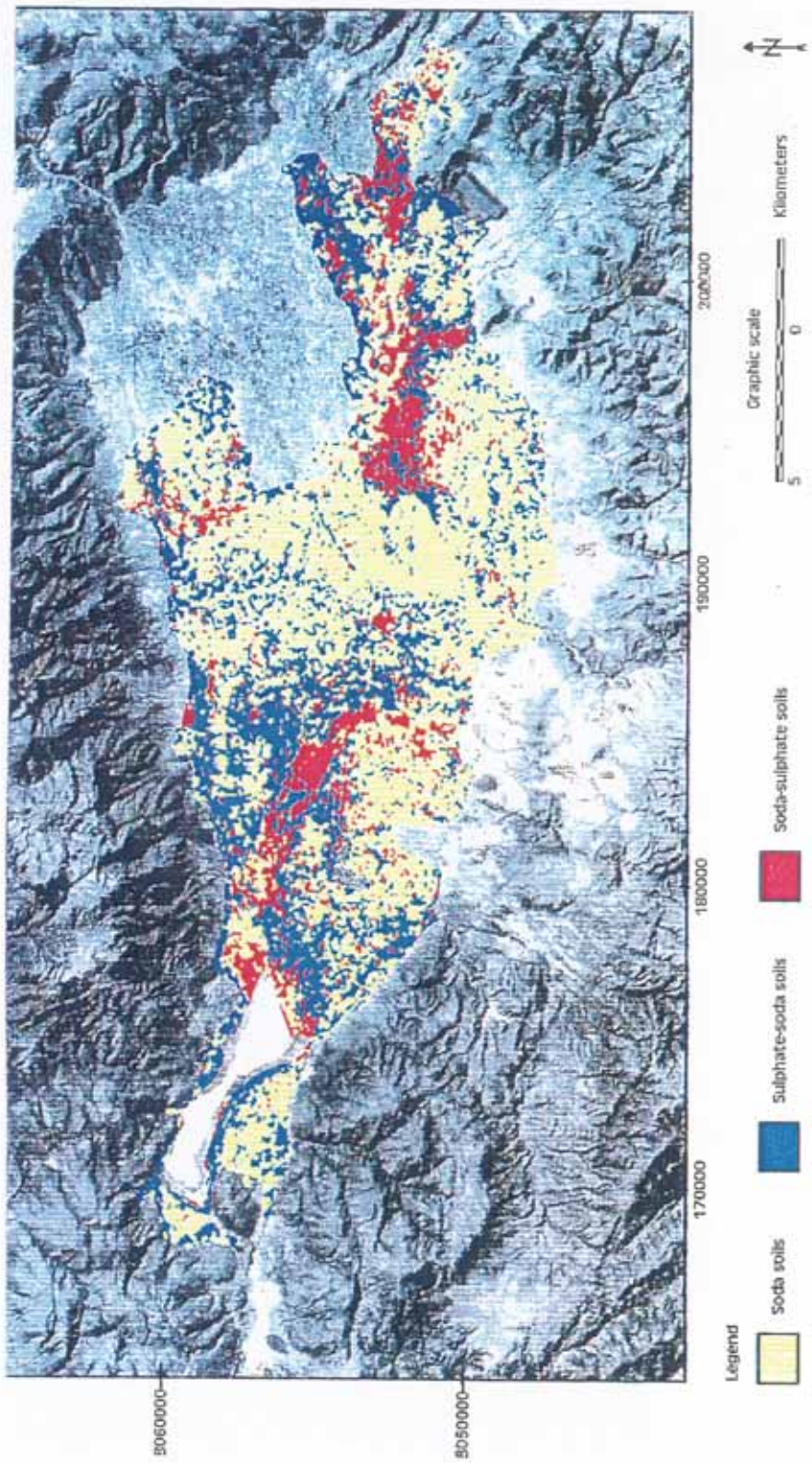

Fig. 6.57: Spatial distribution of soda soils, using a maximum likelihood classifier with prior probabilities and fuzzy modelling of information classes.

(b) Data interpretation

Table 6.30 indicates class reliability and accuracy in labelling sulphate, chloride-sulphate and sulphate-chloride soils. Spatial discrimination of sulphate soils is low, as ground data corresponding to other classes were labelled as sulphate soils on the image. Additionally, the classifier failed to recognize all the sulphate areas. On the contrary, a remarkable improvement was obtained in the distinction between chloride-sulphate and sulphate-chloride soils. In general, the fuzzy set approach improved class accuracy in all the classes. Correct labelling of the ground data increased by 36% for the sulphate-chloride soils (fig. 6.58). Overall accuracy achieved values ranging from 51 to 73%.

Table 6.30: Confusion matrix of sulphate, chloride-sulphate, sulphate-chloride and chloride soils.

CLASSIFIED DATA	REFERENCE DATA				TOTAL	ACC.%
	Sulphate	Chloride-sulphate	Sulphate-chloride	Chloride		
Sulphate	10	40	10	10	70	14
Chloride-sulphate		160	20	20	200	80
Sulphate-chloride	10	20	240	20	290	83
Chloride			20	50	70	71
TOTAL	20	220	290	100	630	
REL.%	50	73	83	50		73

REL.%= class reliability; ACC.%= class accuracy

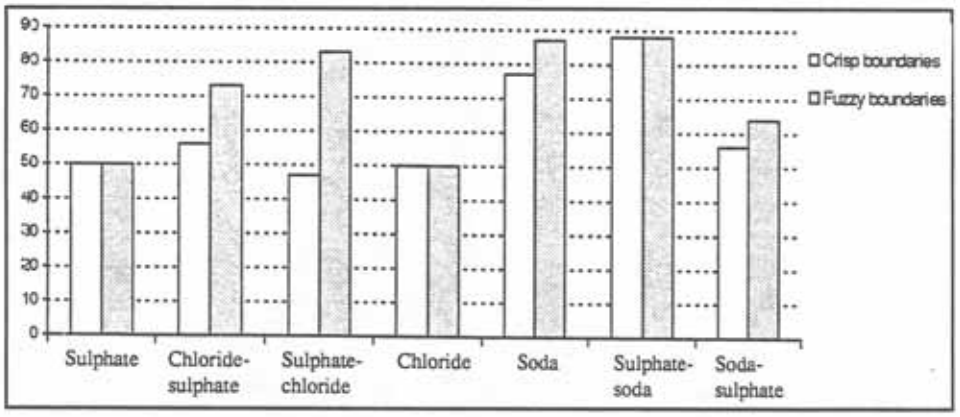

***Fig. 6.58:** Per-class improvements achieved using fuzzy sets and a maximum likelihood classifier with prior probabilities.*

A confusion matrix was also built up for soda, sulphate-soda and soda-sulphate soils (table 6.31). As carbonate contents increase, the probability of correct labelling of ground data also increases. The

identification accuracy of soda-sulphate soils, having relatively higher carbonate contents than the other classes, is 64%.

Table 6.31: Confusion matrix of soda, sulphate-soda and soda-sulphate soils incorporating certainty factors in the classification procedure.

CLASSIFIED DATA	REFERENCE DATA			TOTAL	ACC.%
	Soda	Sulphate-soda	Soda-sulphate		
Soda	260	10	80	350	74
Sulphate-soda	30	70	10	110	64
Soda-sulphate	10	0	160	170	94
TOTAL	300	80	250	630	
REL.%	87	88	64		77

REL.%= class reliability; ACC.%= class accuracy

(3) Evaluation of the classification performance

For chloride-sulphate soils, class accuracy and reliability were low when using crisp class boundaries. This is explained by the fact that chlorides do not have specific absorption bands in the visible, near-infrared and thermal regions of the spectrum. Therefore, absorption features of the sulphates dominate. Fuzzy modelling of the information categories and the incorporation of certainty factors during the classification procedure allowed to overcome these poor results. Identification accuracies improved by as much as 36% for chloride-sulphate and sulphate-chloride soils with similar proportions of both anions.

Higher accuracies were achieved for soda-sulphate soils, since both carbonates and sulphates have absorption features in the infrared and thermal ranges of the spectrum. Slight improvements in feature discrimination were obtained through the application of fuzzy modelling to the information categories.

(4) Relationship between landscape positions and salt type distribution

There is a good correlation between the chloride distribution map, elaborated using field data and geostatistical interpolation techniques (appendix I), and the results obtained by satellite image classification. Chlorides reach their maximum concentration in the playas. Additionally, the classified image evidences the presence of chloride soils in the distal parts of the southern piedmont glacis. Higher lagunary flats have concentrations of sulphate anions below 2% (appendix I). Towards lower positions, the chloride contents increase and reach maximum expression in the low-lying playas. The highest concentrations of chloride anions, between 4-14%, together with EC values higher than 60 dS/m, coincide with the sulphate-chloride and chloride soil distribution. The distribution of chloride-rich soils is according to the following sequence: playa and southwestern distal piedmont glacis > lower and medium lagunary flats > higher lagunary flats (fig. 6.59).

The distribution of soda or carbonate dominated soils, delineated from the classified Landsat TM scene,

correlates satisfactorily with the carbonate, bicarbonate and pH maps obtained by using laboratory data and geostatistical interpolation (appendix I). Similarly, the carbonate distribution map agrees with the soda distribution map. The highest carbonate contents were identified in the southwestern and southern parts of the playas. Sulphate-soda soils, with approximately equal proportions of sulphate and carbonate anions, were mapped in the middle and lower flats as well as on playas. In the places previously occupied by the Angostura reservoir, low amounts of carbonates and chlorides were identified in areas where also low salinity-alkalinity degrees were mapped. The spatial distribution of carbonate-rich soils is according to the following sequence: southwestern playas and distal piedmont glacis > southern lower lagunary flats > middle lagunary flats = higher lagunary flats (fig. 6.60).

The carbonate distribution is controlled by the presence of carbonate-rich parent materials, originated from mountains south of the Punata-Cliza valley, and by the texture of the soils. In the coarse-textured soils of the proximal and central parts of the piedmont glacis, leaching of the carbonates and formation of calcareous concretions and calcic horizons take place. On the contrary, in the fine-textured soils of the playas and lower flats, clayey textures do not facilitate salt migration to lower horizons. High concentrations of carbonates occur on the soil surface, which can be detected from the satellite image because carbonates have specific absorption bands.

Finally, there was an overall high correlation between the salt distribution on the landscape from laboratory data (table 6.2), the maps obtained by geostatistical interpolation of field soil properties and the results of digital image classification. However, the extent of chloride-rich soils was underestimated in the satellite image classification because of the lack of absorption features of the chloride salt.

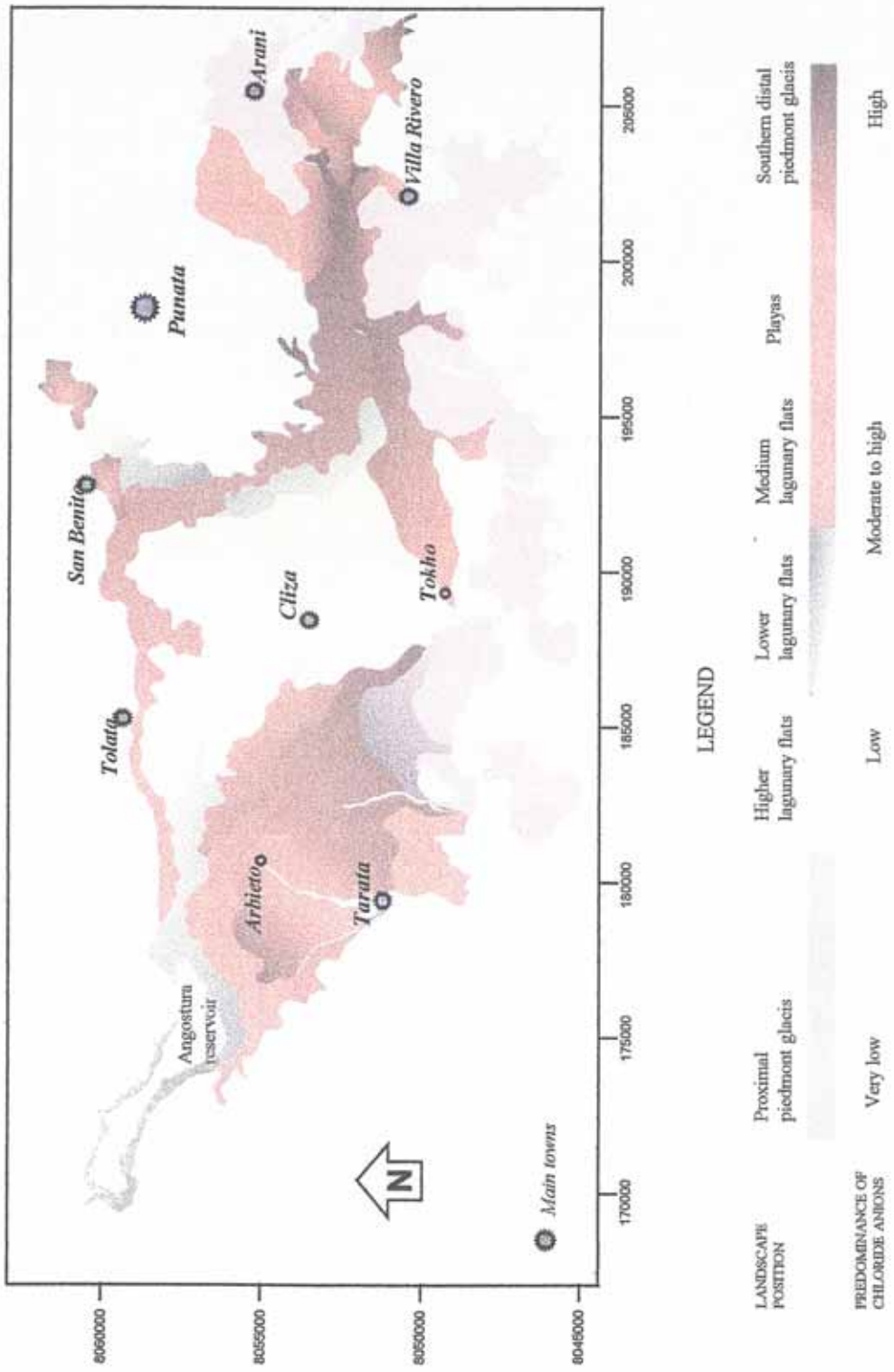

Fig. 6.59: *Spatial distribution of sulphate - chloride soils.*

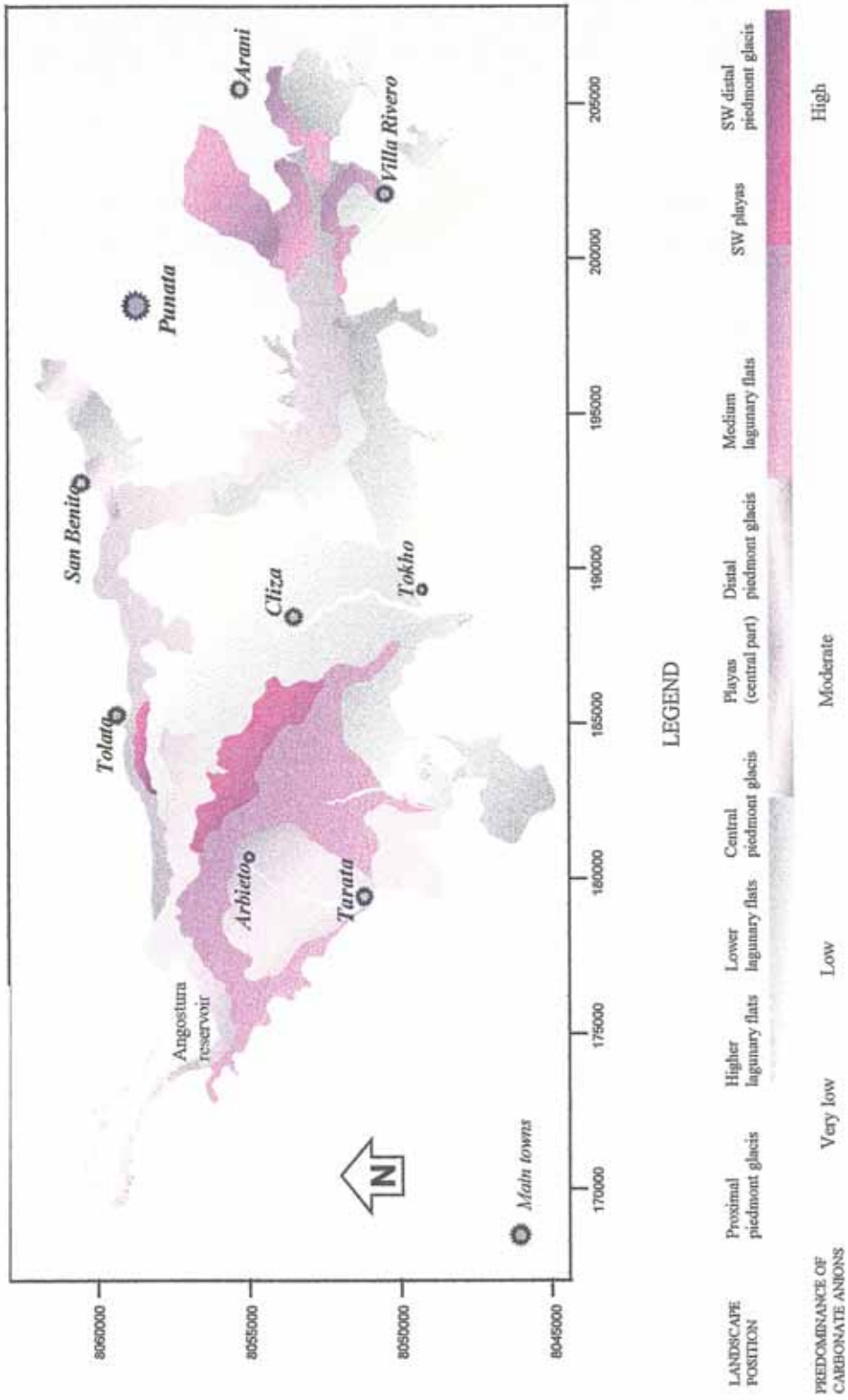

Fig. 6.60: Spatial distribution of soda - sulphate soils.

6.6 MONITORING TEMPORAL CHANGES OF SALINITY AND ALKALINITY

To follow the evolution of the salinity-alkalinity process in the Punata-Cliza valley, a monitoring model was built up (fig. 6.61). The model evaluates the nature, magnitude, rate and reliability of the changes occurred in the area. Model inputs are multi-temporal remote sensing data from 1986 and 1994. Thus, the assessment of temporal changes in salinity-alkalinity spans a period of 9 years. Satellite images are labelled using a pre-determined classification scheme.

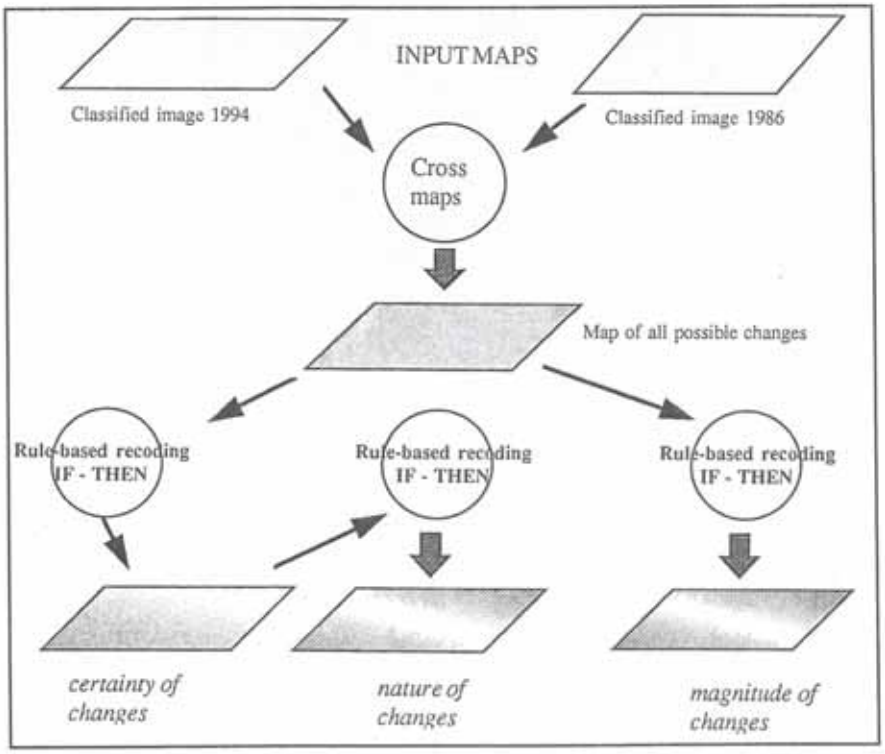

Fig. 6.61: *The monitoring model*

6.6.1 Assessment rules

(1) The likelihood of the changes

Expert knowledge about the possibility of actual changes are incorporated as degree of likelihood of certain events to occur. The expert grades the likelihood of occurrence in terms of certainty factors within a range of 0 to 1 (table 6.32). On the basis of the general trend in the area, it was assumed that salinity and/or alkalinity may increase, rather than decrease, over time (fig. 6.62).

Table 6.32: Likelihood of changes expressed in terms of certainty factors

CLASS	DEGREE OF POSSIBILITY	CERTAINTY FACTOR
1	Absolutely likely	1.0
2	Extremely likely	0.9
3	Likely	0.6
4	Neither likely nor unlikely	0.5
5	Unlikely	0.4
6	Very unlikely	0.2
7	Absolutely unlikely	0.0

Class 1, for instance, clusters areas which did not change through time (9 years), with a total certainty that no changes took place, while class 2 groups areas experimenting extremely likely changes through the monitored period. Ninety different changes could have occurred from 1986 to 1994. Hereafter, some IF-THEN statements used to implement the likelihood of changes are presented

Rule 1:
IF in 1986 an area was 'non-affected' AND in 1994 the area has the same label, THEN the certainty that no change occurred is absolutely likely.

Rule 2:
IF in 1986 an area was 'non-affected' AND in 1994 the same area is 'moderately alkaline, non saline' or 'moderately and strongly saline, non-alkaline', THEN the change is extremely likely.

Rule 3:
IF in 1986 an area was 'non-affected' AND in 1994 the same area is 'moderately and strongly saline-alkaline', THEN the change is likely.

Rule 4:
IF in 1986 an area was 'non-affected' AND in 1994 the same area is 'very strongly saline, non alkaline' or 'strongly alkaline', THEN the change is neither likely nor unlikely.

Rule 5:
IF 1986 an area was 'non-affected' AND in 1994 the same area is 'very strongly alkaline, moderately and strongly saline' or 'very strongly saline, moderately and strongly alkaline', THEN the change is unlikely.

Rule 6:
IF in 1986 an area was 'non-affected' AND in 1994 the same area is 'very strongly saline-alkaline',

THEN the change is very unlikely.

Rule 7:
IF in 1986 an area was 'moderately and strongly saline-alkaline' AND in 1994 the same area is 'non-affected', THEN the change is absolutely unlikely.

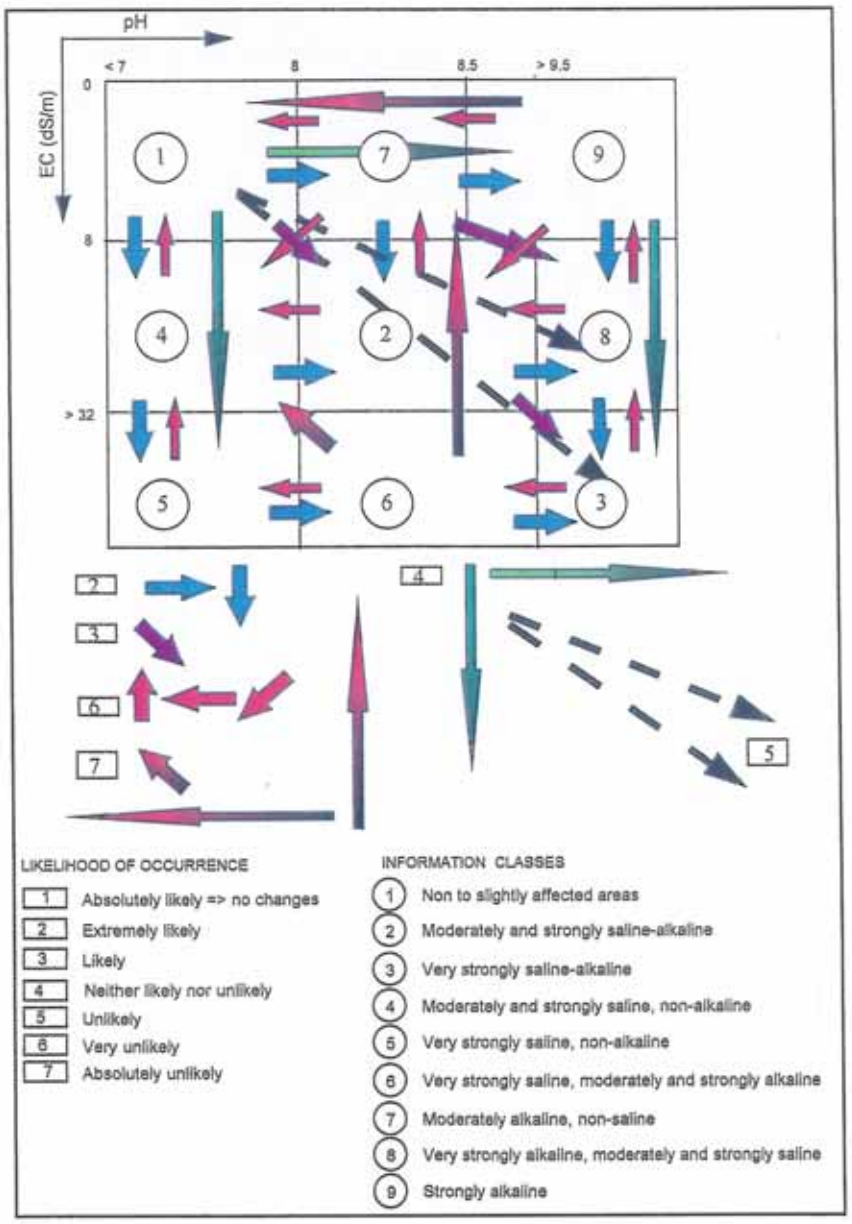

Fig. 6.62: Graphic representation of the likelihood of the changes.

(2) The magnitude of the changes

Changes of one degree in salinity OR alkalinity are said to be extremely likely (rule 2). A change is likely (rule 3) when salinity AND alkalinity increase by one degree. But, if salinity increases by two degrees AND alkalinity by one degree, or vice versa, then the change is neither likely nor unlikely (rule 4). Increases of salinity OR alkalinity by two degrees are unlikely (rule 5). Increments of two degrees in salinity AND alkalinity are seen as very unlikely (rule 6).

The georeferenced soil sample set, used to train the classifier for the 1994 Landsat TM image, was also utilized for the 1986 image classification. It was thus assumed that the soil samples belonged to the same salinity and alkalinity classes at both dates. This assumption is ambiguous, but it was considered as the best approach to label the 1986 image because field data were not available for that date. Considering that the year 1986 was drier than the year 1994 and that the 1986 image was collected in July, one month later than in 1994, surface salinity features might be enhanced on the 1986 image. Additionally, a given soil sample could be at the limit between two classes, being for instance moderately alkaline with a pH of 8.1 in 1994, thus at the boundary between 'non to slightly alkaline' and 'moderately alkaline'. To overcome these two issues, a decrease by one degree of salinity or alkalinity from 1986 to 1994 was not rejected but assumed as very unlikely. More substantial decreases in salinity or alkalinity over the last 9 years were considered absolutely unlikely (rule 7).

Magnitude and likelihood rules can be combined in a matrix of changes (table 6.35). The results of the 1994 classification are column inputs and the information for 1986 is entered in the rows. Magnitude classes considered are listed in table 6.33.

Table 6.33: Magnitude of the changes

CLASS	MAGNITUDE	DEGREE OF POSSIBILITY
1	Not changes	absolutely likely
2	One degree in salinity or alkalinity	extremely likely
3	One degree in salinity and alkalinity	likely
4	Either two degrees in salinity and one degree in alkalinity, or two degrees in alkalinity and one degree in salinity	neither likely nor unlikely

Table 6.34: Information classes used for monitoring temporal changes

CLASS CODE	INFORMATION CLASS
1	Non or slightly saline-alkaline
2	Moderately and strongly saline-alkaline
3	Very strongly saline-alkaline
4	Moderately and strongly saline, non-alkaline
5	Very strongly saline, non-alkaline
6	Very strongly saline, moderately and strongly alkaline
7	Moderately alkaline, non-saline
8	Very strongly alkaline, moderately and strongly saline
9	Strongly alkaline
10	Water body (only for 1986)

Table 6.35: Matrix of changes 1986 - 1994. (Row and column intersections represent the likelihood of changes).

		1994								
	Information classes	***1***	***2***	***3***	***4***	***5***	***6***	***7***	***8***	***9***
	1	1	3	6	2	4	5	2	5	4
	2	7	1	3	6	6	2	6	2	7
	3	7	7	1	7	7	6	7	6	7
1	***4***	6	2	5	1	2	3	7	4	7
9	***5***	7	7	4	6	1	2	7	7	7
8	***6***	7	6	2	7	6	1	7	7	7
6	***7***	6	2	5	6	7	4	1	3	2
	8	7	6	2	7	7	6	7	1	6
	9	7	6	4	7	7	7	6	2	1
	10	2	3	4	3	4	4	2	4	4

(3) The nature of the changes

The model contemplates also that an area may undergo changes to saline, to alkaline, to saline-alkaline or to non-affected, the latter being applicable only to emerged areas resulting from the extent reduction of the Angostura reservoir. Ninety-one unique combinations were obtained after crossing the 1986 and 1994 image classification maps. To produce a map representing the nature of the changes occurred during the 9- year period, combinations were analyzed and recoded using a rule-based system together with the magnitude classes listed in table 6.33 and the information classes listed in table 6.34. Expert rules implemented are explained hereafter.

(a) An area becomes more alkaline (e.g. higher pH) if it changes:

From	*To*
Class 1	class 7 or 9
Class 7	class 9
Class 10 (water bodies)	class 7 or 9

(b) An area becomes more saline if it changes:

From	*To*
Class 1	4 or 5
Class 4	5
Class 10 (water bodies)	4 or 5

(c) An area becomes saline-alkaline if it changes:

From	*To*
Class 1	2 or 6 or 8 or 3
Class 4 or 5	2 or 6 or 8 or 3
Class 7 or 9	2 or 6 or 8 or 3
Class 10	2 or 6 or 8 or 3

(d) The extent of the Angostura reservoir was reduced by more than 1000 hectares between 1986 and 1994. As a consequence, areas formerly covered by water emerged, shifting from class 10 to class 1.

6.6.2 Data interpretation

The 1986 Landsat Thematic Mapper image was classified using the procedure described under point 6.5.1 (1) (fig. 6.63). A 'water bodies' class was added to refer to the area covered by the Angostura reservoir in 1986. For several reasons, including a decrease of the annual rainfall and the construction of several dams in the upper catchment areas, the extent of the Angostura lake was reduced by 1147 hectares in a period of 9 years.

(1) Evaluating the likelihood of the changes

Figure 6.64 compares the areas occupied by the ten salinity/alkalinity classes at the two selected dates. There are some inconsistencies, especially regarding the discrimination of non to slightly affected areas. In 1994, this class covers an area larger than in 1986. This might result from the one-month difference in the acquisition time between the two images, causing an enhancement of the salinity-alkalinity features in 1986, and from the areal reduction of the Angostura reservoir. The overestimation of the non to slightly affected class for 1994 results from the erroneous inclusion of moderately alkaline areas.

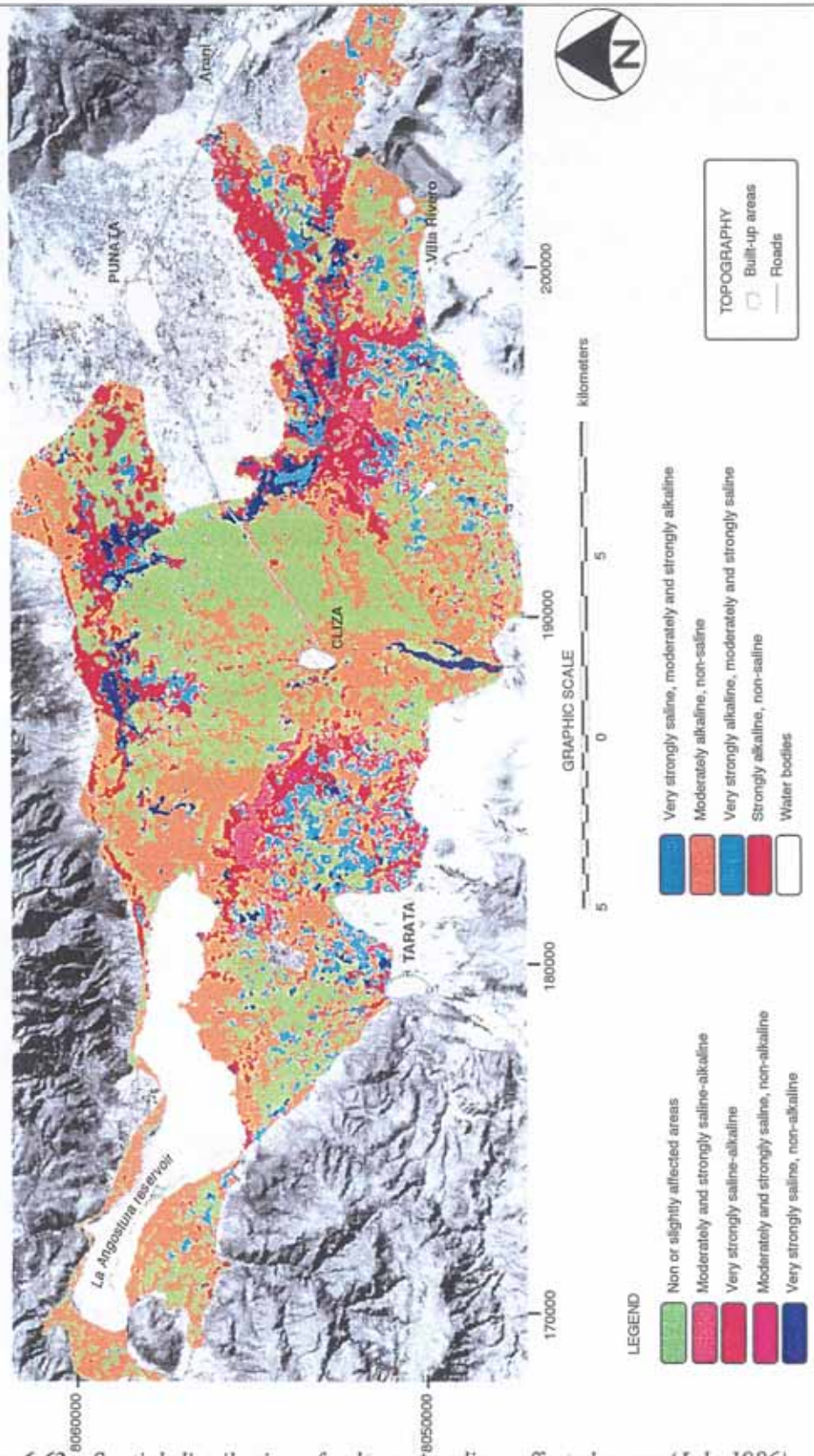

Fig. 6.63: Spatial distribution of salt- and sodium-affected areas (July 1986).

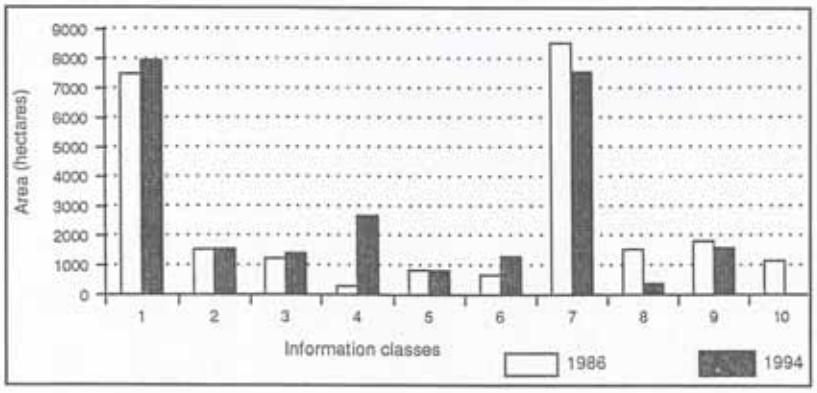

Fig. 6.64: Areal extent of information classes for 1986 and 1994.

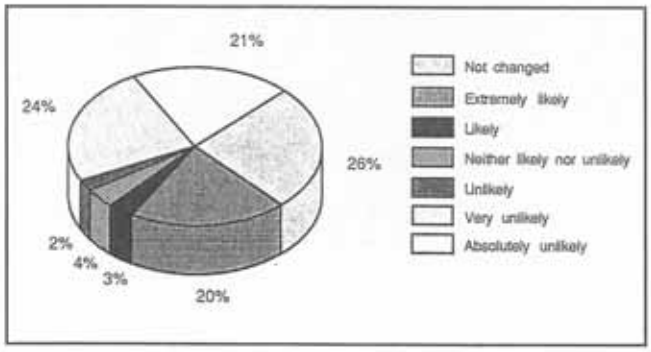

Fig. 6.65: Likelihood of changes

About 26% of the area did not experiment alterations during the period 1986-1994 (figs. 6.65 and 6.66). Likely changes occurred in 30% the area, while very unlikely variations arose in 24% of the area. Nearly 21% of the area classified contains changes considered as absolutely not likely, as for example the reduction of the degree of salinity or alkalinity.

Unlikely changes were classified mainly in the distal parts of the dissected depositional glacis and middle lagunary flats. The higher lagunary flats and the central parts of the playas, between Cliza and Punata, exhibit smaller variations throughout time, while changes qualified as likely occur in the lower lagunary flats and playas.

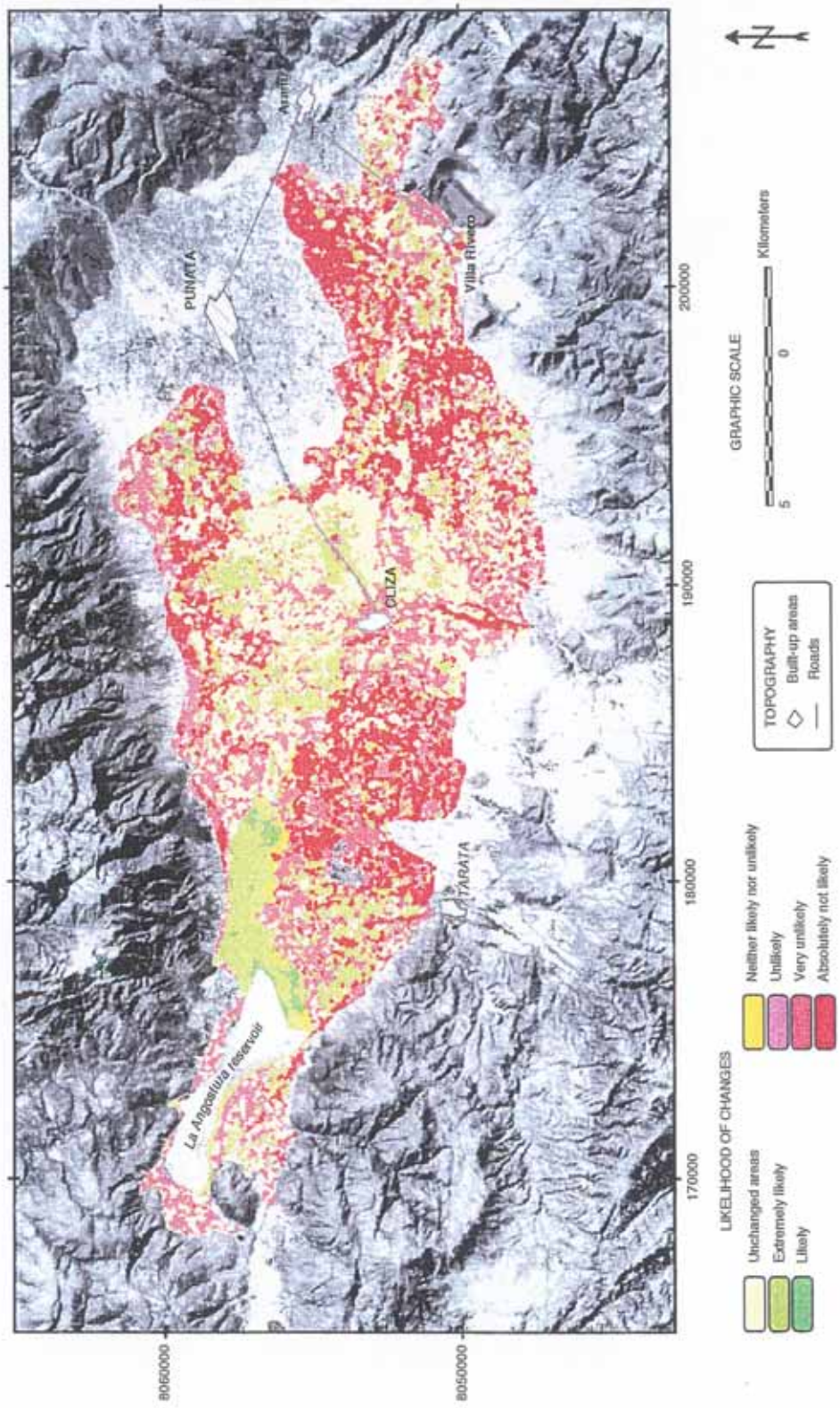

Fig. 6.66: Monitoring the likelihood of changes in salinity-alkalinity (July 1986 - June 1994).

(2) Evaluating the nature of the changes

According to the rule-based system used to evaluate the nature of the changes, 70% of the area changed to alkaline, 15% to saline, 12% to saline-alkaline and 3% to non-affected, the latter being water-free areas resulting from the areal reduction of the Angostura reservoir (fig. 6.67).

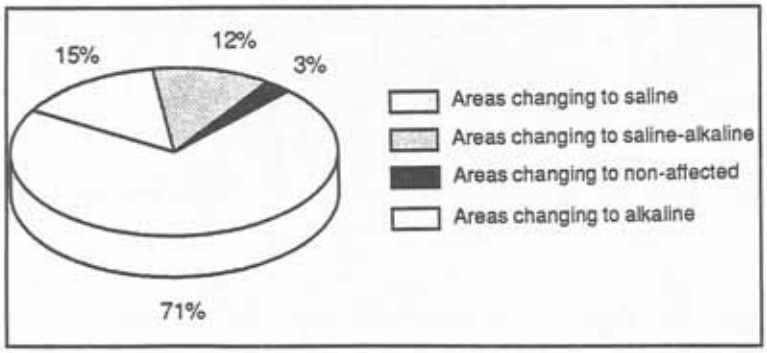

***Fig. 6.67:** The nature of changes*

The tendency is towards increasing alkalinity, especially in the higher lagunary flats (fig. 6.68). This is attributed to the nature of the deposits coming from the carbonate-rich southern mountains (calcareous sandstones). Soil samples from the higher lagunary flats are mainly composed of carbonate anions, although total anion concentrations are low (< 0.3% in table 6.2). As previously mentioned, low amounts of free carbonates are capable of alkaline hydrolysis, raising therefore the pH. Sodium cations are abundant in the area, probably in the form of sodium carbonates and bicarbonates. As a consequence of the former, higher lagunary flats are exposed to potential alkalinization.

About 15% of the classified areas became saline during the monitored period, being located mainly in the lower lagunary flats bordering the Angostura reservoir. Changes towards saline-alkaline classes are spread all over the area, except for the higher lagunary flats and piedmont glacis. They occur more frequently in the margins of the playas and middle lagunary flats, in particular along the contact zone with the distal part of the Punata alluvial fan, where Jordan (1977) reports groundwater rich in chlorides and carbonates of sodium and magnesium, with small amounts of calcium. Because of the difference in permeability, springs are common in the transition zones between the piedmont and the lagunary depressions. Additionally, the level topography of the lagunary flats helps water seepage and saline spots form in the contact areas.

The alkalinization trend is confirmed by the classification based on anion ratios, where most of the area was labelled as soda soils which are alkaline, non to slightly saline soils. Carbonates and bicarbonates, with low amounts of sulphates of sodium, predominate in these soils.

(3) Evaluating the magnitude of the changes

Increases in one degree of salinity or alkalinity occur in the area previously occupied by the Angostura

reservoir (fig. 6.69). Two-degree changes towards salinity and alkalinity are spread in small patches all over the study area.

6.6.3 Hazard prediction

Figure 6.70 integrates the results of the three individual maps depicting the likelihood, nature and magnitude of changes. It displays the areas exposed to increasing salinization and/or alkalinization as well as the areas already affected. It also reflects the evolution of the salinity-alkalinity degradation process during the period 1986-1994 and its dissemination to areas having similar parent materials and landform types.

The spatial coincidence between (1) salt concentration and composition in relation to landscape position, (2) distribution of salt types and salinity degrees, and (3) cartography of anions, pH and electrical conductivity obtained by geostatistical interpolation, was incorporated as a prediction factor. High multi-source data coincidence with observed degradation features allows to establish probabilities of potential development of similar features in areas not yet affected.

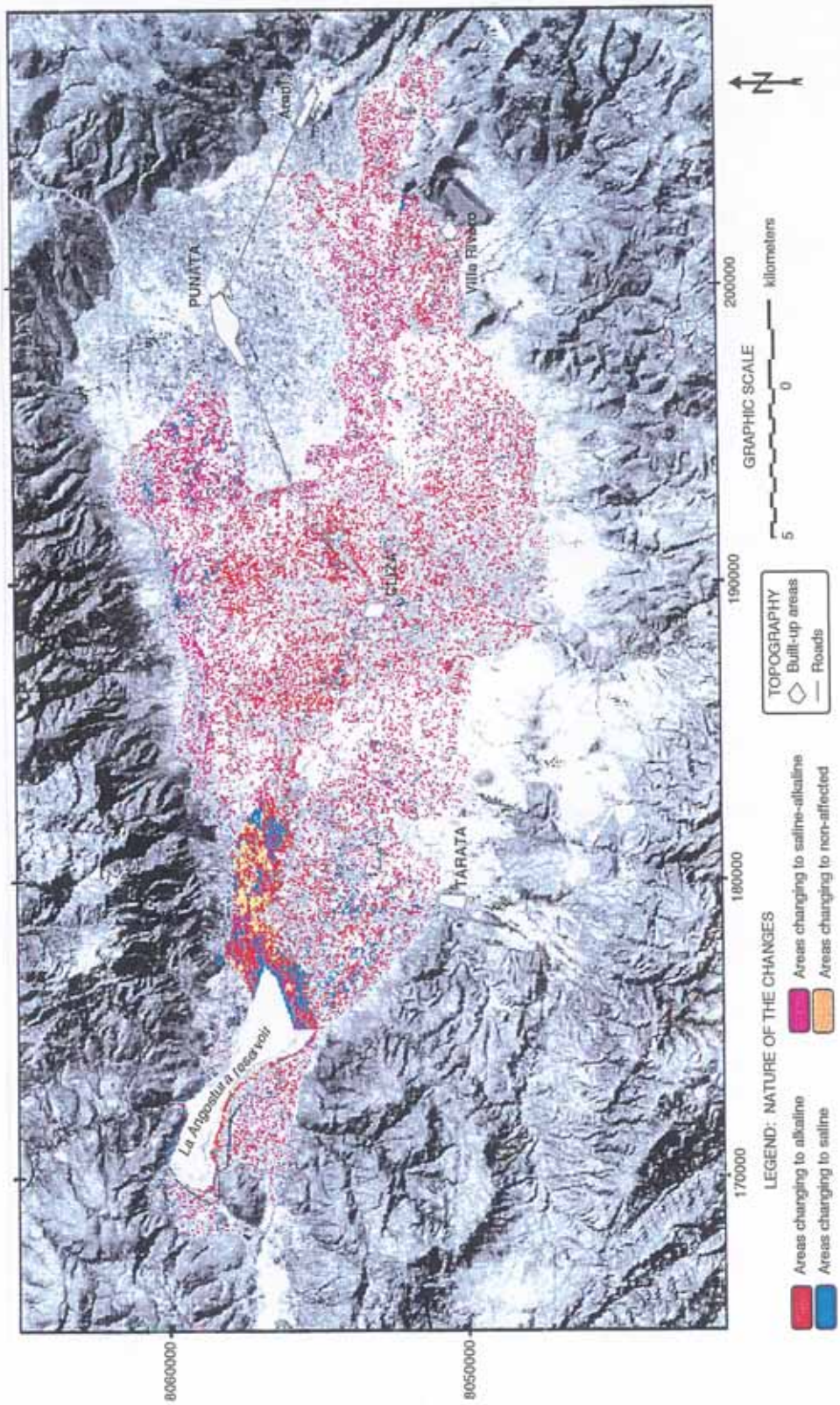

Fig. 6.68: Monitoring the nature of the changes in salinity-alkalinity (July 1986-June 1994).

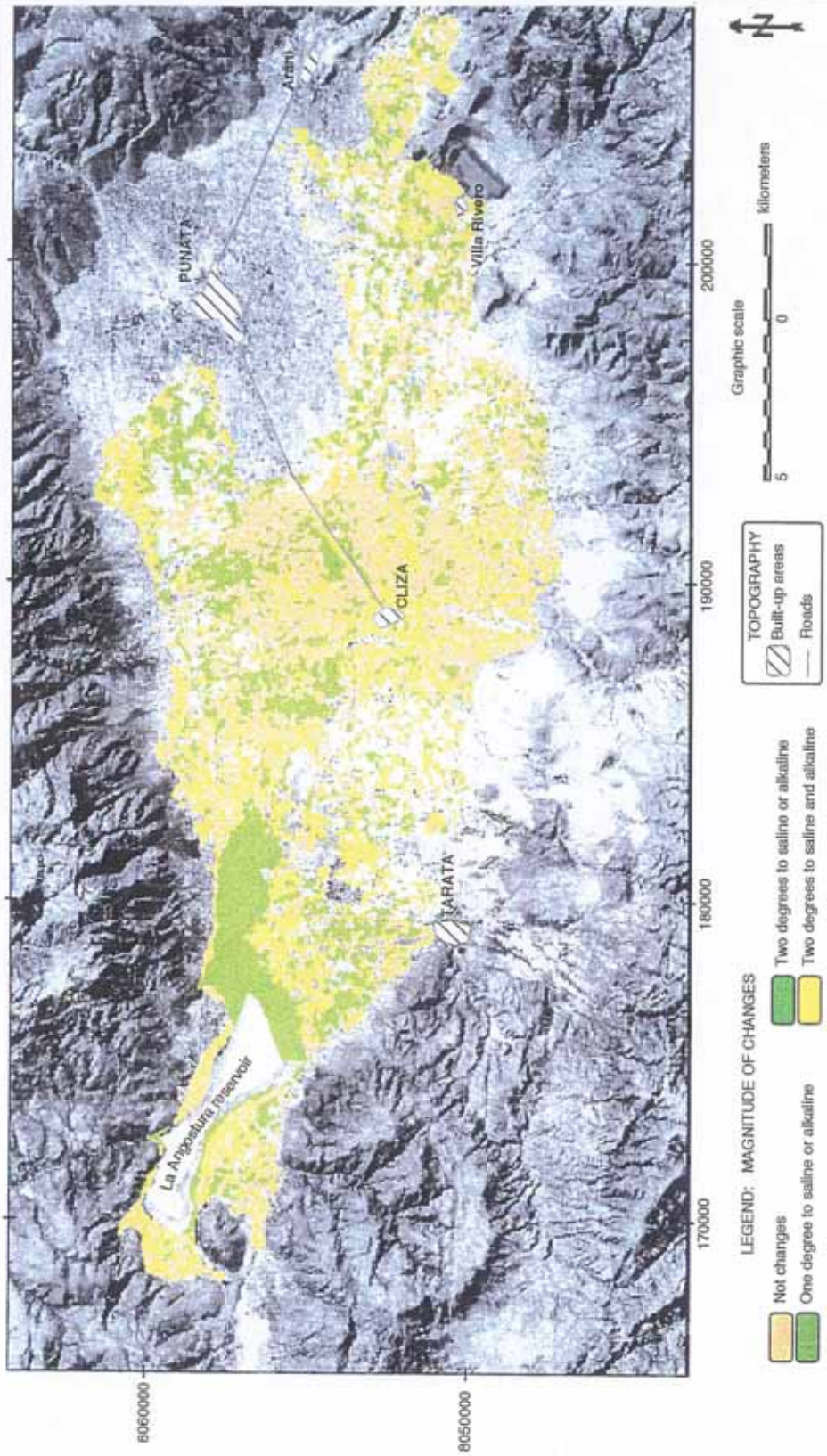

Fig. 6.69: Monitoring the magnitude of the changes in salinity-alkalinity (July 1986-June 1994).

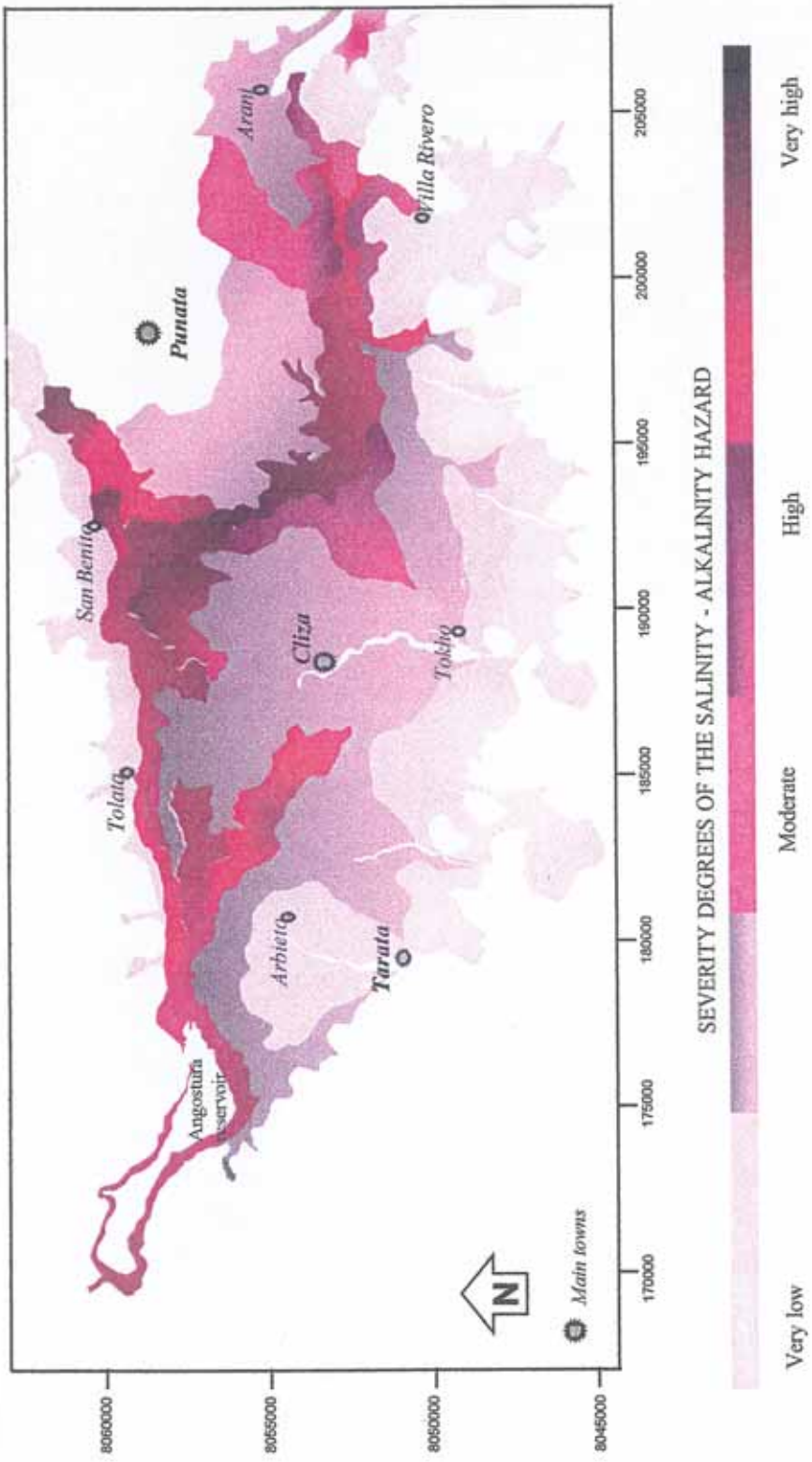

Fig. 6.70: Salinity-alkalinity hazard prediction.

6.7 CONCLUSIONS

(1) Relationship between salinity and spectral band selection

The salts of the Punata-Cliza valley are mainly chlorides and sulphates of sodium and magnesium, with small amounts of carbonates and bicarbonates. The best spectral separability among classes was obtained by the combination of Landsat TM bands 1, 2, 4, 5, 6 and 7, regardless of the classification scheme applied. This results from the chemical composition of the salts and from the influence of the topsoil texture and organic matter, which have specific absorption features in the selected wavelength ranges.

(2) Prediction of soil salinity-alkalinity ranges

It was not possible to predict SAR values from the soil reaction with satisfactory results. Polymodal and asymmetric histograms were obtained. The pH showed the highest correlation with carbonate anions. Instead, it was possible to estimate SAR, electrical conductivity and soil reaction ranges using ground reflectance spectra from the visible and near-infrared regions (450-800nm). High r^2 and F-tests resulted from the stepwise regressions. However, the established regression equations are geographically dependant and may not be applicable to other areas.

(3) Spectral confusion

Main sources of spectral confusion, causing variations in salinity-alkalinity degrees, were found to be: (1) the type and abundance of the salt-tolerant vegetation cover; (2) the surface morphology and soil roughness caused by the salt compounds (e.g. puffy, fluffy or smooth crusts) or the land management practices (e.g. clods, smooth crusts); (3) the topsoil textures, where high amounts of silt and clay mask the effect of variable salt and sodium contents; (4) the mixture of topsoil properties under field conditions, where salts, soil texture, crusting and soil color mutually interfere.

Soil texture seems to have a low influence on images collected from active sensors, unlike those collected from passive satellite sensors. Radar backscattering was affected by the roughness of the surface, produced by land cultivation. This caused erroneous allocation of alkaline and saline-alkaline soils to non-affected areas.

(4) Spectral discrimination of salt types and salinity-alkalinity degrees

Differentiation between sulphate, sulphate-chloride and chloride affected soils was poor. Low class accuracies were obtained because chlorides do not have specific absorption bands in the visible, near-infrared and thermal wavelengths. As a consequence, the sulphate absorption features dominated. Higher accuracies in feature discrimination were achieved for soda, sulphate-soda and soda-sulphate soils because both, carbonates and sulphates, have absorption features in the infrared and thermal ranges of the spectrum. Although the labelling of the above soils was acceptable, none of the classes could be completely isolated with 100% accuracy. This could be attributed, not only to a poor spectral separability among the salinity-alkalinity classes, but also to an erroneous determination of the boundaries of the

information classes.

The conventional approach to map saline, saline-alkaline, alkaline and non-affected areas using SAR or pH and EC values, revealed to be insufficient for the handling of satellite data. Established salinity class boundaries and variable crop tolerance to specific EC values were sources of confusion among categories, when dealing with remote sensing data in the optical as well as in the microwave ranges. Similarly, cultivation practices and surface morphology and roughness greatly affect the energy backscattering, reflection and absorption. As a consequence, many degraded areas were labelled as non-affected areas when subjected to cultivation. This demonstrates the impossibility to differentiate among salinity and alkalinity classes on the sole basis of reflectance and/or backscattering values. Field observations, supported by laboratory data, are necessary to achieve reliable discriminations.

Two approaches were implemented to determine salinity-alkalinity degrees and differentiate soils according to their anion composition. The first is based on crisp class boundaries; the second assumes that natural boundaries between classes of salt types and salinity degrees are not sharp but transitional and, for that purpose, uses fuzzy sets. Class membership functions, defining the grade of membership of a soil sample 'x' in a class 'A', were built up. Sigmoidal and linear membership functions were tested. Fuzzy modelling allowed to achieve higher accuracies in the discrimination of salt degrees and types, but did not improve map readability. Not only the spectral separability among the surface features, but also the correct determination of the class boundaries and the selection of the soil parameters are important to model the classes.

(5) Salt discrimination versus sensor performance

Supervised fuzzy classification of JERS-1 SAR data was most effective to discriminate saline and saline-alkaline areas. On the other hand, the fusion of visible, infrared and microwave data allowed to separate areas non-affected by salinity-alkalinity from alkaline soil surfaces.

In general, lower class reliability and accuracy were obtained when working with Landsat Thematic Mapper data and crisp class boundaries. The highest accuracies were achieved by fully supervised fuzzy classification, including not only fuzzy class boundary definition, but also pixel allocation to certain class. Landsat TM and JERS-1 data fusion, together with the fuzzy modelling of information categories, provided the highest class reliability and accuracy .

(6) Salt distribution on the landscape

Chloride-rich soils are frequent in the playas and southwestern distal piedmont glacis, but decrease towards the lower and medium lagunary flats, and are rare in the higher lagunary flats (fig. 6.59). Carbonate-rich soils, in turn, dominate in the southwestern playas and distal piedmont glacis, but decrease towards the southern lower lagunary flats, and are rare in middle and higher lagunary flats (fig. 6.60).

Carbonate-rich soils are related to calcareous parent materials coming from the mountains south of the Punata-Cliza valley. The coarse-textured soils, in the proximal and central parts of the piedmont glacis, allow the leaching of the slowly soluble carbonates leading to the formation of calcareous concretions and calcic horizons. In the fine-textured soils of the playas and lower flats, where clayey textures do not facilitate salt migration to the lower horizons, higher concentrations of carbonates remain on the soil surface, which can be detected from the satellite images because they have specific absorption bands.

There was a high coincidence between the salt distribution on the landscape derived from laboratory data (table 6.2), the maps obtained by geostatistical interpolation of field soil properties and the results of digital image classification. The extent of chloride-rich soils was underestimated in the satellite image classification because of their lack of absorption features.

The most degraded areas are located in the playa landform. Conversely, non to slightly saline-alkaline areas correspond to the higher lagunary flats (fig. 6.53). Middle and higher lagunary flats are threatened by potential salinization. Parent material, topographic position and the dry climate, which reduces the leaching but increases the migration of soluble salts towards surface horizons, are the main factors controlling the spatial distribution of salt- and sodium-affected areas.

(7) The monitoring model

To monitor changes in salinity-alkalinity over time, a model was designed using fuzzy sets and a rule-based system of if-then statements. Input data were derived from the multi-temporal classification of satellite images. Thus, the accuracy of monitoring depends on the reliability of the image classification. The model capitalizes on expert knowledge about the local salinization-alkalinization. Information on the possibility of actual changes is incorporated as 'degrees of likelihood' of a certain event to occur. The model provides maps displaying the likelihood, nature and magnitude of the changes. It also locates the more hazardous areas, those where the magnitude of the predicted changes is highest.

In the Punata-Cliza valley, the general trend is towards increasing alkalinity, especially in the higher lagunary flats (fig. 6.68). This is attributed to the nature of the deposits coming from the carbonate-rich southern mountains (calcareous sandstones). Soils of the higher lagunary flats are mainly composed of carbonate anions, although total anion concentrations are low (< 0.3%). Therefore, higher as well as middle lagunary flats are threatened by potential salinity-alkalinity expansion. The hazard refers not only to the geographic extension of saline-alkaline areas, but also to the intensification of the process in areas already degraded, specially if the recent tendency towards increased climatic dryness continues.

CHAPTER SEVEN:

ACCELERATED SOIL EROSION BY WATER

Four types of water erosion were found in the piedmont and lagunary depressions of the Sacaba basin: sheet, rill, gully and tunnel-piping erosion. Sheet and rill erosion are caused by overland flow, while subsurface flow within permeable materials originates coalescing pipes which collapse and enlarge into tunnels. Gullies originate either from the deepening of rills by collapse of tunnel roofs, or as combination of both surface and subsurface erosional processes.

The role of the landscape evolution in influencing subsurface processes of piping and tunneling was analyzed in chapter five. Surface erosion through concentrated runoff and overland flow is mainly related to land management practices and rainfall characteristics. In the southern part of the Sacaba valley, rainfed crops are common because of the lack of irrigation schemes. After harvesting, parcels are ploughed and left fallow during the dry season, causing the formation of a structural crust which protects the soil against soil moisture losses. Following the first rains, parcels are tilled to remove the crust and to allow water infiltration. Crust removal favor the development of splash and sheet erosion as there is no protection of the soil surface against raindrop impact and soil particle detachment. As a consequence, rills and sealing develop on the soil surface (fig. 7.1).

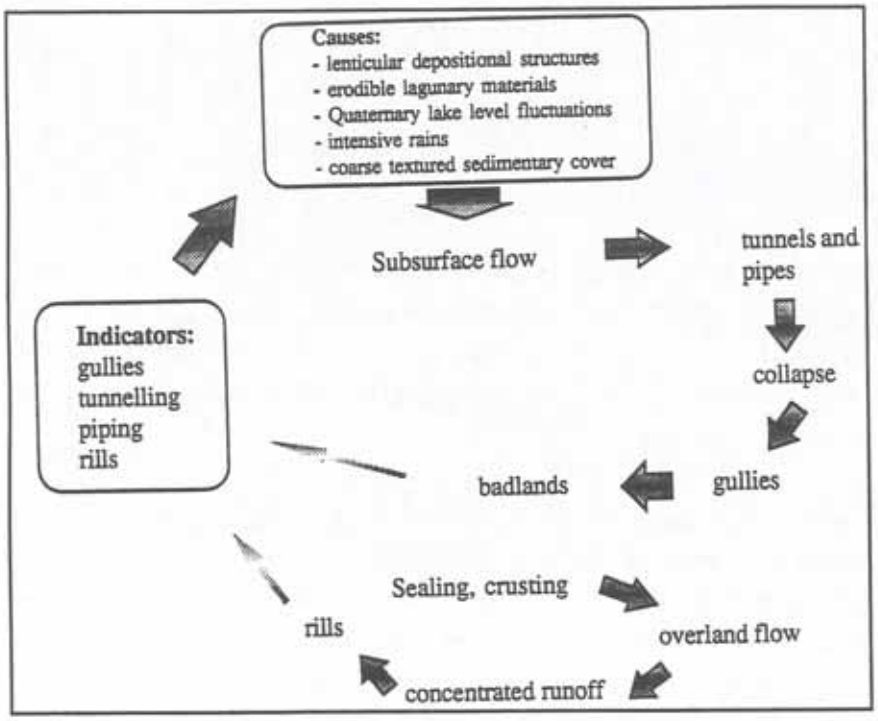

Fig 7.1: Indicators, causes and mechanisms related to water erosion in the Sacaba valley.

7.1 WATER EROSION INDICATORS IN THE SACABA BASIN

The selection of indicators related to soil degradation by water erosion varies according to the scale of survey and the detection and mapping techniques used. At plot level, soil properties such as texture, organic matter content, structure and soil aggregate size are reported as useful to estimate soil erodibility as well as to predict it in areas with similar soil characteristics, if enough observations are available. Interpolation techniques based on geostatistics or inverse square distance can be used for the mapping procedure. Detection and mapping of soil erosion by means of remote sensing techniques require the determination of surface features, which can be correlated to erosion severity.

Features such as rills, gullies, pipes, tunnels, depositional crusts, surface pavements of rock fragments, splash pedestals and exposed buried soils are useful indicators for field identification and rating of erosion severity. In studies at local and regional level carried out with the support of remote sensing techniques, indirect indicators such as soil color and the presence of natural vegetation can be used, together with erosion pavements, gullies, badlands and small channel patterns, easy to recognize by photo-interpretation of aerial photographs at medium and large scales. If studies of erosion severity can rely on field and laboratory determinations, soil properties become suitable indicators of susceptibility to erosion.

Specific features, such as small channels relating to rill erosion or deep coalescing holes relating to piping,

were identified and recorded during the field data collection. Some of these indicators could be related to more than one erosion type; such was the case of piping and tunneling and the formation of pavement-like rock surfaces. The soil properties and surface features selected as indicators to assess and map soil susceptibility to erosion, using laboratory determinations, ground-based radiometric recordings, field observations, photo-interpretation of aerial photographs and satellite image classification, are presented hereafter.

7.1.1 Surface features

(1) Depositional crusts

Depositional crusts form through sedimentation of fine materials on the soil surface as turbid water infiltrates into the soil. They were commonly observed at the bottom of rills and micro-depressions in medium-textured topsoils. Depositional crusts had a bright aspect and smooth surface, causing high reflectances in the visible and near-infrared region of the spectrum. They were thus useful to delineate soil eroded areas by means of remote sensing imagery.

(2) Splash pedestals

Splash pedestal form by the combined action of raindrop splash and rainwash, due to the protection of the underlying soil by rock fragments (Poesen et al., 1994). They were used as a field indicator of surface erosion severity. Their reflectance was also measured.

(3) Rock fragment pavements

Rock fragments at the soil surface can be correlated to soil erosion in different ways. Although they protect the soil surface from detachment by raindrop splash and runoff by forming erosion pavements, they reveal past water erosional processes. Coarse-textured lenses of variable thickness and length are common in the dissected depositional glacis and lagunary depressions of the Sacaba valley. When exposed after removal of the overlying sediments and washing of the fines, the coarse fragments form erosional pavements. In some places, the upper side of the rock fragments was covered by a dark desert varnish resulting from the precipitation of iron and manganese oxides. Field reflectances of variable coverage densities of rock fragments were recorded and used as indicators of soil erosion as detected from the remote sensing imagery.

(4) Rills, gullies, tunnels and pipes

They were used as field indicators to determine erosion severity, following the FAO guidelines for soil description (FAO, 1990). Three classes, namely slight, moderate and severe erosion were set up to analyze and compare the relationship between soil erodibility and soil properties. Gully and rills patterns were also used as surface indicators to identify and delineate erosion severity from the aerial photographs and satellite images.

(5) Natural vegetation

Natural vegetation was used as an indirect parameter of soil erosion, especially to delineate erosion areas from satellite imagery. Areas of moderate or severe erosion, with deep rills, gullies and badlands, are not suitable for agricultural purposes. They are colonized by native species of shrubs, grasses and trees like schinus molle, acacia, jayak and chilka which can be distinguished on the satellite images, particularly during the dry season.

(6) Buried Mollisols

In the southern part of the Sacaba basins, dark-coloured, medium- to fine-textured Mollisols are buried at variable depths by coarse-textured layers (see chapter 5). In some places, Mollisols are at shallow depth or directly exposed at the surface. Their spectral reflectance in the visible and near-infrared ranges of the spectrum was recorded on the ground to be compared with the spectral curves of Aridisols and Entisols, more frequent in the soilscape. Nevertheless, the areal extent occupied by exposed Mollisols was not large enough to allow their discrimination from satellite-borne sensors.

7.1.2 Soil properties

Soil structure, particle size distribution, organic matter content, permeability, aggregate size, bulk density and porosity were determined to analyze the relationship between soil properties, soil susceptibility to erosion and actual surface erosional process.

In addition, soil color was used as a surface feature indicator to identify and map soil erosion from remote sensing documents. For example, whitish spots easily isolated on the satellite images and aerial photographs were related to moderate and severe erosion. Light to white colors, resulting from the combination of low organic matter content and high silt content in the topsoils, produced high reflectance values in the visible and near-infrared regions of the spectrum.

7.2 RELATION BETWEEN SOIL PROPERTIES AND ERODIBILITY

Eighty four topsoils, located in the central and proximal parts of a dissected depositional glacis and lagunary depressions south of the Sacaba town, were selected for field determinations and laboratory analyses. They included 9 coarse loamy, 42 fine loamy, 14 loamy, 10 fine silty, 3 silty, one coarse silty and 5 fine clayey mixed thermic families. Forty four soils were sampled on the central and distal parts of a dissected depositional glacis, twenty five soils on a lagunary flat and fifteen in badlands. The laboratory techniques and field sampling procedures followed for data collection and analyses are described in chapter 3. Erosion types and degrees of the sampled sites were recorded in the field according to the specifications of the FAO guidelines for soil description (FAO, 1990).

Water erosion types present in the selected area are: rills, interrill flow, sheetwash and rainsplash, gullies and tunnels, sometimes in combination. The different erosion types were coded for statistical analysis, such as follows: (1) interrill; (2) rill; (3) gully; (4) tunneling; (5) combined surface erosional processes (eg,

interrill, rill and gully erosion); (6) combined subsurface erosional processes (eg, tunneling and gullies).

Three rates were used for field recording of erosion degrees: (a) slight, if the surface horizon presented some evidence of truncation; (b) moderate, when clear evidence of removal of the surface horizon was observed; and (c) severe, when the surface horizon was completely removed (FA0, 1990). Erosion degree was slight on 48 sites, moderate on 28 sites and severe on 8 sites.

7.2.1 Diagnostic surface and subsurface horizons

Sixty-one percent of the sampled soils classified as Aridisols, 29% as Mollisols with sedimentary covers of variable thickness, 7% as Entisols and 2% as buried Alfisols covered by coarse-textured layers. The following suborders were identified: Orthids, Argids, Orthents, Fluvents, Ustolls and Ustalfs. The Orthids were spread all over the southern Sacaba soilscape, while the Argids occurred only in the proximal parts of the dissected depositional glacis. Orthents and Fluvents, instead, dominated in the badlands and lagunary flats. Ustalfs were found only in the dissected depositional glacis (fig. 7.2).

Most of the soils have a cambic horizon and an ochric epipedon. The frequency of diagnostic subsurface horizons according to landform types is reported in figure 7.3. Argillic horizons were observed only in the proximal and distal parts of a dissected depositional glacis. Some soils in the badlands and lagunary flats lack diagnostic subsurface horizons. Cambic horizons predominated in all soilscapes.

Mollic and ochric epipedons dominated in the area, in more or less equal proportions in the proximal parts of the dissected depositional glacis, badlands and lower lagunary flats. The ochric epipedon was slightly more frequent in the distal parts of the dissected depositional glacis and middle lagunary flats. In all cases, the mollic epipedon was buried by recent depositional layers of variable thickness.

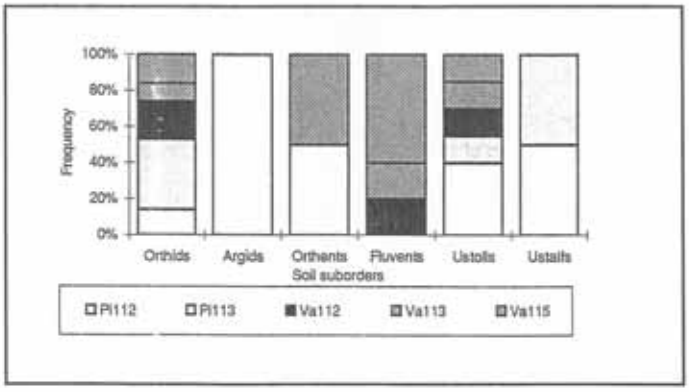

Fig. 7.2: Frequency of soil suborders in the mapped landform types.

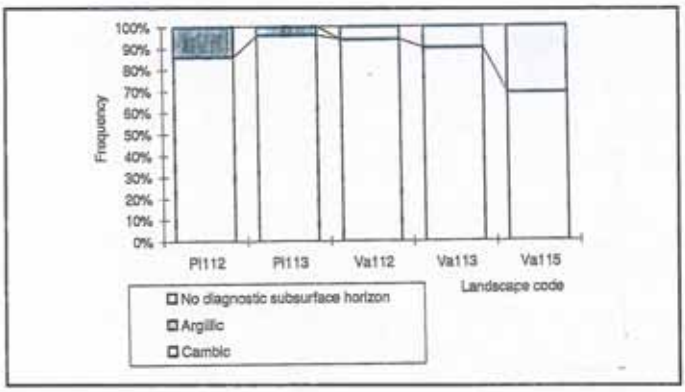

Fig. 7.3: Frequency of diagnostic subsurface horizons in the mapped landform types.

Aridisols with an argillic horizon (Argids) were mainly fine clayey and to a lesser extent silty (fig. 7.4). The Orthids had a wide range of particle size families, including fine loamy (52%), coarse loamy (8%), loamy (14%) and fine silty (12%). Fine silty and fine loamy particle size classes dominated in the Orthents, while those of the Fluvents ranged from coarse loamy (40%) to fine loamy (20%), and from coarse silty (20%) to fine silty (20%). The Ustolls, similarly, presented a wide range of particle size classes, with dominance of fine loamy (53%) and loamy (27%), but including also fine clayey (8%), fine silty (8%) and contrasting particle size classes. Finally, coarse silty (50%) and fine clayey (50%) particle sizes were identified in the Ustalfs.

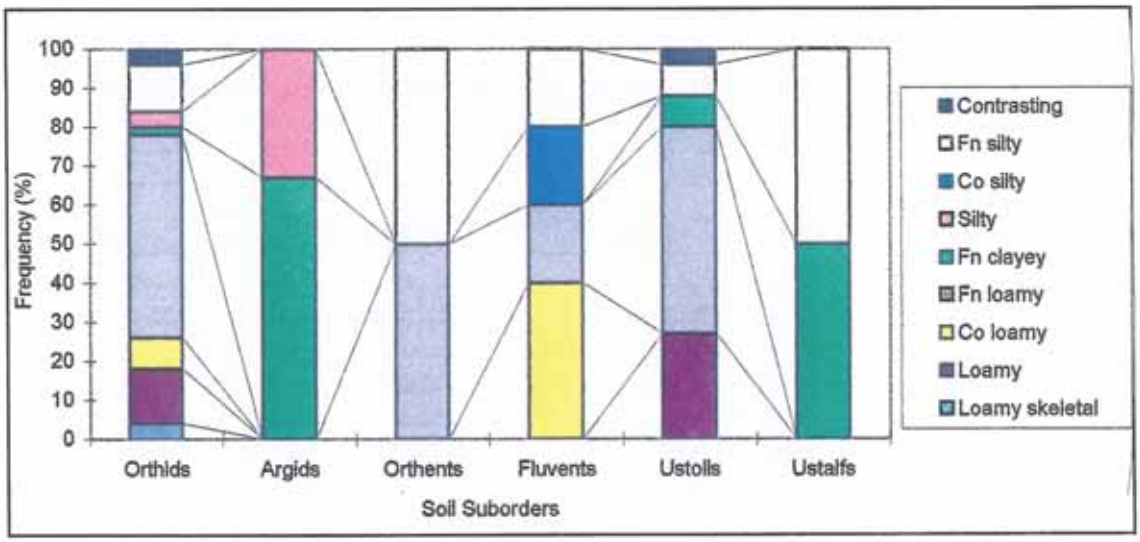

Fig. 7.4: Frequency of particle size classes in the soil suborders of the Sacaba valley.

7.2.2 Estimating relative soil erodibility

Soil susceptibility to erosion is a function of its chemical and physical properties. Table 2.2 (chapter 2) summarizes the attempts to identify the significant soil properties affecting soil erodibility, either directly or indirectly through their influence on aggregate stability, structure or infiltration. Several studies have

tried to isolate the most important soil properties affecting erodibility. However, there is no general agreement on the best set of properties related to erodibility.

The K-factor is a widely used coefficient to assess soil erodibility. It assigns a relative erodibility value between 0 and 1 to each soil on the basis of soil particle size, organic matter, structure and permeability (Wischmeier et al., 1971). The resulting soil erodibility index performs well in medium-textured soils, where the silt percentage does not exceed 60%. Because most of the soils sampled in the Sacaba basin did not surpass this range and the K-factor is one of the indexes most frequently used in soil loss models such as ANSWERS (Beasley et al., 1980), USLE (Wischmeier et al., 1969) and RUSLE, the soil susceptibility to erosion was assessed using this index. The K-factor of the Universal Soil Loss Equation was computed by the following formula (Wischmeier et al., (1971):

$$K= [0.00021*(12-OM)*M^{1.14} + 3.25*(SC-2) + 2.5*(P-3)]/100$$

where:
K = the soil erodibility factor ranging from 0 to 1;
OM = the organic matter content;
M = [(silt% + very fine sand%)*(100 - clay%)];
SC = the soil structure code;
P = the permeability class.
Soil structure was determined from field profile descriptions and soil permeability was estimated from the soil textural classes as described by Horn (1971). Table 7.1 indicates the variability of the parameters used to estimate relative erodibility.

Table 7.1: Variability of the parameters used to estimate the soil K-factor (USLE).

VARIABLE	MEAN	MINIMUM	MAXIMUM	VARIANCE	STANDARD DEVIATION	C.V.(1)
Permeability class	5.3	5	6	0.20	0.45	0.08
Structure code	3.4	2	4	0.32	0.56	0.16
Clay	23.8	12	44	42	6.5	0.27
Fine sand plus silt	65.2	43.4	85.85	133	11.5	0.18
M-textural term	4982.6	2632	7383	1120806	1058.7	0.21
Organic matter	1.44	0.13	3.14	1	0.76	0.52

(1) C.V. =coefficient of variation

A one-way analysis of variance (ANOVA) was carried out (1) to evaluate the correlation between field recorded erosion degrees and the estimated K-factor and (2) to analyze the interaction effects between relative soil erodibility, landscape position and erosion type (eg, interrill, rill, gully). When the *F*-test (the variance ratio) indicated statistical significance, the least significant difference (LSD) test was used to determine which group differences were significant (ie, the means for the compared groups significantly differed from each other). The means of the slight, moderate and high erosion degrees were plotted against the estimated K-values. Figure 7.5 indicates a positive correlation between field determined erosion degrees and the relative erodibility estimated using the K-factor of USLE.

The interaction plot between degrees of erosion, landscape positions and K-values indicates that soil susceptibility to erosion is affected by landscape position and directly correlated to field observed erosion rates. For example, the highest K-values occur in the lagunary depressions (eg, badlands and lower lagunary flats) and, to a lesser extent, in the central and distal parts of the dissected depositional glacis (fig. 7.6).

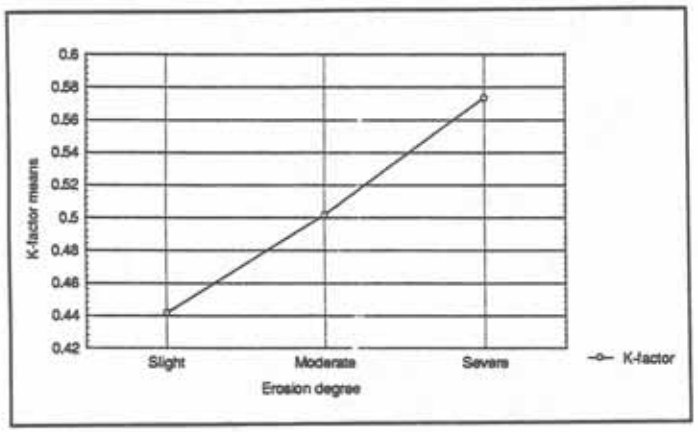

Fig. 7.5: Means of K-factor vs. field erosion rates (ANOVA analysis).

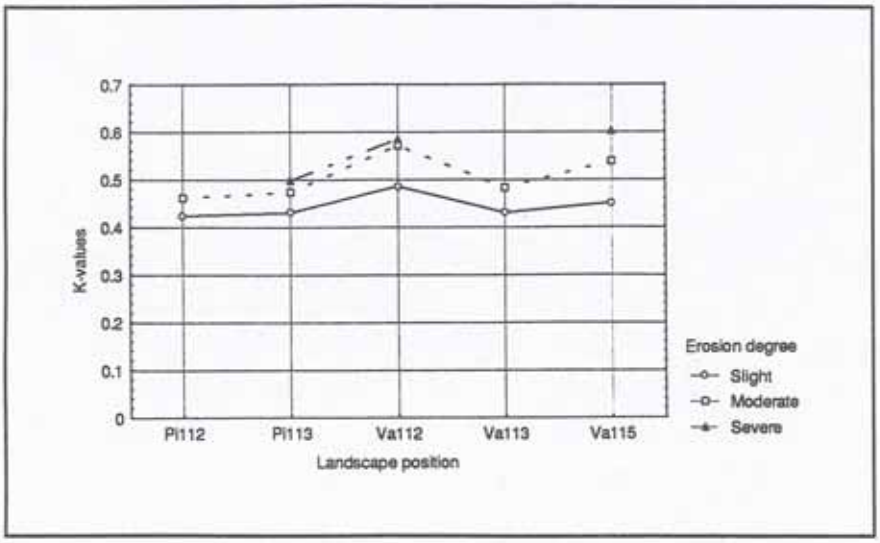

Fig. 7.6: Interaction plot between landscape position, erosion degree and estimated K-values.

Table 7.2: ANOVA results for landscape, erosion type and degree, and the K-values.

Independent variable	SS	d.f.	MS	SS error	d.f. error	MS error	F-ratio	p-value
Landscape position (*)	0.13	4	0.03	0.605	79	0.007	4.49	0.002537
Erosion degree (*)	0.15	2	0.07	0.551	79	0.006	10.67	0.000079
Erosion type	0.25	2	0.01	0.669	77	0.008	1.44	0.243358

(*) significant at $p < 0.05$; d.f.= degrees of freedom

Table 7.2 summarize the results of the analysis of variance performed using the landscape position, erosion type and erosion degree as independent variables and the estimated K-values as dependent variables. Landscape positions were: proximal (Pi111), central (Pi112) and distal (Pi113) parts of a dissected depositional glacis; middle (Va112) and lower (Va113) lagunary flats and badlands (Va115). Descriptions are provided in chapter 4. Slight, moderate and severe erosion degrees were considered. Three types of erosion, namely sheet, rills and combined surface erosional processes were distinguished.

The SS error, or error variance, denotes the within-group variability which could not be explained by the K-factor when analyzing, for example, the clustering according to erosion degrees. The SS (sum of squares), instead, is the variation that can be explained because of the differences in means between the groups. In other words, the group membership explains this variability. The F-ratio refers to the ratio

of the between-groups variability (MS) to the within-groups variability (MS error). The greater the ratio, the larger the differences between the means of the groups (eg, slight, moderate and severe erosion) and the larger the variance explained by the K-factor .

The table indicates that the K-factor means according to the landscape types and erosion degrees are significantly different from each other, and explain thus the variance between, for instance, erosion rates. In contrast, the K-factor does not significantly explain variances between erosion types. The least significant differences test (LSD) denotes that the K-values of the middle lagunary flats and badlands are significantly different from those of the proximal and distal parts of the dissected depositional glacis (table 7.3). Additionally, the LSD test evidences that the means of the estimated K-values are significantly different for the three groups of erosion degrees considered (table 7.4).

Table 7.3: Results of the Least Significant Difference test (LSD) for the landscape positions

LANDSCAPE POSITION	Pi112 (M= 0.43)	Pi113 (M=0.44)	Va112 (M=0.52)	Va113 (M=0.45)	Va115 (M=0.52)
Pi112		0.92	0.0039*	0.645	0.004*
Pi113			0.0036*	0.692	0.004*
Va112				0.552	0.992
Va113					0.0571

M= group mean; (*) differences are significant at $p < 0.05$

Table 7.4: Results of the Least Significant Difference test for the erosion degrees.

EROSION DEGREE	Slight (M=0.44)	Moderate (M=0.50)	Severe (0.57)
Slight		0.0036*	0.00009*
Moderate			0.0353*

M= group mean; (*) differences are significant at $p<0.05$

7.2.3 Relation between erosion severity and soil properties

The one-way analysis of variance was also performed for the erosion degrees as the independent variable (subdivided in slight, moderate and severe groups) against dependant variables such as soil texture, organic matter content, porosity, bulk density, soil structure and percentage of four different aggregate diameters (i.e. 4, 2 ,1 and 0.5 mm).

(1) Particle size distribution

The analysis of variance indicates that silt, coarse sand and fine sand contents are significant to explain variations between slight, moderate and severe erosion levels (table 7.5) . The plot of five selected particle size means shows that silt and fine sand contents are positively correlated to increments in erosion severity. Conversely, there is a decrease in the clay, coarse sand and medium sand contents as the severity of surface erosion increases. The results indicate that fine and very fine sand (50 - 200 µm) behaves more like silt than like the other sand particles, as assumed in the soil texture term (M) of the K-factor in USLE, and that soils with high silt and fine sand contents are the most erodible.

Clay percentage was negatively correlated with medium and fine sand contents, but positively related to organic matter in soils presenting slight erosion degree. There was a significant negative correlation between medium sand and silt contents of soil samples affected by moderate and severe erosion.
In soils exposed to slight erosion, silt percentage was positively correlated with organic matter and clay contents, whereas the reverse relationship occurred when erosion was moderate or severe.

Table 7.5: Analysis of variance of soil particle distribution according to erosion degrees

VARIABLE	SS	d.f.	MS	SS error	d.f.error	MS error	F-ratio	p-value
Clay	50.7	2	25.35	3019.8	79	38.22	0.663	0.518
Silt (*)	189.2	2	94.6	2126.8	79	26.92	3.51	0.034
Fine sand (*)	848.2	2	424	8865.6	79	112.2	3.78	0.027
Medium sand	2.57	2	1.28	90.5	79	1.14	1.12	0.33
Coarse sand (*)	1167.5	2	583.75	100054.4	79	127.2	4.58	0.013

(*) significant at $p < 0.05$

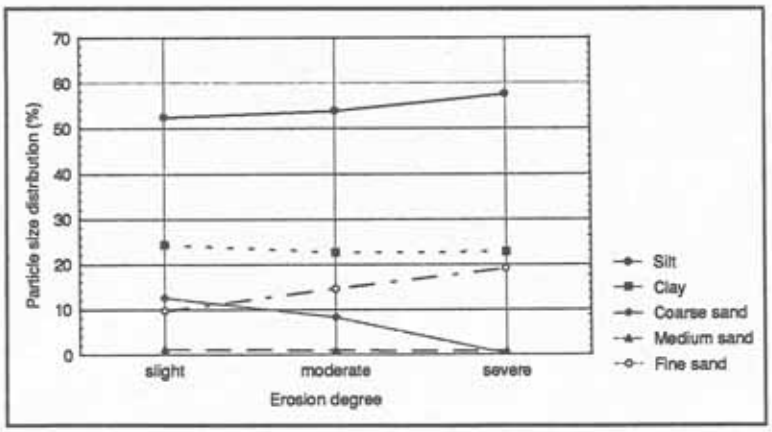

***Fig. 7.7**: Plot of means between erosion severity and soil particle size distribution.*

(2) Organic matter, bulk density and porosity

Organic matter content decreases at higher erosion rates. Bulk density correlates positively with increasing erosion rates (fig. 7.8). Organic matter increases soil cohesion and porosity, through the formation of stable aggregates, and thus contributes to decreasing soil susceptibility to erosion. Strong compaction, reflected by higher bulk density, decreases infiltration and favors water runoff, responsible for the initiation of water erosion.

Simple correlation analysis showed positive relations between organic matter content and clay percentage, and between porosity and soil structure, whereas the opposite trend was observed between silt content, bulk density and organic matter content. Soil porosity was negatively related with clay content, bulk density and erosion severity. Permeability of the surface layer increased with increasing porosity.

(3) Water-stable soil aggregates (WSA)

The percentages 4-mm-size soil aggregates were negatively correlated with erosion severity. In contrast, the percentages of aggregates of 2, 1 and 0.5 mm diameter showed a positive relation with increasing erosion degrees. Soil susceptibility to erosion is higher when the aggregates smaller than 4 mm predominate in the soil material (fig. 7.9). In addition, it was observed that soils exposed to moderate erosion had percentages of WSA 2 and 1 mm size, which negatively correlated with organic matter contents, whereas the reverse relation occurred for aggregates of 4 and 0.5 mm diameter. At slight erosion degree, instead, the percentage of WSA was always positively correlated with organic matter content, independently of their size.

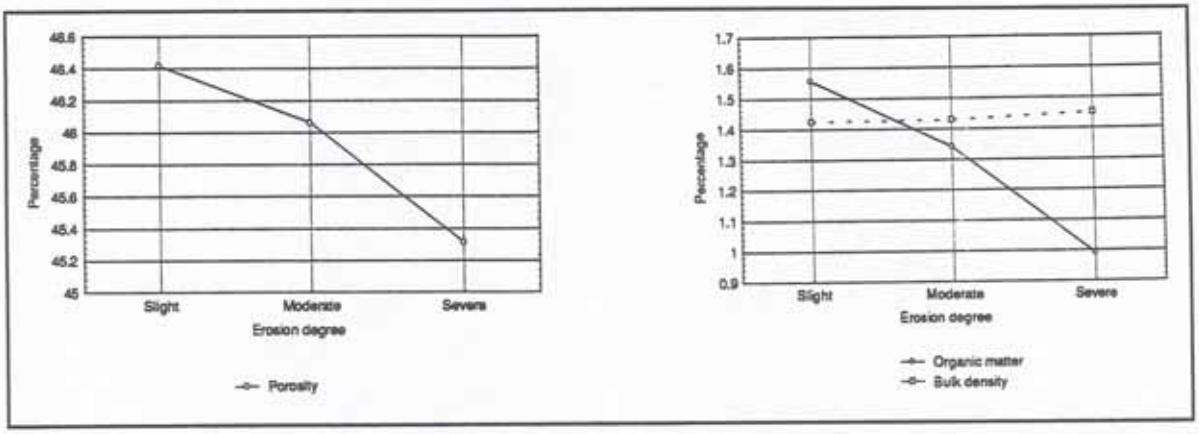

Fig. 7.8: Variation of organic matter, bulk density and porosity in relation to erosion degree.

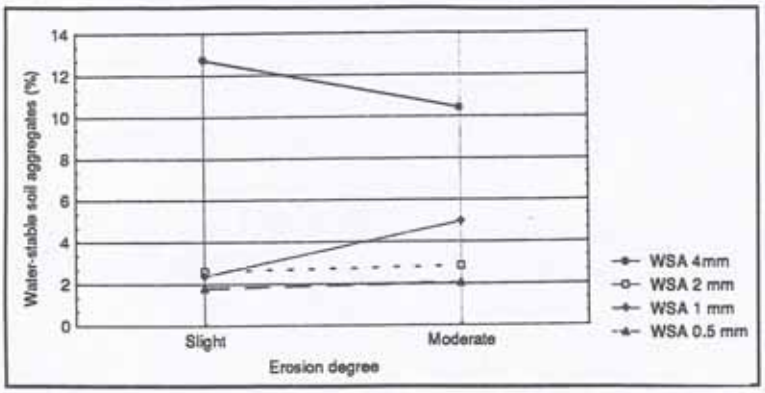

Fig. 7.9: Variation of soil aggregate size and percentage in relation to erosion degree.

(4) Soil structure and permeability

Within -group correlation analysis showed blocky and platy soil structures to develop under increasing clay, silt and organic matter contents and lower sand contents when erosion was slight. At increasing erosion severity, structure strength was negatively correlated to sand and silt contents.

The diagram of the means of structure and permeability showed that, in soils exposed to slight erosion, medium and coarse granular structure predominates, while increasing soil erodibility is more correlated to blocky, platy and massive soil structures (figure 7.10)

Soil permeability showed a positive correlation with erosion severity. Silt, clay and organic matter contents were negatively related to permeability, that is, the higher the silt and clay contents, the lower the soil permeability. In addition, porosity was positively correlated with permeability.

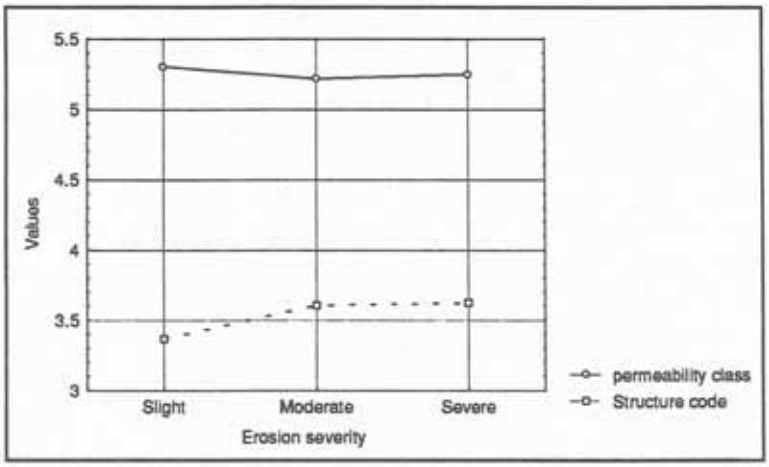

Fig. 7.10: Plot of the means of permeability and soil structure.

7.2.4 Interaction between erosion degree and landscape position

Not only was the interest on the correlation between soil properties and erosion severity, but also on how the landscape position affected the former relation. Therefore, diagrams were constructed to interpret the interaction between landscape position, erosion degree and topsoil properties.

(1) Soil texture and organic matter content

A plot of the organic matter and textures of the sampled topsoils was prepared to analyze the interaction between erosion severity and landscape position (fig. 7.11). Earlier, a positive correlation between silt plus fine sand contents and soil erodibility was found. Figure 7.11 indicates relation between landscape position and erosion severity, since the most erodible soils, with high silt and fine sand contents, are located in the lagunary depressions. Coarse and medium sand contents are lowest in the lagunary flats and highest in the dissected depositional glacis of the piedmont. The central parts of the dissected depositional glacis and the lower lagunary flats do not indicate features of severe erosion.

The severity of erosion increases as clay and organic matter contents decrease, independently of the landscape position. Soils located in the lagunary flats, with slight and moderate erosion, have higher organic matter contents than those situated in the piedmont glacis.

In conclusion, erosion severity is affected by the landscape position because soils with the highest silt plus fine sand contents are located in badlands, middle lagunary flats and distal parts of the dissected depositional glacis.

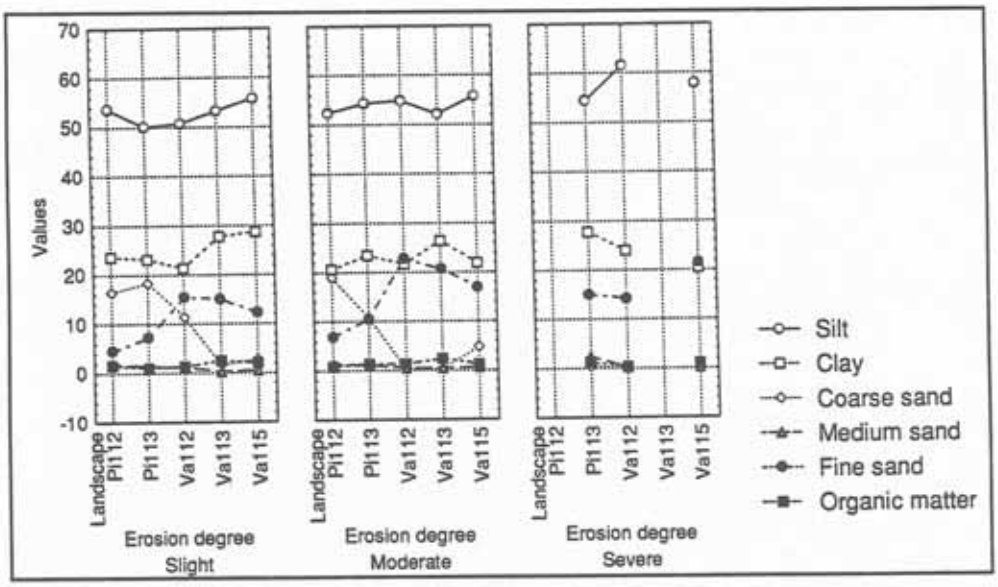

Fig. 7.11: Relation between soil erodibility, soil texture and organic matter content, as controlled by landscape position.

(2) Percentage of soil aggregates

Relationship between erosion degree, landscape position and soil aggregates was analyzed only on the central and distal parts of a dissected depositional glacis. According to earlier conclusions, a positive

correlation between the percentage of aggregates equal or smaller than 2mm and soil erodibility was established. A reverse relation was observed for soil aggregates of 4 mm size, called thus non-erodible.

Figure 7.12 shows the interaction among landscape position, degree of erosion and percentage of soil aggregates of 4, 2, 1 and 0.5 mm diameter. There is a notorious decrease in the percentage of the 4-mm-size aggregates, negatively correlated to erosion severity, from the central towards the distal parts of the dissected depositional glacis. In soils subjected to moderate erosion, higher percentages of aggregates equal and smaller than 1 mm were recorded in the distal parts, respect to the central parts of the glacis, whereas the reverse situation occurred when the degree of erosion was slight.

Soil erodibility increased with the reduction in percentage of the 4-mm-WSA and the increase of aggregates smaller than 2 mm. The aggregate classes are correlated to landscape position, since lower amounts of non-erodible aggregates, 4 mm in diameter, were recorded in the distal parts of the dissected glacis, which also shows a higher erosion degree.

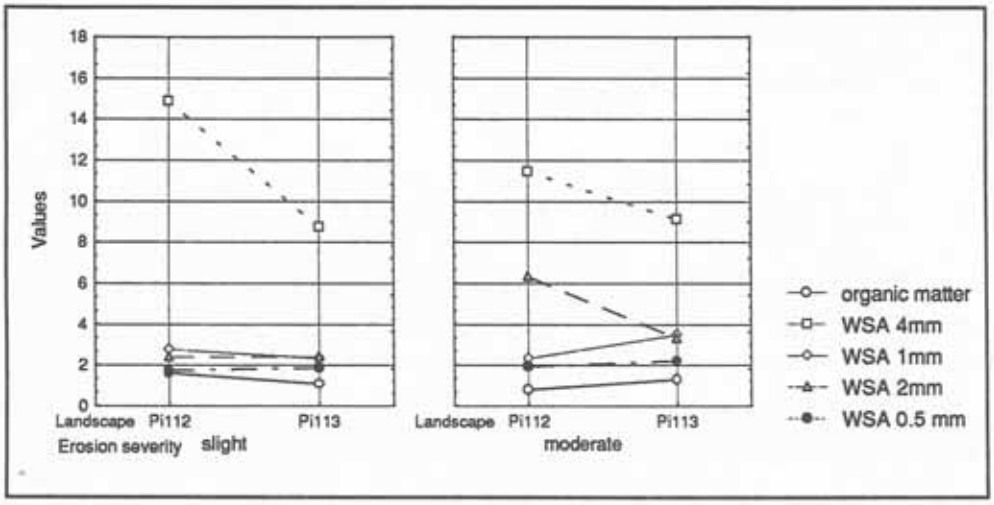

***Fig. 7.12:** Interaction plot among percentage of soil aggregates, landscape position and erosion severity.*

7.2.5 Relationship between erosion type and soil properties

Soil samples were grouped according three erosion types: (1) interrill erosion, determined by unconcentrated wash and raindrop splash; (2) rill erosion, caused by concentrated flow; and (3) combined processes of concentrated and overland flow, characterized by sheet, rill and gully erosion. When soil samples were grouped according to these three erosion types, the analysis of variance indicated significant between-groups differences regarding the coarse plus medium sand contents, as well as the percentage of 1 mm soil aggregates.

(1) Soil texture

The plot of soil particle size and organic matter content indicates a dominance of combined erosional processes with decreasing content of coarse soil particles (fig. 7.13). Relatively lower clay contents seem to favor soil losses by rill erosion. In contrast, higher clay contents generally promote soil aggregation, favoring water intake, and thus reducing overland flow.

High contents of silt and fine sand particles cause rill and combined surface erosion processes rather than interrill erosion. Moreover, comparing rill and interrill erosion, the latter dominates at comparatively higher proportions of clay and coarse plus medium sand contents. Clay and organic matter contents were also significantly correlated, regardless of the erosion type.

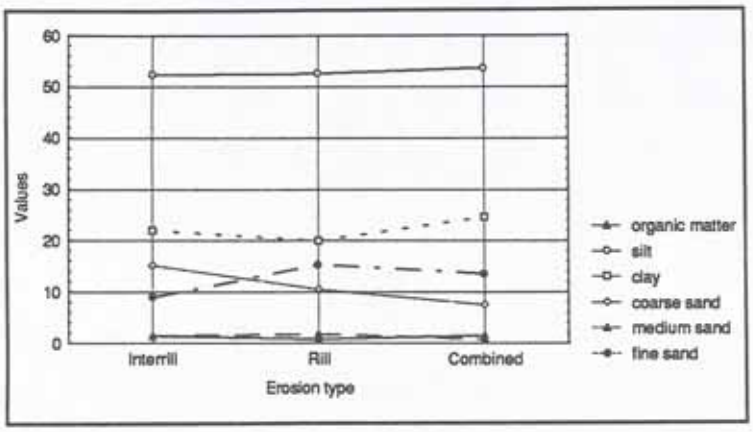

Fig. 7.13: Relationship between soil texture, organic matter content and erosion types.

(2) Soil aggregate size and organic matter content

Figure 7.14 illustrates the relationship between erosion types, soil aggregate diameters and organic matter contents. A positive correlation between the percentage of the 0.5-mm-diameter soil aggregates and organic matter content was found. Soil samples having the lowest organic matter content and highest percentage of 1 mm aggregates showed higher tendency to rill erosion.

Development of interrill and combined surface erosion types was favored by high amounts of 4 mm soil aggregates, low amounts of soil aggregates equal and smaller than 2 mm and relatively higher organic matter percentages (fig. 7.14).

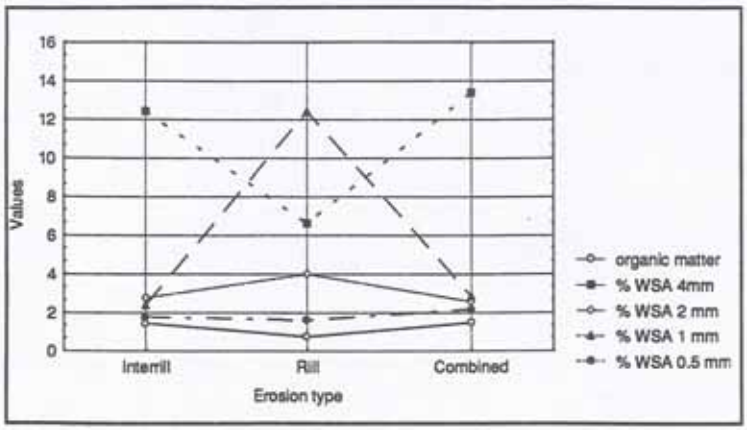

Fig. 7.14: Relationship between soil aggregates, organic matter and soil erosion types.

(3) Other soil properties

Bulk density did not show relationship with a particular soil erosion process (fig. 7.15). Instead, weaker soil structure appeared to favor unconcentrated flow and splash detachment over concentrated flow.

Only two variables, namely the coarse plus medium sand content and the percentage of 1 mm soil aggregates, were found significant to explain different erosion types. In general, organic matter and clay contents promote soil aggregation, especially the formation of non-erodible 4 mm aggregates. Concentrated runoff is reduced under these conditions, while raindrop splash and unconcentrated wash dominate. Interrill erosion was the dominant process in more aggregated soils, where the percentage of 4 mm aggregates was significantly higher, the silt and fine sand contents were relatively lower, and the organic matter, clay and coarse sand content were slightly higher, as compared to places where rill erosion takes place. Rill erosion was favored by high percentages of 1 mm soil aggregates, lower percentages of 4 mm aggregates, low organic matter and clay contents, and relatively higher amounts of silt and fine sand.

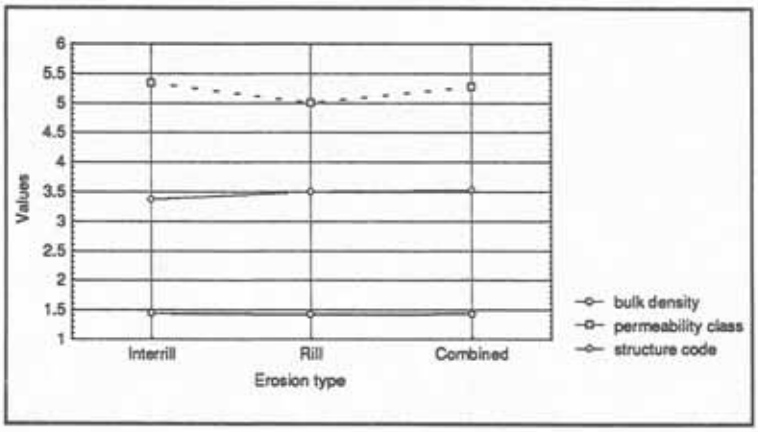

Fig. 7.15: Relationship between structure code, bulk density, permeability class and erosion types.

7.2.6 Interaction between erosion type and erosion degree

Figure 7.16 shows that the overall negative correlation between organic matter content and erosion degree is modified by the erosion type. Soils with the lowest organic matter contents are exposed to slight and moderate rill erosion, while combined erosional processes of different intensity are promoted under increasing amounts of organic matter. Organic matter contents lower than 1% are related to slight and moderate rill erosion, while percentages ranging from 1 to 1.5% are related to interrill erosion.

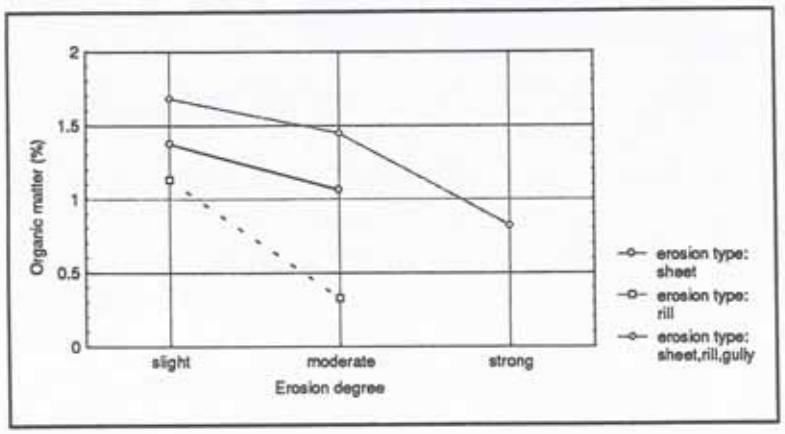

Fig. 7.16: Interaction between erosion degree and erosion type (organic matter content)

Erosion severity increases under the combined action of concentrated and overland flow, causing erosion features such gullies, rills and sheet wash. In soils subjected to sheet and rill erosion, there is a positive correlation between erosion degree and silt and sand contents. Soils with low organic matter and clay contents are exposed to stronger sheet and rill erosion. Previous studies also report a positive correlation between sand content and soil erodibility by splash (Epstein, 1967).

Combined erosional processes occurred in soils having silt percentages higher than 50%. Maximum severity was reached as the silt content increased. A negative relationship between organic matter, clay content and erosion degree was found. Figure 7.17 indicates that, soils were more exposed to sheet, rill and combined surface erosional processes, as silt and fine sand contents increased.

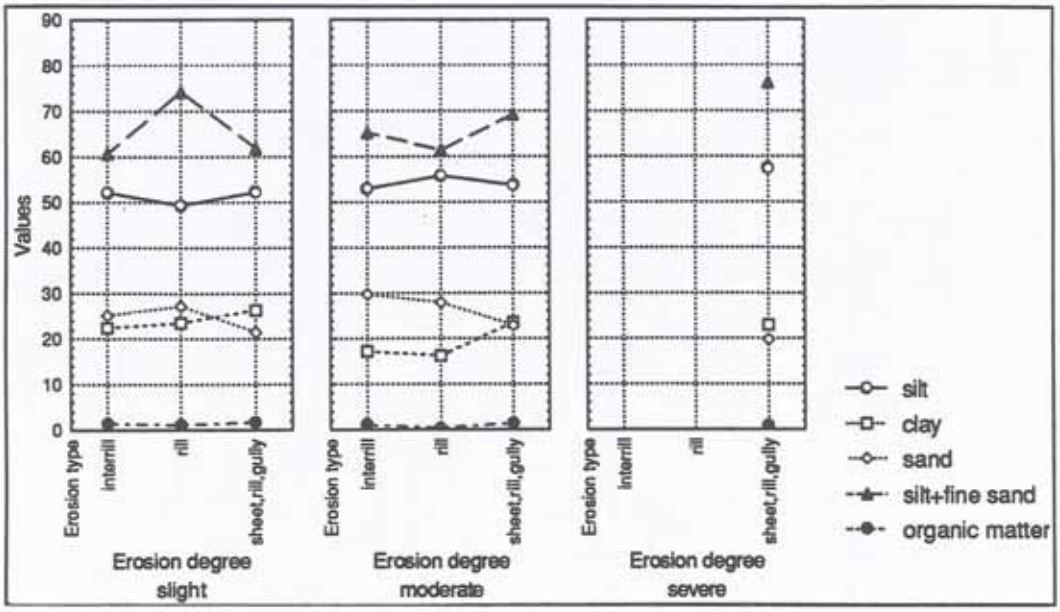

Fig. 7.17: Relationship between erosion degree, erosion type and soil texture (as silt and fine sand contents increase).

7.2.7 An equation to predict erosion severity due to surface erosional processes

After analyzing the one-way variance among soil properties and erosion degrees, a stepwise multiple linear regression was developed using the variables summarized in table7.6. The multiple regression yielded a four-term equation, explaining 31% of the variation in soil erosion degrees. The equation standard error of estimate is 0.56, with 75 degrees of freedom. The F-test provides a ratio of explained to unexplained variance of 8.4.

Erosion severity= 0.42 + 0.0002*(M) - 0.265*(medium sand) - 0.24*(organic matter) + 0.207*(soil structure)

Table 7.6: Equation to predict erosion severity as a function of topsoil properties

Variable	Order of entrance	B	t(75)	p-level
Intercept		0.423450	0.68288	0.496784
M-textural term	1	0.000194	3.01366	0.003519
Medium sand	2	-0.265409	-2.63896	0.10109
Organic matter	3	-0.240266	-2.63268	0.010281
Soil structure	4	0.207176	1.76863	0.081022

Included values were significant at the 0.001 confidence level. The textural M-term from the K-factor explained most of the variance in erosion degrees, thus indicating a positive correlation between erosion severity and the amount of fine sand and silt. The second and third terms correspond by the medium sand and organic matter contents, negatively related to erosion degrees. Soil structure (numerically coded from the soil profile descriptions) was the last parameter entered in the equation and showed to be positively related to erosion degrees. Massive and blocky structures are prone to higher erosion degrees than moderate subangular blocks, but the relation is very low. Wischmeier and Mannering (1969) also report a positive correlation between structure and the K-factor.

The most powerful predictor of erosion severity for the conditions of the Sacaba valley is the M-textural term of the K-factor or USLE erodibility index, included in several soil loss equations such as ANSWERS, USLE, K-MARTIN. Organic matter promotes soil aggregation and therefore reduction in splash detachment. Ekwue (1990) and Verhaegen (1984) found also a negative correlation between organic matter content and soil susceptibility to erosion.

7.3 FIELD REFLECTANCES OF SOIL PROPERTIES RELATED TO ERODIBILITY

Main factors producing a particular reflectance curve shape include soil texture, color, chemical composition, structure and moisture content. In addition, surface cover features like rock fragments, vegetation and depositional or structural crusts modify the reflectance characteristics and curve shape of soil properties.

Field reflectances collected in the piedmont and valley landscapes south of the Sacaba valley, affected

by different erosion degrees, were analyzed under two main aspects: (1) the effects of soil properties on soil reflectance, including variations in soil texture, color and organic matter content; and (2) the variations in soil reflectance because of the type and characteristics of the surface cover, including percentage, shape and size of rock fragments, crusting and vegetation.

The effects of soil moisture on reflectance were excluded from the analysis because the reflectances were measured in dry field conditions, without notorious changes in the humidity contents during the field data collection period. The procedure and geometrical considerations followed to collect ground-based soil reflectance spectra are described in chapter 3.

7.3.1 Soil properties

(1) Topsoil texture

Reflectance in the visible and near-infrared varies inversely to the soil particle size, as clay particles exhibit higher reflectance than sandy ones. Figure 7.18 indicates that variations in clay and sand contents affect soil reflectances when the silt contents are lower than 50%. Clay loam textures have higher reflectances and different curve shape than loam and sandy loam textures.

The lowest reflectance values correspond to the sandy loam topsoils, while the highest reflectances are related to silty clay loam and clay loam textures, having the same silt percentage range (60 to 70%) but differing in clay contents. Reflectance decreases as follows: silty clay loam > clay loam > silt loam=loam > sandy loam.

As the clay content decreases, the spectral curve has a more gentle, monotonically increasing slope. Fine-textured topsoils exhibit three main breaks in the curve shape. The first occurs at 500 nm, followed by a steeper slope in the range from 500 to 600 nm. At 600 nm, the curve flattens and changes to a convex, gently sloping shape from 700 nm on.

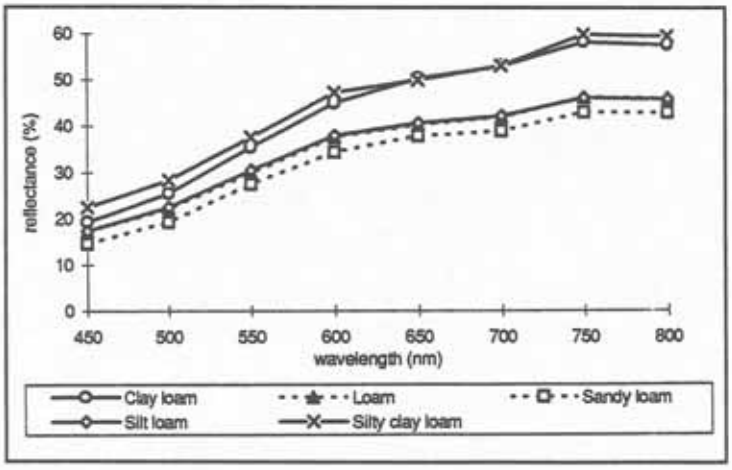

Fig. 7.18: Variations in topsoil reflectance as a consequence of textural changes.

(2) Organic matter

Figure 7.19 illustrates the spectral curves of three soil types common in the Sacaba valley. The highest reflectances correspond to Orthents and Orthids, with organic matter contents below 1%, yellowish colors and medium to coarse textures. The lowest reflectance values correspond to a Mollisol developed under moister past climatic conditions, with organic matter contents above 1%, relatively dark colors (10YR 3/2, 3/3, 4/3) and generally fine loamy textures. In the Cochabamba valleys, Mollisols are relicts buried under the present-day Aridisols and Entisols, unless erosion has removed the sedimentary cover materials.

The relative increase in organic matter content in mollic horizons causes not only an average higher light absorption but also a gentler slope of the spectral curve, resulting in a monotonically increasing linear shape, which resembles the 'organic-affected' curve described by Stoner et al. (1981). The ability of organic matter to flatten the spectral curve was also noted by Escadafal (1994) in soils containing around 1% of organic matter. Organic matter causes stronger light absorption in the range of 500 to 800 nm. This is also reported by Mathew (1973), who found highest correlation between organic matter content and reflectance in the range 500 to 1200 nm. Furthermore, organic matter controls also the soil color, which causes an overall light absorption in the visible range of the spectrum (Orlov, 1964).

Orthids and Orthents have similar spectral curve shapes. The slope rises slightly towards the red-near infrared portion without noticeable inflection. The shape resembles the minimally altered curve, proper of soils with low organic matter content, low iron oxide content and good drainage described by Stoner et al. (1981).

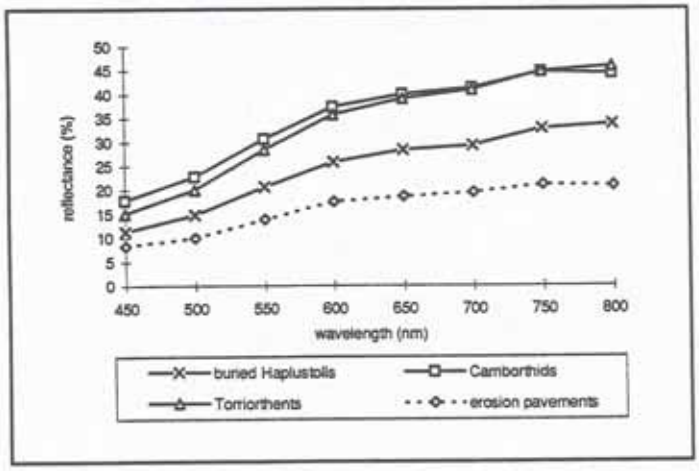

Fig. 7.19: Soil reflectance variations mainly as a function of variations in soil organic matter content.

(3) Soil color

Figures 7.20, 7.21 and 7.22 illustrates variations in soil reflectance due to changes in one of the three variables of the Munsell color system: hue, value or chroma. For soils with constant hue and value but increasing chroma, the reflectance in the red wavelength range (650-700 nm) varies more rapidly than in

the green (500-550 nm), thus a direct relationship between color saturation, expressed by the chroma, and reflectance (fig. 7.20). The 'purer' the soil color, the higher the reflectance, particularly in the yellow to near-infrared wavelength range (550 to 800nm).

Reflectance variations due to changes in color value, expression of the color brightness, are more subtle. Figure 7.21 shows a positive relation between color brightness and reflectance, more accentuated in the near-infrared range (700-800 nm). In figure 7.22, light reflection in the 600-700 nm (orange and red wavelengths) increases as color hue becomes redder. The yellowish 2.5Y hue has overall higher absorption than the reddish 10YR hue. The curve slopes are similar in the blue to yellow range (450 - 600nm), where the 2.5Y spectral curve deflates, while the reddish 10YR curve acquires a stepper slope because of the higher reflectance in the red portion of the spectrum.

Summarizing, color hue and value affect the red and green portions of the spectrum less than the chroma. The blue range is useful only to discriminate variations in color hue.

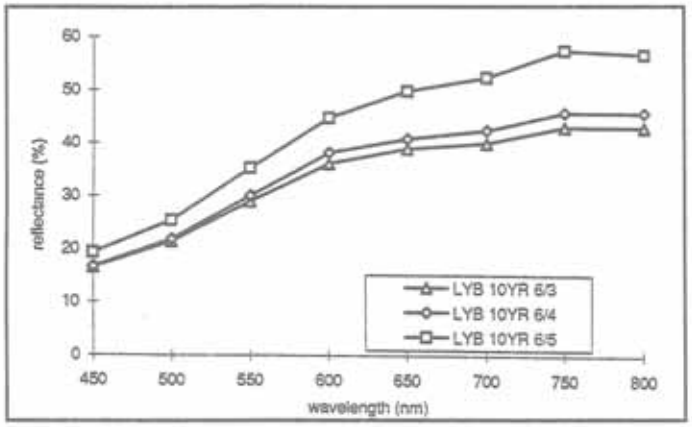

Fig. 7.20: Reflectance variations due to changes in color chroma.

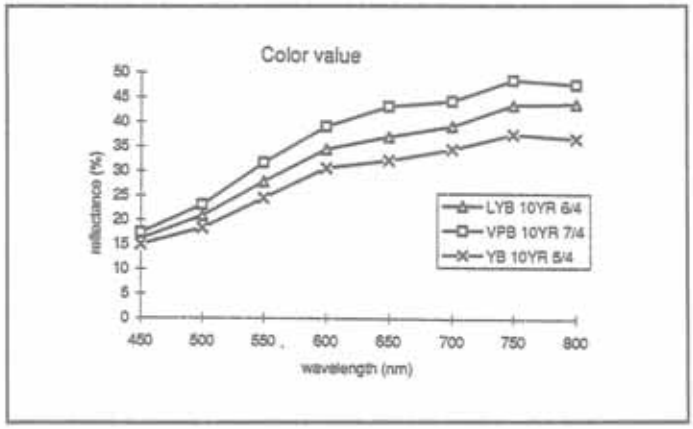

Fig. 7.21: Reflectance variations due to changes in color value.

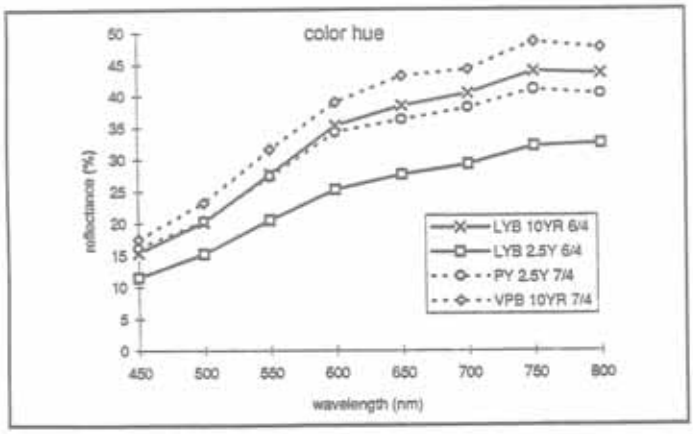

Fig. 7.22: Reflectance variations due to changes in color hue.

7.3.2 Surface features

(1) Surface rock fragments

Coarse fragments, 2 mm or larger in diameter, effect the reflectance of bare soil plots. Not only the cover densities, but also the size and shape of the pebbles produce changes in reflected energy. There is an inverse relation between the percentage of rock fragments and reflectance, especially when the fragments cover more than 60% of the soil surface (fig. 7.23). Rock fragments create a complex, irregular surface with large pore space between the individual pebbles. As the incident flux falls on the pebbles, most of the energy is trapped in the free space between the rock fragments and completely extinguished there.

The shape of the curve evidences a strong influence of the soil background, especially at low fragment density. The curve follows a convex shape, with changes in slope at 500, 600 and about 700 nm. Higher reflectances occur in the yellow, red and near-infrared wavelengths, related to the curve type 2 and the 'minimally altered curve' described by Condit (1972) and Stoner et al., (1981). Increases in rock fragment density mask the reflectance of the soil background, flattening the convex shape of the curve.

The shape and size of the rock fragments also affect surface reflectances. Gravels vary from 2 to 7.6 cm and stones from 25 to 60 cm (USDA, 1986). In figure 7.24, reflectance decreases as the size of the pebbles increases. Furthermore, rounded fragments reflect more energy than angular ones because of their smoother surface. The curves have a convex shape, but above 600nm the slope flattens as rock fragments become larger and more angular.

In conclusion, the percentage of light absorption varies as a function of cover density, shape and size of the coarse fragments. High amounts of fragments, angular shapes and large sizes cause lower reflectance values.

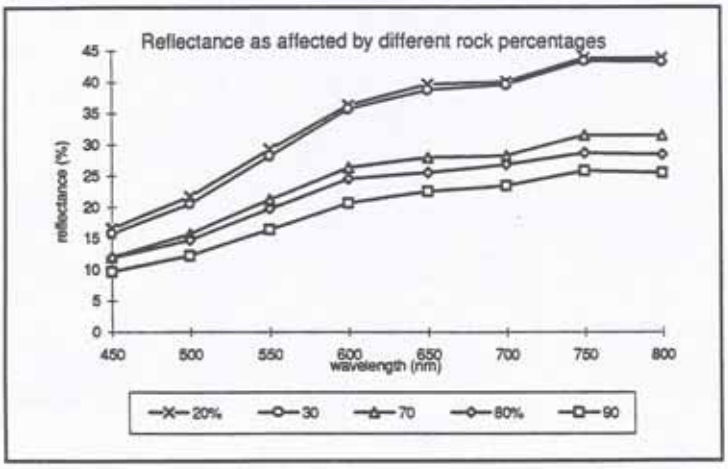

Fig. 7.23: Reflectance as affected by the percentage of surface rock fragments.

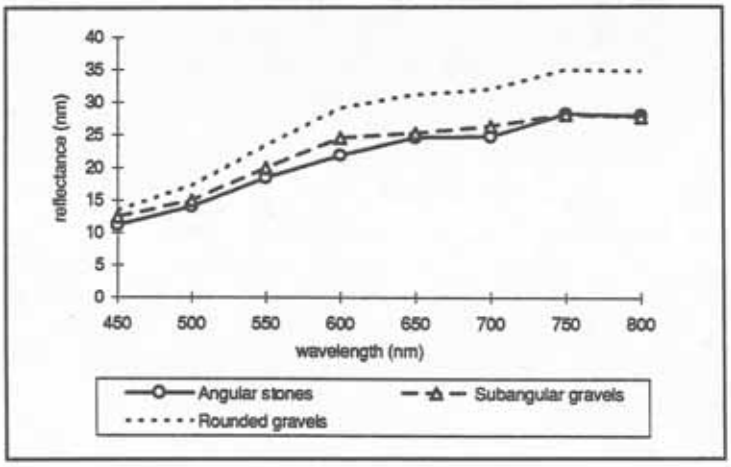

***Fig. 7.24**: Reflectance variations due to changes in rock fragment shape and size.*

(2) Splash pedestals

Splash pedestals are caused by raindrop impact and rainwash. They result from the protection of the underlying soil by rock fragments. The spectral curve has a convex shape and highest reflectance in the near-infrared region of the spectrum (fig. 7.25). Sometimes, the pedestals are covered by dark-colored fungi which strongly absorb the incident energy and lower the reflectance, especially in the yellow and red wavelengths.

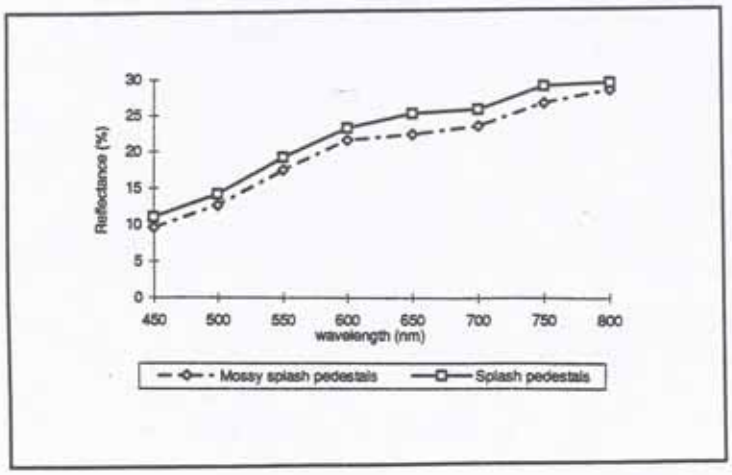

Fig. 7.25: Spectral curve of splash pedestals

(3) Crusts

Bright silt-rich depositional crusts, resulting from the soil particle displacement and sorting, have overall high reflectance. Increase in coarse sand particles of the soil surface causes a slight decrease in reflectance (fig. 7.26). Strongest energy absorption occurs when the crust is covered by dark fungi (fig. 7.28). Also the presence of rock fragments on the crust surface decreases the reflectance (fig. 7.27). This is attributed to higher surface roughness, causing more scattering and trapping of the incoming light flux.

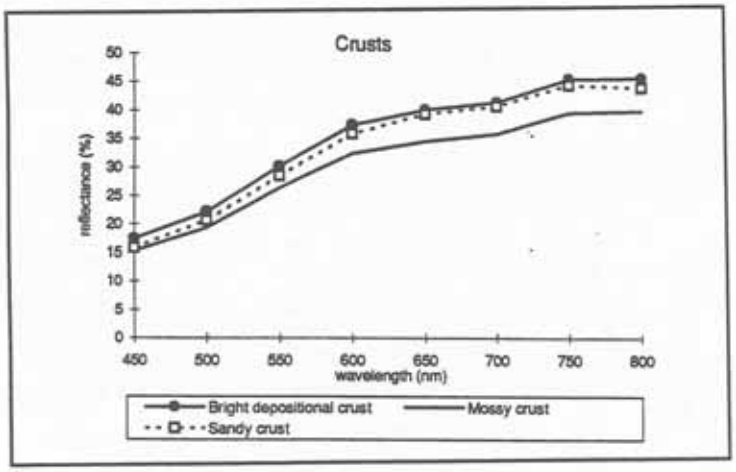

Fig. 7.26: Spectral curve of depositional crusts, mossy crusts and sandy surfaces

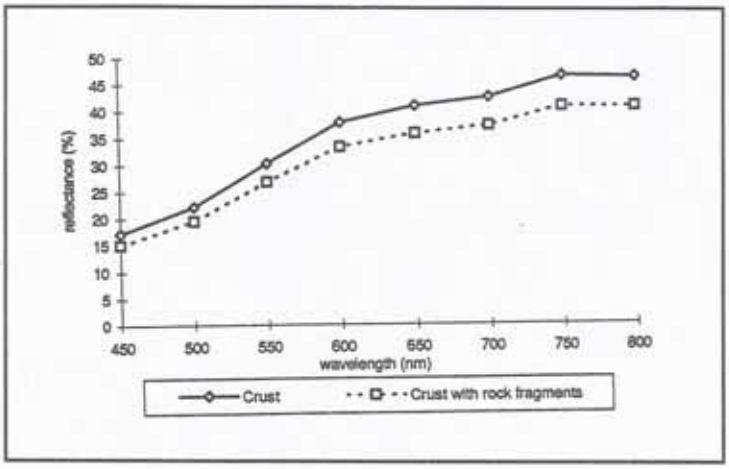

Fig. 7.27: Influence of rock fragments on the spectral reflectance of depositional crusts

Fig. 7.28: Mossy crust

(4) Natural vegetation

Figure 7.29 contains the spectral curves of the main shrubs and trees found in badlands, gullies, ephemeral brooks and moderately eroded areas. There are two main curve types. One corresponds to the green vegetation with absorption features in the blue and red regions of the spectrum and high reflexion in the green and near-infrared ranges. The curve gently slopes in the range of 450-500 nm and has a convex shape between 500 and 600 nm, with a maximum reflection peak at 550 nm. This is followed by another absorption feature due to chlorophyll pigments at 650 nm and further by a very steep slope from 700-750 nm onwards. The second type corresponds to senescent, yellowish vegetation which has a monotonically increasing curve shape, without evidence of energy absorption due to the absence of chlorophyll pigments.

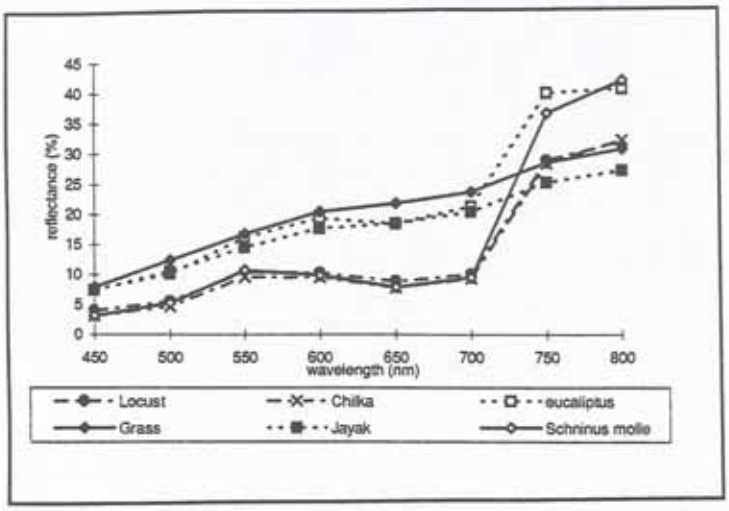

Fig. 7.29: Spectral signatures of natural vegetation types.

7.3.3 Conclusions

The analysis of the spectral behavior of surface features and topsoil properties in the visible and near-infrared regions of the spectrum by ground-based radiometric measurements allows to conclude that the main factors affecting the reflectance of surface components related to the soil susceptibility to erosion are: soil color, organic matter content, silt-rich topsoil textures, coarse fragment surface density, shape and size of the surface rock fragments, and 'bright' depositional crusts.

Low reflectance values are caused by dark-colored mollic horizons. Organic matter contents higher than 1% were enough to decrease the overall reflectance values and flatten the spectral curve shape, compared to the light-colored ochric horizons of Entisols and Aridisols, with very low organic matter contents. By this means, Mollisols could be discriminated from either Aridisols or Entisols, using ground-based reflectance measurements. It was not possible, however, to separate characteristic features of Aridisols and Entisols, as they have similar spectral curves in the range of the spectrum analyzed.

The presence of rock fragments decreased the reflectance of the depositional crusts. Reflectance decreases were positively related to greater amounts of rock fragments of angular shape and larger size. Soil background clearly influenced the shape of the spectral curve when the cover density of rock fragments was lower than 60%.

Reddish color hues had higher reflectances than yellowish ones, especially in the 600 to 800 nm range (orange, red and near-infrared wavelengths). Lower color chromas and/or values caused reflectance decreases, particularly in the range of 600 to 800 nm.
The presence of a gray-greenish fungi, which protect the soil surface against splash erosion, was another feature lowering the overall reflectance of the soil surfaces in the visible and near-infrared ranges, but without effecting the curve shape.

7.4 IDENTIFICATION AND MAPPING OF AREAS AFFECTED BY EROSIONAL PROCESSES

Three different techniques were used to identify and delineate areas affected by erosional processes. The first consisted in interpreting aerial photographs at scale 1:25000 to identify erosion classes on the basis of patterns, shapes and grey tones. Secondly, digital classification of satellite images covering the visible, infrared, thermal and microwave regions of the spectrum was carried out by using statistical pattern recognition techniques. Two objectives were pursued: (1) area labelling by using the Landsat TM data set (visible, infrared and thermal ranges); and (2) class allocation by merging of JERS-1 microwave and Landsat TM data set. The third approach intended to map the abundance of surface components related to erosion severity within one pixel, by unmixing their spectral signatures. A linear mixing and distinctive spectral characteristics were assumed for the surface components mapped.

7.4.1 Mapping erosion severity by interpretation of aerial photographs

(1) Method

Aerial photographs at scale 1:25000 dated June 1976, thus from a period of the year when non-irrigated areas are fallow, were interpreted and compared with the satellite image classification of 1994 to monitor erosion encroachment. Four classes of erosion severity were determined using the following rules:

(1) slightly eroded areas : surfaces with grayish tones, low vegetation cover and very few plots of geometric shape (fallow land) (fig.7.30);

(2) moderately eroded areas: whitish spots and low density rill patterns (fig. 7.31);

(3) highly eroded areas: gullies or dense rill patterns and whitish areas (fig. 7.32);

(4) badlands: white areas and complex patterns of gullies with evidence of natural vegetation or shadow and, in some locations, very steep slopes with gullies (fig. 7.33).

Fig. 7.30: Slightly eroded areas

Fig.7.31: Moderately eroded areas

Fig. 7.32: Strongly eroded areas

Fig. 7.33: Badlands

(2) Results and discussion

The results of the photo-interpretation were digitized, rasterized and entered as input data in the geographic information system to measure the extent of the erosional classes (figures 7.34 and 7.35). In 1976, from a total of 4161 hectares, 2265 hectares were affected by slight erosion, 1261 hectares by moderate erosion and 313 hectares by severe erosion. Badlands occupied 321 hectares.

The determination of classes was subjective and related to field observations and interpreter experience. The delineation of slightly and moderately eroded areas is less accurate than that of highly eroded areas and badlands, which present more conspicuous features.

Slightly eroded areas were mapped in the proximal, central and, to a lesser extent, in the distal parts of the dissected depositional glacis. Moderately eroded areas occupied the proximal part of the dissected depositional glacis, while severely eroded areas coincided with the badlands developed in the lagunary depressions and on the steep slopes in the southeastern part of the Sacaba valley.

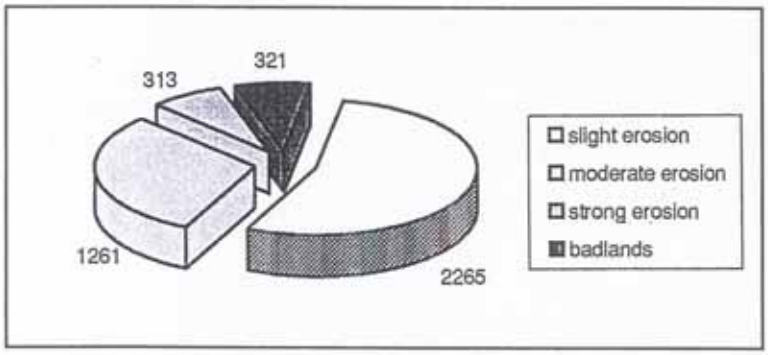

Fig. 7.34: Areal extent of erosional classes for June 1976 (in hectares)

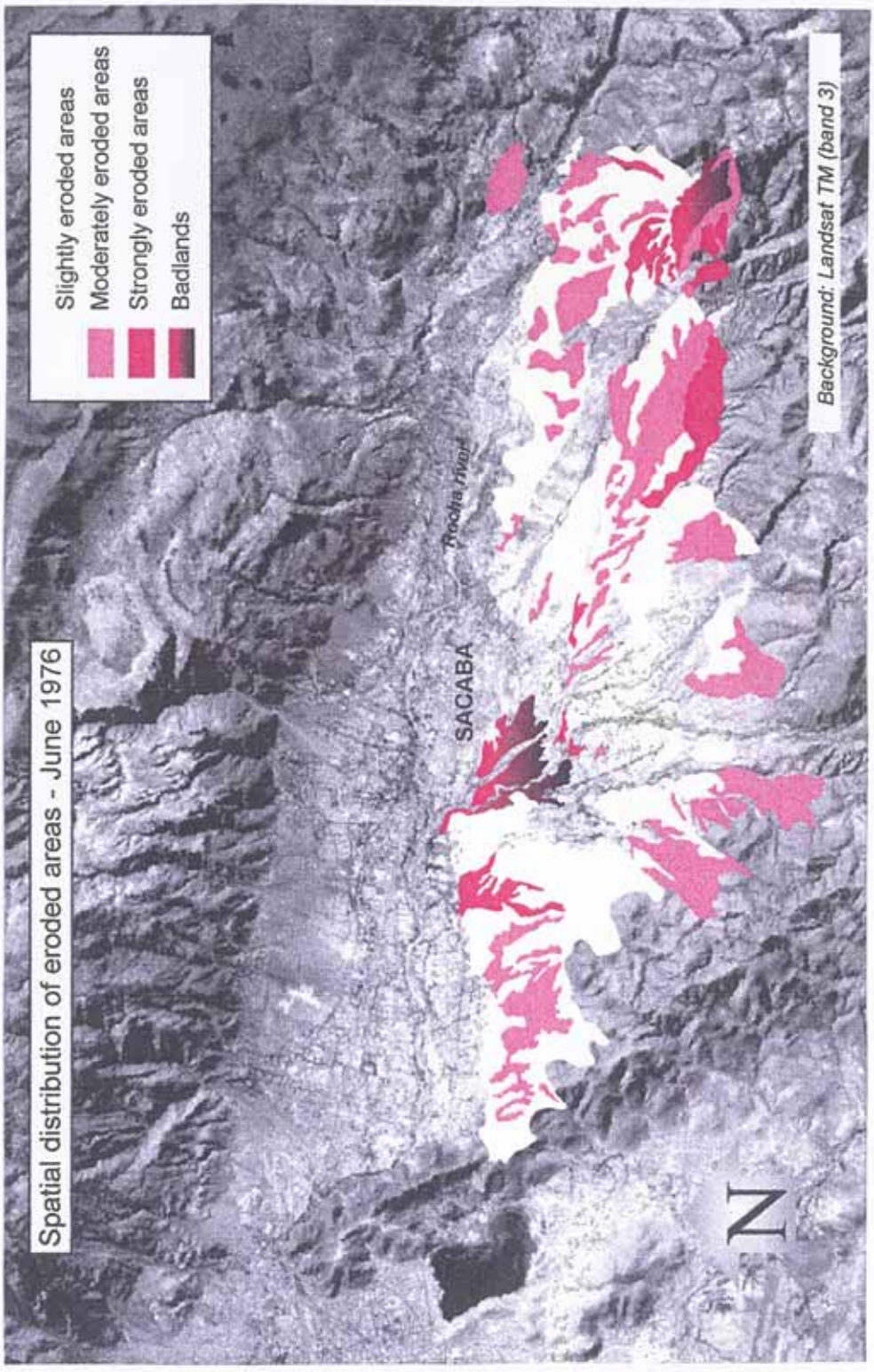

Fig. 7.35: Areas affected by erosional processes in June 1976.

7.4.2 Delineation of eroded areas using satellite-borne sensors

Two different data sets , a seven-band Landsat TM scene acquired on June 1994 and a JERS-1 SAR scene from May 1994, were utilized to identify and map the eroded areas in the southern part of the Sacaba valley. Since the aim was not only to delineate eroded areas but also to assess the improvements achieved by merging microwave and optical data, the same classes and classification techniques were used on both data sets.

Data were acquired contemporaneously to the field data collection. The images were geo-referenced to topographic sheets (see chapter 3) and the field plots spatially referenced using a global positioning system. Erosion degrees were recorded according to the FAO guidelines (FAO, 1990). Field plots showing variable degrees of erosion were used to determine the classes on the satellite images and train the classifier.

The three approaches, namely statistical pattern recognition using Landsat TM data, the fusion of Landsat TM and JERS-1 SAR data sets, and surface feature abundance mapping by linear unmixing of Landsat TM data, were tested in an area south of Sacaba, where field data collection was carried out. To facilitate the analysis and interpretation of the satellite data, a mask was created to extract the area of interest.

(1) Landsat Thematic Mapper

(a) Method

Six classes were considered to characterize the study area, which comprised dissected depositional glacis and lagunary depressions:

(1) Fallow land: non-irrigated agricultural parcels, where only rainfed crops are grown, thus being bare soil surfaces during the dry season, but without field evidence of erosion.

(2) Slightly eroded areas: surface horizons affected by sheet and slight rill erosion.

(3) Moderately eroded areas: clear evidence of removal of the surface horizons, with predominance of rill over sheet erosion features.

(4) Badlands: substantial removal of deeper subsurface horizons, with a mixture of natural vegetation, eroded soils and variable percentages of rock fragments.

(5) Natural vegetation: shrubs, molles and locust trees commonly grown in highly eroded areas and badlands, and thus used as surface features indirectly related to erosional processes; they constitute the only vegetation cover during the dry season (March-October) in non-irrigated areas.

(6) Miscellaneous land: ephemeral brooks and erosion pavements. The brook-beds are covered by rock fragments of variable sizes and shapes. Their reflectance is similar to that of the erosion pavements formed in badlands and highly eroded areas, because they derive from the same geologic material in the mountains south of Sacaba (sandstones, quartzitic sandstones).

A supervised training technique based on area extraction of spectral values, with spatial and spectral

constraints, was used to generate the spectral signatures of the surface components. Figure 7.36 plots the spectral curves of the six selected classes extracted from the seven-band Landsat TM data set. Transformed divergence analysis was used to statistically evaluate the class signature separability and select the best band combination for allocating the image pixels to one of the pre-determined information classes.

(b) Results and discussion

Moderately eroded areas exhibit the highest reflectance values in all the waveband ranges, except the 760-900 nm range (TM-4) where maximum reflectance values correspond to green vegetation. Surface components are spectrally distinct in bands 4, 5, 7 and, to a lesser extent, in band 3. Badlands and vegetation have strong absorption features and are not separable in the range of 450-690 nm. The low reflectance of badlands in the visible and near-infrared ranges could be attributed to a shadow component, related to the depth of the gullies and the irregularities of the surfaces, trapping more of the incoming light and thus reducing the reflectance.

Field evidence in moderately eroded areas showed truncation of the topsoil, rills and sheet erosion. Organic matter contents are very low in most of the soils (classified as Aridisols), causing light-coloured topsoils with overall high reflectance in the visible region of the spectrum. Additionally, the soil dryness and relatively lower clay content, compared to slightly eroded areas, are assumed to cause the high reflectance peak in the middle infrared range (TM-5). Coleman et al. (1993) report a negative relationship between the reflectance in band 5 and clay contents of the topsoil. The spectral signatures of surface components in bands 5 and 7 (middle infrared) show a decrease in reflectance as erosion severity decreases, except for badlands whose spectral plot relates more to the surface roughness compound.

Fallow land, slightly eroded areas and miscellaneous land have similar spectral behavior in the 450-600 nm range (TM1 and TM2). Their spectral curves are slightly distinct in the range of 630 - 690 nm (TM3). Fallow land exhibits comparatively lower reflectance values, which could be attributed to slightly higher organic matter contents and higher surface roughness resulting from the cultivation practices. Reflectance in the near-infrared region is also negatively related to erosion severity (fig. 7.36). The above three types of areas are spectrally distinguishable in the middle-infrared range, coinciding with Landsat TM bands 5 and 7.

As with ground-based reflectances, vegetation presents absorption features around 450 nm (TM-1) and 650 nm (TM-3), and high reflectance in the near-infrared (TM-4). Another strong absorption feature occurs in the middle-infrared, related to the water content of the leaves. The healthier the vegetation, the stronger the absorption. The lowest reflectance values are recorded in the middle-infrared range (TM-7).

In conclusion, eroded areas have overall higher reflectances than fallow land. This agrees with the positive relationship between silt and fine sand contents and soil susceptibility to erosion, and with the

negative relation between increasing amounts of organic matter and soil susceptibility to erosion. Additionally, the analysis of ground-based reflectances acquired over the Sacaba area revealed positive correlations between soil reflectance and increases in silty-like particles as well as decreases in the soil organic matter contents.

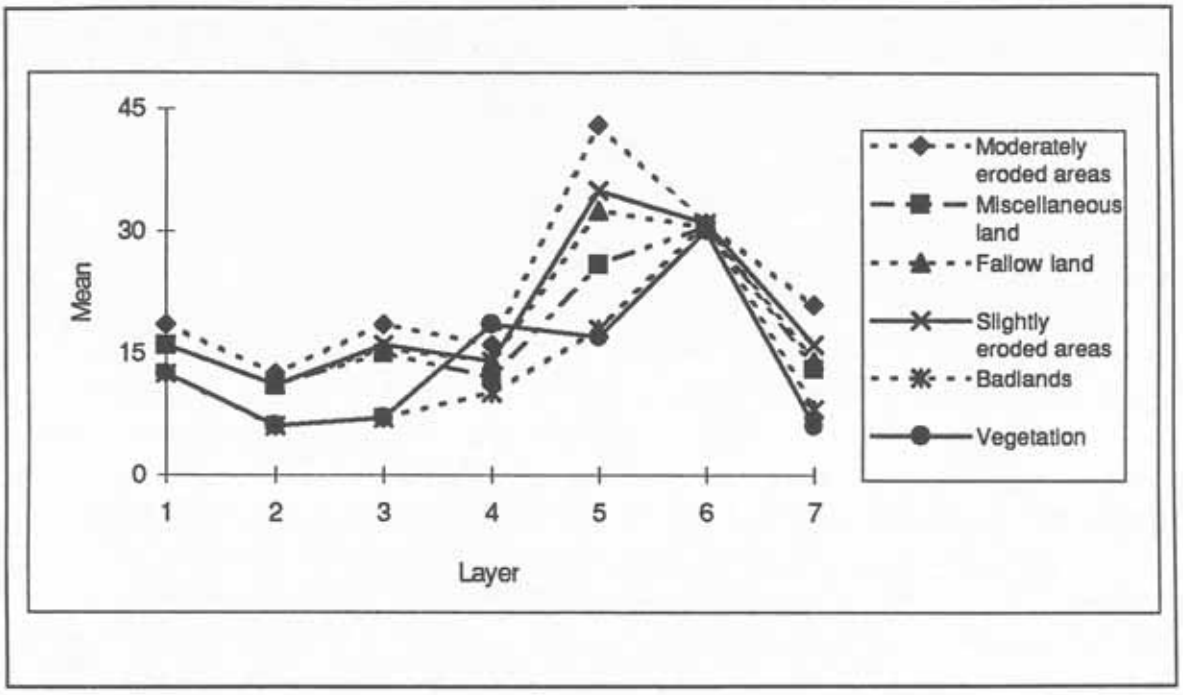

Fig. 7.36: Spectral curves of selected surface components

According to transformed divergence analysis, the set constituted by bands 1, 2, 4, 5, 6 and 7 produced the highest average spectral separability between classes, equal to 1950. The correlation matrix indicates, however, relatively low separability among the spectral signatures of badlands respect to miscellaneous land and slightly eroded areas (1380 and 1586 respectively). Additionally, the spectral separability between fallow land, slightly eroded areas and moderately eroded areas is also relatively low (table 7.7).

Table 7.7: Spectral separability among information classes

CLASSES	Badlands	Miscellaneous land	Slightly eroded areas	Moderately eroded areas	Fallow land	Natural vegetation
Badlands	-	1380	2000	186	2000	2000
Miscellaneous land	-	-	2000	1640	2000	2000
Slightly eroded areas	-	-	-	1885	1385	2000
Moderately eroded areas	-	-	-	-	1604	2000
Fallow land	-	-	-	-	-	2000

The inclusion of TM-1 and TM-2 bands is related to the absorption features of green vegetation, while maximum reflection of green plants correspond to the TM-4 band. On the other hand, the incorporation of Landsat TM bands 4, 5 and 7 could be attributed to yellowish and yellowish red soil colors and the silty nature of the topsoils, causing high reflectances in the red and near-infrared regions of the spectrum. The incorporation of thermal band 6 could be related to the presence of rock fragments which affect the thermal conductivity and heat storage capacity of the soil surface. The latter increase linearly with increasing rock fragment content in dry soils (Childs and Flint, 1990). Rocky soils warm up more rapidly than rock free soils, whose dark grey color cause lower digital numbers on the satellite image.

The relatively lower reflectance of fallow land respect to moderately and slightly eroded areas can be explained by roughness of the soil surface because of tillage operations. Tilled soil surfaces, broken into aggregates of several centimeters in diameter, are usually left as fallow land during the dry season, so that a crust is formed to avoid soil moisture losses. These rough surfaces trap the incoming radiation among the coarse particles, causing a decrease in reflectance. Similar findings were reported by Obukhov et al. (1964), who found well structured plow layers to reflect 15-20% less light energy than structureless soils.

Figure 7.37 presents the spatial distribution of the selected erosion classes. Discrimination accuracy of fallow land is low because part of the moderately and slightly eroded areas were allocated to this class.

On the contrary, soil sites corresponding to fallow land were labelled as moderately eroded areas. Also slightly eroded areas were erroneously labelled as badlands, miscellaneous land and fallow lands, with a consequent diminution in overall accuracy. The extent of the selected information classes, corresponding to a total area of 5680 hectares, is shown in table 7.8.

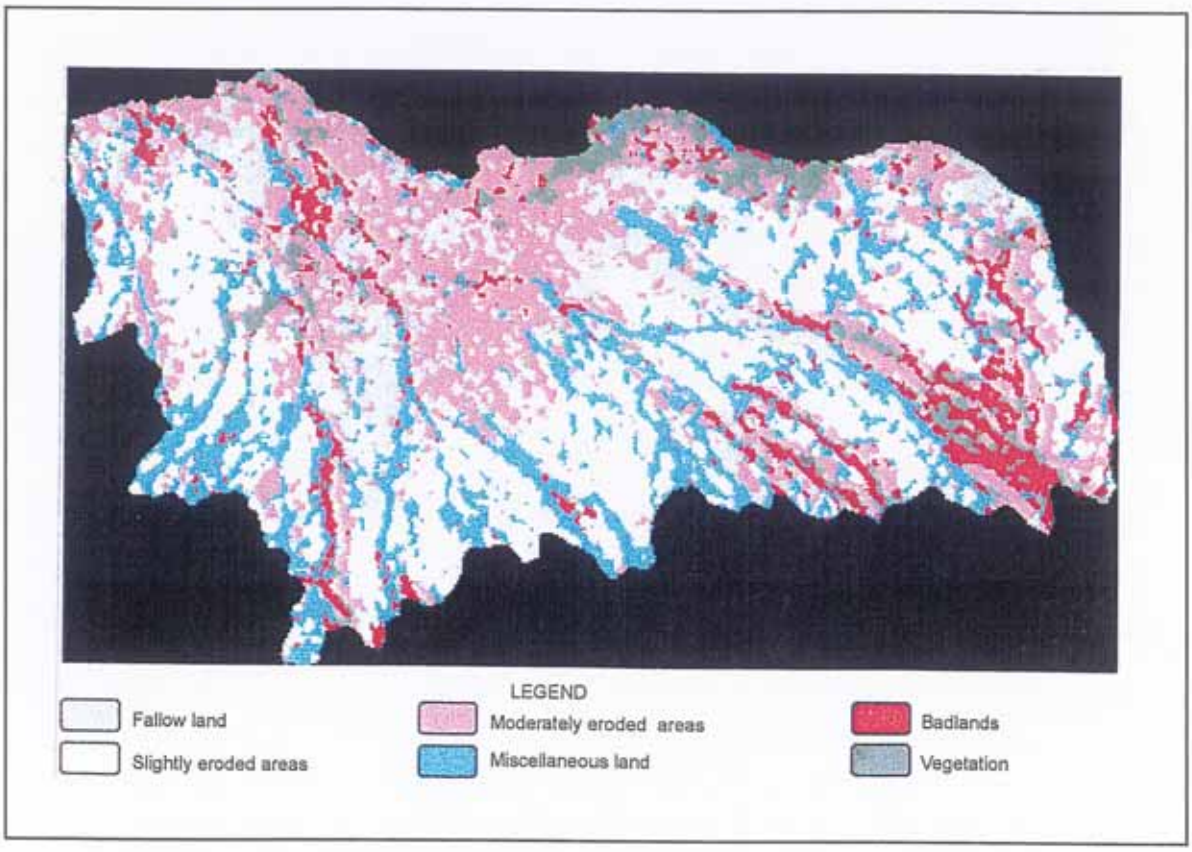

Fig. 7.37: Spatial distribution of eroded areas using Landsat TM data and a maximum likelihood classifier (year 1994).

Table 7.8: Areal extent of the information classes

INFORMATION CLASS	HECTARES
Badlands	543
Moderately eroded areas	1310
Slightly eroded areas	1609
Fallow land	685
Miscellaneous land	1174
Vegetation	359

The most degraded areas are located in the badlands and middle lagunary depressions and, to a lesser

extent, in the distal parts of a dissected depositional glacis. Moderately eroded areas were distributed mainly in the lagunary depressions, but also in the distal and proximal parts of the dissected depositional glacis. Slightly eroded areas predominated on the middle lagunary flats and, to a lesser extent, in the distal parts of the dissected depositional glacis and in the badlands.

In general, fallow land, slightly eroded areas and moderately eroded areas were not spectrally distinct enough to allow for accurate discrimination. Perhaps, soil roughness at a macro-scale is the main factor controlling distinctiveness. The incorporation of microwave data could enhance this soil property and is therefore analyzed hereafter.

(2) JERS-1 SAR and Landsat TM data fusion

(a) Method

After speckle reduction (see chapter 3), the 15 m ground resolution JERS-1 SAR scene was merged to the 30 m ground resolution Landsat TM scene. The data set was resampled to a ground resolution of 15 m, after georeferencing to a common cartographic base. Statistical pattern recognition was applied to allocate the pixels to selected classes. The classes described under point 7.4.2 (1) were used. Badlands were split into two classes, namely badlands proper and steep dissected areas. Badlands were used to label areas with gentle slope, while steep dissected areas referred mainly to the proximal parts of the dissected depositional glacis, southeast of Sacaba. The steep slopes determined a shadow component effecting the reflectance of the badlands. Pixels representative of the considered classes were selected to build up spectral curves and evaluate the spectral behavior in the different wavelengths (fig. 7.38).

(b) Results and discussion

Because information classes did not vary and their spectral behavior in the visible, near-infrared, middle-infrared and thermal ranges was analyzed in the previous section, only the backscattering of the classes, related to the behaviour in the microwave range, will be treated hereafter. The backscattering decreased as follows: fallow land > vegetation > miscellaneous land > badlands > slightly eroded areas and moderately eroded areas (fig. 7.38).

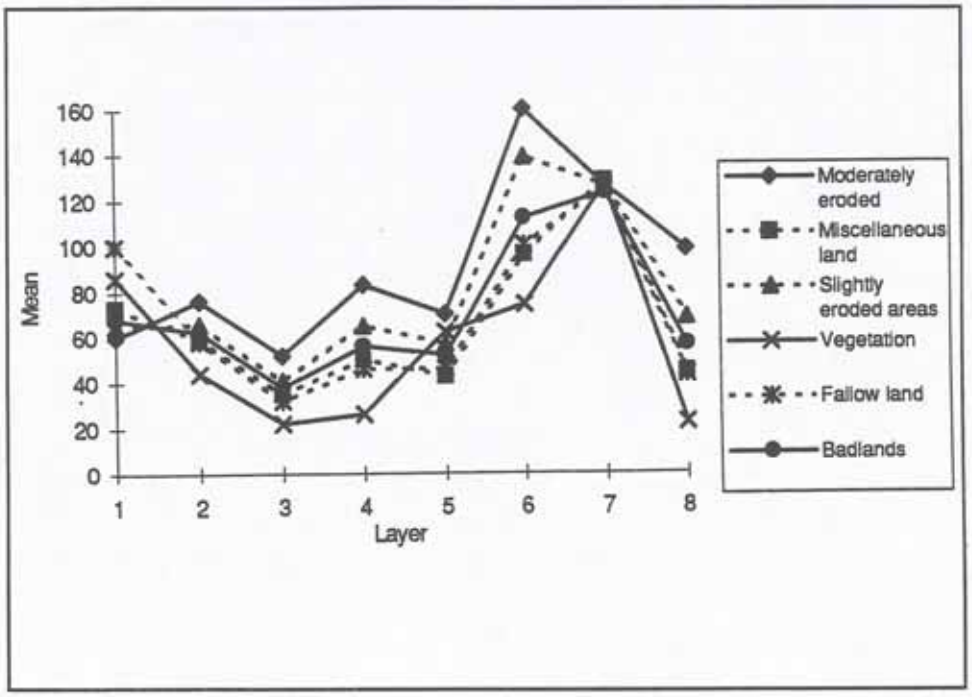

Fig 7.38: Spectral curves of the information classes (microwave, layer 8 and optical data, layers 1 to 7)

Fallow land had the highest backscattering values. The rough surface conditions of the fallow parcels, with large aggregates formed after tillage operations, caused a high amount of energy to backscatter towards the sensor antenna. In the JERS-1 scene, pixels became brighter than in areas of, for example, slight erosion on the TM scene.

In the case of natural vegetation, the incoming wave has usually multiple interactions with ground features such as canopy, trunks and stalks, and produces a volume scattering which relies on the ability of microwaves to penetrate different cover targets and return signals from the surface (Trevett, 1986). The shrubs and trees of the Sacaba valley had high interaction with the incident energy, since the backscattered signal was comparatively the second highest (fig. 7.38).

Rock fragments, in erosion pavements and at the bottom of the ephemeral brooks, presented a relatively smooth surface in the radar sense. Since roughness is a function of the incident wavelength, the surfaces produced by rock fragments were 'rough' for the short wavelengths of the visible and infrared ranges, but relatively smooth for the 23 cm JERS-1 wavelength.

The energy backscattered by badland surfaces was variable but relatively low (fig. 7.38). The signal received by the sensor is the integration of the energy backscattered by the components present within an area of 15 by 15m (resampled pixel size), where surface roughness is very variable due to the heterogeneous composition of the badlands. For example, erosion pavements, natural vegetation and

gullies were mixed with smooth truncated soil surfaces.

Slightly and moderately eroded areas backscattered the lowest amounts of incident energy, with slightly lower values for moderately eroded areas, than for slightly eroded ones. But this relation basically depends on the type of erosional features dominating within the area covered by one pixel. For example, a smooth depositional crust tends to backscatter lower amounts of energy than rilled surface, because the former acts more like a specular surface. Dense rill patterns instead, behave more as rough surfaces, backscattering higher amounts of energy towards the sensor.

The transformed divergence analysis showed the highest separability between classes to occur when taking 8 bands at a time, the JERS-1 band plus Landsat TM bands 1, 3, 4, 5, 6 and 7. Average class separability was 1980. Separability measures lower than 1800 were recorded between spectral plots of badlands and miscellaneous land and between plots of slightly eroded areas and fallow land (table 7.9).

Table 7.9: Transformed divergence analysis to evaluate between-class separability

CLASSES	Badlands	Miscellaneous land	Slightly eroded areas	Moderately eroded areas	Fallow land	Steep dissected areas	Natural vegetation
Badlands	-	1768	2000	2000	2000	2000	2000
Miscellaneous land	-	-	2000	2000	2000	2000	2000
Slightly eroded areas	-	-	-	1746	1764	2000	2000
Moderately eroded areas	-	-	-	-	1998	2000	2000
Fallow land	-	-	-	-	-	2000	2000
Steep dissected areas	-	-	-	-	-	-	2000

Figure 7.39 represents the results of mapping areas subjected to soil erosional processes, fallow land and natural vegetation, using a maximum likelihood classifier and the set of TM bands plus JERS-1 providing the highest between-class separability. To evaluate the contribution of the thermal range to mapping eroded areas, a classification attempt was performed leaving out the thermal band 6. The results were very

poor, especially for badlands which showed to be spread everywhere over the study area. Also fallow land was overestimated. In general, map readability was unsatisfactory.

The post-classification procedure included class merging, application of a majority filter to improve map readability by deleting small patches, and an accuracy assessment by matching the ground reference data with the labels of the classified image.

Table 7.10 shows the accuracy report related to the fusion of JERS-1 and Landsat TM data sets. An overall classification accuracy of 87% was obtained, with 100% reliability in the identification of pixels corresponding to natural vegetation and steep dissected areas. Accuracy in the labelling of pixels related to moderately eroded areas and natural vegetation was 100%. The lowest labelling accuracy was 54%, corresponding to badlands whose extent was overestimated due to the inclusion of moderately eroded areas. The reliability in discriminating moderately eroded areas was only 51%, because the classifier failed to recognize nearly half of the reference data.

Table 7.10: Accuracy report

CLASS NAME	REFERENCE TOTALS	CLASSIFIED TOTALS	NUMBER CORRECT	CLASS RELIABILITY	CLASS ACCURACY
Badlands	20	35	19	95	54
Moderately eroded areas	29	15	15	52	100
Slightly eroded areas	53	50	48	91	96
Miscellaneous land	31	32	28	90	88
Fallow land	62	62	58	94	94
Natural vegetation	4	4	4	100	100
Steep dissected areas	7	8	7	100	88

The incorporation of the microwave data set modified the areal extent of the classes. Badlands and fallow land increased, while moderately eroded areas, slightly eroded areas and miscellaneous land types considerably decreased. Also the areal extent of the natural vegetation was reduced (fig. 7.39).

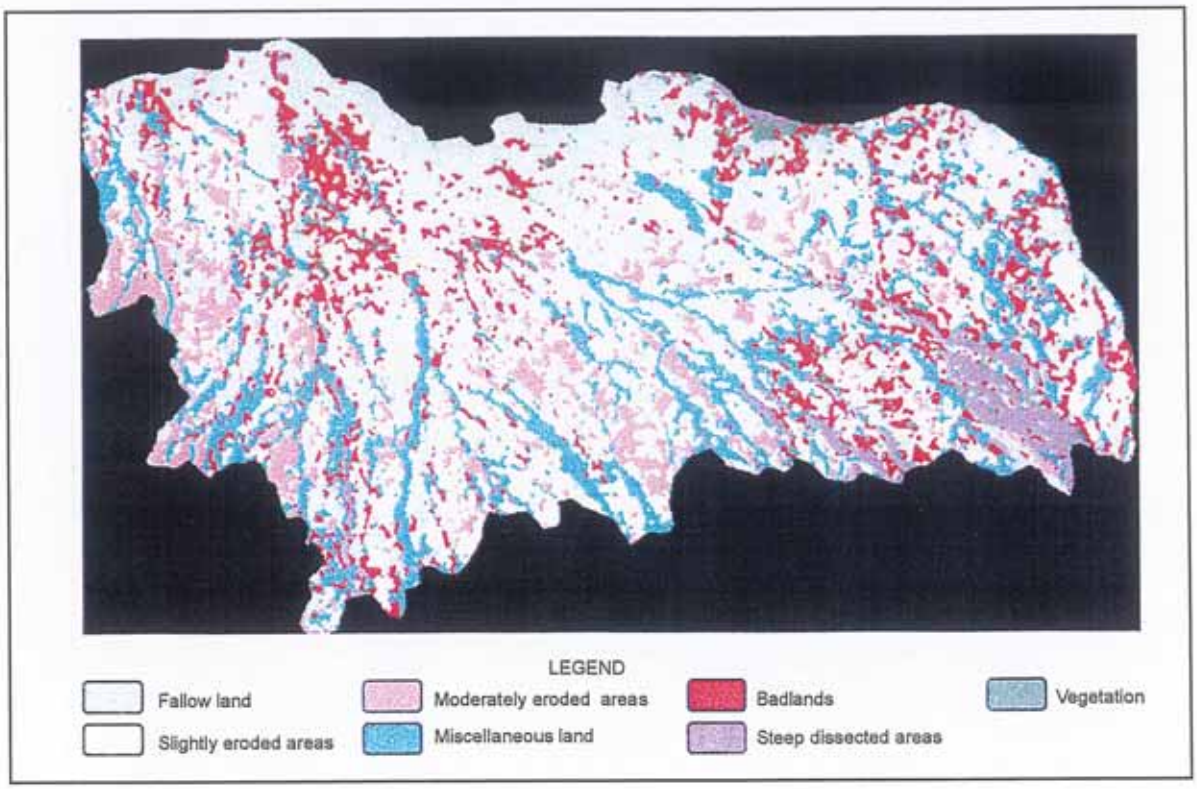

***Fig. 7.39**: Spatial distribution of eroded areas using Landsat TM and JERS-1 data sets and a maximum likelihood classifier (year 1994)*

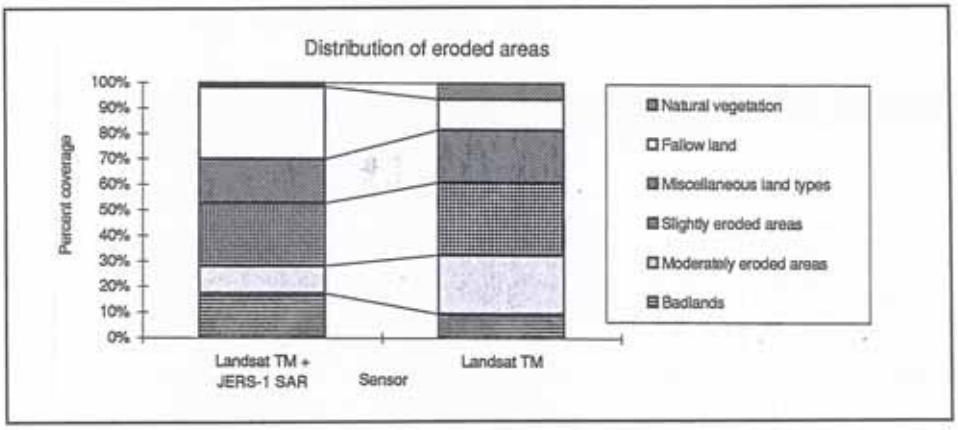

***Fig. 7.40**: Areal extent of the information classes using two data sets.*

(3) Monitoring temporal changes in soil erosion

Figures 7.35 and 7.39 represent the spatial distribution of eroded areas for the dry season of 1976 and 1994. They were matched to evaluate the advances in extent and severity of the erosional processes in the southern and southeastern part of the Sacaba valley for a time interval of 18 years. The comparison of both maps indicates a trend of non-eroded areas to be affected by slight erosion. This is especially

notorious in the proximal part of the dissected depositional glacis south of Sacaba. Moderately eroded areas have extended in the southwestern part of the valley. Also the southern piedmont glacis shows increment in erosion degree.

Globally, non-eroded and slightly eroded areas decreased by 12% and 4% respectively. In contrast, badlands almost duplicated their extent, increasing from 9 to 17% in a period of 18 years. Similarly, moderately eroded areas triplicated their extent, from 3 to 11% of the area under study (fig. 7.41).

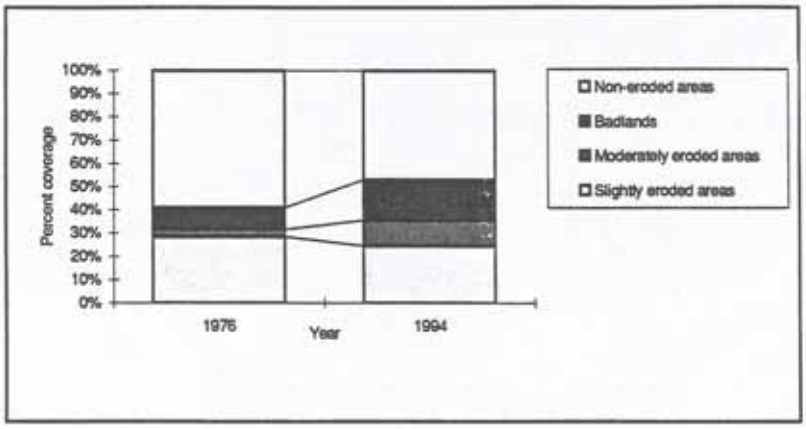

***Fig. 7.41**: Temporal changes in the extent of eroded areas.*

7.4.3 Estimating ground cover proportions by linear mixture modeling

(1) Method

The procedure followed to discriminate and map ground cover proportions at a sub-pixel level using a linear mixture model, is illustrated in figure 7.42. The model produces image outputs in which pixel intensities reflect the proportion of a certain surface component within one pixel. The basis and assumptions of the linear modeling are described in chapter 3. The individual proportion maps can be used as input in a geographic information system for further spatial modelling of erosional processes and as parameters of exploratory models for prediction. The error image is used as input to evaluate the mapping accuracy of surface component proportions.

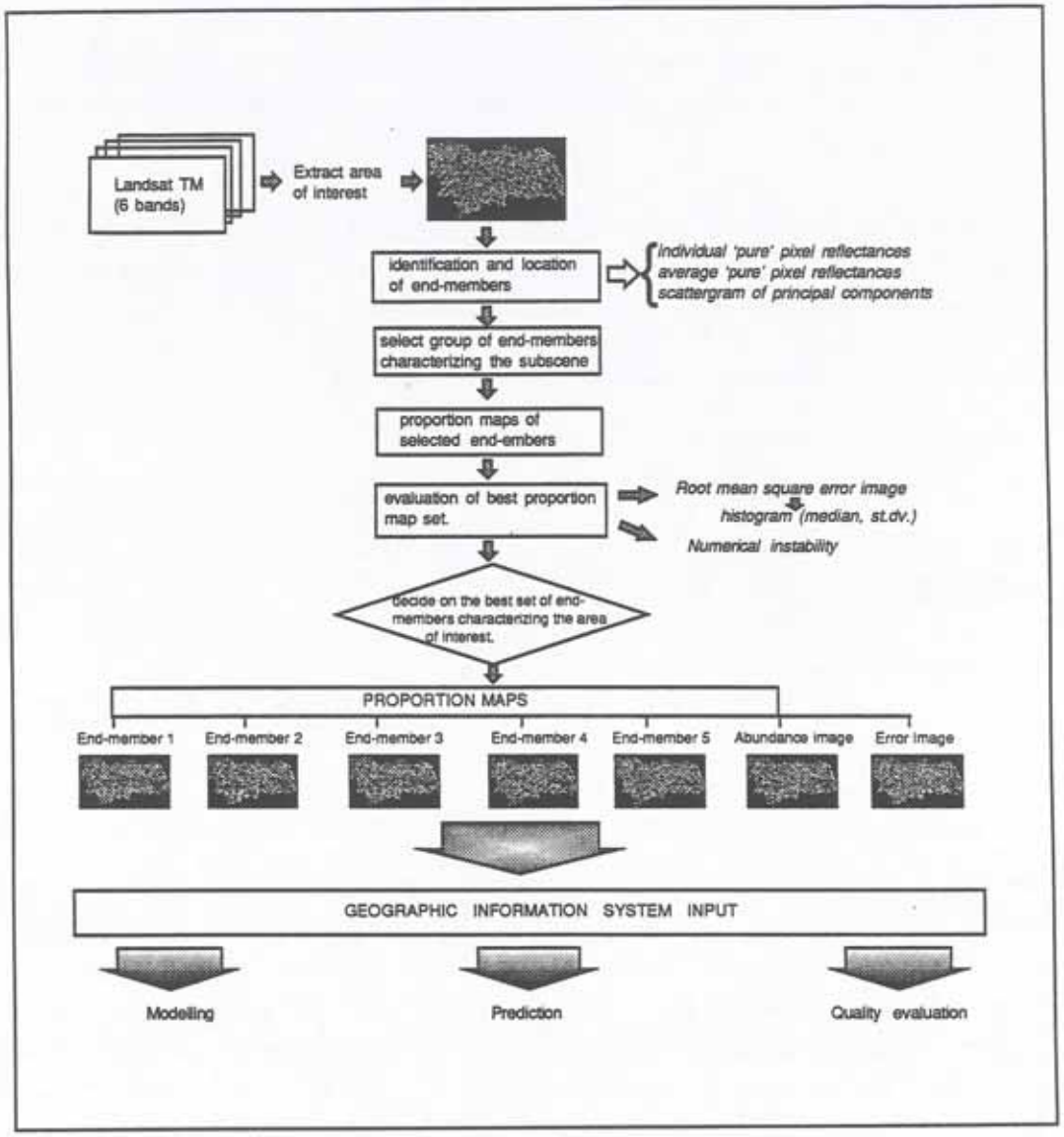

Fig. 7.42: The linear mixture model

The linear mixture model was applied in the southern area of the Sacaba valley. The model allowed to use up to five surface components to characterize the selected area, since six bands (1, 2, 3 4, 5 and 7) of the Landsat TM sensor were used as inputs. As the linear mixture model is applied by a least square fitting of the end-members to all pixels in the image, the software requires end-members to be (n - 1) the number of inputs to solve the equations (see chapter 3).

(2) Identification of surface components (end-members)

Six surface components were identified on Landsat TM false color composites (3,2,1 and 4,3,2) scenes. Aerial photographs at scale 1:25000 and field data were used to locate 'pure' pixels representing the end-

members. Selected end-members characterizing the surface cover in the south of the Sacaba valley, were: natural vegetation, gullies, yellowish brown soils, yellowish soils, whitish topsoils and miscellaneous land.

(a) Natural vegetation (class 1): native weeds, shrubs and trees colonizing moderately and extremely eroded areas (badlands) as well as ephemeral brooks. They were assumed to indicate moderate and severe erosion degrees.

(b) Miscellaneous land (class 2): beds of ephemeral brooks and erosion pavements typical in badlands, resulting from the removal of finer materials from gravel lenses of depositional sequences. Rock fragments of variable sizes and shapes, mainly from greenish-gray sandstones, provided comparatively high reflectance values in the TM-2 (green band). Pure pixels, 100% occupied by this surface feature, were selected in the ephemeral brooks and sampled to estimate the proportions of rock fragments present in badland areas. Presence of these surface features in areas other than brooks were related to badlands (extreme erosion).

(c) Whitish topsoil surfaces (class 3): these overall highly-reflecting surfaces were related to scarcely vegetated areas with truncated topsoils, where soil degradation features such as depositional crusts, coarse loamy textures and very light colors caused by low organic matter contents dominate. Erosion is moderate and severe.

(d) Reddish brown soils (class 4): areas with none to very scarce vegetation cover, observed on the dissected depositional glacis in the southern piedmont of the Sacaba valley. Formed from alluvial depositions of siltstones and greenish-gray to light brown sandstones, soils have a reddish brown color, determining high light reflection in the range of 630- 900 nm (TM-3). Field-recorded reflectances showed high light reflection in this region of the spectrum to be related to the redness of the topsoil, low organic matter contents, loamy textures and low percent coverage of rock fragments and vegetation (see sections 6.4.2, 7.3.1 and 7..3.2). They were related to non-eroded areas.

(e) Yellowish soils (class 5): bare or scarce vegetated topsoil surfaces, having strong absorption in the blue band (TM1) and relatively high reflection in the yellow and red wavelengths (550 -700 nm), related to bands TM-2 and TM-3. Relatively bright color chromas and/or values (5/4, 6/4, 7/3) determine high reflectances and are indicative of very low organic matter contents. Color brightness in the visible range of the spectrum was also related to the presence of smooth depositional crusts (section 7.3.2). These top surfaces corresponded to slightly eroded areas.

(f) Gully areas (class 6): extremely eroded areas, with evidence of removal of the surface horizons and complex topography due to the presence of gullies, rills and surface erosion pavements, where agricultural activities cannot be undertaken. Their spectral signature is a mixture of the reflectances produced by erosion pavements, natural vegetation and whitish eroded soils. In steep sloping areas, shadow effects the

spectral behavior of the badlands.

(3) Location of the end-members

The application of the linear mixture model required to identify 'pure' pixels corresponding to the selected end-members. Among the various methods commonly used to determine end-members from the satellite image, three were selected: (a) identification of one 'pure' pixel representing a particular surface component from false color composites; (b) average of 'pure' pixels to characterize a particular end-member; and (c) a method based on principal components (Smith et al., 1985). The latter assumes that pure end-members lie at the extremes of the distribution of pixel signatures in the principal component features space, the number of extremes equalling the number of spectrally distinct surface components. The extremes are revealed by plotting a scattergram of the first two principal components. Thus the principal components were calculated and plotted for the area of interest. Spectrally distinct end-members were determined and used to locate the corresponding pixels on the image, thus allowing the extraction of end-member signatures from the original spectral bands. For techniques (a) and (b), pixels representing the surface components were selected from false color composites. The subsequent step consisted in computing the proportion maps.

(4) Spectral unmixing and proportion maps

Constrained unmixing was used (Smith et al., 1994; see also chapter 3), thus forcing the proportion estimates for each end-member to be greater or equal to zero and the sum of the abundances less or equal to one. Four spectral unmixing approaches were tested, differing in the way the 'pure' pixels for each end-member are selected and in the type of surface component considered. Although six end-members were determined, only five at a time could be used. In the first test, one 'pure' pixel per end-member was selected, considering natural vegetation, miscellaneous land, whitish topsoils, brownish red soils and gully areas as end-members. The same surface components were adopted in the second approach, but the spectral signature of the end-members was determined by averaging pixel values related to a particular end-member. The third approach was also based on averaging pixel values, but gully areas were replaced by yellowish soils. Finally, in the fourth approach, the purest pixels of each surface component were selected using principal component analysis and considering natural vegetation, whitish topsoils, yellowish soils, brownish red soils and gully areas as the end-members.

The output of the unmixing analysis consisted in a proportion map for each of the considered surface components, one image representing the sum of all the abundances and a root-mean-square (RMS) image. The RMS image represents the error between the original, mixed spectrum and the best-fit spectrum computed from the resulting end-member abundances. The solution of the unmixing is considered valid, when the abundance values across the image are mostly between one and zero, the average RMS error is low and the RMS error image shows a low spatial correlation (van der Meer, 1995).

Histograms of the four error images were built up to compare the standard deviation, mean and median.

These parameters were used, in addition to the analysis of numerical instability, to select the best set of end-members and the best 'pure' pixel selection procedure. The analysis of numerical instability refers to the percentage of image pixels whose abundances violate the imposed constraints and generally indicate that the end-members used do not closely match some region of the image (SIPS, 1992). This drawback can be eliminated either by reducing the area of interest, so that only surfaces represented by the selected end-members will be considered, or modifying the end-members themselves. Table 7.11 resumes the results of these analyses.

Table 7.11: Analysis of the RMS error image, numerical instability and abundance image for the considered approaches

METHOD	BRIEF DESCRIPTION	N.I.(1)	ERROR IMAGE		ABUNDANCE IMAGE		
			Mean	St. dv.	Mean	St.dv.	Median
A (Fig. 7.43)	One 'pure' pixel per end-member. Classes: 1,2,3,4,6	0.74	1.86	2.16	59.9	48.0	99.8
B (Fig. 7.44)	Average 'pure' pixels per end-member. Classes:1,2,3,4,6	0.43	1.46	1.91	59.5	47.7	95.1
C (Fig. 7.45)	Average 'pure'pixels per end-member. Classes:1,2,3,5,6	1.06	1.28	1.79	58.5	47.0	91.2
D Fig. (7.46)	End-members selected from extreme values of scattergram done with PC1 and PC2(*). Classes: 1,2,3,4,5	0.52	5.98	5.96	60.9	99.8	48.5

(*) PC: principal component bands

(1) N.I.: numerical instability, expressed as percentage of the image pixels.

Classes: (1) Natural vegetation; (2) Miscellaneous land; (3)Whitish topsoil surfaces; (4) Reddish brown soils; (5) Yellowish soils ; (6) Gully areas

According to table 7.11 the use of the average pure pixel reflectances to build up the spectral signature of classes 1, 2, 3, 4 and 6 (method B) provided the best characterization in the surface components of the southern part of the Sacaba valley. Method C produced the highest percentage of image pixels violating the imposed constraints (see chapter 3), while the lowest values corresponded to method B, which has also one of the lowest mean and standard deviation errors. Therefore, method B was assumed to best characterize the surface components of the selected area.

The median of the abundance images shows that, in 95 % of the cases, the individual pixel compositions were explained by the selected surface components. Spatial distribution of the errors is also a factor to be considered during the evaluation of the results. A high spatial correlation of errors to certain area indicates that this particular region was not properly characterized by the selected end-members. Figure 7.44(7) represents the error images inherent to the different approaches.

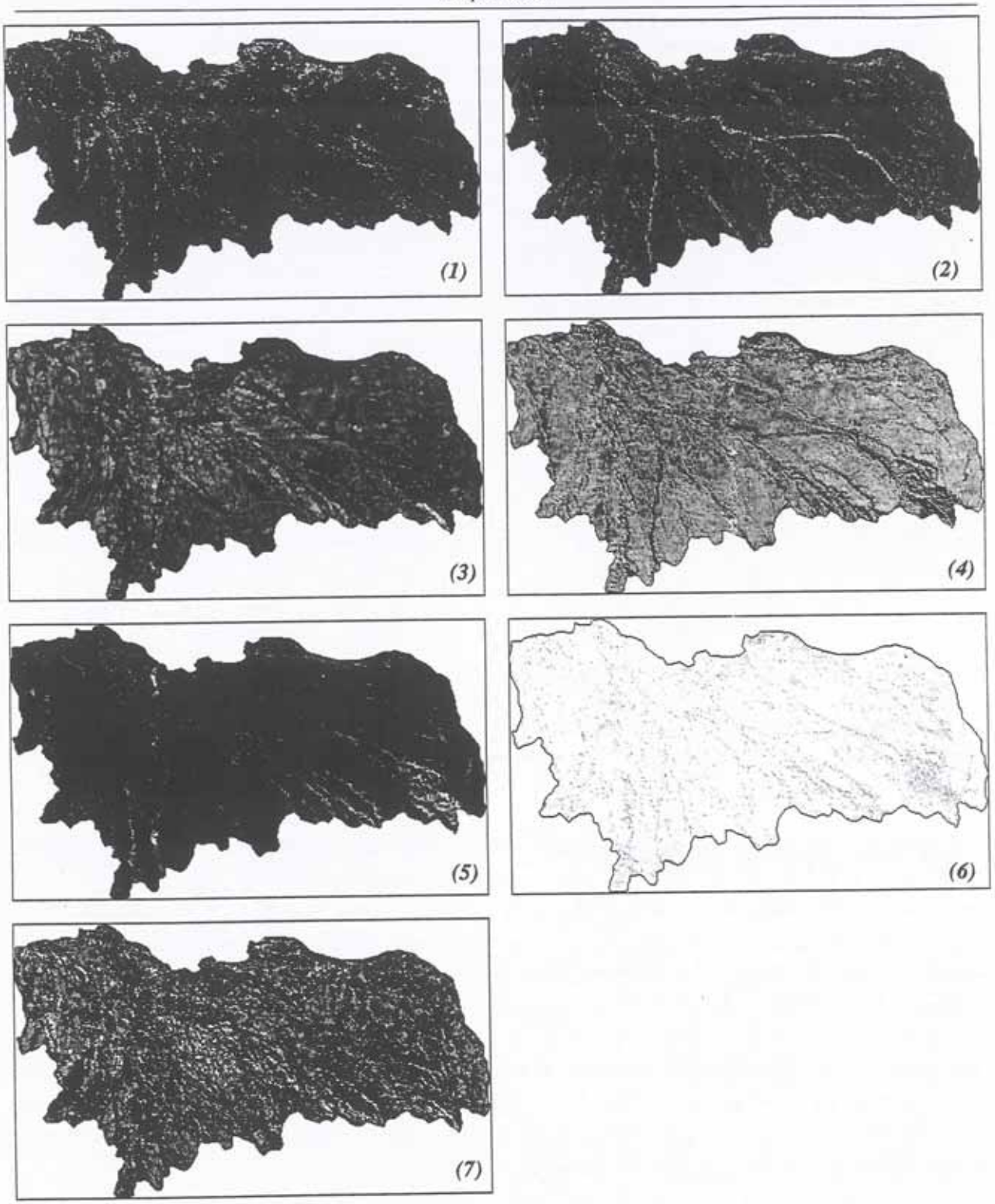

***Fig. 7.43**: Spectral unmixing using one 'pure' pixel to characterize end-members. Classes: natural vegetation (1); miscellaneous land (2); whitish topsoil surfaces (3); reddish brown soils (4) and gully areas (5). Additional: abundance image (6) and error image (7). Method A.*

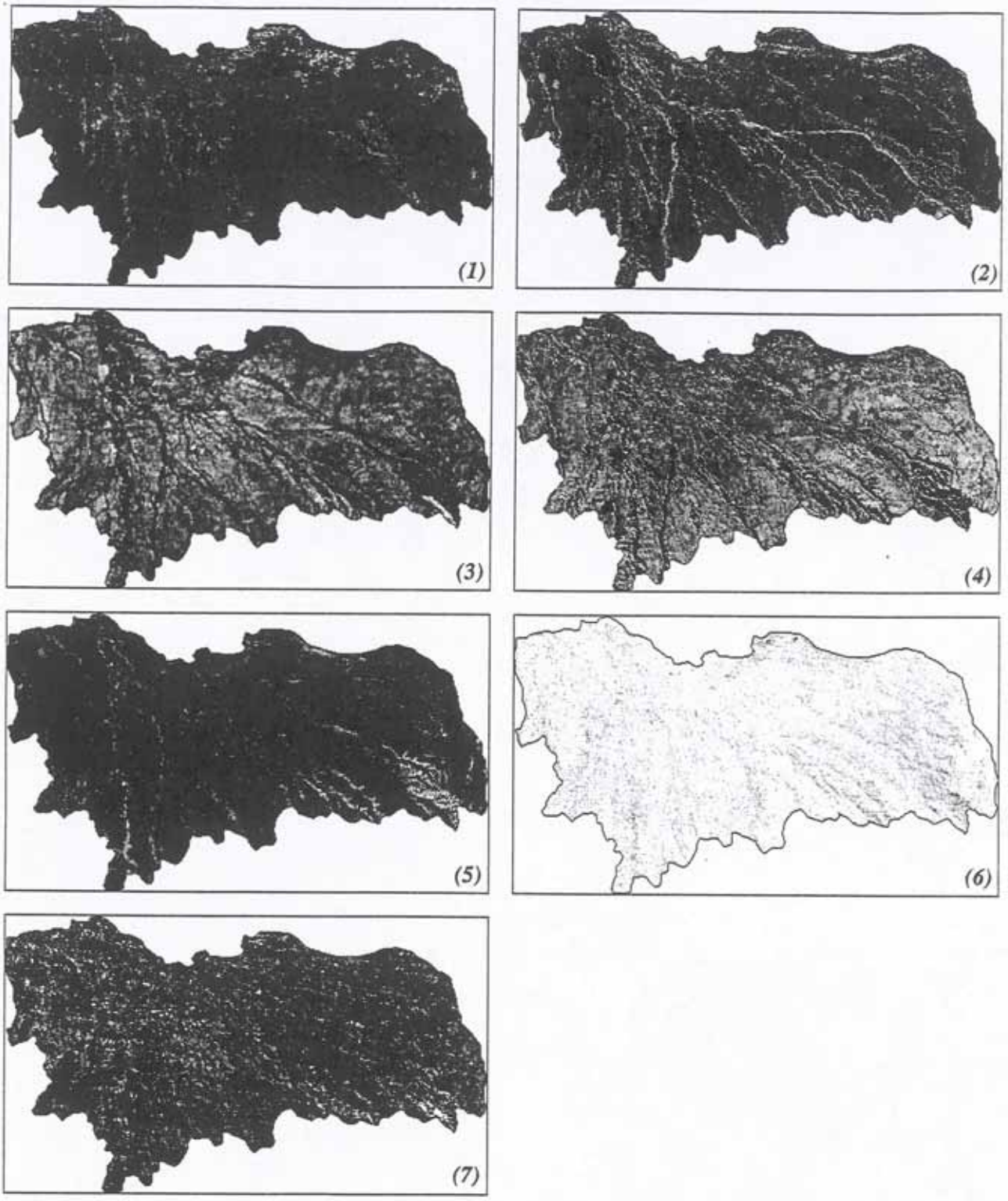

Fig. 7.44: Spectral unmixing using average pixel reflectances to characterize end-members. Classes: natural vegetation (1); miscellaneous land (2); whitish topsoil surfaces (3); reddish brown soils (4) and gully areas (5). Additional: abundance image (6) and error image (7). Method B.

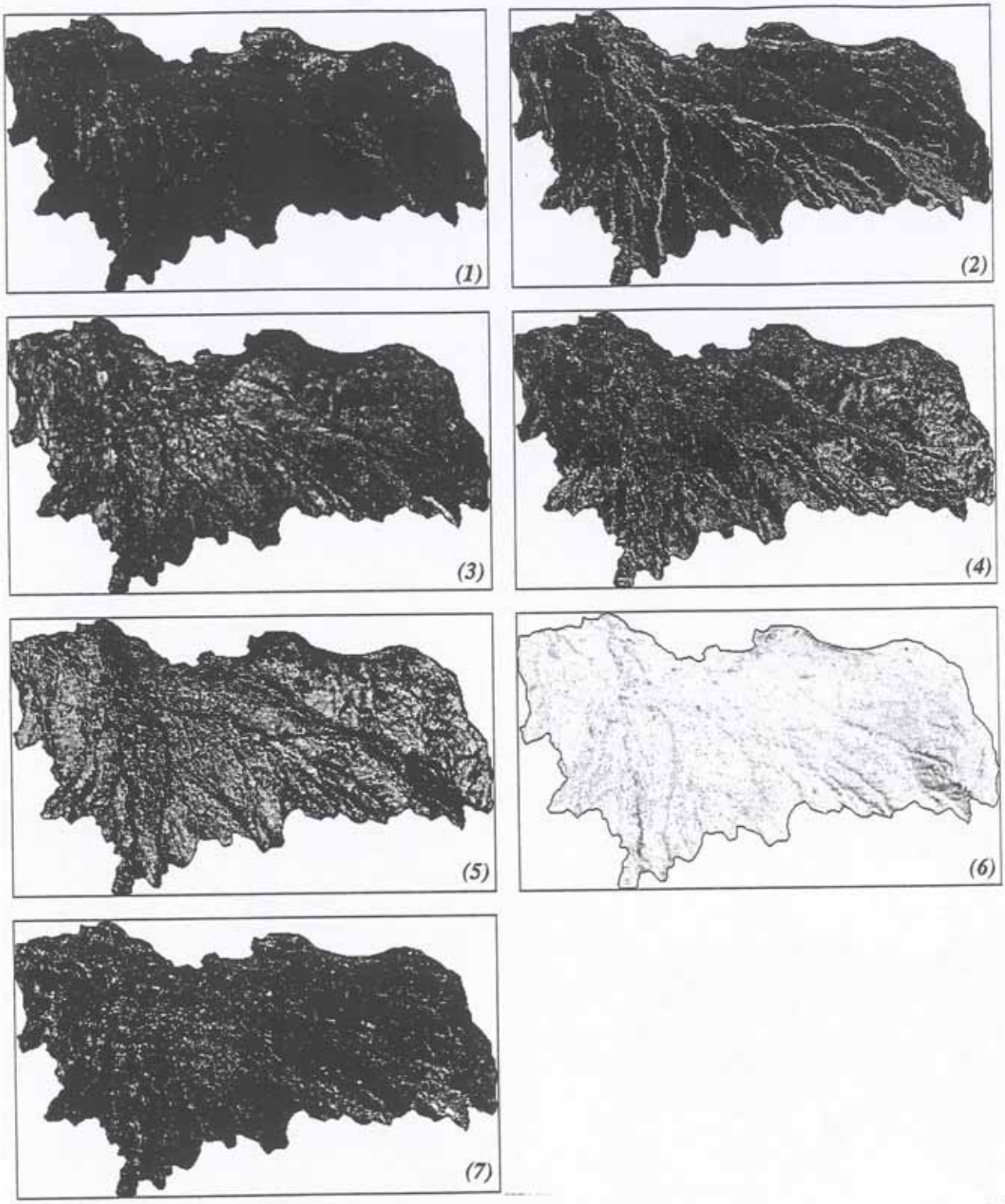

Fig. 7.45: *Spectral unmixing using average pixel reflectances to characterize end-members. Classes: natural vegetation (1); miscellaneous land (2; whitish topsoil surfaces (3); yellowish soils (4) and gully areas (5). Additional: abundance image (6) and error image (7). Method C.*

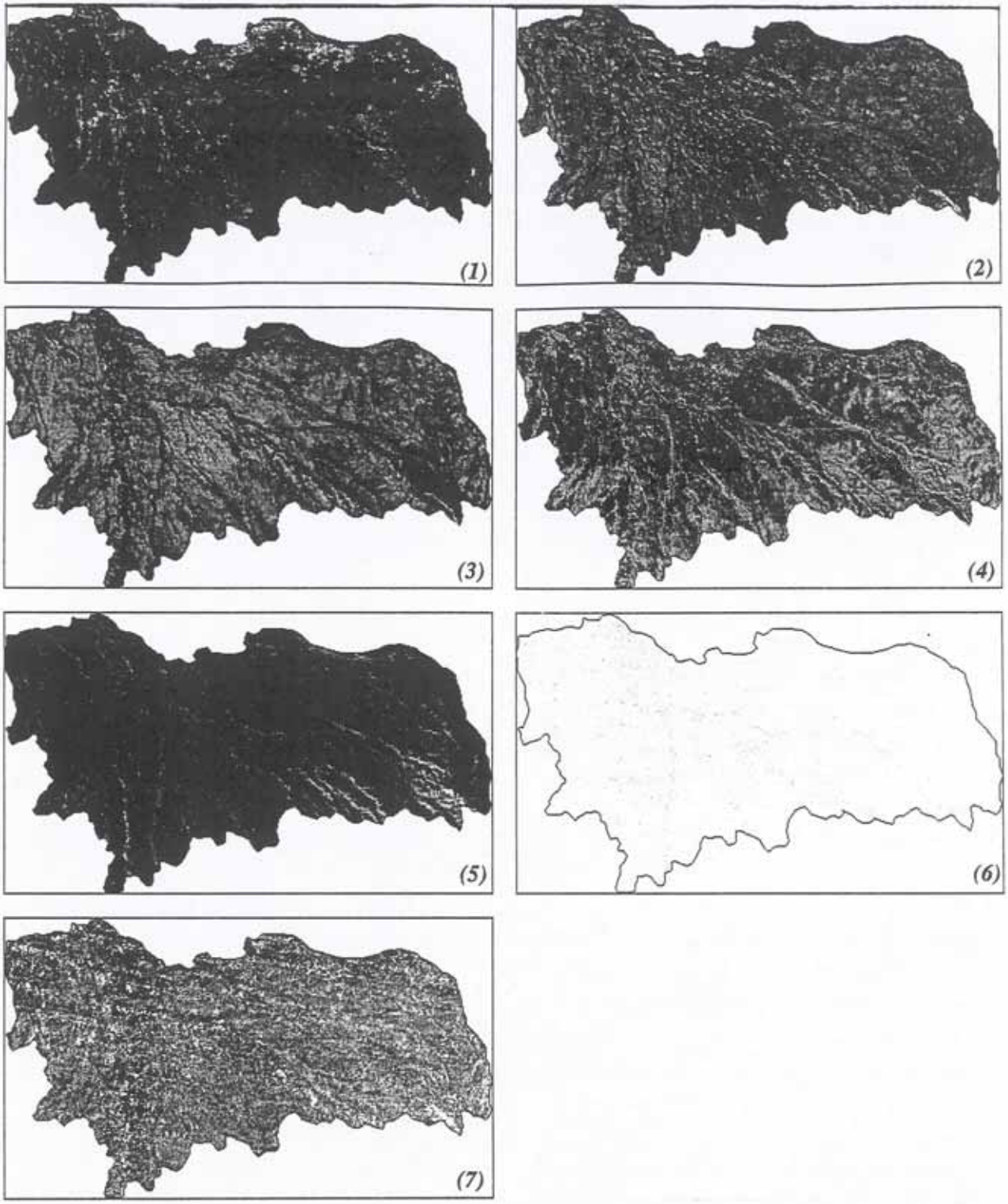

Fig. 7.46: Spectral unmixing using scattergrams from principal components to select end-members. Classes:natural vegetation (1); miscellaneous land (2); whitish topsoil surfaces (3); reddish brown soils (4) and gully areas (5). Additional: abundance image (6) and error image (7). Method D.

(5) Application of linear mixture modelling to map eroded areas

The spatial distribution of (1) natural vegetation, (2) miscellaneous land, (3) whitish topsoils, (4) brownish red soils and (5) gully areas is displayed on figure 7.44 (1 to 5).
Natural vegetation and some agricultural parcels under irrigation are spread east of the Sacaba town. Areas dominated by natural vegetation were delineated mainly along ephemeral brooks, but also in some isolated plots in the piedmont and valley landscapes where farmers use to line the parcel boundaries with eucalyptus which controls the spectral signature.

Rock fragments as miscellaneous land, comprising the riverbed of ephemeral brooks as well as the erosion pavements of badlands, were clearly distinguishable. High proportions of rock fragments were mapped in the Canal Mayu and Crespo Mayu riverbeds and in the badlands near the Sacaba town, the latter being related to surface erosion pavements.

Whitish topsoils, related to moderately eroded areas, dominated in some parts of the lagunary depressions and in the proximal parts of the dissected depositional glacis. Unlike the former two components, they did not show specific geographic distribution and were present in different proportions, reflected by grayish tones, all over the southern part of the Sacaba valley. They were less frequent in the southeastern part, occupied by reddish brown soils.

The reddish brown soils, related to non-eroded areas, have no specific location either. Spatial distribution on the landscape is of medium to low frequency. They do not occur in steep dissected areas.
Lastly, steep dissected areas dominated in the southeastern part of the Sacaba valley, reflected in figure 7.44(4) as whitish tones. The whiter the color, the higher the proportion of the end-member within a pixel.

There is an agreement between the results obtained by using statistical pattern recognition on either the Landsat TM data set alone or on the data set provided by the fusion of Landsat TM with JERS-1 SAR (figures 7.37 and 7.39), whenever the proportion of a certain component clearly dominates within one pixel. This is true mainly for steep dissected areas, miscellaneous land and the badlands located near the Sacaba town. Higher proportions of vegetation resulted in unmixing pixel compositions. Fallow land is composed by proportions of moderately eroded areas (eg, whitish topsoils) and non-eroded areas (eg, reddish brown soils). In addition, areas labelled as slightly eroded are mainly dominated by reddish brown soils and, to a lesser extent, whitish soils.

Therefore, low classification accuracies obtained by using statistical pattern recognition on the Landsat TM data set and mainly related to insufficient discrimination between slightly and moderately eroded areas and badlands, were not only due to spectral similarity between the classes, but also to the mixture of the surface components within one pixel. In such a case, the solution resides either in using unmixing techniques, as done here, or improving the spatial resolution of the data set.

(6) Model validation

The root-mean-square image, representing the error between the original and the best-fitted spectrum computed from the resulting proportions of end-members, was used as input in a geographic information system to verify the spatial distribution of the error ranges within the area (fig. 7.42). The image was re-classified into the following error ranges: 0, 1, 10, 30, 50 and > 50%. Table 7.12 presents the area in hectares and the percentage of the error ranges resulting from unmixing.

Table 7.12: Error levels resulting from unmixing

ERROR RANGE (%)	AREA (HECTARES)	AREA (%)
0 - 1	2068	36
1.1 - 10	3582	63
10.1 - 30	28	1
> 30	0	--

in 36% of the classified area, the error between original and best-fit output proportion maps was equal or lower than 1%. In 63% of the area, end-member proportions were mapped with an error between 1 and 10%. Only 1% of the mapped area had errors between 10 and 30%, corresponding to areas with steep slopes and complex topography in the southeast of the valley. The selected components were not sufficient to fully characterize this particular area. In general, errors equal or lower than 10% are spread all over the area, providing thus a proper characterization of the surface components. However, the inclusion of a sixth end-member could have improved the results. Unfortunately, the SIPS software constrains the number of end-members to be one less than the number of input bands.

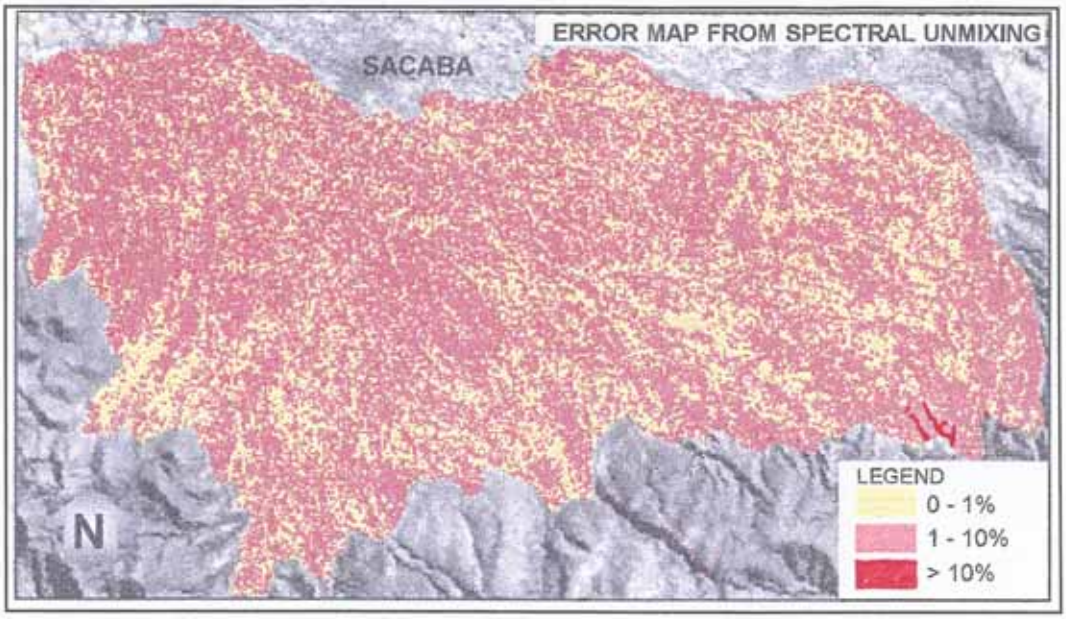

Fig. 7.47: Spatial distribution of the error in the unmixed area.

7.4.4 Conclusions

The incorporation of microwave data improved the separability and thus the discrimination among spectral plots representing fallow land and moderately as well as slightly eroded areas. Surface roughness resulting from soil ploughing caused high backscattering at a macro-scale level. This distinctive feature in the microwave region allowed separation of classes with similar spectral behavior in the visible and infrared wavelengths.

None of the approaches dealing with data fusion provided high class accuracy for badlands, meaning that pixels corresponding to other classes were included. This is not unexpected, since badlands are heterogeneous areas, composed by mixtures of natural vegetation, erosion pavements and eroded topsoils. Thus, this is not a problem related to spectral confusion, but to the presence of more than one surface component within the area covered by a single pixel. Such a problem cannot be solved by the synergy of the different wavelengths. The solution, instead, reside in performing spectral unmixing of the surface components and computing their proportions within a pixel.

7.5 FUZZY KNOWLEDGE-BASED EXPLORATORY MODELS

7.5.1 The concept

Empirical models were designed to answer common user's questions such as:

(a) What is the hazard to accelerated soil erosion in area 'A' , located in the distal part of a dissected depositional glacis, with a slope of about 20%, vegetation coverage less than 30% and 60% of rock fragments on the terrain surface?

(b) What degree of erosion can be expected to occur in an area where the vegetation cover is lower than 80%?
(c) What is the best set of soil degradation indicators to predict soil erosion hazard in a selected area?
(d) Where high erosion can be expected to occur?

Such models explore cause-effect relationships on the basis of the general knowledge about causes and the specific relation between processes and indicators of water erosion in the Sacaba area. The models were designed to investigate the susceptibility of specific areas to erosion by incorporating expert knowledge, in the sense that information on soil properties and/or landscape elements assumed to control accelerated soil erosion could be incorporated into the modelling process. The models are therefore considered region-oriented and exploratory. Fuzzy boundaries were applied to rank the landscape factors, used in modelling the likelihood of an area to be affected by different erosion degrees. For instance, if the user observes highly eroded areas to be strongly related to slope percentage, landscape position and surface rock fragments, these landscape factors can be used to 'explore' the susceptibility to erosion hazard. The model can be formulated as a state factor equation, similar to the established by Jenny (1980) for soil formation or by Vasquez and Zinck (1994) to model gully distribution, such as:
Hazard to accelerated erosion = f (Climate, A, B, C....n)
where A, B, C ... n represent erosion-promoting landscape elements, together with climate, a non-differentiating factor in the study area.

Crisp or fuzzy values for the landscape factors can be extracted from a geographic database where laboratory determinations, field observations and other ancillary data are stored as tables (see chapter 3). By querying the database, the user can extract the data related to a particular parameter (eg, soil property). Proportion maps derived from fuzzy classifications or spectral mixture modelling of remote sensing data are also possible inputs. Information on landscape position, lithology or predominant soil type can be derived from geopedologic maps. Slope gradients can be either obtained from field measurements or from a digital elevation model.

Not all the model inputs are however quantitative, needing therefore the use of linguistic variables such as 'very low', 'low', 'medium', 'high'. These variables have to be mapped into a range of numbers, where the user defines a serie of basic parameters required to build up a membership function representing, for example, the linguistic variable 'moderate'.

The drawback of the exploratory models resides in the fact that a considerable expert knowledge about the erosion causes in the area and general understanding about the erosional process itself are required. Erosion indicators must be correctly related to erosion severity and the most appropriate set of landscape factors related to accelerated soil erosion must be found.

7.5.2 Exploratory models to assess erosion hazard

The exploratory models require the expertise to decide on the following items:

(a) erosion-related landscape elements

(b) the primary terms to represent the susceptibility to soil erosion hazard (eg, low, moderate, high)

(c) type and set of parameters of the membership function. The function is used to compute the certainty factor of the erosion-related parameters to the fuzzy sets representing hazard degrees (low, moderate, high).

(d) the fuzzy production rules (IF-THEN statements). They are implemented by means of fuzzy operators (Zadeh, 1965).

Soil erosion hazard was ranked in five classes, namely very low, low, moderate, high and very high. Three fuzzy sets (low, moderate and high) were determined and the qualitative labels 'very low' and 'very high' were derived by concentration of the fuzzy membership functions low and high, as described by Zadeh (1965), Schmucker (1980) and Binj et al. (1995).

(1) The landscape elements

Vegetation cover percentage, rock fragment density, abundance of whitish topsoils, reddish brown topsoils assumed to reflect the absence of erosion, landscape position and slope gradient were the landscape elements selected to map soil erosion hazard. The inputs for the first four elements were proportion maps derived from the spectral unmixing of a Landsat TM data set, while landscape position was obtained from the geopedologic map and slope gradient computed from a digital elevation model.

High density of vegetation and rock fragments covering the soil surface and high proportions of reddish brown soils were assumed to be related to low soil erosion hazard. On the contrary, high proportion of whitish topsoils, related to current moderate erosion, was hypothesized to reflect a high erosion hazard.

Slope gradient was difficult to model because there was no clear-cut relationship between slope steepness and erosion severity. Field observations and interpretation of aerial photographs showed development of badlands in flat lagunary depressions, with slope percentages lower than 2%, but also in steeper areas with slopes greater than 10%. The photo-interpretation map, delineating areas subjected to variable degrees of soil erosion (fig.7.35), was overlaid onto the slope map derived from a digital elevation model. The overlay revealed that moderate and slight erosion coincided with slope ranges from 2 to 10%. In flatter positions, high erosion might occur in concave topography and alluvial-lagunary materials (see chapter 5). As a consequence of the former, two intervals were selected to correlate slope with high erosion susceptibility, that is 0 to 2% and greater than 10%.

(2) The membership functions

The next step consisted in computing the membership degree of the selected parameters to the fuzzy set representing 'low', 'moderate' and 'high' hazard of accelerated soil erosion. A S-shaped function, as

described by Dombi (1990), was used to determine the degree of membership of the parameters. This was a crucial step, because the membership degree of the selected landscape elements to the low, moderate and high erosion hazard sets depended on the correct determination of the parameters characterizing the membership function (interval, sharpness and inflection points) or the ranges to be correlated to a certainty factor.

Figure 7.48 illustrates the membership functions designed for slope gradient, percentage of vegetation cover, rock fragments, whitish topsoils and reddish brown soils. Table 7.13 contains the values used to represent the membership functions in terms of sharpness, inflection and intervals. Additionally, ancillary data were used to determine the susceptibility of the landscape positions to low, moderate or high erosion hazard. This knowledge was expressed by linguistic variables (eg, very high, low, very low), which were latter on translated into certainty factors (table 7.14).

Table 7.13: Parameters used to compute the membership functions

LANDSCAPE ELEMENT	SHARPNESS			INFLECTION			INTERVAL (%)			STANDARD POINT (%)		
FUZZY SETS	LOW	MOD	HIGH	LOW	MOD	HIGH	LOW	MOD	HIGH	LOW	MOD	HIGH
Rock fragments	5	3	4	0.65	0.7	0.7	0-100	10-90	0-100	100	50	0
Vegetation	5	3	5	0.65	0.8	0.65	0-100	0-100	0-100	100	50	0
Reddish brown soils	4	3	4	0.6	0.7	0.7	0-100	0-100	0-100	100	50	0
Whitish topsoils	3	3	4	0.8	0.7	0.4	0-100	0-60	0-100	0	40	100
Slope	3	3	4	0.8	0.4	0.8	0-12	1-9	0-12	0	5	0, >10

Table 7.14: Certainty factors of the landscape positions related to low, moderate and high erosion hazard

LANDSCAPE POSITION	LOW	MODERATE	HIGH
Proximal part of a dissected depositional glacis (Pi111)	0.8	0.7	0.4
Central part of a dissected depositional glacis (Pi112)	0.6	0.7	0.1
Distal part of a dissected depositional glacis (Pi113)	0.6	0.6	0.7
Middle lagunary flat (Va112)	0.7	0.9	0.8
Lower lagunary flat (Va113)	0.6	0.7	0.1
Badlands (Va115)	0.6	0.7	0.9

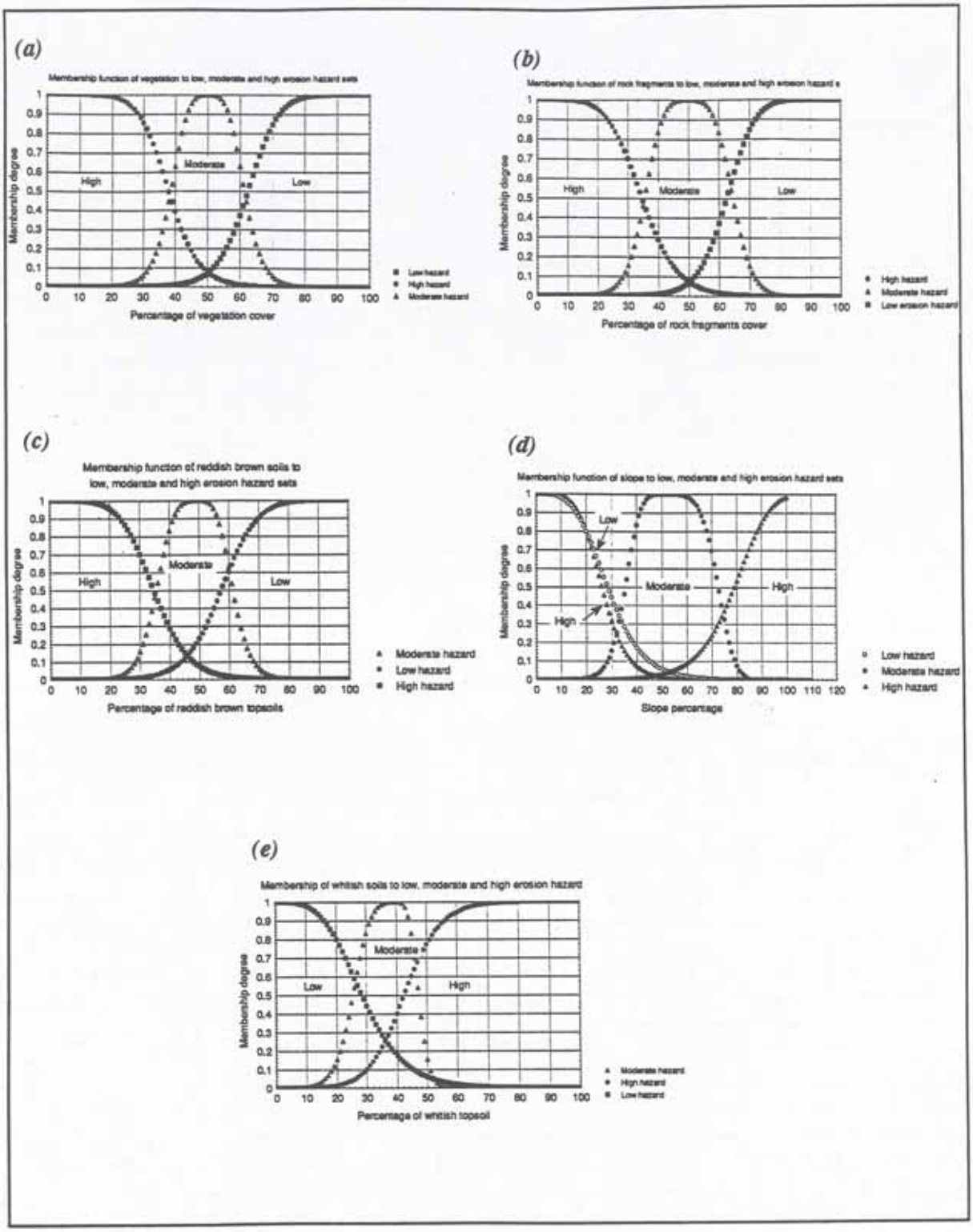

Fig. 7.48: Membership functions of (a)vegetation coverage; (b) surface rock fragments; (c) whitish topsoils; (d) reddish brown soils; and (e) slope gradient to fuzzy sets of low, moderate and high erosion hazard.

(3) Model implementation within a geographic information system

The model was implemented in the ILWIS information system. Five ranges were derived from the membership functions shown in the figure 7.48 for each of the selected parameters (percentage of vegetation, surface rock fragments, whitish topsoils, reddish brown topsoils and slope). The ranges were ranked from 1, expressing very low erosion hazard, to 5 characterizing the susceptibility of an area to very high erosion. For example, if the vegetation covers between 100 and 75% of the soil surface, the susceptibility to erosion is considered 'very low' (eg, the membership degree to the low erosion set was > 0.9) and the code 1 is assigned.

Table 7.13 contains the ranges established for each of the selected model parameters, according to the membership functions depicted in figure 7.48. The proportion maps derived from the spectral unmixing, the landscape position map and the slope map were reclassified using these ranges.
Five maps, expressing degrees of erosion susceptibility from very low, low, moderate, high to very high, resulted from this procedure (figure 7.49). They were used as information layers to produce a final map showing the spatial distribution of erosion severity in the Sacaba valley.

Different exploratory models were build up and implemented by using IF-THEN statements. A total of 40 possible output models could result from combining the six information layers, taking variable numbers of layers at a time. For instance if the user considers the following model:
(1) soil erosion severity= *f* (vegetation coverage), for a ground cell (x) with coverage < 20%, this would result in 'very high' erosion hazard.

$\mu_{\text{soil erosion hazard}}(x) = \mu_{\text{vegetation}}(x)$

$\mu_{\text{soil erosion hazard}}(x) = 5$

The area would be mapped as prone to very high soil erosion, that is, the ground-cell would take the label resulting from reclassifying the vegetation proportion map into the five mentioned ranges .

A second model could be formulated ,where
(2) soil erosion severity= *f* (vegetation coverage, surface rock fragments,landscape position)
This model would be implemented as:
IF the vegetation coverage is very high and the surface rock fragments are moderately dense and the landscape position is very low, THEN the soil erosion hazard is very low. The statement is computed using a fuzzy minimum operator (see chapter 3). This means:

$\mu_{\text{soil erosion hazard}}(x) = \min [(\mu_{\text{vegetation}}(x), \mu_{\text{surface rock fragments}}(x), \mu_{\text{landscape position}}(x)]$

$\mu_{\text{soil erosion hazard}}(x) = \min$ (very high, moderate, very low)

$\mu_{\text{soil erosion hazard}}(x) = \min (5, 3, 1) \Rightarrow \mu_{\text{soil erosion hazard}}(x) = 1$; which corresponds to a 'very low' soil erosion hazard.

Contrasting results are obtained from the implementation of models 1 and 2. Therefore, certain assumptions have to be formulated. In this case, it was assumed that one parameter alone cannot properly characterize the soil erosion hazard and thus a high number of constraints would provide more reliable

results. Models were built up taking 4, 5 and 6 parameters at a time.

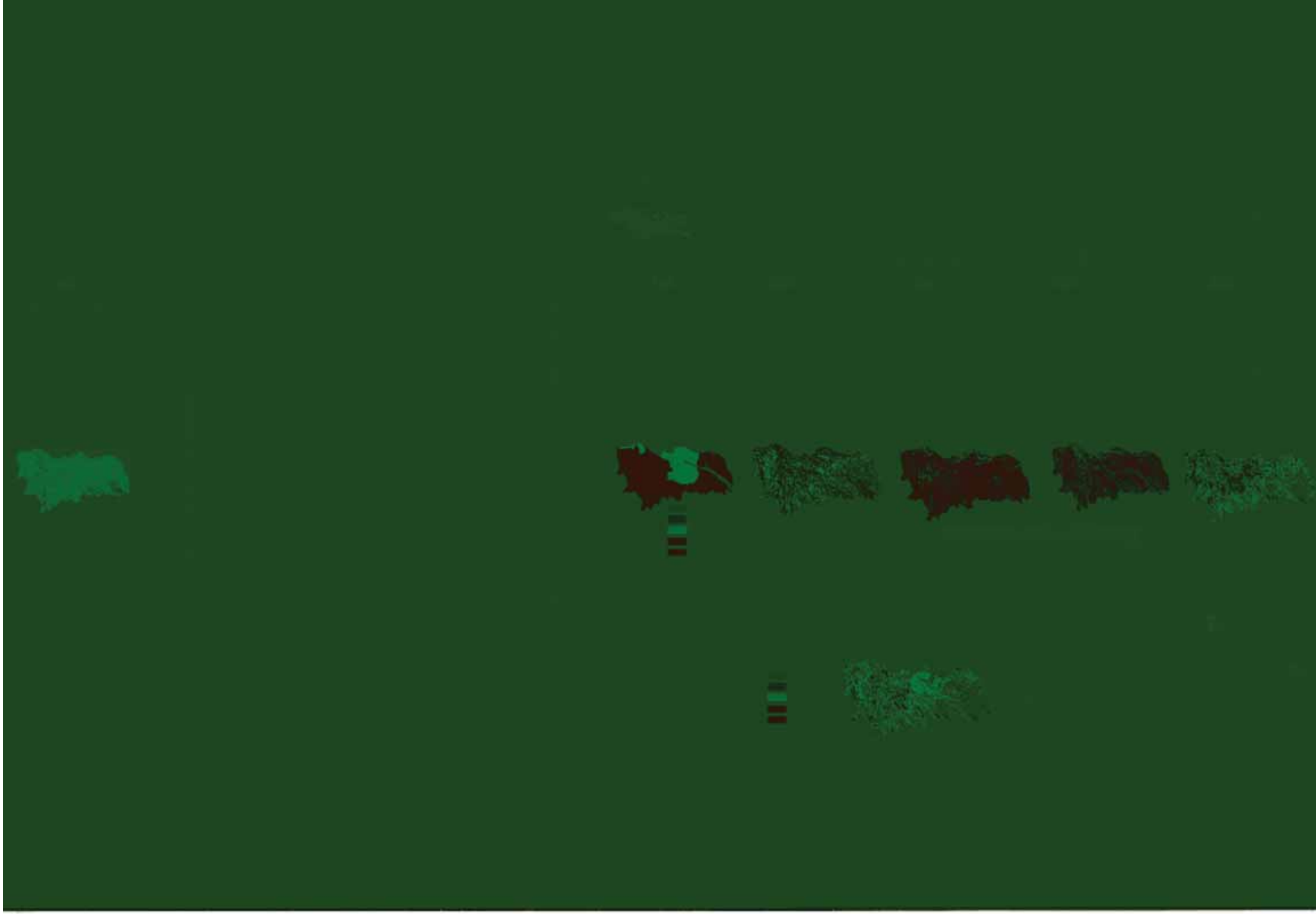

(4) Model evaluation

A total of 15 models was evaluated by comparing the spatial distribution of mapped erosion severity against existing information obtained from diverse sources. The exploratory model incorporating the percentage of vegetation cover, surface rock fragments, whitish topsoils, reddish brown soils and landscape position showed to perform best. Exclusion of the latter element implied an overestimation of erosion severity in the middle lagunary flats. Figures 7.50 and 7.51 illustrate these differences. Both models predict very low erosion hazard in areas occupied by ephemeral streams, high vegetation coverage and badlands. In fact, no further notorious increase in erosion severity can be expected in areas presently occupied by badlands or affected by extreme erosion degree. The riverbeds of ephemeral streams, are covered by more than 90% rock fragments, impeding further erosion.

The incorporation of the landscape position as a model component not only improved the map reliability but also its readability. More homogeneous areas, threatened by different soil erosion severity degrees, were obtained. Moderate hazard of soil erosion is predicted in the distal and central parts of the dissected depositional glacis in the south and southeast parts of the Sacaba valley. High soil erosion hazard is expected to occur in the lagunary flats, especially the middle ones, and in areas located in the glacis close to ephemeral streams. The spatial proximity of badlands and gully areas to brooks was observed in the field and analyzed in chapter five (see figure 5.12). These severely eroded areas are related to subsurface flows causing pipes and tunnels and washing coarse-textured alluvial lenses into the brooks. The collapse of the tunnel roofs originate deep gullies. The process is assumed to continue, especially along the streams oriented SSE-NNW.

The incorporation of the slope layer did not contribute to improve the results. This could be attributed to the difficulty in finding an appropriate membership function to relate erosion severity to slope gradient. Perhaps, a more direct relation could be found between slope shape and erosion severity. This relation could not be tested because of lack of data at a detailed scale. As a consequence of the former, a steep dissected area in the southeastern part of the Sacaba valley, where erosion severity seems more related to slope percentage than to any of the other parameters considered, could not be reliably assessed.

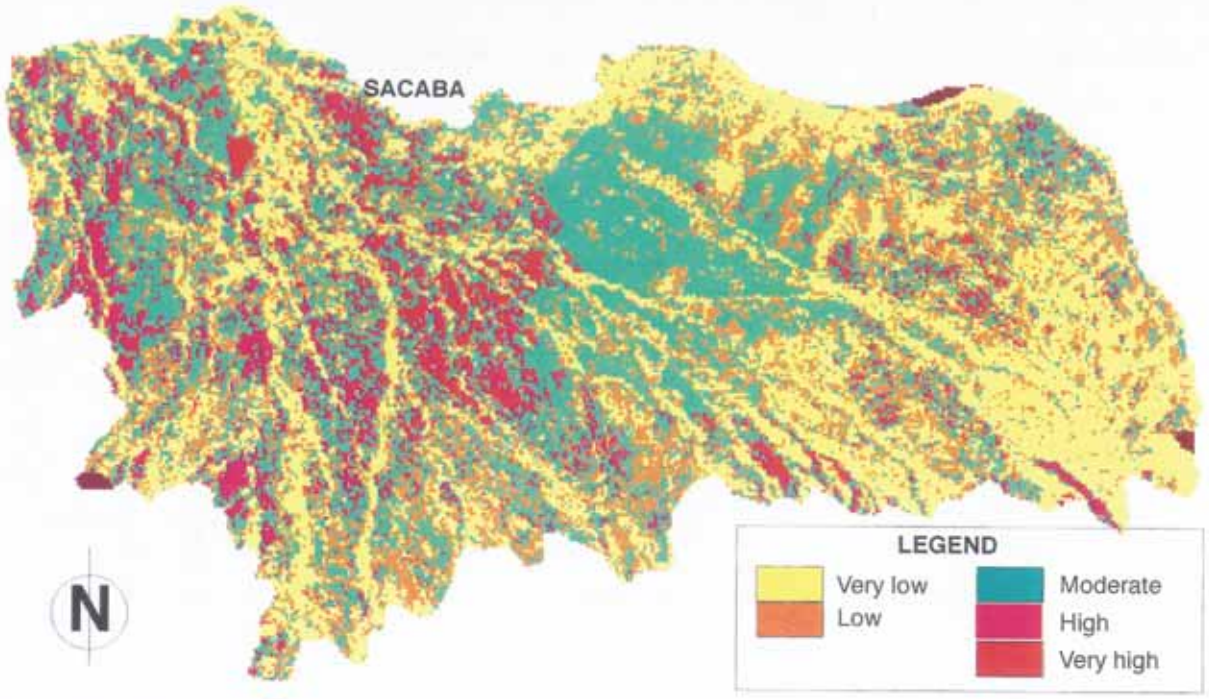

Fig. 7.50: Spatial distribution of areas prone to very low, low, moderate, high and very high soil erosion hazard as a function of vegetation coverage, whitish topsoils, surface rock fragments and landscape position.

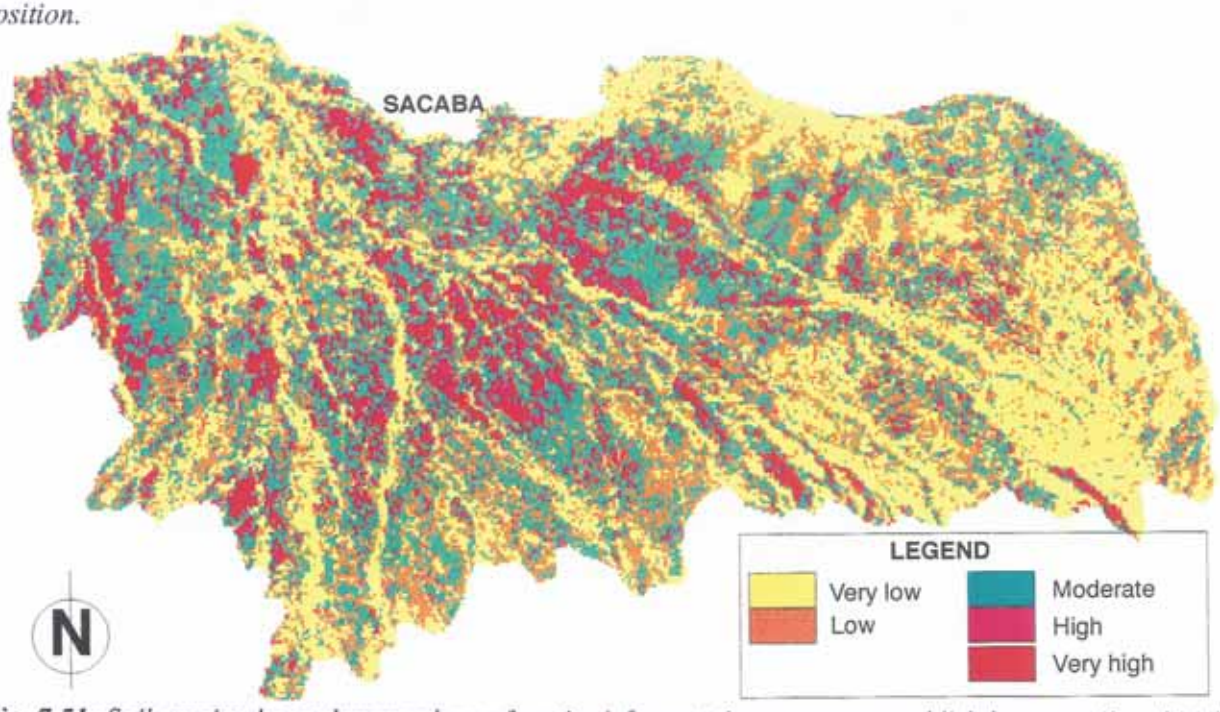

Fig. 7.51: Soil erosion hazard mapped as a function of vegetation coverage, reddish brown soils, whitish topsoils and surface rock fragments.

7.5.3 Soil erosion hazard prediction

(1) A knowledge-based fuzzy model

A second approach was designed implementing a knowledge-based fuzzy model to predict soil erosion susceptibility in the Sacaba valley (fig. 7.52). It differs from the first approach in that maps showing the spatial distribution of the soil parameters considered as suitable predictors are not the unique input. Field observations can be directly introduced as tables in the database. The membership functions already built up (fig. 7.48) are used to attach a certainty factor to each particular parameter included in the low, moderate and high fuzzy sets representing the universe of discourse 'soil erosion hazard'.

The membership degrees of a point (x) to the fuzzy sets low, moderate and high are computed by using a minimum operator. The point will take the label where it has the highest membership degree (ie, closest to 1) by applying a maximum operator (fig. 7.52). For instance, a user likes to know the likely susceptibility to soil erosion of a plot where:
"vegetation coverage is 40%, surface rock fragments cover 40% of the plot located in the distal part of a dissected depositional glacis (Pi113), with slope between 5 and 6%, whitish topsoils are observed in 30% and reddish brown soils in 50% of the plot".
The first step will be to obtain the certainty factors of each of the parameters in the low, moderate and high fuzzy sets. According to the results from the table 7.15, it is absolutely unlikely that low and high erosion hazard would occur in the hypothetical plot, but instead it is likely that moderate soil erosion will occur.

Table 7.15: Hypothetical plot

Parameter	SOIL EROSION HAZARD		
	Low	Moderate	High
Vegetation coverage (40%)	0.0	0.65	0.4
Surface rock fragments (40%)	0.0	0.9	0.3
Landscape position (Pi113)	0.6	0.6	0.7
Slope percentage (5 - 6%)	0	0.9	0.08
Whitish topsoil observed in 30% of the plot	0.4	0.85	0.1
Reddish brown soils observed in 50% of the plot	0.21	1.0	0.08
Likely susceptibility => minimum operator	0.0	0.6	0.08

The likely susceptibility to low, moderate and high erosion is obtained by the equation:

$\mu_{\text{soil erosion hazard}}(x) = \max [\min (\mu_{\text{vegetation}}(x), \mu_{\text{surface rock fragments}}(x)...)]$

The output of the prediction is not directly visualized as a map. It is a crisp value which can be expressed as a linguistic variable of the type likely or very unlikely by using linguistic approximation rules. The correspondence between certainty factors and verbal description of likelihood designed by Drummond (1991) was adopted here (see table 3.5). Scenarios of the type 'what if...' can be designed by using fuzzy rules of the type IF-THEN.

(2) Effect of rock fragments on erosion susceptibility

The effect of rock surface fragments on soil erosion processes has been widely documented. However, except for the K-Römkers, none of the revised soil erodibility indices incorporates rock fragment percentage in soil erosion models (see chapter 2). The model formulated here considers the effect of landscape elements, such as rock fragments, to protect the soil surface against raindrop impact and water entraintment. For instance, a soil covered by 20% of rock fragments will be more exposed to surface erosion than another having 70% of rock fragments on its surface.

(3) Seasonal variations of erosion susceptibility

The model also allows to consider seasonal variations in soil susceptibility to erosion, because of changes in vegetation coverage. In places like the Sacaba valley, the vegetation canopy is very scarce in non-irrigated areas at the beginning of the rainy season and therefore do not cover more than 30% of the surface when intensive rains fall in November-December. The situation is different in February-March when crops cover as much as 80% of the soil surface, depending on the crop type. This variations in canopy density determines changes in the membership degree of the vegetation cover to the fuzzy sets low, moderate and high erosion hazard (table 7.16).

7.5.4 Conclusions

Fuzzy knowledge-based exploratory models were designed to investigate the susceptibility of specific areas to erosion by incorporating expert knowledge, in the sense that information on soil properties and/or landscape elements assumed to control accelerated soil erosion could be incorporated into the modelling process.
The models are therefore considered region-oriented and exploratory. Fuzzy boundaries were applied to rank the landscape factors, used in modelling the likelihood of an area to be affected by different erosion degrees.

The vegetation cover percentage, rock fragments density, abundance of whitish topsoils, reddish brown topsoils assumed to reflect the absence of erosion, landscape position and slope gradient were the landscape elements selected to map soil erosion hazard. Although the model provides qualitative estimations, it showed very useful to explore indicators-causes-processes relationships. In addition, it allowed to test the importance of the individual landscape elements related to soil erosion and select those which best predict soil erosion.

The model considers the effect of rock fragments to protect the soil surface against raindrop impact and water entraintment and seasonal variations in soil susceptibility to erosion because of changes in vegetation coverage.
High soil erosion hazard is expected to occur in the lagunary flats, especially the middle ones, and in areas located in the glacis close to ephemeral streams. The process is assumed to continue, especially along the streams oriented SSE-NNW.

CHAPTER EIGHT:

THE EFFICIENCY OF THE SYNERGISTIC APPROACH

Two land degradation processes, soil erosion and salinization-alkalinization, were studied to identify similarities in terms of landscape position and spectral behavior of selected indicators in two different environments, the Sacaba and Punata-Cliza valleys. This calls now for an evaluation of the level of efficiency at which the different data sources and data processing techniques have performed in identifying, characterizing and discriminating specific surface indicators of land degradation.

Frequently, more than one land degradation process act in the same regional context. Sometimes, one phenomenon creates the appropriate conditions for another to start. For instance, in the Punata-Cliza valley, broken puffy and fluffy saline crusts leave exposed pulverulent soil material which is blown away by the wind. Therefore, the first step in land degradation studies is to relate surface indicators, soil properties and landscape elements to specific land degradation processes. The second step consists in characterizing the indicators to select the data sources and processing techniques for feature identification and delineation. Identified features can be directly labelled to represent certain land degradation intensity classes or used in models to relate the presence and proportions of a feature to a certain land degradation process. Exploratory models, taking advantage of expert knowledge and supported by fuzzy sets, were used in this research to relate and rank the model input parameters. The whole study process is thus based on synergy of data and techniques.

8.1 ISSUES OF FEATURE DISCRIMINATION AND MAPPING

Problems faced in discriminating and mapping surface features related to land degradation are: (a) the one-to-many relationship between surface features and land degradation processes, one feature characterizing many degradation processes; (b) the spectral similarity among surface features; and (c) the differences in spatial resolution of various data sources, including remotely-sensed data, field observations and laboratory determinations.

Land degradation is a complex ensemble of surface processes including, among others, wind and water erosion, salinization and alkalinization. Delineation requires proper feature definition. The relationship of surface feature to land degradation process can be one to one, many to one or one to many. The first two relations do not represent major mapping problems procedures, as far as the indicators can be properly characterized. The latter relation, however, causes monitoring difficulties, especially from remotely-sensed documents.

A complex relation also exists between degradation indicators and their spectral characteristics. Different

land degradation surface indicators have similar spectral signatures, a fact which constitutes a main drawback when working only with remotely-sensed data. Techniques of feature identification based on statistical pattern recognition did not perform suitably in differentiating among intensity classes of salinity-alkalinity. When characterizing a specific indicator by means of remotely-sensing data, problems related to spectral similarity and, depending on the scale of the data source, to the presence of more than one surface component in the minimum ground spatial unit the sensor can discriminate (the pixel), must be solved.

Automated clustering of land degradation indicators on the basis of their spectral signatures did not produce positive results. For satellite-borne sensors, like the Landsat TM, this results from the fact that some features lack specific absorption bands and are highly variable in space. Especially for salt-related features, automated clustering did no provide meaningful classes. Soil texture, crusting, surface roughness, topsoil color showed to effect the spectral signature of features related to salinity-alkalinity, under field conditions.

Land management practices also contributed to confusion between degrees of salinity-alkalinity. Sodium-tolerant crops are cultivated in areas considered moderately alkaline, with soil reaction between 7.5 and 9. As a consequence of cultivation, such areas presented the same surface appearance as non-affected areas, taking therefore that label.

A similar situation occurred when delineating areas affected by water soil erosion. Spectral confusion, in the visible and infrared ranges, occurred among slightly eroded areas, moderately eroded areas, and fallow land.

In conclusion, in the areas of the Cochabamba valleys affected by salinity-alkalinity and soil erosion processes, the use of existing spectral libraries and automated clustering of land degradation indicators did not provide reliable classification of degraded areas.

Another factor indirectly influencing the classification accuracy was the correct determination of information classes. Reliable mapping of areas affected by salinity-alkalinity depends not only on class discrimination, but also on correct class characterization. The use of transitional (fuzzy) boundaries and/or fuzzy class allocation techniques to determine saline, saline-alkaline, alkaline and non-affected areas generated differences in area labelling in comparison with the utilization of crisp class boundaries.

This study mobolizes different types of synergy:

(a) synergy between various data sources, including remotely-sensed, field and laboratory data;
(b) synergy of data from different regions of the electromagnetic spectrum;
(c) synergy of data having different spatial resolutions.

The framework implemented to evaluate the efficiency of the synergistic approach is displayed in figure 8.1.

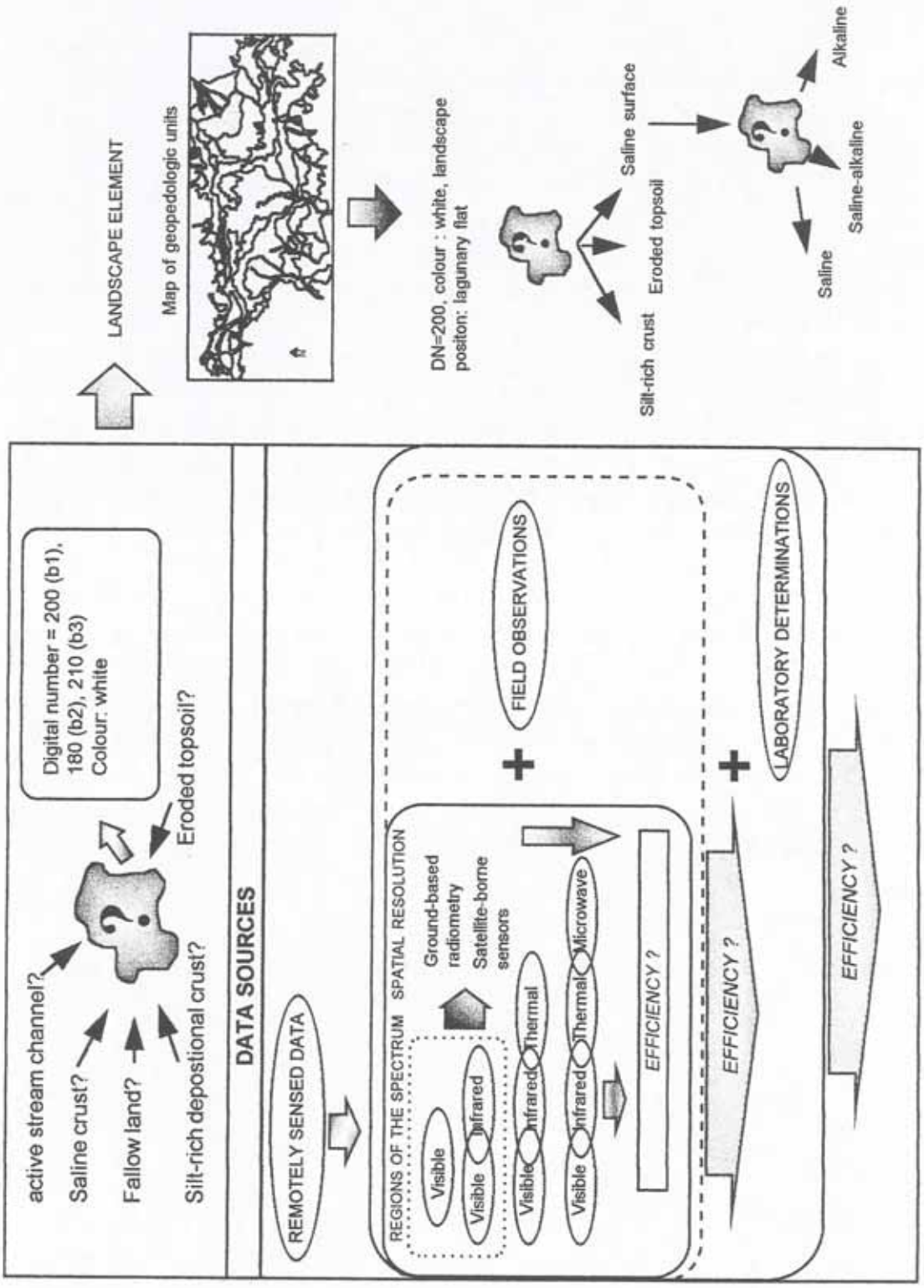

Fig. 8.1: Evaluating the efficiency of the synergistic approach

8.2 SPECTRAL SEPARABILITY OF LAND DEGRADATION FEATURES AT PLOT LEVEL

Reflectances of surface features related to degraded and non-degraded areas were recorded using a ground-based multiband radiometer, with six bands covering the visible region of the spectrum (450 to 700 nm) and two bands located in the near-infrared range (750 to 800nm).

Three qualitative measures were used to assess the efficiency of a region of the spectrum to separate land degradation features of interest: very good, good and poor. If the spectral signature of a feature was distinct in 4 to 6 bands of the visible range, performance was assessed as very good. Spectral differentiation in 3 out of the 6 bands considered marked a good performance. Spectral distinction in 2, 1 or none of the 6 bands determined a poor achievement. Since only 2 bands were located in the infrared, performance was assessed as very good when features were separable in both bands, good if separability was possible in only one band, and poor when the spectral behavior was equal in both bands.

8.2.1 Spectral separability of features between saline-alkaline areas and non-degraded areas

Chapter 6 describes the interaction between reflectance and surface features. The following features related to salinity-alkalinity were selected to assess efficiency: (1) salt crusts; (2) puffy salty crusts, characteristic of sodium sulphate-rich areas; (3) cracked salty crusts; (4) salt-tolerant Chenopodiaceae; and (5) Cynodon dactilon. The latter are salt-tolerant vegetation species, very common in the Punata-Cliza valley. The spectral curves of these features were confronted with features belonging to areas non-affected by salinity-alkalinity, namely: (6) crusted ploughed fields; (7) 'mullido', artificial sealing crusts made by ploughing to protect the soil against moisture losses during the dry season; (8) ploughed fields with large clods; (9) bare soil surfaces from uncultivated land; (10) bright silt-rich crusts.
The results of the analysis are reported in table 8.1 for the separability in the visible range, and in table 8.2 for the separability in the near-infrared range.

Table 8.1: Spectral separability in the visible range between features related to saline-alkaline areas and non-degraded areas at plot level.

Features	2	3	4	5	6	7	8	9	10
1	XXX	XX	XXX	XXX	XXX	XXX	XXX	XXX	XXX
2		XXX	XXX	XXX	XXX	XXX	XX	XX	XXX
3			XXX	XXX	XXX	XXX	XXX	XXX	XXX
4				XX	XX	XXX	XXX	XXX	XXX
5					XXX	XXX	XXX	XXX	X
6						XXX	XXX	XXX	XXX
7							XXX	XXX	XXX
8								XXX	XXX
9									XX

(1) crusted ploughed field; (2) mullido crust; (3) ploughed field; (4) salt crust; (5) bare soil; (6) puffy salty crust; (7) Chenopodiaceae; (8) Cynodon dactilon; (9) cracked salty crust; (10) bright silt-rich crust. XXX: very good; XX: good; X: poor spectral separability.

Table 8.2: Spectral separability in the near-infrared range between features related to saline-alkaline areas and non-degraded areas at plot level.

Features	2	3	4	5	6	7	8	9	10
1	XXX	XXX	XXX	XXX	XXX	XXX	XXX	XXX	XXX
2		XXX	XXX	XXX	XXX	XXX	X	X	XXX
3			XXX	XXX	XXX	XX	XXX	XXX	XXX
4				XXX	X	XXX	XX	XXX	X
5					XXX	X	XXX	XXX	X
6						XXX	XXX	XXX	XXX
7							XXX	XXX	XXX
8								X	XXX
9									XX

(1) crusted ploughed field; (2) mullido crust; (3) ploughed field; (4) salt crust; (5) bare soil; (6) puffy salty crust; (7) Chenopodiaceae; (8) Cynodon dactilon; (9) cracked salty crust; (10) bright silt-rich crust. XXX: very good; XX: good; X: poor spectral separability.

Both tables show an overall very good separability in the visible and near-infrared ranges among features related to areas degraded by salinity and/or alkalinity processes and non-affected areas, at plot level.

The most remarkable confusion in the visible range occurs between bright silt-rich crusts and bare soils. Other spectral confusions arise between the smooth mullido crusts, on the one hand, and Cynodon dactilon

covered surfaces, and cracked salty crusts, on the other. When the vegetation coverage is scarce, a typical situation for salt-tolerant vegetation, the influence of the soil background effects the spectral curves. The formation of cracks alters the smooth, highly reflecting salt crusts. Surface roughness, due to the formation of cracks or puffs, lowers the amount of reflected energy. All these factors contribute to diminishing the separability among degraded and non-degraded areas.

Since the infrared range only covers a short portion of the spectrum, higher confusions occur due to poorer spectral feature characterization. Poor separabilities are reported between mullido crusts and Cynodon dactilon as well as cracked salty crusts. Salt and silt-rich bright crusts are spectrally similar in this region of the spectrum. The near-infrared showed unable to identify salt-tolerant, scarcely vegetated areas. The low chlorophyll content and soil background influences determined a poor separability respect to cracked salty surfaces and bare soils.

The synergy of the visible and near-infrared regions of the spectrum can overcome the spectral confusions between silt-rich bright crusts, bare soil surfaces, salt crusts and salt-tolerant vegetation.

8.2.2 Spectral separability of features between eroded and non-eroded areas

Selected surface indicators to analyze the spectral separability between areas subjected to soil erosion and non-degraded areas were: (1) exposed mollic horizons; (2) crusts with rock fragments; (3) splash pedestals; (4) erosion pavements; (5) bright depositional crusts; (6) locust trees, as natural vegetation commonly present in eroded areas; (7) 'erodible' topsoil textures, including loamy, silt loam and sandy loam textures which are highly correlated to different degrees of erosion in the Sacaba valley.
These features were confronted with the indicators associated to areas non-affected by erosion: (8) ochric topsoils in Camborthids; (9) ochric topsoils in Torriorthents; (10) wheat crop; (11) 'non-erodible' topsoil textures, such as silty clay loam and clay loam.

The poorest separability in the visible range occurred between erodible textures, on the one hand, and ochric topsoils and bright depositional crusts, on the other (table 8.3). They all possess high reflectance values in the visible range, partly due to relatively high silt contents, low organic matter contents and light yellowish brown colors.

The infrared region solved the previous spectral similarities between bright depositional crusts and ochric topsoils in Camborthids. But new sources of mixture appeared between ochric topsoils and non-erodible topsoil textures (table 8.4). Natural vegetation, proper of eroded areas such as gullies and badlands, showed similar high reflectance as crops.

Table 8.3: Spectral separability in the visible range between features related to eroded and non-eroded areas at plot level.

Feature	2	3	4	5	6	7	8	9	10	11
1	XXX	XX	XXX	XXX	XXX	XXX	XXX	XXX	XXX	XXX
2		XXX	XXX	XXX	XXX	XX	XXX	XXX	XXX	XXX
3			XXX	XXX	XXX	XXX	XXX	XXX	XXX	XXX
4				XXX	XXX	X	X	XXX	XXX	X
5					XXX	XXX	XXX	XXX	XXX	XXX
6						XXX	XXX	XXX	XXX	XXX
7							XX	XXX	XXX	X
8								XXX	XXX	X
9									XXX	XXX
10										XXX

(1) exposed/buried mollic horizon; (2) crust with rock fragments; (30 splash pedestals; (4) ochric topsoil in Camborthids; (5) wheat; (6) erosion pavements; (7) ochric topsoil in Torriorthents; (8) bright depositional crust; (9) locust trees; (10) non-erodible topsoil textures; (11) erodible topsoil textures.
XXX: very good; XX: good; X: poor spectral separability.

Table 8.4: Spectral separability in the near-infrared range between features related to eroded and non-eroded areas at plot level.

Feature	2	3	4	5	6	7	8	9	10	11
1	XXX	XXX	XXX	XXX	XXX	XXX	XXX	XXX	XXX	XXX
2		XXX	XXX	XXX	XXX	XXX	XXX	XXX	XXX	XXX
3			XXX	X	XXX	XXX	XXX	X	XXX	XXX
4				XXX	XXX	X	X	XXX	X	XXX
5					XXX	XXX	XXX	X	XXX	XXX
6						XXX	XXX	XXX	XXX	XXX
7							X	XXX	XXX	X
8								XXX	XXX	X
9									XXX	XXX
10										XXX

(1) exposed/buried mollic horizon; (2) crust with rock fragments; (30 splash pedestals; (4) ochric topsoil in Camborthids; (5) wheat; (6) erosion pavements; (7) ochric topsoil in Torriorthents; (8) bright depositional crust; (9) locust trees; (10) non-erodible topsoil textures; (11) erodible topsoil textures.
XXX: very good; XX: good; X: poor spectral separability.

Topsoil textures susceptible to erosion have distinct spectral behavior in comparison to the less susceptible ones (higher clay and organic matter contents) in the visible and near-infrared range. Exposed mollic horizons, crusts with rock fragments and erosion pavements were also spectrally separable in the range considered.

In conclusion, spectral mixing resulting from the presence of more than one surface component related to the same land degradation process, within the minimum recorded surface, could be disentangled when working with ground-based instruments. For features related to salinity-alkalinity and soil erosion, a good to very good spectral separability could be accomplished.

8.2.3 Spectral separability of features between degraded and non-degraded areas

The poorest spectral separability occurred between topsoils of Camborthids, puffy salty crusts and cracked topsoils of salt crusts. Puffs and cracks lower the high reflectance of saline crusts, confused therefore with the topsoils of Camborthids (table 8.5). In addition, the spectral signature of puffy salty crusts is quite similar to erodible topsoil textures. The synergy of the visible and near-infrared ranges could overcome the confusions, as indicated in table 8.6.

Table 8.5: Spectral separability in the visible range between features related to different degradation processes at plot level.

Feature		1	2	3	4	5	6	7	8	9	10	11
		SOIL EROSION FEATURES										
1	SALINITY FEATURES	XXX	XXX	XX	XXX	XX	XXX	XXX	XXX	XXX	XXX	XXX
2		XXX	XX	XXX	XXX	XXX	XXX	XXX	XXX	XXX	XXX	XXX
3		XX	XXX	XX	XXX	XXX	XXX	XXX	XXX	XXX	XXX	XXX
4		XXX	XXX	XXX	XXX	XXX	XXX	XXX	XXX	XXX	XX	XXX
5		XXX	XXX	XXX	XXX	XXX	XXX	XXX	XXX	XXX	XXX	XXX
6		XXX	XXX	XXX	X	XXX	XXX	XXX	XXX	XXX	XXX	X
7		XXX	XXX	XXX	XXX	XX	XXX	XXX	XXX	XXX	XXX	XXX
8		XXX	X	XXX	XXX	XXX	XXX	XX	XXX	XXX	XXX	XXX
9		XXX	XXX	XXX	X	XXX	XXX	XX	XX	XXX	XXX	X
10		XXX	XXX	XXX	XX	XXX	XXX	XXX	XXX	XXX	XXX	XXX

XXX: very good ; XX: good; X: poor spectral separability.

Table 8.6: Spectral separability in the near-infrared range between features related to different degradation processes at plot level.

Feature		1	2	3	4	5	6	7	8	9	10	11
		SOIL EROSION FEATURES										
1	SALINITY FEATURES	XXX	XXX	XX	XXX	XX	XXX	XXX	XXX	XXX	XXX	XXX
2		XXX	XX	XXX	XXX	XXX	XXX	XXX	XXX	XXX	XXX	XXX
3		XX	XXX	XXX	XXX	XXX	XXX	XXX	XXX	XXX	XXX	XXX
4		XXX	XXX	XXX	XXX	XXX	XXX	XXX	XXX	XXX	XXX	XXX
5		XXX	XXX	XXX	XXX	XXX	XXX	XXX	XXX	XXX	XXX	XXX
6		XXX	XXX	XXX	XXX	XXX	XXX	XXX	XXX	XXX	XXX	XXX
7		XX	XXX	XXX	XXX	XXX	XXX	XXX	XXX	XXX	XXX	XXX
8		XXX	XX	XXX	XX	XXX	XXX	XXX	XXX	XXX	XXX	X
9		XXX	XX	XXX	XXX	XXX	XXX	XXX	XXX	XXX	XXX	XXX
10		XXX	XXX	XXX	XXX	XXX	XXX	XXX	XXX	XXX	XXX	XXX

XXX: very good ; XX: good; X: poor spectral separability.

8.3 SPECTRAL SEPARABILITY OF LAND DEGRADATION FEATURES AT REGIONAL SCALE

Differentiation between degraded and non-degraded areas was done by visual and digital interpretation of remotely-sensed data, with reliable discrimination accuracy (table 8.7). For instance, in the visible range of the spectrum, features such as saline patches, moderately eroded soils and silt-rich depositional crusts have all relatively high reflectances, compared to non-degraded areas (fallow land, arable land). However, when the interest is to discriminate among degradation processes and/or intensities such as classes of salt- and sodium-affected areas or classes of eroded soil surfaces, field data are required. It was impossible, for example, to determine if a highly reflective feature would correspond to a moderately eroded surface or a salt-affected area (table 8.7 and 8.8). If, in addition, the interest is to differentiate salinity or alkalinity degrees and/or salt types, laboratory determinations are further required. The more detailed the pursued discrimination is, regarding to type and intensity of degradation processes, the greater are the needs of synergy among remotely-sensed, field and laboratory determinations, especially in salinity-alkalinity studies.

8.3.1 The assessment approach

Spectral separability was analyzed by grouping the pixels, used to train the classifier, according to their correct allocation to non-affected, saline, saline-alkaline and alkaline areas. Spectral separability among

classes was computed taking the Landsat TM bands covering the visible (TM-bands 1,2 and 3), the infrared (TM-bands 4, 5 and 7) and the thermal range (TM-6) of the spectrum. In addition, separability between classes was analyzed using microwave data (L-band) alone, from the JERS-1 SAR radar satellite.

The following approach was adopted to evaluate the separability of different classes in the visible, infrared, thermal and microwave portions of the spectrum:
(a) Compute the number of samples used to build up the spectral signatures of each class (*A1,A2,A3, etc.).*
(b) Compute all possible combinations between classes (B1, B2, B3, etc). Combinations were represented in a two-dimensional table (*A1* composed by 7 samples and *A2* by 5 samples would generate 35 possible combinations *).*
(c) Compute the number of combinations where the transformed divergence analysis showed values below 1000, indicating very poor separability *(C1, C2, C3)*
(d) Compute the number of combinations where the transformed divergence analysis showed values between 1000 and 1600 (*D1, D2, D3, etc.*), assumed as indicative of good between-class separability. Values above 1600 were supposed to express very good between-class separability and therefore excluded from the analysis.
(e) Compute the percentage of all possible combinations with values below 1000 (eg, C1/B1) and the percentage of the combinations with values between 1000 and 1600 (eg, D1/B1).
(f) Compute the average to evaluate the between-class separabilities in the visible, infrared, thermal and microwave ranges. Since values below 1000 were assumed to express very low between-class separabilities, a weighting factor of 1.5 was added to this range.
Average separability= *[(C1/B1)*1.5+(D1/B1)]/2*

Bar graphs were built up to illustrate the results. The Y-axis depicts the percentage of spectral confusion over the total number of samples used to construct the class signature. On the X-axis, were plotted all possible class combinations. The comparison showed the classes which could benefit from the synergy of visible and infrared, or visible and thermal, or visible and microwave, etc. In addition, the graphics show in which range major spectral confusions between the two classes being considered could be expected to occur. The per-spectral range results are presented as matrices expressing qualitative measures: very good, good and poor separability among selected classes. Laboratory determinations were required to establish the classes related to saline-alkaline degradation processes and field observations for soil erosion classes.

8.3.2 Spectral separability between features related to salinity-alkalinity processes

Four classes were used to evaluate the efficiency of the synergistic approach at regional scale. They were: non-affected areas (pH <=7.5, EC <= 8 dS/m), saline areas (pH <= 7.5, EC > 8 dS/m); alkaline areas (pH > 7.5 , EC < 8 dS/m) and saline-alkaline areas (pH > 7.5 and EC > 8 dS/m).

Figure 8.2 illustrates the spectral confusions found among different class combinations. If the region of

the spectrum is not depicted in the graphic or its percentage is very low, this means that it greatly contributes to improve the spectral separability between two specific classes. The microwave region provided the best separability between saline and alkaline areas, non-affected and saline-alkaline areas, as well as among saline and saline-alkaline areas. The visible range, instead, resulted suitable to discriminate among non-affected and saline areas. The infrared range provided the lowest spectral confusion when separating saline-alkaline areas from alkaline ones. Finally, the thermal range was useful to separate among non-affected and alkaline areas.

Synergy of the visible, infrared and microwave ranges could improve the separability between non-affected and saline areas, non-affected and saline-alkaline areas, and the latter respect to the saline and alkaline areas. The thermal range appears to be determinant to improve the separability of alkaline areas. Alkalinity is determined by the amount of free carbonates, which have a strong absorption feature in the thermal range of the Landsat TM-band 6. Synergy of the thermal, microwave and visible ranges improve the separability between saline and alkaline areas.

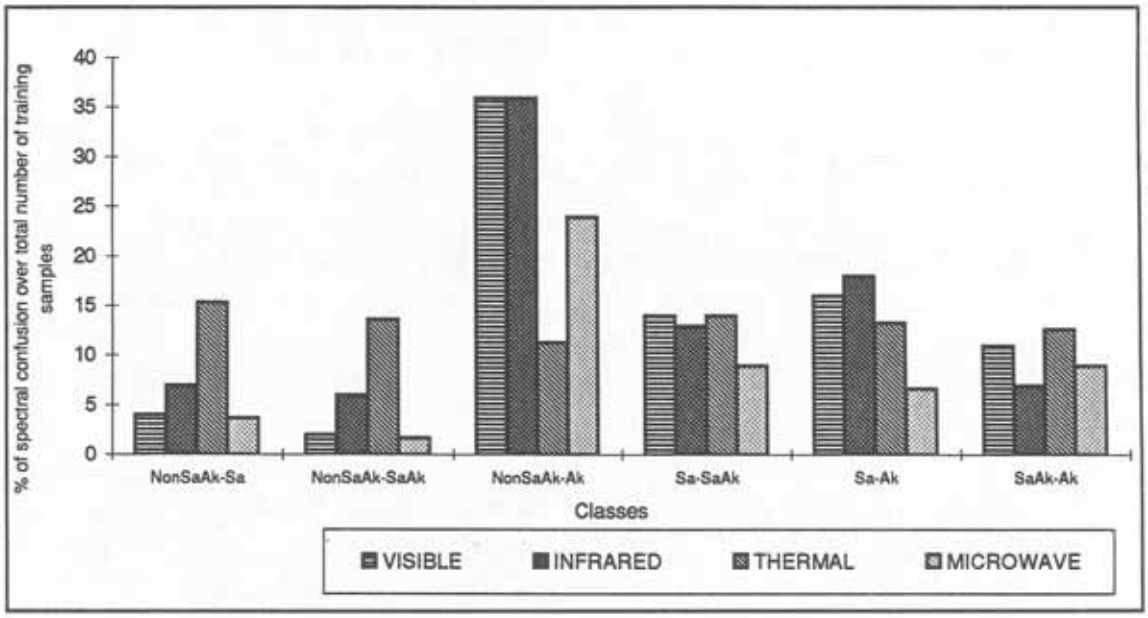

***Fig. 8.2:** Percentage of spectral confusion over the total number of per-class training samples*

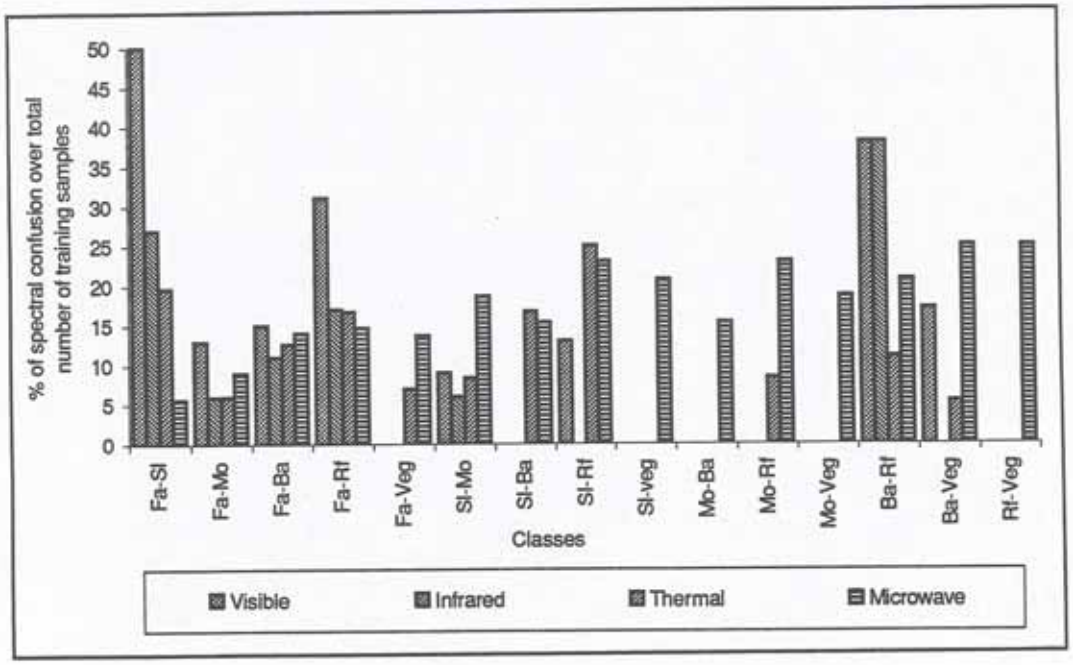

Fig. 8.3: Spectral confusion among surface soil erosion indicators.

8.3.3 Spectral separability between features related to soil erosion processes

Figure 8.3 shows the percentage of spectral confusion in relation to the total number of training samples used to build up the spectral signatures of the erosional classes discriminated in the Sacaba valley. The visible range performs poorly in distinguishing fallow land from slightly eroded areas and from surface rock fragments. The graphic also shows the very poor performance of the visible and infrared ranges to separate badlands from rock fragments.

Table 8.7 expresses the performance of the different wavelength ranges in discriminating among saline and alkaline classes. The synergy of microwave and visible plus infrared ranges seems to be required to overcome problems of spectral separability between saline and saline-alkaline classes. Visible and infrared ranges are capable to discriminate non-affected areas from saline or saline-alkaline ones.

Table 8.7: Efficiency of different regions of the spectrum to discriminate among saline, alkaline, saline-alkaline and non-affected areas.

Classes	Saline	Saline-alkaline	Alkaline	Non-affected
	VISIBLE RANGE (Landsat TM bands 1,2,3)			
Saline		X	XX	XXX
Saline-alkaline			X	XXX
Alkaline				XX
	INFRARED RANGE (Landsat TM bands 4, 5, 7)			
Saline		X	XX	XXX
Saline-alkaline			XX	XXX
Alkaline				XX
	THERMAL RANGE (Landsat TM band 6)			
Saline		X	XX	XX
Saline-alkaline			X	XX
Alkaline				XXX
	MICROWAVE RANGE (JERS-1 SAR L-band)			
Saline		XXX	XXX	XXX
Saline-alkaline			X	XX
Alkaline				X

XXX: very good; XX: good; X: poor spectral separability

Fusion of the visible and infrared ranges with thermal and/or microwave data improves feature separability. Temperature difference between surfaces with and without rock fragments greatly helps distinguish erosion pavements (surfaces densely covered by rock fragments) from badlands and, to a lesser extent, fallow land.

The surface roughness component determines variations in the amount of energy backscattered towards the JERS-1 SAR sensor, causing therefore different spectral signatures for fallow land, slightly eroded areas and rock fragments in the microwave region of the spectrum. The visible range provides enough information to separate vegetation from different erosional classes and fallow land. The infrared range improves the separability between slightly and moderately eroded areas (table 8.8).

Table 8.8: Efficiency of the visible, infrared, thermal and microwave regions of the spectrum to discriminate among surface soil erosion.

Classes	Slightly eroded	Moderately eroded	Badlands	Rock fragments	Vegetation
	VISIBLE RANGE (Landsat TM bands 1,2,3)				
Fallow land	X	XXX	XX	X	XXX
Slightly eroded		XXX	XXX	XXX	XXX
Moderately eroded			XXX	XXX	XXX
Badlands				XX	XXX
Rock fragments					XXX
	INFRARED RANGE (Landsat TM bands 4, 5, 7)				
Fallow land	XX	XXX	XXX	XXX	XXX
Slightly eroded		XXX	XXX	XXX	XXX
Moderately eroded			XXX	XXX	XXX
Badlands				XX	XXX
Rock fragments					XXX
	THERMAL RANGE (Landsat TM band 6)				
Fallow land	X	XX	X	X	XXX
Slightly eroded		XXX	XX	XX	XXX
Moderately eroded			XXX	XXX	XXX
Badlands				XXX	XXX
Rock fragments					XXX
	MICROWAVE RANGE (JERS-1 SAR L-band)				
Fallow land	XXX	X	X	XX	XXX
Slightly eroded		X	XXX	XXX	XX
Moderately eroded			X	X	XXX
Badlands				XX	XXX
Rock fragments					XXX

XXX: very good; XX: good; X: poor spectral separability

8.4 SYNERGY OF DIFFERENT DATA SOURCES: TOWARDS COST-EFFECTIVENESS

Remotely-sensed data alone are not sufficient to distinguish among land degradation types and/or degrees of salinity-alkalinity and soil surface erosion. Perhaps, a reliable distinction between degraded and non-degraded areas could be achieved. But, more accurate discrimination between degradation types and levels requires synergy with field observations and laboratory determinations.

An alternative to discriminate and map surface features, especially soil properties related to land

degradation processes, is by spatial interpolation of laboratory data. A series of items such as the minimum number of samples, sampling strategy, interpolation method are to be decided, and a global positioning system (GPS) is required to spatially locate the observations. In this research, kriging and inverse square distance interpolation techniques were applied to produce topsoil properties maps of the Punata-Cliza and Sacaba valleys. When compared with remotely sensed data maps, supported by field and laboratory determinations, geostatistical interpolation performed better than inverse square distance. However, a minimum of 80 samples was necessary to produce reliable semi-variograms.
A stratified oriented approach was followed for data collection. In places where the observations were not evenly distributed the map reliability was low. The inverse square interpolation techniques, in all cases, caused a 'bull eyes' aspect in the output maps (see appendix I). A good compromise between cost and efficiency might be achieved when applying geostatistics to small areas, at local scale. But, synergy with remotely-sensed data is definitively required to map areas at regional scale, like in the Cochabamba valleys where the three basins comprise approximately 90,000 ha.

In any case, synergy of different data sources produced better results than their individual use. Table 8.9 resumes a cost-effectiveness analysis on the basis of the research findings and the data sets used.
Satellite data collected from the different regions of the spectrum were not enough to accurately map areas affected by land degradation processes and their degrees of severity. The use of existing spectral libraries was insufficient to identify land degradation indicators. This is attributed to the spectral similarities and to the mixing of more than one surface component within a pixel. The latter was partly solved, in the case of soil erosion mapping, by using a linear mixture model to unmix surface components. However, this technique required end-members to be spectrally distinct, a requirement not always possible to be met. Interpretation of aerial photographs alone can discriminate the extent and type of degradation, such as soil eroded areas or saline-alkaline areas. However, the approach becomes less accurate when trying to discriminate salinity-alkalinity degrees and types.

Ground-based radiometry provided good results, but the data are collected at a plot scale and, being point measurements recorded by a non-imaging instrument, they do not allow for visual discrimination of surface features. They can only be used to understand and help interpret data from satellite-borne sensors.

Field observations and/or laboratory data alone would need the use of a global positioning system and further interpolation. Reliable maps require intensive and evenly distributed samples. Field mapping and laboratory determinations are time-consuming and expensive. As indicated in table 8.9, Dfl. 195 were charged per sample for salinity-alkalinity studies. Distributed over an area of about 6,000 hectares, a total of Dfl. 15600 would have to be spent to map that area with reliable results.

Integration of different data sources allows to decrease the number of laboratory determinations and field observations. The use of field observations and/or laboratory determinations alone to produce maps by spatial interpolation is recommended only for small-area surveys. Larger areas can be mapped by

integration of different data sources, at higher reliability and lower costs. This research focused on the advantages and drawbacks of different data sources and scales, and on the capabilities of the different regions of the electromagnetic spectrum to identify and discriminate land degradation surface features.

Table 8.9: Efficiency of different approaches in relation to cost/benefit

USER DEMAND	DATA SOURCES	TECHNIQUE	RELIABILITY	COST	COMMENTS
(A): Degraded - Non-degraded areas	Aerial photographs (AP)	visual interpretation	High -> Medium	Dfl. 1,000 (at 1:50,000)	Semi-detailed scale larger than 1:50000
	Satellite images (RS)	visual and/ or digital analysis	High -> Medium	Dfl. 5,000 (JERS-1 + Landsat TM subscene)	smaller than 1:50000
	AP+RS+field obs.	visual and/or digital analysis	High+	Dfl. 10,000 (approx.)	regional, semi-detailed; stratified random sampling. Multi-scale approach.
(B): Classes - Degraded by soil erosion. - Degraded by salinity-alkalinity processes. - Non-degraded areas	Satellite images (RS)	image enhancement and visual interpretation; digital analysis	Medium	Dfl. 5,000 (JERS-1 and Landsat TM)	Regional scales
	Aerial photographs (AP)	visual interpretation	Medium	Dfl. 1,000	Regional and semi-datailed scale
	AP+RS	visual interpretation; digital analysis	Medium+	Dfl. 6,000	Regional and semi-detailed scale. Large scale photographs could be used in pilot areas to identify surface features.
	AP+RS+field obs.	visual interpretation; digital analysis	High ++	Dfl. 10,000	Regional , checking reduced to pre-determined strata.
	RS + field obs.	visual interpretation; digital analysis	High	Dfl. 8,000	Regional
	AP + field obs.	visual interpretation	High	Dfl. 5,000	Regional
	Field obs + lab. det.	GPS and spatial interpolation	Medium	Dfl 26,000	Many point (> 80) observations are required; only recommended for small areas

Continued

(C): Classes and degrees of erosion - Non-degraded areas - Saline - Saline-alkaline - Alkaline - Slightly eroded - Moderately eroded - Badlands	Satellite images	visual interpretation; digital analysis	Low	Dfl. 5,000	Very difficult to distinguish between classes and/or degrees of soil degradation.
	Aerial photographs	visual interpretation	Low ->Moderate	Dfl. 1,000	
	Field obs. + lab. det.	GPS and spatial interpolation	Moderate	Dfl. 26,000	Accurate, but many observations are required. Sampling strategy has to be decided.
	RS +AP	visual interpretation; digital analysis	Low-> Moderate	Dfl. 6,000	Very difficult to distinguish degrees.
	RS+AP+field obs.	visual interpretation; digital analysis	High	Dfl. 10,000	Selection will mainly depend on the extent of the area and the scale of mapping, as well as hardware and software availability. Mapping at scales larger than 1:30000 is not possible by the current satellite-borne sensors.
	AP+field obs.	visual interpretation; digital analysis	High	Dfl.6,000	
	RS+field obs.	digital analysis; visual interpretation	High	Dfl. 8,000	

* Costs were estimated for a standard area of 40,000 hectares at the rate of June 1994.

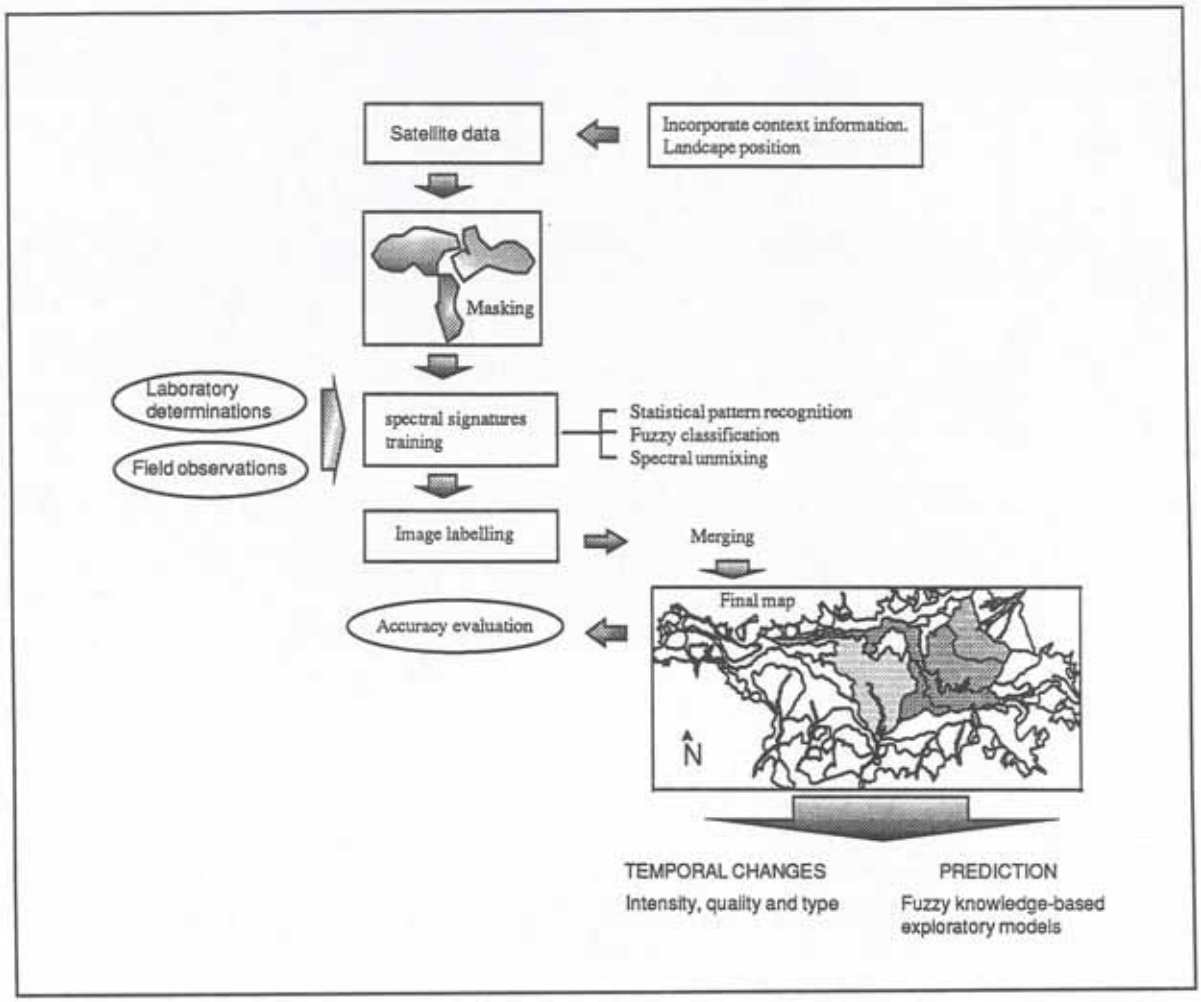

Fig. 8.4: *Incorporation of landscape information, previous to image classification, as a means to reduce spectral confusion.*

Analyzing the landscape evolution of the Cochabamba valleys, it was concluded on a close relationship between depositional environment and causes of land degradation. The research also demonstrated a good relationship between landscape position, lithology and particular land degradation processes. For instance, salt- and sodium-affected areas are closely related to lagunary flats and playas; dominantly calcareous areas are related to dissected depositional glacis. Hence, a first step before attempting satellite image classification should be the elaboration of a map of geomorphic units (fig. 8.4). The resulting units at landscape or relief type level can be digitized and used as masks to classify the scene. In a post-classification procedure, the different masks can be merged to elaborate a final map. This approach allowed to reduce the sources of spectral confusion bewteen land degradation related surface features in the Punata-Cliza valley and, in consequence, improve the classification accuracy. However, overcoming the spectral confusions due to the mixture of different surface components within one pixel was not possible. A linear mixture model had to be implemented to solve the within-pixel mixtures.

CHAPTER NINE:

CONCLUSIONS AND RECOMMENDATIONS

9.1 MAJOR CONTRIBUTIONS

Major contributions of this research are summarized hereafter.

9.1.1. Characteristics of the study area and their relationship to land degradation processes

(1) In spite of their common tectonic origin, the basins of Cochabamba, Sacaba and Punata-Cliza have undergone a different evolution over time, resulting in significant geopedologic variations. Local differences in lithology and tectonics contribute to diversify the taxonomic composition of similar geomorphic units in the three valleys.

(2) The study of the landscape origin and evolution over time facilitates the understanding of the mechanisms of action, location, extent and expansion trends of degradation phenomena. The tectonic and sedimentary history of the basins, the nature of the sediments and the spatial distribution of the geopedologic cover formations determine a differential susceptibility of the valleys to specific land degradation processes. The reworking by fluvial ablation of loose moraine deposits from the last glacial periods, located in the northern parts of the Cochabamba and Sacaba valleys, constitute a permanent threat to urban settlements and agricultural fields in the lowlands. As a consequence, stream avulsion is the main environmental hazard in the Cochabamba valley. In the Sacaba valley, badlands develop through gully formation from collapsing of subsurficial tunnels and pipes. The presence of lenticular gravel and coarse sand depositional strata, the Quaternary lake level fluctuations, and the erodibility of the silty and sandy clay lagunary materials are among the factors controlling the initiation of the erosional processes in the Sacaba area. In the Punata-Cliza valley, topsoil degradation dominates through crusting and surface concentration of salts and sodium compounds, because the lagunary depressions of the valley are characterized by thick, fine-textured lacustrine sequences.

(3) A generalized paleoenvironmental reconstitution of the Holocene period in the Cochabamba valleys, through radiocarbon dating of buried humus-rich soil horizons, suggests that climatic conditions moister than at present reigned in the three valleys during the later part of the middle Holocene, allowing for the development of mollic, argillic and calcic horizons in diverse parent

material and topographic conditions.

9.1.2 Correlation between landscape positions and land degradation processes

(1) Salt distribution in the Punata-Cliza valley

Chloride-rich soils are frequent in the playas and southwestern distal piedmont glacis, decreasing towards the lower and middle lagunary flats, but are rare in the higher lagunary flats. Carbonate-rich soils, in turn, dominate in the southwestern playas and distal piedmont glacis, but decrease towards the southern lower lagunary flats, and are rare in middle and higher lagunary flats.

The most degraded areas are located in the playa landform. Conversely, non to slightly saline-alkaline areas correspond to the higher lagunary flats. However, middle and higher lagunary flats are threatened by potential salinization. Parent material, topographic position and the dry climate, which reduces the leaching but increases the migration of soluble salts towards the surface horizons, are the main factors controlling the spatial distribution of salt- and sodium-affected areas.

The general trend is towards increasing alkalinity, especially in the higher lagunary flats. This is attributed to the nature of the deposits coming from the carbonate-rich southern mountains (calcareous sandstones). Therefore, higher as well as middle lagunary flats are threatened by potential salinity-alkalinity expansion. The hazard refers not only to the geographic extension of saline-alkaline areas, but also to the intensification of the process in areas already degraded, specially if the recent tendency towards increased climatic dryness continues.

(2) Accelerated soil erosion by water in the Sacaba valley

The distal and central parts of the dissected depositional glacis in the south and southeast of the Sacaba valley are exposed to moderate hazard of soil erosion. High soil erosion hazard is expected to occur in the lagunary flats, especially the middle ones, and in areas located in the glacis close to ephemeral streams. The spatial proximity of badlands and gullied areas to brooks is related to subsurface flows causing pipes and tunnels and washing coarse-textured alluvial lenses into the brooks. The process is likely to continue, especially along the streams oriented SSE-NNW.

9.1.3 Data fusion

This study mobilizes different types of synergy:

- synergy between various data sources, including remotely-sensed, field and laboratory data;
- synergy of data from the different regions of the electromagnetic spectrum;
- synergy of data having different spatial resolutions.

(1) Landsat TM and JERS-1 SAR data to identify and map surfaces affected by soil erosion.

The incorporation of microwave data improved the separability and thus the discrimination among spectral plots representing fallow land and moderately as well as slightly eroded areas. Surface roughness resulting from soil ploughing caused high backscattering at macro-level. This distinctive feature in the microwave region allowed the separation of classes with similar spectral behavior in the visible and infrared wavelengths.

Fusion of the visible and infrared ranges with thermal data improved also feature separability. Temperature difference between surfaces with and without rock fragments greatly helps distinguish erosion pavements, densely covered by rock fragments, from badlands and, to a lesser extent, fallow land.

(2) Landsat TM and JERS-1 SAR data to identify and map salt- and sodium-affected areas

The fusion of visible, infrared and microwave data is suitable to map areas non-affected by salinity-alkalinity and discriminate alkaline soil surfaces, at a level of accuracy remarkably superior to the accuracy achieved by Landsat TM and JERS-1 separately (35 to 40% accuracy increase).

Synergy of the visible, infrared and microwave ranges could improve the separability between non-affected and saline areas, non-affected and saline-alkaline areas, and the latter respect to the saline and alkaline areas. The thermal range appears to be determinant in improving the separability of alkaline areas. Alkalinity is determined by the amount of free carbonates, which have a strong absorption feature in the thermal range.

9.1.4. Classification techniques

(1) There was a high coincidence between the salt distribution on the landscape derived from laboratory data, the maps obtained by geostatiscal interpolation of field soil properties and the results of digital image classification.

(2) Neighbourhood-based analysis was useful to overcome high spatial and spectral variability of salinity- and alkalinity-related surface features.

(3) Independently of the classification scheme and classifier used, fuzzy modelling of information categories provided higher discrimination accuracies. Two membership functions were tested: a S-shaped membership function with two parameters to adjust the shape of the membership curves and a linear function.

(4) Linear mixture modelling was applied in the southern area of the Sacaba valley. The model allowed to use up to five surface components to characterize the selected area, since six bands (1, 2, 3, 4, 5 and 7) of the Landsat TM sensors were used as input. In 99% of the area, the selected

end-member proportions were mapped with an error lower than 10%. A sixth end member would have been necessary to fully characterize the area.

(5) In the areas of the Cochabamba valleys affected by salinity-alkalinity and soil erosion processes, the use of existing spectral libraries and automated clustering of land degradation indicators did not provide reliable classification of degraded areas.

9.1.5 Determination of salinity-alkalinity classes

The conventional approach to map saline, saline-alkaline, alkaline and non-affected areas using SAR or pH and EC values, revealed to be insufficient for the handling of satellite data. Established salinity class boundaries and variable crop tolerance to specific EC values were sources of confusion among categories, when dealing with remote sensing data in the optical as well as the microwave ranges. Similarly, cultivation practices and terrain surface morphology greatly affect the energy backscattering, reflection and absorption. As a consequence, many degraded areas were labelled as non-degraded areas when subjected to cultivation. This demonstrates the impossibility to differentiate among salinity and alkalinity classes on the sole basis of reflectance and/or backscattering values.

Reliable mapping of areas affected by salinity-alkalinity depends not only on class discrimination, but also on correct class characterization. The use of transitional (fuzzy) boundaries and/or fuzzy class allocation techniques to determine saline, saline-alkaline, alkaline and non-affected areas generated differences in area labelling in comparison with the utilization of crisp class boundaries.

9.1.6 Modelling: fuzzy knowledge-based exploratory models

Fuzzy knowledge-based models explore cause-effect relationships on the basis of the general understanding about causes and the specific relation between processes and indicators in the study area.

(1) Monitoring salinity-alkalinity

A model was designed using fuzzy sets and a rule-based system of if-then statements. Input data were derived from multi-temporal classification of satellite images. Thus, the accuracy of monitoring depends on the reliability of the image classification. The model capitalizes on expert knowledge about the local salinization-alkalinization status. Information on the possibility of actual changes is incorporated as 'degrees of likelihood' of a certain event to occur. The model provides maps displaying the likelihood, nature and magnitude of the changes. It also identifies the more hazardous areas, those where the magnitude of the predicted changes is highest.

(2) Soil erosion hazard prediction

Fuzzy knowledge-based exploratory models were designed to investigate the susceptibility of specific areas

to erosion by incorporating expert knowledge on the soil properties and/or landscape elements assumed to control accelerated soil erosion. The models are considered region-oriented and exploratory. Fuzzy boundaries were applied to rank the landscape factors, used in modelling the likelihood of an area to be affected by different erosion degrees. A S-shaped membership function and fuzzy overlay analysis were used. Although the model provides only qualitative estimations, it proved useful to explore indicator-cause-process relationships. In addition, it allowed to assess the importance of the individual landscape elements related to soil erosion and select those which best predict soil erosion. The model considers the effect of rock fragments to protect the soil surface against raindrop impact and aggregate detachment. Seasonal variations in soil susceptibility to erosion because of changes in vegetation cover are also taken into account.

9.1.7 Feature discrimination

Problems in discriminating and mapping surface features related to land degradation were face at plot and regional levels.

(1) At plot level

The main factors affecting the reflectance of surface components related to the soil susceptibility to erosion, in the visible and near-infrared regions of the spectrum, were:

- soil color: color hue and value affect the red and green portions of the spectrum less than the chroma;
- organic matter contents higher than 1% were enough to decrease the overall reflectance values and flatten the spectral curve shape;
- silt-rich topsoil textures;
- density, shape and size of the surface rock fragments;
- 'bright' depositional crusts.

Main factors causing reflectance changes of surface features related to salinity and/or alkalinity were identified to be:

- terrain surface morphology and roughness: non-saline crusts have lower reflectance and slightly different curve shape than salty crusts. Surface roughness at a micro-scale explains changes in reflectance as a function of soil particle diameter. In general, reflectance decreases with increasing size of the particles;
- topsoil texture: high silt contents produce variations in reflectance and curve shape. Sandy loam textures have lower reflectance than clayey textures;
- crust color: differences in one point of color value or chroma cause changes in soil reflectance. However, the color chroma seems to control more the overall reflectance behavior of the crusts than the color value. The blue region reacts very little to alterations in color chroma. As the color hue becomes redder, the light reflection in the 600 - 700 nm increases;

- salt-tolerant vegetation decreases the overall reflectance of saline crusts.

The curve shape of the soil spectra studied for salinity-alkalinity features showed to depend mainly on the soil color, the percentage of silt and sand, and the organic matter content. The specific influence of these factors could not be established because measurements under controlled conditions are lacking. Surface roughness and morphology affect mainly the reflectance percentage in the range from 450 to 800 nm, without major changes in the curve shape.

(2) At regional level

(a) Salinity-alkalinity

Spatial discrimination of salt- and sodium-affected areas from space-borne satellite allows the following conclusions:

- 'moderate' classes are difficult to be discriminated, regardless of the data set and modelling technique used;
- discrimination of the very strongly saline class improved by the merging of Landsat TM and JERS-1 SAR data.
- differentiation between sulphate, sulphate-chloride and chloride affected soils was poor. Low class accuracies were obtained because chlorides do not have specific absorption bands in the visible, near-infrared and thermal wavelengths. As a consequence, the sulphate absorption features dominated. Higher accuracies were achieved for soda, sulphate-soda and soda-sulphate soils because both, carbonates and sulphates, have absorption features in the infrared and thermal ranges of the spectrum.

Different salinity-alkalinity degrees were masked by:

- type and abundance of the vegetation cover;
- topsoil textures, specially at high silt and clay contents;
- mixture of topsoil properties under field conditions, where salts, soil texture, crusting and soil color mutually interfere;
- land management practices, when discrimination was done from JERS-1 SAR data.

Soil texture seems to have a low influence on images collected from active sensors, unlike those collected from passive satellite sensors. Radar backscattering was affected by the roughness of the terrain surface, produced by land cultivation.

(b) Surface soil erosion

Fallow land, slightly eroded areas and moderately eroded areas were not spectrally distinct enough to allow for accurate discrimination. The incorporation of microwave data improved the separability among spectral plots representing fallow land and moderately as well as sightly eroded areas. Surface roughness

resulting from soil ploughing caused high backscattering at macro-level. This distinctive feature in the microwave region allowed the separation of classes with similar spectral behavior in the visible and infrared wavelength.

9.2 RECOMMENDATIONS

Further research should be conducted on items which could not be fully covered or even approached in the present work.

9.2.1 Related to the study area

- Analysis and monitoring of the salinization-alkalinization process in the Central valley.

Although at present this land degradation process occurs in both the Cochabamba and Punata-Cliza valleys, most of the studies are concentrated in the latter one. It is thus recommended to carry out a study to analyze the causes, mechanisms and indicators related to the salinization-alkalinization problem in the Cochabamba valley.

- Stream avulsion hazard in the Central and Sacaba valleys.

The reworking and mobilization of the moraine deposits, located in the northern parts of the Cochabamba and Sacaba valleys, constitute a permanent threat to urban settlements and agricultural fields in the lowlands. Further studies should concentrate on the analysis and modelling of buffer zones exposed to stream avulsion hazard in the piedmont area.

- Seasonal changes in salinity-alkalinity.

This research concentrates on long-term increasing salinity-alkalinity trends. Further research should focus on the seasonal variations of soil salinity-alkalinity.

- Relation between salinity-alkalinity and wind erosion in the Punata-Cliza valley.

There is a notorious soil erosion by wind, closely related to salinity-alkalinity problems. Broken puffy and fluffy saline crusts leave exposed pulverulent soil material which is blown away by the wind. Research is required to analyze the relation between both degradation processes and identify indicators of wind erosion for monitoring purposes.

9.2.2 Related to techniques and methods

- Application of a precise model for atmospheric correction.

Application of precise atmospheric correction models to test whether there are improvements in the spectral separability of land degradations indicators, compared to the use of raw remotely-sensed data.

- Fuzzy supervised classification to delineate saline-alkaline areas using Landsat TM data.

The present research only tested the advantages of fuzzy supervised classification of JERS-1 SAR data. Further research is needed to test whether fuzzy sets are suitable for mapping ground cover proportions at a sub-pixel level, compared to linear spectral unmixing techniques.

- Study of salt-related spectral plots under controlled conditions and the use of spectroradiometers covering the middle-infrared region.

Different factors were found to affect the reflectance of saline and alkaline plots. Further study should concentrate on their specific effect altering the spectral behavior of saline and alkaline plots and, also on the behavior of salinity- alkalinity-related surface features in the middle-infrared region.

- Introduce other landscape elements in the modelling process

For example, slope shape and detailed land use cover in fuzzy knowledge-based exploratory models might be relevant landscape elements for determining the spatial distribution of eroded areas.

- The use of fuzzy weighting factors in the modelling process.

Factors related to land degradation do not influence the processes in the same way. This should be accounted for by assigning weights, so that fuzzy layers representing different landscape elements are conferred variable importance during the modelling process.

REFERENCES

Agassi M., Shainberg I. and Morin J. (1981). Effect of electrolyte concentration and soil sodicity on infiltration rate and crust formation. Soil Sci. Soc. America Jnal. 45:848-851.

Agbu P., Fehrenbacker D. and Jansen I. (1990). Soil property relationships with SPOT satellite digital data in east central Illinois. Soil Sci.Soc.Am.J. 54:807-812.

Amos B. and Greenbaum D. (1987). Alteration detection using TM imagery: the effects of supergene weathering in an arid climate. ERIM, 21st. Int. Symp. on Remote Sensing of Environment, Ann Arbor, MI,USA, 1975.

Aubreville A. (1949). Climats, forét et désertification de l'Afrique tropicale. Soc. d'éditions géographiques et coloniales, Paris, 352 pages.

Al-Abbas A.H., Swain P.H. and Baumgardner M.F. (1972). Relating organic matter and clay content to the multispectral radiance of soils. Soil Science, vol.28 (2) 477-485.

Alperovitch N., Shainberg I. and Keren R. (1981). Specific effect of magnesium on the hydraulic conductivity of sodic soils. Jnal. Soil Sci. 32:543-554.

Angstrom A. (1925). the albedo of various surfaces of ground. Geografiska Ann. 7:323.

Anderson H.W. (1954). Suspended sediment discharge as related to streamflow, topography, soil, and land use. In: Trans.AGU, 34th Annual meeting, Washington,D.C. v.35-2:268-281.

Argabright Scott (1991). Evolution in use and development of the wind erosion equation. Jnal. of Soil and Water conservation. pp. 104-105.

Argollo (1982). Evolution du Piedmont Ouest de la Cordillere Royale (Bolivie) au Quaternaire. PhD. thesis, L'Université d'AIX-Marseille II. Faculté des Sciences de Luminy. 110 pages.

Ballivian O., Bles, J. and Servant M. (1978). El Plio-Cuaternario de la región de La Paz (Andes Orientales, Bolivia). Cah. ORSTOM, sér. géol., 10(1):101-114.

Bates R. and Jackson J. (1987). Glossary of geology (3rd. edition). American Geological Institute, Alexandria, Virginia. 787 pages.

Bathke G.R. and Blake G.R. (1984). Effects of soybeans on soil properties related to soil erodibility. Soil Sci. Am. J., vol.48: 1398-1401.

Baumgardner M., Kristof S., Hohannsen C. and Zachary A. (1970). Effects of organic matter on the multispectral properties of soils. Proc. Indiana Acad. Sci. 79:413-422

Baumgardner M., Silva L.F., Biehl L., Stoner E. (1985). Reflectance properties of soils. Advances in Agronomy, vol. 38:1-44.

Beasley D., Huggins L. and Monke E. (1980). ANSWERS: A Model for Watershed Planning. Transactions of the ASAE, vol.23(4):938-944.

Beaty C.B. (1974). Debris flows, alluvial fans and revitalized catastrophism. Zeitschrift für Geomorphology N.F. Suppl., 21:39-51.

Beck R.H., Robinson B.F., McFee W.H. and Peterson J.B. (1976). Info note 81.176 Lab. Applic. remote sensing Purdue Univ. West Lafayete-Indiana.

Bennet H.H. (1926). Some comparisons of the properties of humid-tropical and humid-temperate American soils, with special reference to indicated relations between chemical composition and

physical properties. Soil Science, 21:349-375.

Barnett A. and Rogers J. (1966). Soil physical properties related to runoff and erosion from artificial rainfall. Trans., ASAE 9:123-125,128.

Bergsma E. (1983). Classes of relief susceptibility for surface erosion. In: El-Swaify (Ed), Soil erosion & conserv. Hawaii, pp. 432-436.

Bergsma E. and Valenzuela C.R. (1981). Drop testing aggregate stability of some soils near Mérida, Spain. In: Earth surface processes and landform, vol.6, pp.309-318.

Bergsma E. (1985). Development of soil erodibility evaluation by simple test. In: G.Chisci and R.P.C. Morgan (Eds.). Soil erosion in the European community. Impact of changing agriculture. pp. 213-223.

Bierwirth P.N. (1990). Mineral mapping and vegetation removal via data-calibrated pixel unmixing, using multispectral images. Int.J. Remote Sensing, vol.11:1999-2017.

Black J.M.W and Chanasyk (1989). The wind erodibility of some Alberta soils after seeding: Aggregation in relation to field parameters. In: Can. J. Soil Sci., vol.69, pp.835-847.

Bocco G. and Valenzuela C. (1988). Integration of GIS and image processing in soil erosion studies using ILWIS. ITC Jnal 1988-4, pp.309-319.

Bowers S. and Hanks R. (1965). Reflection of radiant energy from soils. Soils Science 100(2):130-138.

Brackmann P., De Dapper M., Goosens R. and Kidwai A. (1992). Topographical, geomorphological and other ancillary information to classify soil material on satellite imagery, applied on the area of Messinia, Greece. IEEE 1992, pp. 950-952.

Bouyoucos G.J. (1935). The clay ratio as a criterion of susceptibility of soil to erosion. Journal of the American Society of Agronomy, vol.27. pp.738-741.

Bradford J.M., Ferris J.E. and Remley P.A. (1987). Interrill soil erosion processes: II. Relationship of Splash detachment to soil properties. Soil Sci. Soc. AM.J., vol.51:1571-1575.

Braitsch O. (1971). Salt deposits, Their origin and Composition, Springer-Verlag, Berlin, 289 pag.

Breman E. (1981). Paleoecologia de los ostracodos de pozos perforados en el cuaternario de Cochabamba, Bolivia. Revista CIAF vol.6 (1-3), 45-51.

Bronger K.A. and Catt R.J.A. (1989). Paleosols: Problems of definition, Recognition and Interpretation. Catena Supplement 16, pp.1-7.

Bruce-Okine E. and Lal R. (1975). Soil erodibility as determined by raindrop technique. Soil Science vol.119, (2): 149-157.

Bryan R.B. (1976). Considerations on soil erodibility indices and sheetwash. Catena vol.3 (Ed.) pp. 99-111.

Bryan R.B., Govers G. and Poesen J. (1989). The concept of Soil Erodibility and some problems of Assessment and Application. Catena vol.16 (Ed.).pp.393-412.

Bryan R.B. and Poesen J. (1989). Laboratory experiments on the influence of slope length on runoff, percolation and rill development. Earth surface processes and landform, vol.14: 211-231.

Bryan R.B. (1968/69). The development, use and efficiency of indices of soil erodibility. Geoderma, 2: pp.5-26.

Bryan R.B. (1974). Water erosion by splash and wash and the erodibility of some Albertan soils.

Geografiska Annaler vol. 56, 259-281.

Bryan R. (1987). Processes and significance of rill development. Catena supplement 8, pp.1-15.

Bryant R. (1995). Validated linear mixture modelling of Landsat TM data for mapping evaporite minerals on a playa surface. The RSS95 Conference, Southampton, UK, pp.729-736.

BRGM (1990). Evaluación de los recursos de agua y abastecimiento de agua potable de la ciudad de Cochabamba. SEMAPA, Cochabamba.

Bullock P. (1974). The use of micromorphology in the new system of soil classification for England and Wales. In: Rutherford. G.(ed.), Soil Microscopy. The limestone Press, Kingston, Ontario, 607-631.

Bull W. (1961). Tectonic significance of radial profiles of alluvial fans in western Fresno county, California. U.S. Geological Survey Professional Paper, 424-B, pp. 181-184.

Burrough P.A. (1989). Fuzzy mathematical methods for soil survey and land evaluation. Journal of soil science, vol.40,477-492.

Burgess T. and Webster R. (1980). Optimal interpolation and isarithmic mapping of soil properties. the semi-variogram and punctual kriging. Jnal. of Soil Science, vol. 31:315-331.

Campbell I.A. (1989). Badlands and Badland gullies. In: David S.G. Thomas (ed.) Arid zone Geomorphology. Belhaven Press. pp.159-183.

Carneiro Filho A. and Zinck J.A. (1994). Mapping paleo-aeolian sand cover formations in the northern Amazon basin from TM images. ITC Jnal. pp. 270-282.

Catt J.A. (1979). Soils and Quaternary geology in Britain. Jnal. of Soil Science, vol. 30:607-642.

Catt J.A. (1987). Palaeosols. Progress in Physical Geography, vol.ll, pp.487-510.

Catt R.J.A. (1989). Relict properties in Soils of the central and north-west European temperate region. Catena supplement 16, pp.41-58.

CSES-CIRES (1992). Spectral Image Processing System (SIPS) user's manual, version 1.2, University of Colorado, Boulder, 88 pages.

Childs S. and Flint A. (1990). Physical properties of forest soils containing rock fragments. In: S.P.Gessel, D.S. Lacate, F.F. Weetman and R.F. Powers (Eds.). Sustained productivity of forest soils. University of British Columbia, Faculty of Forestry Publ. Vancouver, B.C. pp.95-121.

Chorley R.J. (1959). The geomorphic significance of some Oxford soil. American Journal of Science, vol.257, pp.503-515.

Cipra J., Franzmeier D., Bauer M. and Boyd R. (1980). Comparison of multispectral measurements from some non-vegetated soils using Landsat digital data and a spectroradiometer. Soil Sci.Soc.Am.J. 44:80-84.

Cipra J., Baumgardner M., Stoner E. and MacDonald R. (1971). Measuring radiance characteristics of soil with a field spectroradiometer. Soil Sci.Soc.Am.Proc. 35:1014-1017.

Clapperton C.M. (1979). Glaciation in Bolivia before 3.27 Myr. Nature vol. 277, pp. 375-377.

Clapperton C.M. (1981). Quaternary glaciations in the Cordillera Blanca, Peru, and the Cordillera

Real, Bolivia. Memoria del Primer Seminario sobre el Cuaternario de Colombia, Bogotá, Agosto 25 al 29 de 1980. Revista Centro Interamericano de Fotointerpretación C.I.A.F. (Bogotá), 6, 93-111.

Clapperton, C.M. (1983). The glaciation of the Andes. Quaternary Science Reviews, 2, 83-155.

Coleman T.L. and Montgomery O.L. (1987). Soil moisture, organic matter and iron content effect on the spectral characteristics or selected vertisols and alfisols in Alabama. Photogramm. Eng. remote sens. 53:1659-1663.

Coleman T.L., Agbu P.A., Montgomery O.L. and Prasad S.(1991). Spectral band selection for quantifying selected properties in highly weathered soils. Soil Science 151,5,355-361.

Coleman T.L., Agbu P.A. and Montgomery O.L. (1993). Spectral differentiation of surface soils and soil properties: is it possible from space platforms?. Soil Science, vol. 155, (4): 283-293.

Condit H. (1970). The spectral reflectance of American soils. Photogramm. Eng. 36:955-966.

Congalton R. (1991). A review of assessing the accuracy of classifications of remotely sensed data. Rem.Sens. of Environ. 37:35-46.

Cropscan (1991). Cropscan user's manual, 30 pages.

CORDECO (1991/92). Diagnóstico del efecto de la sequía en el año agrícola 1991-1992. Comisión técnica de emergencia, CORDECO. Cochabamba, Bolivia.

CORDECO-SUBDESAL (1993). Plan general de riego del valle Alto. 6 tomos, Cochabamba, Bolivia.

Cressie N. and Hawkins D. (1980). Robust estimation of the variogram. Mathematical geology. vol.12(2):115-125.

Cross A.M. and Settle J.J. (1991). Subpixel measurement of tropical forest cover using AVHRR data. Int.J. Remote Sensing, vol.12(5)1119-1129.

Csillag F., Pasztor L. and Biehl L. (1993). Spectral band selection for the characterization of salinity status of soils. remote Sens. Environ. 43: 231-242.

Davis P.A.Jr., Grolier M.J., Schultejann P.A. and Eliason P.T. (1982). Discrimination of Phosphate, Gypsum, Limestone, Halide and Quartz-Sand deposits in South-Central Tunisia by cluster analysis of Landsat multispectral data. Presented at the First Thematic Conference: "Remote sensing of arid and semi-arid lands", Cairo, Egypt, January, 1982, pp.337-359.

Dombi J. (1990). Membership function as an evaluation. Fuzzy sets and systems 35. pp. 1-21.

Drake N., Bryant R., Milligton A. and Townshend J. (1994). Playa sedimentology and geomorphology: mixture modelling applied to Landsat Thematic Mapper data of Chott El Djerid, Tunisia. Sedimentology and Geochemistry of Modern and Ancient Saline Lakes. SEPM Special Pub. No.50, pp.126-131.

Driessen P.M. and Schoorl (1973). Mineralogy and morphology of salt efflorescence on saline soil in the great Konya basin, Turkey. Soil Science, vol.24 (4) 436-443.

Driessen P. and Dudal R. (1991). Lecture notes on the geography, formation, properties and use of the major soils of the world. Agricultural University Wageningen-Catholic Univ. Leuven, 295

pages.

Drummond J.E. (1991). Determining and Processing quality parameters in GIS. PhD thesis, University of Newcastle upon Tyne. Chapter 5:Fuzzy subset theory. pp.152-171.

Durand J.M., Gimonet B.J. and Perbos J.R. (1987). SAR data filtering for classification. IEEE Trans. Geoscience and Remote Sensing, 25, pp.629-637.

Eghbal M.K., Southard R.J. and Whitting L.D. (1989). Dynamics of evaporite distribution in soils on a fan-playa transect in the Carrizo plain, California. Soil Sci.Am.J., vol.53: 898-903.

Ekwue E.I. (1990). Effect of organic matter on splash detachment and the processes involved. Earth surface proc. and landform, vol.15, 175-181.

Elliot W.J., Laflen J.M. and Kohl K.D. (1989). Effect of soil properties on soil erodibility. Paper No.89-2150. Am.Soc.Agr.Engs., St. Joseph, Mich., 24 pages.

El-Swaify S. and Dangler E. (1976). Erosion of selected Hawaii soils by simulated rainfall. Soil Sci. Soc. Am., Ankeny, Iowa, pp.105-114.

Ellenberg, H. (1981). Desarrollar sin destruir. I.E., La Paz, Bolivia.

Epema G. (1986b). Processing thematic mapper data for mapping in Tunisia. ITC Journal 1986-1, pp.30-34.

Epema G. (1990a). Diurnal trends in reflectance of bare soil surfaces in southern Tunisia. Geocarto International 4:33-39.

Epema G. (1990b). Effect of moisture content on spectral reflectance in a playa area in southern Tunisia. Proc. of the Int. Symp. on Remote Sensing Water Resources, IAH, Enschede, The Netherlands, pp. 301-308.

Epema G. (1993). Mapping surface characteristics and their dynamics in a desert area in southern Tunisia with Landsat Thematic Mapper. PhD. thesis, Agricultural University of Wageningen.

Epstein E. and Grant W.J. (1971). Soil erodibility as affected by soil surface properties. Transaction of the ASAE, vol.14, 647-648.

Escadafal R. (1989). Caractérisation de la surface des sols arides par observations de terrain et par téledétection. PhD. thesis, University of Paris, 317 pp.

Escadafal R. (1992). Remote sensing of soil color: principles and applications. Remote sensing reviews.

Escadafal R. and Huete A. (1992). Soil optical properties and environmental applications of remote sensing. Int. Arch. Photogramm. Rem. Sens., vol 29(B7), 709-715.

Escadafal R. and Courault M. (1989). Munsell soil color and soil reflectance in the visible spectral bands of Landsat MSS and TM data. Remote Sens. Environ. 27:37-46.

Escadafal R. (1994). Soil spectral properties and their relationships with environmental parameters. Examples from arid regions. In: Imaging Spectrometry - a tool for environmental observations. Hill J. and Mégier J. (Eds.), ECSC, EEC, EAEC, Brussels and Luxembourg, pp. 71-87.

Evans R. (1980). Mechanics of water erosion and their spatial and temporal controls: an empirical viewpoint. In: Kirby, M. and Morgan, R. (eds.), Soil Erosion, Wiley, New York, pp.109-128.

Evans R. (1989). Mechanic of Water Erosion and their Spatial and Temporal Controls: An empirical viewpoint. In: Kirkby and Morgan (Ed.) Soil Erosion. John Wiley & Sons. pp.109-128.

Everitt J., Escobar D., Gerbermann A. and Alaniz M. (1988). Detecting saline soils with video imagery. Photogrammetric Engineering and Remote Sensing, 54:1283-1287.

FAO (1990). Guidelines for soil description. 3rd. Edition. 70 pag.

Fernandez J., Bluck B.J. and Viseras C. (1993). The effects of fluctuating base level on the structure of alluvial fan and associated fan delta deposits: an example from the Tertiary of the Betic Cordillera, Spain. Sedimentology 40,879-893.

Fisher P.F. and Pathirana S. (1990). The evaluation of fuzzy membership of land cover classes in the suburban zone. Remote sensing environ., vol.34:121-132.

Foody G. (1994). Fuzzy modelling of vegetation from remotely sensed imagery. Ecological modelling, in press.

Foster G.R. (1982). Modelling the erosion process. In: Haan et al.(eds), Hydrologic modelling of small watersheds. ASAE Monograph number 5, 297-380.

Foster G. R. (1987). Modelling soil erosion and sediment yield. In: Lal, R. (ed.), Soil erosion research methods, 97-117. Soil and Water Conservation Society, Ankeny, Iowa.

Foster G.R. (1991). Advances in wind and water erosion prediction. Journal of Soil and Water Conserv. vol.46 (1): 27-44.

Frenkel H. and Meiri A. (1985). The effect of salinity and sodicity on the physical properties of soils. In: Frenkel H. and A. Meiri (Eds.), Soil salinity. Two decades of research in irrigated agriculture. pp.53-61.

Frenkel H., Goertzen J.O. and Rhoades J.D. (1978). Effects of clay type and content, exchangeable sodium percentage, and electrolyte concentration on clay dispersion and soil hydraulic conductivity. Soil Sci. Soc. America Jnal. 42:32-39.

Fryrear D.W., Krammes C.A., Williamson D.L. and Zobeck T.M. (1994). Computing the wind erodible fraction of soils. Journal soil and water cons. 49 (2): 183-188.

Frost V., Stiles J., Shanmugan K. and Holtzman J. (1982). A model for radar images and its application to adaptive digital filtering of multiplicative noise. IEEE Trans. on Pattern Analysis and Machine Intelligence, vol. PAMI-4, No.2, pp.157-165,

Gajem Y., Warrick A. and Myers D. (1981). Soil Science Soc. Am. Jnal. vol 45:709-715.

Gabriels D. and De Boodt M. (1975). A rainfall simulator for soil erosion studies in the laboratory. In: Pedologie, XXV, 2, pp.80-86.

Gates D., Keegan H., Schleter J. and Weidner V. (1965). Spectral properties of plants. Applied Optics vol. 4:11-20.

GEOBOL-ONU (1977/1978). Investigaciones de aguas subterráneas en las cuencas de Cochabamba. Proyecto integrado de recursos hídricos, Cochabamba. Informe Técnico. PNUD/Octubre Bol/73/008.

Gedroitz K.K. (1955). Selected papers in soil science (Russian), vol.1., Soil colloids and exchange properties of soils; vol.ll. Chemical analyses of soils; vol. lll. Use of fertilizers. Soil amelioration and field experiments, Sel'-Khozgiz, Moscow.

Gore R.S. and Bhagwat K.A. (1991). Saline degradation of Indian agricultural lands: A case study in

Khambhat Taluka, Gujarat State (India), using satellite Remote Sensing. Geocarto International (3):5-13.

Gorte B. and Koolhoven W. (1990). Interpolation between isolines based on the Borgefors distance transform. ITC Jnal. 1990-3, pp. 245-247.

Gouzes R. and Delpont G. (1990). Evaluación de los recursos de agua y abastecimiento en agua potable de la Ciudad de Cochabamba, Bolivia. B.R.G.M./SEURECA,France, 45 pag.

Graf K. (1977). Nuevos datos Palinológicos del Cuaternario alto de Bolivia. Boletín de GEOBOL, Serie A, vol.1(1):1-14. La Paz.

Graf K. (1981). Palynological investigations of two post-glacial peat bogs near the boundary of Bolivia and Peru. Journal of Biogeography vol.8:353-368.

Graf K. (1983). A quaternary pollen profile from the upper valley of Cochabamba (Bolivia). INQUA Sym. on the Genesis and Lithology of Quaternary deposits/USA 1981/Argentina 1982, pp.365-372.

Grunblatt J., Ottichilo W. and Sinange R. (1992). A GIS approach to desertification assessment and mapping. Jnal. of Arid Environments. 23(1):81-102.

Hansen B., Wright H. and Bradbury J. (1984). Pollen studies in the Junín area, central Peruvian Andes. Geological Society of America Bulletin, vol. 95:1454-1465.

Hanan N.P., Prince S.D. and Hiernaux P.H.Y. (1991). Spectral modelling of multicomponent landscapes in the Sahel. Int.J. Remote Sensing, vol.12(6):1243-1258.

Harvey A.M. (1989). The occurrence and role of Arid zone Alluvial Fans. In: David S.G. Thomas (ed.) Arid zone geomorphology. Belhaven Press.

Harvey A.M. (1978). Dissected alluvial fans in southeast Spain. Catena, vol.5, 177-211.

Harvey A.M. (1990). Factors influencing Quaternary alluvial fan development in southeast Spain. In: Rachocki A. and Church M. (eds.), Alluvial Fans. A field approach, pp.247-270.

Hare F. (1985b). Climate variations, drought and desertification. WMO 653:35.

Hastenrath S. and Kutzbach (1985). Late Pleistocene climate and water budget of the South American Altiplano. Quaternary research 24,249-256.

Henderson T., Szilagyi A., Baumgardner M., Chen C. and Landgrebe D. (1989). Spectral band selection for classification of soil organic matter content. Soil Sci.Soc.Am.J. 53:1778-1784.

Hilgard E.W. (1906). Soils: Their formation, properties, composition and relations to climate and plant growth in the humid and arid regions. Macmillan, New York.

Hill J. (1993). Land degradation and soil erosion hazard mapping in Mediterranean environments with operational earth observation satellites. Symposium Operazionalization of Remote Sensing, April 1993, Enschede, The Netherlands, pp.41-51.

Holdridge, L.R. (1947). Determination of world plant formations from simple climatic data. Science, vol. 105, No.2027, pp.367-368.

Horn M. (1971). Estimating soil permeability rates. Proc. ASAE (IR2):263-273.

Hutchinson D. and Pritchard H. (1976). Resource conservation glossary. In: Jnal. of Soil and Water Conservation, 31(4). 63 pages.

Hunt G.R. (1980). Electromagnetic radiation: The communication link in remote sensing. In: B.Siegal & A.Gillespie (Eds.) Remote Sensing in Geology, New York, Wiley: 5-46.

Hunt G., Salisbury J. and Lenhoff C. (1971). Visible and near-infrared spectra of minerals and rocks: IV. Sulphides and sulphates. Modern Geology, vol 3. pp. 1-14.

Hunt G.R. and Salisbury J.W. (1971). Visible and near-infrared spectra of minerals and rocks: II. Carbonates. Modern Geology, vol.2, pp. 23-30.

Huete A. and Escadafal R. (1991). Assessment of biophysical soil properties through spectral decomposition techniques. Remote Sens. Environ. 35:149-159.

Instituto Nacional de Estadística, INE (1984). Reporte del censo nacional de población, La Paz, Bolivia.

ITC-CUMAT-UMSS (1989). Levantamiento de suelos a nivel de reconocimiento de la zona del valle Alto, Cochabamba, Bolivia. 98 páginas.

ITC (1993). ILWIS User's manual. ITC, Enschede, The Netherlands.

IDRISI for Windows (1995). User's manual, version 1.0. Clark University, USA.

Jensen J. (1986). Introductory digital image processing. Prentice Hall, New Jersey, USA, 379 pages.

Jenny H. (1980). The soil resource. Origin and behaviour. Ecological studies, vol. 37, Springer-Verlag, New York.

Jiang B., Ormeling F. and Kainz W. (1995). Visualization support for fuzzy spatial analysis. ACSM/ASPRS Conf., Charlotte, North Caroline, pp.291-300.

Jiang Bin (1996). Fuzzy overlay and visualization in Geographic Information Systems. PhD. thesis. Utrecht University, 165 pages.

Jones J. (1987). The initiation of natural drainage networks. Progress in physical geography vol. 11,pp.207-245.

Jordán D.L. (1977). Caracteristicas hidroquímicas de las unidades hidrogeológicas de la cuenca Cliza-Punata. Servicio Geológico de Bolivia.14 pag.

Journel A. and Huijbregts C. (1978). Mining geostatistics. London, 600 pages.

Justusson B. (1978). Noise reduction by median filtering. Proc. 4th. Int. Conference Pattern Recognition. Kyoto, Japan, pp.502-504.

Justice C., Dugdale g., Townshend J., Narracott A. and Kumar N. (1991). Synergism between NOAA-AVHRR and Meteosat data for studying vegetation in semi-arid West Arica. Int. Jnal. of Remote Sensing, vol.12, pp. 1349-1368.

Kahle A.B. (1982). Spectral remote sensing of rocks in arid lands. In: First Conf.: R. Sen. of Arid and semiarid lands, Cairo, Egypt, January, 1982.

Kamphorst A. (1987). A small rainfall simulator for the determination of soil erodibility. Netherlands Journal of Agricultural Science 35: pp.407-415.

Kazman Z., Sainberg I. and Gal M. (1983). Effect of low levels of exchangeable sodium and applied phosphogypsum on the infiltration rate of various soils. Soil Sci. 135:184-192.

Karmonova L. (1981). Effect of various iron compounds on the spectral reflectance and color of soils.

F. Lumumba University, Moscow. Sov. Soil Sci. 13:53-60.

Kennan L., Lamb S. and Rundle C. (1995). K-Ar dates from the Altiplano and Cordillera Oriental of Bolivia: implications for Cenozoic stratigraphy and tectonics. J.of South Am.Earth Sci.,vol.8:2:163-186.

Key J.R., Maslanik J.A. and Barry R.G. (1989). Cloud classification from satellite data using a fuzzy sets algorithm: A polar example. Int.J. Rem. Sensing vol.10,12:1823-1842.

Kirkby M.J. (1989). The problem. In: Kirkby M.J. and Morgan R.P.C. (Ed.). Soil Erosion. John Wiley & Sons. pp.1-12.

Klir G.J. and Folger T.A. (1988) Fuzzy Sets, Uncertainty and Information. Ed. Prentice-Hall International,Inc. 347 pages.

Krishnan P., Alexander J., Butter B. and Hummel J. (1980). Reflectance techniques for predicting soil organic matter. Soil Sci.Soc.Am.J. 44:1282-1285.

Kovda V.A. (1977). Arid land irrigation and soil fertility. Problems of salinity, alkalinity and compaction, in arid land irrigation in developing country, Pergamon Pres, New York, 211.

Kovda V.A. (1947). Origin and regime of Salt-Affected soil (Russian), vols. 1 and 2, Izd.Ak. Nauk SSSR, Moscow.

Kust G.S. (1992). Desertification assessment and mapping in the pre-aral region. Desertification bulletin Nº21, pp.38-43.

Laflen J.M., Foster G.R., Hagen L.J. and Lane L.J. (1980). Replacement of the wind and water erosion prediction equations. In: Conser. and Erosion data Base. 5th. International Soil Cons. Conf., Bangkok. pp. 509-515.

Lal, R. (1988). Erodibility and erosivity. In: Lal, R. (ed.), Soil erosion research methods. SWCS/ISSS, Wageningen, 140-160.

Lal R. and Stewart B. (1990). Soil degradation: a global threat. In: Lal and Stewart (eds.), soil degradation. Springer-Verlag, New York, 345 pages.

Lal R. and Elliot W. (1994). Erodibility and erositivity. In: R. Lal (Editor), Soil erosion research methods. pp. 181-210.

Larney F. and Bullock M. (1994). Influence of soil wetness at time of tillage and tillage implement on soil properties affecting wind erosion. Soil and Tillage Research , vol 29, pp. 83-95.

Latz K., Weismiller R., van Soyoc G. and Baumgardner M. (1984). Characteristic variation in spectral reflectance of selected eroded Alfisols. Soil Sci.Soc.Am.J. 48:1130-1134.

Lauer, W. and Rafiqpoor, M. (1986). Die jungpleistozäne Vergletscherung der Apolobamba-Kordillere (Bolivien). Erdkunde, 43:228-231.

Lavenau A. (1986). Etude Tectonique et neotectonique de l'altiplano et de la cordellere orientale des andes boliviennes. PhD. thesis, Universite de Paris-Sud, Centre D'Orsay, 393 pages.

Lavenau A. and Ballivian O. (1979). Estudios neotectónicos de las cuencas de las regiones de Cochabamba, Sucre, Tarija, Cordillera Oriental. Bolivia. Rev. Ac. Nac. Cien. Bol., año 2, No.3,pp.107-129.

Lee K., Lee G. and Tyler E. (1988a). Determination of soil characteristics from Thematic Mapper data of a cropped Organic-Inorganic soil landscape. Soil Sci.Soc.Am.J. 52:1100-1104.

Lee J. (1986). Speckle supression and analysis form synthetic aperture radar images. Optical Engineering 25(5):636-643.

Lee J. and Juerkevich I. (1989). Segmentation of SAR images. IEEE Trans. on Geoscience and Rem.Sens., vol 27(6):674-680.

Lee K. (1990). characterization of forest stands using spaceborne radar and optical remote sensor data. Ph.D. thesis, Colorado University, U.S.A., 206 pages.

Le Bissonais Y. (1990). Experimental Study an Modelling of Soil Surface Crusting Processes. In: Rorke B. Bryan (Ed.) Soil Erosion -Experiments and Models. Catena Supplement 17. pp.13-28.

Le Bissonnais Y., Singer M.J. and Bradford J.M. (1993). Assessment of soil erodibility: the relationship between soil properties, erosion processes and susceptibility to erosion. In: S. Wicherek (Ed.). Farm Land Erosion: In temperate Plains Environment and Hills. Elsevier Science Publishers B.V. pp.87-96.

Lindsay J. and Gumbs F. (182). Erodibility indices compared to measured values of selected Trinidad soils. Soil Sci.Soc.Am.J. 46:393-396.

Lo A., El-Swaify S.A. and Rose C.W. (1988). Comparing empirical and process-based indices of Soil susceptibility to erosion. 5th. Intern. Soil Conservation. Conference Bangkok 1988, pp.403-417.

Lopez A., et al., (1990). Maximum a posteriori speckle filtering and first order texture models in SAR images. IGARSS' 90, vol.III, Washington.

Lopez A., Touzi R. and Nezry E. (1990). Adaptive Speckle filters and scene heterogeneity. IEEE Trans. on Geoscience and Remote Sensing, vol.28, No.6.

Lozano F. (1988). Analysis of synergistic effects of a combined spaceborne multispectral scanner and L-band multiple incidence angle radar set. PhD. thesis, Purdue University, 241 pages.

Luk S.H. (1979). Effect of Soil properties on Erosion by Wash and Splash. Earth Surface Processes, vol.4, pp.241-255.

Luk Shiu-hung (1977). Rainfall erosion of some Alberta soils a laboratory simulation study. Catena, vol.3, pp.295-309.

Lyles L. and Tatarco J. (1986). Wind erosion effects on soil texture and organic matter. Jour. of Soil and Water Conser., vol.41, (3): 191-192.

Mabbut J.A. (1977). Desert Landform. The MIT Press, Cambridge, Masachusetts, 340 pages.

Mabbutt J.A. (1986). Desertification in Australia. In: Arid land development and the combat against desertification: an integrated approach. UNEP-UNEPCOM, Moscow, pp.101-112.

MACA-SUBDESAL (1993). Proyecto de desarrollo alternativo Sacaba. Tomo 6: Estudio de suelos. 101 páginas.

Mainguet M. (1991). Desertification. Natural Background and Human Mismanagement. Springer-Verlag, Berlin. 306 pages.

Maizels, J. (1993). Long-term palaeochannel evolution during episodic growth of an exhumed Plio-Pleistocene alluvial fan, Oman. In: Alluvial fans. A field approach. Rachocki A. and Church M. (Eds.), John Wiley & Sons, Chichester, England. pp.271-304.

Manrique L.A. (1988). Land erodibility assessment methodology. In: LEAM, Using soil survey data based in soil taxonomy. Ed. & Publication SHOP, Honolulu, Hawaii, USA, 28 pag.

Manzilla L.W. (1979). Geologia del Plio-Cuaternario de la cuenca de Sacaba-Cochabamba. Tesis de Grado, Univ. Mayor de San Andres, 76 pag.

Martin D.C., Piteau D.R., Pearce R.A. and Hawley P.M. (1984) Remedial measures for debris flows

at the agassiz mountain institution, British Columbia. Can. Geotech. J., vol. 21, pp.505-517.

Martin W. (1988). Die erodierbarkeit von böden unter simulierten und naturlichen regen und ihre abhangigkeit von bodeneigenschaften. Thesis. Technical University Munchen, 160 pages.

Martz L. (1992). The variation of soil erodibility with slope position in cultivated Canadian prairie landscape. In: Earth surface proc. and landform, vol.17, pp.543-556.

Mathers P. (1986). Computer processing of remotely sensed images. An introduction. Wiley&Sons, Chichester, 352 pages.

Matheron G. (1963). Principles of geostatistics. In: Economic geology 51246-1266.

Matheron G. (1965). Les variables regionalisees et leur estimation. Une application de la theorie des functions aleatoires aux sciences de la nature, Paris.

McBratney A. and Webster (1981). Spatial dependence and classification of the soil along a transect in northeast Scotland. Geoderma, vol.26:63-82.

Mathews H.L., Cunningham R.L. and Petersen G.W. (1973). Application of multispectral remote sensing to soil survey in southern Pennsylvania. Soil Science Soc.Am.Proc. Madison-West Lafayete-Indiana.

McConnell S.G. (1989). Potential wind and water erodibility of four Land-Use Systems in South-Eastern Montana, USA. In: Agric., Ecosys. and Envir., vol. 25 (1989), pp. 207-215.

Meer van der F. (1995). Imaging spectrometry and the Ronda peridotites. PhD thesis, Univ. Wageningen. Chapter 8: Mineral mapping and automatic feature extraction from imaging spectrometer.pp.197-232. Chapter 9: Imaging spectrometry and the Ronda peridotites. pp.237-274.

Mercer, J.H. and Palacios, M.O. (1977). Radiocarbon dating of the last glaciation in Peru. Geology, 5, 600-604.

Merzouk A., Blake R.G.R. and St Paul (1991). Indices for the estimation of interrill erodibility of Moroccan soils. Catena,vol.18 pp. 537-550.

Metternicht G. (1993). A comparative study on the performance of spatial filters for speckle reduction in ERS-1 SAR data. Proc. of the 13th EARSeL Symposium, Dundee, Scotland, U.K., pp.275-283.

Meyer L.D. and Harmon W.C. (1984). Susceptibility of Agricultural Soil to Interrill Erosion. Soil Sci. Am. J., vol.48, pp. 1152-1157.

Middleton H.E. (1930). Properties of soil which influence soil erosion. In: Tech.Bulletin Nº 178, U.S. Depart. of Agriculture, Washington, D.C. pp. 1-16.

Moore D.C. and Singer M.J. (1990). Crust formation effects on soil erosion processes. In: Soil Sci. Soc. Am. J. 54: 1117-1123.

Moree L. (1975). Estudio hidrometeorológico del area de los Valles de Cochabamba. Ed. PIRHC. PP. 4-35.

Mougenout B., Pouget M. and Epema G. (1993). Remote sensing of salt affected soil. Remote Sensing Reviews, vol.7, 241-259.

Mueller P. and Hoffer R. (1989). Low pass filtering of satellite radar data. Photogrammetric Engineering and Rem. Sens. 55(6):887-895.

Mulders M.A. (1987). Remote Sensing in Soil Science. Elsevier (Ed.) 379 pag.

Mulders M. and Girard M. (1993). Remote sensing of soils in warm arid and semi-arid lands. Remote Sensing Reviews, vol. 7, 341-363.

Naveh Z. (1989). The challenges of desert landscape ecology as a transdisciplinary problem-solving oriented science. Journal of arid Env. 17: 245-253.

Negoita C.V. (1985). Expert systems and fuzzy systems. Ed. The Benjamin/Cummings Publishing Company,Inc. pp. 47-93.

Nezry E., Lopez A. and Touzi R. (1991). Detection of structural and textural features for SAR images filtering. IEEE Trans. Geoscience and Remote Sensing, 30, pp.2169-2172.

Nicodemus F., Richmond J., Hsia J., Ginsberg I. and Limperis (1977). Geometrical considerations and nomenclature for reflectance. NBS Monograph 160, U.S. Dept.of Commerce, Washington, D.C.

Nickling W.G. and Fitzsimons J.G. (1983). Relationship of soil type and agricultural systems to wind erosion in southwestern Ontario. In: El Swaify (Ed), Soil erosion & conserv., Hawaii, pp.34-50.

OAS (1991). Primer on Natural Hazard Management in Integrated Regional Development Planning. Washington D.C.

Olsson, L. (1985). An integrated study of desertification. Application of remote sensing, GIS and spatial models in semiarid Sudan. Lund Studies in Geography, Serie C, No.13, 170 pages.

Oberlander T.M. (1974). Landscape inheritance and the pediment problem in the Mojave Desert of southern California. American J. of Sci., 274: 849-875.

Obi M.E, Salako F.K., Lal N.R. and Ibadan (1989). Relative susceptibility of some Southeastern Nigeria soils to erosion. In: Catena, vol.16, pp.215-225.

Olson T.C. and Wischmeier W.H. (1963). Soil - Erodibility for soils on the Runoff and erosion stations. In: Soil Science Soc. Of A@erica Procceding, vol.27, 1963.

Onstad C.A. and Young R.A. (1982). Erosion characteristics of Three Northwestern soil. In: Transactions of the ASAE 1982, pp. 367-371.

Ovando S.J.A. (1982). ! Detener las torrenteras! Proyecto original del Parque Tunari. In: Ecología y Recursos naturales en Bolivia, Centro pedagógico y cultural portales, pp. 105-119.

Obukhov A and Orlov D. (1964). Spectral reflectivity of the major soil groups and possibility of using diffuse reflection in soil investigations. Sov.Soil Sci. 2:174-184.

Pan H. (1990). A spatial structure theory in machine vision and its application to structural and textural analysis of remotely sensed images. PhD. thesis, Twente University, Enschede, The Netherlands, 230 pages.

PCI Inc. (1994). PCI User's manual.

Plicht J.van der and Mook W.G. (1989). Calibration of Radiocarbon ages by computer. Radiocarbon, vol.31(3):805-816.

Poesen J., Torri D. and Bunte K. (1994). Effects of rock fragments on soil erosion by water at different spatial scales: a review. Catena vol. 23:141-166.

Poesen J. and Lavee H. (1994). Rock fragments in top soils: significance and processes. Catena vol. 23, pp. 1-28.

Plyusnin I.I. (1969). Reclamative Soil Science. Ed. Foreign Languages Pub. House - Moscow, 398 pages.

Rapp A. (1974). A review of desertization in Arica-water, vegetation and man. Secretariat Int. Ecol., Stockholm, Sweden, 77 pages.

Ramesh P., Dickinson W.T., Green D. and McGirr R. (1982). Impacts of soil characteristics on soil erodibility. In: Proceedings of the Exeter Symposium, July 1982. IAHS Publ. Nº137. pp.39-47.

Rao B.R.M., Dwivedi R.S., Venkataratnam L., Ravishankar T., Thammappa S.S., Bhargawa G.P., Singh A.N. (1991). Mapping the magnitude of sodicity in part of the Indo-Gangetic plains of Uttar Pradesh, Northern India using Landsat-TM data. In: Int.J. Remote Sens., vol. 12 (3): 419-425.

Retallack, G. (1981). Fossil soils: indicators of ancient terrestrial environments. In: Niklas, K.(ed), Paleobotany, paleoecology and evolution, vol. 1. New York: Praeger, pp.55-102.

Richards (1986). Remote Sensing digital image analysis. An introduction. Springer-Verlag, Berlin, 277 pages.

Römkens M.J.M. (1983). The soil erodibility factor: A perspective. In: El-Swaify (Ed). Soil erosion & conservation, Conf. Hawaii, pp. 445-461.

Römkens M.J.M., Prasad S.N. and Poesen J.W.A. (1986). Soil erodibility and properties. XIII. Congress of the Intern. Soc. of Soil Sci., vol.(v) 492-504.

Römkens M.J.M., Poesen J.W.A. and Wang J.Y. (1988). Relationship between the USLE soil erodibility factor and soil properties. In: 5th. Int.Soil Conservations Conf. Bangkok,1988, pp. 371-385.

Römkens M.J.M., Roth C.B. and Nelson D.W. (1977). Erodibility of selected Clay Subsoils in relation to physical and chemical properties. In: Soil Sci. Soc. Am. J., vol. 41, pp.954-960.

Roo, A. de (1993). Modelling surface runoff and soil erosion in catchments using geographical information systems. Validity and applicability of the ANSWERS model in two catchments in the lower area of South Limburg (The Netherlands) and one in Devon (UK). PhD. thesis, University of Utrecht, The Netherlands, 293 pages.

RÖthlisberger, F. (1987). 10,000 Jahre Gletschergeschichte der Erde, Verlag Sauerlander, Aarau, 348 pages.

Rozanov, B. (1984). Principles of the doctrine on environment. IGU, Moscow, 273 pages.

Ruhe R. (1956). Geomorphic surfaces and the nature of soils. Scoil Science, vol 82:441-455.

Sanz, A. (1994). El suicidio de cochabamba. Diario Opinion, 25.05.94. Cochabamba.

Salski A. (1992). Fuzzy knowledge-based models in ecological research. Ecological Modelling, 63,103-112.

SENAMHI (1994). Datos de Precipitación, Cochabamba, Bolivia

Semapa (1994). Plan maestro para el abastecimiento de agua potable de la ciudad de Cochabamba y diseños finales de obras de rehabiltiación y ampliación. Estudios hidrogeológicos. Cochabamba, 1994.

Soil Survey Staff (1992). Keys to soil taxonomy. SMSS Technical Monograph No.19. Pocahontas Press, Inc. Blacksburg, Virginia, 529 pages.

Schmucker K. (1982). Fuzzy sets, natural language computations and risk analysis. Computer Science Press, 189 pages.

Sehgal J. and Abrol L.P. (1992). Land degradation status: India. In: Desertification Bulletin, Nº21, 1992.

Seltzer G.O. (1990). Recent glacial history and paleoclimate of the Peruvian-Bolivian Andes. Quaternary Science reviews, vol.9,pp.137-152.

Semmel A. (1989). Paleopedology and Geomorphology: examples from the western part of central Europe. In: Bronger A. and Catt J. (eds.), Paleopedology: nature and application of paleosols. Catena supplement 16, pp.143-162. Catena Verlag, W.Germany.

Servant M. (1978). El cuadro estratigráfico del Plio-Cuaternario del Altiplano de los Andes tropicales de Bolivia. Rev.de Geoc.UMSA, vol.1 (1)23-29.

Shainberg I., Rhoades J.D., Suarez D.L. and Prather R.J. (1981). Effect of mineral weathering on clay dispersion and hydraulic conductivity of a sodic soil. Soil Sci. Soc. America Jnal, 45: 273-277.

Sherard J.L., Dunnigan L.P., Decker R.S. and Steele E.F. (1976). Identification and nature of dispersive soils, Journal of the Geotechnical Division, A.S.C.E., vol. 102, Nº GT4, pp.187-301.

Sheridan (1981). Desertification of the United States. Conc. Environ. Qual, 142 pp

Singh R.P. and Srivastav S.K. (1990). Mapping of waterlogged and salt-affected soils using microwave radiometers. In: Int. J. Rem. Sen., vol. 11, (10): 1879-1887.

Singh A.N. (1994). Monitoring change in the extent of salt-affected soils in northern India. In: Int. J. Remote Sen., vol. 15 (16): 3173-3182.

Skidmore E.L., Hagen L.J., Armbrust D.V., Durar A.A., Fryrear D.W., Potter K.N., Wagner L.E., Zobeck T.M (1994). Methods for investigating basic processes and conditions affecting wind erosion. In: R. Lal (Editor) Soil erosion research methods. pp. 295 - 330.

Skidmore E.L. (1994). Wind erosion. In: R. Lal (Editor), Soil erosion research methods. pp.265-294.

Smith M., Johnson P. and Adams J. (1985). Quantitative determination of mineral types and abundances from reflectance spectra using principal component analysis. Jnal. of Geophysical research, vol. 90, supplement, pp. C797-C804.

Smith D., Ustin S., Adams J. and Gillespie A. (1990a). Vegetation in deserts. I. A regional measure of abundance from multispectral images. Remote Sensing of Environment, 31:1-26.

Stein A. (1993). Introduction to geostatistics. Lecture notes, Wageningen, 40 pages.

Stoner E. (1979). Physicochemical, site, and bidirectional reflectance factor characteristics of uniformly moist soils. Ph.D. dissertation, Purdue Univ., West Lafayette, Ind. (Libr. Congr. Card. No.Mic.80-15525).

Stoner E.R. and Baumgardner (1981). Characteristic variations in reflectance of surface soil. Soil Sci.Am.J., vol.45,1161-1165.

Stoner E., Baumgardner M., Weismiller R., Biehl L. and Robinson B. (1980). Extension of laboratory measured soil spectra to field conditions. Soil Sci.Soc.Am.J. 44:1161-1165.

Swain P. and Davis s. (1978). Remote sensing: the quantitative approach. Mc.Graw Hill, USA. 395

pages.

Szabolcs, I. (1988). Salt-affected soils. CRC Press, Inc. Boca Raton, Florida. 261 pages.

Szabolcs I. (1992). Salinization of soil and water and its relation to desertification. Desertification Bulletin No. 21 pp.32-37.

Terrazas U.W. (1982). El deterioro de los valles Mesotermicos. In: Ecología y recursos naturales en Bolivia. Centro pedagógico y cultural portales. pp. 121-123.

Torrent J., Schwertmann U., Fechter H. and Alferez F. (1983). Quantitative relationships between soil color and hematite content. Soil Science 136(6):354-358.

Townshend J. (1977). A framerwork for examining the role of remote sensing in monitoring the Earth's environment. In: Monitoring environmental changes by remote sensing, ed. by Remote Sensing Soc. (van Genderen and Collins), Cambridge, pp.1-15.

Trott K.E. and Singer M.J. (1983). Relative erodibility of 20 California range and forest soils. Soil Sci. Soc. Am. J., vol.47: 753-759.

Troll C. and Finsterwalder R. (1935). Die karten der Cordillera Real und des Talkessels von La Paz (Bolivien). Pet. Geogr. Mitt., 81:393-399 and 445-455.

Trangmar B., Yost R. and Uehara G. (1985). Application of geostatistics to spatial studies of soil properties. Advances in agronomy, vol. 38: 45-95.

UNEP-UNCOD (1977). United Nations Conference on Desertification. 29 Aug-9Sept 1977. Round-up, plan of action and resolutions, New York, 43 pages.

UN-UNCED (1992). Conference on Environment and Development, Río de Janeiro, Brazil, June 1992.

UMSS-GEOBOL-ORSTOM (1981). Geomorfología y suelos de la cuenca de Cochabamba. Suelos No.32, 75 páginas.

United States Salinity Laboratory Staff (1954). Diagnosis and improvement of saline and alkali soils. Agriculture Handbook No. 60. United States Department of Agriculture. Ed. L.A. Richards. 160 pages.

Van der Meer, F. (1995). Imaging spectrometry and the Ronda peridotites. PhD. thesis. Wageningen Agricultural University. 309 pages.

Van Reuwijk P. (1988). Introduction to physico-chemical aspects of soil formation. Lecture notes, ITC, Enschede, The Netherlands, 89 pages.

Vazquez-Selem L. and Zinck J.A. (1994). Modelling gully distribution on volcanic terrains in the Huasca area, central Mexico. ITC Jnal., vol. 3, pp. 252-263.

Veit, H. (1992). Estudio geológico de los sedimentos plio-cuaternarios de la cuenca de Cochabamba. Convenio Aleman-Boliviano de aguas subterráneas (CABAS), Cochabamba, 24 pages.

Verhaegen T.H. (1984). The influence of soil properties on the erodibility of Belgian loamy soils: A study based on rainfall simulation experiments. Earth surface processes and landform, vol.9: 499-507.

Verma K.S., Saxena R.K., Barthwal A.K. and Deshmukh. (1994). Remote sensing technique for mapping salt affected soils. Int. J. Remote Sen., vol.15, (9): 1901-1914.

Voznesensky A.S. and Artsruui A.B. (1940). A laboratory method for determining the anti-erosion stability of soils. In: Soils Fertilizers, vol.10: 289 pag.

White K. and Drake N. (1993). Mapping the distribution and abundance of gypsum in south-central Tunisia from Landsat Thematic Mapper data. Z. Geomorph.N.F., vol.37(3):309-325.

Wang F. (1990). Improving Remote sensing image analysis through fuzzy information representation. Photogrammetric Engineering and Rem. Sensing, vol.56,8:1163-1169.

Wang F. (1990). Fuzzy supervised classification of remote sensing. IEEE Transactions on geoscience and remote sensing, vol.28,2:194-201.

Webster's (1989). Webster's Encyclopedic Unabridged Dictionary of the English language. New York: Portland House.

Webster R. and Oliver M. (1992). Sample adequately to estimate variograms of soil properties. Jnal. of Soil Science, vol.43:177-192.

Wirrmann D. and De Oliveira A.L.F. (1987). Low holocene level (7700 to 3650 years ago) of lake Titicaca (Bolivia). Palaeogeography, Palaeoclimatology, Palaeoecology, vol.59: 315-323.

Wischmeier W. and Manering J. (1969). Relation of soil properties to its erodibility. Soil Sci.Soc.Amer.Proc., vol. 33:131-137.

Wischmeier W., Johnson C. and Cross B. (1971). A soil erodibility nomograph for farmland and construction sites. Jnal. Soil and Water Conservation, vol. 26:189-193.

Wonnacott T.H. and Wonnacott R.J. (1990). Multiple regression. Introductory Statistics, second edition. Ed. Wiley International edition, pp.287-480.

Woodburn R. and Kozachyn J. (1956). A study of relative erodibility of a group of Mississippi Gully soil. Transaction, American Geophysical Union. vol.37, N°6. pp. ???????

Woodruff N. and Siddoway F. (1965). A wind erosion equation. Soil Science Soc. of America Proceedings 29:602-608.

Yamamoto T. and Anderson H.W. (1973). Splash erosion related to soil erodibility indexes and other forest soil properties in Hawaii. In: American Geophysical Union (Ed.) Water Resources Research. Vol.9, N°2. pp.336-345.

Yaalon, D. (1971). Soil-forming processes in time and space. In: D.H. Yaalon (ed.), Paleopedology. Origin, nature and dating of paleosols. International Soc. of Soil Science and Israel Universities Press, Jerusalem.

Yaron B. and Thomas G.W. (1968). Soil Hydraulic Conductivity as affected by sodic water. Water Resources Research 4:545-552.

Yoder R.E. (1936). A direct method of aggregate analysis of soils and a study of the physical nature of erosion losses. J. of Am. Soc. of Agron., vol.28 (5): 337-351.

Young R.A. and Mutchler C.K. (1977). Erodibility of some Minnesota soils. In: Journal of Soil.and Water Cons. vol.32 (3): 180-182.

Yost R.. Loague K. and Green R. (1993). Reducing variance in soil organic carbon estimates; soil classification and geostatistical approches. Geoderma, vol.57:247-262.

Zadeh L. (1965). Fuzzy sets. Information and Control, vol. 8. pp.338-353.

Zadeh L. (1975). The concept of a linguistic variable and its application to approximate reasonin, I-Information Sci. 8:199-250, 301-375; 9:43-80.

Zinck J.A. (1988). Physiography and soils. ITC Int. publication, Enschede, The Netherlands.

Zinck J.A. and Valenzuela C. (1990). Soil Geographic Database: structure and application examples. ITC Jnal. 1990-3, pp.270-294.

Zobeck T.M. (1991). Soil properties affecting wind erosion. Jour. of Soil and Water Conser.,vol.46 (2): 112-118. Sens. of arid and semi-arid lands, Cairo, Egypt, pp. 279-295.

Zubieta (1977). Estudio hidrogeológico en el sector oriental de la cuenca Cliza-Punata. GEOBOL, Cochabamba, Bolivia. 23 páginas.

APPENDIX 1:

Maps of topsoil properties.
Punata - Cliza and Sacaba valleys.

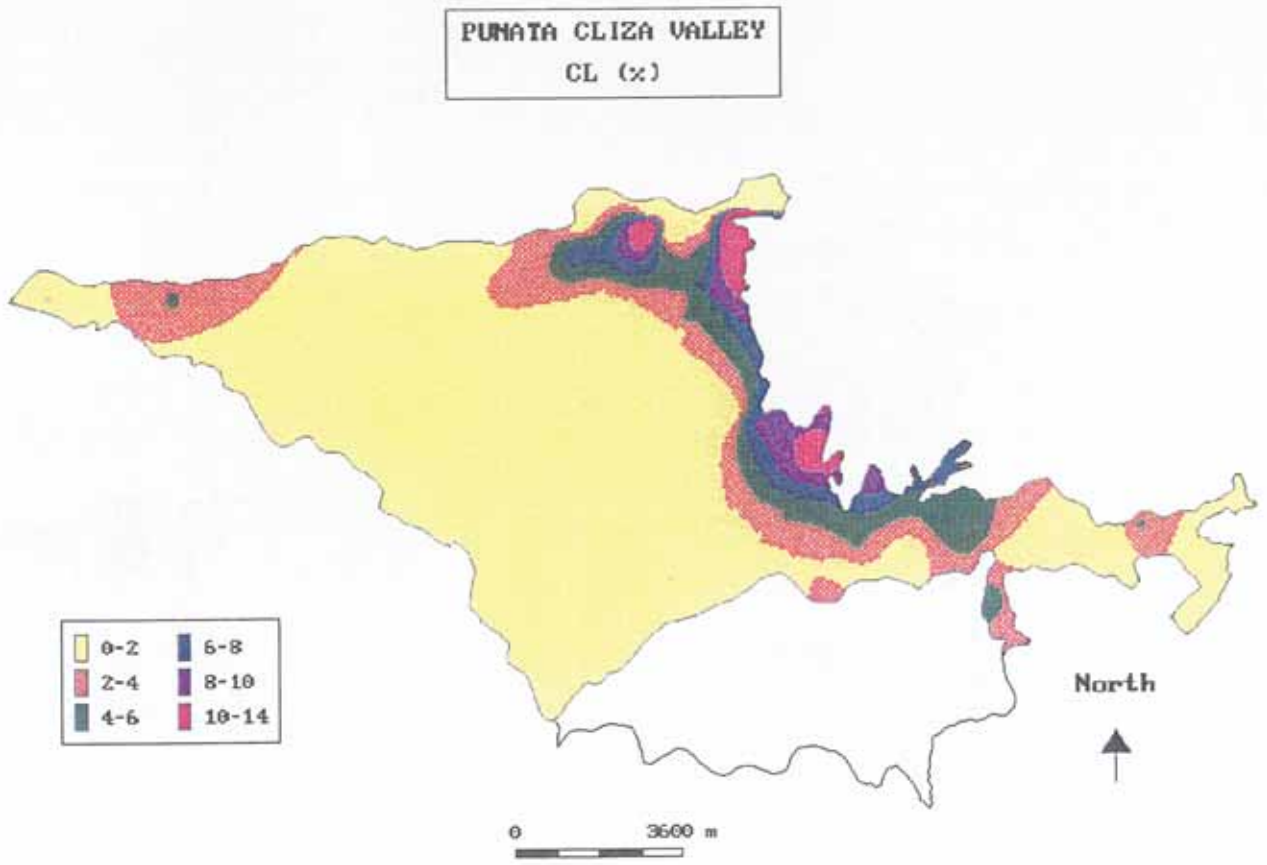
PUNATA CLIZA VALLEY
CL (%)
0-2
2-4
4-6
6-8
8-10
10-14
North
0
3600 m

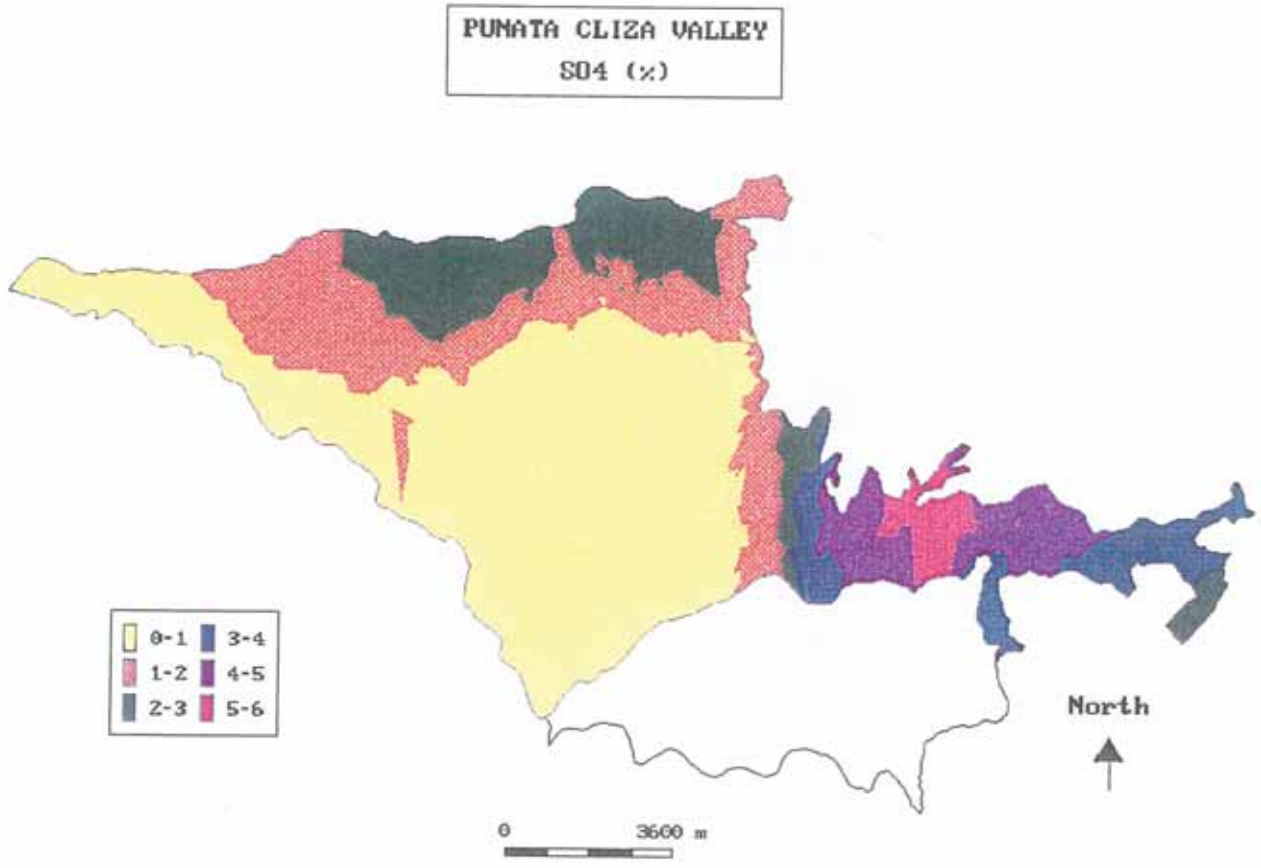
PUNATA CLIZA VALLEY
SO4 (%)
0-1
1-2
2-3
3-4
4-5
5-6
North
0
3600 m

PUNATA CLIZA VALLEY
CO3 (%)

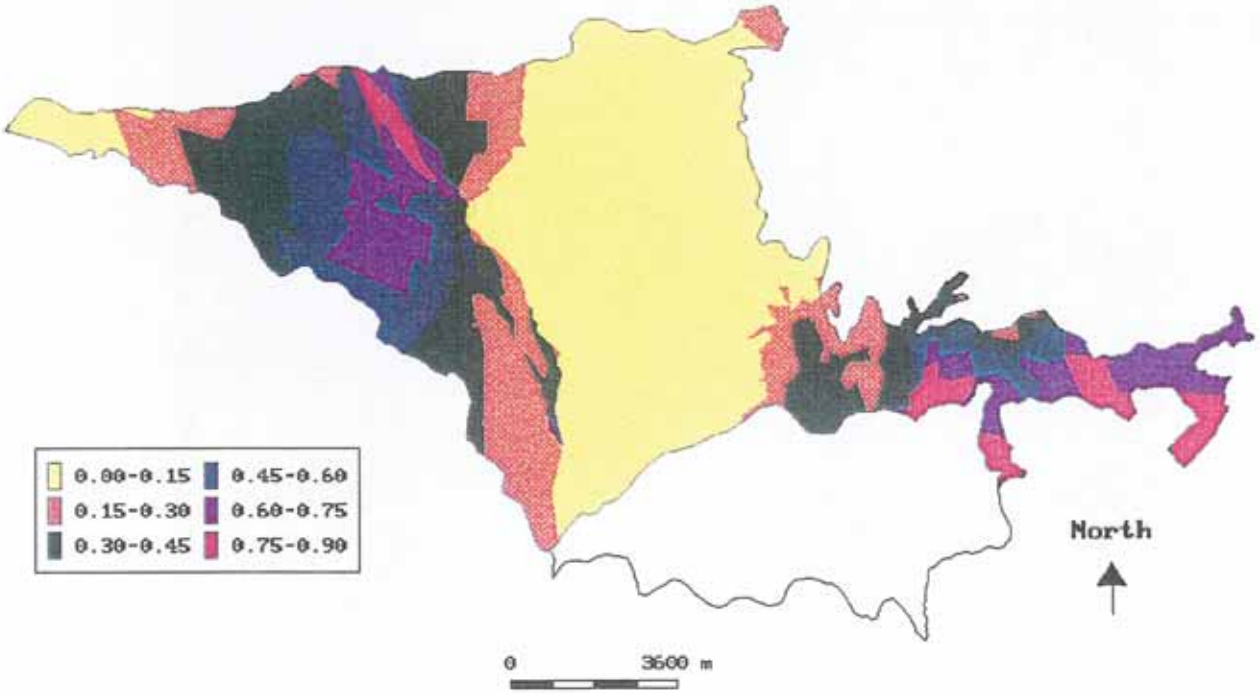

PUNATA CLIZA VALLEY
HCO3 (%)

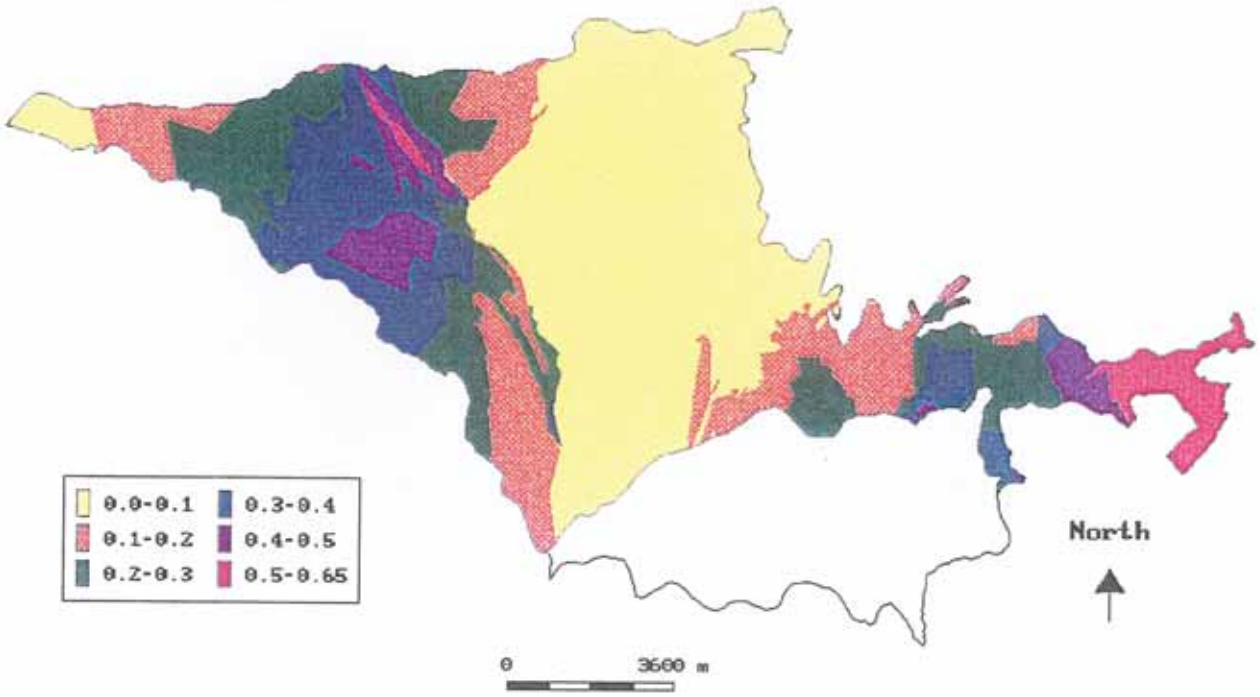

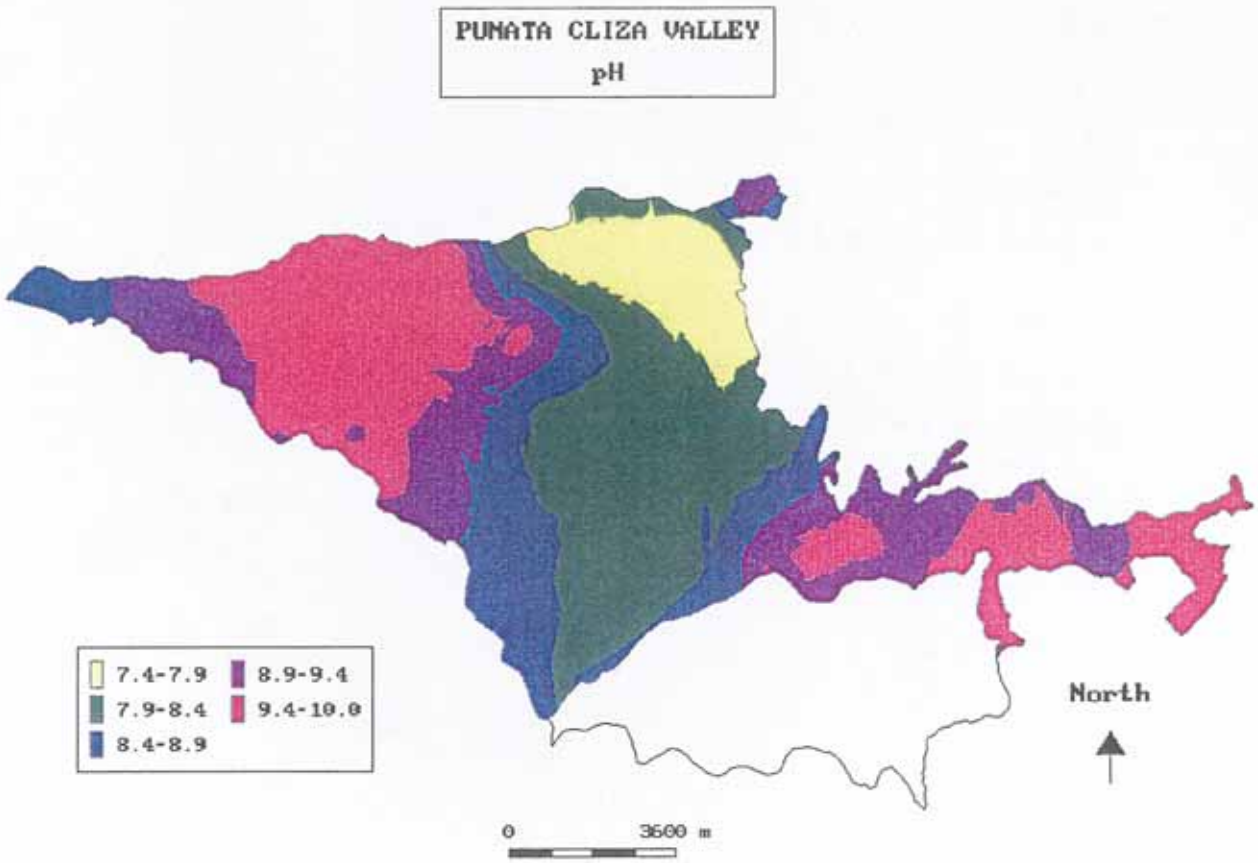
PUNATA CLIZA VALLEY
pH
7.4-7.9
7.9-8.4
8.4-8.9
8.9-9.4
9.4-10.0
North
0
3600 m

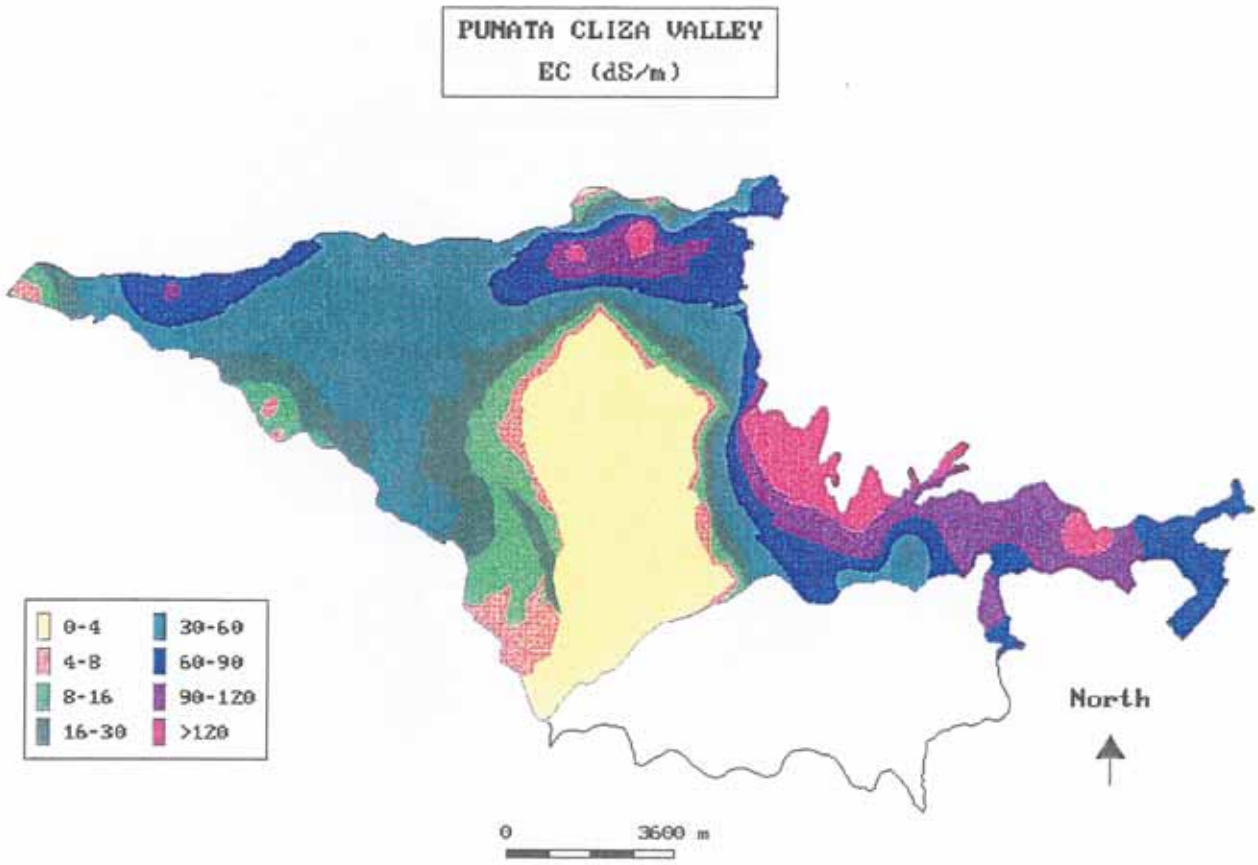
PUNATA CLIZA VALLEY
EC (dS/m)
0-4
4-8
8-16
16-30
30-60
60-90
90-120
>120
North
0
3600 m

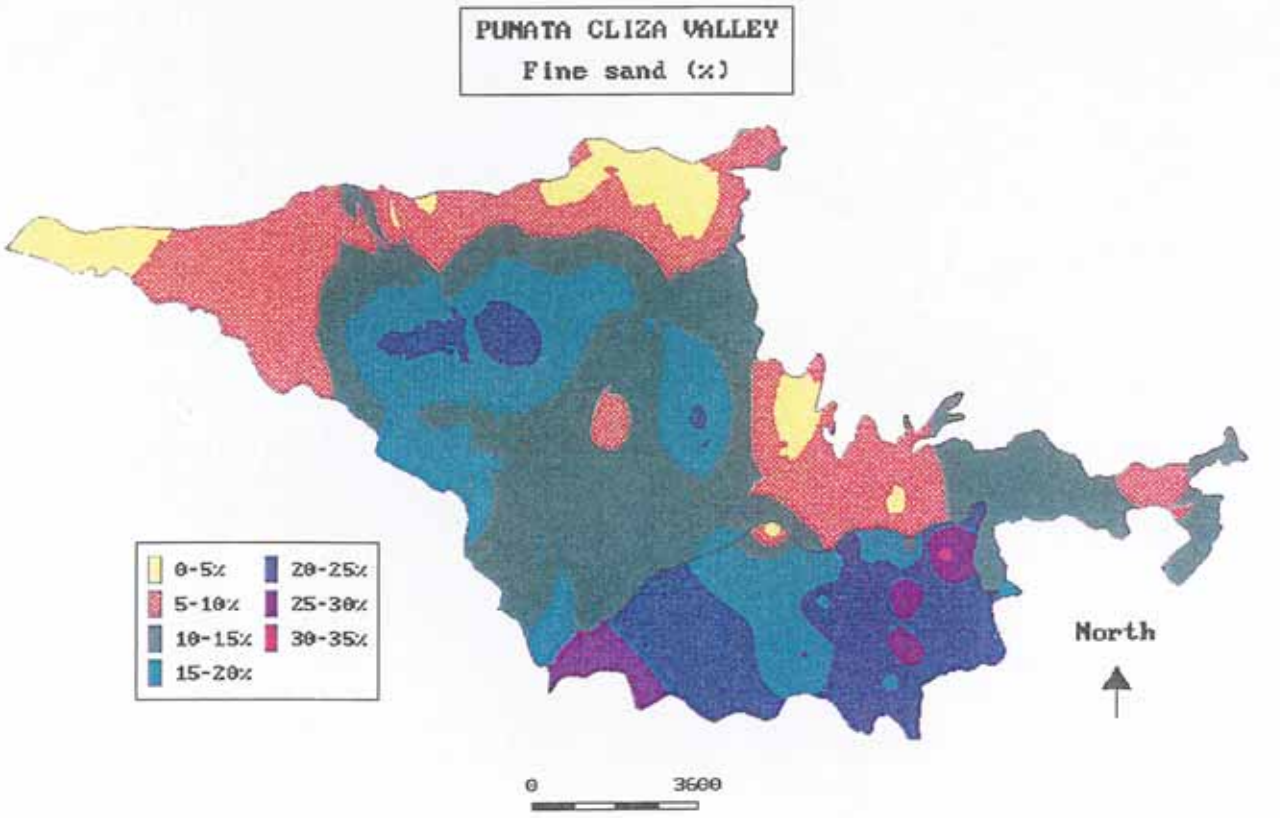
PUNATA CLIZA VALLEY
Fine sand (%)
0-5%
5-10%
10-15%
15-20%
20-25%
25-30%
30-35%
North
0
3600

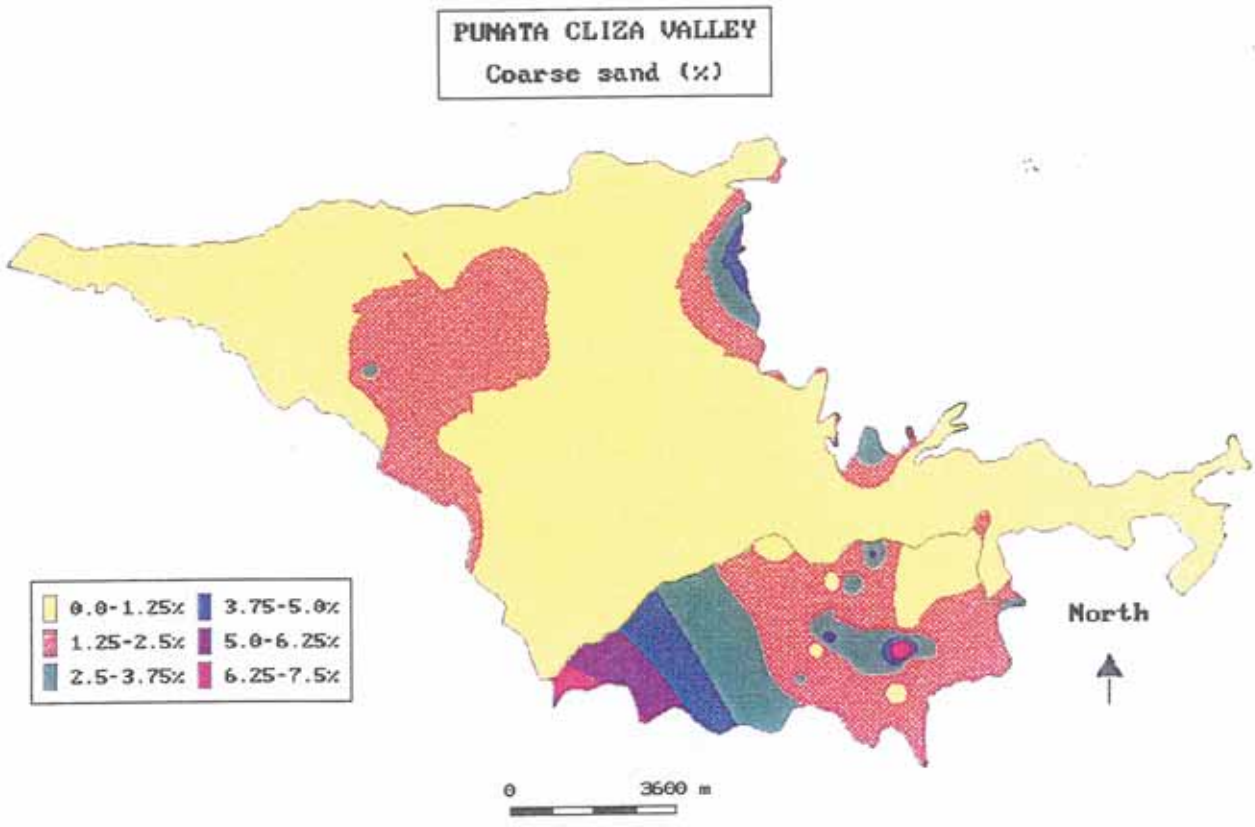
PUNATA CLIZA VALLEY
Coarse sand (%)
0.0-1.25%
1.25-2.5%
2.5-3.75%
3.75-5.0%
5.0-6.25%
6.25-7.5%
North
0
3600 m

PUNATA CLIZA VALLEY
Organic matter content (%)

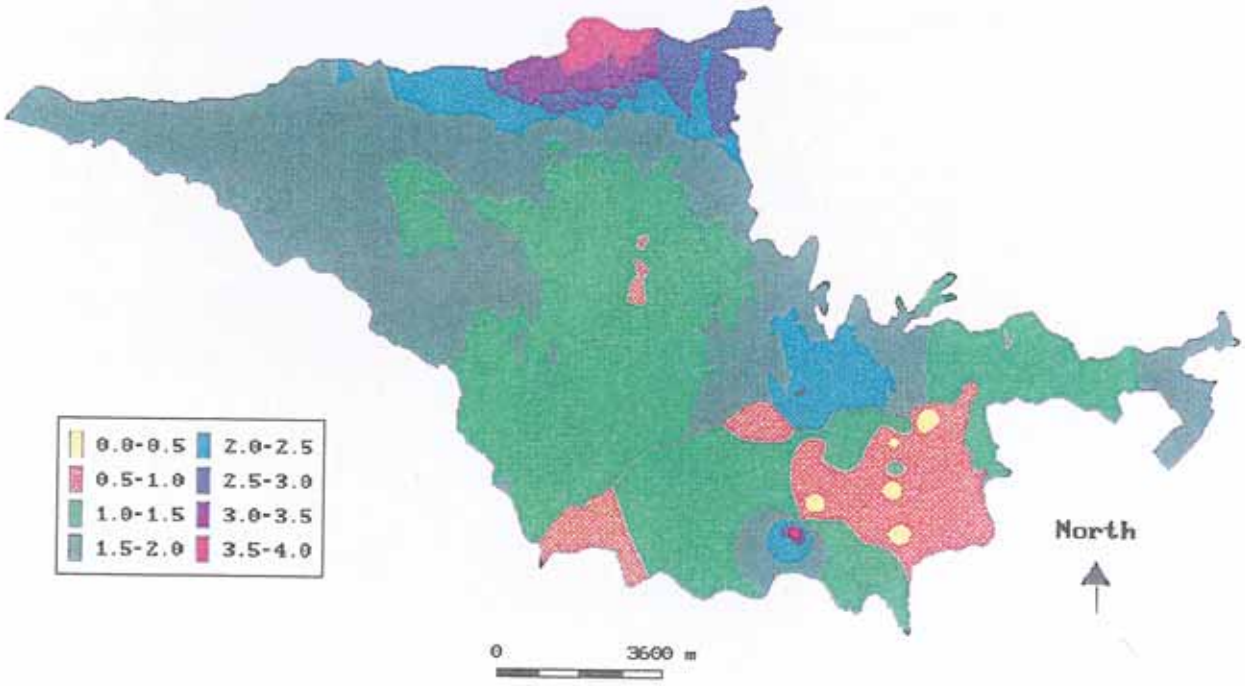

PUNATA CLIZA VALLEY
Error in organic matter content (squared %)

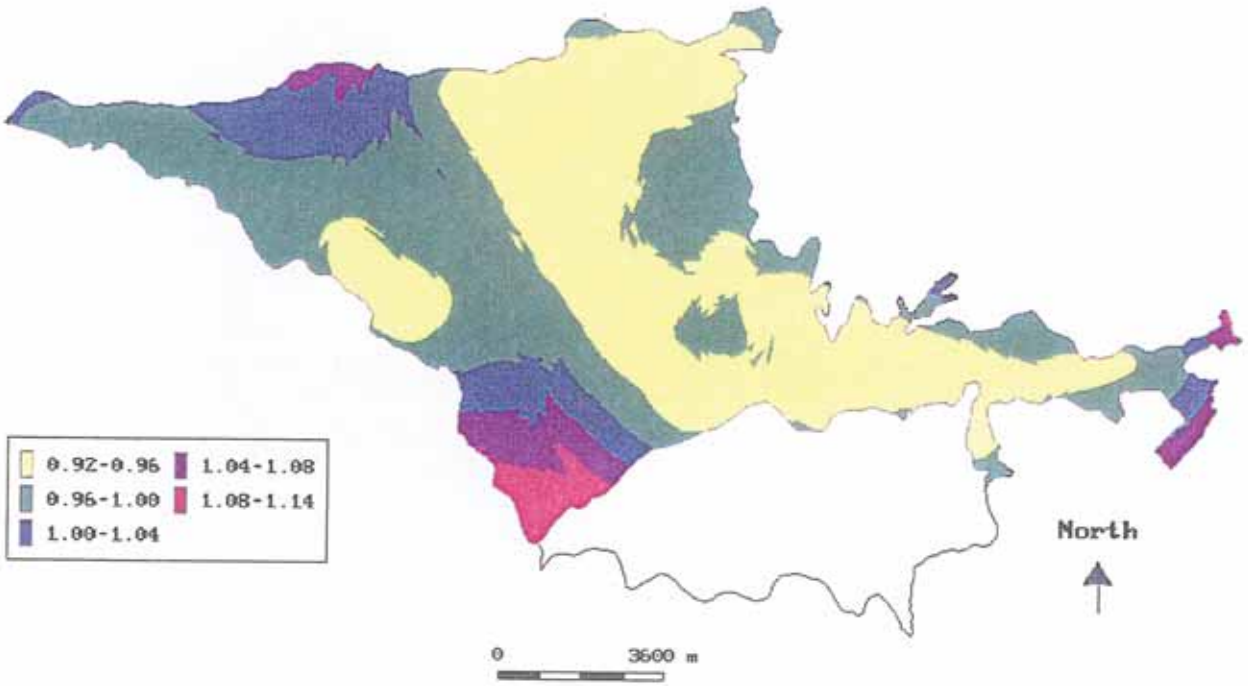

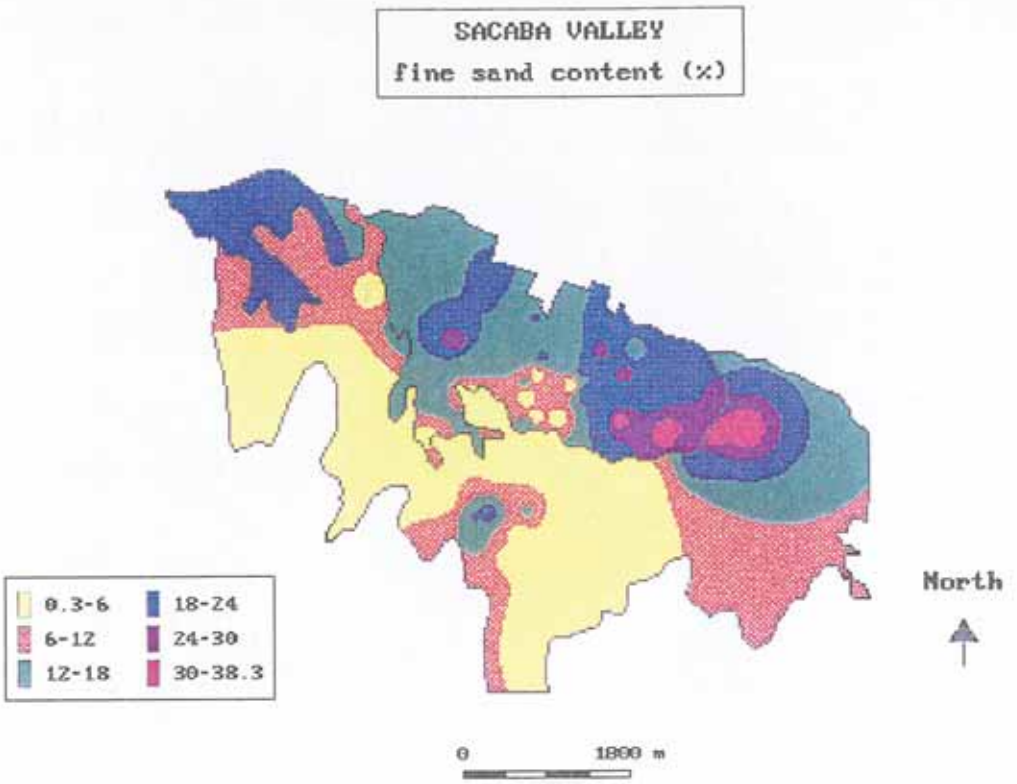
SACABA VALLEY
fine sand content (%)
0.3-6
6-12
12-18
18-24
24-30
30-38.3
North
0
1800 m

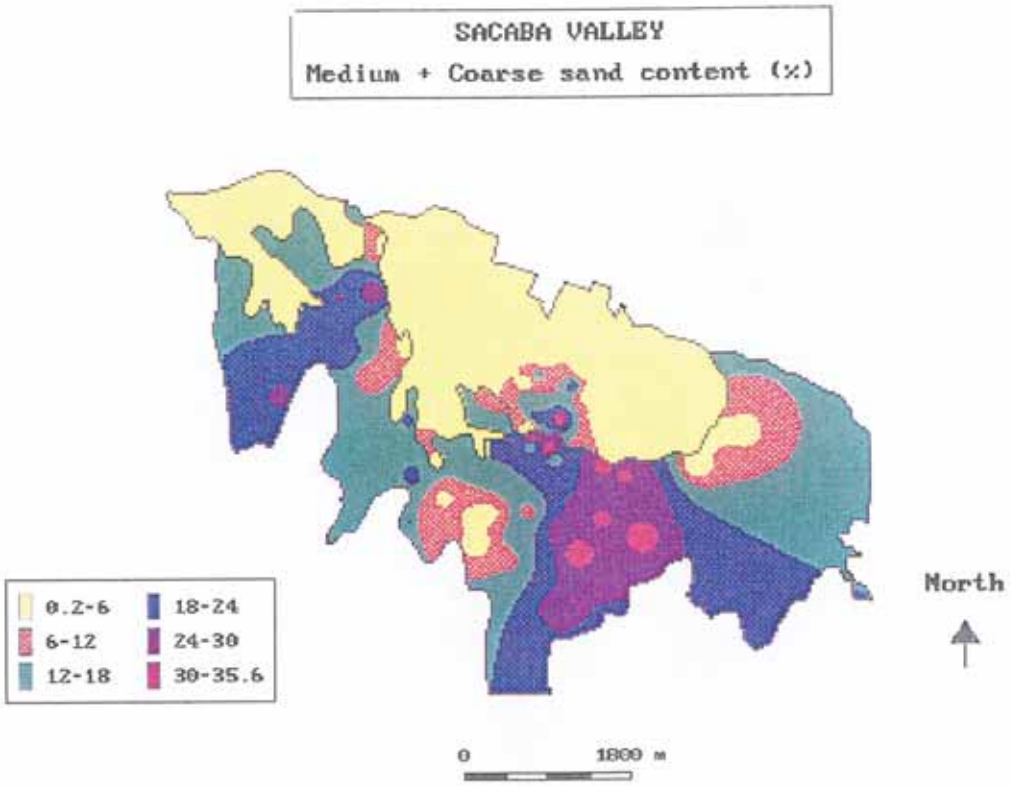
SACABA VALLEY
Medium + Coarse sand content (%)
0.2-6
6-12
12-18
18-24
24-30
30-35.6
North
0
1800 m

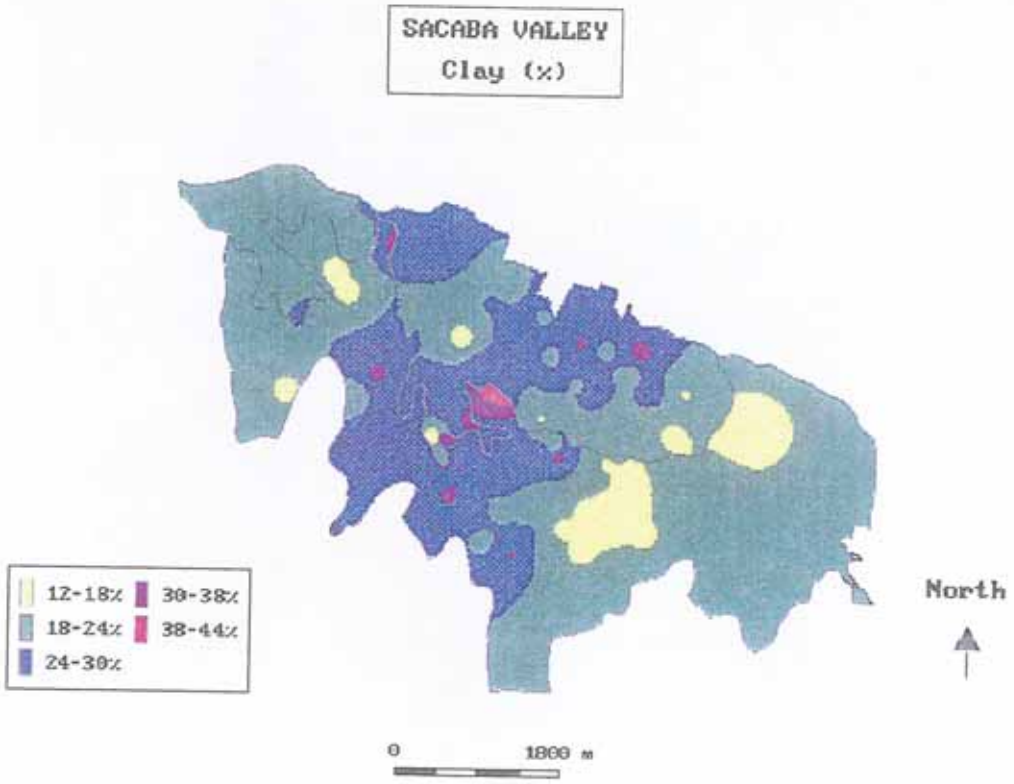
SACABA VALLEY
Clay (%)
12-18%
18-24%
24-30%
30-38%
38-44%
North
0
1800 m

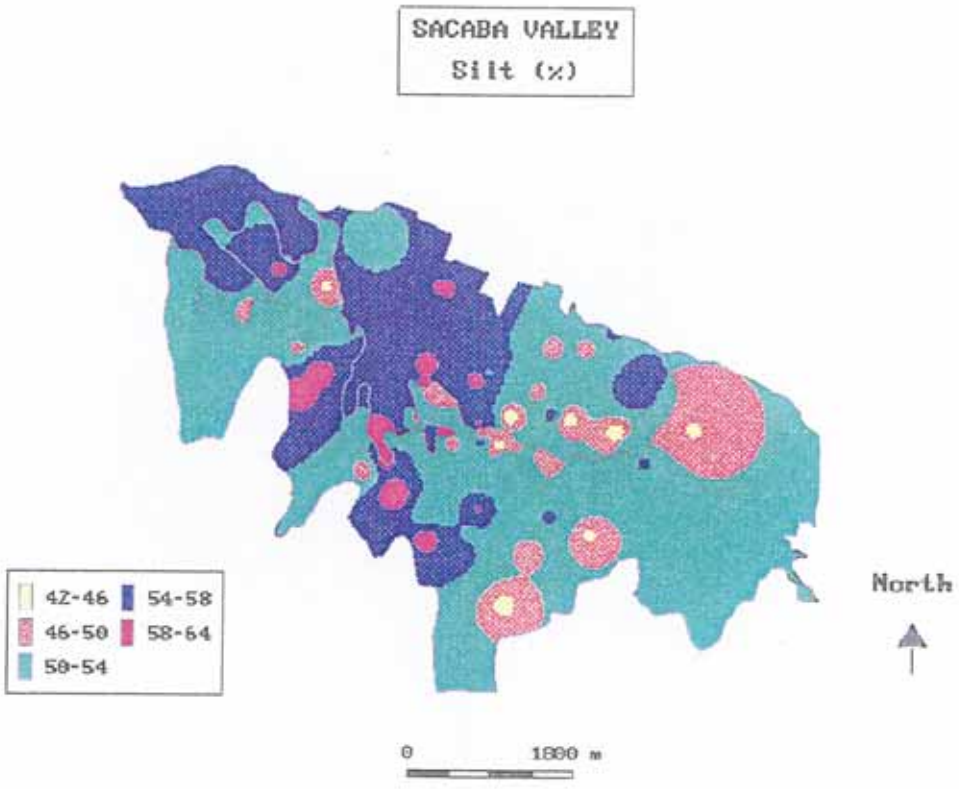
SACABA VALLEY
Silt (%)
42-46
46-50
50-54
54-58
58-64
North
0
1800 m

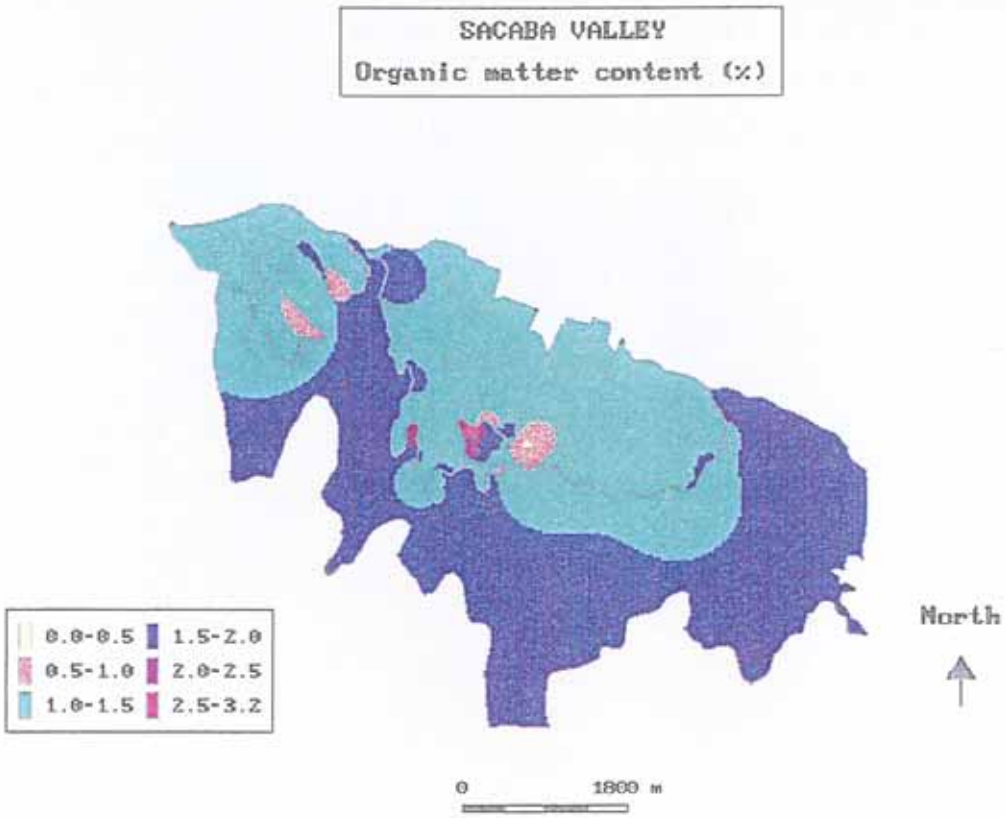
SACABA VALLEY
Organic matter content (%)
0.0-0.5
0.5-1.0
1.0-1.5
1.5-2.0
2.0-2.5
2.5-3.2
North
0
1800 m

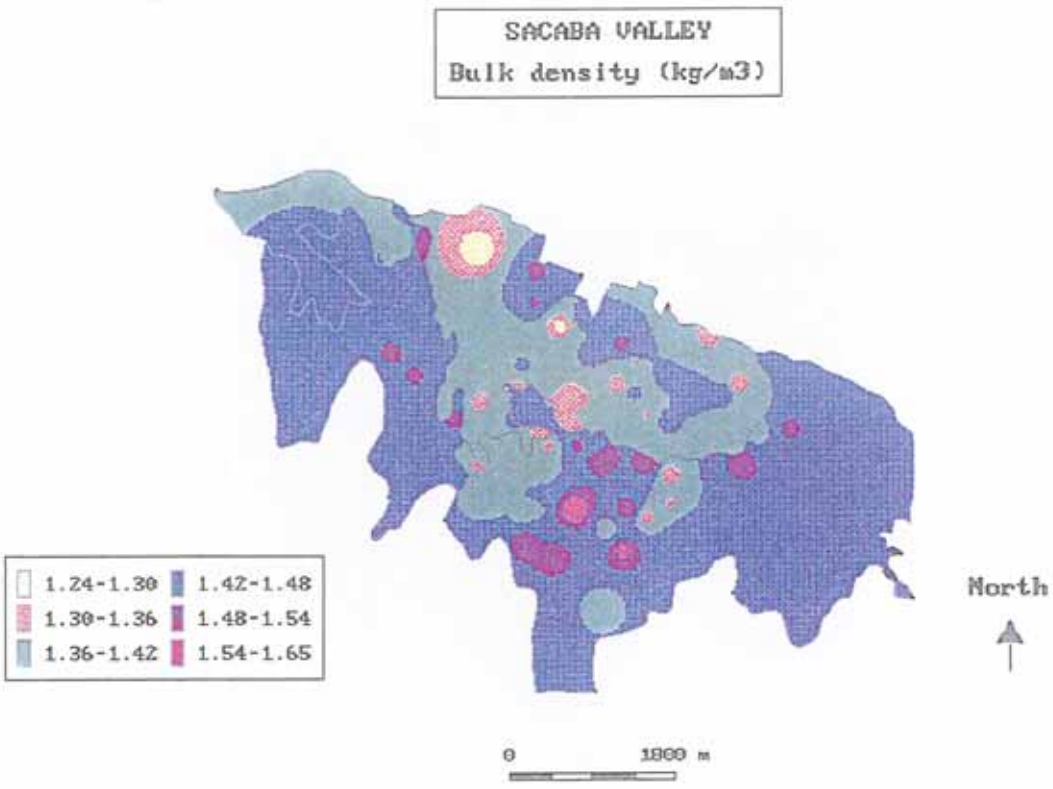
SACABA VALLEY
Bulk density (kg/m3)
1.24-1.30
1.30-1.36
1.36-1.42
1.42-1.48
1.48-1.54
1.54-1.65
North
0
1800 m

Semi-variograms. *Gaussian model*

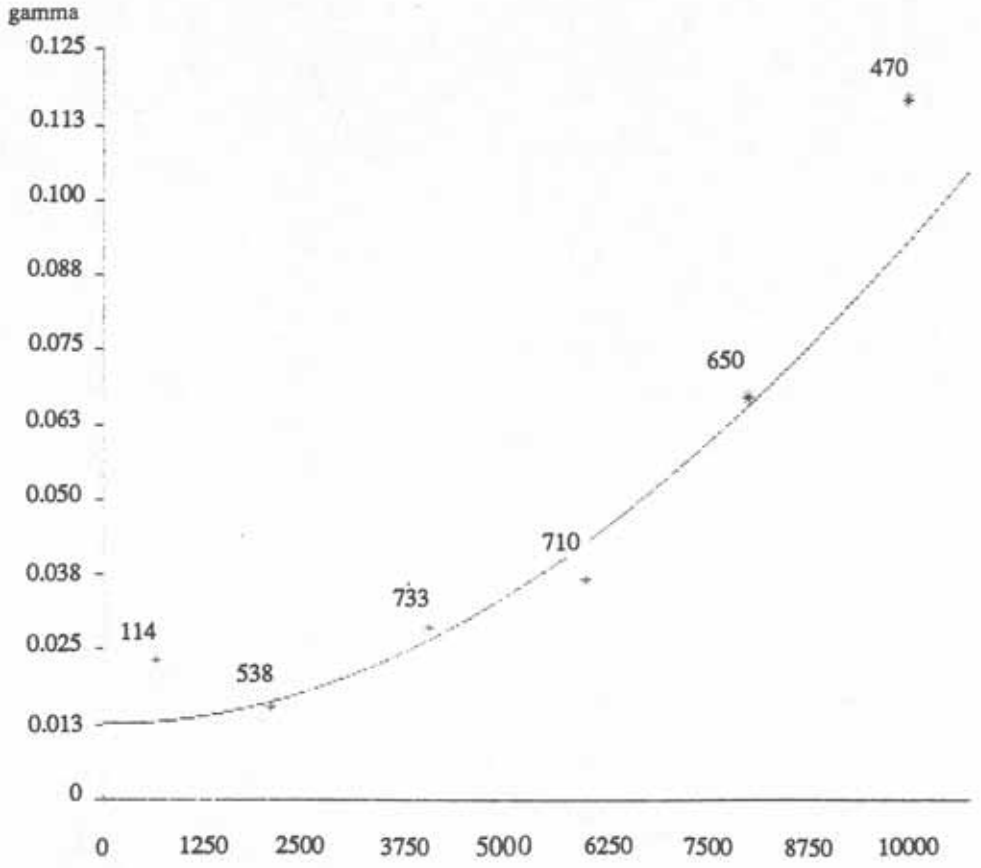

input file: vario\spat14.res = CO_3 (%)
model type: gaussian
direction: total
c0= 1.26e-0004 c=5.44E-0001 r=2.49E+0004
SSD/SST= 0.079

Semi-variograms. *Exponential model*

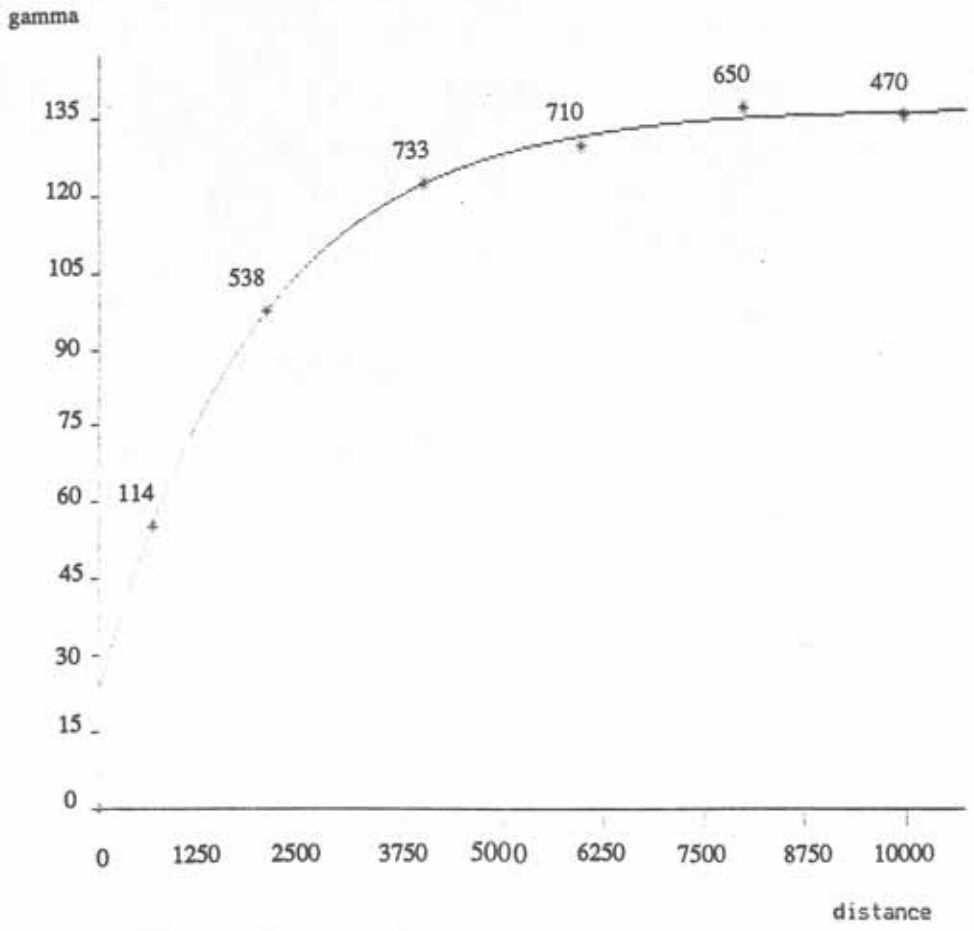

input file: vario\spat4.res=silt (%)
model type: exponential
direction: total
c0= 2.28E+0001 c=1.14E+0002 r=1.95E+0003
SSSD/SST=0.001

Semi-variograms. *Spherical model*

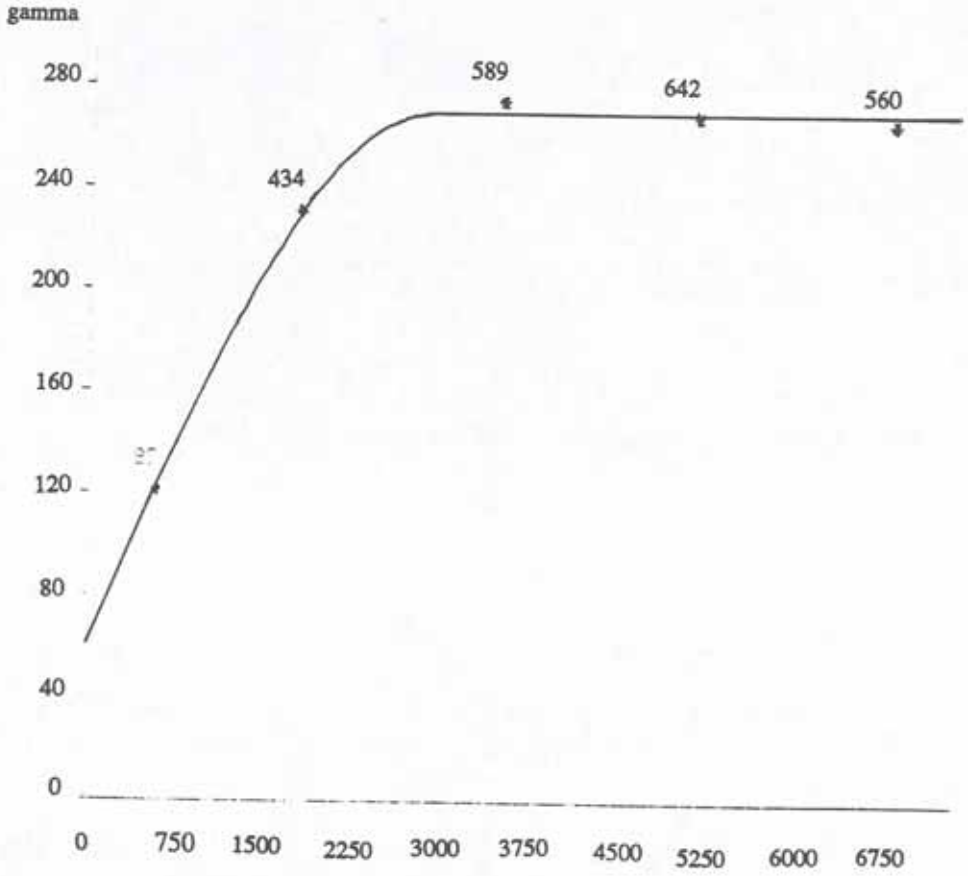

input file: vario\spat3.res = clay (%)
model type: spherical
direction: total
c0= 5.91E+0001 c=2.09E+0002 r= 2.86E+0003
SSD/SST= 0.003

SAMPLING POINTS LOCATION

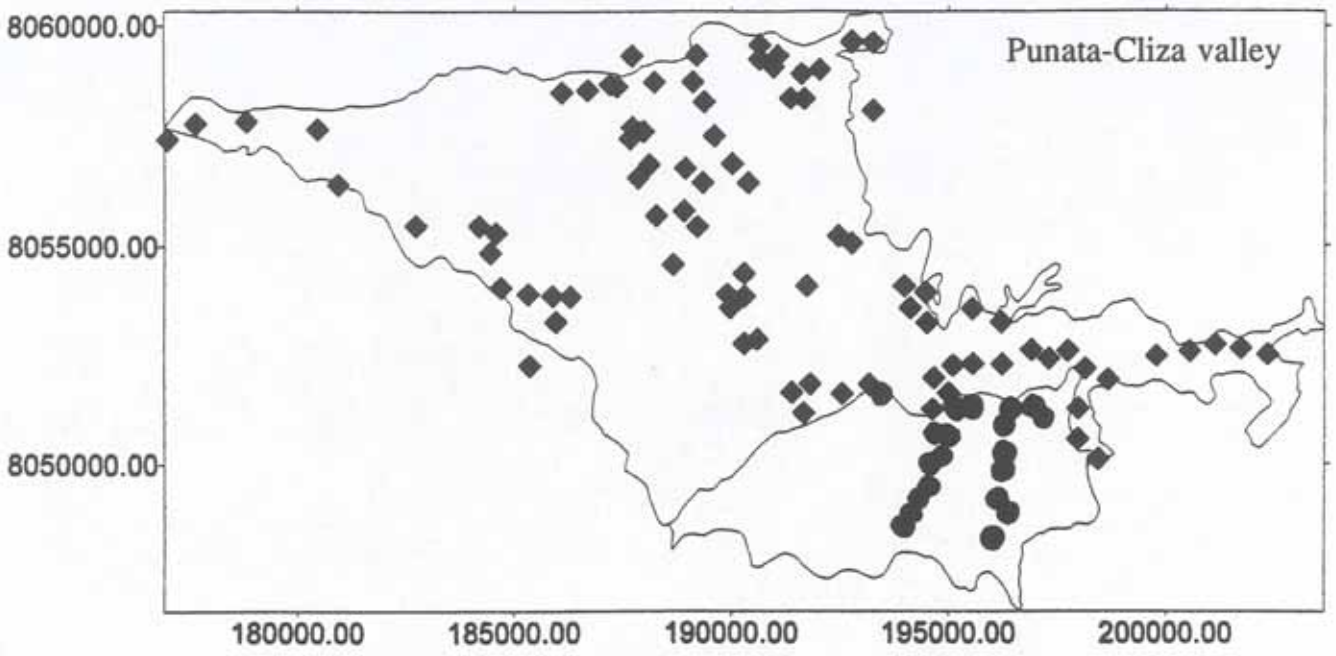

● sampling points in Piedmont units ■ sampling points in Valley units

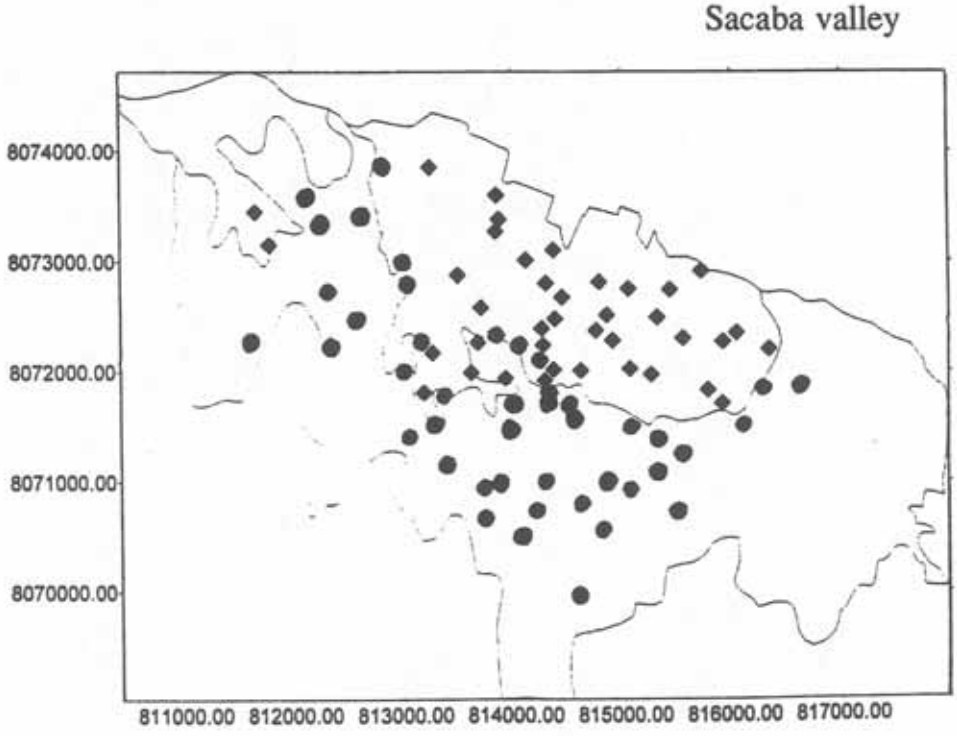

● sampling points in Piedmont units ■ sampling point in Valley units

Table 1: Number of observations per unit

LANDFORM	No. OF OBSERVATIONS	
	Sacaba valley	Punata-Cliza valley
Higher lagunary flats (Va111)	--	15
Middle lagunary flats (Va112)	16	1
Lower lagunary flats (Va113)	10	18
Badlands (Va115)	16	--
Playas (Va124)	--	56
Central part of the dissected depostional glacis (Pi112)	22	7
Distal part of the dissected depostional glacis (Pi113)	25	13

STATISTICAL ANALYSIS OF VALLEY AND PIEDMONT UNITS

CHARACTERISTIC FEATURES OF THE SEMI-VARIOGRAMS OF THE VALLEY AND PIEDMONT UNITS OF THE SACABA AND THE PUNATA CLIZA VALLEY

PUNATA CLIZA VALLEY

Playa unit

variable	model	nugget	sill	range	ssd/sst
clay	exp	76	656	7290	0.017
silt	lin	54			0.017
fnsand	sphe	27	51	2280	0.115
mcsand	exp	0.2	1.3	19400	0.081
om	lin	1.1			0.671
cl⁻	sphe	1.8	13	8860	0.011
so4⁻	declining semivariogram				
co3⁻	sphe	0	0.1	1770	0.022
hco3⁻	sphe	0.01	0.04	3280	0.097
pH	lin	0.2			0.009
EC	sphe	603	3923	13700	0.013

Lagunary-alluvial units

variable	model	nugget	sill	range	ssd/sst
clay	gaus	64	118	4090	0.132
silt	gaus	33	79	6330	0.31
fnsand	sphe	0	58	1580	0.017
mcsand	gaus	0.01	3.2	19400	0.021
om	gaus	0.4	1.3	5630	0.015
cl⁻	gaus	153	139159	14900	0.536
so4⁻	gaus	0	137708	19600	0.532
co3	gaus	2.4	2542	14900	0.28
hco3⁻	gaus	12	1325	19600	0.047
pH	gaus	0.1	0.5	5710	0.007
EC	gaus	2.1	1012	14900	0.646

All valley units

variable	model	nugget	sill	range	ssd/sst
clay	sphe	39	268	2850	0.004
silt	exp	23	137	1920	0.001
fnsand	gaus	25	67	1560	0
mcsand	exp	0.04	0.3	2690	0.039
om	sphe	0.8	1.8	18900	0.003
cl⁻	exp	0	8.3	4110	0.008
so4⁻	gaus	1.8	29	23600	0.036
co3⁻	gaus	0.01	0.6	24900	0.079
hco3⁻	gaus	0.01	0.07	14500	0
pH	exp	0.3	1.9	8830	0.01
EC	exp	54	8034	14500	0.01

SACABA VALLEY

Valley units

variable	model	nugget	sill	range	ssd/sst	
clay	exp	-0.4	31	431	0.009	
silt	exp	7.1	31	484	0.002	
fnsand	exp	36	115	696	0	
mcsand	gaus	0.2	1.8	3020	0.003	declining
OM	gaus	0.5	0.6	1030	0.007	
por	sphe	5.7	8.5	1060	0.163	
dens	sphe	0	0.01	1490	0.001	

Piedmont units

variable	model	nugget	sill	range	ssd/sst	
clay	gaus	18	91	1420	0	
silt	exp	9.5	32	5520	0.002	
fnsand	sphe	-3.4	69	3160	0	
mcsand	sphe	-15	190	1830	0.007	
OM	sphe	0.3	0.6	811	0.026	
por	gaus	11	-2.8	5220	0.213	declining
dens	gaus	0.01	0.01	1030	0.019	declining
pH	exp	0.1	0.2	1070	0.008	
EC	gaus	0	0.01	928	0	

PUNATA CLIZA VALLEY

Piedmont units

variable	model	nugget	sill	range	ssd/sst	
clay	sphe	3.4	47	2330	0.198	
silt	gaus	27	617	24500	0.267	
fnsand	gaus	16	79	3620	0.09	
mcsand	gaus	3.2	2.5	1950	0.687	declining
OM	gaus	0.3	2.5	8220	0.07	
por.	gaus	13	25	21200	0.918	
dens	sphe	0.01	0.01	3640	0.687	

Improving 3 variograms by deleating one , not fitting. lag gives

clay	sphe	0.4	45	2020	0.096
fnsand	gaus	17	78	3940	0
dens	gaus	0.01	0.02	14700	0.047

APPENDIX II:

RADIOCARBON DATINGS AND SOIL PROFILE DESCRIPTIONS

SOIL SAMPLES USED FOR ^{14}C ANALYSIS

Identification	Horizon designation	Depth (in cm)
Sb1 (6)	3A2b	97-126
Sb2 (4)	-A2b	818-863
Sb3 (3)	2Ab	71 - 88
Sb88 (4)	2Bw2	84 - 144
Va68 (4)	2BAb	44 - 54

PROFILE DESCRIPTIONS

Profile No.: Sb1
Classification: Typic Camborthid loamy, mixed, thermic (cover)
Aridic Haplustoll loamy, mixed, thermic (buried)
Date of examination: 22.03.94 (end of rainy season)
Author: Metternicht
Location: Sacaba (south), cemetery road, in the exposed bed wall of Canal Mayu river (top of the deposicional section).
Elevation: 2720 m.a.s.l
Landscape: piedmont
Relief form: disseccted depositional glacis
Lithology: alluvial
Landform: distal part of dissected depositional glacis
Topography: almost flat
Slope: 1% N.
Landuse and/or vegetation: molle, eucaliptus, grama
Climate: semi-arid
Soil temperature regime: thermic
Soil moisture regime: aridic
Parent material: alluvial (from shale, sandstone, siltstones)
Drainage class: well drained
Depth to water table: more than 10 meters
Moisture conditions in profile: dry throughout the profile
Erosion: severe gully erosion, moderate sheet and rill erosion and moderate tunnelling erosion.
Human Influence: ploughing and "tepeo" in the sorroundings
Surface stones: no

Profile description

A1 0 - 12 cm. light yellowish brown (10YR 6/4 dry) and dark yellowish brown (10YR 4.5/4 moist); silt loam to silty clay loam; moderate coarse subangular blocky structure; 0.5 cm surface crust of laminar structure; hard dry, very friable moist, slightly sticky and slightly plastic; many fine tubular horizontal pores and few fine roots; clear smooth boundary.

A2 12 - 24 cm. yellowish brown (10 YR 5/4 dry) and dark yellowish brown (10YR 3/4 moist); silt loam; moderate to strong coarse subangular blocky structure; hard to very hard dry, very friable to friable moist, slightly sticky and nonplastic; many fine tubular pores; common to few fine roots; clear smooth boundary.

2Bw 24 - 54 cm. pale olive (2.5 Y 6/4 dry) and dark yellowish brown (10YR 4/4 moist); sandy loam; moderate coarse subangular blocky structure; hard dry, very friable moist, nonsticky and nonplastic; many fine horizontal and few vertical tubular pores; abrupt smooth boundary.

2C 54 - 70 cm. yellowish brown (10YR 5.5/4 dry) and dark yellowish brown (10YR 4/4 moist); loamy sand to sandy loam; structureless; slightly hard to hard dry, loose moist, nonsticky and nonplastic; fine stratification of sand; abrupt smooth boundary.

3A1b 70 - 97 cm. brown (10YR 5/3 dry) and dark brown (10 YR 3/3 moist); silty clay loam; prismatic structure breaking into strong coarse subangular blocky structure; very hard dry, firm moist, slightly sticky and slightly plastic; many very fine and common fine horizontal tubular pores; clear smooth boundary.

3A2b 97 - 126 cm. dark grayish brown (10YR 4/2 dry) and very dark grayish brown (10 YR 3/2 moist); silty clay loam to silty clay; prismatic structure breaking into strong coarse subangular blocky structure; very hard dry, extremely firm moist, slightly sticky and slightly plastic; many fine horizontal tubular pores; clear smooth boundary.

3Bw1b 126 - 150 cm. brown (10YR 4/3 dry) and dark brown (10YR 3/3 moist); silt loam; strong coarse subangular blocky structure; very hard dry, firm moist, slightly sticky and slightly plastic; few fine random tubular pores; clear smooth boundary.

3Bw2b 150 - 162 cm. dark yellowish brown (10YR 4/4 dry) and dark yellowish brown (10YR 4/3 moist); silt loam to loam; strong coarse to medium subangular blocky structure; hard dry, firm moist, slightly sticky and plastic; many very fine horizontal tubular pores; gradual smooth boundary.

4Cb 162 - 194 cm. brown (10YR 4/3.5 dry) and dark brown (10 YR 3/3 moist); silty clay loam with 10% fine and medium gravel; strong coarse subangular blocky structure; hard dry, friable moist, slightly sticky, plastic; many fine tubular horizontal pores; clear smooth boundary.

5Cb 194 - 232 cm. yellowish brown (10 YR 5/4 dry) and dark yellowish brown (10 YR 4/4 moist); silt loam; strong coarse subangular blocky structure; hard dry, very friable moist, nonsitcky and nonplastic; many fine and very fine tubular horizontal pores.

Remarks: No effervescence to HCl in all horizons.

Diagnostic horizons: ochric epipedon and cambic horizon (cover); mollic horizon (buried)

Profile No.: Sb2
Classification: Typic Haplustalf fine loamy, mixed, thermic (buried)
Date of examination: 23.03.94
Author: Metternicht
Location: Sacaba (south), cemetery road, in the exposed bed wall of Canal Mayu river, starting description at 7mts from the surface (bottom of the depositional section).

Elevation: 2720 m.a.s.l
Landscape: piedmont
Relief form: dissected depositional glacis
Lithology: alluvial
Landform: distal part of dissected depositional glacis
Topography: almost flat
Slope: 1% N.
Landuse and/or vegetation: molle, eucaliptus
Climate: semi-arid
Soil temperature regime: thermic
Soil moisture regime: aridic
Parent material: alluvial (from shale, sandstone, siltstone)
Drainage class: well drained
Depth to watertable: more than 10 meters
Moisture conditions in profile: dry throughout the profile
Erosion: severe gully erosion on the top of bed wall
Human Influence: no
Surface stones: no

Profile description: (starting at 7 meters from the surface below the Sb1 profile)

-C1 700 - 740 cm. light yellowish brown (2.5Y 6/4 dry) and dark yellowish brown (10 YR 4/4 moist); silt loam; strong medium to coarse subangular blocky; hard dry, friable moist, slightly sticky and slightly plastic; many very fine tubular horizontal pores; gradual smooth boundary.

-C2 740 - 750 cm. yellowish brown (10YR 5.5/4 dry) and brown (10YR 4/3 moist); loam to silt loam; strong coarse subangular blocky structure; slightly hard dry, friable to firm moist, sligthly sticky and slightly plastic; common very fine horizontal and few fine vertical tubular pores; clear smooth boundary.

-A1b 750 - 818 cm. brown (10 YR 4/3 dry) and yellowish brown (10 YR 5/4 dry), and dark brown (10 YR 3/3 moist); silty clay loam; moderate to strong medium subangular blocky structure; slightly hard to hard dry, firm moist, sligtly sticky to sticky and slightly plastic; common very fine random tubular pores; clear smooth boundary.

-A2b 818 - 863 cm. dark grayish brown (10YR 4/2 dry) and very dark grayish brown (10 YR 3/2 moist); silty clay loam; moderate medium subangular blocky structure; very hard dry, firm moist, slightly sticky and slightly plastic; many fine horizontal and few random fine tubular pores; clear smooth boundary.

-Btb 863 - 903 cm. brown (7.5 YR 4/3 dry) and dark brown (7.5 YR 3/4 moist); clay loam; moderate medium subangular blocky structure; hard dry, firm moist, sticky and plastic; distinct moderately thick broken clay cutans on pedfaces and root channels; common to few horizontal tubular pores; radual wavy boundary.

-Cb 903 - 928 cm. yellowish brown (10YR 5.5/6 dry) and dark yellowish brown (10YR 4/4 moist); loam to sandy clay loam; moderate medium subangular blocky structure; hard dry, firm to friable moist, sligthly sticky and slightly plastic; few fine horizontal tubular pores.

Remarks: the section lying between the bottom of the Sb1 profile (232 cm.) and the top of the Sb2 profile (700 cm.) could not be described due to inaccesibility of the river bed wall.

No effervescence to HCl in all horizons.

Diagnostic horizons: ochric epipedon and argillic horizon.

Profile No.: Sb3
Classification: Ustochreptic Camborthid fine loamy, mixed, thermic (cover)
Date of examination: 24.03.94
Author: Metternicht
Location: Sacaba (south), Kererani zone; 260 m west of road starting from the cemetery and 900 m after crossing the Crespo Mayu river south direction.
Elevation: 2700 m.a.s.l
Landscape: piedmont
Relief form: disssected depositional glacis
Lithology: alluvial (from shale, sandstone, siltstone)
Landform: central part of the dissected depositional glacis
Topography: gently undulating
Slope: 2% N.
Landuse and/or vegetation: barley, wheat, maiz, beans. Molle, eucaliptus
Climate: semi-arid
Soil temperature regime: thermic
Soil moisture regime: aridic
Parent material: alluvial (from shale, sandstone, siltstones)
Drainage class: well drained
Depth to watertable: 16 meters
Moisture conditions in profile: slightly humid throughout the profile
Erosion: slight sheet and rill erosion
Human Influence: ploughing
Surface stones: very few medium and coarse gravel (rounded)

Profile description:

Ap 0 - 17 cm. yellowish brown (10 YR 5.5/4 dry) and brown (10YR 4/3 moist); silt loam to silty clay loam (some mica); moderate to weak coarse subangular blocky structure; hard dry, friable moist, sligthly sticky and sligthly plastic; many very fine horizontal tubular pores, common very fine vertical tubular pores; comon very fine and few medium roots, very few coarse roots; broken thin silt cutans on pedfaces; diffuse smooth boundary.

Bw 17 - 71 cm. yellowish brown (10YR 5.5/4 dry) and dark yellowish brown (10YR 4/4 moist); silt loam; moderate medium subangular blocky structure; hard dry, friable moist, slightly sticky and slightly plastic; common very fine and fine tubular horizontal pores; few very fine and very few fine roots, abrupt smooth boundary.

2Ab 71 - 88 cm. dark grayish brown (10YR 4/2 dry) and very dark gray (10YR 3/1 moist); loam with many (30%) medium rounded gravels; moderate medium subangular blocks; slightly stickly, slightly plastic, friable moist, hard dry; common very fine tubular horizontal pores and

few fine vertical pores, very few fine random tubular pores, clear smooth boundary.

3Cb 88 - 114cm brown (10YR 5/3 dry) and very dark grayish brown (10YR 3/2.5 moist); dominant (85%) fine and medium rounded gravel and many (15%) coarse subrounded gravel in sandy loam matrix; structureless; slightly hard dry, loose moist, nonsticky and nonplastic; very few very fine roots; clear smooth boundary.

4Cb 114 - 162 cm. brown (10YR 4/3 dry) and dark brown (10YR 3/3.5 moist); silt loam; strong medium subangular blocky structure; very hard dry, firm moist, slightly sticky and plastic; many fine horizontal tubular pores and few fine random tubular pores.

Remarks: No effervescence to HCl in all horizons.

Diagnostic horizons: ochric epipedon and cambic horizon. The buried soil does not meet thickness requirements for mollic epipedon.

Profile No.: Sb88
Classification: Fluventic Camborthid fine silty, mixed, thermic (loamy depositional phase)
Date of examination: 19.05.94
Author: Metternicht
Location: South of Sacaba, 100 m west of cementery
Elevation: 2740 m.a.s.l
Landscape: valley
Relief form: depression
Lithology: alluvial
Landform: lagunary flat
Topography: flat
Slope: 0.2%
Landuse and/or vegetation: natural grasses
Climate: semi-arid
Soil temperature regime: thermic
Soil moisture regime: aridic
Parent material: alluvial (from sandstone, siltstones)
Drainage class: well drained
Depth to watertable: 16 meters
Moisture conditions in profile: dry throughout the profile
Erosion: slight sheet erosion and moderate rill erosion
Human Influence: tepeo
Surface stones: no

Profile description:

A1 0 - 15 cm. pale brown (10YR 5.5/3 dry) and brown (10YR 4/3 moist); silt loam (fine loamy); moderate coarse subangular blocky structure; sligtly hard dry, very friable moist, sligthy sticky and plastic; many very fine roots; many very fine vesicular and tubular random pores; clear smooth boundary; pH 6.5; cover phase.

2A2 15 - 62 cm. brown (10YR 4.5/3 dry) and dark brown (10YR 3.5/3 moist); silty clay loam (fine silty); strong coarse subangular blocky structure; very hard dry, firm moist, sticky and

plastic to very plastic; many pedotubules; undecomposed organic rests; common to many fine and very fine tubular random pores; clear smooth boundary; pH 7.8.

2Bw 62 - 84 cm. yellowish brown (10YR 5/4 dry) and dark yellowish brown (10YR 4/4 moist); silt loam (fine loamy); moderate coarse subangular blocky structure; sligthly hard to hard dry, friable moist, sticky and plastic to very plastic; undecomposed organic rests; many fine and very fine tubular pores; wavy diffuse boundary; pH 8.2.

2Bw2 84 - 144 cm. yellowish brown (10YR 5/4 dry) and dark yellowish brown (10YR 4/4 moist) (60%), brown (10YR 5/3 dry) and brown (10YR 4/3 moist) (40%); silt loam (fine loamy); strong coarse subangular blocky structure; hard dry, friable to firm moist, sticky and plastic; pedotubules, undecomposed organic rests; many fine and very fine tubular pores; gradual irregular boundary; pH 8.2.

3C 144 - X cm. yellowish brown (10YR 5.5/6 dry) and dark yellowish brown (10YR 4/4 moist); 80% rounded and subrounded coarse gravel in sandy loam matrix (loamy skeletal); weak fine subangular blocky structure; slightly hard dry, very friable moist, nonsticky and sligthly plastic; common very fine discontinuous tubular pores; pH 7.4.

Remarks: No effervescence to HCl in all horizons.

Diagnostic horizons: Cambic horizon and ochric epipedon

Profile No.: Va68
Classification: Aquic Haplargid clayey, mixed, thermic (loamy depositional cover phase)
Date of examination: 17.06.94
Author: Metternicht
Location: Valle Alto, Tolata-Cliza road, 1 km south of Tolata.
Elevation: 2700 m.a.s.l
Landscape: valley
Relief form: lagunary depression
Lithology: lagunary
Landform: playa
Topography: level
Slope: 0%
Landuse and/or vegetation: algarrobo, grama (Cynodon dactylon)
Climate: semi-arid
Soil temperature regime: thermic
Soil moisture regime: aridic
Parent material: lagunary
Drainage class: moderatelly well drained
Depth to watertable: 3 meters
Moisture conditions in profile: slightly humid throughout the profile
Erosion: slight eolic erosion
Human influence: overgrazing
Surface stones: no

Profile description:

A1 0 - 17 cm. light yellowish brown (2.5Y 6.5/4 dry) and dark ywllowish brown (10YR 4.5/4 moist) (50%), very pale brwon (10YR 7/3 dry) and brown (10YR 5/3 moist) (50%); silty clay loam (fine silty); moderate fine platy structure; firm moist, sticky and plastic; many fine horizontal pores; moderately calcareous; clear smooth boundary; pH 9.7.

C1 17 - 33 cm. light yellowish brown (2.5Y 6/4 dry) and olive brown (2.5Y 4.5/4 moist), yellowish brown (10YR 5/4 dry) and pale brown (10YR 6/3 moist), very pale brown (10YR 7/3 dry) and light yellowish brown (10YR 6/4 moist) (laminar distribution, 33% each); silt loam (coarse loamy); weak medium and fine platy structure; friable moist, slighlty sticky and slightly plastic; many horizontal fine pores; slightly calcareous; clear smooth boundary; pH 9.6.

C2 33 - 44 cm. light yellowish brown (2.5Y 6/4 dry) and light olive brown (2.5Y 5/4 moist); silt loam to loam (fine loamy); weak medium platy structure; friable to firm moist, sligthly sticky and slightly plastic; few to common fine horizontal pores; slightly calcareous; abrupt smooth boundary; pH 9.7.

2BAb 44 - 54 cm. light brownish gray (2.5Y 6.5/2 dry) and dark grayish brown (2.5Y 4/2 moist); clay (very fine clayey); strong coarse subangular blocky structure; very firm moist, sticky and very plastic; thin broken clay skins on root channels; pedotubules; few undecomposed organic rests; many fine and very fine random pores; moderately calcareous; clear smooth boundary; pH 9.7.

2Btgb 54 - 73 cm. light yellowish brown (2.5Y 6/3 dry) and olive brown (2.5Y 4.5/3 moist); clay to sandy clay (fine clayey); strong coarse and medium subangular blocky structure; firm moist, sticky and plastic; thin patchy clay skins on rooth channels; undecomposed organic rests; few fine distinct Fe mottling strong brown (7.5YR 5/8), few to common fine soft Mn motting black (5YR 2.5/1); many fine and very fine random pores; slightly calcareous; gradual smooth boundary; pH 9.6.

2BCgb 73 - 90 cm. light yellowish brown (2.5Y 6/4 moist) (50%) and brown (10YR 5/3 moist) (50%); sandy clay loam to loam (fine loamy); strong medium subangular blocky structure; firm moist, slightly sticky and plastic; common to many fine distinct Fe mottling strong brown (7.5YR 5/6), few to common fine distinct Mn mottling black (5YR 2.5/1); many fine and very fine pores; no effervescence to HCl; clear smooth boundary; pH 9.6.

3Btg1b 90 - 104 cm. light yellowish brown (2.5Y 6/4 dry) and brown (10YR 5/3 moist)(50%), pale yellow (2.5Y 7/3 dry) and yellowish brown (10YR 5/4 moist) (50%); clay (fine clayey); strong medium subangular blocky structure; firm moist, sticky and plastic; patchy thin clay skins on root channels; common to many fine distinct Mn mottling black (5YR 2.5/1), common fine distinct Fe mottling strong brown (7.5YR 5/6); many fine random pores; slightly calcareous; gradual smooth boundary; pH 9.8.

3Btg2b 104 - 127 cm. light yellowish brown (2.5Y 6/3 dry) and light olive brown (2.5Y 5/3 moist); sandy clay loam to sandy clay (fine loamy); strong coarse subangular blocky structure; firm moist, slightly sticky to sticky and plastic; thin patchy clay skins on

pedfaces; many medium distinct Mn mottling black (5YR 2.5/1), few fine distinct Fe mottling strong brown (10YR 5/8); many very fine random pores; slightly calcareous; clear smooth boundary; pH 9.7.

4BCg 127 - 151 cm. light yellowish brown (2.5Y 6/4 dry) and yellowish brown (10YR 5/4 moist) (60%), yellowish brown (10YR 5/4 dry) and brown (10YR 5/3 moist) (40%); sandy loam (coarse loamy); moderate medium subangular blocky structure; firm moist, nonplastic and nonsticky; patchy thin clay skins on root channels; many madium Mn mottling black (5YR 2.5/1), few medium distinct Fe mottling strong brown (10YR 5/8); many very fine random pores; moderately calcareous; pH 9.8.

Diagnostic horizons: argillic horizon and ochric epipedon

Radiocarbon calibration of the soil sample Sb1(6). Profile No. Sb1

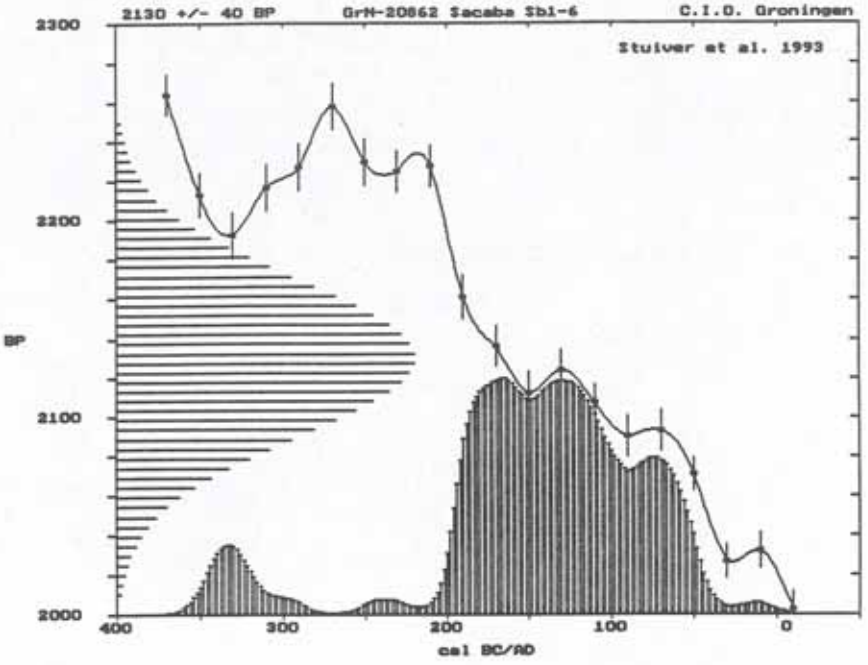

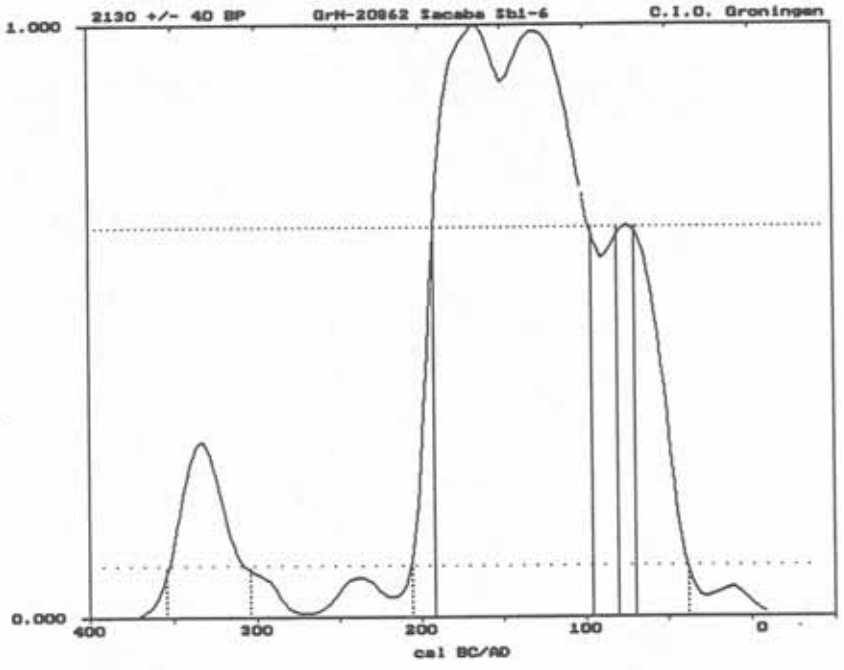

Radiocarbon calibration of the soil sample Sb3(3). Profile No. Sb3

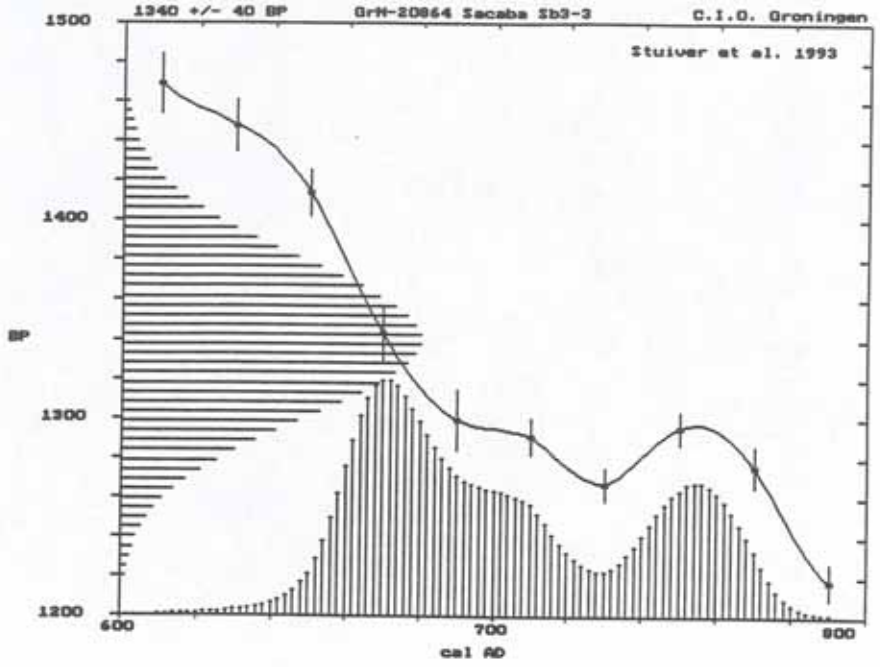

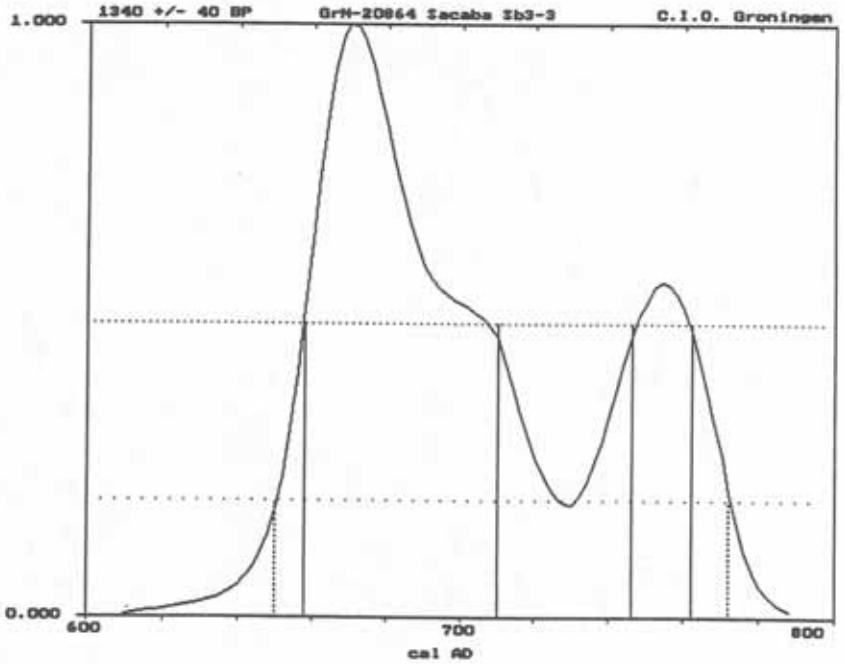

Radiocarbon calibration of the soil sample Sb88(4). Profile No. Sb88

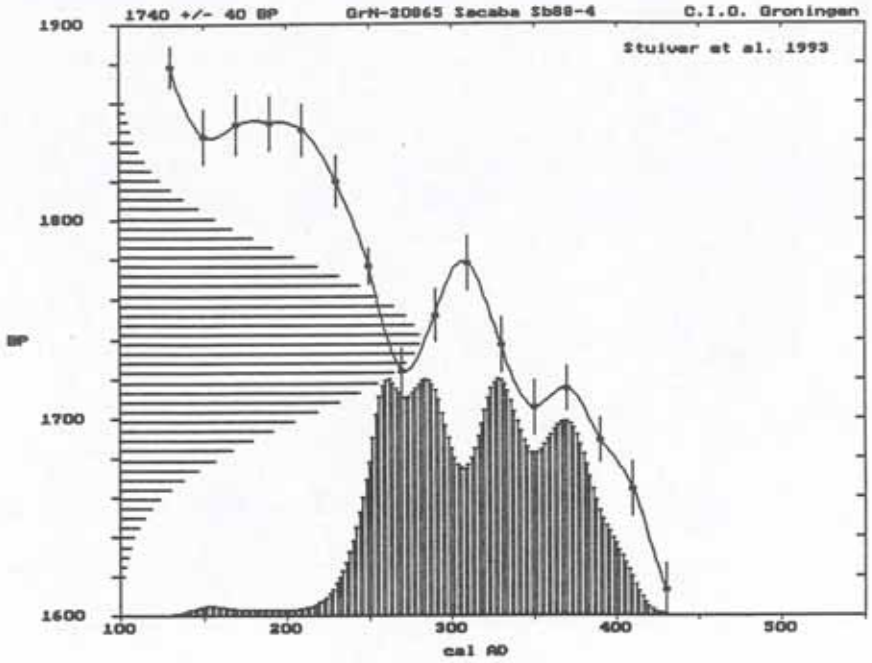

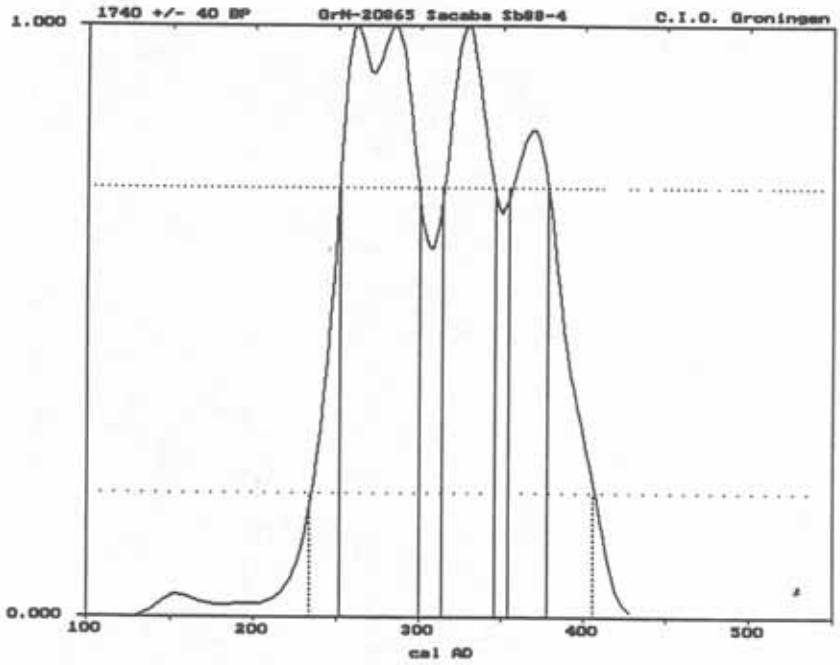

Radiocarbon calibration of the soil sample Va68(4). Profile No. Va68

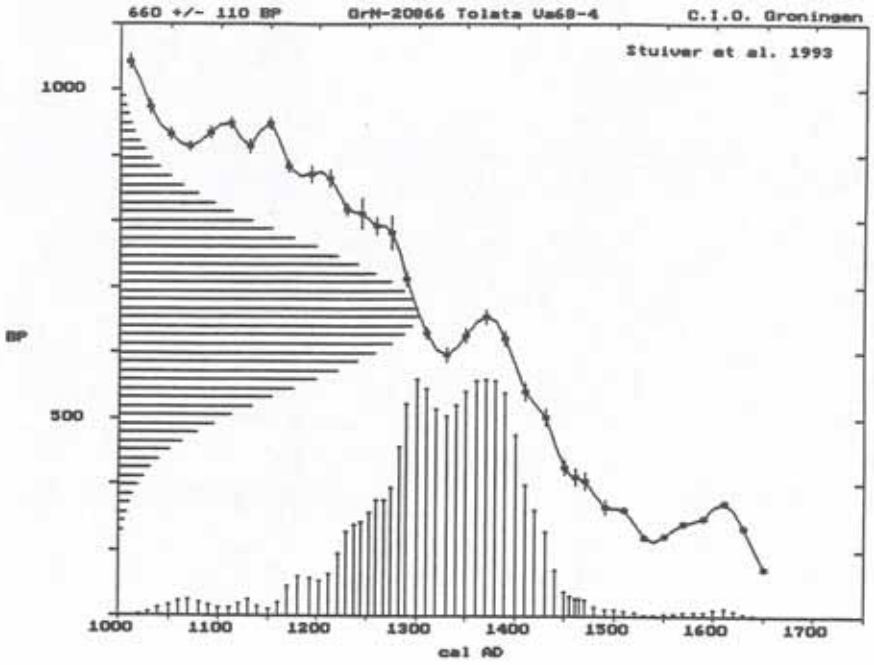

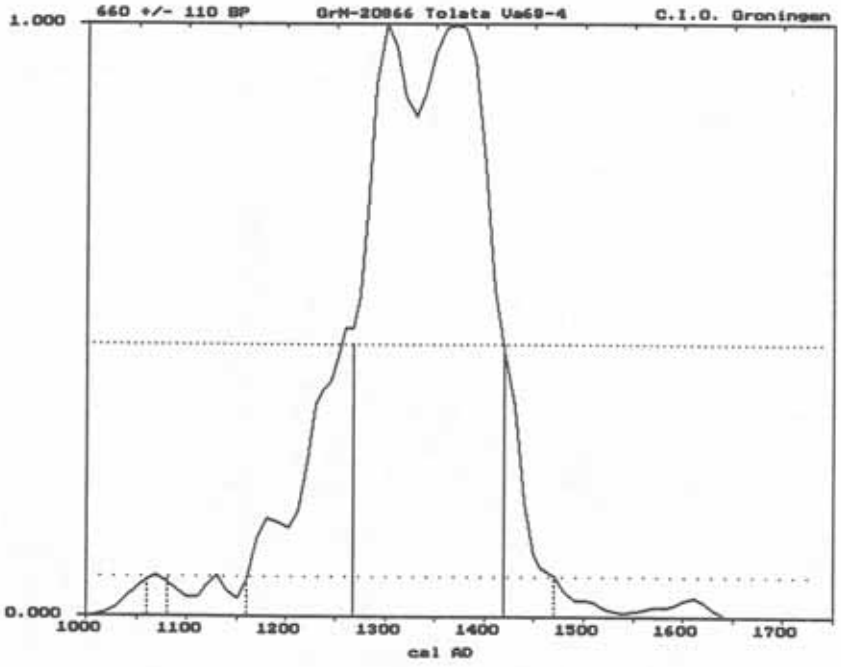

APPENDIX III:

GEOPEDOLOGIC MAP OF THE SACABA VALLEY

GEOPEDOLOGIC MAP OF THE PUNATA - CLIZA VALLEY

GEOPEDOLOGIC MAP OF THE COCHABAMBA VALLEY

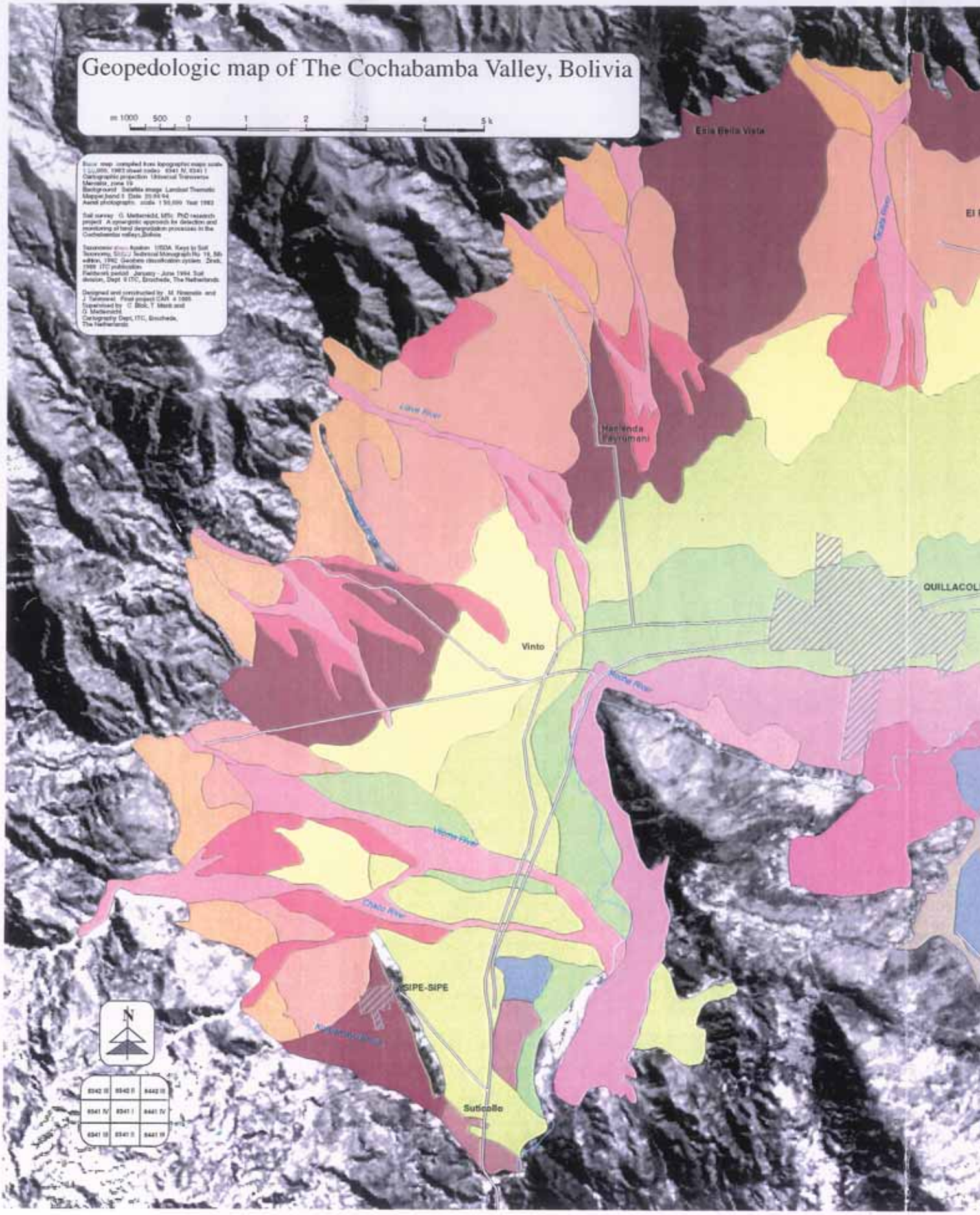
Geopedologic map of The Cochabamba Valley, Bolivia
m 1000 500 0 1 2 3 4 5 k
Base map compiled from topographic maps scale 1:50,000, 1983 sheet codes: 6341 IV, 6341 I
Cartographic projection Universal Transverse Mercator, zone 19
Background Satellite image Landsat Thematic Mapper,band 5 Date: 20-09-94
Aerial photographs scale 1:50,000 Year 1992
Soil survey G. Metternicht, MSc PhD research project A synergistic approach for detection and monitoring of land degradation processes in the Cochabamba valleys,Bolivia
Taxonomic sheet Soil Taxonomy, USDA Keys to Soil Taxonomy, SMSS Technical Monograph No 19, 5th edition, 1992 Geogenic classification system Zinck, 1988 ITC publication
Fieldwork period January - June 1994 Soil division, Dept. of ITC, Enschede, The Netherlands
Designed and constructed by M. Ninomiya and J. Tatewawa Final project CAR 4 1995
Supervised by C. Blok, T. Mank and G. Metternicht
Cartography Dept, ITC, Enschede, The Netherlands
Esta Bella Vista
Hacienda Payrumani
Vinto
QUILLACOL
SIPE-SIPE
Suticollo
N
6342 III
6342 II
6342 III
6341 IV
6341 I
6441 IV
6341 III
6341 II
6441 III

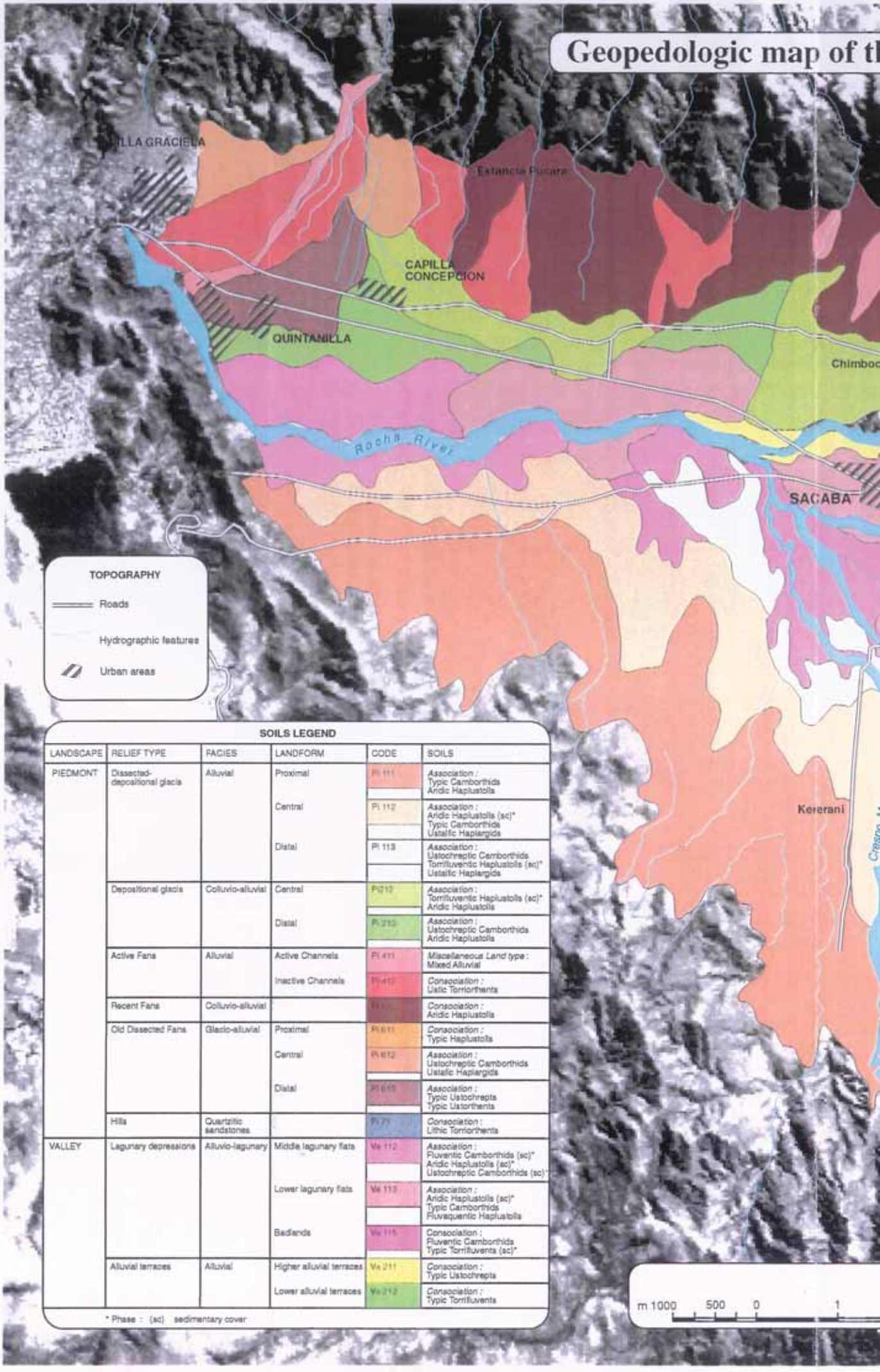

SOILS LEGEND

LANDSCAPE	RELIEF TYPE	FACIES	LANDFORM	CODE	SOILS
PIEDMONT	Dissected-depositional glacis	Alluvial	Proximal	Pi 111	*Association :* Typic Camborthids Aridic Haplustolls
			Central	Pi 112	*Association :* Aridic Haplustolls (sc)* Typic Camborthids Ustalfic Haplargids
			Distal	Pi 113	*Association :* Ustochreptic Camborthids Torrifluventic Haplustolls (sc)* Ustalfic Haplargids
	Depositional glacis	Colluvio-alluvial	Central	Pi212	*Association :* Torrifluventic Haplustolls (sc)* Aridic Haplustolls
			Distal	Pi 213	*Association :* Ustochreptic Camborthids Aridic Haplustolls
	Active Fans	Alluvial	Active Channels	Pi 411	*Miscellaneous Land type :* Mixed Alluvial
			Inactive Channels	Pi 412	*Consociation :* Ustic Torriorthents
	Recent Fans	Colluvio-alluvial		Pi [illegible]	*Consociation :* Aridic Haplustolls
	Old Dissected Fans	Glacio-alluvial	Proximal	Pi 611	*Consociation :* Typic Haplustolls
			Central	Pi 612	*Association :* Ustochreptic Camborthids Ustalfic Haplargids
			Distal	Pi 613	*Association :* Typic Ustochrepts Typic Ustorthents
	Hills	Quartzitic sandstones		Pi 71	*Consociation :* Lithic Torriorthents
VALLEY	Lagunary depressions	Alluvio-lagunary	Middle lagunary flats	Va 112	*Association :* Fluventic Camborthids (sc)* Aridic Haplustolls (sc)* Ustochreptic Camborthids (sc)*
			Lower lagunary flats	Va 113	*Association :* Aridic Haplustolls (sc)* Typic Camborthids Fluvaquentic Haplustolls
			Badlands	Va 115	*Consociation :* Fluventic Camborthids Typic Torrifluvents (sc)*
	Alluvial terraces	Alluvial	Higher alluvial terraces	Va 211	*Consociation :* Typic Ustochrepts
			Lower alluvial terraces	Va 212	*Consociation :* Typic Torrifluvents

* Phase : (sc) sedimentary cover

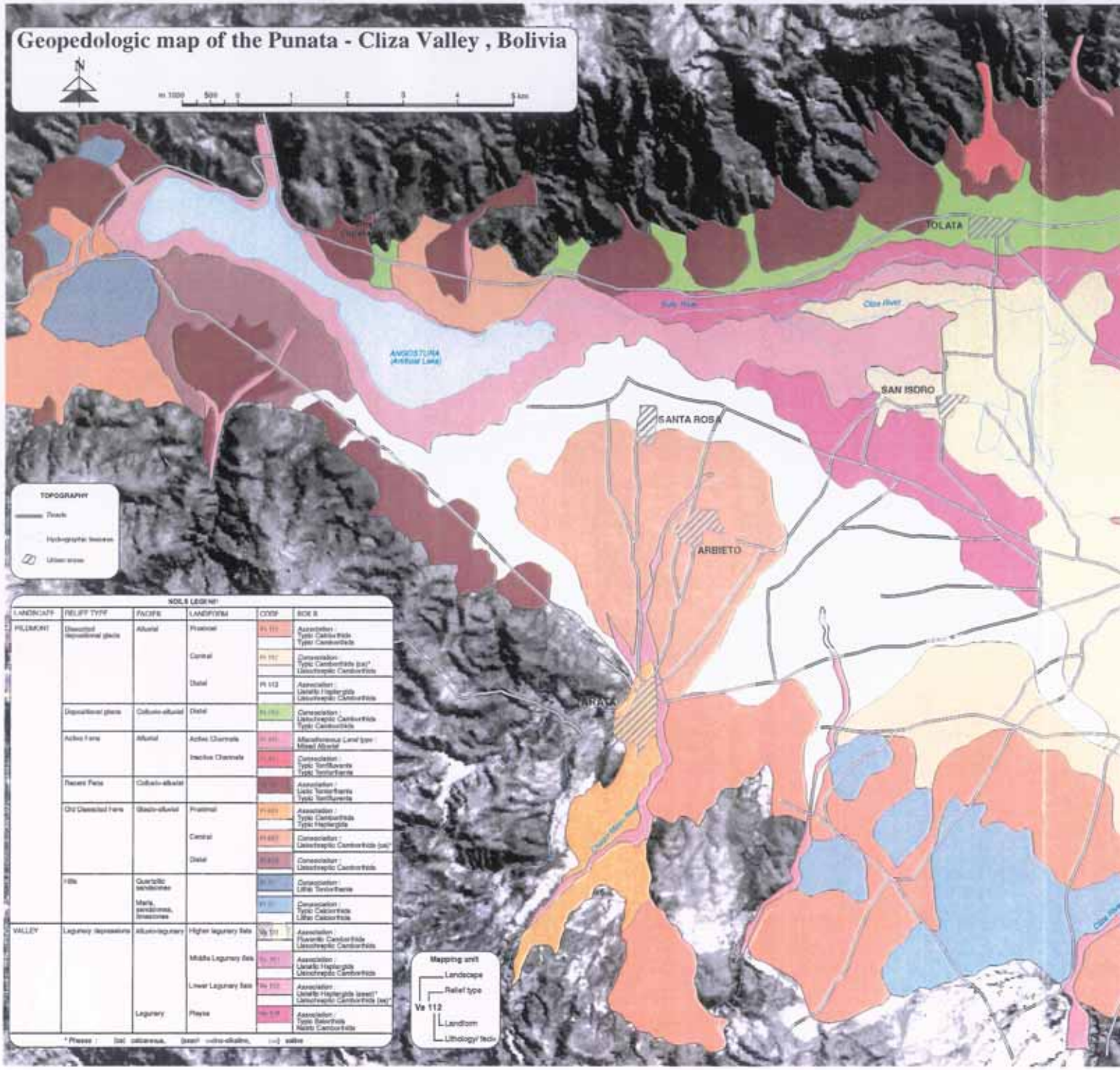
Geopedologic map of the Punata - Cliza Valley , Bolivia
TOLATA
SAN ISIDRO
SANTA ROSA
ARBIETO
ANGOSTURA
(Artificial Lake)
TOPOGRAPHY
SOILS LEGEND
LANDSCAPE
RELIEF TYPE
FACIES
LANDFORM
CODE
SOILS
PIEDMONT
VALLEY
Mapping unit
Landscape
Relief type
Va 112
Landform
Lithology/ Texture

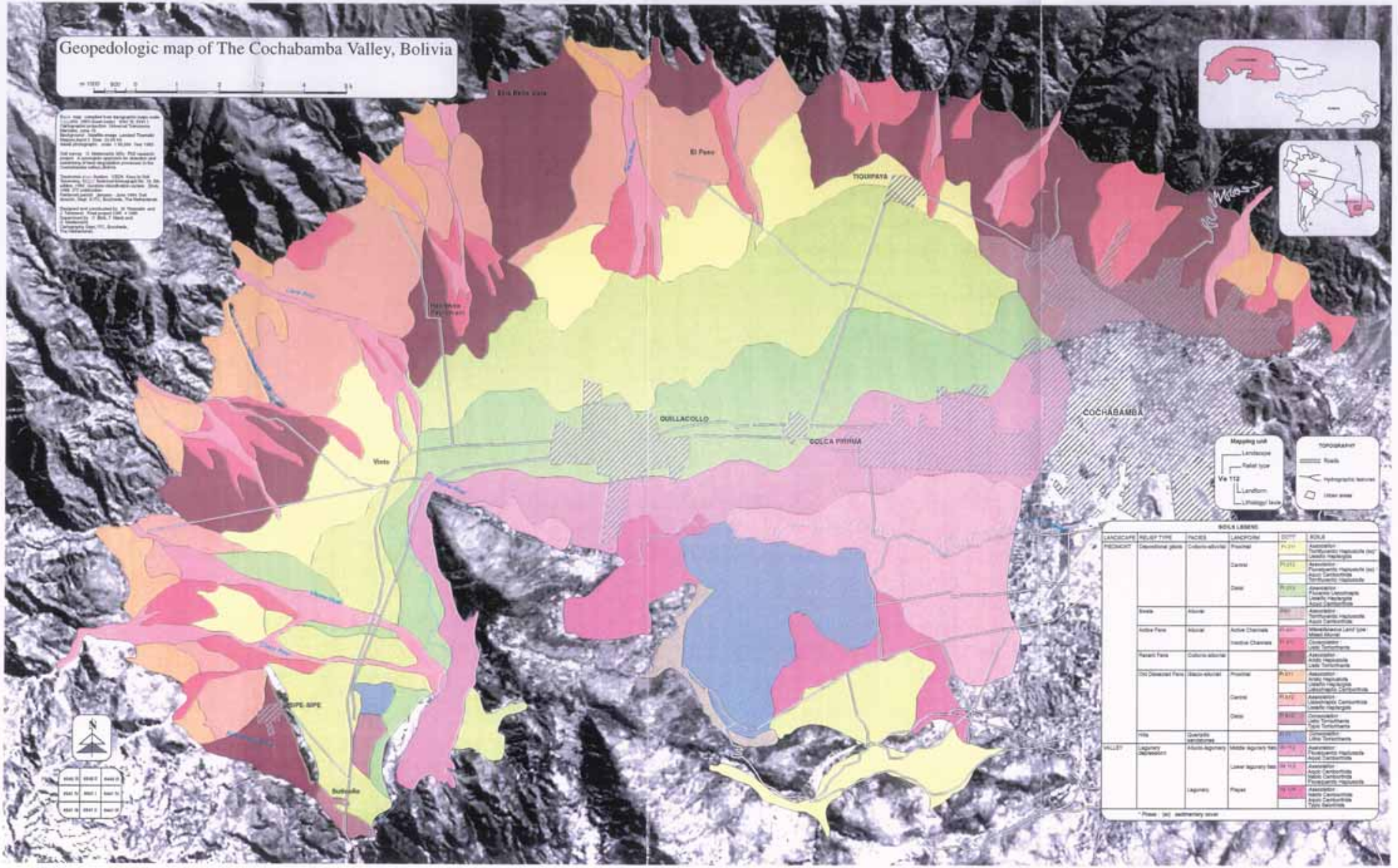
Geopedologic map of The Cochabamba Valley, Bolivia
El Paso
TIQUIPAYA
QUILLACOLLO
COCHABAMBA
SOLCA PAMPA
Vinto
SIPE SIPE
Sacaba
Mapping unit
Landscape
Relief type
Ve 112
Landform
Lithology/ facie
TOPOGRAPHY
Roads
Hydrographic features
Urban areas
SOILS LEGEND
LANDSCAPE
RELIEF TYPE
FACIES
LANDFORM
SOILS

Geopedologic map of the Sacaba Valley , Bolivia

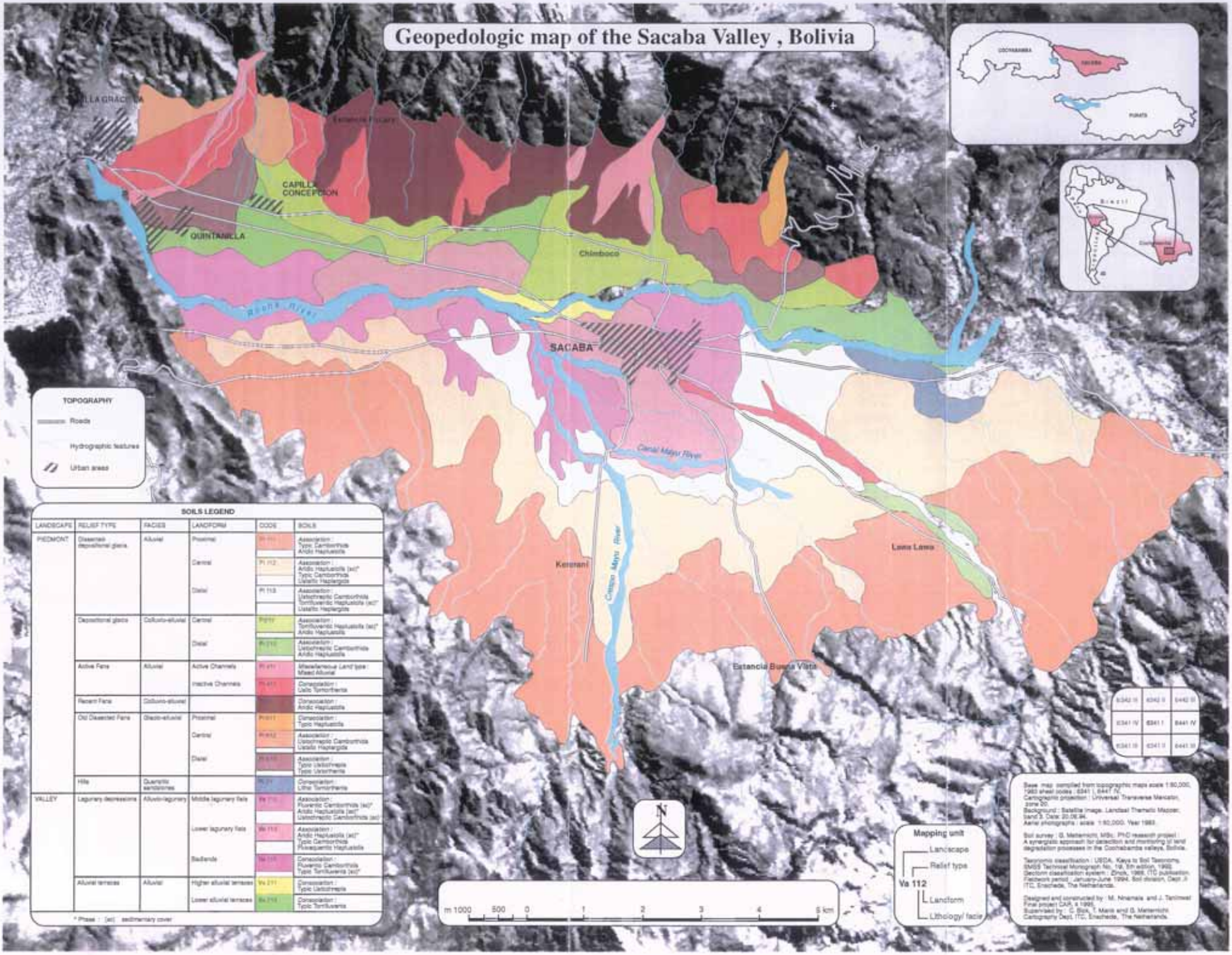

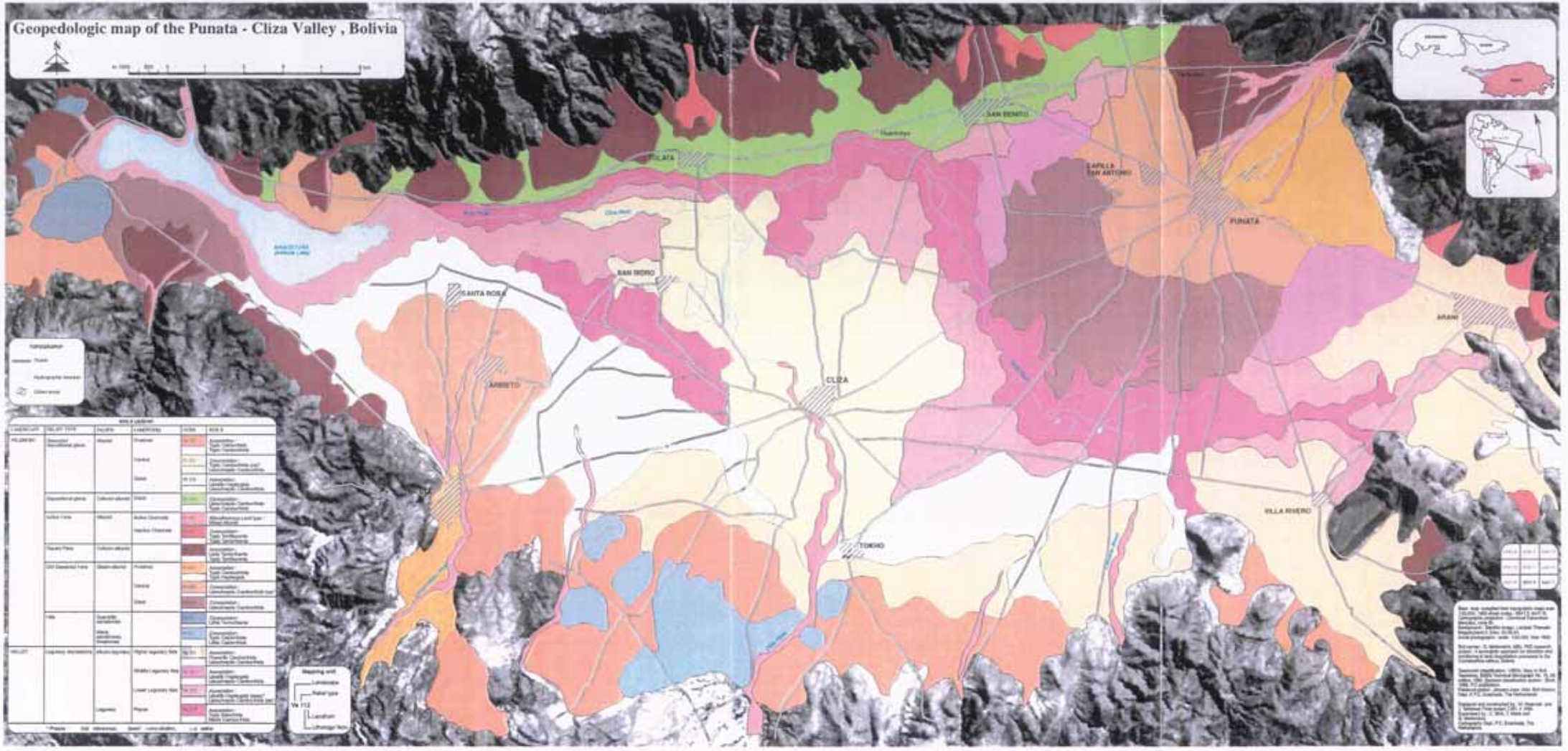
Geopedologic map of the Punata - Cliza Valley , Bolivia
CLIZA
SAN BENITO
CAPILLA SAN ANTONIO
PUNATA
SAN ISIDRO
SANTA ROSA
ARBIETO
ARANI
VILLA RIVERO
TOKKO